10th International Probabilistic Workshop

15 / 16 November 2012 in Stuttgart

Edited by
Christian Moormann
Maximilian Huber
Dirk Proske

Institut für Geotechnik der Universität Stuttgart

2012

Mitteilung 67
des Instituts für Geotechnik
Universität Stuttgart, Germany, 2012

Herausgeber:
Univ.-Prof. Dr.-Ing.habil. Christian Moormann
Institut für Geotechnik
Universität Stuttgart
Pfaffenwaldring 35
D - 70569 Stuttgart

Druck: DCC Siegmar Kästl e.K, Stuttgart, Deutschland, 2012

ISBN 978-3-921837-67-2

Preface

Safety, reliability and risk are key issues in a world with continuously increasing complexity. Road and railway accidents, tunnel fires or natural hazards like hurricanes, floods or earthquakes show the vulnerability of our technical facilities and the natural and social environment. Therefore the consideration of safety and risk is without doubt a very important issue during the design of technical facilities, such as civil engineering structures and infrastructure works. Questions about the analysis and treatment of safety and risk arise, as well as questions about optimal safety levels or questions about acceptable values.

In 2012 we celebrate 10 years of the symposium "International Probabilistic Workshop". This series of probabilistic workshops on safety and risk in civil engineering were organized starting 2003/2004 in Dresden, followed 2005 in Vienna, 2006 in Berlin, 2007 in Ghent, 2008 in Darmstadt, 2009 in Delft, 2010 in Szczecin and 2011 in Braunschweig. During all this symposiums more than 200 presentations were given and thousands of pages were written for the conference proceedings. The covers of the proceedings of these former symposiums can be seen on the next page. Besides the proceedings, special issues of the journals "Structure and Infrastructure Engineering", "Beton- und Stahlbetonbau" and "Georisk" based on expanded papers from symposiums were published.

This series is continued with the 10th Probabilistic Workshop at University of Stuttgart, which is organised jointly by the Institute of Geotechnical Engineering of the University of Stuttgart and the Institute of Natural Hazards, University of Natural Resources and Applied Life Sciences-Vienna.

Four internationally renowned keynote speakers will lecture on risk, reliability and probability methods in mechanical engineering, geotechnical engineering, financial engineering and clinical economics. This year the conference programme includes 21 contributions from prestigious authors coming form all over the world, which have been reviewed by the scientific committee in order to guarantee the quality of the work.

Finally, the organizers are grateful to all those who have helped and contributed to the organisations of this event. The largest part of the credit for theses

proceedings goes to the authors, speakers and the reviewers, not only for this conference, but for all conferences in this series.

We look forward to the interesting presentations, animated discussions and gracious meetings at our conference. Furthermore the editors hope that this set of papers can be a useful reference for many readers.

Christian Moormann, Maximilian Huber & Dirk Proske

Editors

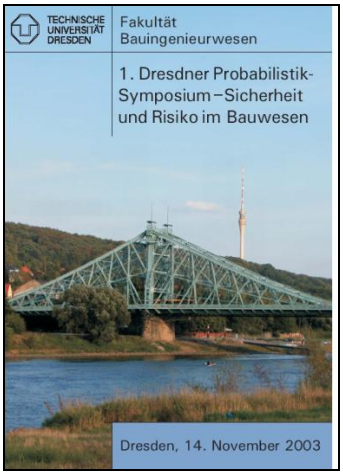
TECHNISCHE UNIVERSITÄT DRESDEN
Fakultät Bauingenieurwesen
1. Dresdner Probabilistik-Symposium – Sicherheit und Risiko im Bauwesen
Dresden, 14. November 2003

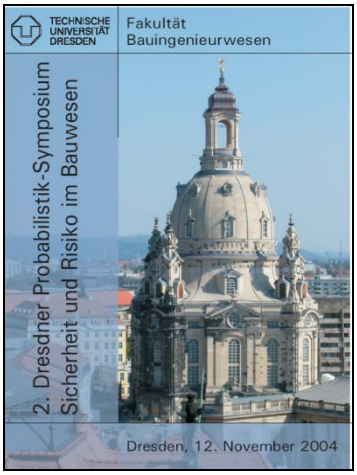
TECHNISCHE UNIVERSITÄT DRESDEN
Fakultät Bauingenieurwesen
2. Dresdner Probabilistik-Symposium
Sicherheit und Risiko im Bauwesen
Dresden, 12. November 2004

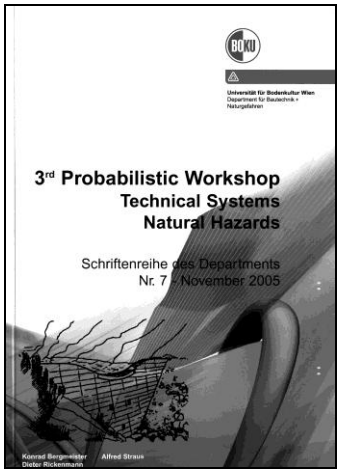
3rd Probabilistic Workshop
Technical Systems
Natural Hazards
Schriftenreihe des Departments
Nr. 7 / November 2005

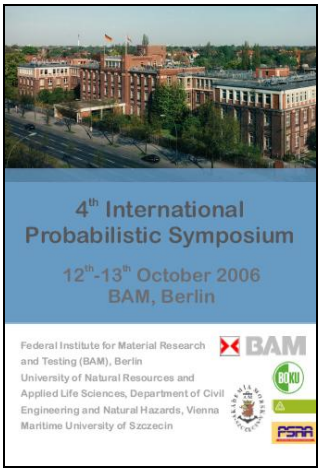
4th International
Probabilistic Symposium
12th-13th October 2006
BAM, Berlin
Federal Institute for Material Research and Testing (BAM), Berlin
University of Natural Resources and Applied Life Sciences, Department of Civil Engineering and Natural Hazards, Vienna
Maritime University of Szczecin
BAM

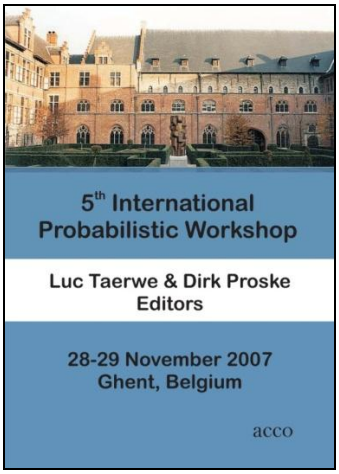
5th International
Probabilistic Workshop
Luc Taerwe & Dirk Proske
Editors
28-29 November 2007
Ghent, Belgium
acco

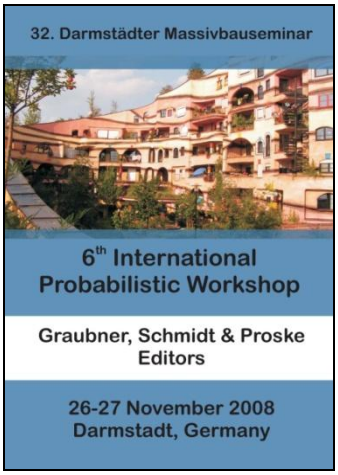
32. Darmstädter Massivbauseminar
6th International
Probabilistic Workshop
Graubner, Schmidt & Proske
Editors
26-27 November 2008
Darmstadt, Germany

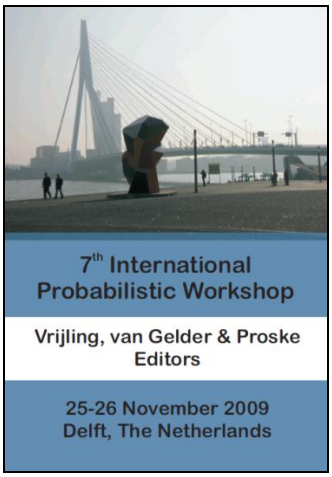
7th International
Probabilistic Workshop
Vrijling, van Gelder & Proske
Editors
25-26 November 2009
Delft, The Netherlands

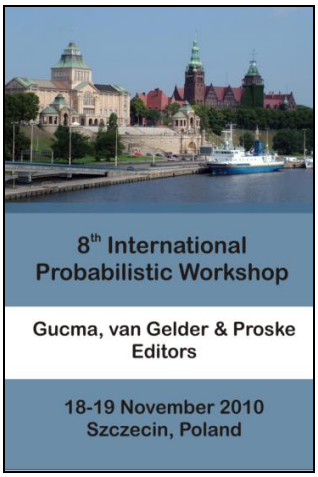
8th International
Probabilistic Workshop
Gucma, van Gelder & Proske
Editors
18-19 November 2010
Szczecin, Poland

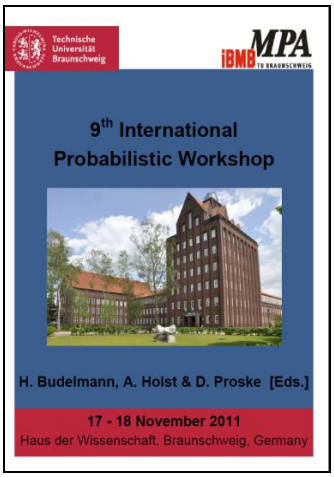
Technische Universität Braunschweig
iBMB MPA
9th International
Probabilistic Workshop
H. Budelmann, A. Holst & D. Proske [Eds.]
17 - 18 November 2011
Haus der Wissenschaft, Braunschweig, Germany

Table of contents

Recent Developments in Applied Mechanics with Uncertainties

Isaac Elishakoff
Department of Ocean and Mechanical Engineering
Florida Atlantic University
Boca Raton, FL 33431-0991, U.S.A.

It has been recognized during past decades that deterministic mechanics as such cannot answer all problems that arise in engineering. For example, the safety factor that is being utilized in engineering design cannot possibly be justified within deterministic mechanics. Thus, the uncertainty analysis is introduced in deterministic analysis 'via the back door.' The realistic analysis and design of structures demands the introduction of uncertainty analyses. To accomplish this goal, until very recently the only methodology used was the probabilistic analysis. It is interesting to note that the first attempt to do so, appears to have been a dissertation by Max Mayer titled Die Sicherheit der Bauwerke und ihre Berechnung nach Grenzkraeften astatt nach zulaessigen Spannungen, published in 1926 by Springer. In this spirit the lecture reviews first the safety factor idea and then the most common method that is applied in stochastic analysis of nonlinear structures, namely the stochastic linearization technique.

Then the lecture deals with alternatives to probability analysis: interval and ellipsoidal analyses and shows which one should be used in which circumstances .In these analyses no probability or fuzzy measures are needed to be known. These analyses depend on scarce knowledge—that is often the case-for involved uncertain variables. Instead the bounds--as either intervals or ellipsoids--are incorporated into the analysis. The notion of combined optimization and anti-optimization will be discussed. At the last part the lecture reviews the notion of the fuzzy safety factor.

Many researchers prefer to use one of these techniques exclusively and maintain that only one of these methods is useful. In fact it appears that there is, as it were, a Babel Tower erected between different methodologies of uncertainty analyses. As pragmatic creatures engineers appear to be in need to know each of these techniques and use them in different circumstances depending on the character and the amount of available data.

References

Elishakoff, I., Probabilistic Theory of Structures, Dover, Mineola, NY, 1999.

Elishakoff, I., Safety Factors and Reliability: Friends or Foes, Kluwer, Dordrecht, 2004.

Elishakoff, I. and Ohsaki M., Optimization and Anti-Optimization of Structures under Uncertainty, Imperial College Press, London, 2010.

A finite cell approach for discretization of random fields

Wolfgang Betz[1], Iason Papaioannou, Daniel Straub
Engineering Risk Analysis Group, Faculty of Civil Engineering and Geodesy,
Technische Universität München, Germany

Abstract: A new method for discretization of Gaussian random fields with only a small number of random variables in the representation is introduced. The method is based on the Karhunen-Loève (KL) expansion, which is optimal among series expansion methods with respect to the global mean square truncation error. The resulting integral eigenvalue problem in the KL-expansion is discretized using a finite cell (FC) approach; i.e. the domain of computation is extended beyond the physical domain up to the boundaries of an embedding domain with a primitive geometrical shape. Higher order polynomials are used as FC shape functions. The approach is useful for random fields defined on domains with complex geometries since it shifts the problem from the mesh generation to the integration of discontinuous functions defined over a fictitious domain. A suitable approach for numerical integration is described. The presented method is compared to the Expansion Optimal Linear Estimation (EOLE) method and to the finite element discretization of the KL-expansion with respect to the mean error variance and in terms of computational costs. On the one hand, the proposed approach shows an exponential rate of convergence in terms of the dimension of the matrix eigenvalue problem to solve for a fixed number of random variables. On the other hand, obtaining a solution for the random field approximation takes considerably longer than with the EOLE method. However, the generation of a realization of the random field representation with the finite cell approach is computationally more efficient than with EOLE.

1 Introduction

A stochastic analysis of structures in civil engineering often requires the modeling of input parameters that vary randomly in space (e.g. load distributions or material parameters). This type of uncertainty is modeled by means of ran-

[1] With the support of the Technische Universität München - Institute for Advanced Study, funded by the German Excellence Initiative.

dom fields. A random field represents a random quantity at each point of a continuous domain, and, thus, consists of an infinite number of random variables. For computational purposes, the random field has to be expressed using a finite number of random variables. This step is referred to as random field discretization.

The efficiency of a random field discretization method depends on its ability to approximate the original random field accurately with a minimum number of random variables. Accuracy is to be defined with respect to a certain error measure such as the global mean square truncation error. It is advantageous to keep the number of random variables in the representation of the random field small, since it can have a considerable influence on the computational costs of a subsequent stochastic analysis. An example is finite element reliability analysis [2] where, for instance, a first-order reliability method (FORM) is employed to obtain an estimate of the failure probability of the investigated system. Another example is the spectral stochastic finite element method [4]. For this method, the size of the problem to solve is a function involving factorials of the input random variables and, thus, the problem size increases drastically with increasing number of random variables. An overview of random field discretization methods is given in [9].

The Karhunen-Loève (KL) expansion of random fields is optimal in the global mean square truncation error with respect to the number of random variables in the representation [5]. However, its analytical solution is available only for primitive geometries and for a few selected autocovariance functions. For complex-shaped geometries, a finite element based approach can be chosen to approximate the solution of the KL expansion. However, this requires a spatial decomposition of the domain.

The requirements to a good random field mesh are not the same as the requirements to a good mesh of the corresponding mechanical system (see [9]). Consequently, two different meshes might be necessary. However, working with different meshes is a handicap in writing efficient algorithms for post-processing the random field (e.g. evaluating the realization of the field at every finite element Gauss-point). A possible remedy is to use the elements in the FE mesh as a basis for the random field mesh, and to adapt the mesh by either refining individual elements or by coalescing different elements. This approach becomes impractical for two- or three-dimensional problems if the physical domain is of complex geometrical shape. This includes domains with curved boundaries, domains with holes, and porous media. Therefore, meshless approaches appear to be favorable on complex shaped domains.

The Expansion Optimal Linear Estimation (EOLE) method [6] does not require a mesh; the domain of the field is approximated by a number of points. Consequently, the shape of the physical domain is of minor importance, since the selection of points can be easily performed on a fictitious domain containing the actual physical domain, where all points outside of the physical domain are neglected. Another meshless approach [7] is to embed the physical domain in a larger domain of primitive geometrical shape. The KL expansion is then solved for the primitive domain, either analytically or numerically. However, the optimality of the KL expansion with respect to the mean square truncation error is lost in this approach since the expansion is solved on a domain that is larger than the actual physical domain.

The finite cell (FC) method [8] is a fictitious domain approach, developed as an extension of the finite element method. Following this approach, the physical domain is embedded in elements of primitive geometrical shape. Higher order shape functions are of crucial importance for the applicability of the method because they yield a fast rate of convergence [8]. The finite cell method shifts the problem of complex geometries from the mesh generation to the integration.

In this work, a finite cell like approach is utilized to discretize the spatial domain of the random field and, thus, to approximate the solution of the Karhunen-Loève expansion numerically. The proposed method inherits the efficiency of the KL expansion if the error in the numerical integration is negligible and if the eigenmodes of the KL expansion can be approximated well by the chosen shape functions. The presented method is compared to the EOLE method and to the finite element discretization of the KL-expansion. The proposed approach shows an exponential rate of convergence with respect to the size of the matrix eigenvalue problem to solve. On the other hand, obtaining a solution for the random field approximation takes considerably longer than with the EOLE method. However, the generation of a realization of the random field representation with the finite cell approach is more efficient in terms of computational cost than with EOLE.

2 Discretization of random fields

A continuous random field $H(\mathbf{x},\theta)$ may be loosely defined as a random function that describes a random quantity at each point $\mathbf{x}\in\Omega$ of a continuous domain $\Omega\subset\mathbf{R}^d$, $d\in\mathbf{N}_{>0}$. $\theta\in\Theta$ is a coordinate in the sample space Θ, and (Θ,F,P) is a complete probability space. If the random quantity attached to each point $\mathbf{x}$ is a random variable, the random field is said to be *univariate* or

real-valued. If the random quantity is a random vector, the field is called *multivariate*. The dimension d of a random field is the dimension of its topological space Ω. One usually distinguishes between a *one-* and a *multidimensional* random field, the former one is also referred to as *random process*. The field is said to be Gaussian if the distribution of $(H(\mathbf{x}_1,\theta),\ldots,H(\mathbf{x}_n,\theta))$ is jointly Gaussian for any $(\mathbf{x}_1,\ldots,\mathbf{x}_n)\in\Omega$ and any $n\in\mathbf{N}_{>0}$. It is completely defined by its mean function $\mu(\mathbf{x}):\Omega\to\mathbf{R}$ and auto-covariance function $Cov(\mathbf{x},\mathbf{x}'):\Omega\times\Omega\to\mathbf{R}$. In the following, we will restrict ourselves to continuous univariate multidimensional Gaussian random fields.

The approximation $\hat{H}(\cdot)$ of a continuous random field $H(\cdot)$ by a finite set of random variables $\{\chi_i(\theta), i=1,\ldots,M\}$ is referred to as *random field discretization*.

2.1 Error measures

Different error measures are available to quantify the error resulting from the discretization of a random field. For a given outcome θ, the *truncation error* $\varepsilon_H(\cdot)$ is defined at position $\mathbf{x}$ as the difference between the random field and its approximation:

$$\varepsilon_H(\mathbf{x},\theta) = H(\mathbf{x},\theta) - \hat{H}(\mathbf{x},\theta). \tag{1}$$

In the context of this work, we will assume that the mean function of the approximated random field can be modeled precisely, i.e. $\mathrm{E}\left(\varepsilon_H(\mathbf{x},\theta)\right)=0\ \forall\,\mathbf{x}\in\Omega$.

In general, the truncation error can only be evaluated if the exact representation of the random field is known explicitly. This is usually not the case. In the following, an error estimator is introduced which circumvents this problem. $\varepsilon_\sigma(\mathbf{x})$ is known as the *error variance* and has been commonly used in the literature; it is defined as:

$$\varepsilon_\sigma(\mathbf{x}) = \frac{\mathrm{Var}\left(H(\mathbf{x},\theta)-\hat{H}(\mathbf{x},\theta)\right)}{\mathrm{Var}\left(H(\mathbf{x},\theta)\right)} = \frac{\mathrm{Var}\left(H(\mathbf{x},\theta)-\hat{H}(\mathbf{x},\theta)\right)}{\sigma^2(\mathbf{x})}, \tag{2}$$

where $\sigma(\mathbf{x})$ is the standard deviation function of the random field $H(\mathbf{x},\theta)$.

Pointwise measures are of little use when making a quantitative assessment of the quality of the overall random field approximation. Therefore, the following global error norm $\bar{\varepsilon}_\sigma$, known as the *mean error variance*, is used here:

$$\bar{\varepsilon}_\sigma = \frac{\int_\Omega \varepsilon_\sigma(\mathbf{x})\,\mathrm{d}\,\mathbf{x}}{|\Omega|} \tag{3}$$

where $|\Omega| = \int_\Omega \mathrm{d}\,\mathbf{x}$. Besides the mean error variance, other global error measures haven been used in the literature. For example, in [6] the supremum norm of the error variance was used to compare different random field discretization methods. It has been noted in [10] that different global error measures might favor different discretization methods. In this work, we will only investigate convergence with respect to the mean error variance.

2.2 Karhunen-Loève expansion

The KL-expansion is a series expansion method for the representation of a random field. The expansion is based on the spectral decomposition of the covariance function of the field. It states that a random field can be represented exactly by the following expansion:

$$H(\mathbf{x},\theta) = \mu(\mathbf{x}) + \sum_{i=1}^{\infty} \sqrt{\lambda_i}\,\varphi_i(\mathbf{x})\,\xi_i \tag{4}$$

where $\mu(\mathbf{x})$ is the mean function of the field, ξ_i are independent standard normal random variables, and λ_i, $\varphi_i(\mathbf{x})$ are the eigenvalues and eigenfunctions of the covariance kernel obtained from solving the integral eigenvalue problem:

$$\int_\Omega \varphi_i(\mathbf{x})\,\mathrm{Cov}(\mathbf{x},\mathbf{x}')\,\mathrm{d}\,\mathbf{x}' = \lambda_i \varphi_i(\mathbf{x}) \tag{5}$$

The eigenfunctions are by definition orthonormal, i.e. $\int_\Omega \varphi_i(\mathbf{x})\,\varphi_j(\mathbf{x})\,\mathrm{d}\,\mathbf{x} = \delta_{ij}$, where δ_{ij} is the Kronecker delta.

2.2.1 Truncated Karhunen-Loève expansion

The truncated KL-expansion is obtained by arranging the eigenvalues and eigenfunctions in a descending series with respect to the magnitude of the eigenvalues, and truncating the ordered expansion after M terms. The truncated KL-expansion does no longer represent the random field $H(\mathbf{x})$ exactly, but provides an approximation $\tilde{H}(\mathbf{x})$ of the field. Hence, the truncated KL-expansion is a random field discretization method. The discretized random field is written as:

$$\tilde{H}(\mathbf{x},\theta) = \mu(\mathbf{x}) + \sum_{i=1}^{M} \sqrt{\lambda_i}\,\varphi_i(\mathbf{x})\xi_i \tag{6}$$

An important property of the truncated KL-expansion is that the global mean square error is minimized with respect to any other complete basis of $L^2(\Omega)$ [5].

2.2.2 Error variance

For the truncated KL-expansion, the error variance can be expressed as [9]:

$$\varepsilon_\sigma(\mathbf{x}) = 1 - \frac{\sum_{i=1}^{M} \lambda_i \varphi_i^2(\mathbf{x})}{\sigma^2(\mathbf{x})} \tag{7}$$

2.3 Finite element approximation of the KL-expansion

The KL-expansion involves solving the integral eigenvalue problem given in equation 5. Equation 5 can be solved analytically only for a few covariance functions and geometries (see [5]). Therefore, for general problems with arbitrary geometries and covariance functions, a numerical approach is necessary. This involves a spatial discretization of the integral eigenvalue problem. Obviously, this introduces yet another approximation to the representation of the random field. The obtained eigenvalues $\hat{\lambda}_i$ and eigenfunctions $\hat{\varphi}_i(\mathbf{x})$ are, therefore, approximations to the eigenvalues λ_i and eigenfunctions $\varphi_i(\mathbf{x})$ of the analytical solution of the KL-expansion. The approximation of the random field can be expressed as:

$$\hat{H}(\mathbf{x},\theta) = \mu(\mathbf{x}) + \sum_{i=1}^{M} \sqrt{\hat{\lambda}_i}\,\hat{\varphi}_i(\mathbf{x})\xi_i \tag{8}$$

In the finite element approximation of the KL-expansion (in the following referred to as *FE-KL method*), the eigenfunctions are approximated as:

$$\hat{\varphi}_i(\mathbf{x}) = \sum_{n=1}^{N} d_n^i N_n(\mathbf{x}) = \mathbf{N}^{\mathrm{T}}(\mathbf{x})\,\mathbf{d}_i \tag{9}$$

where N is the number of shape functions, $N_n(\mathbf{x}) \in L^2(\Omega)$ are the global shape functions forming a basis in a chosen sub-space of the set of all Lebesgue square-integrable functions on Ω, and $d_n^i \in \mathbf{R}$ are the coordinates of the *i*th eigenfunction in the basis formed by all shape functions. $\mathbf{N}^{\mathrm{T}}(\mathbf{x})$ is a vector function of $\mathbf{x}$ with elements $N_n(\mathbf{x})$, and $\mathbf{d}_i$ is a vector containing the coeffi-

cients d_n^i. It is important to note that the eigenfunctions are by definition orthonormal and, therefore, the vectors $\mathbf{d}_i$ have to be scaled appropriately.

The approximation of the integral eigenvalue problem defined in equation 5 by means of equation 9 introduces an error term, denoted $\varepsilon_N^i(\mathbf{x})$. The coefficients of the vectors $\mathbf{d}_i$ are selected such that the error term $\varepsilon_N^i(\mathbf{x})$ becomes orthogonal to the space spanned by the shape functions. A solution to this problem is given by the matrix eigenvalue problem:

$$\mathbf{B}\mathbf{d}_i = \hat{\lambda}_i \mathbf{M}\mathbf{d}_i \tag{10}$$

The coefficients B_{kn} of the matrix $\mathbf{B}$ are defined as:

$$B_{kn} = \int_{\mathbf{x}\in\Omega} N_k(\mathbf{x}) \int_{\mathbf{x}'\in\Omega} N_n(\mathbf{x}') \operatorname{Cov}(\mathbf{x},\mathbf{x}') \,\mathrm{d}\mathbf{x}' \,\mathrm{d}\mathbf{x} \tag{11}$$

The coefficients M_{kn} of the matrix $\mathbf{M}$ are defined as:

$$M_{kn} = \int_{\mathbf{x}\in\Omega} N_k(\mathbf{x}) \, N_n(\mathbf{x}) \,\mathrm{d}\mathbf{x} \tag{12}$$

The error variance of the FE-KL approach can be expressed as [1]:

$$\varepsilon_\sigma(\mathbf{x}) = 1 + \frac{\sum_{i=1}^{M} \hat{\lambda}_i \hat{\varphi}_i^2(\mathbf{x}) - 2 \cdot \sum_{i=1}^{M} \hat{\varphi}_i^2(\mathbf{x}) \int_\Omega \operatorname{Cov}(\mathbf{x},\mathbf{x}') \hat{\varphi}_i(\mathbf{x}') \, d\mathbf{x}'}{\sigma^2(\mathbf{x})} \tag{13}$$

In case of a constant standard deviation σ within the domain of the field, the mean error variance reduces to (compare [1]):

$$\bar{\varepsilon}_\sigma = 1 - \frac{1}{\sigma^2 \cdot |\Omega|} \cdot \sum_{i=1}^{M} \hat{\lambda}_i \tag{14}$$

2.4 Finite cell approximation of the KL-expansion

The finite cell method [8] was developed as an extension to the finite element method for the solution of linear elasticity problems. Let $\Omega \subset \mathbf{R}^d$ be the domain of interest and $\Omega^* \subset \mathbf{R}^d$ a geometrically simpler domain with $\Omega \subseteq \Omega^*$. The geometrically simpler domain Ω^* is called *primitive domain*, and the original domain Ω is called *physical domain*. Furthermore, let the shape functions $N_n^*(\mathbf{x}) \in L^2(\Omega^*)$ form a basis of a subspace in $L^2(\Omega^*)$. We are searching a solution of the integral equation defined on Ω, and approximate it with functions defined on Ω^*.

The spatial decomposition of the problem is performed on the primitive domain Ω^* (this is illustrated in figure 1). Since Ω^* is by definition of primitive geometrical shape (e.g. a hyperrectangle), the meshing of the domain is a triv-

ial task. However, the region $\Omega^* \cap \overline{\Omega}$ is not part of the physical domain. In order to solve the original, i.e. physical, problem, the non-physical part of the extended domain Ω^* must not influence the solution. For this reason, we introduce the mapping $\alpha : \Omega^* \to \{0,1\}$ as:

$$\alpha(\mathbf{x}) = \begin{cases} 1 & \forall\, \mathbf{x} \in \Omega \\ 0 & \text{otherwise} \end{cases} \tag{15}$$

In order to solve the problem defined in equation 10 we have to assemble the matrices $\mathbf{M}$ and $\mathbf{B}$. The integral in equation 12 can be transformed to an integral over Ω^* as:

$$M_{kn} = \int_{\mathbf{x} \in \Omega^*} \alpha(\mathbf{x})\, N_k(\mathbf{x})\, N_n(\mathbf{x})\, \mathrm{d}\mathbf{x} \tag{16}$$

In a similar way, the integral in equation 11 can be written as:

$$B_{kn} = \int_{\mathbf{x} \in \Omega^*} \alpha(\mathbf{x})\, N_k(\mathbf{x}) \int_{\mathbf{x}' \in \Omega^*} \alpha(\mathbf{x}')\, N_n(\mathbf{x}')\, \mathrm{Cov}(\mathbf{x}, \mathbf{x}')\, \mathrm{d}\mathbf{x}'\, \mathrm{d}\mathbf{x} \tag{17}$$

In the finite cell approach, the shape functions are defined locally on the cells Ω_e, see Figure 1. Higher order hierarchical shape functions based on the integrated Legendre polynomials [11] are used, compare [8]. Note that the integrals in equations 16 and 17 are smooth over the domain Ω but not even continuous over the domain Ω^*. Therefore, it is important to use appropriate numerical integration schemes in order to keep the integration error small.

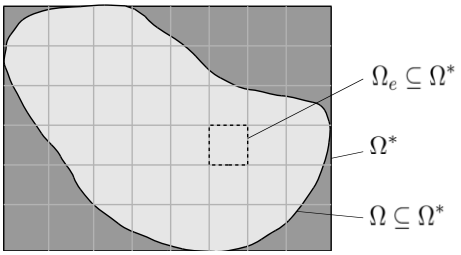

Figure 1. Notation for the finite cell approach.

A staggered Gaussian integration scheme is proposed. The principal idea of this integration scheme is illustrated in figure 2. For staggered Gaussian integration, a tree-based mesh refinement is used to mesh the domain of the finite cell for integration. For one-, two- and three-dimensional elements, a binary-, quad- and oct-tree is used, respectively. Gaussian integration is applied in the leaf elements of the tree. A tree-element is refined if it is cut by the boundary of the physical domain and if the element level is smaller than the maximum tree-depth. The element level of the finite cell itself is zero.

In the context of this work, the number of Gauss-points used on the respective levels of the tree is decreased with an increasing level. This is contrary to the approach presented in [8] and [3], where all sub-cells were integrated with a full number of Gauss-points. However, in the cut-cells the function to integrate is discontinuous and, therefore, cannot be approximated well using polynomials. Moreover, the influence area of the individual Gauss-points is not directly observable and not necessarily accumulated around the corresponding point.

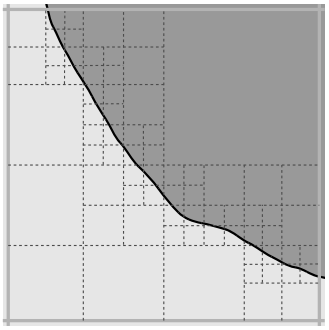

Figure 2. Staggered Gaussian integration: mesh for integration on a cut finite cell.

Assuming the integration error is small enough, $\varepsilon_\sigma(\mathbf{x})$ and $\bar{\varepsilon}_\sigma$ can be computed according to equation 13 and 14, respectively.

2.5 EOLE method

The EOLE method [6] is a series expansion method that is based on an optimal linear estimation using discrete points of the field and carries out a spectral decomposition of the covariance matrix $\mathbf{\Sigma}_{\chi\chi}$ corresponding to these points. The coefficients of the covariance matrix are defined as $\left(\mathbf{\Sigma}_{\chi\chi}\right)_{ij} = \mathrm{Cov}\left(\chi_i, \chi_j\right)$ with $i, j \in \{1,2,\ldots N\}$, where each χ_i is a random variable associated with a point $\mathbf{x}_i \in \Omega$.

The points $\mathbf{x}_i$ are used to discretize the domain Ω of the random field pointwise. Consequently, the domain is represented approximately by a finite number of points and no finite element mesh is required. The distribution of the points $\mathbf{x}_i$ has an influence on the random field approximation, especially if the field is approximated by a minimal number of points.

The random field representation in case of the EOLE method writes:

$$\hat{H}(\mathbf{x},\theta) = \mu(\mathbf{x}) + \sum_{i=1}^{M} \frac{\mathbf{\Phi}_i^T \mathbf{\Sigma}_{\chi\mathbf{X}}(\mathbf{x})}{\sqrt{\omega_i}} \xi_i \tag{18}$$

where ω_i and $\mathbf{\Phi}_i^T$ are the M largest eigenvalues and their corresponding eigenvectors of the covariance matrix $\mathbf{\Sigma}_{\chi\chi}$, the ξ_i are independent standard normal random variables; $\mathbf{\Sigma}_{\chi\mathrm{X}}(\mathbf{x})$ is a vector function whose coefficients are defined as $\left(\mathbf{\Sigma}_{\chi\mathrm{X}}(\mathbf{x})\right)_j = \mathrm{Cov}\left(\mathbf{x}_j, \mathbf{x}\right)$ with $j \in \{1,2,\ldots,N\}$. The EOLE method minimizes the mean square error pointwise given values of the random field at the set of points $\{\mathbf{x}_1, \mathbf{x}_2, \ldots, \mathbf{x}_N\}$. For the EOLE method, the error variance can be expressed as [6]:

$$\varepsilon_\sigma(\mathbf{x}) = 1 - \frac{1}{\sigma^2(\mathbf{x})} \sum_{i=1}^{M} \frac{\left(\mathbf{\Phi}_i^T \mathbf{\Sigma}_{\chi\mathrm{X}}(\mathbf{x})\right)^2}{\omega_i} \tag{19}$$

3 Numerical convergence study

The convergence behavior of the proposed finite cell approach with respect to the mean error variance is investigated by means of a numerical example. The random field is modeled for a squared domain with a circular hole in its center. The length of a side of the square is four and the diameter of the circular hole is two, as shown in figure 3. The Gaussian random field has a constant mean value and standard deviation of $30 \cdot 10^3$ and $6 \cdot 10^3$, respectively.

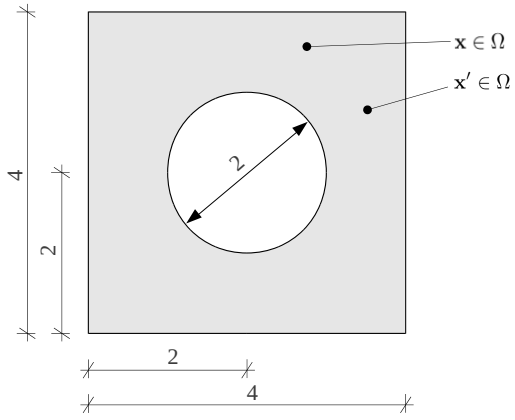

Figure 3. Domain used for the numerical convergence study.

Three different types of correlation coefficient functions are considered:

$$\text{Type A}: \quad \rho(\mathbf{x}, \mathbf{x}') = \exp\left(-\left(\frac{|\mathbf{x} - \mathbf{x}'|}{\delta_A} \right)^2 \right) \tag{20}$$

$$\text{Type B}: \quad \rho(\mathbf{x}, \mathbf{x}') = \exp\left(-\frac{|\mathbf{x} - \mathbf{x}'|}{\delta_B} \right) \tag{21}$$

$$\text{Type C}: \quad \rho(\mathbf{x},\mathbf{x}') = \frac{1}{1+\left(\frac{|\mathbf{x}-\mathbf{x}'|}{\delta_C}\right)^{1.2}} \tag{22}$$

The correlation lengths δ_A, δ_B and δ_C used in the numerical study were chosen such that the reference mean error variances $\bar{\varepsilon}_{\sigma,\text{ref}}$ are close to ten percent for 100 random variables in the expansion. This reference value is the error from the truncation of the KL-expansion and was calculated with a uniform 10x10 finite cell mesh and a maximum polynomial order of the shape functions of ten. The so obtained reference value was verified with a uniform 14x14 finite cell mesh and a maximum polynomial order of eight. The applied correlation lengths and their corresponding reference mean error variances are $\delta_A = 0.3325$, $\delta_B = 1.08$, $\delta_C = 0.725$, $\bar{\varepsilon}_{\sigma,\text{ref,A}} = 0.099781$, $\bar{\varepsilon}_{\sigma,\text{ref,B}} = 0.099853$ and $\bar{\varepsilon}_{\sigma,\text{ref,C}} = 0.09953$. The correlation coefficient functions corresponding to the chosen correlation lengths are depicted in figure 4.

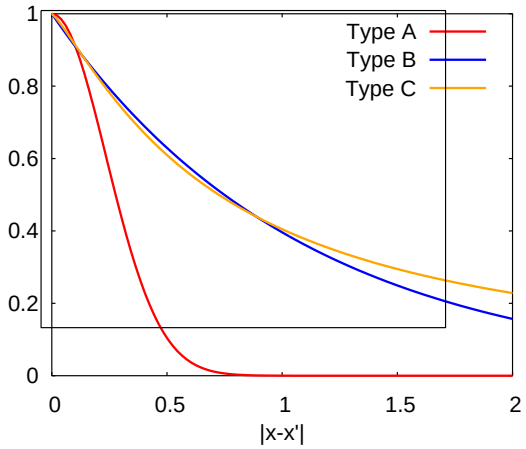

Figure 4. Plot of the investigated correlation coefficient functions.

For the convergence study, the following relative error is defined:

$$\varepsilon_{\text{rel,N}} = \frac{\left|\bar{\varepsilon}_{\sigma,\text{N}} - \bar{\varepsilon}_{\sigma,\text{ref}}\right|}{\bar{\varepsilon}_{\sigma,\text{ref}}} \tag{23}$$

where $\bar{\varepsilon}_{\sigma,\text{N}}$ is the mean error variance for a given size *N* of the matrix eigenvalue problem to solve.

The errors obtained by the finite cell approximation of the KL-expansion (FC), the finite element approximation of the KL-expansion using linear shape functions (hFEM), and the EOLE method are shown in figure 5. For the FC-approach, a uniform 2x2 finite cell mesh is used. The size *N* of the matrix eigenvalue problem to solve is increased by increasing the maximum poly-

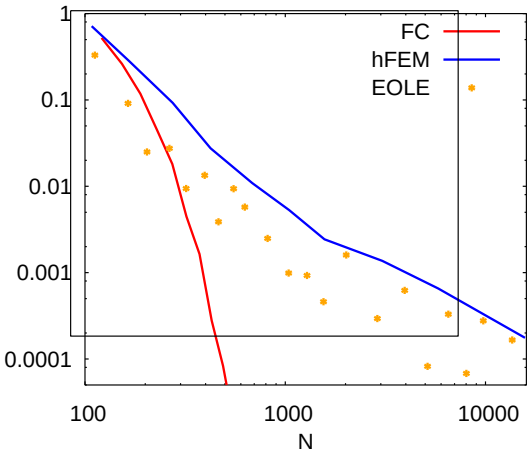

(a) convergence (Type A)

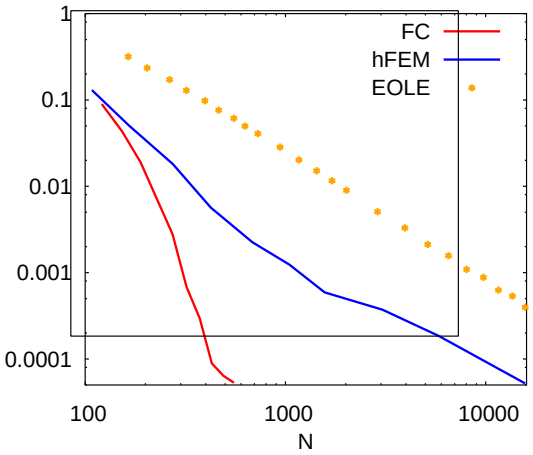

(b) convergence (Type B)

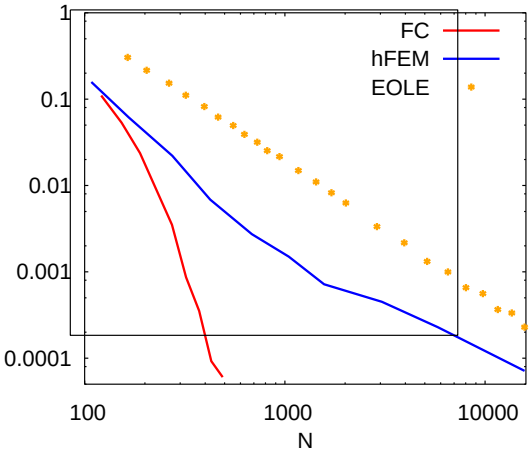

(c) convergence (Type C)

Figure 5. Convergence in the relative error w.r.t. the size of the size of the problem.

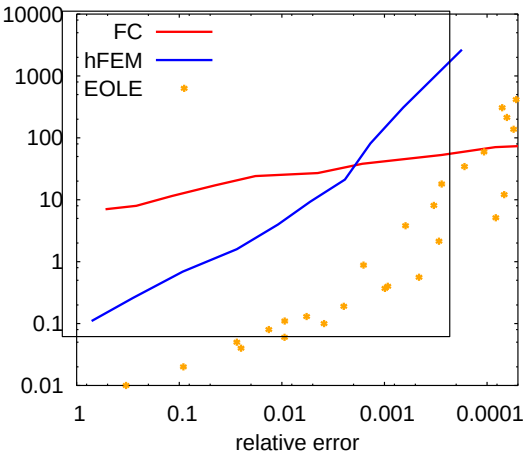

Figure 6. Time needed to converge to a certain relative error. (Type A)

nomial order of the shape functions. The maximum polynomial order in each coordinate direction is the same. For the hFEM-approach, the actual physical domain is meshed using four node quadrilateral elements. The problem size N is increased by refining the mesh. In case of the EOLE-method, the problem size N is equivalent to the total number of points used to discretize the field. The points were distributed uniformly over the domain.

The plots (a), (b) and (c) in figure 5 show the relative error defined in equation 23 for an increasing size N of the matrix eigenvalue problem to solve. The FC-approach shows an exponential rate of convergence for all three types of correlation coefficient functions. The convergence rate of the hFEM-method and the EOLE method is approximately linear in the log-log plots. The EOLE-method converges faster than the hFEM-method for the correlation coefficient function of type A. For the correlation coefficient functions of type B and C, the hFEM-method converges faster than the EOLE-method.

Figure 6 shows the time needed for the methods to converge to a certain relative error for the correlation coefficient function of type A. To obtain a reasonably well converged solution, the FC-approach needs considerably more time than the hFEM-method and the EOLE-method. For this particular correlation coefficient function, the EOLE-method solves the problem around one order of magnitude faster than the hFEM-method.

In a next study, the time required to evaluate a realization of the random field at a given position $\mathbf{x}$ is analyzed. This is of importance when the random field is used as input to finite element reliability analysis, because a realization of the field has to be evaluated at every finite element Gauss-point. In case of the hFEM-approach, the time needed to evaluate a realization of the random field at one position $\mathbf{x}$ does not depend on the mesh, because the number of shape functions per element remains constant. Consequently, it remains constant with increasing N. This time is denoted t_{hFEM} in the following. On the other hand, the time needed to obtain a realization depends in case of the FC-approach on the maximum polynomial degree of the shape functions, and for the EOLE-method on the number of points used to discretize the domain.

In the log-log plot depicted in figure 7, the time needed to obtain a realization of the random field is weighted by t_{hFEM} and plotted in terms of the relative error defined in equation 23. A correlation coefficient function of type A was employed to generate the plot. It is shown that a realization of the random field can be computed several times faster with the FC-approach than with the EOLE-method.

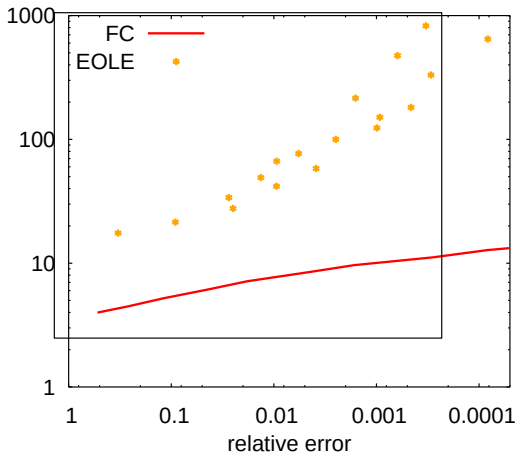

Figure 7. Time needed to compute a realization of the random field. Comparison between FC-approach and EOLE-method. Time is given relative to the time needed with the hFEM-method.

4 Summary and Conclusion

The proposed FC-approach exhibits an exponential rate of convergence with respect to the mean error variance. However, it is relatively expensive to compute a random field approximation. This effect will be even more severe for three-dimensional problems. On the other hand, compared to the EOLE-method, the proposed approach is computationally very efficient in obtaining a random field realization. This is advantageous, if many realizations of the random field have to be generated.

Compared to the hFEM method, the proposed approach is computationally more expensive in obtaining a random field realization. Therefore, for domains which are meshed with a linear finite element mesh that is fine enough to represent the correlation structure of the random field reasonably well, the hFEM-method is to be preferred. However, the FC-approach is useful for problems that do not require a mesh on the physical domain, e.g. meshless approaches or FC methods.

References

[1] Betz, W.: Quasi meshless discretization of random fields based on the Karhunen-Loève expansion. TU München, 2012 – Master's thesis

[2] Ditlevsen, O.; Madsen, H.O.: *Structural Reliability Methods*. Chichester: John Wiley & Sons Ltd, 1996

[3] Düster, A.; Parvizian, J.; Yang, Z.; Rank, E.: The finite cell method for three-dimensional problems of solid mechanics. Comp. Methods Appl. Mech. Engrg. 197 (2008), p. 3768-3782

[4] Ghanem, R.-G.; Spanos, P.-D.: Polynomial chaos in stochastic finite elements. *Applied Mechanics* 57 (1990), p. 197-202.

[5] Ghanem, R.-G.; Spanos, P.-D.: *Stochastic Finite Elements - A Spectral Approach*. New York: Springer, 1991

[6] Li, C.-C.; Der Kiureghian, A.: Optimal discretization of random fields. *Journal of Engineering Mechanics* 119 (1993), p. 1136-1154

[7] Papaioannou, I.: *Non-intrusive Finite Element Reliability Analysis Methods*. TU München, 2012 – Dissertation

[8] Parvizian, J.; Düster, A.; Rank, E.: Finite cell method. *Computational Mechanics* 41 (2007), p. 121-133

[9] Sudret, B.; Der Kiureghian, A.: Stochastic finite element methods and reliability – a state-of-the-art report. *Technical Report UCP/SEMM-2000/08*, Department of Civil & Environmental Engineering, Univ. of California, Berkeley, November 2000

[10] Sudret, B.: Uncertainity propagation and sensitivity analysis in mechanical models - Contributions to strucutral reliability and stochastic spectral methods. Université BLAISE PASCAL - Clermont II, 2007 – Habilitation.

[11] Szabó, B. A.; Düster, A.; Rank, E.: The p-version of the finite element method. In: Stein E, de Borst R, Hughes TJR (eds) Encyclopedia of computational mechanics, Vol. 1, Chapter 5. Wiley, New York (2004), pp. 119–139

Bayesian estimation of the covariance function of random fields based on a limited number of measurements

Pieterjan Criel, Robby Caspeele, Luc Taerwe
Magnel Laboratory for Concrete Research, Ghent University, Ghent

Abstract: A Bayesian response surface updating procedure is applied in order to update covariance functions for random fields based on a limited number of measurements. Formulas as well as a numerical algorithm are presented in order to update the parameters of complex response surfaces using Markov Chain Monte Carlo simulations. In case of random fields, the parameters of the covariance function are often based on some kind of expert judgment. However, a Bayesian updating technique enables to estimate the parameters of the covariance function more rigorously and with less ambiguity. Prior information can be incorporated in the form of vague or informative priors, and the latter can be based on e.g. expert judgment. The proposed estimation procedure is evaluated through numerical simulations and the influence of the position of measurement points is investigated.

1 Introduction

The parameters of the covariance function of random fields are often based on some kind of expert judgment, certainly in cases where only a few measurements are available. However, Bayesian updating techniques enable to estimate the parameters of the covariance function more rigorously and with less ambiguity as these can be used to update previously obtained information regarding parameters of similar random fields. Markov chain Monte Carlo (MCMC) simulations can be used to incorporate Bayesian updating based on limited samples in the response surface estimation. Prior information (vague or informative) can then be used to update the covariance function based on available monitoring data or measurement results. Of course, the sample pattern according to which the measurements are obtained plays an important role for optimizing the Bayesian estimation method in case only a few measurements can be obtained.

2 Random fields and their covariance function

A random field $H_{\underline{x}}$ is a function whose values are random variables for any position $\underline{x}$. In general, their characteristics can differ for each position $\underline{x}$ in the random field. Some of the phenomena that can be represented by random fields are: the bathymetry of the sea, the earth's surface temperature, concrete properties in structural elements, etc. resulting from a distributed disordered system that displays complex patterns of variation in space and/or time [15].

For numerical applications random fields are most often defined on a discrete domain, e.g. on a lattice grid (lattice process). A continuous random field can be obtained by interpolation methods, e.g. Kriging [3]. In many cases the random field is defined on a surface and can be decomposed into a mean value or trend surface and a residual variation with mean 0. This residual variation usually exhibits some spatial structure, described by a covariance function $C(x_i, x_j)$. The covariance function is a measure of the correlation between two positions in the field. When a random field is considered to be homogeneous, isotropic and ergodic the covariance function is only dependent on the distance τ between two positions in the field, hence:

$$C(x_i, x_j) = C(\tau) \tag{1}$$

Random fields are called Gaussian if the random variables which describe the field follow a Gaussian distribution. An advantage of such fields is that they can be transformed into a field described by standard normal distributed variables. As such, further in this paper only standard normal distributed random fields need to be considered.

A standard normal field is characterized by its mean 0 and its covariance function and can be presented by a multivariate standard normal distribution:

$$f_H = (2\pi)^{-N/2} |\Sigma|^{-1/2} \exp\left(-\frac{1}{2} (H - \underline{\mu})^T \Sigma^{-1} (H - \underline{\mu}) \right) \tag{2}$$

where N is the amount of positions x in the field, $\underline{\mu}$ the mean value of the field and Σ the covariance matrix, whose elements (i, j) are equal to the covariance between position x_i and x_j:

$$\Sigma_{ij} = C(x_i, x_j) \tag{3}$$

Practical simulation methods to obtain random fields can be found in [3]. In Figure 1 an example of a such a field is given.

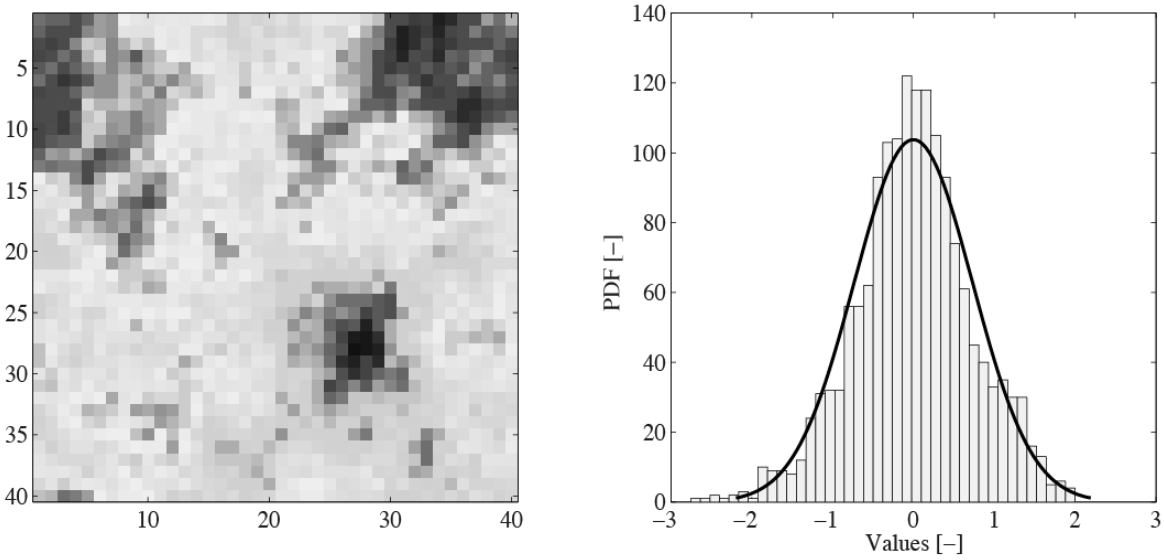

Figure 1. Realization of a standard normal distributed random field on a lattice grid, 40 by 40 positions (left) and the associated histogram of realizations (right)

The correlation between two positions decreases if the distance between them increases. Because only ergodic fields are considered $\lim_{\tau \to \infty} C(\tau) = 0$ [3]. Different models for the covariance function are suggested in literature. The most commonly used models are the exponential, squared exponential and Matérn covariance function. The exponential and squared exponential covariance functions are described by only one parameter, namely the correlation length β, defined as [1]:

$$\beta = \frac{\int_0^\infty \tau\, C(\tau) d\tau}{\int_0^\infty C(\tau) d\tau} \tag{4}$$

The Matérn covariance function additionally incorporates a smoothness parameter ν. A comparison of the different covariance functions is given in Figure 2.

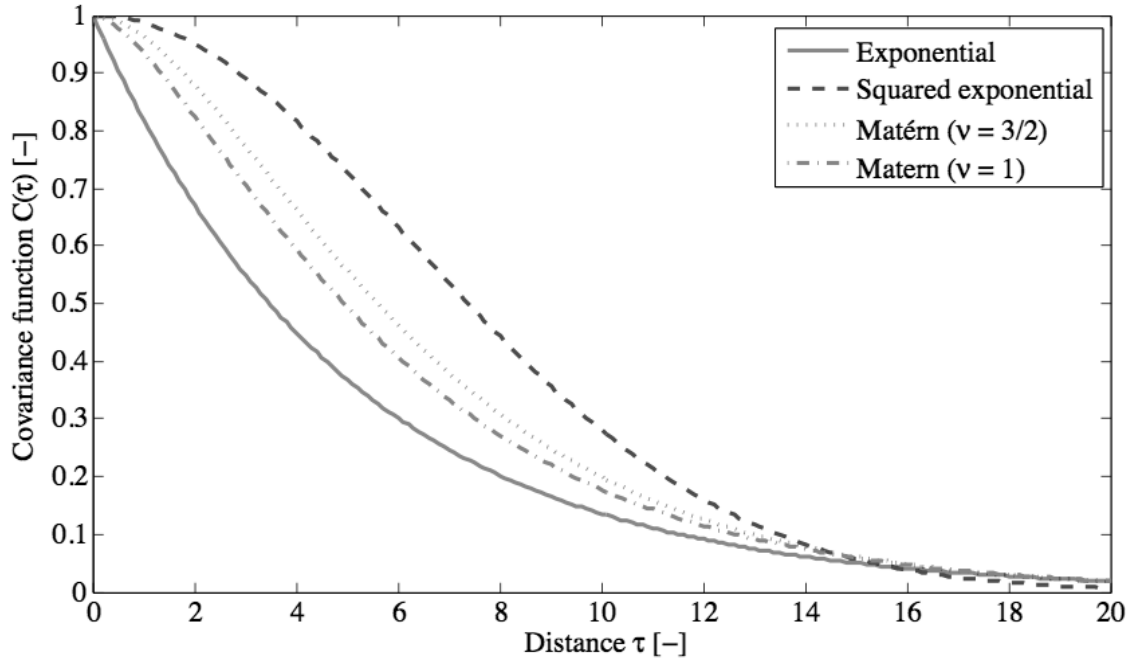

Figure 2. Comparison of covariance functions with correlation length $\beta = 5$

3 Bayesian estimation of response surface parameters

Bayesian estimation of linear regression models is well-described in literature, e.g. in [2, 4-7, 9]. However, in most cases observational data is modelled as a nonlinear combination of multiple model parameters and variables. Available literature on Bayesian nonlinear regression is rather limited (see e.g. [5, 7]).

Assume that the true value of the response variable $\tilde{y}$ can be predicted by a mathematical model *M* which is a nonlinear function of R parameters β_r (r = 1,…,*R*) and depends on a vector $\underline{x}$ which represents a *m*-dimensional set of input variables. If this model would be "perfect" and the true values $\underline{\tilde{x}}$ are exactly known, the model would be able to predict the true response value $\tilde{y}$ exactly. However, due to the existence of uncertainties, the true value is given by:

$$\tilde{y} = y + \varepsilon = M(\underline{x}) + \varepsilon \tag{5}$$

where the error term can be considered as a realization of a Gaussian random variable (with mean 0 and variance σ_ε^2), representing the measurement and model uncertainties. Hence:

$$\varepsilon \propto N(0, \sigma_\varepsilon^2) \tag{6}$$

where the variance of the error term is assumed to be constant in the domain of the input variables.

If N independent test results y_i are available for the response variable of N sets of corresponding input variables $\underline{x}_i$, the likelihood of the experimental data can in general be written as:

$$L(y_1,...,y_N|\sigma_\varepsilon,\beta_1,...,\beta_R)=\prod_{i=1}^{N}\frac{1}{\sigma_\varepsilon}\phi\left(\frac{y_i-M(\underline{x}_i)}{\sigma_\varepsilon}\right) \tag{7}$$

where $\phi(.)$ is the probability density function (PDF) of the standard normal distribution.

Based on the Bayesian principle, the prior information (either vague or informative) is given as the joint prior distribution $f'_B(\sigma_\varepsilon,\beta_1,...,\beta_R)$ of the standard deviation σ_ε of the error term and the model parameters $(\beta_1,...,\beta_R)$. This prior distribution can be updated towards a posterior distribution $f''_B(\sigma_\varepsilon,\beta_1,...,\beta_R)$ by using the likelihood function as follows:

$$\begin{aligned} & f''_B(\sigma_\varepsilon,\beta_1,...,\beta_R) \\ &= \frac{f'_B(\sigma_\varepsilon,\beta_1,...,\beta_R)\,L(y_1,...,y_N|\sigma_\varepsilon,\beta_1,...,\beta_R)}{\int_B f'_B(\sigma_\varepsilon,\beta_1,...,\beta_R)\,L(y_1,...,y_N|\sigma_\varepsilon,\beta_1,...,\beta_R)\,d\sigma_\varepsilon\,d\beta_1...d\beta_R} \\ &= c\; f'_B(\sigma_\varepsilon,\beta_1,...,\beta_R)\,L(y_1,...,y_N|\sigma_\varepsilon,\beta_1,...,\beta_R) \end{aligned} \tag{8}$$

with c a normalizing constant and B the domain of the parameters $(\sigma_\varepsilon,\beta_1,...,\beta_R)$ that have to be updated. Equation (8) can be difficult or impossible to solve analytically. Therefore MCMC simulations are applied (i.e. using the Metropolis-Hastings algorithm) to estimate values for the model parameters and the standard deviation of the error term.

4 MCMC Bayesian updating of response surface parameters using a 'cascade' Metropolis-Hastings algorithm

Markov chain Monte Carlo methods (MCMC) form a class of numerical algorithms that allow to obtain samples from probability distributions based on the construction of a Markov chain. A Markov chain is defined in probability theory as a sequence of random variables x_i for which the distribution of x_i,

conditioned on past realizations x_{i-1}, x_{i-2}, …, depends only on the previous sample x_{i-1}, i.e. not on x_{i-2}, x_{i-3}, etc. [5]. Thus, these methods allow to draw a discrete-time homogeneous chain of samples from the posterior distribution [13]. The idea is to generate iteratively samples of a Markov chain, which asymptotically behaves as the probability density function (PDF) which has to be sampled. More specifically, the Metropolis-Hastings algorithm [8, 12] is commonly used for generating such Markov chains. The practical adaptation of this algorithm for the Bayesian estimation of response surface parameters is explained hereafter. More profound information on MCMC simulations can be found in e.g. [4-6, 10, 14].

Considering a certain PDF $f_X(\underline{x})$ which is a function of an input vector $\underline{x}$, MCMC realizations $\underline{x}_S$ are generated sequentially and independently, starting from an arbitrary chosen starting vector $\underline{x}_0$. In each step, the transition between the states $\underline{x}_S$ and $\underline{x}_{S+1}$ is given according to (see e.g. [5]):

$$\underline{x}_{S+1} = \begin{cases} \underline{\tilde{x}} \propto q(\underline{\tilde{x}}|\underline{x}_S) & \text{with probability } \alpha(\underline{x}_S, \underline{\tilde{x}}) \\ \underline{x}_S & \text{else} \end{cases} \tag{9}$$

where $\underline{\tilde{x}}$ is a candidate vector, $q(\underline{\tilde{x}}|\underline{x}_S)$ is called the transition or proposal distribution and the acceptance probability $\alpha(\underline{x}_S, \underline{\tilde{x}})$ given by (see e.g. [5]):

$$\alpha(\underline{x}_S, \underline{\tilde{x}}) = min\left\{1, \frac{f_X(\underline{\tilde{x}})}{f_X(\underline{x}_S)} \frac{q(\underline{x}_S|\underline{\tilde{x}})}{q(\underline{\tilde{x}}|\underline{x}_S)}\right\} \tag{10}$$

Practically, in order to select a candidate $\underline{\tilde{x}}$ – calculated according to Equation (5) – a random number r_s is generated (i.e. from a uniform distribution $U[0;1]$) and $\underline{\tilde{x}}$ is accepted as the next draw from $f_X(\underline{x})$ with a probability $\alpha(\underline{x}_S, \underline{\tilde{x}})$ in case $r_S \leq \alpha(\underline{x}_S, \underline{\tilde{x}})$ or rejected in the other case. This way, a sequence of random draws $\underline{x}_S$ from $f_X(\underline{x})$ is generated, even when no analytical solution is available for $f_X(\underline{x})$.

By using the random walk algorithm to propose values for the parameters the transition distribution is symmetrical and Equation (10) can be simplified to:

$$\alpha(\underline{x}_S, \underline{\tilde{x}}) = \min\left\{1, \frac{f_X(\underline{\tilde{x}})}{f_X(\underline{x}_S)}\right\} \tag{11}$$

In case of the Bayesian estimation of response surface parameters, the transition between 2 estimates $(\sigma_{\varepsilon,s},\beta_{1,s},...,\beta_{R,s})$ and $(\sigma_{\varepsilon,s+1},\beta_{1,s+1},...,\beta_{R,s+1})$ for the posterior set of response surface parameters can be rewritten as:

$$(\sigma_{\varepsilon,s+1},\beta_{1,s+1},...,\beta_{R,s+1}) = \begin{cases} (\tilde{\sigma}_{\varepsilon},\tilde{\beta}_1,...,\tilde{\beta}_R) \propto q(\tilde{\sigma}_{\varepsilon},\tilde{\beta}_1,...,\tilde{\beta}_R \mid \sigma_{\varepsilon,s},\beta_{1,s},...,\beta_{R,s}) \\ \quad \text{with probability } \psi \\ (\sigma_{\varepsilon,s},\beta_{1,s},...,\beta_{R,s}) \\ \quad \text{else} \end{cases} \tag{12}$$

where $q(\tilde{\sigma}_{\varepsilon},\tilde{\beta}_1,...,\tilde{\beta}_R \mid \sigma_{\varepsilon,s},\beta_{1,s},...,\beta_{R,s})$ is the transition distribution. A common choice for the transition distribution is a random walk, more specifically by adding a random increment to the previous estimate according to:

$$(\tilde{\sigma}_{\varepsilon},\tilde{\beta}_1,...,\tilde{\beta}_R)^T = (\sigma_{\varepsilon,s},\beta_{1,s},...,\beta_{R,s})^T + (\varsigma_0,\varsigma_1,...,\varsigma_R)^T \tag{13}$$

with $(\varsigma_0,\varsigma_1,...,\varsigma_R)$ a random vector that does not depend on the previous chain. In practice, it is common to choose the values ς_i according to a normal or uniform distribution with mean 0 and variance σ_{ς}^2. The latter value determines how fast the MCMC algorithm will converge to yield the posterior response surface parameters.

Further, the probability ψ is the joint acceptance probability based on the prior probability and the likelihood function or in other words the probability that a random sample $u_P \propto U[0;1]$ from a uniform distribution (defined for values between 0 and 1) is accepted according to the prior distribution and that a random sample $u_L \propto U[0;1]$ is accepted according to the likelihood function. Based on the "cascade" principle as described in [2,7], this probability is generalized for Bayesian estimation of response surface parameters according the following equations:

$$\psi = \text{Prob}[(u_P \le \alpha_P) \cap (u_L \le \alpha_L)] \tag{14}$$

$$\begin{aligned} \alpha_P &\equiv \alpha_P[(\sigma_{\varepsilon,s},\beta_{1,s},...,\beta_{R,s}),(\tilde{\sigma}_{\varepsilon},\tilde{\beta}_1,...,\tilde{\beta}_R)] \\ &= min\left\{1,\frac{f'_B(\tilde{\sigma}_{\varepsilon},\tilde{\beta}_1,...,\tilde{\beta}_R)}{f'_B(\sigma_{\varepsilon,s},\beta_{1,s},...,\beta_{R,s})}\right\} \end{aligned} \tag{15}$$

$$\alpha_L \equiv \alpha_L\left[\left(\sigma_{\varepsilon,s},\beta_{1,s},...,\beta_{R,s}\right),\left(\tilde{\sigma}_{\varepsilon},\tilde{\beta}_1,...,\tilde{\beta}_R\right)\right] = \min\left\{1,\frac{L\left(y_1,...,y_N\left|\tilde{\sigma}_{\varepsilon},\tilde{\beta}_1,...,\tilde{\beta}_R\right.\right)}{L\left(y_1,...,y_N\left|\sigma_{\varepsilon,s},\beta_{1,s},...,\beta_{R,s}\right.\right)}\right\} \tag{16}$$

with the likelihood $L\left(y_1,...,y_N\left|...\right.\right)$ according to Equation (7) in case of sequentially independent response measurements.

5 Bayesian estimation of the covariance function based on limited measurements

Consider a random field with an exponential or a squared exponential covariance function. In this case there is only one parameter which has to be estimated, namely the correlation length β. Instead of fitting a covariance function to an empirical covariance function, it is fitted to a semi-variogram. A semi-variogram $\gamma\left(x_i,x_j\right)$ or variogram $2\gamma\left(x_i,x_j\right)$ is – like the covariance function – a function describing the degree of spatial dependence in a random field. It is defined as the variance of the difference between two values of the field. For homogeneous and isotropic fields the semi-variogram is only depending on the distance between those two positions, hence:

$$2\gamma\left(x_i,x_j\right)=2\gamma\left(\left\|x_i-x_j\right\|\right)=2\gamma(\tau) \tag{17}$$

For second order stationary random fields the following relation between the semi-variogram en the covariance function holds [3]:

$$2\gamma(\tau)=2\left(C(0)-C(\tau)\right) \tag{18}$$

with $\gamma(\tau)$ the semi-variogram and $C(\tau)$ a covariance function.

The semi-variogram has the advantage that the mean value of the field - assumed constant (if necessary after a trend correction) - does not have to be known to compose the empirical semi-variogram.

This strategy is also applied in other methods for estimating the correlation length based on measurement data, e.g. the maximum likelihood estimation (MLE) and the least squares method (LSQ) [3]. However, these methods do not consider prior information on the covariance function, i.e. prior information on the correlation length β. As such, the bias and uncertainty of the

estimation can be very large in case of limited data. When considering prior knowledge this can however be ameliorated. The method presented in section 4 can be applied to update the model parameters of the covariance function based on a limited amount of measurements considering the empirical semi-variogram derived from the measurements. Prior informative is given as the joint distribution (either vague or informative) of the error term and the parameters that define the covariance function. In case a uniform distribution is assumed for the error term and lognormal distributions for the correlation length, the prior distribution becomes:

$$f'(\beta,\sigma_\varepsilon) = \begin{cases} \frac{1}{b-a}\frac{1}{\beta\delta\sqrt{2\pi}} exp\left(-\frac{1}{2}\left(\frac{ln(\beta/\xi)}{\delta}\right)^2\right) & \text{if } a \le \sigma_\varepsilon \le b \\ 0 & \text{else} \end{cases} \quad (19)$$

with ξ and δ the parameters of the lognormal distribution.

Rewriting Equation (5) in terms of the semi-variogram yields:

$$\bar{\gamma}(\tau) = \gamma(\tau \mid \beta) + \varepsilon \quad (20)$$

where $\bar{\gamma}(\tau)$ is the empirical semi-variogram, $\gamma(\tau \mid \beta)$ the semi-variogram model and ε the error term as defined in Equation (6).

There are different methods commonly available to compose an empirical semi-variogram based on measurement data [3]. In this paper the method-of-moments estimator defined by Matheron [11] is adopted:

$$\bar{\gamma}(\tau) = \frac{1}{2|T(\tau)|}\sum_{T(\tau)}(h_i - h_j)^2 \quad (21)$$

$$T(\tau) \equiv \left\{(h_i, h_j) : \|h_i - h_j\| = \tau; i, j = 1,\ldots,N\right\} \quad (22)$$

where $T(\tau)$ is a set defined by Equation (22), $|T(\tau)|$ is the number of elements in the set $T(\tau)$ (i.e. the number of available measurements for a certain distance τ) and h_i, h_j are the values of the measurements. Other methods can be found in [3].

$\bar{\gamma}(\tau)$ is not continuous as there are only a finite number of distances between the measurement points. In order to obtain sufficient samples per set $T(\tau)$ for constructing a semi-variogram in practice, similar distances are grouped in distance classes by adding a tolerance on the distance τ. Hence, the set of elements corresponding to a distance class τ are described as follows:

$$T(\tau) \equiv \left\{ \left(h_i, h_j \right) : \tau - e \le \left\| h_i - h_j \right\| \le \tau + e; i, j = 1, \ldots, N \right\} \tag{23}$$

The tolerance e should be carefully chosen so that the empirical semi-variogram is not biased and there are enough combinations available in each distance class.

In the case of an exponential covariance function (i.e. with two unknown parameters, namely the correlation length β and the standard deviation σ_ε of the error term), the likelihood function defined in Equation (7) in terms of the semi-variogram can be rewritten as:

$$L\left(\bar{\gamma}_1, \ldots, \bar{\gamma}_N \middle| \beta, \sigma_\varepsilon\right) = \prod_{i=1}^{N} \frac{1}{\sqrt{2\pi}\sigma_\varepsilon} \exp\left(-\frac{1}{2} \frac{\bar{\gamma}(\tau_i) - \gamma(\tau_i \mid \beta)}{\sigma_\varepsilon^2} \right) \tag{24}$$

By using a symmetrical transition distribution the simplified acceptance probability can be used in the MCMC simulation. The acceptance probabilities α_P and α_L as given in Equation (14) and (15) respectively can then be rewritten as:

$$\alpha_P = min\left\{ 1, \frac{f'\left(\tilde{\beta}, \tilde{\sigma}_\varepsilon\right)}{f'\left(\beta_s, \sigma_{\varepsilon,s}\right)} \right\} \tag{25}$$

$$\alpha_L = min\left\{ 1, \frac{\prod_{i=1}^{N} \frac{1}{\sqrt{2\pi}\tilde{\sigma}_\varepsilon} exp\left(-\frac{1}{2} \frac{\bar{\gamma}(\tau_i) - \gamma\left(\tau_i \mid \tilde{\beta}\right)}{\tilde{\sigma}_\varepsilon^2} \right)}{\prod_{i=1}^{N} \frac{1}{\sqrt{2\pi}\sigma_{\varepsilon,s}} exp\left(-\frac{1}{2} \frac{\bar{\gamma}(\tau_i) - \gamma(\tau_i \mid \beta_s)}{\sigma_{\varepsilon,s}^2} \right)} \right\} \tag{26}$$

As an example the traditional LSQ method and the currently developed MCMC method are compared. Both methods (MCMC method based on 25 measurement points on a domain of 32 x 32 positions and LSQ method based on 25 or 1024 measurement points on the same domain size) are applied to

find the correlation length β of a random field on a lattice grid (40 by 40 positions). For each method 100 standard normal distributed random fields with a correlation length β = 10 are generated. In case of the MCMC method a lognormal prior distribution for β is considered with $\mu_\beta = 8$ and $\sigma_\beta = 2$. The results are shown in Figure 3. Hence, the prior distribution used for the correlation length was biased. Figure 3(C) shows the prior and posterior PDF of the correlation length in case of the MCMC method.

Compared to the LSQ method, the MCMC method provides a less uncertain estimation (due to the incorporation of prior information). The LSQ estimation improves when more measurement points are available, however a large number of measurement points are necessary for achieving a similar accuracy as provided by the MCMC method. 1024 or more measurement points are of course impossible to achieve in common structural engineering applications, hence indicating the importance of the proposed MCMC method.

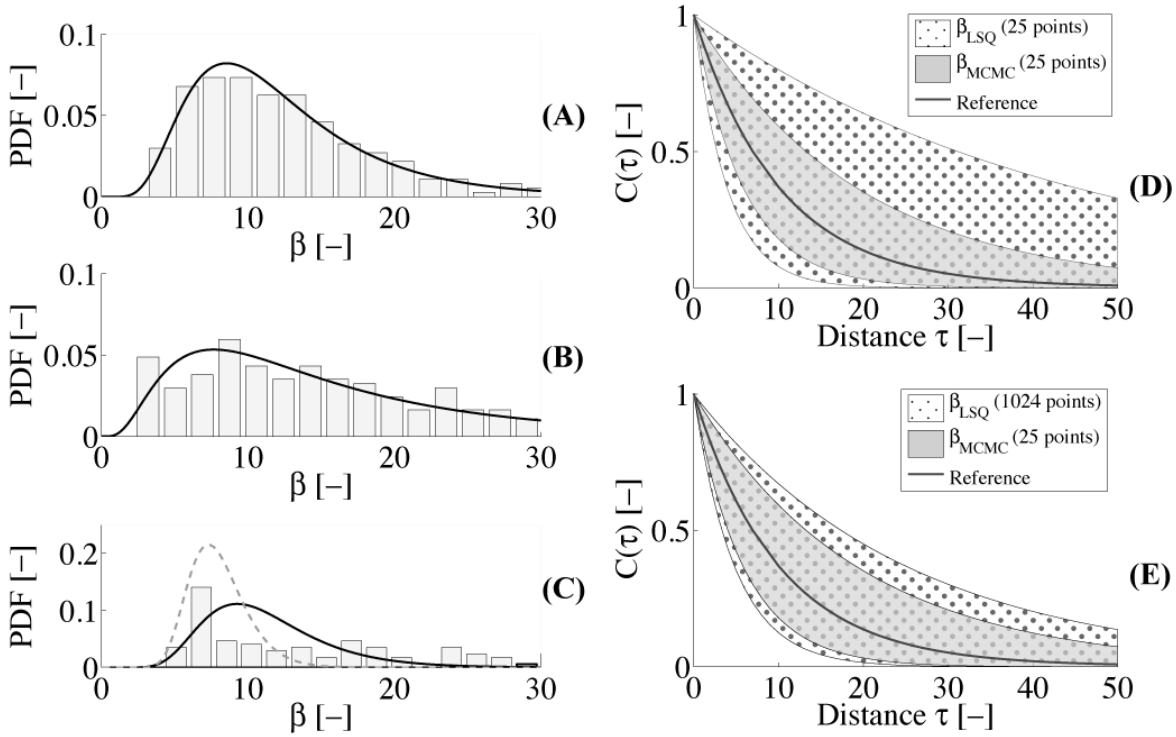

Figure 3. (A) Probability density function (PDF) of β in case of the LSQ method considering 1024 measurement points. (B) PDF of β in case of the LSQ method considering 25 measurement points. (C) PDF of β in case of the MCMC method considering 25 measurement points and prior information. (D) 90% confidence intervals for the LSQ and MCMC method when considering 25 points. (E) 90% confidence interval for the LSQ method when considering 1024 points compared to the MCMC method when considering 25 points.

6 Study of the influence of the sample pattern

In order to optimize the information which can be obtained from a limited number of measurement points, the sample pattern according to which the measurements are obtained plays an important role for the efficiency of the Bayesian estimation method. Two patterns are considered in the following, namely patterns with a constant distance between the measurement points (linear regular pattern) and a pattern where de distance between the measurement points grows exponentially (logarithmic regular pattern), see Figure 4.

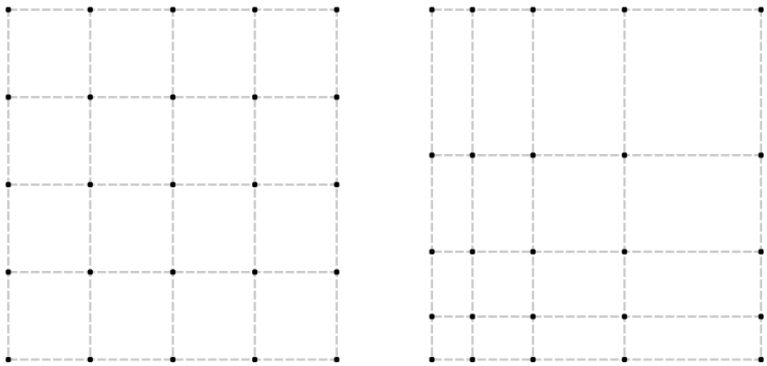

Figure 4. Linear regular pattern (left) and logarithmic regular pattern (right)

For the linear regular pattern a larger amount of measurement couples per distance class are available, while in case of the logarithmic regular pattern a larger amount of different distance classes is represented, although less measurements per distance class are available. A linear regular pattern will have the advantage that there are more measurements available for each distance class, while the logarithmic pattern samples according to a larger number of distance classes. However, in the latter case less measurement points are available per distance class, which leads to a less informative likelihood function.

In order to compare the influence of both sample patterns, the performance of the MCMC method for estimating the correlation length β of a standard normal random field defined on a lattice grid (40 by 40 positions) is quantified for a specific example. For both suggested sample patterns 100 standard normal distributed random fields with a correlation length $\beta = 10$ are generated. A lognormal prior distribution for β is considered with $\mu_\beta = 10$ and $\sigma_\beta = 2$. In case 25 measurement points are considered according to both

sample patterns over the same domain (15 by 15 positions), the results are shown in Figure 5.

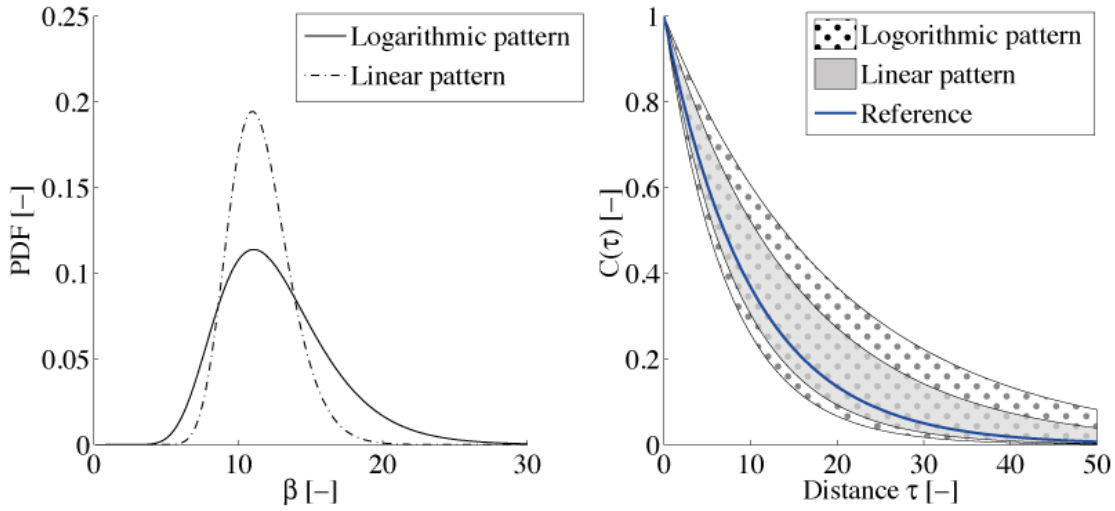

Figure 5. PDF of β for the logarithmic and linear pattern (left) and 90% confidence interval for the logarithmic and linear pattern (right)

From Figure 5 it can be concluded that in case the prior information is consistent with the simulation reference and the sample patterns have the same span, a more informative likelihood function is obtained according to a linear sample pattern (as discussed above), which consequently results in a smaller confidence interval of the estimated correlation length.

7 Conclusions

- By assuming homogeneous, isotropic and ergodic properties for random fields, the spatial characteristics are determined by the covariance function.
- A methodology based on Markov chain Monte Carlo (MCMC) simulations is developed in order to estimate the covariance function of random fields from empirical semi-variograms and considering Bayesian updating of prior information.
- When only a limited amount of measurement data is available, the MCMC method enables to obtain a more accurate estimation of the correlation length of random fields compared to the commonly used LSQ method.
- With respect to constructing a semi-variogram, the use of a linear sample pattern results in a smaller confidence interval for the estimated cor-

relation length in case the prior information is consistent with the simulation reference and the sample patterns have the same span.

8 References

[1] Baecher, G.B. and J.T. Christian, *Reliability and Statistics in Geotechnical Engineering*. 2003: John Wiley & Sons.

[2] Box, G.E.P. and G.C. Tiao, *Bayesian inference in statistical analysis*. 1992: Wiley.

[3] Cressie, N.A.C., *Statistics for spatial data*. 1993: J. Wiley.

[4] Gamerman, D. and H.F. Lopes, *Markov Chain Monte Carlo: Stochastic Simulation for Bayesian Inference, Second Edition*. 2006: Taylor & Francis.

[5] Gelman, A., et al., *Bayesian Data Analysis*. 2003: Chapman & Hall/CRC.

[6] Ghosh, J.K., M. Delampady, and T. Samanta, *An Introduction to Bayesian Analysis: Theory and Methods*. 2010: Springer.

[7] Gregory, P., *Bayesian Logical Data Analysis for the Physical Sciences: A Comparative Approach with Mathematica® Support*. 2005: Cambridge University Press.

[8] Hastings, W.K., *Monte Carlo sampling methods using Markov chains and their applications.* Biometrika, 1970. **57**(1): p. 97-109.

[9] Lee, P.M., *Bayesian Statistics: An Introduction*. 2012: Wiley.

[10] Liu, J.S., *Monte Carlo Strategies in Scientific Computing*. 2008: Springer.

[11] Matheron, G., *Traité de géostatistique appliquée*. Technip ed. Vol. 14. 1962, Paris.

[12] Nicholas, M., et al., *Equation of State Calculations by Fast Computing Machines.* The Journal of Chemical Physics, 1953. **21**(6): p. 1087-1092.

[13] Perrin, F., et al. *Comparison of Markov chain Monte Carlo simulation and a FORM-based approach for Bayesian updating of mechanical models*. in *10th int. Conf. on Applications of Statistics and Probability in Civil Engineering*. 2007. Tokyo: Taylor & Francis Group.

[14] Robert, C. and G. Casella, *Monte Carlo Statistical Methods*. 2010: Springer.

[15] VanMarcke, E., *Random Fields: Analysis and Synthesis*. 2010: World Scientific.

Assessing the prediction quality of coupled partial models considering coupling quality

Holger Keitel
Research Training Group 1462, Bauhaus-Universität Weimar,
Berkaer Str. 9, 99423 Weimar, Germany

Abstract: The process of analysis and design in structural engineering requires the consideration of different partial models of loading, structural material, structural elements, and analysis type, among others. The various partial models are combined by coupling of their several components. Due to a large number of available partial models describing similar phenomena many different model combinations are possible to simulate the same quantities of a structure. The challenging task of an engineer is to select a model combination that ensures a sufficient reliable prognosis. In order to achieve this reliable prognosis of the overall structural behaviour, on the one hand a high individual quality of the partial models and on the other hand an adequate coupling of the partial models is needed. Several methodologies have been proposed so far to evaluate the quality of partial models for their intended application, but a detailed study of the coupling quality is still lacking. This paper proposes a new approach to assess the quality of coupled partial models in a quantitative manner taking into account directly the coupling quality. In order to achieve a global measure for the quality of the coupled partial models existing methods based on graph theory and variance based sensitivity analysis are extended to include the quality of coupling. The functionality of the algorithm is demonstrated using an example of structural engineering.

1 Introduction

The models used in structural engineering to design for serviceability and the ultimate limit state are composed of several partial models (PM) and their couplings (C). A partial model describes a component of the global model, e.g. loading, material, or the level of abstraction. For each class of PMs, e.g. the material behavior of steel, several possibilities of modeling are available. If the material model is relevant for the structural behavior, the structural engineer needs to decide, whether a linear or a non-linear material model should

be used and whether further effects, e.g. long-term behavior, have to be considered. Apart from the selection of appropriate partial models the coupling of the individual PMs is a key issue. Some partial models might interact with each other, thus a coupling is substantial and the quality of this coupling influences the quality of the global model.

In recent years, strategies to estimate the quality of partial models, [4], [5], and to quantify the influence of the partial models on the global model prognosis [3] have been developed. Furthermore, the quantification of the prognosis quality of a global model, neglecting the influence of coupling quality, is described in [3]. The assessment of software coupling has been shown in [1], but does not apply to partial models directly. Altogether, the evaluation of partial model coupling and its influence on the prognosis of a global model has not been addressed so far.

In the scope of this paper a method to quantify the quality of data coupled partial models is presented. The basis of the procedure is the consistency of data belonging to the coupled partial models. Besides the pure data integrity the influence of the coupling on the partial models' output is taken into account within the framework of the evaluation algorithm. Further, a quantitative measure for the prediction quality of the global model taking into account the individual qualities of the partial models, their influence on the output quantity, and coupling quality is derived.

2 Basic Methods and Principles

2.1 Graphical Representation of Coupled Partial Models

Global models used in engineering consist of several partial models. Figure 1 depicts a structure of a simply supported beam, connected to a clamped column with a footing. Exemplarily several partial models are shown. On the left side the overall structure is presented all in one, on the right side the structural parts are decoupled.

Stein, Lahmer, and Bock [8] show that a global model can be represented schematically by a graph, consisting of vertices – symbolizing the partial models – and edges – symbolizing the coupling. This idea is extended within the scope of this paper. The global model in Figure 1, represented by the graph in Figure 2, is separated into its structural components; beam, column, and foundation. Due to the numerical calculation, a discretization of the struc

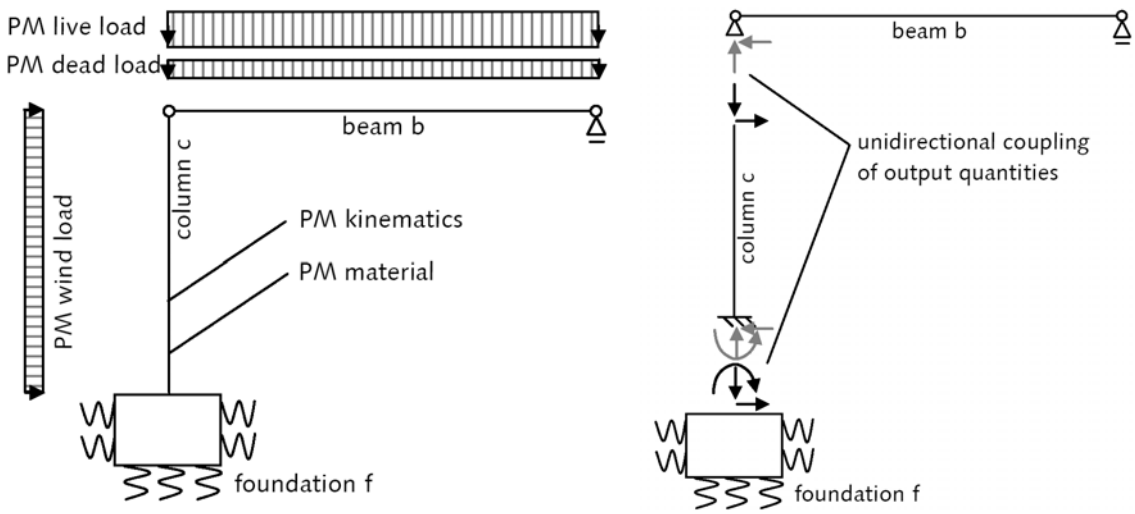

(a) Complete coupled system (b) Decoupled system

Figure 1. System of coupled partial models (PM).

tural parts is necessary. Each of the structural parts consists of several classes of partial models, which are arranged according to the sequence of the analysis. These classes of partial models may include several different representations – partial models - of a phenomenon, for example material behavior. Only one partial model of a class can be used at the same time when modeling a global system.

Within Figure 2 the coupling of partial models or structural parts is illustrated by arrows. These coupling are distinguished into unidirectional and bidirectional coupling [1]. If unidirectional coupling is applied, for example coupling beam and column, the output of the beam is the input of the column, but the output of the column is not the input of the beam. In case of bidirectional coupling, the output of the column is also considered as input of the beam.

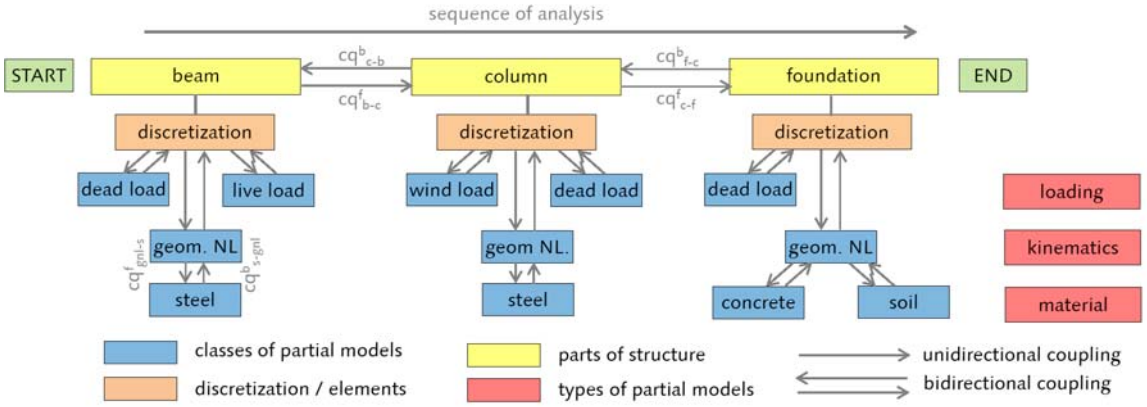

Figure 2. Representation of coupled partial models by a graph.

2.2 Sensitivity Analysis applied to Partial Models

Sensitivity analyses quantify the influence of input parameters on the output of a model. As proposed in [3], variance-based global sensitivity analysis can also be used to study the influence of partial models on the output of the global model. This procedure detects the most influential classes of partial models. Consequently, when evaluating the quality of the global model, the individual quality of the partial models with high influences on the system's behavior is crucial for the overall prognosis quality. This algorithm to quantify the influence of classes of partial models is the basis of this investigation of coupling quality as well as total prediction quality and is described in the following.

Each of the classes of partial models *i, j* is represented by a uniformly distributed, discrete random parameter

$$X_i \in \{0,1\},\ X_j \in \{0,1\},... \tag{1}$$

A value of $X_i=0$ denotes the deactivated partial model class *i*, for example geometric non-linearity is not included, and $X_i=1$ denotes the activated partial model class *i*. The global model *Y* is calculated for all possible combinations of the number of N_p partial model classes. Using these model results all required sensitivity indices can be calculated.

The exclusive influence of the parameter X_i is quantified by the first-order sensitivity index S_i, defined in detail in [7].

In order to take into account coupling effects, the total-effects sensitivity index S_{Ti} was introduced by Homma and Saltelli [2]. Besides the exclusive influence of the parameter X_i on the variance of the response, the S_{Ti} index considers the interaction of X_i with all other parameters $\boldsymbol{X}_{\sim i}$. These interactions are quantified by the difference of S_i and S_{Ti}. Further, when using high-order indices S_{ij}, these interactions can be directly apportioned to specific parameters/classes *i* and *j* of partial model. For details see [6].

In the present case of discrete input parameters all first-order, total-effects, and high-order indices can be calculated directly from the results of model *Y* for the *N* combinations of input parameters without the usual need of specific sensitivity estimators, which require high computational effort.

3 Coupling Quality

3.1 Quality of Data Coupling

Within the scope of this paper, coupling is defined as data coupling and the quality of coupling is related to the quality of data transfer. Let α and β be quantities appearing in both partial models k and l at the same point on the structure, for example forces or displacements. A perfect data coupling ensures consistent data in both models, e.g. $\alpha^k=\alpha^l$, which refers to data coupling quality of $cq^f_{\alpha,k\text{-}l}=1$. The index f denotes the forward coupling according to the sequence of partial models within the graph, whereas b denotes the backward-coupling, for example $cq^b_{\beta,l\text{-}k}$. As the differences in transferred data increases, the quality of the coupling decreases down to a quality of zero when no data is transferred. This leads to the following definition of data coupling quality:

$$cq^{\mathrm{f}}_{\alpha,k-l} = 1 - \frac{\left|\alpha^k - \alpha^l\right|}{\max\left\{\left|\alpha^k\right|, \left|\alpha^l\right|\right\}} \quad \text{and} \quad cq^{b}_{\beta,l-k} = 1 - \frac{\left|\beta^k - \beta^l\right|}{\max\left\{\left|\beta^k\right|, \left|\beta^l\right|\right\}}. \tag{2}$$

The data coupling quality depends on the quantity being compared. As a coupling might consist of numerous data, the mean quality of N_f forward and N_b backward transferred data is derived with

$$\overline{cq}^{f}_{k-l} = \frac{1}{N_f}\sum_{\alpha=1}^{N_f} cq^{\mathrm{f}}_{\alpha,k-l} \quad \text{and} \quad \overline{cq}^{b}_{l-k} = \frac{1}{N_b}\sum_{\beta=1}^{N_b} cq^{b}_{\beta,l-k}. \tag{3}$$

An example of coupling is the data transfer of the support forces of the column to the foundation in Figure 1, when both structural parts are analyzed seperately. The forward quantities normal force, shear force, and bending moment are transferred to the foundation, and the backward quantities deformation in vertical direction u_z and horizontal direction u_x as well as the rotation φ_y, that occur due to the flexibility of the soil, are transferred back to the column support and are considered pre-deformations of the column at the support.

3.2 Influence of Coupling on Data

Independent from the quality of data coupling, the question of the influence of coupling on the data needs to be answered. For this reason, variance-based sensitivity analysis according to Section 2 is applied. In the current section the sensitivity of the forward coupled data quantities with respect to the partial models is explored, which is in contrast to the usual algorithms used when the sensitivity of certain structural quantities of the global system is determined.

For this analysis the partial models need to be distinguished based on their position in the sequence of the analysis: partial models arranged before the investigated coupling, denoted as $PM \leq k$, and models arranged after the investigated coupling, denoted as $PM \geq l$. If the coupling quality of column-foundation needs to be determined for the graph in Figure 2, $PM \leq k$ refers to all models directly linked to the beam and the column, and $PM \geq l$ refers to all models directly linked to the foundation.

Using high-order indices, the influence of partial models on the transferred data can be apportioned to each model and to several groups of models. In the present case we are interested in the sensitivity of the transferred data with respect to all $PM \leq k$ and all $PM \geq l$. The sum of high-order indices for the groups of models becomes

$$\sum_{PM \leq ,k} S_\alpha = \sum_{i \leq k} \sum_{j \leq k} S_{ij,\alpha} \quad \text{and} \quad \sum_{PM \geq l} S_\alpha = \sum_{i=1}^{N_p} S_{Ti,\alpha} - \sum_{PM \leq k} S_\alpha . \tag{4}$$

In $\sum_{PM \leq k} S_\alpha$ no first-order or higher-order indices referring to any $PM \geq l$ are included. This value is a measure of the importance of forward coupling for quantity α. In contrast to this, $\sum_{PM \geq l} S_\alpha$ indicates the importance of backward coupling and includes all first-order for $PM \geq l$ and all high-order terms referring to any $PM \geq l$. The need for bidirectional coupling increases with an increasing influence of backward coupling. Hence, the coupling quality is more and more dependent on the quality of the backward coupling.

3.3 Quality of Partial Model Coupling

In order to derive the quality of PM coupling, the data coupling quality and the influence of coupling are combined. The final application of the derived

coupling quality is the consideration within the framework of model evaluation, thus the quality of coupling is defined with this motive. In order to do so, the coupling quality depends on the position of the output quantity in the graph, for which the influence of coupling is investigated for.

When the coupling quality is evaluated for coupled PMs that are after the investigated output quantity in the sequence of the analysis, a backward coupling is essential; otherwise no information of the partial models arranged after the coupling can be transferred back to the PMs that are before in the sequence of the analysis. In this case, quality of coupling becomes

$$CQ_{k-l} = \overline{cq}^{f}_{k-l} \times \overline{cq}^{b}_{l-k}. \tag{5}$$

If one of the forward or backward data coupling quality is zero, the total quality is zero as well.

When coupling quality is evaluated for coupled PMs that are arranged before the investigated output quantity, the backward coupling might influence the coupled quantities to some extent, but it is not obligatory. In this case the quality is defined as

$$CQ_{k-l} = \frac{\frac{1}{N_f}\sum_{\alpha=1}^{N_f}\left(cq^{f}_{\alpha,k-l}\sum_{PM\le k} S_{\alpha_f}\right) + \overline{cq}^{b}_{l-k}\,\frac{1}{N_f}\sum_{\alpha=1}^{N_f}\left(\sum_{PM\ge l} S_{\alpha}\right)}{\frac{1}{N_f}\sum_{\alpha=1}^{N_f}\sum_{PM} S_{\alpha}}. \tag{6}$$

The forward data coupling quality $cq^{f}{}_{\alpha}$ is directly linked to the sensitivity indices of α. For backward data coupling quality this is not possible, because it cannot be determined which of the backward coupling quantities β has an influence on α. Furthermore, the number of forward and backward coupling quantities might differ. Hence, the mean value of sensitivity indices of α is multiplied with the mean of backward data coupling quality $\overline{cq}^{b}_{l-k}$.

3.4 Global Model Quality

The prediction quality of the global model for an output quantity γ depends on the quality of partial models, their influence on the quantity of interest, and

the coupling quality. The quality of partial model *i*, MQ_i, is weighted by the influence of partial model *i* on quantity γ, quantified by S^{γ}_{Ti}, with respect to the sum of all S^{γ}_{Ti} of the N_{PM} partial models involved. In addition, the quality contribution of each partial model is multiplied by coupling quality, CQ_c, of each of the $N_{c,i,\gamma}$ couplings that are necessary to transfer data from PM_i to the quantity of interest γ. For example, to transfer data from the beam to the foundation, Figure 1 and 2, two couplings, beam-to-column and column-to-foundation, are necessary. This means, $N_{c,i,\gamma}$ is equal to two. The resulting model quality of the global model *GM* for quantity γ becomes

$$MQ^{\gamma}_{GM} = \sum_{i=1}^{N_{PM}} \left[\frac{S^{\gamma}_{Ti}}{\sum_{j=1}^{N_{PM}} S^{\lambda}_{Tj}} MQ_i \prod_{c=1}^{N_{c,i,\gamma}} CQ_c \right]. \tag{7}$$

The coupling quality CQ_c of the partial models *a* and *b* being coupled is once more distinguighed into two cases, depending on the position of the output quantity γ within the sequence of the graph:

$$CQ_c = \begin{cases} CQ^{a}_{a-b} & \text{if } \gamma \text{ is after coupling } c \text{ (coupling } a \text{ with } b) \\ CQ^{b}_{a-b} & \text{if } \gamma \text{ is before coupling } c \text{ (coupling } a \text{ with } b). \end{cases} \tag{8}$$

4 Example

4.1 Partial Models and First Results

In the following, an example depicted in Figure 3 is analyzed with respect to coupling quality and the total prediction quality. The considered partial models are: live load beam (PM1), non-linear material behavior of the steel columns (PM2), geometric non-linear behavior of the steel column (PM3), and elastic behavior of soil (PM4). Coupling positions of the structural parts are between beam and column, denoted as 1, and between column and foundation, denoted as 2. Further parameters are depicted in the figure.

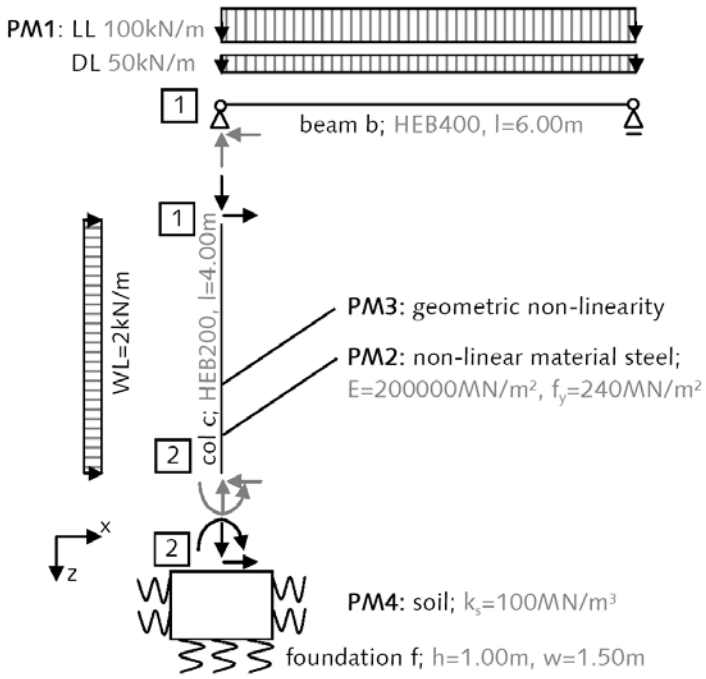

Figure 3. Example of coupled partial models.

First, the system is calculated considering perfect model coupling and the resulting major forces, moment, displacements, and rotations of the three structural parts are given in Table 1. From these numbers the qualitative influence of the several classes of partial models is derived, e.g. the influence of geometric non-linearity PM3 on the bending moment at column support, $M_{y2,c}$. The quantity $s_{z,f}$ denotes the maximum settlement of the foundation, resulting from vertical displacement and rotation.

Table 1. Results for different model classes, perfect bidirectional coupling.

X_{PM1}	X_{PM2}	X_{PM3}	X_{PM4}	$F_{z1,b}$ [kN]	$F_{z2,c}$ [kN]	$M_{y2,c}$ [kNm]	$u_{x1,c}$ [mm]	$\varphi_{y2,c}$ [E-3]	$\varphi_{y2,f}$ [E-3]	$s_{z,f}$ [mm]
0	0	0	0	150	150	16.0	5.5	0.00	0.00	0.00
0	0	0	1	150	150	16.0	9.9	-0.86	-0.86	1.64
1	0	0	0	450	450	16.0	5.5	0.00	0.00	0.00
1	0	1	0	450	450	19.3	7.3	0.00	0.00	0.00
1	0	0	1	450	450	16.0	9.9	-0.97	-0.97	3.65
1	0	1	1	450	450	21.7	13.3	-1.06	-1.06	3.80
1	1	1	1	450	450	21.7	13.3	-1.06	-1.06	3.80

Second, Table 2 shows the results of different couplings of the structural parts, distinguished into uni- and bidirectional coupling. Furthermore, bidirectional coupling with a limited number of iterations between the structural subsystems is given. From these numbers the relationship between the couplings are found. For example the support force of the beam $F_{z1,b}$ is independent

from these couplings. This is in contrast to the support moment of the column $M_{y2,c}$, which depends on the type of column-foundation foundation.

Table 2. Results for different coupling types, all partial models considered.

coupling b-c	coupling c-f	$F_{z1,b}$ [kN]	$F_{z1,c}$ [kN]	$M_{y2,c}$ [kNm]	$M_{y2,f}$ [kNm]	$\varphi_{y2,c}$ [E-3]	$\varphi_{y2,f}$ [E-3]	$s_{z,f}$ [mm]
unidirectional	unidirectional	450	450	19.3	19.3	0.00	-0.97	3.74
bidirectional	unidirectional	450	450	19.3	19.3	0.00	-0.97	3.74
unidirectional	bidirectional	450	450	21.7	21.7	-1.06	-1.06	3.80
bidirectional	bidirectional	450	450	21.7	21.7	-1.06	-1.06	3.80
bidirectional	bidirectional, only 1 iteration	450	450	21.5	21.5	-0.97	-1.05	3.80

4.2 Influence of Partial Models

The influence of the partial models is determined by means of sensitivity analysis according to [3], applying a perfect data coupling. The resulting high-order sensitivity indices for selected output quantities are given in Table 3. The output $F_{z1,b}$ depends only on PM1 live load beam, thus no interaction effects with other PMs occur. Contradictory to this, $M_{y2,c}$ depends on several partial models and an interaction of these PMs is quantified by the high-order indices, for example an interaction of live load PM1 and geometric non-linearity PM3 with S_{13}=0.181. The quantity $M_{y2,c}$ depends also on the soil model PM4. This effect can only occur when backward coupling from the foundation to the column exists, thus a higher demand for this coupling is present, in contrast to the beam-column coupling.

Table 3. Sensitivity indices of specific model responses.

	$F_{z1,b}$	$F_{z2,c}$	$M_{y2,c}$	$u_{x1,c}$	$\varphi_{y2,f}$	$s_{z,f}$
S_1	1.000	1.000	0.181	0.035	0.002	0.113
S_2	0.000	0.000	0.000	0.000	0.000	0.000
S_3	0.000	0.000	0.536	0.104	0.005	0.000
S_4	0.000	0.000	0.037	0.801	0.984	0.773
$S_{13}= S_{31}$	0.000	0.000	0.181	0.035	0.002	0.000
$S_{14}= S_{41}$	0.000	0.000	0.014	0.005	0.002	0.113
$S_{34}= S_{43}$	0.000	0.000	0.037	0.014	0.005	0.000
$S_{134}= S_{314}= S_{413}$	0.000	0.000	0.014	0.005	0.002	0.000
S_{T1}	1.000	1.000	0.389	0.081	0.007	0.226
S_{T2}	0.000	0.000	0.000	0.000	0.000	0.000
S_{T3}	0.000	0.000	0.768	0.158	0.013	0.001
S_{T4}	0.000	0.000	0.102	0.826	0.992	0.887
$\Sigma S_{PM \leq k}$	1.000	1.000	1.079	0.209	1.011	1.114
$\Sigma S_{PM \geq l}$	0.000	0.000	0.181	0.856	0.000	0.000
ΣS_T	1.000	1.000	1.260	1.065	1.011	1.114

4.3 Coupling Quality

Within this section the coupling quality is estimated considering all four partial models of the example. Different couplings of beam-column and column-foundation are investigated. The further couplings, e.g. the material behavior with the kinematics, do not provide any data loss and have a quality of one. The qualities for specific quantities are given in the Tables 4 and 5. As mentioned earlier, the quality of partial model coupling *CQ* depends on the quantity of interest, in particular on the position of the quantity of interest within the sequence of the analysis. Hence, *CQ* is calculated for the different involved partial models/structural parts, denoted for example as CQ^c for coupling quality of the column.

Table 4. Results for coupling quality beam-column.

coupling b-c	cq^f_{Fz1}	cq^b_{uz1}	$\sum_{PM\leq 1} S_{Fz1}$	$\sum_{PM\geq 2} S_{Fz1}$	$\frac{1}{2}\sum_{f=1}^{2}\left(\sum_{PM\geq 2} S_{\alpha_f}\right)$	CQ^b_{b-c}	CQ^c_{b-c}
unidirectional	1.00	0.00	1.00	0.00	0.00	0.00	1.00
bidirectional	1.00	1.00				1.00	1.00

Table 5. Results for coupling quality column-foundation.

coupling c-f	cq^f_{My2}	$cq^f_{\varphi y2}$	$\sum_{PM\leq 3} S_{My2}$	$\sum_{PM\geq 4} S_{My2}$	$\frac{1}{3}\sum_{f=1}^{3}\left(\sum_{PM\geq 4} S_{\alpha_f}\right)$	CQ^c_{c-f}	CQ^f_{c-f}
unidirectional	1.00	0.00				0.00	0.94
bidirectional	1.00	1.00				1.00	1.00
bidirectional, only 1 iteration	1.00	0.92	1.08	0.18	0.06	0.92	0.99

The coupling beam-column consists of two output quantities of the beam, $F_{z1,b}$ and $F_{x1,b}$, and two output quantities of the column, $u_{z1,b}$ and $u_{x1,c}$. The forward coupling quality is always one, as the output quantities of the beam are directly applied to the column and no data loss occurs. In case of unidirectional coupling the data coupling quality of the backward coupling is zero. Analyzing the sensitivity indices reveals that the output quantity $F_{z1,b}$ depends only on PM1, thus no backward coupling is necessary when *CQ* is analyzed for the column and this results to $CQ^c_{b\text{-}c}=1.0$ according to Eq. (6). When analyzing the quality for quantities of the beam according to Eq. (5), values of $CQ^b_{b\text{-}c}=0.0$ and $CQ^b_{b\text{-}c}=1.0$ for the unidirectional and bidirectional case are obtained. The zero coupling quality for unidirectional interaction results from necessity of backward coupling for the beam in order to take into account output quantities of the column.

The coupling column-foundation consists of three output quantities of the column, $F_{z2,c}$, $F_{x2,c}$ and $M_{y2,c}$, as well as three output quantities of the foundation, $u_{z2,f}$, $u_{x2,f}$ and $\varphi_{y2,f}$. The forward coupling quality is still always one and the backward coupling quality is always zero in case of unidirectional coupling. As already mentioned, $M_{y2,c}$ depends to some extent on PM4. This is pointed out when comparing the sum of the sensitivity indices of all $PM \leq 3$ before and all $PM \geq 4$ after the coupling, 1.08 and 0.18. Hence, the coupling quality of the partial models depends on the quality of the forward and backward coupling even for response quantities that are after the coupling. The data coupling quality of the support moment is given in Table 5. The resulting coupling qualities are also shown in this Table 5 for two response quantities: first belonging to the column $CQ^{c}_{c\text{-}f}$, which is before coupling and calculated according to Eq. (5), and second for the foundation $CQ^{f}_{c\text{-}f}$, which is after the coupling analyzed according to Eq. (6). The value of $CQ^{c}_{c\text{-}f}$ is zero in the unidirectional case, as no information of PM4 can be transferred back to the column. When analyzing $CQ^{f}_{c\text{-}f}$ it is observed that a unidirectional coupling still leads to a quality of $CQ^{f}_{c\text{-}f}$=0.94, as the output quantities of the column are mainly defined by the forward coupling and only relatively small parts of the output quantities are influenced by the backward coupling. In case of bidirectional coupling with only one iteration between the structure of the column and foundation, a high value of $CQ^{f}_{c\text{-}f}$=0.99 is determined, thus one iteration already gives satisfying results.

4.4 Global Model Quality of the Prediction

Exemplarily, the prediction quality is calculated for the output quantity support moment of the column $M_{y2,c}$ and the maximum settlement of the foundation $s_{z,f}$. This example focuses on the effect of coupling type and the consequences from the choice of coupling type. Thus, the quality of the PM1, PM2, and PM3 are chosen not to influence the results and are considered as perfect, $MQ=1.0$. For PM4 (soil) two different models are considered: a simple approach PM4s with $MQ_{PM4s}=0.7$ and an advanced formulation with $MQ_{PM4a}=1.0$. Apart from the coupling beam-column and column-foundation all other couplings are perfect, $CQ=1.0$.

The example shall demonstrate the trade-off for choosing a simple soil model, which allows for an iterative bidirectional coupling due to a time-efficient calculation, and an advanced soil formulation only allowing for unidirectional coupling.

First, the prediction quality for $M_{y2,c}$ is calculated according to Eq. (7). In case of bidirectional coupling and applying the worse soil model MQ_{GM} becomes

$$MQ_{GM,PM4s}^{M_{y2,c}} = \frac{0.389}{1.260} \cdot 1.0 \cdot 1.0 + \frac{0.000}{1.259} \cdot 1.0 \cdot 1.0 + \frac{0.768}{1.260} \cdot 1.0 \cdot 1.0 + \frac{0.102}{1.260} \cdot 0.7 \cdot 1.0 = 0.976,$$

and in opposite applying the advanced soil model and unidirectional coupling

$$MQ_{GM,PM4a}^{M_{y2,c}} = \frac{0.389}{1.260} \cdot 1.0 \cdot 1.0 + \frac{0.000}{1.259} \cdot 1.0 \cdot 1.0 + \frac{0.768}{1.260} \cdot 1.0 \cdot 1.0 + \frac{0.102}{1.260} \cdot 1.0 \cdot 0.0 = 0.919.$$

It is shown that the selection of the simple soil model with a bidirectional coupling leads to a higher prediction quality than the advanced soil model with a unidirectional coupling. This is a consequence of the missing data transfer from the foundation to the column in case of unidirectional coupling.

Second, the prediction quality for the settlements $s_{z,f}$ are calculated. In case of bidirectional coupling and applying the worse soil model MQ_{GM} becomes

$$MQ_{GM,PM4s}^{s_{z,f}} = \frac{0.226}{1.114} \cdot 1.0 \cdot 1.0 \cdot 1.0 + \frac{0.000}{1.114} \cdot 1.0 \cdot 1.0 \cdot 1.0 + \frac{0.001}{1.114} \cdot 1.0 \cdot 1.0 \cdot 1.0 + \frac{0.887}{1.114} \cdot 0.7 \cdot 1.0 = 0.762,$$

and in opposite applying the advanced soil model and unidirectional coupling

$$MQ_{GM,PM4s}^{s_{z,f}} = \frac{0.226}{1.114} \cdot 1.0 \cdot 1.0 \cdot 0.94 + \frac{0.000}{1.114} \cdot 1.0 \cdot 1.0 \cdot 0.94 + \frac{0.001}{1.114} \cdot 1.0 \cdot 1.0 \cdot 0.94 + \frac{0.887}{1.114} \cdot 1.0 \cdot 1.0 = 0.988.$$

In contrast to the support moment, the quality analyzed for the settlements is different, as the influence of the bidirectional coupling on the settlements is less than the influence on the support moment. Thus, the advanced soil model provides the higher quality, due to the better individual partial model quality.

The conclusion from an engineering point of view is that the use of a simple soil approach is sufficient enough for the calculation of the column. The results of this first analysis can be used to study the settlements more detailed applying unidirectional coupling and the sophisticated soil model.

5 Conclusions

This paper presented a method to calculate data coupling quality and to quantify the influence of coupling on the output data in the case of coupled partial models. By doing so the determination of coupling quality of partial models in the context of a global system is accounted for. Further, a measure for the

prediction quality of a global system taking into account coupling quality, individual quality of the partial models, and their influence on the output are taken into account.

The method provides a useful tool to determine the necessity to couple partial models in a uni- or bidirectional manner. Doing so, the algorithm allows for a reduction of complexity of global systems when bidirectional coupling is less important.

Acknowledgements

This research is supported by the German Research Institute (DFG) via Research Training Group "*Evaluation of Coupled Numerical Partial Models in Structural Engineering (GRK 1462)*", which is gratefully acknowledged by the author.

References

[1] Fröbel, T.: *Data coupled civil engineering applications: modeling and quality assessment methods*. Bauhaus-Universität Weimar, Verlag der Bauhaus-Universität Weimar, 2012 - Dissertation

[2] Homma, T.; Saltelli, A.: Importance measures in global sensitivity analysis of nonlinear models. *Reliability Engineering and System Safety* 52 (1996), p. 1-17

[3] Keitel, H.; Karaki, G.; Nikulla, S.; Lahmer, T.; Zabel, V.: Evaluation of coupled partial models in structural engineering using graph theory and sensitivity analyses. *Engineering Structures* 33 (2011), p. 3726-3736

[4] Lahmer, Z.; Knabe, T.; Nikulla, S.; Reuter, M.: Bewertungsmethoden für Modelle des konstruktiven Ingenieurbaus. *Bautechnik Sonderheft* 88 (2011), p. 60-64

[5] Most, T.: Assessment of structural simulation models by estimating uncertainties due to model selection and model simplification. *Computers and Structures* 89 (2011), p. 1664-1672

[6] Saltelli, A.; Ratto, M.; Andres, T.; Campolongo, F.; Cariboni, J.; Gatelli, D.; Saisana, M.; Tarantola, S.: *Global sensitivity analysis. The primer*. John Wiley and Sons, 2008

[7] Sobol, I.: Sensitivity estimates for nonlinear mathematical models. *Mathematical Modeling & Computational Experiment* 1 (1993), p. 407-414.

[8] Stein, P.; Lahmer, T.; Bock, S.: Synthese und Analyse von gekoppelten Modellen im konstruktiven Ingenieurbau. *Bautechnik Sonderheft* 88 (2011), p. 8-11

Dependent load combination

T. Poutanen
Department of Civil Engineering, Tampere University of Technology
Tampere, Finland

Abstract: A universal theory on combining loads in structural design is lacking. Current codes include three methods: dependent, semi-dependent and independent. These methods are mutually contradicting and inconsistently applied. The dominant assumption is that loads are combined independently if the loads are independent, dependently if the loads are dependent and other loads are combined semi-dependently. However, the permanent loads are independent but combined always dependently in the current codes contrary to the basic assumptions. The permanent load and the variable load are combined sometimes independently and sometimes dependently in the failure state but always dependently in the serviceability state. Variable loads are combined usually semi-dependently but sometimes dependently.
This paper explains that the structural loads must always be combined dependently i.e. the fractile load of the combination load distribution is obtained by adding up the related fractile loads of the partial load distributions. The basic reason is that the distributions in the structural design must be the extreme distributions. Many other arguments are presented, too.
In order to combine variable loads the distributions must be first converted simultaneous i.e. the loads must be active at the same time. This distribution alteration induces a combination factor ψ_0.

1 Introduction

The load combination is the key issue in the safety factor and the combination factor γ_G, γ_Q, γ_M, ψ_0 calculation. The dominant theory is that the loads are combined independently if the loads are independent, dependently if the loads are dependent and other loads are combined semi-dependently. However, the permanent loads are independent but combined always dependently. The

permanent load and the variable load are combined sometimes independently and sometimes dependently in the failure state but always dependently in the serviceability state. Variable loads are combined usually semi-dependently but sometimes dependently.

An explanation is missing why different combination methods are used. A uniform theory on the load combination was lacking.

Arguments are presented in this paper that loads must always be combined dependently. The primary argument is that the combination distribution must be the extreme distribution. The dependent load combination is universal and consistent in all cases.

1.1 Current theory

The current load combination theory and its code implementations are disclosed in references [1, 2, 3, 4, 5, 6, 10, 11].

The basic load combination theory is revealed by MADSEN ET AL [6], MADSEN [5] and TURKSTRA [11]. Much theoretical research is paid to find out how variable loads are combined and how the load configuration affects on the load combination. The current variable load combination is based on Turkstra's method TURKSTRA [11]: The combination load is the higher load which is obtained when one load is constant and the other load has a random value. In this load combination, the load configuration has no effect.

The theoretical references [5, 6, 11] and references [1, 2, 3, 4, 10, 11] explaining the actual load combination in the code, describe that the loads are stochastic and combined independently. However, this concept is not consistently applied. No reference explains why permanent loads are combined dependently although these loads are independent?

If there are many loads, e.g. imposed loads of a multi storey house[1] or many permanent loads, the independent load combination results in an unrealistic outcome as the reliability vanishes. The current load combination theory does not address this contradiction either.

The references [1, 2, 3, 4, 5, 6, 10, 11] do not address several other significant issues of the load combination:

[1] The unrealistic outcome of the independent load combination is recognized in an Eurocode background document: *Imposed loads on floors and roofs* (1990) "The storey-dependent reduction formulas of the code-draft are not scientifically derived…".

- The extreme function, i.e. the rule of the maximum load combination.
- The correlation of the loads due to the equality design equation.
- The correlation of the loads when the loads are proportions of another load.
- The load losing and the uneven failure probability of the independent combination.
- The independent combination contradicts the linearity and Hook's law.

1.2 Dependent, semi-dependent and independent load combination

Two loads are combined dependently by adding up the distributions by fractiles i.e. a load X with an item x_i in fractile i and a load Y with an item y_i in the same fractile i are combined dependently to obtain the combination load XY with an item xy_i in fractile i by adding up x_i and y_i, i.e. $xy_i = x_i + y_i$, POUTANEN [7, 8]. If the Monte Carlo simulation is used to combine the loads, in the dependent combination one seed number is used. The same combination load is obtained when several random load pairs x_i , y_i are generated and the combination load distribution is constructed from these load pairs considering the extreme function i.e. the maximum load rule. If the convolution equation is used to combine the loads, the deviation of the combination load is fixed in a way the combination distribution crosses the crossing point of the partial distributions POUTANEN [7, 8]. In the dependent combination, the action of a new load in the combination is independent of other loads in the load combination. When the loads are combined dependently in the actual structural design, the design values of the partial loads are added up as such without any reductions, combination factors etc. and without any load losing.

The semi-dependent combination is an imprecise abstraction. Several semi-dependent combination methods exist, e.g. Turkstra's method, TURKSTRA [11], where one load has a constant value and the other load has a random value. The semi-dependent combination should lie between the dependent and independent combination. This is normally true at least at high fractiles[1]. In the current codes the semi-dependent combination is carried out by Turkstra's load combination model TURKSTRA [11] to combine variable loads. In the actual code two loads are added up with a combination factor ψ_0 in the lesser load. Turkstra's load combination model is approximate. This combination is

[1] Turkstra's combination load depends on how the constant value is defined. It is normally the mean value (or approximately the mean value) when Tukstra's combination is less than the independent combination load and also less that the dependent combination load (as the dependent combination load is the highest one).

a discontinuous[1] function of partial loads and it does not include two relevant concepts in the load combination: the load duration and the simultaneity. Turkstra's load combination includes a load losing.

In the independent combination, the loads are combined randomly e.g. by using the convolution equation or by using Ferry Borges – Castanheta's method, ISO 2394 [4], or by using the Monte Carlo simulation and two seed numbers without the extreme function i.e. the maximum load combination rule. In the independent combination, the action of the new combination load depends on the earlier loads in the combination[2]. The independent combination is often applied in the combination of the permanent and the variable load and to define the material safety factor γ_M. A part of the load, ca 0...10 %, vanishes in this combination and therefore the safety factor γ_M includes a reduction factor of ca 0.9...1.

In the semi-dependent and in the independent combinations, each new load in the combination decreases the total safety factor. If the number of loads is infinite, there is no safety and the total load is the sum of the mean partial loads.

The current terms dependent and independent combination are misleading as in the independent combination the partial loads may be independent or dependent but the combination load is dependent of the partial loads and in the dependent combination vice versa. Therefore it would be clearer to use other terms. The independent combination may be called "indefinite" or "random" summation. Correspondingly, the dependent combination may be called "definite" or "accumulation" summation.

1.3 Load combination in current codes

Loads are combined in the current codes in three ways:

- Permanent loads are always combined dependently.
- A permanent and a variable load are combined in the failure state sometimes dependently and sometimes independently but in the serviceability state always dependently.

[1] The actual load is the function of the load ratio $F(\alpha)$, it is continuous but its derivative $dF(\alpha)/d\,\alpha$ is discontinuous.

[2] This is a clear argument that the independent load combination is wrong. It is impossible, for instance, that the effect of the snow load on a roof would depend on the permanent load of the roof and the effect was different on a light and a heavy roof.

- Two variable loads are always combined semi-dependently if these loads are the first and the second variable load in the load combination, but always dependently if the loads are third, fourth etc. load in the load combination.

EUROCODE [1] includes three options to combine the permanent and the variable load, 6.10, 6.10a,b and 6.10a,mod. The first one is dependent and the others are independent. Finnish Eurocode is based on 6.10a,mod.

1.4 Contradictions in current codes

The basis of the current load combination theory is questionable as three contradicting combination methods exist and these methods are applied inconsistently:

- The permanent *G* and the variable *Q* load are usually considered independent but they are independent only during one year and virtually fully correlated and dependent during the service time of a structure, 50 years[1].

- Permanent loads are independent and according to the current load combination hypotheses, these loads should be combined independently but they are always combined dependently. Permanent loads cannot be combined independently as the outcome was unrealistic.

- Eurocode includes three load combination rules 6.10, 6.10a,b and 6.10a,mod. The first one is dependent, and the others independent. The code writer cannot give a clear directive about the load combination.

- In the current codes, permanent and variable loads are combined in the failure state sometimes dependently and sometimes independently but in the serviceability state always dependently. It is evident that the loads must be combined consistently in the same way in all cases.

- Variable loads are combined semi-dependently if the loads are the first and the second load in the load combination but thereafter the loads are combined always dependently.

[1] All *Q*-load values below fractile 0.98 occur during 50 years. Whichever the *G*-load is below the fractile 0.98 there is a *Q*-load at the same fractile.

2 Arguments for dependent load combination

Next nine arguments are presented that the structural loads must be combined dependently.

2.1 Extreme function, rule of maximum load combination

In the structural design the load distributions denote the extreme load values of a specific probability at a selected reference time. Consequently, the load combination must also consist of the extreme values of the combination loads. When the loads are combined independently, the load distribution is the sum of the extremes when the maximum load rule is ignored but it must be the extreme of the extremes when the maximum load rule is considered. This is the key error of the independent combination demonstrated by combining loads *G* and *Q* in Figure 1.

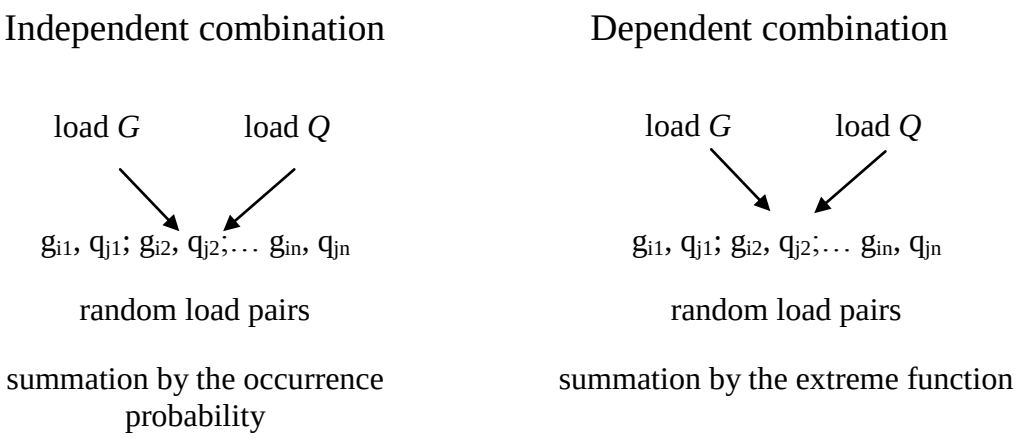

Figure 1. Illustration of the independent and the dependent load combination of loads *G* and *Q*. The loads can be combined by processing several random loads pairs and the combination load is constructed from these loads pairs by considering the extreme function i.e. the maximum load rule with the highest loads combined first, then the next highest etc. In this combination, the loads are combined dependently i.e. the loads of the same fractiles of the partial loads are added up to obtain the load of the related fractile value of the combination load.

The independent combination applies to one random load pair only. However, the combination of structural loads always applies to many loads. The load distribution is fixed to one-year loads only but the design must cover all loads during the working time, normally 50 years. When several adjacent roof girders are designed, it is not sufficient to consider loads in one girder only but in all girders in the roof. Thus, the load combination always applies to a

group of loads, thus the maximum load combination and the dependent combination must be employed.

2.2 Common sense reasoning

The dependent combination can be deduced by common sense reasoning: Assume a material (or a structure) has the survival probability S and the resistance 1 for the permanent load G alone and the variable load Q load alone. Now, if the material is loaded by $0.5G$ and $0.5Q$ and the loads are combined independently, the material has the resistance of ca 1.1[1] and if combined dependently, it is 1. The independent combination is unrealistic. It is impossible that the effect of one load decreases if the other load is present. The reason for the high resistance, if the loads are combined independently, is the load losing.

2.3 Equality equation

The basic design equation of the structural design with the permanent load G, the variable load Q and the material property M is

$$\gamma_G \cdot G + \gamma_Q \cdot Q \leq \frac{M}{\gamma_M} \tag{1}$$

If we apply an equality equation, a definite dependence and correlation exists between the distributions G, Q as the material property M is constant regarding the loads. G and Q have a full negative correlation. When one load is increased the other decreases correspondingly. Due to this correlation the loads G and Q must be combined dependently regardless of whether they are independent or dependent otherwise.

2.4 Linearity, Hook's law

Hook's law directs one basic rule in the structural design, linearity: when a load has a certain effect at one load level, the same effect occurs by the same load at any other load level. The independent load combination is in contrast with the Hook's law and the linearity:

One realization of the independent load combination is the combination rule 6.10a,mod of Eurocode. In this load combination with low permanent load when the variable load increases no effect occurs.

[1] In Eurocode more precisely 1.0646, $V_{G,normal} = 0.09147$, $V_{Q,gumbel} = 0.4$, $\beta = 3.826$, combination rule 6.10.

The independent combination theory contradicts the linearity and the Hook's law in the same way: Assume the loads *G* and *Q* act in a tension bar, A = 1000 mm^2, the target reliability is 0.98 and the distribution functions are normal. Table 1 includes 5 load cases. We see in Table 1 and the load case 5 with the independent combination that ca 10 % load vanishes; the linearity and Hook's law are not valid.

Table 1. Five load cases of the permanent *G* and the variable *Q* load. The load case 5 shows that the independent combination results in a load losing of ca 10 %, the linearity and the Hook's law are not valid.

load	load [kN]		stress [N/mm^2]	
case	*G*	*Q*	depend.	independ.
1	1	0	1	1
2	0	1	1	1
3	0.2	0	0.2	0.2
4	0	0.2	0.2	0.2
5	0.2	0.2	0.4	0.37

We can put this example to another form: Assume the permanent load is 1 kN and the variable load 1 kN, too. It is evident that the stress on the bar is 1 N/mm^2 when the loads act alone. It is also obvious that the stress is 2 N/mm^2 when the loads act together. However, if the loads are combined independently the stress is ca 1.8 N/mm^2. The independent combination is wrong. It is impossible that the effect of one load decreases if another load is present.

2.5 Load losing

The independent load combination results in a load losing. We see in Table 1 and load case 5 that ca 10 % of the combination load vanishes. In the current codes the material safety factors are sometimes calculated by combining the loads independently which results in up to 10 % too low safety factors for this reason.

The semi-dependent load combination by Turkstra [11] results in a load losing, too.

2.6 Rule of maximum load combination

One basic rule of the structural design is that the loads must be combined to obtain the maximum load. According to this rule, all loads should be combined dependently as the dependent combination results in the highest

load. This rule is valid and must always be obeyed. In the current theory, this rule is sometimes ignored as the independent loads are wrongly considered demanding the independent load combination.

2.7 Imposed loads

Imposed loads on the floors of a multi storey house are different from other loads as they are proportions of another load, the total imposed load in the house. Therefore the imposed loads on the floors are correlated and must be combined dependently.

2.8 Permanent loads

Permanent loads are independent but combined in all codes always dependently i.e. correctly contrary to the current load combination theory. Permanent loads cannot be combined independently as the result was unrealistic. The safety would vanish in case of many loads.

2.9 Many loads

If loads are combined independently or semi-dependently, each new load in the combination decreases the total safety. In case of many loads, e.g. permanent or imposed loads of a multi storey house, the safety vanishes, which is unrealistic.

3 Combination of variable loads

The combination of variable loads *A* and *B* is like the combination of the permanent and the variable loads *G* and *Q*, POUTANEN [9]. The distribution of one load is converted to the active time of this load when it becomes analogous to the permanent load. The distribution conversion induces a combination factor ψ_0. This load and the other variable load are combined dependently without any further combination factors or reductions which would induce a load losing. The loads *A* and *B* may have different active times; therefore each load must be converted in turn to its active time and the greater load combination is selected.

4 Consequences

Material safety factors γ_G of current Eurocode are presented In Figure 2 with loads combined independently and dependently according to the combination rule 6.10, $\gamma_{G,\,normal} = 1.35$, $\gamma_{Q,\,Gumbel} = 1.\,5.\,\beta = 3.286$.

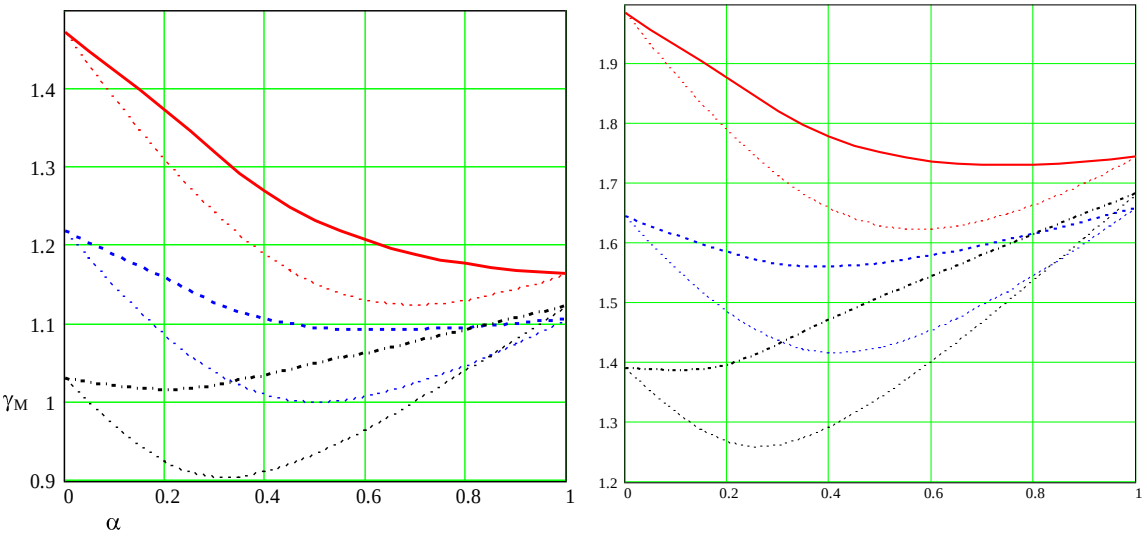

Figure 2. Material factors γ_M of Eurocode, $\beta = 3.826$[1], $\gamma_G = 1.35$, $\gamma_Q = 1.5$ as the function of the load ratio α ($Q/G+Q$, permanent load G only $\alpha = 0$, variable load Q only $\alpha = 1$), left Figure. Red solid line $V_M = 0.3$ (sawn timber); blue dashed line $V_M = 0.2$ (glue lam); black dash-dotted line $V_M = 0.1$ (steel). The dotted lines denote to the corresponding independent load combination. The right Figure denotes to γ_M according to a corresponding design value code $\gamma_G = \gamma_Q = 1$.

We see in Figure 2 that the independent and the dependent safety factors are the same if these loads act alone. The dependent material safety factor γ_M is approximately a linear interpolation of the partial loads. On the other hand, the independent combination has a downward bow from the linear interpolation and results in ca. 10 % less safety factor at $\alpha = 0.3...0.5$ in comparison with the safety factors of the dependent combination. The design outcome was precisely equal if the partial safety factor design $\gamma_G = 1.35$, $\gamma_Q = 1.5$ and material factors γ_M of the left Figure or the design value method design $\gamma_G = \gamma_Q = 1$ and material factors γ_M of the right Figure were used regardless whether the loads are combined independently or dependently. For example, when $\alpha = 0.8$ and $V_M = 0.2$ i.e. glue lam, the dependent and the independent material factor γ_M in the partial load factor method, left Figure, are 1.09 and 1.05, consequently, the total safety factors are correspondingly

[1] This reliability approximately corresponds to actual material safety factors, but is less than one-year reliability recommended in Eurocode $\beta_1 = 4.7$, thus the safety factors γ_G for $\beta_1 = 4.7$ are higher.

$\gamma_{GQ}\cdot\gamma_M$, 1.62 and 1.54 which are equal to the total safety factors of the design value method, right Figure. However, in the actual design minor variations occur as the current codes do not include the concrete material safety factors γ_M but these factors are approximated but constants i.e. the curved and inclined lines are horizontal lines.

The dependent load combination in the actual design are summarized as follows:

- The combination rules including two permanent load factors e.g. the rules 6.10a,b and 6.10a,mod of Eurocode are induced from the independent load combination and these combination rules should be deleted.

- The total safety factor calculated from *G* and *Q* loads $\gamma_t = \gamma(\gamma_G, \gamma_Q, \gamma_M)$ is up to 10 % too low, if the permanent and the variable load is combined independently. The safety factors of the current codes are normally higher than the target safety factors and the actual error is less. However, in some cases this error has its full effect.

- Two variable loads are currently combined semi-dependently, which results in up to ca 30 % too low combination factors ψ_0 POUTANEN [9].
  The combination factor ψ_0 for the snow load is currently 0.5...0.7 but should be adjusted according to the duration of the snow load: one week $\psi_0 \approx 0.75$; one moth $\psi_0 \approx 0.85$ and two moths, $\psi_0 \approx 0.90$. As this factor is close to unity a feasible approximation is to set it at unity, $\psi_0 = 1$.
  The combination factor ψ_0 of a short duration load e.g. imposed load and wind load combined with each other or with snow (except imposed load – imposed load) depends on the duration of the load: one minute, $\psi_0 \approx 0.55$; 10 minutes, $\psi_0 \approx 0.6$; ten hours, $\psi_0 \approx 0.65$; one day, $\psi_0 \approx 0.7$ and one week, $\psi_0 \approx 0.75$, POUTANEN [9].
  The current imposed load factor is $\psi_0 = 0.7$ but it should be 1. The reason is that the imposed loads on floors are dependent and proportions of the whole imposed load of the house[2].

- The unsafe error of the reliability model due to the independent and the semi-dependent load combination is up to ca 15 % in two loads and up to ca 20 % in three loads. The unsafe error of the actual code is less, up to ca 15 %, as the safety factors are often selected higher than obtained from the independent and semi-dependant calculation.

The dependent combination affects on the safety and the combination factors only, not the design equations and the design processes.

[1] $\gamma_{GQ} = 0.2\cdot1.35 + 0.8\cdot1.5 = 1.470$

[2] The characteristic imposed loads in current codes are high enough to compensate the ψ_0 error.

The dependent load combination results in a partial safety factor code with one permanent load factor e.g. combination rule 6.10 of Eurocode or a unity load factor code $\gamma_G = \gamma_Q = 1$. A partial safety factor code including one permanent load factor can always be converted in a unity load factor code $\gamma_G = \gamma_Q = 1$ with an equal reliability and equal design outcome. This change does not affect the current limit state design concept. Thus the option $\gamma_G = \gamma_Q = 1$ is attractive as it simplifies the code and decreases the calculation work. If we set $\gamma_G = \gamma_Q = 1$ with γ_M semi-variable in variable *G*-*Q*-loads (constant in normal load cases), such code has far better reliability accuracy with less calculation work than any current code, $\gamma_G \neq \gamma_Q \neq 1$, constant γ_M.

5 Conclusions

Structural loads must be combined dependently. It is the consistent and the universal load combination in all cases:

- The permanent loads with each other *G* – *G* and the permanent load and the variable load *G* – *Q* are combined dependently as such i.e. without combination or reduction factors which would induce a load losing.
- The variable loads *Q* – *Q* are combined dependently, too after the distributions are altered in a way the loads are simultaneous i.e. they are active with each other at the same time. The distribution alteration induces a combination factor ψ_0.
- If variable loads are proportions of another load (e.g. imposed loads of a multi storey house), they are combined dependently i.e. without a combination factor, $\psi_0 = 1$.
- The maximum load combination rule, the equality equation, Hook's law, the linearity and the load losing demand the dependent load combination.
- A good option is to set $\gamma_G = \gamma_Q = 1$ and semi-variable γ_M. This setting results in much better reliability accuracy than in current codes with less calculation work and simpler code.
- The current terms dependent and independent combination are misleading. It would be clearer to use terms "accumulation" or "definite" summation and "random" or "indefinite" summation.
- The accumulation summation of loads is reliable, it is simple and the required design work is little.

Acknowledgement

When writing this paper I have got valuable comments from Professor Keijo Ruohonen, Tampere University of Technology.

References

[1] CodeCal, A soft ware for reliability calculation, 2002, http://www.jcss.ethz.ch

[2] *EN 1990:2002 Eurocode – Basis of structural design*, European Committee for standardization, Bruxelles

[3] Gulvanessian H., Calgaro J-A., Holicky M., *Designer's Guide to EN 1990, EUROCODE: Basis of structural design*, Thomas Telford Publishing, London, 2002

[4] ISO 2394, *General principles on reliability for structures*, International Organization for Standardization, Geneva, Switzerland, 1996

[5] Madsen H., O., *Load Models and Load Combination*, Technical University of Denmark, Rapport nr R 113, 1979

[6] Madsen H., O., Krenk S., Lind N., C., *Methods of Structural Safety*, Prentice-Hall Inc. NJ, USA, 1986

[7] Poutanen T., *Safety factors and design codes*, Joint IABSE – fib Conference, Dubrovnik, May 3-5, 2010

[8] Poutanen T., *Calculation of partial safety factors*, Applications of Statistics and Probability in Civil Engineering – Faber, Köhler & Nishijima (eds), Taylor & Francis Group, London, 2011

[9] Poutanen T., *Combination factors ψ_0 in structural design*, A journal article submitted for review, 2011

[10] *Probabilistic Model Code*, Part 1, Basis of Design, http://www.jcss.ethz.ch

[11] Turkstra C., J., *Theory of Structural Safety*, SM Study No. 2, Solid Mechanics Division, University of Waterloo, Waterloo, Ontario, 1970

Reliability-based design optimization of damage-tolerant elastoplastic frames

Dimos C. Charmpis
Department of Civil and Environmental Engineering, University of Cyprus,
75 Kallipoleos Str., P.O. Box 20537, 1678 Nicosia, Cyprus

Abstract: This work is concerned with the explicit treatment of progressive collapse resistance within the process of structural design optimization under uncertainty. Progressive collapse resistance is associated with the damage tolerance of a structural system and controls the ability of the system to sustain local damage (e.g. loss of a structural component) by minimizing the potential of triggering system failure (progressive partial/full collapse). The present work focuses on the reliability-based optimum design of damage-tolerant elastoplastic steel frames with correlated random member properties. For this purpose, additional reliability constraints concerning the structure with artificial local damage are incorporated into the Reliability-Based Design Optimization (RBDO) formulation, which –in its classical form– takes only one reliability constraint associated with the intact (non-damaged) structure into account and aims in minimizing structural cost (or material volume/weight). The direct Monte Carlo simulation procedure is employed to perform structural reliability analyses, while a specialized heuristic random number generator is used to sample from multivariate probability distributions with their marginals being the distributions of the arbitrarily distributed and intercorrelated random member properties. The resulting RBDO approach, which is implemented using a discrete Simulated Annealing optimizer, is capable of producing cost-effective designs for elastoplastic frames with acceptable system damage tolerance.

1 Introduction

Reliability-Based Design Optimization (RBDO) is the most common approach applied to structural design optimization problems taking into account uncertainties in material properties, geometric parameters, loads etc. The optimization process aims in detecting the optimum design by minimizing the weight or cost of a structure subject to constraints ensuring adequate performance for the structural members and/or the overall system. In RBDO, typically one structural reliability constraint is incorporated by pre-specifying the

maximum allowable failure probability of the structure for the finally achieved design.

The present work is concerned with the reliability-based optimum design of elastoplastic steel frames, which consist of members with correlated random structural properties. In the framework of the implemented RBDO process, the reliability constraint is imposed by adopting a maximum allowable collapse probability of the elastoplastic frame designed.

In addition to the above reliability constraint focusing on the system resistance of an intact (non-damaged) frame, additional probabilistic design requirements on the system resistance of the frame suffering artificial local damage are considered. The term 'artificial local damage' is used to refer to a scenario of local structural failure, which may trigger progressive collapse of the structure. Insensitivity to such local failures is an important property of the structure, which can be considered during the design process. In this work, additional constraints are included in the RBDO procedure, in order to control the reliability (i.e. the non-collapse probability) of the structure under any assumed damage scenario(s). A method based on the notional removal of key-members of a frame is used to define local damage scenarios in an effort to direct the optimizer towards identifying a structural design, which provides adequate alternate load paths (and therefore sufficient structural reliability) when local failure occurs in the structure.

Structural reliability analyses are conducted in this paper with the direct Monte Carlo (MC) simulation procedure combined with the Response Surface method. A specialized random number generation procedure is utilized to handle the task of sampling from a multivariate probability distribution with arbitrarily distributed and intercorrelated marginals, in order to obtain the random realizations required to perform MC simulations. A discrete Simulated Annealing (SA) optimizer is employed to handle the RBDO problem for the steel frames considered. The numerical results obtained for a test example demonstrate the effectiveness and significance of the proposed optimization approach.

2 Structural reliability analysis

This section describes the approach employed in the present work to conduct structural reliability analysis, i.e. to estimate the probability of partial/full collapse (failure probability) of an elastoplastic steel frame.

2.1 Direct Monte Carlo (MC) simulation

The direct MC simulation method, which is utilized in this paper, is the most well-known approach for handling structural reliability problems [6]. Based on samples simulated following the joint probability density function of the random variables of the problem at hand, the failure probability is simply estimated as the expectation of an indicator function denoting structural failure or non-failure. Direct MC simulation is a general method that is applicable to any structural problem, for which a deterministic solver can be invoked, in order to determine output samples for the response quantities of interest by performing a deterministic structural analysis for each MC simulation.

The convergence rate of the MC simulation procedure is independent of the number of random variables considered, their distribution functions and their intercorrelations. Therefore, this procedure seems to be suitable for reliability calculations with several arbitrarily distributed and intercorrelated random variables, as is the case in the present work. On the other hand, the convergence rate depends on the value of the failure probability to be calculated and the number of simulations to be performed. As a consequence, low failure probabilities can be estimated with acceptable accuracy only by conducting rather large numbers of simulations, which is a computationally very demanding task, especially when it has to be repeatedly executed in the framework of the RBDO process.

In order to alleviate the aforementioned high computational workload, deterministic structural analysis results are approximated by employing the Response Surface (RS) method. The deterministic solver utilized in this paper calculates the collapse load factor of the structure under consideration by executing a limit elastoplastic frame analysis [15]. Hence, using this solver, a small number of deterministic limit elastoplastic analyses are conducted for the structure, in order to produce data points for the regression calculations required to determine unknown coefficients involved in the RS function. Then, the collapse load factor of the structure is conveniently and inexpensively estimated at each MC simulation by evaluating a simple RS expression instead of performing a time consuming limit elastoplastic frame analysis.

2.2 Multivariate Random Number Generation (RNG)

For the elastoplastic steel frames considered in the present work, correlations are assumed among random yield strengths at different structural components. These statistical dependences among material properties of different steel members depend on the way these members are constructed at site or manu-

factured at a factory, the sources of their raw materials, the countries/regions the members and/or the raw materials are taken from, etc. For example, high correlations may arise among material properties of members of similar geometries taken from the same lot. On the other hand, lower correlation degrees are expected among material properties of members obtained from different manufacturers in various geographical regions, who make use of different fabrication and quality control processes and have quite different raw material sources. Such correlations among random structural properties typically have a severe effect on the results of structural reliability analyses [4].

Following the above discussion, the random yield strengths of the members of a steel frame are assumed to jointly follow a multivariate probability distribution. Each marginal of the multivariate distribution is associated with the probability distribution of the random material property of a member or a group of members of the frame. The statistical dependences among the random member properties are specified in the correlation matrix of the multivariate distribution. Thus, in the framework of the MC simulation procedure, we are confronted with the task of generating random numbers by sampling from the arbitrarily distributed and intercorrelated marginals of a multivariate distribution.

This multivariate RNG task is effectively handled with the heuristic approach proposed by CHARMPIS and PANTELI [5]. According to this approach, which is schematically illustrated in Fig.1, a specialized two-step sampling procedure is followed:

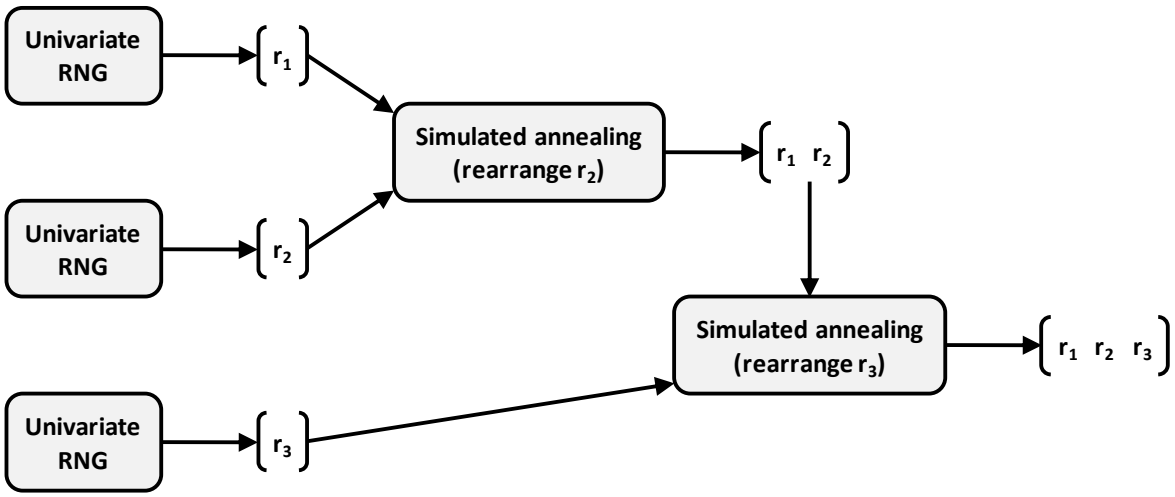

Figure 1. Illustration of the utilized heuristic approach for multivariate RNG (example for a 3-variate distribution).

1. First a univariate random sample is independently generated from each specified member property's distribution (i.e. from each marginal probability distribution) – e.g. see the generated univariate random samples $\mathbf{r}_1$,$\mathbf{r}_2$,$\mathbf{r}_3$ in Fig. 1. Any specified statistical dependences are not taken into account yet, therefore zero-correlations are typically obtained among the marginals of the multivariate random sample produced in this first step.
2. The univariate random samples of the first step are appropriately rearranged by a discrete Simulated Annealing (SA) optimization algorithm, in order to induce the desired correlations among the marginals of the generated multivariate sample – e.g. see the finally obtained correlated multivariate random sample [$\mathbf{r}_1$ $\mathbf{r}_2$ $\mathbf{r}_3$] in Fig. 1. The SA optimizer is invoked to rearrange the generated univariate samples one after the other (only the first univariate sample $\mathbf{r}_1$ is left unchanged): the marginal sample $\mathbf{r}_i$ is rearranged to become appropriately correlated with $\mathbf{r}_1$,$\mathbf{r}_2$,...,$\mathbf{r}_{i-1}$ before processing the next sample ($\mathbf{r}_{i+1}$). The random numbers generated for the univariate samples in the first step are not altered by the SA procedure, only the positions of these numbers within each univariate sample vector are changed until reaching the required correlation structure. The correlation accuracy attained is monitored through the objective function minimized by the SA algorithm, which is an error index measuring the difference between the target and achieved correlations.

The above multivariate RNG procedure is distribution-free, as it allows us to handle actually any type of marginal distribution, for which a corresponding univariate random number generator is available. Moreover, the SA optimizer can induce any values and patterns of target correlations. The details of this generally applicable heuristic multivariate RNG approach can be found in [5].

3 Gaining progressive collapse resistance through alternate load paths

Treating the progressive collapse resistance of a structure during the design phase is generally not a straightforward task. Although the importance of this task is recognized by many design engineers and there are already design guidelines (e.g. [8,7]) and even codes (e.g. [12]) that include provisions/requirements associated with progressive collapse resistance, it is not clear how to enhance the quality of structural designs, in order to achieve improved tolerance against local damage.

The requirement for progressive collapse resistance is handled in the present work by applying the alternate path method. According to this method, the designer aims in specifying a structural design that, in the event of local failure (e.g. loss of certain columns and/or beams of a building), allows the redistribution of the loads acting on the damaged structure, in order to be safely transferred to the ground through alternate load paths employing the remaining undamaged members. In order to achieve such structural designs, the designer can consider an artificial local failure caused by the notional removal of certain column(s) [8,7]. The response of the artificially damaged structure may then be assessed, in order to determine the remaining structural resistance capabilities of the structure, which is required to be able to withstand certain actions that may arise after the occurrence of local damage.

In order to enhance the collapse resistance of the artificially damaged structure, its structural members need to be adequately strengthened, because they will have to carry additional loads in the event of column(s) loss. A straightforward implementation of the alternate path method is to create a 'bridge' over the damaged region by strengthening respective beams (over the damaged region) and columns (beside and below the damaged region). Then, an obvious disadvantage of this approach is that it results in a local type of strengthening, since it is directly linked to a particular failure scenario. Clearly, in the event of a column loss at a storey-level that is higher than that of the 'bridge' formed, the bridge will practically have no effect on the collapse resistance of the structure given the particular local failure.

The aim of the present work is to investigate the application of the alternate path method in a way that progressive collapse requirements are satisfied with minimum additional cost. Through the proposed RBDO implementation it is possible to 'discover' how to meet such requirements in an optimal way by learning from optimization results.

4 Reliability-Based Design Optimization (RBDO)

Structural design optimization is typically formulated as a single-objective optimization task aiming at the minimization of the cost (or material volume/weight) of the structure considered. In RBDO, structural reliability (i.e. failure probability) is explicitly taken into account through a related constraint. The RBDO formulation considered in the present work is as follows:

$$\text{minimize} \quad C(\mathbf{d})$$

$$\text{subject to} \quad P_f(\mathbf{d}) \leq P_{f,\max}$$

$$d_i \in D,\ i=1,\ldots,n_d \tag{1}$$

In the above formulation, **d** is the vector of design variables d_i (i=1,2,…,n_d), which may take values only from a given set D representing the available design options (D is often referred to as the 'design space'), while $C(\mathbf{d})$ denotes the objective function to be minimized (i.e. the structural cost or material volume/weight). $P_f(\mathbf{d})$ is the structural failure probability expressed as a function of the design variables and $P_{f,\max}$ is the maximum allowable failure probability. Thus, RBDO aims in gaining control over output tail probabilities, which are directly associated with structural failure states and their probability to happen. RBDO remains an active research topic and various related approaches can be found in the literature (e.g. [11,10,1,2,14,16]).

Most efforts addressing progressive collapse resistance at the design stage of a structural system have not been implemented in the framework of a structural optimization procedure [13,12,3]. Recently, an approach has been proposed to incorporate a deterministic requirement on progressive collapse resistance in the design optimization process [9]. In the present work, the progressive collapse resistance requirement is probabilistic and is simply added to the RBDO formulation (1) as one more reliability constraint:

$$\begin{aligned} &\text{minimize} && C(\mathbf{d}) \\ &\text{subject to} && P_f(\mathbf{d}) \le P_{f,\max} \\ &&& P_{fd}(\mathbf{d}) \le P_{fd,\max} \\ &&& d_i \in D,\ i=1,\ldots,n_d \end{aligned} \tag{2}$$

In this new formulation, $P_{fd}(\mathbf{d})$ is the structural failure probability given a particular damage scenario (i.e. the failure probability of the structure with certain column(s) removed) and $P_{fd,\max}$ is the maximum allowable failure probability for the damaged structure. The two constraints of formulation (2) ensure that the design yielded by the optimizer has acceptable collapse resistance both when the structure is intact and when it is (artificially) damaged. Additional reliability constraints corresponding to other damage scenarios can be optionally appended to formulation (2).

The failure probability of an elastoplastic frame is calculated as the probability that the carrying capacity (collapse resistance) of the structure is lower than a pre-selected threshold. For an intact frame in particular, we evaluate the probability that the collapse load factor α_c of the structure is lower than some critical value $\alpha_{c,\mathrm{cr}}$, i.e. failure (collapse) of the structure is assumed when $\alpha_c<\alpha_{c,\mathrm{cr}}$: $P_f=P(\alpha_c<\alpha_{c,\mathrm{cr}})$. Similarly, for a damaged frame, we evaluate the probability that the collapse load factor α_{cd} of the damaged structure is lower than

some other critical value $\alpha_{cd,\mathrm{cr}}$, i.e. failure (collapse) of the damaged structure is assumed when $\alpha_{cd}<\alpha_{cd,\mathrm{cr}}$: $P_{fd}=P(\alpha_{cd}<\alpha_{cd,\mathrm{cr}})$. The failure probabilities P_f and P_{fd} are computed by applying the direct MC simulation procedure (once for each of the two probabilities) for any design **d**. The designer's demands for collapse resistance (P_f) and progressive collapse resistance (P_{fd}) of a structural system are imposed and controlled through the user-specified parameters $\alpha_{c,\mathrm{cr}}$ and $\alpha_{cd,\mathrm{cr}}$, respectively.

Problems of the form (1) or (2) can be handled with the use of optimization algorithms, which are invoked to automatically explore the design space, in order to detect the minimum-cost design that satisfies the imposed constraints. The objective and constraints of this optimization problem are generally non-linear functions of the design variables and need to be evaluated for any candidate optimum design considered by the optimizer. Each design variable corresponds to the cross-sectional shape and dimensions of a structural component or group of structural components. This sizing optimization problem is effectively handled in the present work with a discrete Simulated Annealing optimization algorithm.

5 Numerical example

The test example used to examine the presented RBDO approach is the 3-storey multi-bay elastoplastic steel frame of Fig. 2. The frame consists of 27 members and is subjected to three deterministic concentrated loads, which are variable for the purpose of limit load elastoplastic analysis (parameter α in Fig. 2 is the load factor).

All members of the frame have random yield strengths σ_y following a lognormal distribution with mean value 250MPa and standard deviation 25MPa. A Random Variables (RVs) configuration is defined by dividing the members of the frame into 12 groups, as shown in Fig. 2: 9 groups for columns (groups 1,2,...,9) and 3 groups for beams (groups 10,11,12). One RV is associated with each of these groups, thus totally 12 RVs are assigned. Hence, the members of each group have their own common σ_y-value at each MC simulation. A 12×12 target correlation matrix $\mathbf{c}^*$ is specified to model the statistical dependences among RVs. The j-th row/column of $\mathbf{c}^*$ is associated with the RV of the j-th members-group of Fig. 2. The terms c^*_{kl} (k,l=1,2,…,12) of the target correlation matrix are given as:

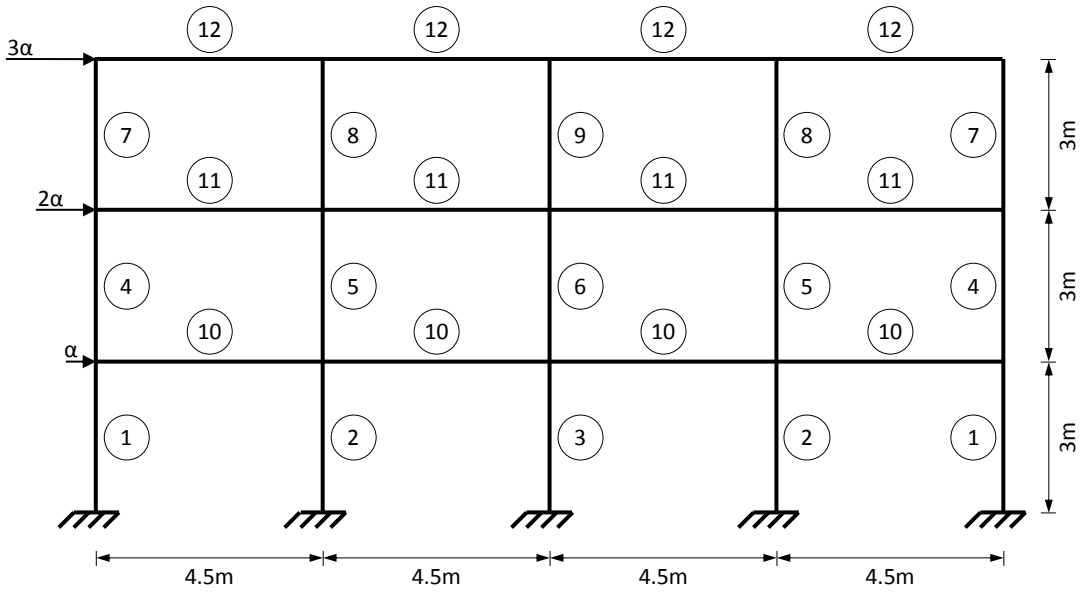

Figure 2. Test example: the intact 3-storey multi-bay frame (applied loads are in kN).

$$\mathbf{c}_{kl}^{*} = \begin{cases} 1.0 & \text{if } k = l \quad \text{(diagonal terms)} \\ 0.9 & \text{if } k, l = 1, 2, \ldots, 9 \wedge k \neq l \end{cases}$$

To justify this correlation pattern, it is assumed that the members of a group (all of the same geometry) are taken from the same lot, therefore it is reasonable for all these members to share a common σ_y-value at each MC simulation. The correlation values in $\mathbf{c}^*$ model the statistical dependences among the RVs of the member groups. For example, a high correlation value could refer to two groups with members of similar geometries fabricated from a single manufacturer using the same raw materials; a low correlation value could arise when the structural members of the groups are taken from manufacturers residing at different countries/regions; intermediate correlation values (e.g. of the order of 0.7) could be assigned if the structural members of the groups are purchased from the same manufacturer but are of different geometries and/or are not made of the same raw materials (e.g. because the members have been fabricated at various periods of time using different raw material sources). In the $\mathbf{c}^*$-matrix specified above, high degrees of statistical dependence between the 9 column-groups are assumed, therefore coefficients equal to 0.9 are adopted. Beam-groups are treated similarly: prescribed correlation coefficients equal to 0.9 denote strong statistical interdependences among the RVs of beam properties. The prescribed correlation coefficients equal to 0.7 imply weaker (but still relatively strong) statistical dependences between the RVs of column and beam groups.

Each member group corresponds to one cross-sectional category of I-shape: standard HEB-sections are considered for columns and IPE-sections for beams. Thus, totally 12 design variables taking discrete values are defined for the optimized frame. The objective function employed in the design optimization process is the total steel weight of the structural members of the frame.

In the local damage scenario examined for this frame, the loss of a corner column at storey 1 is assumed. The 'damaged' frame, in which the aforementioned column is (artificially) removed, is illustrated in Fig. 3. The damaged frame has the same member properties, variable loads and support conditions with the non-damaged structure of Fig. 2.

The RBDO results presented in this section are based on formulation (2) and have been obtained using the following values:

- $P_{f,\max}$=1.0E-3 and $\alpha_{c,\mathrm{cr}}$=140 for the intact structure (Fig. 2) and
- $P_{fd,\max}$=1.0E-2 and $\alpha_{cd,\mathrm{cr}}$=120 for the damaged structure (Fig. 3).

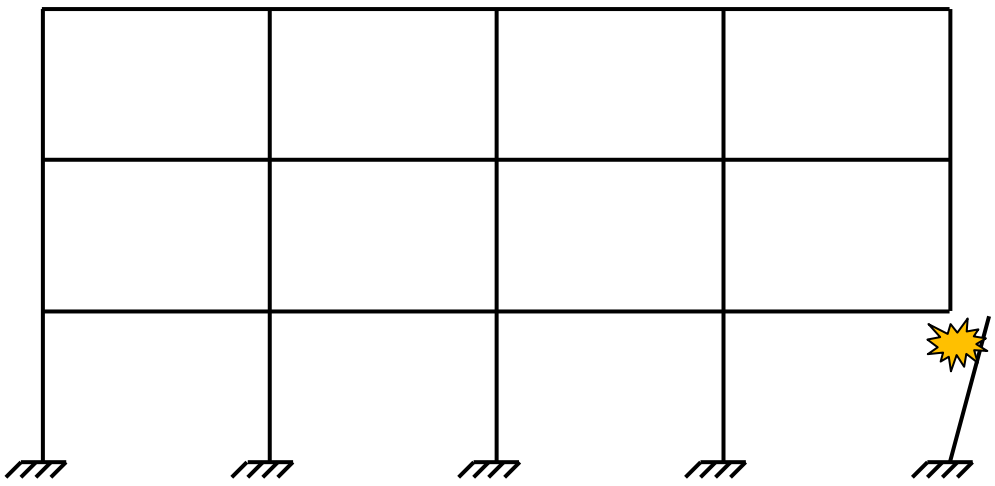

Figure 3. Test example: the 3-storey multi-bay frame with artificial local damage (loss of a corner column).

For this purpose, two multivariate samples have been generated for the 12 correlated RVs, in order to obtain the random realizations required for the MC simulations performed for each candidate optimum design:

- one multivariate sample with 11,100 random realizations for the case of $P_{f,\max}$=1.0E-3 and
- one multivariate sample with 1,100 random realizations for the case of $P_{fd,\max}$=1.0E-2.

These numbers of random realizations have been specified, in order to attain a Coefficient Of Variation (COV) of 30% (an acceptable value usually adopted in MC simulation runs) when computing failure probabilities $P_f = P_{f,\max}$ and $P_{fd} = P_{fd,\max}$, respectively. It is also noted that, using the heuristic multivariate RNG approach of subsection 2.2, 5-digit accuracy between target and achieved correlations has been ensured in the two multivariate random samples produced. The above numbers of random realizations are considered to be adequate for evaluating reliabilities for any candidate optimum design during an RBDO run. E.g., if a failure probability P_f higher than $P_{f,\max}$ is to be evaluated, then the 11,100 random realizations will lead to a P_f -result with COV<30%, i.e. to a rather accurate P_f -estimation. On the other hand, if a probability P_f lower than $P_{f,\max}$ is to be evaluated, then the 11,100 random realizations will lead to a P_f -estimation of poor accuracy (COV>30%); however, the information we need in the framework of the RBDO process is only whether $P_f \leq P_{f,\max}$ and not an accurate P_f -result; the lower the exact value of P_f is, the less probable it is that a false conclusion $P_f > P_{f,\max}$ will be reached.

Based on the above, an RBDO run has been performed for the design of the steel frame according to formulation (2). The total steel weight of all structural members of the finally achieved feasible design is 7,289kg. Fig. 4 depicts the optimal material allocation to the 12 member categories of the frame.

According to the results reported, the optimizer introduces rather strong columns at storey 1 and less strong columns at higher elevations. The internal columns of groups 2, 5 and 8 form the strongest vertical load paths to the ground, while the corner columns of groups 1, 4 and 7 are also strong, but not as much as the internal columns. Notice that strong columns of group 1 are chosen by the optimizer despite the fact that one of these is missing when assessing the 'damaged' frame. The central columns 3, 6 and 9 are strong at storeys 1 and 3 and relatively weak at storey 2. Having column 6 with lower strength than column 9, which is just above, is obviously an undesirable outcome of the optimization process, which can be prohibited in a new RBDO run by appropriately controlling the way design variables take values.

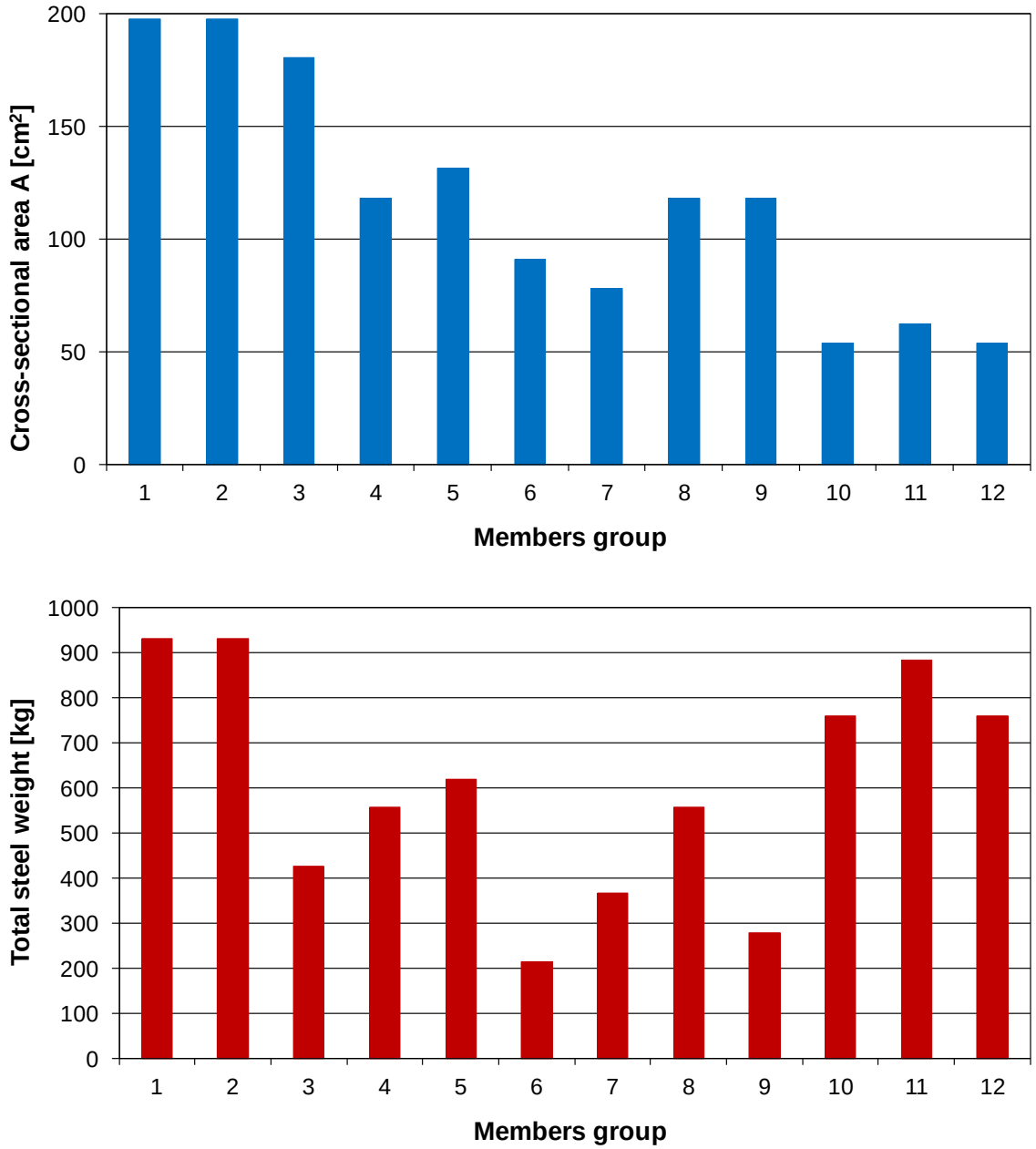

Figure 4. Test example: Optimal material allocation to member groups (design variables) achieved by the RBDO process.

Moreover, rather strong beams all over the height of the structure are selected by the RBDO procedure. Thus, the formation of a 'bridge' over the damaged region of the structure does not appear to be the choice of the optimizer. Instead, the optimizer invests substantial amount of material in the beams of all storeys, in order to horizontally link the vertical load paths formed by strong columns. The intention of the optimizer to activate the structural system against the damage effect (and not just the members at the neighbourhood of the damaged region) is evident.

6 Concluding remarks

The aim of this work is to study the effect from the incorporation of collapse resistance requirements into the reliability-based design optimization process of elastoplastic steel frames. The resulting optimization approach is capable of producing cost-effective designs with acceptable structural system performance under uncertainty.

Inevitably, additional design requirements on system reliability against local failure will lead to increased structural cost due to the need for extra material volume/weight. This increase can be quantitatively explored with the presented RBDO approach and the structural elements can be detected, which need extra material, in order to produce a damage-tolerant structural system.

The results obtained for the test example considered indicate that requirements on reliability against local failure are satisfied in the most cost-effective way by globally activating the structure as a system instead of merely strengthening members at the neighbourhood of the damaged region. It is practically impossible to know a-priori the amount and allocation of additional material, in order to optimally satisfy such requirements. Thus, it appears that an optimization procedure will have to be invoked to cost-effectively handle any new design problem, as its optimal solution depends on the structural system considered and its material/geometric properties, the loads acting on the structure, the demand on collapse resistance and damage tolerance, etc.

References

[1] Agarwal, H.; Renaud, J.E.: Reliability based design optimization using response surfaces in application to multidisciplinary systems. *Engineering Optimization* 36 (2004), pp. 291–311

[2] Allen, M.; Maute, K.: Reliability-based design optimization of aeroelastic structures. *Structural and Multidisciplinary Optimization* 27 (2004), pp. 228–242

[3] American Society of Civil Engineers (ASCE): *Recommendations for designing collapse-resistant structures*. Structural Engineering Institute, Draft Terminology and Procedures Sub-Committee, 2010

[4] Charmpis, D.C.: Probabilistic structural analysis using random samples with correlations induced by simulated annealing. In: Proceedings of *The 2nd International Conference on Soft Computing Technology in Civil, Structural and Environmental Engineering (CSC 2011)*, Chania, Crete, Greece, 2011

[5] Charmpis, D.C.; Panteli, P.L.: A heuristic approach for the generation of multivariate random samples with specified marginal distributions and correlation matrix. *Computational Statistics* 19 (2004), pp. 283-300

[6] Charmpis, D.C.; Schuëller, G.I.: Coping with physical uncertainties in structural mechanics: uncertainties modeling, methods of analysis and applications. In: Marti, K.; Ermoliev, Y.; Makowski, M.; Pflug, G. (editors): *Coping with Uncertainty – Modeling and Policy Issues*. Vol. 581 of Lecture Notes in Economics and Mathematical Systems, Springer, 2006, pp. 67-83

[7] Department of Defence (DoD): *Unified facilities criteria (UFC), design of buildings to resist progressive collapse*. UFC 4-023-03, Washington D.C., 2005

[8] General Services Administration (GSA): *Progressive collapse analysis and design guidelines for new federal office buildings and major modernization projects*. Washington D.C., 2003

[9] Kontogiannis, A.; Charmpis, D.C.: Sizing optimization of collapse-resistant frames. In: Proceedings of *7th GRACM International Congress on Computational Mechanics (GRACM 2011)*, Athens, Greece, 2011

[10] Papadrakakis, M.; Lagaros, N.D.: Reliability-based structural optimization using neural networks and Monte Carlo simulation. *Computer Methods in Applied Mechanics and Engineering* 191 (2002), pp. 3491-3507

[11] Royset, J.O.; Der Kiureghian, A.; Polak, E.: Reliability-based optimal design of series structural systems. *ASCE Journal of Engineering Mechanics* 127 (2001), pp. 607-614

[12] Sørensen, J.D.; Christensen, H.H.: Danish requirements for robustness of structures: background and implementation. *Structural Engineering International* 16 (2006), pp. 172-177

[13] Starossek, U.; Wolf, M.: Design of collapse-resistant structures. In: Proceedings of *JCSS and IABSE Workshop on Robustness of Structures*, Building Research Establishment, Garston, Watford, UK, 2005

[14] Tsompanakis, Y.; Papadrakakis, M.: Large-scale reliability-based structural optimization. *Structural and Multidisciplinary Optimization* 26 (2004), pp. 429–440

[15] Wong, M.B.: *Plastic analysis and design of steel structures*. Butterworth-Heinemann, Elsevier, 2009

[16] Yi, P.; Cheng, G.; Jiang, L.: A sequential approximate programming strategy for performance-measure-based probabilistic structural design optimization. *Structural Safety* 30 (2008), pp. 91-109

Seemingly contradictory: influence of stress-reduction-methods on the strength of bonded joints composed of brittle adherends

Till Vallée[1], Thomas Tannert[2] & Cordula Grunwald[1]
[1]Fraunhofer-Institut für Fertigungstechnik und Angewandte Materialforschung, IFAM, Wiener Straße 12, 28359 Bremen/Germany
[2] The University of British Columbia, 2424 Main Mall, Vancouver, BC, V6T1Z4, Canada

Abstract: Adhesively bonded joints are increasingly considered for structural applications in engineering. Because of the associated mechanical singularity, their dimensioning remains a challenge, especially if considering brittle adherends. The influence of stress-reduction-methods on their strength was investigated herein: experimental and numerical investigations were carried out on two types of brittle adherends considering three different stress-reduction methods. Although numerical analyses showed that the stress peaks are reduced, the experimental evidence lacked the corresponding strength increase, despite intuition and common sense. A probabilistic strength prediction method subsequently applied explains most of the seemingly contradictory findings. The presented work allows for a better insight into the relation between stress-reduction and strength increase of adhesively bonded joints, which is greatly affected by the brittleness of the adherends.

1 Introduction

Adhesively bonding represents a joining technique that is increasingly competing with mechanical fasteners (bolts, rivets) and welding. Initially pushed by the aeronautical and automotive industries, adhesively bonding is gradually considered in civil engineering applications, especially in combination with fibrous and anisotropic materials as composites and timber. Since load trans-

fer in adhesively bonded joints is characterized by sharp stress peaks they challenge the common civil engineer practice because of the almost exclusive focus on stress based design encountered in codes and standards, particularly if combined with brittle materials as composites and timber. This article aims to show how stress-based common sense is tricked out a relatively simple mechanical system in the case of adhesively bonded joints, where a series of intuitive methods aimed to reduce the stress level fails to yield in the expected higher joint performance.

Owing to the complexity of the mechanical system, adhesively bonded joints, are almost inaccessible to simple analytical analyses, unless considered at a very basis level, VOLKERSEN [1], GOLAND and REISSNER [2]. When it comes to the quantification of the influence of parameters that deviate from very strict idealizations [3–5], only numerical methods can be used. Finite Elements Analysis (FEA) is particularly suited to analyse complex joint geometries; its use in the context of bonded joints goes back to Adams et al. [6–7] in the 1970's.

All aforementioned studies, either analytical or numerical, indicate that the load transfer in bonded joints, including the double-lap-joints subsequently considered in this study, is characterized by sharp stress peaks that ultimately trigger failure and define joint strength. **It is thus legitimate to expect that techniques to reduce these stress peaks will yield corresponding increases in joint strength**, thus research has focused on tracking down the influence of stress-reduction-methods on the strength of bonded: three of the most intuitive techniques are described in the following.

1.1 Fillets

Adhesive spew fillets, in essence shaping the adhesive at the end of the overlaps in order to ensure a smoother flow of stresses, have been investigated by several researchers: ADAMS and PEPIATT [6] on triangular spew fillet which reduces the maximal principal stress by around 40%, if compared to a configuration which does note exhibit this stress-reduction-method; ADAMS and HARRIS [7] on adhesively bonded joints proved that rounding the corners removes the mechanical singularity point thus smoothing the stresses. Beyond these theoretical considerations, DORN and LIU [8] have also investigated the influence of fillets on the stresses in adhesively bonded joints composed of metallic and plastic adherends and also found a beneficial effect of these stress-reduction-methods regarding the magnitude of stresses. Later, TSAI and

MORTEN [9] numerically investigated the influence of triangular spews on the stress distribution of composite adherends, and also concluded that spews do reduce the magnitude of stresses. LANG and MALLICK [10] extended the considerations on triangular spew fillets to other forms of fillets, and concluded that these relatively simple methods ensures a much smoother flow of stresses, which in turn reduces their magnitude. Recently, VALLÉE et al. [11], investigated adhesively bonded joints composed of composite adherends and epoxy, showed, using FEA, that both shear and out-of-plane stresses were significantly reduced at the end of the overlaps, when varying the radius of the adhesive rounding.

1.2 Chamfers

Considering the effect of tapering or chamfering the adherend ends, i.e. locally reducing the bending stiffness, expectable stress reduction effects have been reported. ADAMS et al. [12], using numerical methods, have shown that tapering the metallic outer adherends greatly reduced the stresses; the resulting experimentally gathered joint strengths increased more than twofold. Similar numerical results were obtained by HILDEBRAND [13] on single lap joints composed of composite and metallic adherends: the strengths should increase by 90 to 150%. The almost evident effect of tapering/chamfering on the reduction of stresses at the end of the overlaps of bonded joints was subsequently, mostly numerically, confirmed by other researchers [14-17]. DA SILVA et al. [18] rightfully stated that FEA is a convenient technique to find the optimum adherend shape, although he did not define if the optimization target is the stress reduction or the resulting joint strength.

1.3 Graded adhesive layer

Another repeatedly reported intuitive method to reduce the stress peaks at the ends of the overlaps is to grade the adhesive layer, i.e. using adhesives of different stiffnesses (subsequently defined as adhesive grading, although the term mixed adhesive joints is also used [18]). The idea is to associate strain peaks towards the end of the overlap to lower adhesive stiffness, while the less stressed inner part is associated to a stiffer adhesive. The objective is to achieve a more even stress distribution, and consequently expect higher joint strengths. The concept can be traced back to the 1970's [19-21] and is still pursued today [22-24].

1.4 Caveats

When reviewing these works, two important caveats have to be made: firstly, numerical investigations usually point out the stress reduction effect of adhesive grading **and suggest or conclude** that there ought to be a beneficial outcome for the strength issue; secondly, experimental validation has been, in most of the cases, performed on **metallic adherends** which does not exhibit significant brittleness. Unlike the case of metallic adherends, for which there is explicit experimental evidence that stress reductions translate in strength increase, the situation for bonded joints involving brittle adherends has not yet received much attention.

This is, for a great part, due to the fact that joints strength prediction methods involving brittle adherends were just recently formulated, namely for Fibre Reinforced Polymers [25] and for Timber [26]. In both cases, experimental and numerical evidence lead to the conclusion that the strength of adhesively bonded joints it is best described using a probabilistic approach based on a WEIBULL description of the material resistance coupled with the consideration of size-effects.

2 Experimental investigations

2.1 Specimen description

Symmetrical double-lap joints with rectangular sections were fabricated. The joints consisted of two outer and two inner adherends, either FRP or timber, connected by a layer of adhesive. The inner profiles were always twice as thick as the outer ones to keep the cumulative cross-section constant.

The effect of three of the stress-reduction-methods listed in the introduction, namely adhesive roundings, chamfering and adhesive grading; the respective temps being defined in the introduction. Five different combinations of materials and stress-reduction-methods were investigated, the corresponding experimental series are subsequently labelled S1–S5, and defined further in the text, and for which Fig. 1 details the used nomenclature.

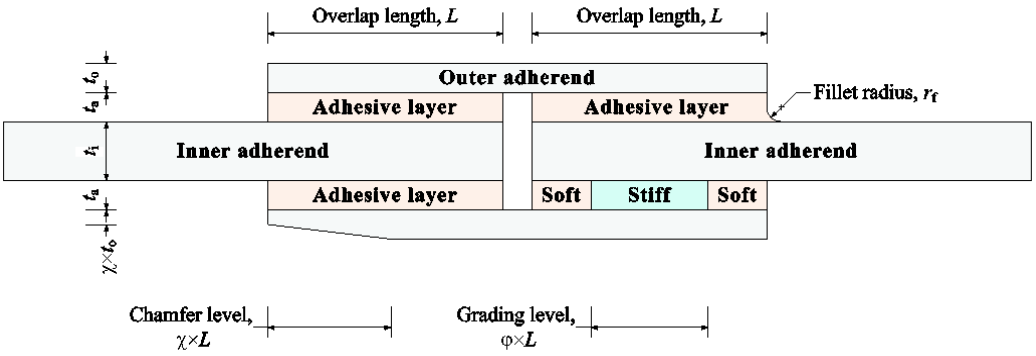

Figure 1. Nomenclature used for the bonded double lap joints and the stress-reduction-methods (not to scale.)

2.2 Material properties and specimen geometry

In the frame of the investigations reported herein, three different cold-curing two-component adhesives were used: a stiff and brittle epoxy adhesive, SikaDur330, not exhibiting any kind of plastic behaviour; a polyurethane exhibiting some level of plasticity, SikaForce7851; and finally a very soft acrylic adhesive exhibiting major plasticity, SikaFast5221. All three adhesives were experimentally characterized in tension according to EN ISO 527-2 [27]: Fig. 2, which represents the stress-strain relationship in tension of the three adhesives best emphases these fundamentally different adhesives; Table 1 lists all the relevant mechanical parameters, as they will be used in the further numerical modelling.

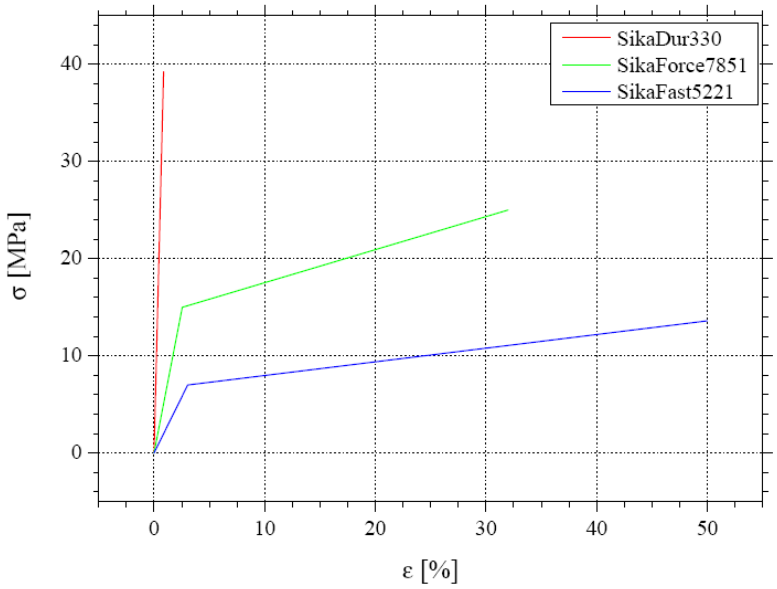

Figure 2. Idealized mechanical description in tension of the adhesives used.

Table 1. Material properties.

Material	E_x [GPa]	$E_y = E_z$ [GPa]	ν_{xz} [–]	ν_{yz} [–]	f_1 [MPa]	$f_2 = f_3$ [MPa]	f_{12} [MPa]
FRP	**32.5**	**3.5**	**0.3**	**0.09**[a]	**325.4**	**8.1**	**20.4**
Timber	**17.9**	**1.1**	**0.4**	**0.04**[a]	**98.2**	**4.5**	**16.5**
SikaDur330	**4.56**[b]		**0.37**		**39.0**		□[d]
SikaForce7851	**0.58**[b]		**0.42**		**25.3**[c]		□[d]
SikaFast5221	**0.14**[b]		**0.40**		**11.8**[c]		□[d]

[a]: assumed according to literature; [b]: isotropic; [c]: beyond elastic limit; [d]: not determined

Pultruded Fibre Reinforced Polymer profiles, subsequently referred to as FRP, were used. The elastic properties of the profiles, listed in Table 1, were determined through full-scale tensile tests, in which the profiles presented an almost linear behaviour up to failure. The strength of the FRP material used herein was determined using a shear-tensile interaction device (cf. [11] for more details) which allows measuring material strength values under any combination of through-thickness tensile and shear stresses. Fifty-five tests were performed on coupons cut from 10 mm thick pultruded FRP flat profiles, corresponding to the locus of failure as subsequently observed on the bonded joints. These samples were 40×40 mm in size, and corresponded to the inner adherend's material, in which failure was initiated by combined through-thickness tensile, σ_z, and shear stresses, τ_{xz}, best described by Eq. (1):

$$\frac{\sigma_z^2}{f_2^2} + \frac{\tau_{xz}^2}{f_{12}^2} = 1 \tag{1}$$

with σ_z and τ_{xz} the through-thickness and shear stresses,
f_2, and f_{12} the resulting average values of the pure through-thickness tensile and shear strengths,
Values listed in Tab. 1

The timber used was Spruce (*Picea abies*) cut from high quality defect-free boards and conditioned to 12% moisture content prior to manufacturing of the specimen and then again stored in constant climate until testing. The elastic properties of the timber required for the numerical investigations (longitudinal modulus of elasticity E_x, the transverse modulus of elasticity E_y and the shear modulus G_{xy}) were determined on small clear specimens from the same boards that were used to produce the joints. Table 1 summarizes the average values and standard deviations; these values are at the high end of the values stated in the literature [28], the difference is explained by the use of high quality timber. The strength of the timber was characterized based upon the

NORRIS failure criterion [29], which has, in a two-dimensional stress state, the form given by Eq. (2):

$$\frac{\sigma_X^2}{f_1^2} - \frac{\sigma_X \sigma_Z}{f_1 f_2} + \frac{\sigma_Z^2}{f_2^2} + \frac{\tau_{XZ}^2}{f_{12}^2} = 1 \therefore \frac{\sigma_X^2}{f_1^2} = 1 \therefore \frac{\sigma_Z^2}{f_2^2} = 1 \quad (2)$$

with f_1, f_2, and f_{12} strength parameters,
values listed in Tab. 1

Before bonding the FRP specimen, the adherent surface veil was mechanically abraded with a sander until the first mat fibres became visible and the surfaces were then cleaned and degreased with acetone. Regarding the timber specimen, the surface was mechanically planed and subsequently residual dust was removed. The adhesive layer thickness was enforced using PVC washers that were put at a significant distance from the ends of the overlaps, to ensure they would not influence the joint strength. In all cases, the adhesive cured at laboratory temperature (22±2°C) for at least a week.

2.3 Test series

The effect of adhesive roundings was investigated on joints involving FRP adherends and the epoxy adhesive; the corresponding series is labelled S1. The rounding was achieved by placing calibrated round aluminium bars at the end of the overlaps, which were removed after hardening. Fig. 3(a) shows typical roundings on double lap joints after the curing. A series of double lap joints (t_i = 5mm, ta = 10mm) with overlaps of L = 100 mm, adhesive layer thicknesses of t_a = 10 mm, and exhibiting 5 different adhesive roundings was investigated. The magnitude of the roundings was varied from r_f = 2 mm to 10 mm in steps of 2 mm.

The effect of adhesive grading was investigated on bonded joints consisting of both FRP and timber adherends, resulting in two different experimental series. Series S2 composed of FRP adherends and Series S3 involved timber adherends. Adhesive grading was achieved by using two different adhesive types for the bonded splice: a stiff adhesive (SikaDur330) in the centre part, in both series defined herein the 2C epoxy adhesive; and a softer adhesive towards the ends of the overlap (SikaForce7851for the FRP, resp. SikaFast5221 for the timber) The adhesive grading level was defined as the ratio of the stiffer adhesive related to the full overlap. S2 exhibited a width of b_2 = 35 mm, overlapping by L = 100 mm, and an adhesive layer thicknesses of t_a = 1 mm, in which levels of adhesive grading, i.e. percentage of stiff adhesive in the inner part of the overlap, from 0% to 100% were varied in steps

of 20%. S3 was b_3 = 50 mm wide, with a constant overlap of L = 100 mm and an adhesive layer thicknesses of t_a = 1 mm.

In the frame of the investigations of **the influence of chamfers** on the strength of bonded joints, the outer lamellas were chamfered. The sole geometrical parameter varied within the two series, labelled herein S4 and S5, was the level of chamfering; both series were bonded using SikaDur330. For series S4, involving FRP adherends, an overlap length L = 100 mm and an adhesive layer thickness t_a = 1 mm, three different chamfer levels were considered: 0%, 50% and 100%, for the definition of the chamfer level see Fig. 1; in series S5, featuring timber adherends, L = 100 mm and t_a = 1 mm, the chamfer level, defined by Fig. 1 and depicted in Fig. 3(b), was varied in four steps: 0%, 33%, 66% and 100%.

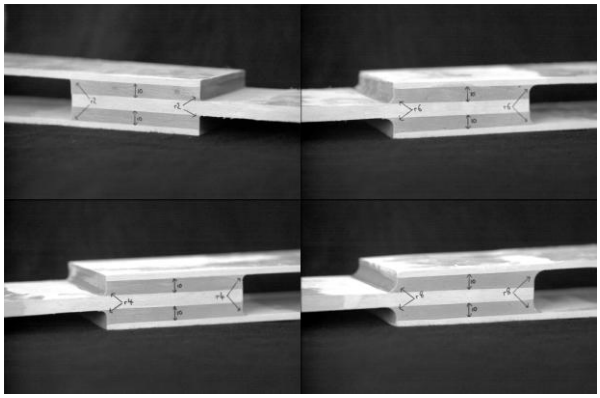

(a) Adhesive roundings series S1

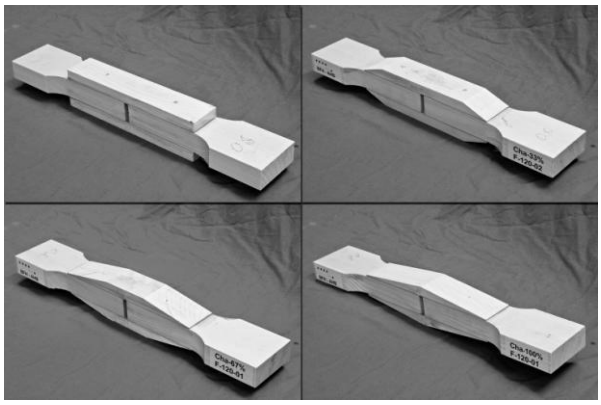

(b) Different chamfering levels for series S5

Figure 3. Selected specimens before being tested.

2.4 Experimental results

All tests were carried out on Zwick universal testing machines with a capacity of 250 kN. Quasi-static axial tensile tests were performed under a displacement-controlled rate of 0.5 mm/s for the FRP joints, respectively of 5 mm/s for the timber joints, in all cases up to failure load. Because of their much weaker through-thickness stiffness and strength, the timber specimen had to be cut in dog-bones shapes, to allow for the tensile force to be introduced.

All individual tests were repeated three times to allow for a minimal statistical significance. All investigated adhesively bonded joints, featuring FRP or timber adherends, failed in a brittle manner, independently on the fact if they involved brittle or ductile adhesives. The FRP joints almost always failed by splitting just below the end of the overlap, usually at depths between 0.5 and 1.5 mm, corresponding to the resin richer layer (cf. [11] which gives more insights into the failure mode of the considered FRP.) The specimen involv-

ing timber adherends also failed at the end of the overlaps. The experimentally gathered strengths for each series are displayed in Fig. 4. Statistical analyses using analysis of variance (ANOVA) were carried out to evaluate the effect of the stress-reduction-methods on the joint strength. P-values were calculated and compared to the significance level, α, chosen herein as < 0.05 [30], which validated the statistical significance of the conclusion drawn.

2.5 Numerical modelling

All experimentally investigated joint configurations were numerically modelled using the FEA package Ansys v11 [31]. Both the FRP and the timber were modelled as linear-elastic orthotropic materials; SikaDur330 was modelled as being a linear-elastic isotropic material, while both SikaForce7851 and SikaFast5221 were idealized as exhibiting a bi-linear plasticity; all material properties are listed in Table 1. In all cases, the mesh was significantly refined at the loci of potential stress peaks.

3 Probabilistic strength prediction

3.1 Principles

As stress-based approaches, due to the huge stress peaks generated at the ends of the overlaps, are deemed to fail regarding the strength prediction of adhesively bonded joints, a probabilistic method has been pursued herein. The prediction method takes into consideration the scale sensitivity of the material strength, considering not only the magnitude of the stress fields, but also the volume over which they act.

For a general overview on size effects and its relations to strength, the reader is kindly redirected to BAŽANT [32-33]. For the purpose of this publication, the following is reminded: probabilistic strength prediction methods assume that the investigated material exhibits brittle failure, and that the material strength is then usually statistically described as being WEIBULL-distributed.

Further, for the implementation of any strength prediction method, including the ones based on probabilistic concepts, a failure criterion for the material in needed. Failure criteria ordinarily used for isotropic materials do not apply to orthotropic and anisotropic materials and their use usually result in incorrect stress state interpretation.

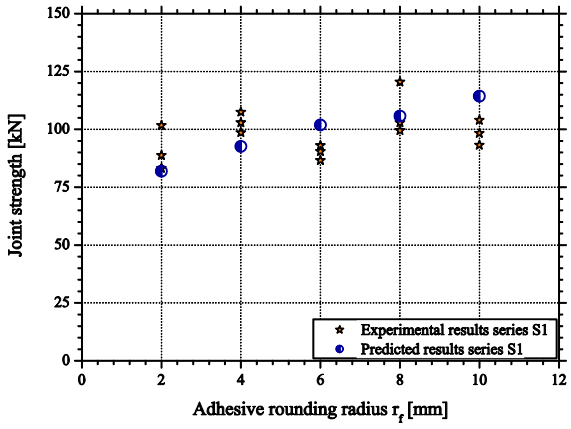

(a) Adhesive roundings series S1, FRP

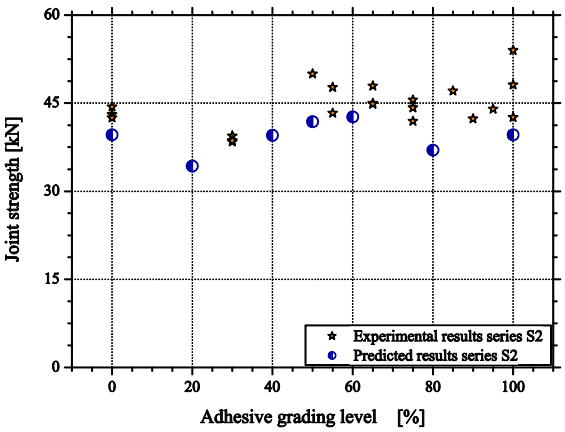

(b) Adhesive grading series S2, FRP

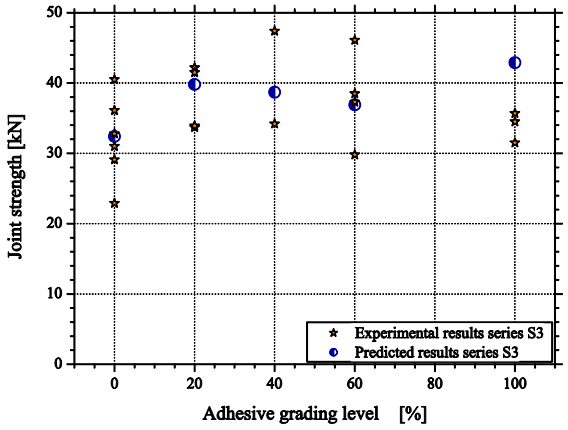

(c) Adhesive grading series S3, timber

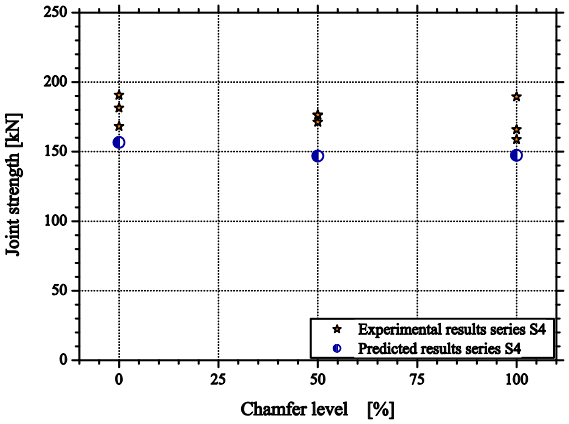

(d) Adherend chamfer, series S4, FRP

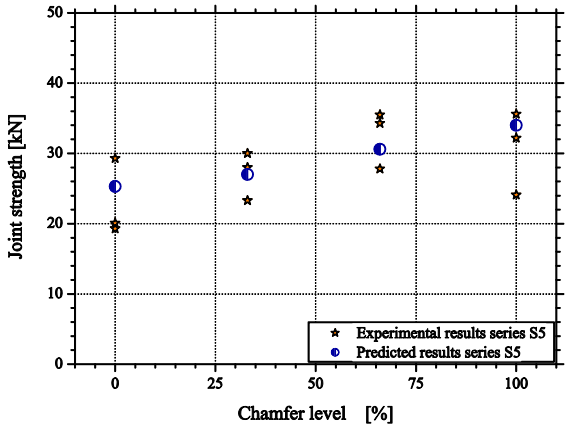

(e) Adherend chamfer, series S5, timber

Figure 4. Joint strength, experimental and predicted values.

3.2 Implementation

Idealizing the joints under consideration as being constituted by n elements that could potentially and independently fail its survival depends on the simultaneous non-failure of all elements $i \leq n$. As a result, for a given applied load, F, the probability of survival of the joint can be calculated by Eq. (3):

$$P_S(F) = \prod_{i=1}^{n} P_{S,i}(F) \tag{3}$$

with σ_z and τ_{xz} the through-thickness and shear stresses,
f_2, and f_{12} the resulting average values of the pure through-thickness tensile and shear strengths,
Values listed in Tab. 1

The function P_s stands for the probability of survival of the constituent element i corresponding to a load level F. Most commonly, for brittle materials, P_s is expressed by a WEIBULL distribution. Herein a two-parameter WEIBULL distribution has been considered, which is mathematically formulated using Eq. (4):

$$P_s = \exp\left[-\int_V \left(\frac{\sigma}{m} \right)^k dV \right] \tag{4}$$

with *σ is the stress acting over a volume V, m is the characteristic stress or scale parameter and k is the shape parameter that gives a measure of the strength variability*
Values listed in Tab. 1

One consequence of Eq. (4) is that for two volumes V_1 and V_2 submitted to constant stresses σ_1 and σ_2 at failure, assuming equal probabilities of survival, the relationship given by Eq. (5) is obtained, which mathematically defines statistical size-effects.

$$\frac{\sigma_1}{\sigma_2} = \left(\frac{V_2}{V_1} \right)^{\frac{1}{k}} \tag{5}$$

with *$\sigma_{1,2}$ resistances acting over volume $V_{1,2}$, k is the shape parameter that gives a measure of the strength variability*
Values listed in Tab. 1

Although initially established for main stresses, WEIBULL theory has since then been extended for any stress operator that defines failure [34]. Herein the failure criteria of FRP, Eq. (1), respectively timber, Eq. (2), can be interpreted

as being stress operators governing the failure of the respective materials. Consequently, if each constituent element i, with a volume V_i is subjected to a constant value of the failure function $\phi_{F,i}$, which in the current case correspond to the failure criterion (Eqs. 1, resp. 2), the probability of survival of the whole member is given by Eq. (6):

$$P_S = \prod_{i=1}^{n} \exp\left[-\frac{V_i}{V_0} \cdot \left(\frac{\phi_{F,i}}{m} \right)^k \right] = \exp \sum_{i=1}^{n} \left[-\frac{V_i}{V_0} \cdot \left(\frac{\phi_{F,i}}{m} \right)^k \right] \tag{6}$$

with $\sigma_{1,2}$ *resistances acting over volume* $V_{1,2}$, *k is the shape parameter that gives a measure of the strength variability*
Values listed in Tab. 1

3.3 Application

Eq. (6) has been implemented in a post-processing routine for FEA results and the strength of timber members was predicted as the load of equal probability of survival or failure, i.e. for $P_S = 0.5$. Accordingly computed joint strengths for all series, S1–S5, are displayed in Fig. 4, where they are compared to the corresponding experimental results.

4 Discussion

4.1 Influence of adhesive rounding

Increasing the size of the fillet radius considerably reduced the tensile and shear stress peaks, τ_{xz}, and through-thickness stress peaks, σ_z, as indicated in Figs. 5(a-b). However, the stress decrease by 50% (considering the shear stresses, τ_{xz}) corresponding to the increase of r_f from 2 to 10 mm only led to a nearly insignificant increase in joint strength of 8%. Assuming a correlation between stress magnitude and joint strength, a much higher increase in strength would have been expected. Although stress levels were reduced with an increasing fillet radius, the volume of the material subjected to higher stresses increased.

Applying the probabilistic method, this apparent contradiction is relieved, as the joints strengths corresponding to the different adhesive roundings are predicted with a good accuracy, both in their magnitude as in the general trend.

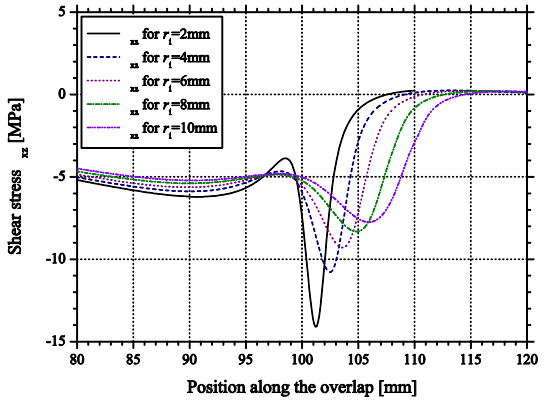

(a) Shear stresses, τxz, in dependence of the fillet radius;
series S1 at a reference load of 100 kN

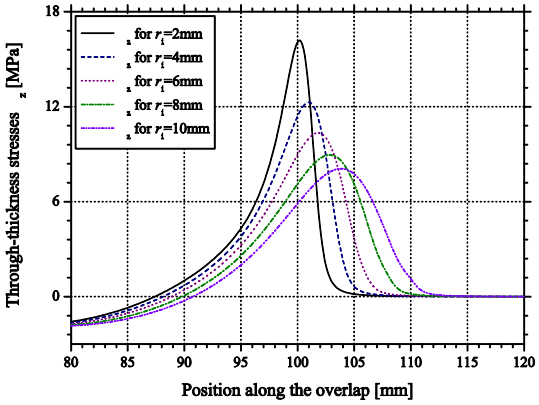

(b) Through-thickness stresses, σz, in dependence of the fillet radius;
series S1 at a reference load of 100 kN

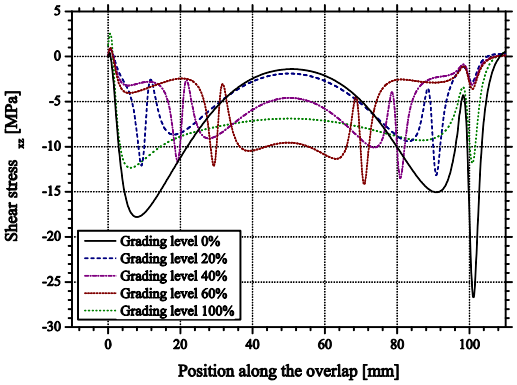

(c) Shear stresses, τ_{xz}, in dependence of the adhesive grading;
series S2 at a reference load of 100 kN

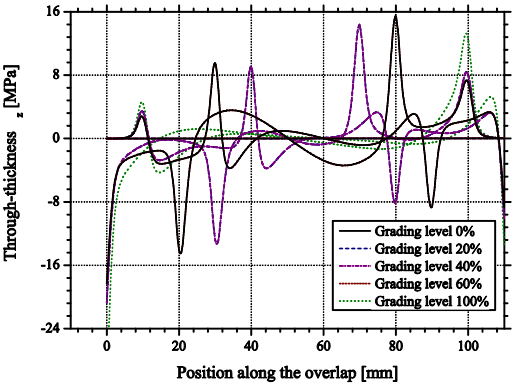

(d) Through-thickness stresses, σ_z, in dependence of the adhesive grading;
series S2 at a reference load of 100 kN

Figure 5. Representative stresses along the overlap for two selected stress-reduction-methods.

4.2 Influence of adhesive grading

The (complex) influence of adhesive grading on the stress distribution is displayed in Figs. 5(c-d), for the specimen of series S2. The two extreme grading levels, i.e. the grading levels 0% and 100%, which correspond to a splice completely made up of SikaDur330, respectively SikaForce7851, are representative for the influence of the adhesive stiffness; it can be seen that the stiffer SikaDur330 leads to higher stress peaks, compared to the softer SikaForce7851, with maximal stress magnitudes lower by around one third. This lowering would have, in the stress based context, yielded in a corresponding strength increase; the experimental evidence, however shows that strength is almost independent from the chamfering level.

The probabilistic method on the other hand delivers predictions that are reasonably consistent with the experimental data.

4.3 Influence of chamfering

Similarly to the adhesive rounding, chamfering does significantly reduce the magnitude of the shear stress peaks, τ_{xz}, and through-thickness stress peaks, σ_z, (not shown for constraints of space in this paper.) For the case of FRP: by approx. 40% if comparing the shear stresses, τ_{xz}, of the joints exhibiting no chamfering relatively to a chamfering level of 100%. However, the corresponding experimentally determined joint strengths were not affected by this particular stress reduction, as clearly indicated by Figs. 4(d-e).

Here again, taking into account the fact that the joint strength is not only driven by the magnitude of stresses, but also by their distribution, i.e. applying a probabilistic approach, sheds light onto this apparent inconsistency by predicting joint strengths that are in good agreement with the experimental values.

5 Conclusion

Adhesively bonded joints are characterized by sharp stress peaks towards the ends of the overlaps, which trigger failure, thus defining strength. A repeatedly reported and at first sight intuitive method to increase the strength of these elements is to reduce the stress peaks by either acting on the geometry, e.g. chamfering the adherends or implementing fillets in the adhesive layer, or on the adhesive, e.g. using ductile adhesives or grading them.

Regarding brittle adherends, i.e. FRP and timber, three commonly reported methods to reduce stress magnitudes, i.e. chamfering, ductile adhesives, and adhesive grading, were experimentally and numerically investigated. These investigations, pursued on a wide range of parameters resulting in five different experimental series, allowed for the following observations:

1. All of the investigated stress-reduction-methods do, according to FEA, lead to significant stress reductions, yet the so reduced stresses act on larger volumes of the adherends;
2. All experimentally investigated adhesively bonded joints failed in a brittle manner, so the materials they were constituted of;
3. None of the investigated stress-reduction-method, neither for FRP nor for timber, did significantly increase the experimentally determined joint strength.

The latter listed observations did allow drawing the following conclusions:

4. There is no direct correlation between stress magnitude and failure, even considering a verified failure criterion, when dealing with brittle materials;
5. Thus, direct stress based approaches to predict the strength of adhesively bonded joints composed of brittle adherends are not suited for dimensioning purposes.

Considering the aforementioned, the authors computationally developed a probabilistic strength prediction method, which implemented a statistical based formulation of size-effects. The probabilistic method not only offers a comprehensive a mechanically coherent for the seemingly contradictory relation between stress reduction and lack of corresponding joint strength increase, it also delivers consistently accurate joint strength estimates for all considered experimental series which makes it useful for their dimensioning.

6 Literature

[1] O. VOLKERSEN, Recherches sur la théorie des assemblages collés, *Constr. Metall.* (1965) 4:3-13.

[2] M. GOLAND, E. REISSNER, The stresses in cemented joints, *J. Appl. Mech.* (1944) A17-27.

[3] C. RAPHAEL, Variable-adhesive bonded joints, *Appl. Polym. Symp.* 3 (1966) 99-108.

[4] L.J. HART-SMITH, Analysis and design of advanced composite bonded joints. *NASA CR-2218*, 1974.

[5] W.J. RENTON, J.R. VINSON, The efficient design of adhesive bonded joints, *J. Adhes.* 7 (1975) 175-193.

[6] R.D. ADAMS, N.A. PEPIATT, Stress analysis of adhesive bonded lab joints, *J. Strain Anal*. 9 (1974) 185-196.

[7] R.D. ADAMS, J.A. HARRIS, The influence of local geometry on the strength of adhesive joints. *Int. J. Adhes. Adhes.* 7 (1987) 69-80.

[8] L. DORN, W. LIU, The stress state and failure properties of adhesive bonded plastic/metal joints, *Int. J. Adhes. Adhes.* 13 (1993) 21-31.

[9] M.Y. TSAI, J. MORTON, The effect of a spew fillet on adhesive stress distributions in laminated composite single-lap joints, *Compos. Struct*. 32 (1995) 123-31.

[10] T.P. LANG, P.K. MALLICK, Effect of spew geometry on stresses in single lap adhesive joints. *Int. J. Adhes. Adhes*. 18 (1998) 167-77.

[11] T. VALLÉE, J.R. CORREIA, T. KELLER, Probabilistic strength prediction for double lap joints composed of GFRP profiles, Part I: experimental and numerical Investigations. *Compos. Sc. Tech*. 66 (2006) 1903-1914.

[12] R.D. ADAMS, R.W. ATKINS, J.A. HARRIS, A.J. KINLOCH, Stress-analysis and failure properties of carbon-fiber-reinforced-plastic steel double-lap joints, *J. Adhes.* 20 (1986) 29-53.

[13] M. HILDEBRAND, Non-linear analysis and optimization of adhesively bonded single lap joints between fibre-reinforced plastics and metals, *Int. J. Adhes. Adhes.* 14 (1994) 261-267.
[14] S. AMIJIMA, T. FUJII, A simple stress analysis method for adhesive bonded tapered joints, *Int. J. Adhes. Adhes.* 9 (1989) 155-160.
[15] E. SANCAKTAR, P. NIRANTAR, Increasing strength of single lap joints of metal adherends by taper minimization, *J. Adhes. Sc. Tech*. 17 (2003) 655-675.
[16] R. KAYE, M. HELLER, Through-thickness shape optimisation of typical double lap-joints including effects of differential thermal contraction during curing, *Int. J. Adhes. Adhes.* 25 (2005) 227-238.
[17] T. KELLER, T. VALLÉE, Adhesively bonded lap joints from pultruded GFRP profiles, Part I: stress-strain analysis and failure modes. *Compos. Part B: Eng.* 36 (2005) 331-340.
[18] L.F.M. DA SILVA, A. ÖCHNSER, Modeling of adhesively bonded joints, Springer, Berlin, 2008.
[19] S. SEMERDJIEV, Metal to metal adhesive bonding, Business Books Limited, London, 1970.
[20] S. SRINIVAS, Analysis of bonded joints, *NASA TN D-7855*, 1975.
[21] R.L. PATRICK, Treatise on adhesion and adhesives, Vol. 4, Marcel Dekker, New York, 1976.
[22] I. PIRES, L. QUINTINO, J.F. DURODOLA, A. BEEVERS, Performance of bi-adhesive bonded aluminium lap-joints. *Int. J. Adhes. Adhes.* 23 (2003) 215-23.
[23] M.D. FITTON, J.G. BROUGHTON, Variable modulus adhesives: an approach to optimized joint performance, *Int. J. Adhes. Adhes.* 25 (2005) 329-336.
[24] E. SANCAKTAR, S. KUMAR, Selective use of rubber toughening to optimize lap-joint strength, *J. Adhes. Sc. Tech.* 14 (2000) 1265-1296.
[25] T. VALLÉE, J.R. CORREIA, T. KELLER, Probabilistic strength prediction for double lap joints composed of GFRP profiles, Part II: strength prediction. *Compos. Sc. Tech.* 66 (2006) 1915-1930.
[26] S. HEHL, T. VALLÉE, T. TANNERT, Y. BAI, A probabilistic strength prediction method for adhesively bonded joints composed of wooden adherents. *Key Eng. Mat.* 417-418 (2010) 533-536.
[27] EN ISO 527-2 Plastics - Determination of tensile properties - Part 2: Test conditions for moulding and extrusion plastics, 1993.
[28] D.W. GREEN, J.E. WINANDY, D.E. KRETSCHMANN, Mechanical properties of wood, in: Wood handbook - wood as an engineering material, Chapter 4, Forest Products Laboratory, Madison, 1999.
[29] G.B. NORRIS, Strength of orthotropic materials subjected to combined stress, Report No. 1816. US Department of Agriculture, Forest Research Laboratory. Madison, 1950.
[30] D.C. MONTGOMERY, G.C. RUNGER, Applied statistics and probability for engineers, third ed. John Wiley & Sons, 2003.
[31] ANSYS, Release 11.0, Documentation for ANSYS: http://www.ansys.com, 2007.
[32] Z.P. BAŽANT, Size effect on structural strength: a review, *Arch. App. Mech.* 69 (1999) 703-725.
[33] Z.P. BAŽANT, Scaling of structural strength, second ed., Elsevier, London, 2005.
[34] A. TOWSE, K.D. POTTER, M.R. WISNOM, R.D. ADAMS, The sensitivity of a WEIBULL failure criterion to singularity strength and local geometry variations, *Int. J. Adhes. Adhes*. 19 (1999) 71-82

Risk Management in Health Care
Lessons learned from Clinical Economics

Franz Porzsolt
Health Services Research at the Department of General and Visceral Surgery, University Hospital Ulm and
Clinical Economics at the Institute of History, Philosophy and Ethics in Medicine, University of Ulm, 89075 Ulm, Germany

Abstract: Increasing safety is the general goal of risk management. The lessons learned from health care are presented here and include the important differences between being safe and feeling safe, a description of risk-management failures and mapping of the effectiveness of risk management in health care, the management of real and of virtual risks, as well as special aspects of managing health-care risks. The second section describes two risks when managing health care, confusing economization with commercialization and two strategies for failure management in health care. The third section describes the difference between Health Economy (HE) and Clinical Economics (CE). Both are essential to understand the difference between economization and commercialization and the need to include both disciplines in the curriculum of medical education. The fourth section describes the road map of risks in health care and, finally, presents seven examples of risks emerging from conflicts of interest in health care. As health is a public as well as a private good, the emerging conflicts in risk management may apply to many other areas in which properties of public and private goods are intertwined.

1 Lessons learned from risk management

1.1 Being safe and feeling safe

The primary goal of risk management in road and railway accidents, tunnel fires or accidents caused by natural hazards is to guarantee a maximum of safety. In these situations, all players, the provider of safety (insurer), the payer, and the users of safety (beneficiary), strive for the same two goals: to be safe and to feel safe [1]. Somebody who feels safe will not necessarily be in a safe condition, and somebody who is in a safe condition may, in fact, not necessarily feel safe. Examples of the first constellation (feeling safe in an unsafe

condition) are people who lose money on the share market or cause car accidents by high-risk manoeuvers. Examples of the second constellation (feeling unsafe in a safe condition) include actions undertaken to prevent bovine spongiform encephalopathy (BSE) in 1990, influenza virus H5N1 infection in 2006, infection with Entero-Hemorrhagic Escherichia Coli (EHEC) in 2011 or the actions to prevent a disaster like the 2011 Fukushima catastrophe in Germany. These examples confirm that, in addition to the existing risks, the perception of safety is an important aspect of risk management.

1.2 Risk-management problems and mapping the effectiveness of prevention

Risk management can fail in two ways. It fails if people are in unsafe conditions or feel un-safe. Lack of being safe, i.e. lack of safety, correlates with too little prevention, indicated by an increased risk of accidents. Lack of feeling safe may correlate with too much or too little prevention, where too much prevention corresponds to harm caused by overprotection.

Too little prevention is easy to detect when accidents happen. It is more difficult to detect too much prevention, as accidents may not happen due to a very low risk of accidents or due to effective prevention. The likelihood of overprotection will be the higher, the lower the risk of accidents is.

Mapping the effectiveness of prevention on a cardinal scale is possible when the event rate with and without prevention is known. If the event rate without prevention is unknown, like in many situations, it is possible to rank the effectiveness of prevention on an ordinal scale. One may assume that mapping on a cardinal scale and ranking on an ordinal scale will be meaningless if the incidence is too low for statistical analyses even if the damage caused by an accident is significant. In these situations, the psychological perception of safety will be much more important because decisions depend on perceived safety signals.

1.3 Management of experience-based and virtual risks

Accidents will happen if a system fails to recognize risks, to develop strategies and to implement them to reduce risks. Consequently, we spend time and resources identifying and reducing the risks that may cause accidents. According to the above four scenarios, it is important to differentiate experience-based from suspicion-based (virtual) risks. In the case of past accidents, the identification of potential causes of the accident is essential for the construction of appropriate barriers to prevent the progression of hazards to accidents [2]. The suspected or virtual accidents and the corresponding lack of perceived safety depend on the information provided. In these situations, the risk

management has to analyze and decide about costs and consequences of counteracting the provided information that causes the unsafe feeling.

The first step in risk management is to identify risks and to recognize the possibilities of risk reduction. In a second step, we associate values to risks and possible risk reduction. As a third step, we make decisions based on these values [3]. In many situations, we cannot define risks and possible risk reduction, but can express whether we feel safe or not. In these situations, we use the value of perceived safety to make decisions [4]. If we base our decisions on perceptions instead of on facts, we may replace adequate risk management by overprotection. We address this problem by analyzing the consequences that were derived from the four above-mentioned health-care challenges (BSE, H5N1, EHEC, and the Fukushima disaster). None of the above scenarios – except H5N1 –confirm whether the prevention was necessary and effective or was not necessary and possibly ineffective. Only the example of H5N1 demonstrates that the preventive intervention (offering the drug) was obviously neither necessary nor effective, as no noteworthy infections occurred although the ordered drug was not used. This example suggests that risk management should differentiate between experience-based risks, i.e. risks based on past accidents, and suspicion-based risks, i.e. risks based on potential accidents, which have never happened.

1.4 Special aspects of risk management in health care and the focus of this paper

Two aspects are different in health-care accidents and road or rail accidents or natural disasters: road or rail accidents usually affect several people and will be noticed by the public. In contrast, health-care accidents usually affect only single individuals, and the public will notice these accidents only in exceptional situations. Low public awareness explains the high risk that a health-care accident will be ‘brushed under the carpet’ and the reasons for the accident will never be analyzed. Without rigorous systematic analyses of accidents and failures, it will be impossible to develop effective strategies for risk management.

As a complete reduction of risks will never be possible, the risk management has to balance the costs and consequences of risk reduction. In other words, economic analyses will be helpful for risk management. It may be important to discuss the significance of economic analyses of decisions on the management of virtual risks. Different actions will be necessary to optimize risk management. The providers, payers, and beneficiaries of safety should try to differentiate between virtual (suspicion-based) and actually-existing (experience-based) risks. If the expected risk actually exists, some accidents will happen despite the best possible risk management. This means that the sustainability of risk management will not only depend on the effectiveness of

risk reduction, but also on the analysis of failures associated with the risk management.

This paper discusses the differences in risk-management strategies from the perspectives of health care. It provides the necessary information to understand the emerging conflicts and considers changes that may solve the existing problems.

2 The risk of managing health care

2.1 Commercialization or economization of health care

Conflicts emerging from health care and commercialization are frequently correlated. In addition, commercialization is often confounded with economization, and economization is frequently associated with virtual risks. Commercial principles are important to bring products to the market and to make profit, while economic principles are generally essential to make decisions. Economization will benefit health care, while commercialization will harm it. An economic analysis includes three components, the description of the input or costs (including any costs/burdens that have to be accepted, not only monetary costs), the description of the output or outcome[1] or of consequences and, finally, the comparison of both cost and consequences.

Although most costs are monetary costs, two types of costs are important in health care, tangible and intangible costs. The intangible costs, such as a reduction in quality of life (e.g. anxiety or loss of physical abilities or loss of participation in social life), are hard to express in monetary units. Most of us will agree that life-threatening risks must be reduced as far as possible. However, there will be a considerable discussion about the limitation of these expenditures. The lower the residual risk is, the higher the costs (or the lower the value) of further risk reduction. For a thirsty person, the first glass of water has a higher value than the second glass, and the value of the second glass will be higher than that of the third glass. The value of each additional unit of a good -here a glass of water- will be lower than the value of the previously provided unit of the good. This principle of marginal costs and consequences is described as Gossen's law [5] and predicts that the costs for the same risk reduction will be higher, the smaller the residual risk. When commercial principles instead of economic principles prevail, the society will manage virtual risks or will provide low-value and overpaid services. In other words, the health system becomes inefficient

[1] Following an intervention, output is a directly measurable result (usually a surrogate parameter), such as the reduction of elevated blood pressure in hypertensive patients, while the outcome is the intended goal, such as prevention of renal failure, blindness, stroke or heart attack in patients with hypertension.

2.2 Strategies of failure management in health care.

Inefficient health care will also emerge when we manage accidents by solving the actual case without reducing the risk of repeating exactly the same mistake or accident. From the perspective of risk management, it makes more sense to interpret an accident as an indicator of a system failure than as an indicator of an individual person's mistake [2]. If the failure management is focused on identifying of the guilty individual – unfortunately a favored strategy in most societies – it will be possible to punish somebody, but the risk of the same failure or accident will remain unchanged. Using the system approach, any possible hazard in a complex system that may lead to an accident is identified. Complex systems contain many hazards. Identification of these hazards is necessary to construct efficient barriers to prevent accidents. This is a core task of Clinical Economics (CE).

3 Differences of Health Economy (HE) and Clinical Economics (CE)

HE and CE are complementary disciplines – both apply economic principles to achieve the same goals in health care, i.e. to guarantee efficiency. As HE emerged from economics and CE from health care, these two disciplines approach the same goal from different origins (Table 1). The science of HE described in several textbooks, which differ in volume and content [6-10], is older than CE, which is a very young discipline, and has been described in only a few books so far [11, 12, 13].

'CE' was established by American colleagues in the 80th and discussed traditional models for the monetary assessment of health services without considering differences in values [14, 15]. As values change during the phases of our lives and are the basis of our decisions [3], societal values should be milestones when constructing a health system. There are at least ten criteria that illustrate the differences between HE and CE.

- The general goals are different, as HE is based on economic analyses, while CE is more concerned with describing the added value of health services.
- The specific goals are the demonstration of cost containment and cost-effectiveness in the case of HE while CE provides solutions to health problems and provides safety as a basic human need and a moral value.
- In HE, decisions are based on costs and societal values. In CE, decisions are based on individual values and the four principals of medical ethics, i.e. autonomy, non-maleficience, beneficience, and justice [16].

- The primary outcome in HE is monetary costs, while it is the quantity and quality of life in CE.
- The necessary basic education and knowledge in HE is macro- and micro-economics, but is medicine or nursing and clinical epidemiology in CE
- HE usually applies models and sensitivity analyses that can only rarely be falsified. CE uses studies that can be falsified.
- The specific tools of HE are various forms of cost-effectiveness analyses in which the costs are expressed in monetary units and the effects or consequences in variable dimensions. When comparing two possible actions, the ratio of difference in costs and difference in consequences is called 'Incremental Cost Effectiveness Ratio (ICER)'. The specific tools in CE are explanatory and pragmatic trials as well as quality of life studies.
- Budget limitations are self-evident in HE, but are a problem in CE because of two aspects. The decisions in CE depend on the problems of individual patients and are practice-oriented, while decisions in HE are theory-based. Second, in HE, usually well-defined tasks have to be completed, while in CE poorly-defined problems have to be solved. Fixed budgets are acceptable for completion and management of well-defined tasks, but can hardly be applied for solving problems where too many unpredictable variables influence the outcome [17].
- The relation between cost and benefit can be clearly defined in theoretical models used in HE. This does not apply to the real-world situation of CE because the explicitly presented perspective, e.g. the benefit to the patient from the provider's point of view, is not necessarily identical with the implicit perspective, e.g. the patient's point of view.
- Finally, the asymmetric distribution of information is a basic component and well accepted in a commercial environment. When negotiating health services, asymmetric information is only acceptable when compatible with ethical principles. As examples, fatal diagnoses have to be communicated by experienced health-care professionals, as more harm than good can be caused by inexperienced doctors. Professionals will never exactly predict fatal outcomes, such as 'your husband will have no longer than two more weeks to live', because biologic variation in most cases far exceeds the imagination of experts.

These ten differences indicate that health-care professionals with different educational backgrounds, like economists and medical doctors, strive for different values, focus on different aspects of the health-care system, use different methods and come to different conclusions. Optimal solutions require the inclusion of different perspectives and different values. The idea of a twin faculty in health care, i.e. a faculty that is chaired by two professionals, one from economics and another from health care, might provide more mature solutions than a faculty chaired by a hybrid expert who is perceived as medical by his economist colleagues and as an economist by his medical colleagues. The first step would be the inclusion of CE in the curriculum of medical education.

4 Road map of risks in health care

Health care is an example for such a complex system. The complexity of the system is usually under-estimated, as the number of existing risks exceeds the awareness of it. These risks can be identified along the "blue highways" that connect the major academic science laboratories to the physicians and patients in primary-care offices across the United States. We used the picture of a roadmap from Westfall and colleagues [18] to categorize the existing risks according to four groups of stakeholders and four types of actions (Table 2). The three existing groups of stakeholders (input-researchers, practitioners, patients) are supplemented by a fourth group, the outcome-researchers. Correspondingly, the three existing types of actions (publication, recommendation, and application) are supplemented by a fourth group, evaluation.

For efficient risk management in health care, knowing the characteristics and actions of the stakeholders is essential. 'Input-researchers' are colleagues (university- or industry-based) who publish and recommend new solutions (Table 2). Practitioners would implement these solutions, in contrast to `outcome-researchers', who evaluate the cost-effectiveness of the implemented solutions. `Input-researchers' in health care are usually educated in natural science, medicine, psychology or sociology, while outcome researchers are usually educated in economics, but rarely in any other of the above scientific fields. This difference in education and socialization between those who theoretically *discuss* the recommendation, provision and assessment of health care and those who in fact *apply* the recommendations and *assess* the outcomes of these recommendations often results in conflicting perspectives [19, 20].

The four types of actions taken by the four groups of stakeholders are associated with specific risks. The 'input-researchers' generate health-care innovations under experimental conditions, publish these innovations, and the publications induce the demand for these innovations. These innovations can be either a new diagnostic tool, or a new preventive measure, or a new thera-

py, or to alter a new application of an already known tool or method. The common and unpleasant feature of these innovations is their resource-binding nature. In other words, innovations in health care will always be associated with an increase in health-care expenditures, although not all of these innovations generate additional value. The true challenge associated with innovations is actually the demonstration of effectiveness. Demonstrating effectiveness means that an innovation which was efficacious under ideal study conditions – and consequently promises that this effect will also be detectable under real-world conditions – can in fact demonstrate this effect under real-world conditions. This leaves two unsolved problems: the ideal methods to conduct confirmatory trials under real-world conditions (also called pragmatic trials) are not yet established. Second, the assessment of validity in efficacy studies is time consuming, costly, requires special skills and knowledge and is not too attractive. These two unsolved problems may explain why the validity of publications and recommendations for practice are challenged only superficially, resulting in low-validity recommendations to general practitioners, who have to establish outcome research urgently.

The first type of risk addressed in our roadmap (Table 2) emerges at the interface of input-researchers and practitioners. These researchers sometimes publish reports that do not meet the criteria of high validity reports. Practitioners do not have the time, the knowledge or the interest to complete critical appraisals of the published literature. They have to trust these reports and base their treatment decisions on them. There is sufficient evidence that critical reading of medical scientific literature is absolutely necessary [19] because the validity of many scientific communications is rather low [21, 22, 23]. The Medical Advisory Service of the German Health Insurance (MDS) summarized data indicating that estimates on the proportion of evidence-based health services range from 4% -20%, while the results of studies suggest that 11% - 80% of services are evidence based [24]. This uncertainty between promise and confirmation represents the risk practitioners take when they just read and apply the published results without first making a critical appraisal.

The second type of risk emerges when medical guidelines and recommendations are based on poorly checked scientific literature. This risk includes the ‘empowerment of flaws’. Empowerment of flaws describes a sequence of socially-desired steps which help to establish flawed standards. First, it is easier to publish a positive than a negative result (publication bias); second, it is easier to confirm than to criticize a published result; and third, authors of guidelines and recommendations avoid including skeptical comments so as not to jeopardize the credibility of their own recommendations.

The third type of risk is related to the application of services recommended by ‘input-researchers’ or requested by the public. Based on our impressions from

traditional risk management in health care, one would predict that the majority of accidents relate to the application of services. This impression may be wrong because accidents in this risk category happen to individual patients and should be easy to detect. As many accidents and errors in health care are either not detected or are not reported and the culture of reporting is only slowly improving 25, 26, 27, 28], we cannot yet decide if the application or the selection of services entails higher risks. In selected prevention programs, systematic mistakes are difficult to detect because the results of prevention will be available only some 15 years after initiating the program. Examples are prevention programs in metabolic syndromes (central obesity, elevated blood pressure, dyslipidemia), as well as programs for prevention of colorectal and prostate cancer.

The fourth type of risk is related to the quality assurance of outcomes. Quality assurance of outcomes is part of the business in any service company or production plant. The companies have a considerable interest in guaranteeing the quality criteria of their products or services. This concept can only partially be transposed into health care due to the expected success rate, which is 100% in service companies or production plants, but not in health care. In health care, we do not have enough data to describe the expected success rates even for the most frequent treatments of the most frequent subgroups of diseases. The unsolved problem is finding the optimal method for data retrieval. These data should describe, but not influence, day-to-day conditions. Ideal but artificial study conditions, like randomized controlled trials, introduce too many artifacts to describe real-world data. A summary of these artifacts and a possible solution of the problem has been submitted for publication.

5 Seven examples for risks of health care emerging from conflicts of interest

Although we identified only four types of risks along a roadmap (Table 2), there actually exist many more risks that may affect the safety of health care. In Table 3 we present seven scenarios, each representing a conflict of interest (COI 1-7) from the perspectives of the provider, payer, or user of health care. These COIs reduce the safety of health care and should, therefore, be identified and be a matter of concern.

The first COI is caused by the low validity of many scientific publications, as shown in several experiments investigating validity criteria [21, 22]. Other groups tried to identify the proportion of evidence-based scientific publications and observed a very high variation in the results [22]. The only conclusion that can be drawn from these data is the existing uncertainty. The providers of health care don’t know the exact validity of their reports, as clinical scientists have neither the necessary time nor the interest to spend hours

assessing the validity of publications. For payers of health services, it is very hard if not impossible to assess the validity of scientific publications. Real-world data which can solve this problem are usually not available. The users of health care - the patients - are primarily interested in getting help, but not in validity checks. Poor validity entails a considerable risk of providing ineffective and inefficient health care.

- The problem can be solved by mandatory and independent registers that meet quality criteria of pragmatic controlled trials [13, 29].

The second COI is caused by claims. Health-care providers create the impression that 'personalized medicine (PM)' is more effective than 'conventional medicine'. PM means the identification of the subpopulation of patients that will respond to a very specific treatment or a very specific treatment that can successfully be used in a very small group of patients. Especially patients with serious health problems who clamor for help are sensitive to such promising statements. The scientific problem may be illustrated by a virtual example. Even if a very rare disease can be identified in a few patients by using modern bio-molecular technology, nobody can tell if these few patients will benefit from a proposed highly-specific treatment because nobody has had the chance to compare conventional and new therapies in these few patients. A helpful effect may be expected due to the 'perceived safety' [30-36] and the positive perspective that is offered to these patients. These psychological effects may be extremely valuable, but are not adequate to support the concept of 'PM' [37-39]. Payers of health services are very much interested in the concept of PM, as the efficiency of health care can be increased by reducing the proportion of unsuccessful treatments.

- The problem can be solved if PM is evidence-based, i.e. if conventional treatments and the 'personalized treatment' can be compared in a specific group of patients who have been identified by molecular markers i.e. 'Evidence-Based Personalized Medicine (EBPM)'

The third COI describes the general problem in health care that the provider and evaluator of health care are often the same institution. This lack of control should be considered a high risk. Health-care providers often claim they have to see the outcomes to detect potential losses in quality. This is correct, but not sufficient, as the provider tends to confirm the quality of its own work rather than to criticize it. Constructive criticism is an absolutely necessary part of the production process, whose value is frequently underestimated. The user of health care is not the right person to evaluate it, as there exist mutual dependencies between health-care professionals and patients which handicap the function of the evaluator.

- External evaluation will probably not solve the problem, as professional teams will never accept rigorous control of their decisions, actions and outcomes. We consider a feasible solution when the team carefully selects and hires an independent member of the team who has to ask 'Y-questions', i.e. "Why are we doing it this way?" The ideal member would be a highly-qualified and especially-trained nurse, as recently published [40]. The details of the Y-nurse concept still must be defined and its effectiveness tested in a scientific project.

The fourth COI is related to the information provided about risks and chances of health care. As higher chances are usually associated with higher risks, the right balance between these two has to be found. This balance will depend very much on the goals of the decision-maker. As the goals depend on values, the balance of chances and risks will finally depend on the values of the decision-maker.

In health care – like in any other area of life – everybody defends his/her territory and will avoid information that could jeopardize this territory. An example is the publication bias, i.e. authors whose data confirm the expected results will be published more often than authors with contradictory results. Correspondingly, reviewers will more often accept manuscripts that confirm than contradict the expected results. This form may be called 'passive publication bias' in contrast to the above mentioned 'active publication bias'. Examples of passive publication bias are manuscripts that were rejected several times before being accepted for publication and subsequently confirmed by additional evidence, such as the spontaneous regression of cancer [41] confirmed by a second trial [42], the low value of mammography [43, 44], or the ineffectiveness of adjuvant therapy of gastric cancer [45]. Unless better options are offered, neither the users nor the providers of health care will be interested in critical publications because users expect a solution to their health problems and providers want to help and sell their services. The payers for health care are the only group which is interested in critical reports because these reports help increase the efficiency of their services.

- Ideal solutions to the information problem on chances and risks have to provide positive perspectives to all stakeholders in the system - the providers, payers, and users. As the values of these stakeholders are different, each stakeholder will expect specific information. Patients want to feel safe, doctors want to solve health problems, and managers want to make cost-effective decisions. Unfortunately, the specification induces a new risk, the risk of asymmetric distribution of information, which may be acceptable from the perspective of economy, but may

present a serious problem from the perspectives of medicine and ethics. These different facets of distributing information illustrate the complexity of the problem and the high risk of COI.

The fifth COI is related to the acceptance of 'perceived safety' as an added value. Payers of health care consider safety a reduction in risks, but refuse to accept perceived safety as an added value. In contrast, health-care providers and users consider perceptions more important than probabilities, as our decisions in daily life depend more on perceptions (perceived safety) than on probabilities (risk reduction). The perceived risks of H5N1, BSE, EHEC or of a nuclear-power accident were estimated higher than the probabilities of these risks. Consequently, it was the perceived risks that influenced the political decisions in Germany to meet the demand of 'perceived safety'. There are no data to confirm that these political decisions reduced the health risks in Germany, but there are many data indicating that the political decisions had unpleasant economic consequences.

- These examples demonstrate the need to discuss the societal significance, as well as the societal hazards, associated with 'perceived safety'. It is necessary to discuss the power of information as a modulator of perceived safety and the ethical aspects associated with the distribution of information.

The sixth COI is related to two types of prevention, the prevention of accidents which have already happened (i.e. experienced accidents) and accidents which have never happened, but are expected to happen (i.e. anticipated accidents). Providers want to offer prevention of both types, experienced and anticipated accidents, payers often offer the prevention of both types of accidents as a marketing instrument, and users warmly accept these offers as long as no additional contributions, such as continuing exercise or diet or co-payments, will be requested.

- The example demonstrates that each player in the system makes decisions based on perceived utility and values. The consumers' behavior confirms their willingness to pay and is a reliable indicator of perceived values. The consumer's behavior should be analyzed more intensively by health-services research to generate the knowledge needed for political decisions in health care and the design of appropriative incentives.

The seventh COI is related to differences in the perceptions of stakeholders related to the strong influence of study designs and study outcomes by preferences. Strong and weak preferences of patients influence the generation of knowledge in health care differently. Doctors and patients with strong prefer-

ences refuse participation in randomized trials. These decisions cause an effect described in the literature as 'sampling bias' [46]. Patients with weak preferences may agree to be included in a randomized trial, but will influence the result of this trial under two conditions. The result will be influenced by the patients' preference if they know whether they will get the preferred treatment or not and if the preferences for the different treatments are not equally distributed (i.e. 50:50 in case of two treatments or correspondingly 33:33:33 in case of three treatments). Patients in any arm of a trial will have the same preferences (this is guaranteed by the randomization), but will not get the same treatment. Patients who get the preferred treatment are more likely to demonstrate a positive study outcome than patients who do not. These psychological effects lead to overestimation of the preferred effects described in the literature as 'performance bias' 47].
The COI emerges because providers of health care will respect patient preferences when selecting the provided care, payers will be concerned about the effects of preferences, and users will rarely accept a non-preferred treatment.

- This means that the effectiveness of health care, i.e. investigating health care under real-world conditions cannot be adequately described by studying efficacy, i.e. investigating health care under ideal study conditions. It will be necessary to use different methods to study efficacy and effectiveness and to accept that efficacy and effectiveness provide different information, which leads to different conclusions.

6 Discussion

Risk management in the health system seems to be different from other systems because health is a meritorious good – like roads, education, and culture - that have properties of private, as well as public, goods. In theory, public goods are not excludable and non-competitive, which means individuals cannot be excluded from use, and use by one individual does not reduce the availability to other individuals [48]. As many goods appear to have properties of both public and private goods, the experience in risk management derived from the health system is valuable to other systems.

The primary goal of risk management is providing safety in two dimensions – being safe and feeling safe. The more safety we request, the higher the consumed resources for safety. The reduction of risks, i.e. providing 'real safety' and the verification of feeling safe, i.e. providing 'virtual safety' will consume resources. Economic analyses are helpful to balance the costs and consequences of the different types of safety.

The examples and scenarios presented in this paper clearly demonstrate the important difference between the economization and the commercialization of health care. Economization is necessary and will improve the quality of health care, while commercialization is harmful for the current form of health care. Health care will benefit from commercialization if the society agrees on a clear separation between private and public health services. Commercialization will not benefit public services associated with the principle of solidarity. In a private health-care system, access and costs are clearly regulated by the market. Commercialization, i.e. making profit by selling health care, fits this concept. A public health system based on the concept of solidarity will be destroyed by commercialization. Management in health care can be ambiguous. It may express both economization and commercialization.

To avoid the confusion between economization and commercialization, we established 'CE', which focuses on the outcomes of health care from the users' perspective. Its sister discipline, HE, focuses on the costs of health care from the payers' perspective. Prevention is a good example to illustrate the confusion between economization and commercialization. Economization requires the selection of cost-effective measures (see 6th COI) from the users' perspective, while commercialization strives for profit by selling cost-effective health care from the providers' perspective.

Only recently a few reports confirmed the successful implementation of a measure, such as the Critical Incidence Reporting System (CIRS) [49], which can improve the quality of health care [50. 51]. The slow progress in the risk management of health care suggests that a new safety culture has to be established. This new culture has to recognize two types of health-care researchers, the 'input-' and 'outcome-researchers' described in the roadmap of risks in health care. These two families of researchers should, but cannot yet, communicate due to differences in their education and socialization. The lack of communication promotes the emerging COIs.

Alternatively, health care can learn from other systems. There is almost no other system, besides health care, in which a COI exists because the provider also evaluates the quality of the provided service. Accordingly, there is no other system which does not systematically assess the outcomes of the provided services. Health care lacks efficient outcomes research. Consequently, it will remain rather difficult to detect and improve poor outcomes unless the necessary data for evaluation of day-to-day services is recorded systematically [52].

According to a recent study, the distinction between evidence-based and non-evidence-based services is a pipe dream [24]. The most appropriate interpretation of these data is probably that 'evidence-based' is an academic certificate with a rather wide variation. The conduct of this research is excellent. The

problem is the definition of 'evidence'. We consider a treatments evidence based if data confirm a (partial) solution of a defined clinical problem. An extensive analysis of adherence of intensive-care services to the international guidelines of the surviving sepsis campaign indicated that adherence is primarily a function of disease severity, but neither an indicator of service quality nor of scientific foundation. Adherence is no appropriate indicator to confirm the quality of a treatment [53]. These data also support the urgent need of outcomes assessments.

The report cannot provide solutions to the huge variety of management problems that require a solution in health care, but may add some suggestions to trigger the ongoing discussion. A first efficient step on this path could be the integration of CE in the curriculum of medical students to specify the difference between the economization and the commercialization of health care.

6.1 Tables

Table 1: Differences between Health Economy (HE) and Clinical Economics (CE). Specific tools in HE are the cost minimization analysis (CMA), cost effectiveness analysis (CEA), cost utility analysis (CUA), cost benefit analysis (CBA), and incremental cost effectiveness ratio (ICER). Specific tools in CE are the randomized controlled trial (RCT), pragmatic controlled trial (PCT), quality-of-life instruments (QoL), number needed to treat (NNT), and likelihood ratio (LR). *The four principals of medical ethics are autonomy, non-maleficience, beneficience, and justice (Beauchamp)

	Health Economy (HE)	**Clinical Economics (CE)**
Goal (general)	Comparing costs and consequences of alternative actions	Demonstrating the added value for individuals and society related to the accepted costs
Goal (specific)	Cost containment, cost-effectiveness	Solution of health problems, safety as a basic human need and moral value
Decisions are based on	Costs and societal values	Individual values and principals of medical ethics*
Primary outcomes	Monetary costs	Quantity and quality of life
Basic education and knowledge	Macro- and micro-economics	Medicine or nursing and clinical epidemiology
Tools (general)	Models (cannot be falsified)	Trials (can be falsified)
Tools (specific)	CMA, CEA, CUA, CBA, ICER	RCT, PCT, QoL, NNT, LR
Budget limitations	Cannot be avoided	Accepted for completion of tasks, but not for solving problems

Cost-benefitrelation	Higher costs are related to more benefit and vice versa	More benefit is related to higher costs, but not necessarily vice versa
Asymmetric distribution of information	Acceptable for commercial reasons	Acceptable for ethical reasons

Table 2: Roadmap of risks in health care according to the systems' stakeholders and their actions. Input-researchers are usually educated in natural science, medicine, psychology or sociology. Practitioners are doctors, nurses, psychologists, physiotherapists, social workers and others providing health-care services. Outcome researchers are usually educated in economics, but rarely in any other scientific field. The examples marked 1 – 7 are related to the described types of risks. The examples 1, 3, 5, and 6 are each related to the first, second, third and fourth type of risk. Example 2 is related to the first and second type of risk, example 4 to the second and third type of risk, and example 7 (not shown in this table) is related to all four types of risks.

		Actions of stakeholders			
		Publication (experiment)	**Recommendation (Institutional review/guideline)**	**Application (intervention)**	**Evaluation (appraisal)**
Stakeholders	**Input-researcher**	Publishing the results of experiments under ideal conditions	Recommending (researcher and practitioner) and requesting (patient) the application of published results		
	Practitioner	Reading/applying the published results		Applying published and requested recommendations in daily practice	
	Patient				Evaluating the outcomes in daily practice
	Outcome-researcher				
Examples		1 2 3	4 5	6	

Table 3: Seven examples of conflicts of interest (COI) that increase the risk of safety in health care shown from the perspectives of health-care providers, payers and users. IC: informed consent.

Risk inducing conflicts of interest (A – G)	**Perspectives of providers, payers, and users of health care**		
	Providers	**Payers**	**Users**
(1) Conflict of interest COI caused by low validity of many scientific publications	No time, experience, or interest in checking validity	It is hard to identify and even harder to replace by valid data	Interested in getting the service, but not in checking validity
(2) COI induced by 'personalized medicine'	Personalized service is an important aspect in marketing	Increasing efficiency by limiting therapies to responders	Request the optimal treatment for any individual patient
(3) COI if the same person provides and evaluates health care	Provider has to be in charge of quality of the provided care	Same person should not provide and evaluate health care	Perception of a COI depends on provider-user confidence
(4) COI associated with publication bias and acceptance bias	Reluctant in providing information on risks and chances	Interested in existing risks and chances	Balance of accepted risks and chances depends on goals
(5) COI on the acceptance of perceived safety as an indicator of added value	Want to provide both risk reduction and perceived safety	Safety is not accepted as added value unless risk reduction is shown	Perceived safety is an important value in health care
(6) COI in the prevention of experienced or suspected accidents	Want to provide both types of prevention	Use prevention as a marketing tool	Accept any prevention if no own contribution is necessary
(7) COI induced by preferences affects study designs and outcomes	Respect patient preferences when selecting the provided care	Preferences cause bias in sampling, randomization & effectiveness	Preferred treatments are superior to non-preferred therapies

7. Literature

[1] Porzsolt, F.; Leonhardt-Huober, H.; Kaplan, RM.: Aims and Value of Screening: Is Perceived safety a Value for Which to Pay? In: Porzsolt, F.; Kaplan, RM (eds.) Optimizing Health – Improving the Value of Healthcare Delivery. Springer, New York, 2006, pp 199-204

[2] Reason, J.: Human error: models and management. BMJ. 2000; 320:768-770.

[3] Gray, JAM.: Evidence-based policy making is about taking decisions based on evidence and the needs and values of the population. BMJ 2004; 329:988–989

[4] Porzsolt, F.; Polianski, I.; Görgen, A.; Eisemann, M.: Safety and security: the valences of values. Journal of Applied Security Research 2011,6:4,483-490. http://dx.doi.org/10.1080/19361610.2011.604069

[5] Gossen, HH.: Entwickelung der Gesetze des menschlichen Verkehrs, und der daraus fließenden Regeln für menschliches Handeln, Vieweg, 1854, Braunschweig.

[6] Kielhorn, A.; Graf von der Schulenburg, J-M.: The health economics handbook. Adis International Ltd. Chester / UK. 2000

[7] Donaldson, C; Mugford, M.; Vale, L.: Evidence-based Health Economics. London. BMJ.books.2002

[8] Breyer, F.; Zweifel, P.; Kifmann, M.: Gesundheitsökonomik. 5. Überarbeitete Auflage, Berlin, Heidelberg New York. Springer. 2005

[9] Drummond, MF.; Sculpher, MJ.; Torrance, GW.; O'Brien, BJ.; Stoddart, GL.: Methods for the Economic Evaluation of Health Care Programmes. 3rd ed. Oxford University Press. 2006

[10] Graf von der Schulenburg, JM; Greiner W.: Gesundheitsökonomik. 2. Auflage, Mohr Siebeck, Tübingen. 2007

[11] Porzsolt, F; Williams, AR.; Kaplan, RM. (eds): Klinische Ökonomik. Effektivität und Effizienz von Gesundheitsleistungen. Ecomed Verlagsgesellschaft 2003.

[12] Porzsolt, F; Kaplan, RM. (eds.): Optimizing Health – Improving the Value of Healthcare Delivery. Springer, New York, 2006

[13] Porzsolt, F. (Hrsg): Grundlagen der Klinischen Ökonomik. Schriftenreihe PVS Verband Band 11, 1.Auflage. Berlin 2011

[14] Eisenberg, JM. New drugs and clinical economics: analysis of cost effectiveness in the assessment of pharmaceutical innovations. Rev Infect Dis. 1984;6 Suppl 4:S905-908.

[15] Schulman, KA.; Ohishi, A.; Park, J. et al.: Clinical economics in clinical trials: the measurement of cost and outcomes in the assessment of clinical services through clinical trials. Keio J Med. 1999;48:1-11.

[16] Beauchamp, TL.; Childress, JF. Principles of Biomedical Ethics. OUP, Oxford, 2001.

[17] Dörner, D., Kreuzig, H.W., Reither, F. & Stäudel, T. (Hrsg). Lohhausen. Vom Umgang mit Unbestimmtheit und Komplexität. Bern, Hans Huber, 1983.

[18] Westfall, JM.; Mold, J.; Fagnan, L.: Practice-based research-"Blue Highways" on the NIH roadmap. JAMA. 2007;24:403-406

[19] Du Prel, JB.; Röhrig, B.; Blettner, M.: Critical appraisal of scientific articles: part 1 of a series on evaluation of scientific publications. Dtsch Arztebl Int. 2009 106:100-105.

[20] Belli, G.: Bridging the research-practitioner gap: views from different fields. In: Reading C (Ed.), Data and context in statistics education: Towards an evidence-based society. Proceedings of the Eighth International Conference on Teaching Sta-

tistics, 2010, Ljubljana, Slovenia. Voorburg, The Netherlands: International Statistical Institute.

[21] Porzsolt, F.; Kajnar, H.; Awa, A.; Fässler, M. ; Herzberger, B.: Validity of Original Studies in Health-Technology Assessment (HTA) Reports: Significance of Standardized Assessment and Reporting. Int. J. Technol. Assess. Health Care 2005;21/3:1-4

[22] Porzsolt F, Bonotto de O.Costa, IC.; Thomaz, TG. for the SHUFFLE group.: Advantages and Limitations of Twin Assessement of Clinical Trials (TACT). J Publ Health 2009;17:425-435.DOI 10.1007/s10389-009-0283-4

[23] Bjordal, JM.; Lopes-Martins, RA.; Klovning, A.: Is quality control of Cochrane reviews in controversial areas sufficient? J Altern Complement Med. 2006;12:181-183.

[24] Neises, G.; Windeler, J.: How much is "evidence-based"? An overview of the state of the art in research. [Article in German] Z Arztl Fortbild Qualitatssich 2001;95:95-104.

[25] Elder, NC.; Von der Meulen MB. ; Cassedy, A.: The Identification of Medical Errors by Family Physicians During Outpatient Visits. Ann Fam Med 2004; 2:125-129

[26] Henriksen, K.; Battles, JB.; Marks, ES.; Lewin, DI. (Eds).: Advances in Patient Safety: From Research to Implementation (Volume 1: Research Findings). Agency for Healthcare Research and Quality (US), Rockville/MD, 2005, Publication No.: 05-0021-1

[27] http://www.ahrq.gov/qual/patientsafetyix.htm. Last access

[28] Meyer-Massetti, C.; Conen, D.: Assessment, frequency, causes, and prevention of medication errors - a critical analysis [Article in German]. Ther Umsch. 2012;69:347-352.

[29] Porzsolt, F.; Geier, J.: Bedeutung der Terminologie in der Versorgungsforschung. 11. Deutscher Kongress für Versorgungsforschung, Dresden 2012.

[30] Porzsolt, F.; Kilian, R.; Eisemann, M.: Gefühlte Sicherheit – Ein neuer gesellschaftlicher Wert. Gesundh ökon Qual manag 2007;12:7-10

[31] Porzsolt, F.: Gefühlte Sicherheit – Ein Entscheidungskriterium für Patienten. Z Allg Med 2007; 83: 501– 506

[32] Porzsolt, F.: Gefühlte Sicherheit – ein neuer gesellschaftlicher Wert. Implicon plus – Gesundheitspolitische Analysen 2007;7:1-8

[33] Porzsolt, F.: Prävention aus Sicht der Klinischen Ökonomik – Eine lebensnotwendige Konsequenz der Zivilisation oder „gefühlte Sicherheit“? In: Kirch, W.; Middeke M.; Rychlik, R. (Hrsg): Aspekte der Prävention. Thieme, Stuttgart, 2010, pp 46-55

[34] Porzsolt, F.; Polianski, I.; Görgen, A.; Eisemann, M.: Safety and security: the valences of values. Journal of Applied Security Research 2011,6:4,483-490. http://dx.doi.org/10.1080/19361610.2011.604069

[35] Porzsolt, F.: Sicherheit und „Gefühlte Sicherheit“. In: Porzsolt, F. (Hrsg).: Grundlagen der Klinischen Ökonomik. Schriftenreihe PVS Verband Band 11, 1.Auflage. Berlin 2011, pp 170-174.

[36] Porzsolt, F.: Das Laborprofil zwischen Ärztlicher Professionalität und Kommerzieller Medizin - Gefühlte Sicherheit. Editorial. Ärzteblatt Baden-Württemberg 2012;01:4

[37] Sutton, AJ.; Cooper, NJ.; Abrams, KR.; Lambert, PC.; Jones, DR.: A Bayesian approach to evaluating net clinical benefit allowed for parameter uncertainty. J Clin Epidemiol. 2005;58:26-40.

[38] Porzsolt, F.: Personalisierte Medizin zwischen wissenschaftlicher Evidenz und Innovation im Gesundheitssystem. Berliner Seminare Biomet 2011;2: 15-16

[39] Windeler, J.: Individualized medicine - our (lack of) understanding.[Article in German]. Z Evid Fortbild Qual Gesundhwes. 2012;106:5-10. Epub 2011 Sep 22.

[40] Porzsolt, F.: The Y-nurse –pain in the neck or blessing for the team. BMJ blog by BMJ group, December 29, 2010

[41] Zahl, PH.; Mæhlen, J.; Welch HG (2008): The natural history of invasive breast cancers detected by screening mammography. Arch Intern Med 168:2311-2316

[42] Zahl, PH.; Gøtzsche, PC.; Mæhlen, J. (2011): Natural history of breast cancers detected in the Swedish mammography screening programme: a cohort study. Lancet Oncol 12:1118-1124

[43] Goetzsche, P. et al.: Why mammography screening has not lived up to expectations from the randomised trials. Cancer Causes Control 2012;23:15-21

[44] Goetzsche, P. et al.: The breast screening programme and misinforming the public. JR Soc Med 2011;104:361-369

[45] Cunningham, D.; Allum, WH.; Stenning, SP. et al.: Perioperative chemotherapy versus surgery alone for resectable gastroesophageal cancer. N Engl J Med 2006;335:11-20

[46] Metge, CJ.: What comes after producing the evidence? The importance of external validity to translating science to practice. Clin Ther. 2011;33(5):578-580.

[47] Jüni, P.; Altman, DG.; Egger, M.: Systematic reviews in health care: Assessing the quality of controlled clinical trials. BMJ. 2001;323:42-46.

[48] Varian, HR.: Microeconomic analysis. WW Norton, New York, 1992

[49] CIRS Critical incident reporting system in Germany http://www.kh-cirs.de/

[50] Tudini, M.; Palluzzi, E.; Cannita, K.; Mancini, M.; Santomaggio, A.; Bruera, G.; Baldi, PL.; Pelliccione, M.; Ricevuto, E.; Ficorella, C.: Modulation of GemOx chemotherapy according to CIRS in elderly patients with advanced pancreatic cancer. Oncol Rep 2012;27:423-432

[51] Wingenfeld, C.; Abbara-Czardybon, M.; Arbab, D.; Frank, D.: Patient safety in orthopaedics: implementation and first experience with CIRS and team time-out [Article in German]. Z Orthop Unfall. 2010;148:525-531

[52] Porzsolt, F.: Notwendige Analyse-Schritte. Dtsch Arztebl 2012;109:A1559

[53] Weiss, M.; Lautenschlager, F; Porzsolt, F.: Surviving Sepsis Campaign Bundles Adherence and Their Limits in Surgical Patients with Septic Shock in an ICU. BJMMR 2012

Uncertainty quantification of pipe flow systems using advanced approximation methods

Daniele Casali, Athanasios Kolios[1], Nikos Asproulis
[1]Offshore, Process and Energy Engineering, Cranfield University, UK

Abstract: Methods for deterministic assessment for pipe flow systems are currently well established and adequately documented in design standard and engineering practices. Optimization of the design and operation of such systems, constitute a probabilistic approach necessary for the evaluation of the probability that the performance of a system remains within acceptable limits. Towards this, efficient incorporation of uncertainties seems essential. This paper will employ non-intrusive formulations for reliability assessment and will document the development of a novel method, called 'Dynamically Kriged Response Surface Method', that allows handling of complicated, non-linear limit states with a large number of variables treated stochastically. The bespoke and newly proposed methods will be applied for the case of a single-phase flow pipe system, benchmarking accuracy and computational requirements.

1 Introduction

Pipe flow systems are used in a vast variety of applications, ranging from large scale oil and gas and refineries pipelines to ultra-small scale applications such as those used for medical applications. Design of such systems is currently governed by standards and practices derived through experience that although provide systems of adequate safety, they do not allow a systematic assessment of their real-time performance due to presence of various sources of uncertainty. A more detailed analysis aiming to incorporate and quantify the impact of these uncertainties can lead to a more efficient design of components and systems with reduced maintenance requirements [18]. Surface roughness, pressure drop coefficients, flow properties, corrosion deterioration etc, are only few of the variables governed by a high degree of randomness. Single and two phase flow systems are indicative applications where such practices can allow optimization of design and operation.

Among available methods for calculation of reliability, intrusive and non-intrusive methods can be identified [6], based on whether or not they interfere into the numerical simulation procedure of the corresponding deterministic simulation. Present work will focus mainly on the latter category, extending work that has been done earlier in cases of structural reliability problems [19; 21].

This paper will present different numerical methods for quantification of inherent uncertainty allowing a better understanding of system performance towards well-informed decision making on the operation and maintenance of individual system components. Further a new method will be documented, developed by the authors and referred to as 'dynamically kriged response surface method-DynKRSM' that combines Surrogate Modelling with Stochastic Response Surface and First Order Reliability Methods. The methodology derived, non-intrusive in nature, allows use of established specialised tools for detailed initial numerical simulations and can be applied in problems when very low probabilities of failure need to be calculated accurately. The methods presented will be applied on a one-phase pipe flow system benchmarking their performance in accuracy and computational requirements. The novel methodology that is developed herein can be extended for different relevant problems encountered in engineering and scientific applications.

2 Probabilistic assessment in pipe flow systems

Among literature and common practice effort has been put in qualitative approaches of probabilistic assessment in pipe flow systems developing case-dependent methodologies based on historical data (WOAD, Oreda etc) and personal experience. Some of these techniques such as RAM (Reliability Availability and Maintainability analysis), RCM (Reliability-Centered Maintenance), FMEA/FMECA (Failure Modes, Criticality and Effect Analysis) and FTA (Fault Tree Analysis) are examples of widely established technics in practice. Together with innovative techniques such as R6 and GO-FLOW they can derive a qualitative estimate of the reliability of a system. Even though these are rigorous procedures, their output is highly subjective and hence biased. Overall these procedures are suitable for already known systems for which past data are available and the qualitative evaluation is time consuming and does not provide reliable estimates.

Some quantitative analysis has been done using cumbersome simulation methods such as Monte Carlo Simulation technique, which is easy-to-

implement and uses a simple algorithm but has the drawback of a long simulation time. Other relevant quantitative studies have been carried out with the support of high fidelity software tools in [7], mainly to solve the joint probability integral of the probability of failure. A Markov model has been developed in [9] for the analysis of in-service inspection strategies for nuclear power plant piping systems which has been focusing on the transition probability between states of the system (success, flow, leak and rupture).

Corrosion is another main issue in the operability of piping systems, highly stochastic in modelling, especially in cases of offshore pipeline applications where both the harsh environment and the fluid flowing in the pipe, with several and different mechanisms contribute to pipe deterioration. In literature extensive material is found to estimate pipe wall corrosion and a lot of work is carried out to assess the reliability and safe operability of worn out pipe walls in ASME B31G-2009 and in [2-5]. Most of the times the assessment is based on inspection and no stochasticity of variables is considered. In some cases quantitative assessment is performed but only direct simulation techniques are employed. Further published data can be found on corrosion rates estimation, for example for CO2 corrosion (e.g. corrosion due to CO2 content in natural gas flowing in the pipe).

Summarizing, the following can be concluded for pipe flow systems:

- no systematic analytical quantitative methods are extensively applied;
- qualitative methods are widely applied, based on use of historical data, which is a limiting factor for the development of innovative systems;
- some quantitative techniques are available but they imply unacceptable simulation times and are not effective with low probabilities of failure (e.g. 10^{-3}, 10^{-4}).

3 Reliability Analysis

3.1 Fundamentals

Reliability is defined as “the ability of a system to fulfil its design functions under designated operating and environmental conditions for a specified period of time”. Theoretically is defined as the complementary to 1 of the probability of failure. The probability of failure can be seen as the probability for which a limit state for a system is exceeded. This can be expressed for a multi-variable system $X = \{x_1, x_2, x_3, \dots x_k\}$ using a Limit State Function as:

$$g(X) = L(X) - V(X) \quad (1)$$

where *L* is the limit and *V* the actual value of the limited variable.

According to the definition of the Limit State Function given above, the probability of failure can be mathematically defined as the probability for the limit state condition to be unsatisfied: $P_f = P[g(X) < 0]$. Hence the probability of failure can be rewritten as:

$$P_f = \int_{-\infty}^{0} f_g dg = \int_{g(X)<0} f_g dg \quad (2)$$

The reliability index β can be defined as a geometric measure of the distance of the limit state surface from the axis intersection of a multi-dimensional normalized space. The mathematic connection between the two quantities is:

$$P_f = 1 - \Phi(\beta) \quad (3)$$

The joint Probability Density Function of the limit state *g(X)* in the case of multiple variables should be expressed as follows.

$$P_f = \int \dots \int f_X(x_1, x_2, x_3, \dots x_k) dx_1 dx_2 dx_3 \dots dx_k \quad (4)$$

The solution of this integral is in most cases very difficult or even impossible to be analytically derived hence approximation methods are often employed characterised by different computational requirements and accuracy. Such methods approximate the stochastic variables through equivalent geometrical representation of the same. Originally two main methods were adopted: First Order Second Moment (FOSM) and Second Order Second Moment (SOSM); which employ Taylor expansion (up to first or second order) around the mean value under the failure condition $g(X) = 0$. Such methods are suitable for low levels of accuracy and relatively simple limit states therefore second order approximation and a different formulation of the methods need to be employed [13] This last formulation is widely known as First Order Reliability Method (FORM) and an analytical derivation of the methodology is given in the next section.

3.2 Monte Carlo Simulations

Monte Carlo simulation is widely used in several engineering and non-engineering applications due to the fact that it does not require much knowledge and statistical understanding of the problem. The algorithm is easy to implement and consists of launching several times the deterministic model

with different inputs and checking each time if one or more thresholds are exceeded or not. The resultant failure probability is calculated as:

$$P_f = \frac{N_f}{N} \tag{5}$$

where N_f is the frequency of failures and N the total number of runs. Typically an accurate result should be derived after two orders of magnitude more iterations than the reciprocal of the probability of failure to be estimated [6]. Therefore, disadvantage of the method is that it is not suitable for low probabilities of failure as it becomes computationally demanding. Even if this can be limited applying variance reduction techniques it can face restrictions in cases of multiple variables.

3.3 First Order Reliability Methods

The First Order Reliability Methods, transform the problem of estimation of probability of failure to that of the identification of the minimum distance of the transformed limit state surface in the intersection of the normalized domain axis following the following transformation:

$$Z_j = \frac{X_j - \mu_j}{\sigma_j}, \qquad X \sim N(\mu_X, \sigma_X) \rightarrow Z \sim N(0,1) \tag{6}$$

Identifying the most prone to fail point and measuring its distance to the origin will give value for reliability expressed in standard deviation units defined with the reliability coefficient β, which gives a measure of how safe the design and operation of the system is. Approximating the initial curve with a First Order Taylor expansion in $\mathbf{Z^*}$ and expressing it explicitly:

$$\tilde{g}(Z) \cong g(Z^*) + \sum \frac{\partial g}{\partial Z_j}\bigg|(Z^*) \cdot (Z_j - Z^*_j) \tag{7}$$

According to the definition of β the minimum distance from the origin to the surface can be given as:

$$\beta = \frac{g(Z^*) - \Sigma \frac{\partial g}{\partial X_j}\Big|(X) \cdot \sigma_{X_j} \cdot Z^*_j}{\sqrt{\Sigma\left(\frac{\partial g}{\partial X_j}\Big|(X) \cdot \sigma_{X_j}\right)^2}} \tag{8}$$

Defining the coordinates of the MPP in the normalised design space

$$Z_j = \beta \cos\theta_{X_j} \tag{9}$$

where the cosine is the direction cosine. This trigonometric variable expresses the influence of the *j*-th variable on the total variation or in other words how the curve changes moving along the *j*-th axis. Direction cosine, can be expressed as:

$$\alpha_j = cos\theta_{X_j} = \frac{\frac{\partial g}{\partial X_j}\Big|(X) \cdot \sigma_{X_j}}{\sqrt{\Sigma\left(\frac{\partial g}{\partial X_j}\Big|(X) \cdot \sigma_{X_j}\right)^2}} \tag{10}$$

The resultant value of β will be derived once this iterative procedure converges.

FORM approximation provides adequate results when the limit-state surface has only one minimal distance point and the function is nearly linear close to the design point. For cases where the failure surface has large or irregular curvatures (high nonlinearity), the failure probability estimated by traditional FORM, using the safety-index β, may give unreliable and inaccurate results. Introducing second-order Taylor series expansions (or other polynomials) may overcome this problem.

4 Stochastic Response Surface Method and Surrogate Modelling

4.1 General

The complexity of problems in engineering design applications is often reduced by system approximations, creating models/expressions that represent the relationship between inputs and outputs. Among several techniques suggested two large and potentially overlapping categories can be distinguished: Response Surface (RSM) and Surrogate Modelling methods (SM). Even if in literature a uniform definition to distinguish them does not exist, RSM are used mostly to simplify a known model while SM attempt to find some relation between inputs and outputs. Often approximation methods start from some given scarce data because the object variable is hard to measure and data hard to collect. In the RSM, polynomial regression techniques (MPR) and generalised linear models (GLM) can be identified while in SM techniques such as kriging and radial basis functions (RBF) [16].

Approximating the system under analysis using such expressions facilitates analysis allowing both optimization and reliability analysis since objective and Limit State functions can be approximated with such techniques. Response surface methods, in particular SRSM, have already been employed

successfully both in optimization and reliability analysis [17; 20] as well as kriging [10; 14].

4.2 Introduction to kriging

Among the interpolating techniques several approximate the original function by means of combination of simple functions. Such functions are called basis function and have various forms [15; 16]. An evolution of simple Gaussian radial basis functions is represented by kriging, which was first developed by mining engineer Danie Krige to predict the concentration of minerals. The basis function is expressed as:

$$corr\left[Y\left(x^{(i)}\right), Y\left(x^{(l)}\right)\right] = e^{-\left(\sum_{j=1}^{k} \theta_j \left|x_j^{(i)} - x_j^{(l)}\right|^{p_j}\right)} \tag{11}$$

Which represents the correlation between two sample points. Mainly two parameters differentiate this basis function from the Gaussian radial basis one. One is the smoothness coefficient p_j that represents how fast the function is and how quickly tends to infinite and zero. The other one is θ_j the 'activity or width parameter' and gives information about how much the output is affected by the corresponding input. The prediction at a new point is assumed to follow the same correlation. Finding the parameters values is a procedure done maximizing the likelihood of the sample set which is partially achieved through analytical differentiation and partially by direct search (e.g. genetic algorithms, simulated annealing etc). The predictor is expressed as:

$$y^*(x) = \hat{\mu} + \psi^T \Psi^{-1} (y - \mathbf{1}\hat{\mu}) \tag{12}$$

Where ψ is the correlation vector between the samples and the prediction point, Ψ is the correlation matrix, $\hat{\mu}$ the MLE estimate of the mean of the sample responses and $\mathbf{y}$ the sample responses.

Kriging also incorporates a procedure to eliminate noise in the sample set [11]. Sampling and tuning are also of key importance for kriging. Sampling can be done properly through LSH and tuning strategies can be found in literature.

4.3 Reliability assessment through direct simulations

The direct simulation method can be applied to explicitly modelled systems. The way to proceed with this in order to obtain reliable results is to start from few runs (e.g. 10^3) and increase the number of runs by one order of magnitude until the result converges. Rules of thumb on how high to go with the number of iterations is already been given in this work. As previously stated it is diffi-

cult to calculate low probabilities of failure without any variance reduction technique but this remains the most reliable approach because the results are not affected by any kind of approximation (neither on the system nor on the probabilistic side).

4.4 Stochastic Response Surface based Methods

In order to speed up the reliability analysis procedure, approximation techniques can be applied to the system initially retaining MCS as reliability analysis tool. The weakness of this approximation procedure is that some failure points are not detected. Further this technique remains inaccurate for low probabilities of failure. This method is applicable when a unified numerical simulation procedure is employed to model the system and it is not necessary to use FORM.

Introducing further approximation on the reliability method and employing FORM, the simulation time drastically drops to few seconds per each limit state evaluation. This is the fastest procedure among the ones analysed but also the one involving the most approximations. This method is suitable for highly continuous systems with a limited number of variables.

4.5 Surrogate Modelling based Methods

For a more accurate approximation of the system (still faster than the direct simulation) kriging can be applied instead of SRSM. Then for every MCS run a random prediction point can be created and the function predicted and evaluated. The kriging function has to be built before running MCS according to evenly spread sample points.

In actual applications the limit state is, mostly represented by a second order polynomial in *k* variables. Kriging parameters obtained though kriging approximations performed on the reference system can be used to directly work out the limit state expressing through the kriging predictor. What can be obtained from second term of the predictor is a single value that represents the deviation from the mean value. In the expression of this matrix multiplication one part of the formula dependent on the new prediction point, which is ψ^T and a second part independent from this, $\mathcal{G} = \Psi^{-1}(y - 1\hat{\mu})$ can be distinguished. $\mathcal{G}$ is a *nx1* matrix where each line can be expressed as:

$$\mathcal{G}(i,1) = \Psi^{-1}(i,1)(y_1 - \hat{\mu}) + \Psi^{-1}(i,2)(y_2 - \hat{\mu}) + \cdots + \Psi^{-1}(i,n)(y_n - \hat{\mu}) \quad (13)$$

The multiplication $\psi^T\mathcal{G}$ can also be expressed as

$$\psi^T \mathcal{G} = \psi^T(1,1)\mathcal{G}(1,1) + \psi^T(1,2)\mathcal{G}(2,1) + \cdots + \psi^T(1,n)\mathcal{G}(n,1) \quad (14)$$

Where, $\psi^T(1,i) = e^{-\{\theta_1|x_{1,i}-x_1|^2+\cdots+\theta_1|x_{k,i}-x_k|^2\}}$

The previously analysed procedure is referred to as Limit State definition. The relevant algorithm is shown in Figure 2.

5 Dynamically kriged response surface method

The methodology developed here is referred to as 'dynamically kriged response surface method-DynKRSM', illustrating the dynamic nature of the method with regards to the continuous change in the limit state through Kriging prediction and local approximation through RSM.

Kriging has the ability to 'reach' all sample points, unlike RSM. Moreover kriging is very good in predicting function values. If a small domain around a local point is considered then SRSM becomes able to map the function accurately. Kriging function's complexity increases with the number of samples making numerical manipulation hard. SRSM is shown inefficient globally but performs better locally. Therefore the positive features of the two methods can be combined together combining accuracy in representation with ease in numerical modelling. An illustrative example to show the sequence of the local approximation starting from a 'kriged' surface is highly non-linear 'Sombrero' test (Figure 1).

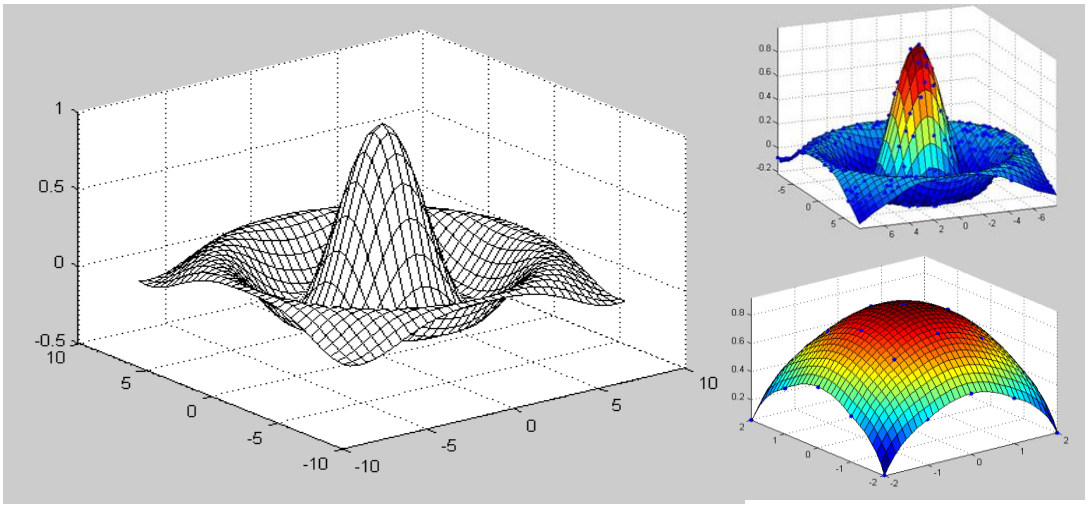

Figure 1. Global (kriging) and local approximation (SRSM) – 'Sombrero' test

The methodology proposed considers prediction of some points around the current design point using kriging and approximate this 'local' curve using SRSM. Then a quick FORM iteration can be done using this quadratic polynomial as the LSF because it is much less demanding computationally than the analytical kriging. Through the FORM iteration a new design point can be

calculated around which some new values will be predicted, building an SRSM and proceed for the next iteration. This procedure algorithm is showed in Figure 3. An intelligent point from which the algorithm can be initiated (as in a normal FORM-HL optimisation algorithm) is the mean point (i.e. the mean value point for each variable). Following the *2k+1* combination rule for sampling we can get the *n* samples to build the SRSM.

$$x_{j,\ ith\ sample} = \mu_{x_j} + f\sigma_{x_j} \tag{15}$$

The *f* factor can be termed as 'amplitude' of the domain mapped by kriging and approximated by SRSM. This also gives the size of the area considered in the following FORM iteration. For this reason it can be considered as an 'horizon factor' giving a measure of how far the FORM iteration goes to search for the optimum point. The bigger f the farther the research can go and the quicker we can get to the optimum point since we do 'bigger steps' iteration by iteration. The smaller the horizon factor the closer we stay to the design point, the more accurate the approximation of the function, the smaller and more the steps towards the optimum point. In this second case the simulation time will definitely increase but the accuracy of the result obtained will be higher. A sensitivity study on this factor has been carried out with values from 0.001 to 1.8 and good results have been obtained with values between 0.2 and 0.4.

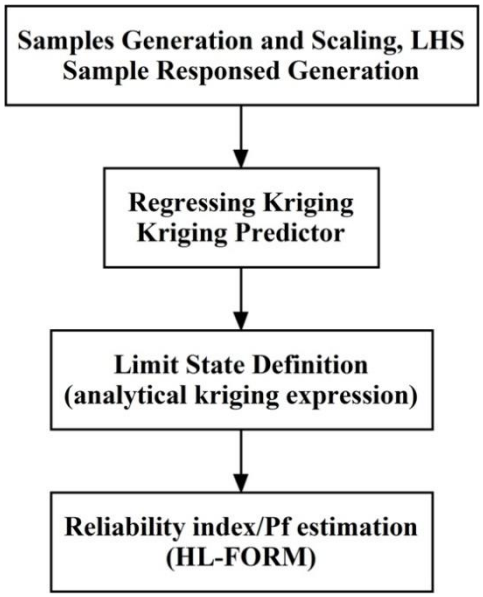

Figure 2. Analytical kriging-FORM

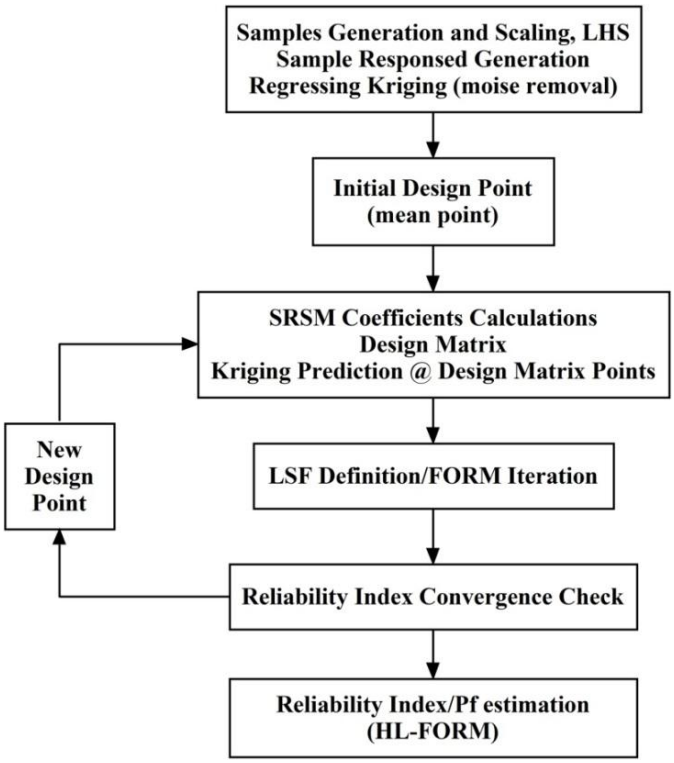

Figure 3. Dynamically kriged RSM algorithm

algorithm

6 Uncertainty of pipe flow systems

6.1 Description of the reference system

For the scope of this study, a system has been modelled initially deterministically using different tools for validation purposes: Matlab and Pipe Flow Expert 2010. Since both a global solution of the system (from differential pressure to flow rate) and a partial solution (from flow rate and one pressure to the missing one) are needed, two generic analytical models were developed. The models built in Matlab are based on well-known fluid mechanics basic equations. Having a system, or a sub-system, delivering a flow from an inlet node to an outlet node its geometry can be defined specifying the basic quantities: length *L*, elevation *h*, diameter *D*, roughness ε, number and type of bends and valves, component losses k_{comp}, pump characteristic, pressure, flow rate and temperature. The elevation is considered positive if increasing moving from the inlet node to the outlet node. The pipe roughness is dependent from the material and can change during the system life introducing a source of uncertainty. Bends and valves in a piping system have a significant variability and building a code taking into account even half of them is first of all useless and second of all too cumbersome. A free variable is introduced where a total sum of all other component losses can be considered. A pump characteristic can be defined with half a parabolic curve symmetrical to the y-axis and concave downwards, hence only two coefficients are needed to define its behaviour (pump head vs. flow rate). No heat loss is considered from the pipe (temperature constant). Table 1 presents the statistical properties of the stochastic variables while Figure 4 illustrates the PID of the reference flow system.

Table 1. Typical Coefficients of Variation

	CoV	**Reference**
Pressure	0.50%	[8]
Temperature	0.20%	[8]
Flow rate	0.50%	[8]
Roughness	10.9%	[23]
Level	0.5%	[12]
Pump characteristic	10.1%	[1]
Valve pressure drop	1.54%	[22]

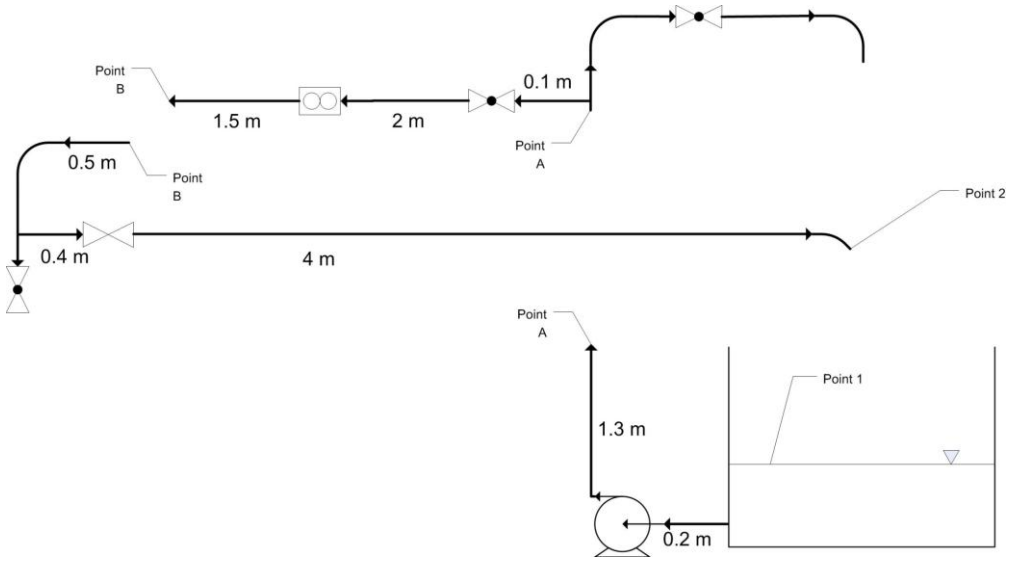

Figure 4. One phase-flow system

6.2 Limit states considered

For the safe and efficient operability of a pipe flow system all failure modes need to be investigated. In this work 4 different scenarios exploring 3 failure modes can be identified: maximum allowable pressure (in a pipe and in a flange-gasket-flange, point A and B respectively), minimum efficiency allowable for the pump, minimum pressure difference for pressure-driven flow. Limits for scenario 1A and 1B are taken from pipe characteristic catalogues and set to 280,000 Pa and 200,000 Pa respectively, limit for pump efficiency is set to 61% and the one for scenario 3 is set to the condition of having more than atmospheric pressure at outlet point.

6.3 Simulation Results and Discussion

Figure 5 and 6 show the results from the techniques employed and developed. As it can be shown, simple SRSM-FORM can estimate well the reliability index in some of the scenarios but not for 1B where the probability of failure is largely under-estimated. Focusing on this and trying to understand if the low accuracy is introduced by SRSM or by FORM further analyses have been carried out excluding those two techniques once at a time. Using SRSM-MCS results are still insufficient but better than previously, implying that inaccuracy is due to SRSM. Performing analysis using kriging and MCS this trend can be confirmed. Removing both SRSM and MCS from the analyses combining kriging and FORM using the innovative and previously illustrated techniques the results match the ones obtained through direct MCS.

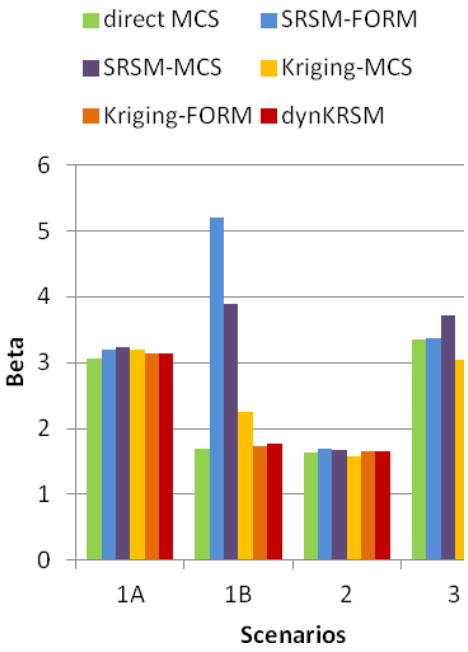

Figure 5. Safety index results

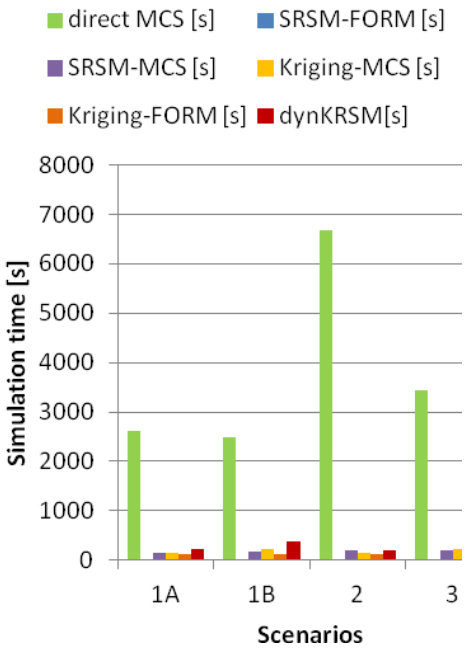

Figure 6. Computation time (sec)

It can also be concluded that Dyn-KRSM and kriging-FORM methods present a simulation time comparable to the surrogates MCS and largely lower than direct simulation. Analysing scenario 1A only and formulating the LS in order to explore more extreme situations (limit pressure moved up to 327,000 Pa) it is possible to test the ability to accurately calculate lower probabilities of failure of the newly developed methodologies. Benchmarking is still done using MCS up to 10^7 runs as seen in figures to follow (Figure 7 and 8).

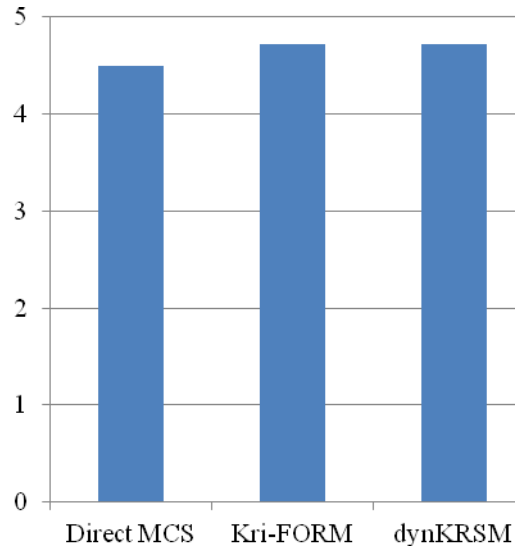

Figure 7. Safety index results for high β calculation

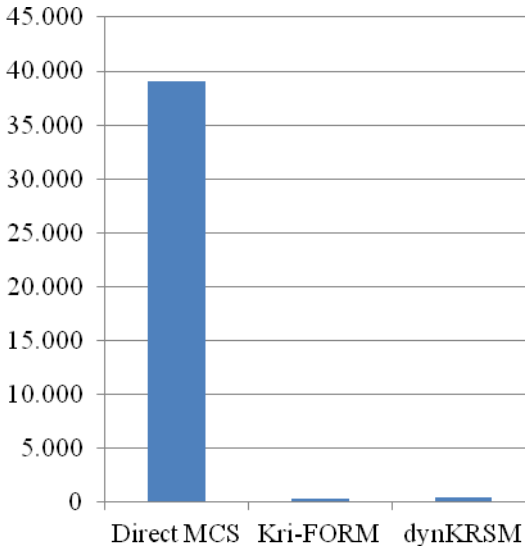

Figure 8. Simulation times for high β calculation (sec)

7 Conclusions

This paper has documented probabilistic assessment methods combining stochastic response surface and surrogate modelling methods to MCS and FORM methods for assessment of uncertainties. The methods developed extent current practice coupling kriging with FORM and suggesting a combination between kriging and SRSM in order to allow estimation of very low probabilities of failure in relatively simple to model non-intrusive methods.

Application of the method in a typical single flow pipe system has shown that the newly proposed methods perform very well both in aspects of accuracy and in computation requirements. The same method has already been applied by the authors for the case of a two phase flow system and highly non-linear limit states with similarly good performance.

8 References

[1] *ISO 9906:2012. Rotodynamic pumps - Hydraulic performance acceptance tests- Grades 1*(2012), .

[2] Alfon, P., Soedarsono, J.W., Priadi, D. and Sulistijono, (2012), *Pipeline material reliability analysis regarding to probability of failure using corrosion degradation model*.

[3] Bai, Y., Moe, E. T. and Mork, K. (1994), "Probabilistic assessment of dented and corroded pipeline", *Proceedings of the International Offshore and Polar Engineering Conference*, Vol. 2, pp. 93.

[4] Bai, Y. and Referex (2001), *Pipelines and risers*, Elsevier, Amsterdam.

[5] Belov, D.A., Coupe, P., Fukuhara, M. and Myalo, E.V., (2011), *Material-loss estimation for pipes*.

[6] Choi, S., Grandhi, R.V., Canfield, R.A. and SpringerLink, (2007), *Reliability-based structural design*, Springer, London.

[7] Edwards, John, Mork, K., Norske, D. and Sydberger, T. (1996), "Reliability Based Design of CO2 Corrosion Control", 24-29 March 1996, NACE International, .

[8] Elster Metering , available at: http://www.elster.com/en/index.

[9] Fleming, K. N. (2004), "Markov models for evaluating risk-informed in-service inspection strategies for nuclear power plant piping systems", *Reliability Engineering & System Safety*, vol. 83, no. 1, pp. 27-45.

[10] Forrester, A. I. J., Sóbester, A. and Keane, A. J. (2006), "Optimization with missing data", *Proceedings of the Royal Society A: Mathematical, Physical and Engineering Sciences*, vol. 462, no. 2067, pp. 935-945.

[11] Forrester, A.I.J., Sóbester, A. and Keane, A.J., (2008), *Engineering design via surrogate modelling*, Wiley, Chichester, UK.

[12] Fulford, J. M., et al. (2006), *Accuracy of radar water level measurements, available at www.waterlog.com/media/pdfs/USGS-Study.pdf, accessed August 2012*.

[13] Hasofer, A. M. and Lind, N. C. (1973), *An exact and invariant First-Order Reliability format*, Solid Mechanic Division, University of Waterloo, Waterloo, Ontario, Canada.

[14] Jeong, S., Yamamoto, K. and Obayashi, S. (2004), "Kriged-Based Probabilistic Method for Constrained Multi-Objective Optimization Problem", *AIAA Journal,* , no. 6437.

[15] Jones, D. R. (2001), "A Taxonomy of Global Optimization Methods Based on Response Surfaces", *Journal of Global Optimization*, vol. 21, no. 4, pp. 345-383.

[16] Khuri, A.I., (2001), *An overview of the use of generalized linear models in response surface methodology*.

[17] Melchers, R. E. (1999), *Structural reliability analysis and prediction*, 2nd ed, John Wiley, Chichester.

[18] Onoufriou, T. and Frangopol, D. M. (2002), "Reliability-based inspection optimization of complex structures: a brief retrospective", *Computers & Structures*, vol. 80, no. 12, pp. 1133-1144.

[19] Proia, S. and Kolios, A. (2012), "Reliability assessment of complex structures in composite materials under stochastic loading", *World Journal of Mechanics*, vol. 2, pp. 162-170.

[20] Queipo, N. V., Haftka, R. T., Shyy, W., Goel, T., Vaidyanathan, R. and Kevin Tucker, P. (2005), "Surrogate-based analysis and optimization", *Progress in Aerospace Sciences*, vol. 41, no. 1, pp. 1-28.

[21] Quinio, A. and Kolios, A. (2010), "A stochastic finite element based approach to the design optimization of a truss structure.", *International Probabilistic Workshop*, The Netherlands, .

[22] Sandalci, M., Mançuhan, E., Alpman, E. and Küçükada, K. (2010), "Effect of the flow conditions and valve size on butterfly valve performance", *Isi Bilimi Ve Teknigi Dergisi/ Journal of Thermal Science and Technology*, vol. 30, no. 2, pp. 103-112.

[23] Wyant, J. C. and Creath, K. (1990), "Absolute measurement of surface roughness", *Proceedings of SPIE - The International Society for Optical Engineering*, Vol. 1319, pp. 568.

Probability of corrosion detection with small anodes

Sylvia Kessler, Christoph Gehlen
Centre for Building Materials, TU München, Germany

Abstract: For realistic and accurate description of the corrosion progress in reinforced concrete structures, the inspection results from detection of on-going corrosion are of vital importance, in particular for the probabilistic service life prediction. The crucial factor of the combination of inspection data and probabilistic service life prediction is the knowledge about the accuracy of the measurement method itself. The Probability of Detection (PoD) is a main descriptor of the accuracy of qualitative inspection methods. Commonly, a PoD curve describes the rate of detecting a defect with given defect size s, PoD(s). In the case of potential mapping, the defect size is the anode area. In this research, an approach based on numerical models is pursued to obtain a PoD of potential mapping for small anode areas. It is expected that through the integration of the potential mapping data the condition of the structure and correspondingly the service life time can be predicted more accurately.

1 Background

The corrosion of the reinforcement is often the major cause for the end of service life of reinforced concrete structures. When cracks due to corrosion are visible, the deterioration process is already advanced and cost intensive repair is necessary. The only measurement method, which is able to distinguish non-destructively between active or passive reinforcement before cracks occur, is the potential mapping method. Figure 1 shows a modified Tuutti diagram with the degree of deterioration due to corrosion in dependence of time.

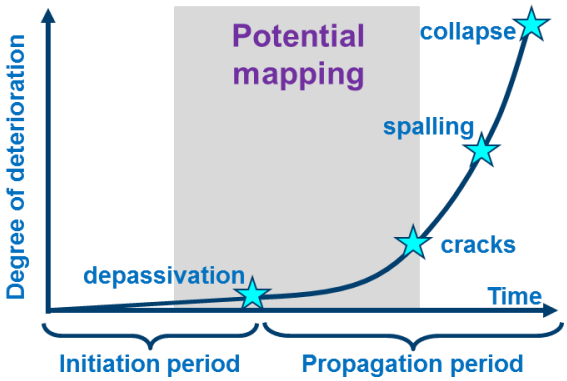

Figure 1. Modified Tuutti diagram with the optimal application time for potential mapping

The grey background indicates the time-span respectively the condition stage of a structure when the application of potential mapping makes sense. It is unreasonable to apply potential mapping at an early structure age because it takes time till depassivation of the reinforcement starts. On the other hand when cracks due to corrosion are visible it is too late for a cost-effective and pro-active maintenance strategy [5].

Additionally potential mapping results indicate whether and where the probabilistic service life models for the initiation period [1] or for the propagation period [10] have to be applied for a comprehensive service life prediction. But first an update of the actual service life prediction with the inspection data of potential mapping has to be performed applying Bayes' rules according to equation (1) [7].

$$\Pr(condition \,|\, inspection) = constant \cdot \Pr(inspection \,|\, condition) \cdot \Pr(condition) \tag{1}$$

The Bayesian approach can combine pre-existing knowledge coming from service life prediction, Pr(*condition*), with inspection data represented by the likelihood function Pr(*inspection* | *condition*) and allows updating the prior knowledge. In the present case the likelihood function can be described as Pr(*potential mapping results* | *corrosion condition state*). This likelihood function is the probability of detection of potential mapping. This paper presents an approach to evaluate the probability of detection of potential mapping to enable the updating of service life predictions.

1.1 Potential mapping

Potential mapping is an effective inspection method for detecting active corroding areas in reinforced concrete structures. During potential mapping po-

tential differences are measured between an external reference electrode and the reinforcement (Figure 2, left). With grid-like displacement of the reference electrode potential differences of a whole structural element can be gathered. The detection of corroding areas is possible due to the fact that passive and active surfaces of the reinforcement are different electrodes, which vary in free corrosion potential and polarisability. If conductivity and oxygen level in concrete is sufficiently high, active-passive elements will be developed and their potential differences can be measured at the concrete surface.

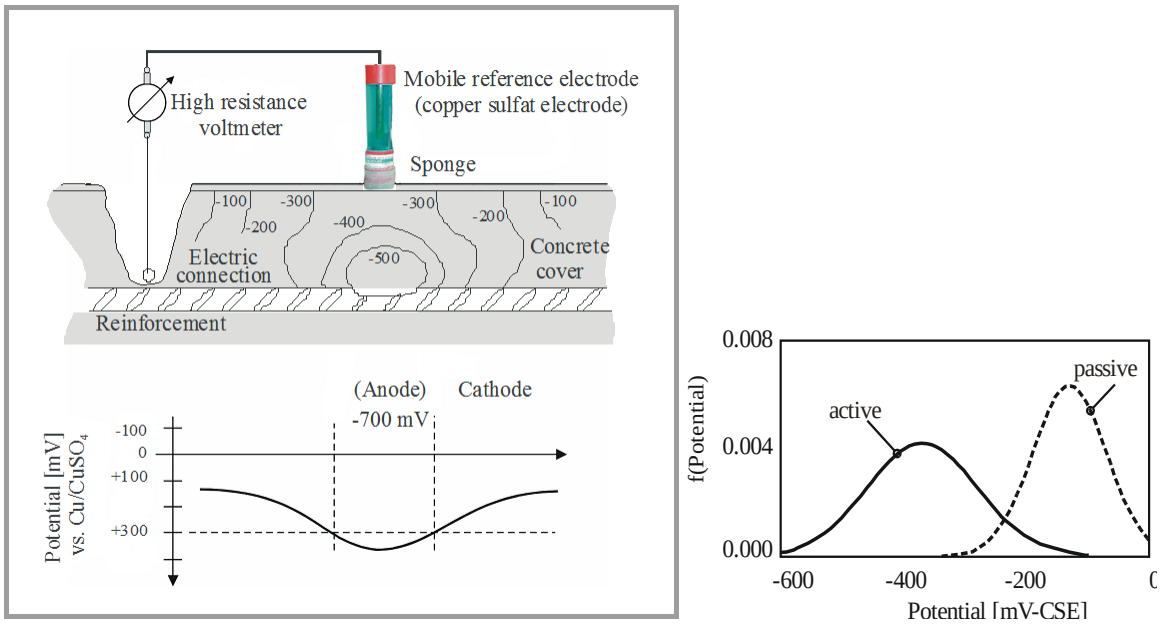

Figure 2. Principal scheme of potential mapping measurement (left), active and passive density functions of potential differences (right)

The aim of the evaluation of potentials is to distinguish where the reinforcement is either active or passive. All potential differences have to be divided into an active and a passive potential difference density (Figure 2, right) by using the Maximum-Likelihood-Estimate (MLE) [1]. It is assumed that both densities are normally distributed.

Low potentials are an indicator for corrosion and with increasing potentials, the probability of corrosion decreases. Figure 2 (right) shows a domain where the active and the passive distribution overlap each other. In these areas there is a higher probability of planning the wrong measures: either a repair is executed although it is not necessary or a wrong all-clear may bring further damages and additional costs in future.

1.2 Evaluation of qualitative test results

For qualitative test methods, as the potential mapping is one of them, the probability of detection (PoD) is the determining factor for describing the

measurement accuracy. The higher PoD, the higher is the reliability of potential mapping. The probability can also be expressed by a probability of detection curve and the curve is defined by the rate of detecting a defect with defect size s, PoD(s), like the anode area in the case of potential mapping.

It is necessary to compare potential measurements of reinforced structures with the true corrosion condition state to obtain a PoD curve for potential mapping. During the comparison of the true corrosion condition state with the inspection result four indications (TP, FN, TN, FP) are possible (Figure 3).

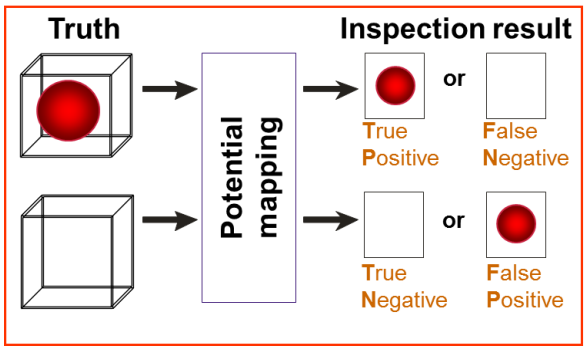

TP: "true positive" indication = present defect correctly indicated (hit)
FN: "false negative" indication = present defect not indicated (miss)
TN: "true negative" indication = not present defect correctly indicated
FP: "false positive" indication = not present defect indicated (false alarm)

Figure 3. Comparison: true condition state – inspection result [4]

After the comparison of the true condition state with the inspection result the probability of detection can be calculated according to equation (2).

$$PoD = P(positive\ \det ected / true\ positive) = \frac{Number\ of\ true\ positive}{Number\ of\ true\ positive + Number\ of\ false\ negative} = \frac{TP}{TP + FN} \quad (2)$$

Figure 4 presents possible resulting PoD(s) curves. The left side shows a perfect inspection which is a step function and the right side shows a PoD(s) of an imperfect inspection which is normally influenced due to the probe, the operator, the procedure etc..

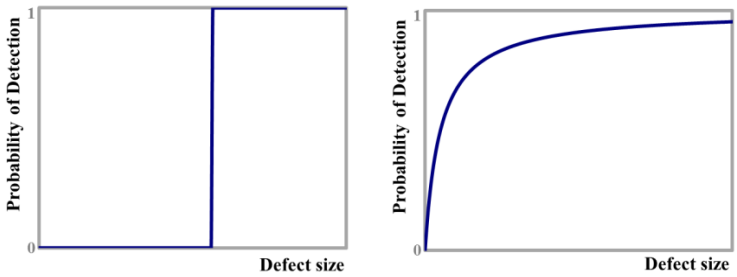

Figure 4. Examples of possible PoD(s) curves [9]

The true corrosion condition state is only identifiable by replacement of concrete cover and visual inspection of the reinforcement. In general, owners will not agree to open a whole structure for evaluating the accuracy of an inspection method. As a solution to this problem a numerical approach is used for evaluating the PoD of potential mapping.

1.3 Numerical modelling of potential fields

Basically the corrosion processes inside an electrolyte and so the resulting potential distributions are controlled by two different physical laws. The first law is known as Ohms law (equation (3)). This law describes the flow of an electrical charge in a medium as a result of a potential field. The current density is proportional to the gradient of the potential and inversely proportional to the resistivity. The Laplace-equation (equation (4)) is the second law. This equation calculates the propagation of the potentials field under steady-state conditions.

Ohms law:
$$\vec{i} = -\frac{1}{\rho}\nabla\Phi \tag{3}$$

Laplace-equation for the electrolyte:

$$\Delta\Phi = 0 \tag{4}$$

with Φ potential [V]
$\vec{i}$ current density [A/m²]
ρ resistivity [Ωm]

The Laplace equation is a partial differential equation of second order. An analytical solution for this equation can only be derived in case of certain geometries and boundary conditions. This is not possible for arbitrary geometries; one has to use numerical means to calculate an appropriate approximation [15].

The kinetics of the chemical reactions at the interface between concrete and steel can be quantified by current density-polarization-curves (equation (5)).

$$i_N = f(\Phi) \tag{5}$$

with i_N current density [A/m²]

These curves describe how much current is produced or consumed at the steel surface as a function of potential. These functions are usually non-linear and represent the boundary conditions for the solution of the Laplace-equation.

They can be obtained by experimental testing. Usually the polarization curves are different for active and passive areas of the reinforcement.

The advantage of numerical simulation is that the corrosion condition of numerical models can be varied. The presented numerical calculations are realized with the Boundary Element Method software BEASY [17]. This simulation software is validated in [6], [8] and [13].

2 Probability of detection of potential mapping

2.1 Numerical model

One of the most important chloride exposed construction component is a reinforced concrete plate like a bridge deck or a garage ceiling. Therefore it was decided to model the probability of detection of a plate first. That's why the numerical model is comparable to a section of a reinforced concrete plate. The dimension of the numerical model has to be bigger than the expansion of the macro cell element of the corrosion process. This condition is fulfilled when no corrosion current takes place at the model boundary. Otherwise the modelled corrosion process would be limited by a lack of cathodic areas and this case isn't realistic for plates.

The expansion of the macro cell element is approximately 1.0 m according to Warkus [13]. The anode area is located at the centre of the model. So taking into account the expansion of the macro cell element the quadratic numerical model has a side length of 2 m. The model contains four reinforcement layers with a diameter of 10 mm and a rod distance of 20 cm. Figure 5 shows the numerical model.

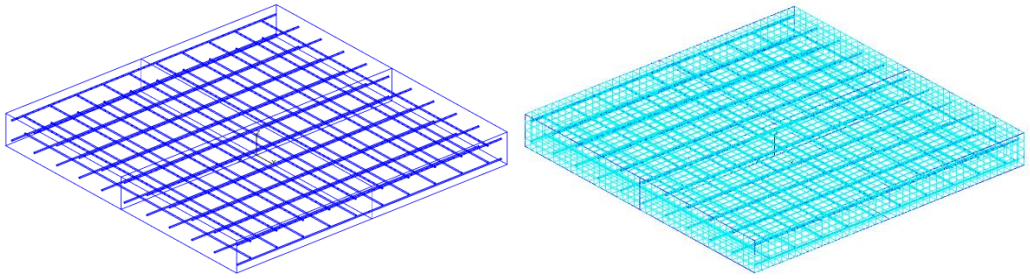

Figure 5. Numerical model of the section of a reinforced concrete plate (left), with elements (right)

It is modelled only a quarter of the plate to take the advantage of the model symmetry. Figure 6 presents a typical result of a numerically simulated potential field.

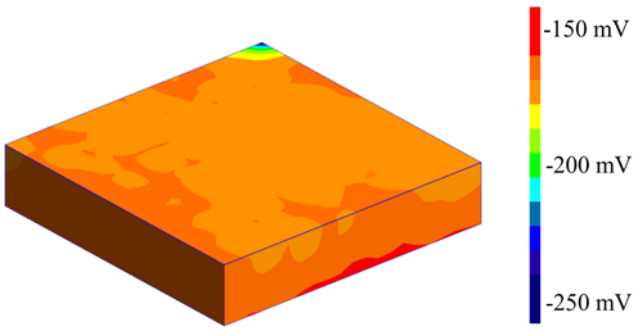

Figure 6. Numerical determined potential field of the quarter section of a reinforced concrete plate

Polarization curves are input parameters to simulate the electrochemical behaviour at anodic and cathodic areas at the metal surface. The chosen polarization curves were taken from literature [1]. The polarization curves were determined potentiodynamically with a velocity of 1 mV/s. According to the climate of exposed structures the anodic polarization curves of 76 % relative humidity and 10°C were chosen. The cathodic polarization is dependent on the oxygen availability at the reinforcement and the oxygen availability is correlated to the humidity. Concrete is not a homogenous electrolyte and the humidity changes from place to place. So four different cathodic polarization curves (100 %, 93 %, 76 %, 66 % RH) were distributed over the numerical model. The mean driving potential averages 380 mV according to [16].

Several factors are influencing the potential field measurement [6] and so these factors are also influencing the probability of corrosion detection. The influencing factors which can be analysed numerically are varied in this research according to Table 1.

Table 1. Variation of the numerical input parameters

Parameter	Unit	Variation
Concrete cover	mm	10, 20, 30, 40, 50
Concrete resistivity	Ωm	100, 400, 700
Anode area	cm²	0.78, 1.56, 2.3, 3.1, 3.9

The values for the concrete cover are in the range of real concrete covers from poor construction work up to structures which were built in accordance with the design standards. The concrete resistivity values represent structures exposed to weathering with ordinary Portland cement CEM I as well as blast furnace cement CEM III [11]. The element size for the discretization of the numerical model determines the anode area variation.

Besides all these influencing material parameters the procedure of the potential mapping especially the grid size and the grid size combination have to be

taken into account. It is evaluated if the reference electrode is placed directly above the anode or as far as possible. The grid size combination is also relevant for the probability of detection. The grid size X x X_Y appendix "Y" indicates the position between anode and reference electrode. The appendix "0" means that the reference electrode is placed directly above the anode (Table 2).

Table 2. Parameters of the evaluation of the grid size

Parameter	Unit	Variation	Distance anode – reference electrode
Grid size	cm²	5 x 5; 10 x 10; 15 x 15; 25 x 25	
X x X_0	cm²		0
X x X_1	cm²		5
X x X_2	cm²		10
X x X_3	cm²		15

The guideline B3 [3] of potential mapping recommends a standard grid size of 0.25 x 0.25 m² and at most a grid size of 0.5 x 0.5 m². In the technical bulletin of SIA [14] grid sizes are between 0.15 x 0.15 m² and 0.25 x 0.25 m² for field measurements. RILEM [12] states grid sizes of 0.15 x 0.15 m². These grid sizes are recommended for the reason that even small corroding areas can be detected with potential mapping. But a quantitative investigation about the ideal grid size in dependence of material condition is missing in literature. That's why a huge range of grid sizes is analysed.

2.2 Numerical evaluation of PoD

The evaluation of the simulated parameter study is performed by the following procedure. The elements from the surface of the model, which are situated directly above the anode, were defined as indicators of corrosion – True state (see Figure 3). Than the potentials from the surface was analysed like shown in Figure 2 and the threshold potential is determined to $U_{threshold}$ = -180 mV. Than the decision of the threshold potential was compared to the true state of the model. This comparison was made with each surface element.

Figure 7 summarises the PoD values in dependence of the chosen grid sizes (5 x 5; 15 x 15; 25 x 25 cm²) with resistivity R = 400 Ωm and concrete cover d_c = 50 mm.

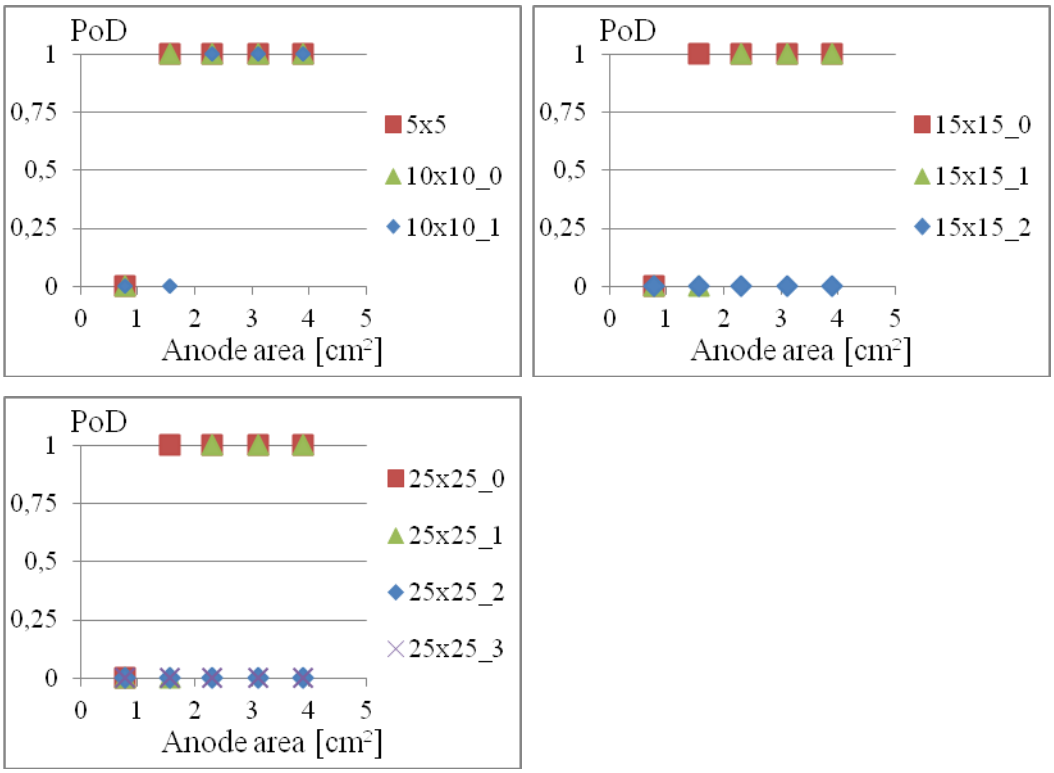

Figure 7. PoD in dependence of the grid size: Resistivity R = 400 Ωm, concrete cover d_c = 50 mm

The PoD value is always 0 or 1. Under the simulated conditions the PoD of potential mapping is a perfect PoD curve according to [9] (Figure 4 left).

The PoD values strongly depend on the grid size. The detectability of corrosion decreases with increasing grid size. Anode areas with 1.56 cm² are detectable if the reference electrode is placed above the location of corrosion (grid size combination X x X_0). But with increasing grid size and increasing distance between reference electrode and anode the corroding areas in the simulated range cannot be indicated.

Figure 8 shows the PoD results with varying concrete resistivity.

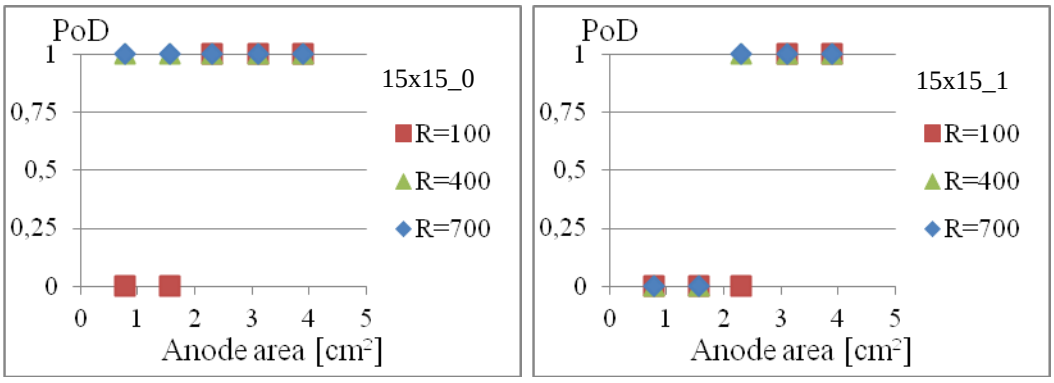

Figure 8. PoD in dependence of the resistivity: concrete cover d_c= 40mm, grid size 15 x 15_0 cm² (left side); 15 x 15_1 cm² (right side)

The detectability of anode areas decreases with low concrete resistivity (100 Ωm). Anode areas lower or equal than 1.56 cm² cannot be detected when the resistivity is 100 Ωm even when the reference electrode is placed directly above the anode. If the resistivity is higher than 400 Ωm its impact on the PoD is negligible. This effect can be explained due to the expansion of the potential field in concrete. If the resistivity is low more cathodic areas will be activated further away from the anode. As a conclusion the equipotential lines are very flat and the potential gradient on the concrete surface is relatively weak. Conversely, high resistivity leads to pronounced gradients at the concrete surface and to a better PoD. So, with lower resistivity a smaller grid size is required to achieve a high detectability.

The following Figure 9 presents the PoD in dependence of the cover depth.

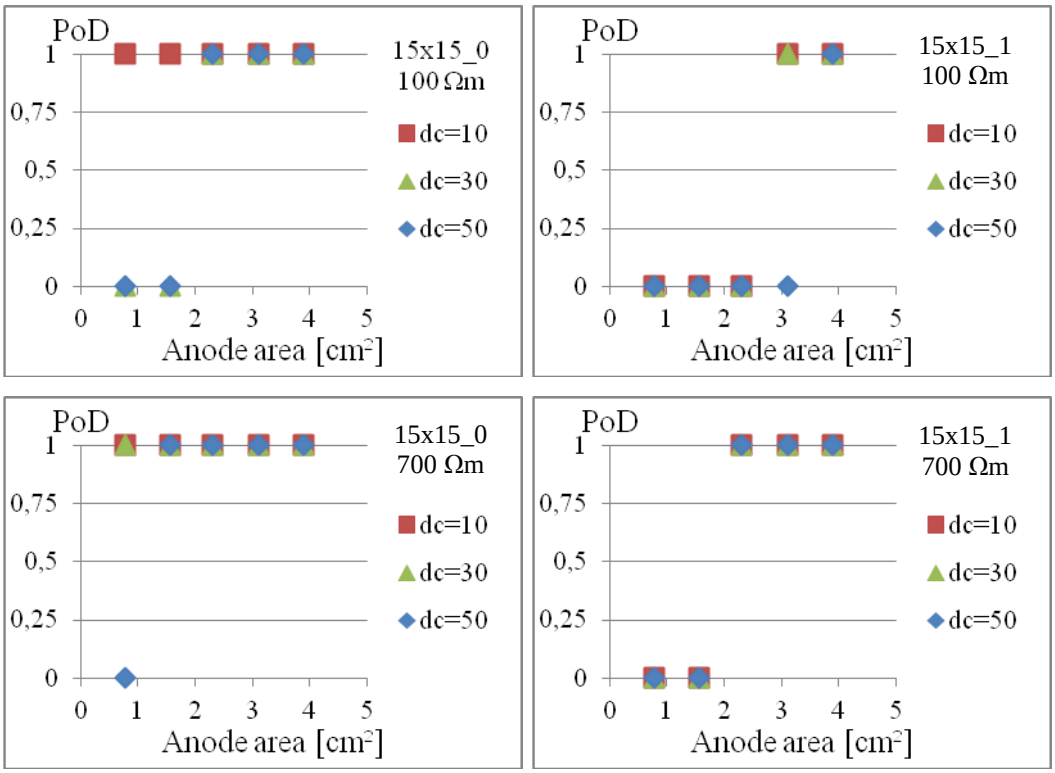

Figure 9. PoD in dependence of the concrete cover: resistivity R = 100 Ωm (above), R = 700 Ωm (below) grid size 15 x 15_0 cm² (left side); 15 x 15_1 cm² (right side)

The PoD values also depend on the concrete cover. But this effect has minor impact and is connected to the concrete resistivity. The detectability arises with smaller concrete cover and higher concrete resistivity. So the influence of the concrete cover is only noticeable with lower concrete resistivity.

3 Conclusions and outlook

This paper presents a numerical approach to evaluate the probability of detection of small anodes with potential mapping. The probability of detection is analysed in dependence of concrete cover, concrete resistivity, grid size and grid size combination.

Under the simulated boundary condition the PoD seems to be a perfect one its values are always 0 or 1. It wasn't always possible to achieve PoD(s) = 1 with the simulated variations. So, bigger anode areas have to involve in the numerical evaluation to determine all PoD boundaries.

Major influence on the PoD has the grid size and the grid size combination. The PoD values increase with smaller grid size and with lower distance between anode area and reference electrode. The impact of the concrete resistivity is negligible for high resistivity. But low resistivity leads to poor detectability. The concrete cover has only an impact in combination with low resistivity. As a result the measurement procedure is more important than the concrete characteristics. The results from this numerical parameter study show, that a grid size of 10 x 10 cm² is reliable to detect small anode areas under the chosen boundary conditions for low resistivity and a grid size of 15 x 15 cm² for high resistivity. But for all investigating structures the question arises: which anode area has to be detected because of its risk for the load bearing capacity? When the engineer has solved this question he can adapt the necessary grid size in dependence of the concrete characteristics.

In the used numerical model the concrete properties like resistivity or concrete cover are totally homogenous. But in reality no concrete has this characteristic. It is assumed that with increasing inhomogeneity the probability of detection decreases and the PoD of a perfect inspection changes into an imperfect one.

Besides the varied factors other influencing factors like the rod distance, structural geometries (columns, walls) or carbonated layers have to be investigated.

For reasons of simplicity as a preliminary test case it was considered one single anodic area. Now, it has to be investigated the interaction of different anode areas in one system and their resulting potential field. The following question rises up: Is the probability of detection of potential mapping sensitive enough for small anodes, when several anodes are in the neighbourhood?

Naturally the PoD has to be validated at existing concrete structures in the next step. The final aim is to describe the probability of detection of potential

mapping mathematically in dependence of their most influencing parameters. When this aim is achieved it simplifies the updating of service life prediction with potential mapping data.

4 References

[1] Brem, M. (2004) *Numerische Simulation der Korrosion in Stahlbetonbauteilen*, Diss. ETH Nr. 15567, Zürich

[2] Ditlevsen, O.: Uncertainty modeling: With applications to multidimensional civil engineering systems. New York: McGraw-Hill, 1981. – ISBN 0-07-017046-0

[3] DGZfP Merkblatt B3 2008 *Elektrochemische Potentialmessungen zur Detektion von Bewehrungsstahlkorrosion* (in German)

[4] Gehlen, C.: *Probabilistische Lebensdauerbemessung von Stahlbetonbauwerken – Zuverlässigkeitsbetrachtungen zur wirksamen Vermeidung von Bewehrungskorrosion* Dissertation, RWTH Aachen (in German), 2001

[5] Gehlen, C. et al.: *Condition Control and Assessment of Reinforced Concrete Structures Exposed to Corrosive Environments (Carbonation / Chlorides)*, fib bulletin 59, 2011

[6] Keßler, S.; Ebell, G.; Gehlen, C.; Burkert, A.: Die Aussagegenauigkeit der Potentialfeldmessung, In, *Beton- und Stahlbetonbau* Volume 106, Issue 7, p. 481–489, 2011 (German)

[7] Keßler, S; Fischer, J.; Straub, D.; Gehlen, C.: Updating of service life prediction of reinforced concrete structures with potential mapping, ICDC, *International conference on durability of concrete*, Trondheim Norway June 18-21, 2012

[8] Kessler, S.; Gehlen, C. (2010) Potential mapping – Possibilities and limits 8th fib PhD Symposium in Kgs. Lyngby, Denmark

[9] MIL-HDBK-1823A, Department of Defense Handbook, Nondestructive Evaluation System Reliability Assessment, 7. April 2009

[10] Osterminski, K.; Schießl, P.: Design model for reinforcement corrosion. *Structural Concrete*, Vol. 13, No. 3, 2012.

[11] Osterminski, K., Tian, W., Schießl, P., Gehlen, C.: Elektrolytwiderstand von Beton und Korrosion in gerissenem Beton. In: „Dauerhaftigkeitsbemessung von Stahlbetonbauteilen auf Bewehrungskorrosion – Teil 1: Systemparameter der Bewehrungskorrosion“ *Schriftenreihe des Deutschen Ausschusses für Stahlbeton e. V., Heft 601*, Beuth Verlag, Berlin, 2012 (German).

[12] RILEM Technical Committees Elsener, B. Andrade, C. Gulikers, J. Polder R. and Raupach, M. 2003 Half-cell potential measurements – potential mapping on reinforced concrete structures. *Materials and Structures*, 36: 461–471

[13] Schießl, P., Osterminski, K., Isecke, B., Beck, M., Burkert, A., Raupach, M., Harnisch, J., Warkus, J., Tian, W.: Deterioration model and input parameters for reinforcement corrosion. *Structural Concrete*, Vol. 13, No. 3, 2012.

[14] SIA 2006 *Durchführung und Interpretation der Potentialfeldmessung an Stahlbetonbauteilen* Zürich (in German)

[15] Warkus, J.; Raupach, M.; Gulikers, J. (2006), Numerical modeling of corrosion – Theoretical backgrounds - *Materials and Corrosion, 57, No. 8*

[16] Warkus, J. Raupach, M. (2009) Modelling of reinforcement corrosion – geometrical effects on macrocell corrosion, *Materials and Corrosion, 61, Issue 6, p. 494–504*

[17] www.beasy.com

Investigation of Reliability Model for Cracking in South African Reinforced Concrete Water Retaining Structures

C.H. M^{c}Leod, J.A. Wium, J.V. Retief
University of KwaZulu-Natal, Durban & University of Stellenbosch, Cape Town, South Africa

Abstract: The development of a design code of practice for concrete water retaining structures (WRS) in South African is presently underway, along with the revision of the code of practice for reinforced concrete structures (SANS 10100). This paper discusses part of the research undertaken in the development of the new design code for WRS, namely, the serviceability limit state of cracking due to loads and/or restrained deformations. The basic crack model considered here is that utilized by Eurocode EN1992-1-1 (2004) and EN1992-3 (2006) which predicts the maximum crack width using a basic compatibility relationship between strain and cracking. This crack width is then compared to a limiting crack width value. A reliability model for load-induced cracking is presented in this paper using the EN1992 crack model applied to South African conditions. The influence of the variables, including model uncertainty on the reliability of the crack model is investigated.

1. Introduction

This paper presents a portion of the research carried out in the development of a South African design standard for water retaining structures (WRS). South African designers currently use the British codes in the design of reinforced concrete water-retaining structures (WRS) as a South African design code for WRS does not exist at present.

As the serviceability limit state (SLS) of cracking tends to be dominant in the design of WRS, with failure to meet this limit state resulting in a loss of function of the structure, a reliability model was developed to assess the EN1992 crack model [5] for cracking due to loading effects applied to South African conditions, using

the First Order Reliability Method (FORM). This paper presents the investigation of the parameters of the reliability model for cracking in reinforced concrete. Two cases of load-induced cracking were considered, namely, those due to pure tension and pure bending. SANS10160-2011[12] was referred to in determining the loads and serviceability reliability levels for the crack model, with SANS10100-2000[10] used as the basis for the material properties used in the model. The reliability crack models were set up and analysed using Microsoft EXCEL.

2. Development of reliability models for tension and flexural cracking

Limiting crack width

The current practice in designing WRS for SLS cracking in South Africa using BS8007 [3] is to specify a limiting crack width of 0,2 mm. A limit of 0,1 mm may also be used, for aesthetic concerns. EN1992-3[6] specifies limits from 0,2 mm to 0,05mm depending on the hydrostatic ratio of depth of water to wall thickness (h_D/h) for cracks passing through the section and where the existence of a compression zone cannot be guaranteed. Therefore the results of reliability analyses with crack widths of 0,2 mm, 0,1 mm and 0,05mm are presented here.

Structural configuration of models for tension and flexural cracking

Representative structural models were used for both serviceability pure tension and flexural cracking in a WRS. The load case considered was for a permanent load due to hydrostatic pressure to SANS10160-2011 [12].

2.2.1 Example of pure flexure in a WRS

For the flexural case, consider a 1 m section of wall of a rectangular reinforced concrete water-retaining structure, designed as a vertical cantilever. The wall is subject to flexure about a vertical axis due to water pressure. The maximum liquid load is $L_k = H.\ \gamma_w$ where γ_w is 9,81 kN/m^3. The wall height (H) was taken as 5m and 7m, resulting in water pressures of 49,1 and 68,7 kN/m^2 per m of wall and corresponding maximum bending moments of 204,6 and 401,0 kNm.

2.2.2 Example of pure tension in a WRS

For the tension case, a 1 m section of wall in a circular reservoir is considered. The

wall is subject to hoop tension due to water pressure (L_k) in the horizontal plane. A reservoir diameter of 28 m is selected. The maximum nominal tensile forces of 686,7kN and 961,4 kN for wall heights of 5 m and 7 m, respectively, is obtained.

Development of limit state equation for reliability crack model

The first step in setting up the reliability model for cracking using FORM was to define the limit state (LS) equation. The SLS criterion for cracking will be met if the calculated crack width is less than the specified crack width limit. Thus the LS equation is:

$$g = w_{lim} - \theta . w_m \quad (1)$$

where w_{lim} is the limiting crack width, θ is model uncertainty and w_m is the crack width. The crack width, w_m, is determined from the basic compatibility equation,

$$w_m = S_{rm} \, . \, \varepsilon_m \quad (2)$$

where S_{rm} is crack spacing and ε_m is average strain.

The crack spacing S_{rm} is determined from the equation developed for EN1992, as described by BEEBY et al [1]:

$$S_{rm} = 2c + 0{,}25 k_1 k_2 \varphi / \rho_{p,eff} \quad (3)$$

where c is concrete cover, $k_1$is a coefficient for high tensile reinforcement bond, k_2 is a coefficient for stress distribution, φ is bar diameter and $\rho_{p,eff}$ is the effective reinforcement ratio.

The average strain for reinforced concrete as given by EN1992 [5] is:

$$\varepsilon_m = \varepsilon_{sm} - \varepsilon_{cm} = \frac{\sigma_s - k_t f_{ct,eff}(1+\alpha_e \rho_{eff})/\rho_{eff}}{E_s} \quad (4)$$

where ε_{sm} is steel strain, ε_{cm} is concrete strain, σ_s is steel stress, E_s is the steel modulus of elasticity, k_t is a coefficient for duration of loading, $f_{ct,eff}$ is effective concrete tensile strength and α_e is the modular ratio, $E_s/E_{c,eff.}$ The modular ratio, α_e, is the ratio E_s/E_c where E_c is the effective concrete modulus. The effective reinforcement ratio is defined as:

$$\rho_{p,\,eff} = A_s / A_{ct,eff} = A_s/(b.h_{c,eff}) \quad (5)$$

where A_s tension reinforcement area, $A_{ct,eff}$ is the effective area of concrete in tension, b is the cross sectional width and $h_{c,eff}$ is the effective depth of concrete in tension.

The effective depth of concrete in tension, $h_{c,\,eff}$, as defined by EN1992 [5], is the lesser of either (h – x)/3, h/2 or 2,5(h - d). In the flexural cracking case, (h – x)/3 was found to be limiting, while in the tension cracking case, the limiting equation was dependent on the combination of section thickness (h), concrete cover (c) and bar diameter (φ), being either h/2 or 2,5 (c + φ/2). Thus, as the former equation is in terms of the basic variable section thickness only and the latter in terms of the basic variable cover (and independent of section thickness), two reliability models were set up for tension cracking.

The equations (1) to (5) are expressed in terms of the basic random variables of section thickness (h), concrete cover (c), liquid load (L_k) and concrete tensile strength ($f_{ct,eff}$).

2.4 Parameters of the reliability crack model

Typical values used for the parameters of the reliability model were obtained from current industry practices in South Africa [13]. Statistical data was obtained from sources such as the JOINT COMMITTEE FOR STRUCTURAL SAFETY [8] and HOLICKY [7]. Table 1 summarises the statistical data used for all parameters in the reliability models for tension and flexural cracking. The reinforcement area (as a deterministic value) was used as the basis for comparison.

The database for model uncertainty with regard to concrete cracking is very small, so some assumptions were made based on the available information. A general value used for the model uncertainty coefficient of variation (CoV) is 0,1 in structural reliability models, as used by HOLICKY [7], and was taken to be the lower limit and the reference level. A maximum value of 0,3 has been suggested in research as being appropriate to cracking in reinforced concrete beams by QUAN et al [9] and was therefore considered here to be the maximum limit. To investigate the effect of model uncertainty variation on the cracking models, reliability analyses were performed for a range of values for the CoV from 0,1 to 0,3.

Level of Reliability, β

The level of reliability was measured using the FORM reliability index, β. The reference level in the study for β was 1,5, in keeping with that used by SANS10160 [12] for the irreversible serviceability limit state of cracking for a design life of 50 years. This is the same value as that recommended by EUROCODE [4].

Table 1: Basic variables used in reliability crack model

Variable	Symbol	Units	PDF	Characteristic Value	Mean μ_x	Std Dev. σ_x
Height of wall	H	m	Det	5	5	0
Water pressure, L_k	L_k	kN/m^2	N	49.1	49.1	2.45
Concrete cube strength	f_{cu}	MPa	Det	37	37	0
Concrete cylinder strength	f_{ck}	MPa	Det	30	30	0
Concrete tensile strength	$f_{c,t}$	MPa	LN	2.00	2.89	0.55
Concrete modulus (long term)	$E_{c,eff}$	GPa	Det	13.7	13.7	0
Steel modulus	E_s	GPa	Det	200	200	0
Concrete modulus (SANS10100)	E_c	GPa	Det	27.4	27.4	0
Concrete creep factor	ϕ	-	Det	1	1	0
Reinforcement diameter	φ	mm	Det	20	20	0
Reinforcement area	A_s	mm^2	Det	varied	varied	0
Wall thickness	h	mm	N	250 - 450	250 - 450	2.5 - 4.5
Wall width	b	mm	Det	1000	1000	0
Cover	c	mm	LN	40	40	6
Limiting crack width	w_{lim}	mm	Det	0.2 /0.1/0.05	0.2 /0.1/0.05	0
Model Uncertainty	θ_w	-	LN	1	1	0.1-0.3

Note: LN = log-normal PDF, N = normal PDF, Det = deterministic value.
Concrete strength to SANS0100 as cube strength, f_{cu} ($f_{ck} \sim 0{,}8\ f_{cu}$)

3. Results and discussion

Flexure

The results of the reliability analysis for flexural cracking showing the influence of the parameters of section thickness, crack width limit, liquid load and model uncertainty are presented as the required amount of steel to achieve the target reliability. Table 2 is a summary of selected data obtained from the analysis of the flexural model for a reliability index, β, of 1,5.

Table 2. Summary of reliability analysis data for flexural cracking for β of 1,5

H (m)	w_{lim} (mm)	h (mm)	CoV θ	$\%A_s$
5	0.20	250	0.10	1.43
5	0.20	450	0.10	0.372
			0.15	0.375
			0.20	0.377
			0.25	0.383
			0.30	0.387
5	0.10	450	0.10	0.61
			0.15	0.62
			0.20	0.63
5	0.05	450	0.10	1.06
			0.15	1.08
			0.20	1.12
7	0.20	450	0.10	0.93

3.1.1 Influence of section thickness, h

Referring to Figure 1, the gradients of the graphs steepen as section thickness increases.

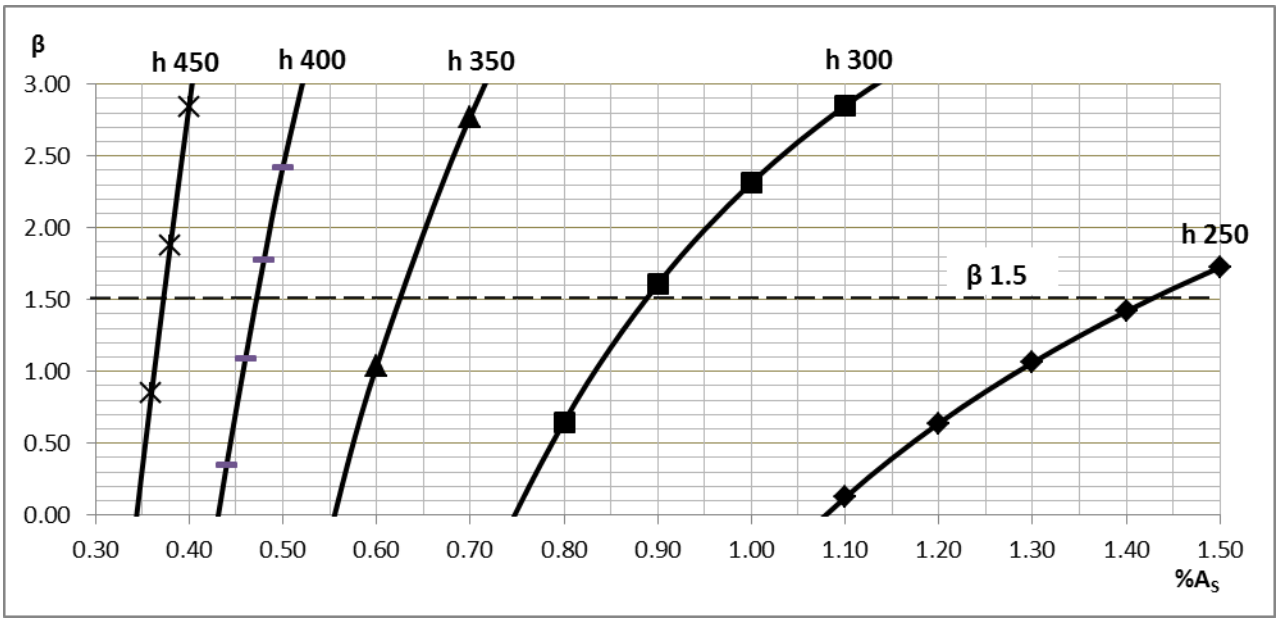

Figure 1. Effect of wall thickness on variation of reliability with reinforcement area (w_{lim} 0,2mm)

A given reinforcement will then result in a higher β for the thicker sections. Conversely, less reinforcement would be required for a 450 mm section than a 250 mm section to achieve the same level of reliability, with an associated small increase in cost. An optimisation process could be performed to determine the best combination of reliability and geometry. Section thickness is not considered to a dominant variable for the reliability of thicker sections under flexural loading.

3.1.2 Load due to water pressure, L_k

The height of the wall, H, and thus the liquid load have a large influence on the physical crack model as the bending moment is proportional to the liquid load by H^2 and to wall height by H^3. In addition to the reliability analyses for a depth of water of 5 m, analyses were performed for a 7m wall height. Referring to Figure 2 and considering the steep gradients of the reliability curves, reliability can be improved for the wall heights considered, and therefore liquid load, for a relatively low cost of increasing the reinforcement area.

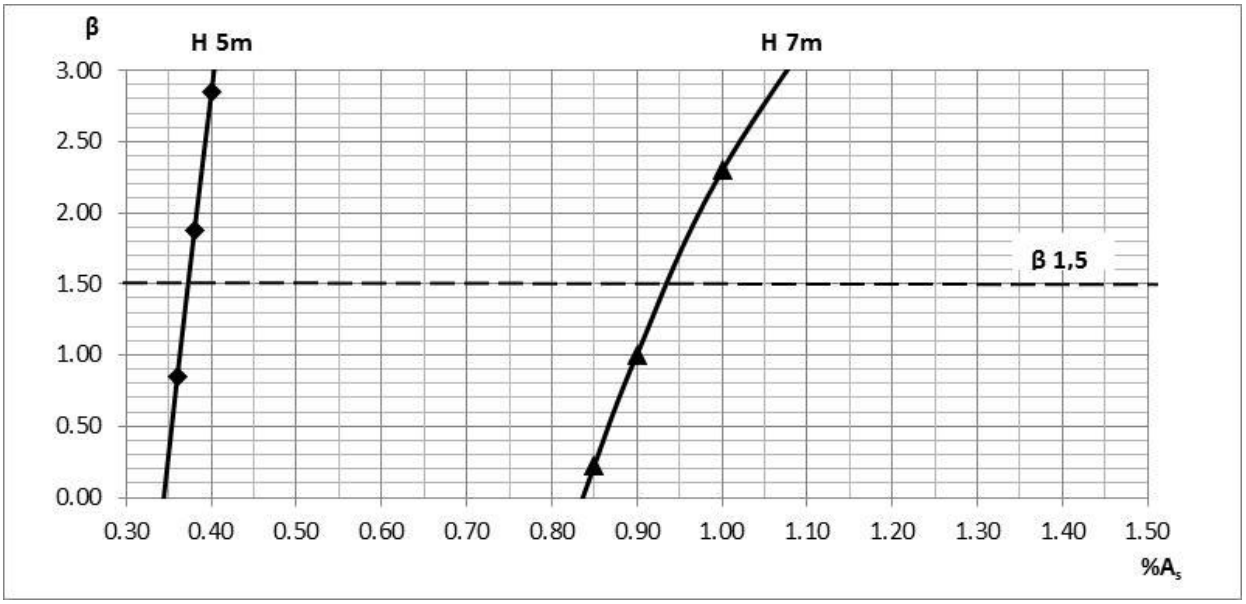

Figure 2. Influence of Load on reliability (w_{lim} 0,2 mm)

3.1.3 Influence of model uncertainty, θ

Referring to Table 2, reliability decreases with increasing model uncertainty, although the increase is small for flexural cracking. Therefore, it can be concluded that model uncertainty does not appear to have a great influence on reliability in this case. Figure 3 illustrates this point for a crack width limit of 0,2 mm. However, it was noted that the model uncertainty has a somewhat greater influence as the crack width limit decreases.

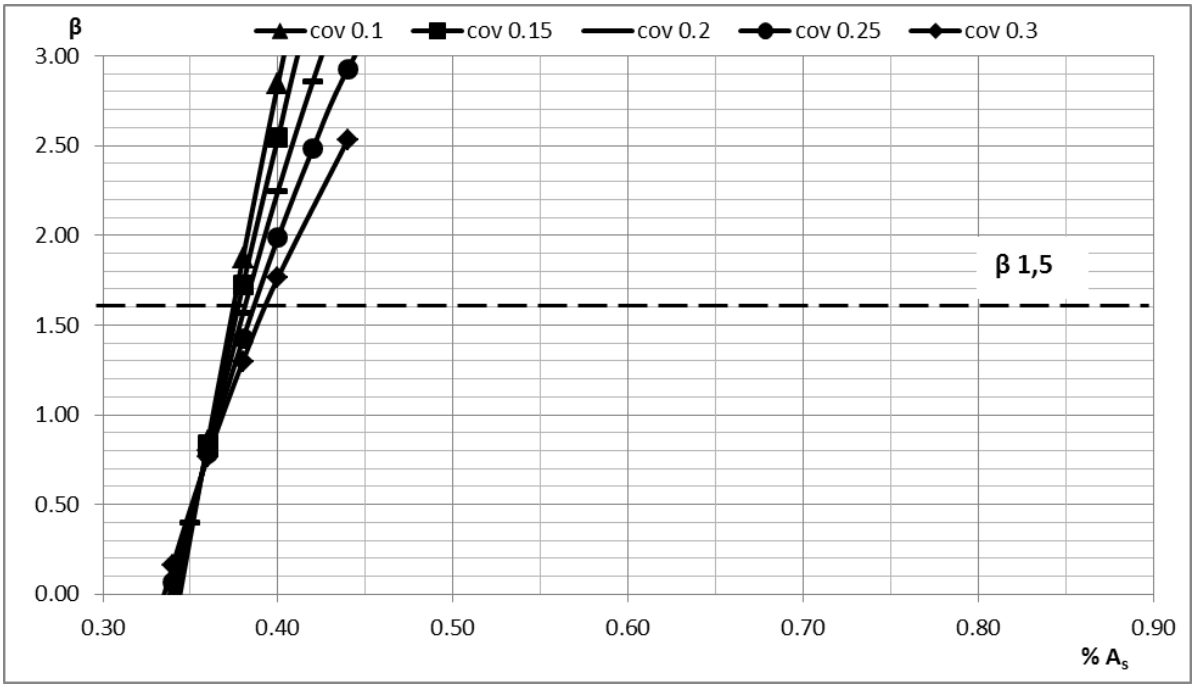

Figure 3. Influence of model uncertainty on reliability for flexural cracking (wlim 0.2mm).

3.1.4 Influence of crack width limit, w_{lim}

The South African industry generally uses a 0,2 mm crack width limit for WRS. With the possibly of a more onerous crack width limit of 0,05 mm specified by Eurocode, it was desired to determine the effect of this lower limit on the reliability and thus the design of WRS. Referring to Table 2, the level of reliability was found to decrease considerably with a decreasing crack width limit for a given reinforcement quantity and model uncertainty CoV. Reducing the crack width limit from 0,2 mm to the more onerous value of 0,05 mm set by EN1992-3 (a decrease by a factor of 4) will result in an increase in the reinforcement required by a factor of about 2,8 for flexural cracking.

Reliability sensitivity to the crack width limit increases as the crack width limit decreases. Referring to Figure 4, the graphs have decreasing gradients as the crack width limit decreases. This means that a change in $\%A_s$ will result in a smaller change in reliability for a crack width limit of 0.05 mm than for a limit of 0.2 mm. Conversely, therefore, a smaller limiting crack width will require a greater increase in reinforcement to achieve the same increase in reliability at a larger crack width.

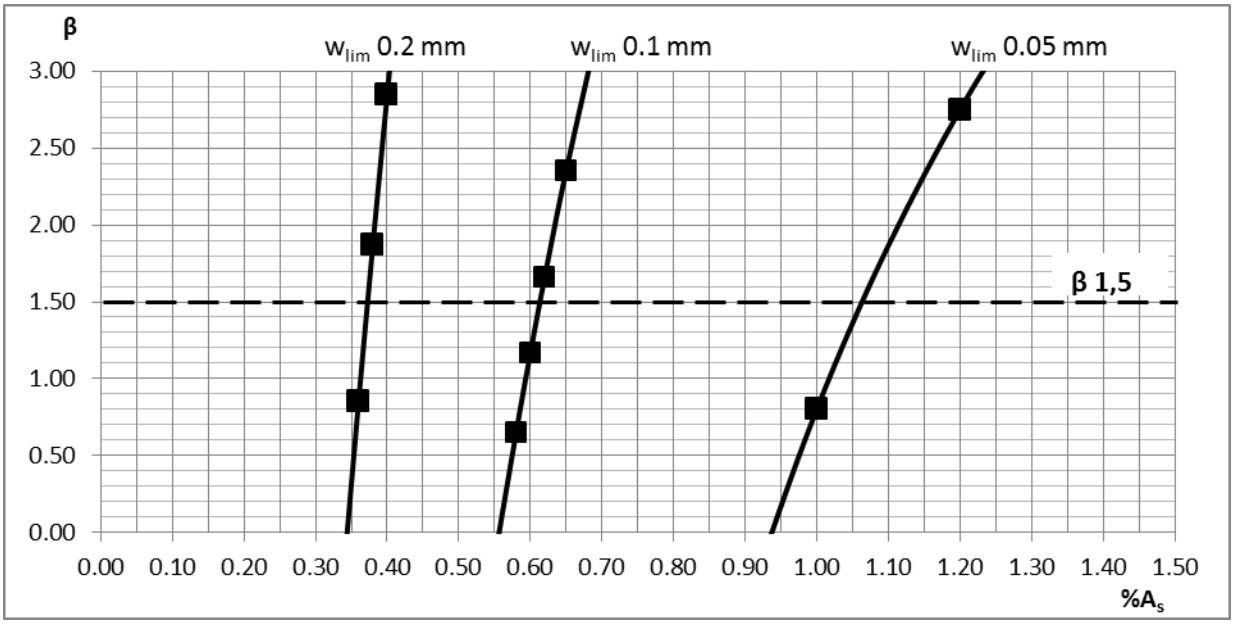

Figure 4. Influence of crack width limit on reliability for flexural cracking (h 450mm)

Tension cracking

The tension cracking model was found to have two possible formulations, depending on the EN1992 limiting equation for the effective depth of the tension zone ($h_{c,eff}$), namely, h/2 or 2,5 (c + φ/2), which in turn depends on the combination of cover, bar diameter and wall thickness chosen. The results for the tension cracking model are therefore presented in terms of influence of the effective depth of the tension zone, the limiting crack width and model uncertainty.

3.2.1 Influence of effective depth of tension zone, $h_{c,eff}$

To evaluate which equation applies, $h_{c,eff}$ was calculated for various values of cover, bar diameter and wall thickness. The results are presented in Table 3. In terms of the reliability analysis of the EN1992 crack equation for tension loading, section thickness, h, and cover, c, are basic random variables whilst bar diameter is taken as a deterministic value. The effective depth of the tension zone determined by h/2 is independent of cover and bar diameter. Bar diameter and cover then only appear directly in the EN1992 crack equation, both variables having a limited effect on the reliability model. However, if the effective depth is determined using 2,5(c + φ/2), the effective depth of the tension zone is expressed in terms of cover (as a random variable) and bar diameter (deterministic value).

Table 3: Calculation of effective depth of the tension zone, $h_{c,eff}$, for tension cracking

Cover (mm)	h	Bar dia 16 mm d	h/2	2,5(h-d)	Bar dia 20 mm d	h/2	2,5(h-d)	Bar dia 25 mm d	h/2	2,5(h-d)
40	250	202	125	**120**	200	**125**	**125**	197.5	**125**	131.25
	300	252	150	**120**	250	150	**125**	247.5	150	**131.25**
	350	302	175	**120**	300	175	**125**	297.5	175	**131.25**
	400	352	200	**120**	350	200	**125**	347.5	200	**131.25**
	450	402	225	**120**	400	225	**125**	397.5	225	**131.25**
	500	452	250	**120**	450	250	**125**	447.5	250	**131.25**
50	250	192	**125**	145	190	**125**	150	187.5	**125**	156.25
	300	242	150	**145**	240	**150**	**150**	237.5	**150**	156.25
	350	292	175	**145**	290	175	**150**	287.5	175	**156.25**
	400	342	200	**145**	340	200	**150**	337.5	200	**156.25**
	450	392	225	**145**	390	225	**150**	387.5	225	**156.25**
	500	442	250	**145**	440	250	**150**	437.5	250	**156.25**

Note: values in bold are the limiting effective depth of the tension zone in concrete.

The cover has a greater influence on the reliability model. The latter limiting equation and the calculated crack width are independent of h. The reliability model is therefore influenced by which equation is limiting. Generally, $2{,}5(c + \varphi/2)$ tends to be the limiting equation, particularly for thicker sections. However, there are some combinations of section thickness, cover and bar diameter which result in the same value for $h_{c,eff}$ calculated by both equations. Referring to Table 3, this occurs for the combination of a 250 mm section thickness, a 20 mm bar diameter and 40 mm cover, for example, giving an $h_{c,eff}$ of 125 mm for both equations. FORM analyses were performed using these values at a crack width limit of 0,2 mm. The results of these analyses are illustrated by Figure 5 showing the variation of the reliability index with $\%A_s$ for $h_{c,eff}$ determined using h/2 and $2{,}5(c + \varphi/2)$.

The effective depth, $h_{c,eff,}$ determined using $2{,}5(c + \varphi/2)$ results in a higher reliability for a given reinforcement area than using h/2. For example, referring to Figure 5, at a $\%A_s$ of 1,55, reliability levels of about 1,7 and 1,5 are obtained for $h_{c,eff}$ determined using $2{,}5(c + \varphi/2)$ and h/2, respectively. Conversely, for a given reliability, using $2{,}5(c + \varphi/2)$ requires less reinforcement than if $h_{c,eff} = h/2$ is used. At a β of 1,5, values of about 1,52% for $h_{c,eff} = 2{,}5(c + \varphi/2)$ and 1,55% for $h_{c,eff} = h/2$ are obtained. Thus, the equation h/2 results in the crack width model being more conservative than $2{,}5(c + \varphi/2)$ and more sensitive to changes in the amount of reinforcement provided, as evident from the flatter gradient of the graph in Figure 5. Hence it can be concluded that the manner in which $h_{c,eff}$ is determined has an effect on the reliability of the crack model for tension cracking.

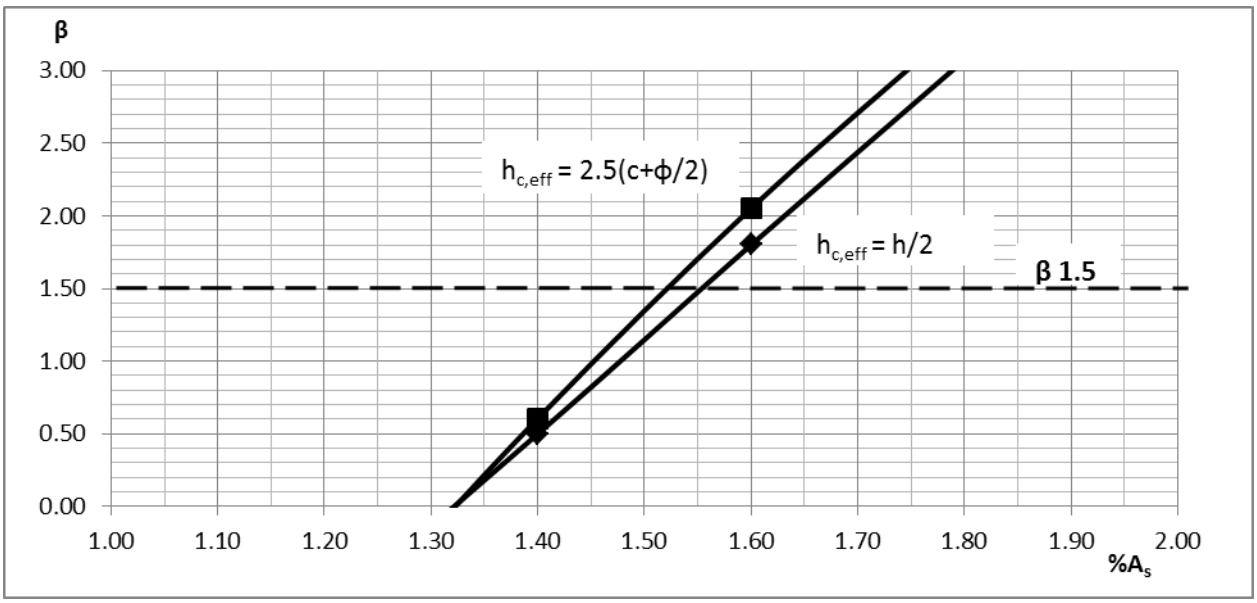

Figure 5. Influence of $h_{c,eff}$ on the reliability of the tension crack model (h 250 mm, w_{lim} 0.2 mm)

3.2.2 Influence of model uncertainty

Model uncertainty has a greater effect on the reliability of the tension cracking model than on the flexural case, with a greater decrease in the graph gradients and thus in the relative decrease in β for a given $\%A_s$ as model uncertainty variation increases, as is shown in Figure 6.

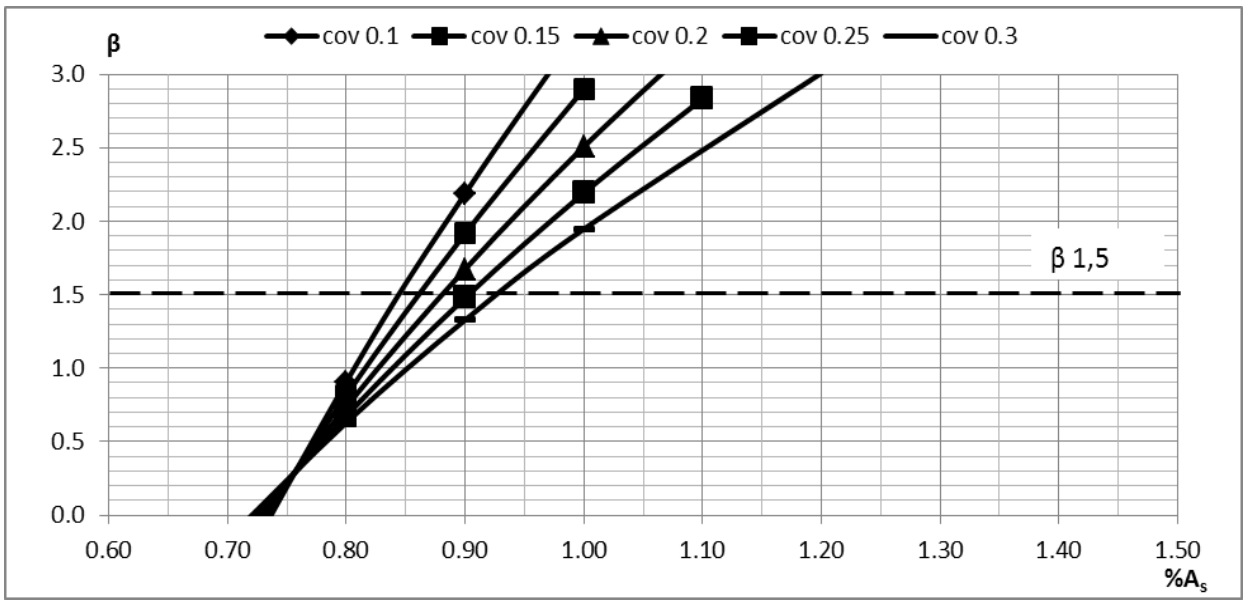

Figure 6. Effect of model uncertainty on reliability for tension cracking (w 0.2 mm, h 450 mm)

The graphs intersect at a β of about 0,30 and a 0,75 $\%A_s$. The sensitivity of reliability increases as model uncertainty increases above β of 0,30. Results for the required steel for β of 1,5 for various cases investigated are summarized in Table 4. The analysis was performed using $2{,}5(c + \varphi/2)$ for $h_{c,eff}$.

Table 4: Influence of crack width and model certainty on reliability for tension cracking

w_{lim} (mm)	Cov of θ	$\%A_s$
0.2	0.10	0.84
	0.15	0.86
	0.20	0.88
	0.25	0.90
	0.30	0.93
0.1	0.10	1.22
	0.15	1.24
	0.20	1.28
0.05	0.10	1.76
	0.15	1.78
	0.20	1.82

3.2.3 Influence of crack width limit

The influence of the crack width on reliability for tension cracking is illustrated by Figure 7 which shows the variation of reliability with $\%A_s$ for a 450 mm wall thickness and a decreasing crack width limit from 0,2 mm to 0,05 mm. The graphs for each crack width are approximately linear, with the gradient decreasing as the crack width decreases, as in the case of flexural cracking.

Referring to both Figure 7 and Table 4, there is a substantial increase in reinforcement required to achieve the same level of reliability as the limiting crack width decreases for tension cracking. It can be concluded that the crack width limit has a substantial influence on the level of reliability for tension cracking. Reducing the crack width limit from 0,2 mm to the more onerous value of 0,05 mm set by EN1992-3 (a decrease by a factor of 4) results in an increase in the reinforcement required by a factor of about 2,1 at a reliability level of 1,5 and model uncertainty cov of 0,1.

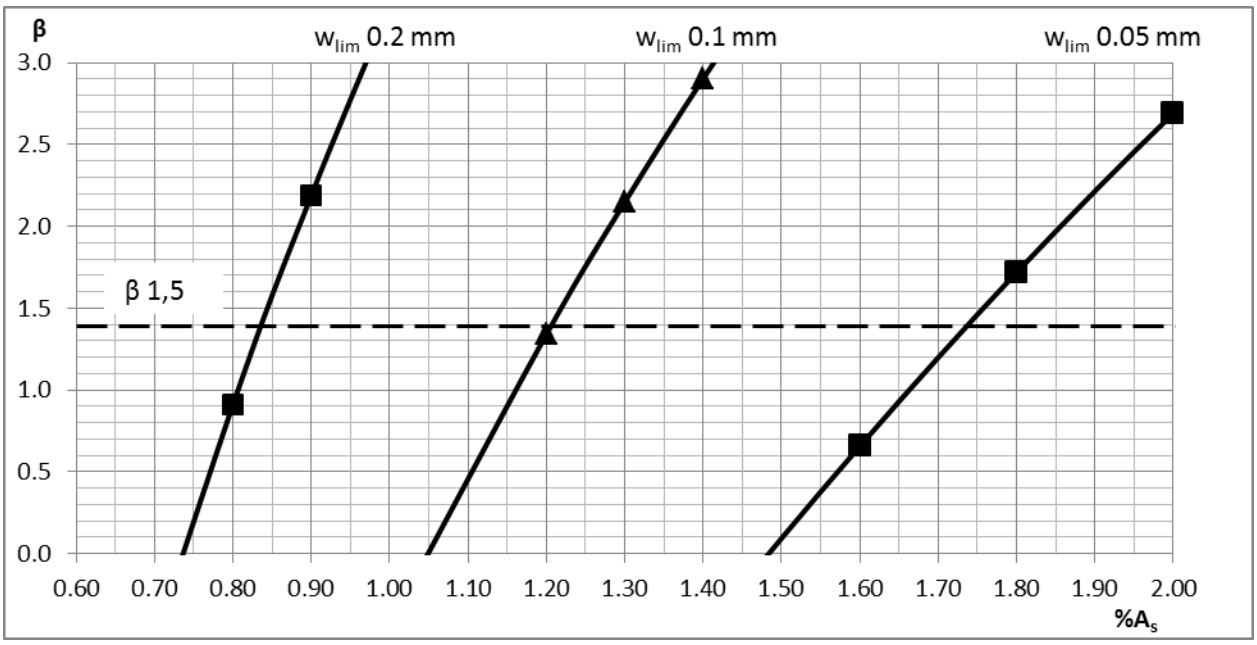

Figure 7. Effect of crack width limit on reliability for tension cracking (h 450 mm)

4. Conclusions

Summarising from the results and discussion:

- The crack width limit has a significant effect on the probabilistic model. As the crack width limit is reduced, the reinforcement required increases and the reliability, and therefore the performance of the structure, decrease. In addition, reliability sensitivity is less for smaller crack widths with a greater increase in reinforcement required to improve reliability.
- Model uncertainty treated here parametrically does have an effect on the reliability of the model, particularly for the tension cracking case. A comparison of the reliability analysis to experimental data on flexural and tension cracking needs to be done to improve the statistical data for crack widths and model uncertainty.
- The reliability model for tension load cracking is influenced by the limiting equation for the effective depth of the tension zone, $h_{c,eff}$ which, in turn is dependent on the geometry of the member considered, in particular the combination of section thickness, bar diameter and cover chosen.

References

[1] Beeby AW, Narayanan RS (2005). *Designer's guide to EN1992-1-1 and EN1992-1-2: Design of concrete structures. General rules and rules for buildings and structural fire design.* Thomas Telford.

[2] BS 8007: *Design of concrete structures for retaining aqueous liqu*ids. BSI 1987

[3] BS EN 1990: *Eurocode 0: Basis of structural design*. BSI 2002.

[4] BS EN 1992-1: *Eurocode 2: Design of concrete structures – Part 1: General requirements.* BSI 2004.

[5] BS EN 1992-3: *Eurocode 2: Design of Concrete Structures – Part 3: Liquid Retaining and Containment Structures.* BSI 2006.

[6] Holicky M (2009). *Reliability analysis for structural design*. SUN Media Stellenbosch.

[7] Joint Committee on Structural Safety. *Interpretation of Uncertainties and Probabilities in Civil Engineering Decision Analysis. Background documents on risk assessment in engineering*. Document No. 2. JCSS, Zurich 2008. http://www.jcss.ethz.ch/.

[8] Quan Q, Gengwei Z (2002). *Calibration of reliability index of RC beams for serviceability limit state of maximum crack width.* Journal of Reliability Engineering and System Safety. No. 75 (2002), pg 359 – 366.

[9] SANS 10100-1: *The structural use of concrete: Part 1: Design.* South African Bureau of Standards. Pretoria 2000.

[10] SANS 10100-3(Draft): *Design of concrete water retaining structures*. WRC Project group with the Institute of Structural Engineering. 2010

[11] SANS 10160: *Basis of structural design and actions for buildings and industrial structures.* South African Bureau of Standards. Pretoria 2011.

[12] Wium, JA (2008). Report April 2008: *Basis of design and materials. The development and calibration of South Africa's National Standards for water retaining structures.* WRC Project No. K5/1764, Water Research Commission of South Africa, Pretoria, SA

Challenges in modelling in banking: behaviour

Remko Riebeek
Integrated Risk Management
ABN AMRO Bank N.V.*

Abstract: In this paper we argue that behavioural phenomena are at the heart of improvements that risk modelling requires to overcome the weaknesses that have been laid bare in the credit crisis. These behavioural aspects need to be addressed both in the models themselves and in the processes around the use of the models.

1 Introduction

The credit crisis in 2007/2008 is closely connected to risk models and, in particular, the use of these models in the financial sector. On the one hand are risk models seen as one of the causal factors for the crisis, on the other hand is the impact of the credit crisis profound on the modelling landscape. In this paper, we will touch upon the most important issues that have become apparent from the credit crisis that are related to the models. We will argue that an important concept that is required to solve these issues is the understanding of behavioural aspects related to how people act under uncertainty.

This is important because one of the consequences of the credit crisis is that decision makers in financial institutions (but, in particular, also in the political surroundings thereof) have lost confidence in the statistical toolkit, thereby relying stronger on their intuitions and gut feelings. One can only question whether or even when this approach will lead to new disasters. In stark contrast with the above we find that regulators and supervisors are continuously and quickly increasing the pressure on financial institutions to lift their standards of risk modelling. These contrasting views are already an enormous challenge for risk modellers and risk managers, but it is even enlarged by another: the current macro-economic climate, with its extremely volatile financial markets and uncertainty (e.g. in the Eurozone). This situation is located on the

* The opinions expressed in this paper are the author's and do not necessarily reflect the policy or position of ABN AMRO.

extreme end of existing risk models, where data is scarce and confidence intervals are difficult to determine.

The science of behavioural economics is not new, but has gained popularity over the last years. The ground breaking research in this area was done by the duo of Amos Tversky and Daniel Kahneman, the latter of them, as a psychologist, receiving the Nobel prize for economics for their research in this area in 2002. It must be mentioned that already Keynes was very aware that economics was a behavioural science. It may even be said that a lot of the problems that led to the credit crisis were the result of the trend in economics to consider the economy as an ergodic system, thereby being able to use "physics resembling" mathematical models to describe the economic reality. Recently, Kahneman published an excellent book that brings forward the whole field of behavioural aspects of judgement and action under uncertainty in an uncomplicated fashion without sacrificing the required nuancing depth. The application of behavioural aspects in finance were pioneered by Hersh Shefrin, see e.g. [8].

In the following chapters we will treat three important topics for risk modellers to address in the world after the credit crisis.

First, we will look at why, when using the models developed to estimate the risks of financial instruments, the risks in the financial world could build up with the collapse of Lehman Brothers and its aftermath as a result. We will see that *excessive optimism*, *overconfidence* and, possibly, *loss aversion* were key ingredients and that understanding these phenomena is necessary to write a "manual" for any financial risk model.

Second, we will look at the risk types that are the current focus of modelling in financial institutions and conclude that more emphasis should be put in modelling operational risk and strategic risk. Currently, both these risk types are measured with a strong use of expert opinion. It is clear that debiasing these expert opinion (especially when performed in groups) is key. Furthermore, both risk types are caused by actions and interactions and beliefs of people: another clear reference for applying behavioural aspects.

Third, we will take a look at risk management in extreme (crisis) situations. In almost all cases we see that group dynamics take over from rationality. Understanding how this works will be necessary to understand and predict the current economic situation and to act wisely.

2 Failed Models or Failed Model Use

If the credit crisis has taught us one thing, it is that models are used by humans and made by humans. Finding the boundaries and holes of models, tweaking models, "gaming the system", ignoring model constraints, misusing models outside of the context are all part of real corporate life, as well as giving in to pressures to implementing unsound statistics and cleaning calibrating data from undesirable elements.

Stories exist all over the place of managers demanding models to provide more optimistic results and risk managers and their modelling teams giving in to these demands or, if not, being fired. It is clear that many AAA-rated financial products were not that risk-free and that capital models were underestimating the capital required to protect the company against insolvency *with a 99.95% or 99.98% confidence level*. Note that this 99.9x% already in itself is a difficult notion to get a mental grasp on and that it is often explained as a 1 in 2000 years event. In terms of ordinary people this translates to extremely unlikely or, better said, too unrealistic to feel the need to prepare for. Remembering that 2000 years ago we were in the times of the Roman Empire and so many unpredictable revolutions happened afterwards, this should also not come as a surprise.

Banks, insurance companies, investors, regulators and supervisory bodies all relied heavily on these (economic) capital models and the Basel II regulation made it possible to use internal models in an attempt to make regulatory constraints more risk sensitive. The fact that less required capital equals more profit (in the short term) is a strong incentive to construct models that reduce capital needs to a minimum. The before mentioned "1 in 2000 years" explanation does not help to feel the need to suppress this incentive and the many parameters an internal and complex model has, can be used by the modeller to give companies the ability to play with capital models.

It seems that regulators have overlooked or underestimated the adverse effects of the allowance of internal risk models to compute required capital, in particular of how it influences the behaviour of managers. It also seems that managers themselves have underestimated the risks of their companies' strategies. The literature suggests that this behaviour often comes from an *illusion of control*: overestimation of one's own degree of control over potential adverse situations.

To protect the value of their profession, the key challenge for modellers in risk management is to unmistakably and comprehensibly define and describe

* The opinions expressed in this paper are the author's and do not necessarily reflect the policy or position of ABN AMRO.

the intended use of the designed models, thereby including knowledge on potential misuse.

The current Basel III proposals (e.g. the introduction of leverage ratio and the return to core equity capital) show that regulators seek to use simpler, centrally designed models to determine the size of regulatory capital in banks. This will relieve risk modellers in those companies somewhat as their modelling efforts will less impact the amount of required regulatory capital.

3 Models that matter

Banks have traditionally focused their risk modelling efforts on their core processes: credit risk and, later, market risk. Regulation has followed these developments (in particular with the so called Basel agreements), the focus until recently being on credit risk and market risk. Only with the revision to Basel II ([1]) from 2006, operational risk has become another important topic of interest, with limited attention also for other risk types. It must be said that in practice modelling operational risk remains a difficult task. With the development of Basel III also other risk types, such as liquidity risk, have gotten to the forefront. It is interesting to see whether these are indeed the most important risk types for a bank's solvability.

James Lam and others [6] have done research on why companies underperform. Their results are summarised in the table below:

Table 1. Strategic risk identified as the major cause for financial distress (copied from [6])

Organization	Research Methodology	Key Findings
James Lam & Associates (2004)	▸ S&P 500 (1982-2003) ▸ One month stock price decline of 30% or greater relative to the S&P 500	▸ 61% were exposed to strategic risks ▸ 30% were exposed to operational risks ▸ 9% were exposed to financial risks
The Corporate Executive Board (2005)	▸ Fortune 1000 companies (1998-2002) ▸ Top 20% of companies with the greatest market value declines	▸ 65% were exposed to strategic risks ▸ 20% were exposed to operational risks ▸ 15% were exposed to financial risks
Deloitte Research (2005)	▸ Thomson Financial Global 1000 Companies (1994-2003) ▸ One-month stock price decline relative to the Morgan Stanley Financial	Among the 100 largest declines: ▸ 66 involved strategic risks ▸ 62 involved external events ▸ 61 involved operational risks

World Index	▸ 37 involved financial risks

The conclusion that can be drawn from this research is that strategic risk and operational risk are the risk types that should require the most attention and that these are undervalued in the regulatory framework.

One of the reasons for not including these risk types in the regulatory framework is the apparent difficulty in modelling them. The difficulty lies for the larger part in the behavioural aspects of both of these risk types. These aspects can be seen in two parts of the modelling process.

First, the decisions taken that lead to operational or strategic disasters often possess a behavioural character. As an example of strategic risks, we can think of the decision process to enter a new market or the decision to develop a new corporate image that can be marred by *excessive optimism* and *overconfidence*. As examples of operational risks, we can think of the Barings/Nick Leeson disaster in 1995 and the enormous trading loss in the Jérôme Kerviel/Société Générale case in 2008 (see [9]) or, more recently, the JP Morgan case that were allegedly caused by a combination of *sure loss aversion* and interactions between traders, back office and control functions.

Second, the current practice of estimating the risks is the intensive use of expert opinions, often in group settings. In these workshop sessions, experts are asked to estimate likelihood and impact of a number of identified risks. Both the biases and heuristics of the experts as well as the group settings are a bowl full of behavioural problems that make the outcome of the estimates questionable if there is no structural attention for the influence of these aspects on the outcomes. As examples we mention *availability bias*: the phenomenon that people overvalue information that is readily available (e.g. an incident that just occurred) and *groupthink*: the phenomenon that consensus leads to not exploring other paths of potential developments.

In my opinion, these phenomena will have to play an important role in the development of models for these risk types, given the influence these have on the outcomes.

4 Models in extreme situations

After the Lehman Brothers collapse on September, 15th 2008, the financial markets are in a state of continuous high tension. The uncertainty of the creditworthiness of sovereigns, financial institutions and companies is perceived high and (therefore?) any newsflash and rumour has a high impact on market

* The opinions expressed in this paper are the author's and do not necessarily reflect the policy or position of ABN AMRO.

sentiment. This market sentiment is a typical subject of study of behavioural risk management.

A common behavioural phenomenon in stress situations is for example *sure loss aversion*: people and financial institutions hold on to assets that have decreased considerably in value betting on the small chance that their value will increase again into profitable terrain, thereby seeing the asset values drop further.

A key element in (not) predicting this extreme situation has been the limited historic horizon (there are almost no known implementations that use data that goes all the way back to the great crash in 1929) that is being used in simulation and stress testing exercises that are often based on replaying historical stress events, thereby limiting the influence of other types of potential events. We now see a move by regulation (e.g. EBA [4] and FED [2]) to rely more and more on stress testing. This development can be an important improvement of risk models as it may estimate extreme events more reliably. Of course, questions still exist around the methodology of stress testing. Some are mentioned in [7]. Again, a high level of human judgement is involved in designing and performing stress testing scenarios, which leads us back to the main theme of this paper.

As a final remark, the Eurozone sovereign and financial sector problems of the last years have shown that politicians play an important role in the direction crises take. The impact of the dynamics of political discourse on the financial markets is high. This political uncertainty is most often included in risk management by analysing several outcomes of scenarios into stress testing exercises. Nevertheless, even though a company should be prepared for various outcomes of scenarios assigning probabilities to these scenarios, it is in practice a topic of heavy discussion. Therefore, the study of interactions of actors in negotiations (i.e. game theory) could be another topic of interest for risk modellers. It is suggested by [3] that probabilities of this type can be predicted with a reasonable level of confidence.

4.1 Literature

[1] Bank of International Settlements: *Basel II: Revised International Capital Framework*, http://www.bis.org/publ/bcbsca.htm , 2006

[2] Board of Governors of the Federal Reserve: Comprehensive Capital Analysis and Review 2012: Methodology and Results for Stress Scenario Projections, http://www.federalreserve.gov/newsevents/press/bcreg/bcreg20120313a1.pdf, March 13, 2012

[3] Bruce Bueno de Mesquita: *The Predictioneer's Game*, 2009

[4] European Banking Authority: *EU-wide stress testing*, http://www.eba.europa.eu/EU-wide-stress-testing.aspx

[5] Kahneman, Daniel: *Thinking, fast and slow*, 2011

[6] Lam, James: *ERM and Corporate Strategy – Driving Business Performance through Risk Intelligence*, webinar (July 17, 2012)

[7] John Lester, Peter Reynolds, Til Schuermann, Dylan Walsh: *Strategic Capital; Defining an effective real-world view of capital*, http://www.oliverwyman.com/strategic-capital-defining-an-effective-real-world-view-of-capital.htm, 2012

[8] Shefrin, Hersh: *Behavioral Corporate Finance – Decisions that Create Value*, 2007

[9] Shefrin, Hersh: *Ending the Management Illusion*, 2008

* The opinions expressed in this paper are the author's and do not necessarily reflect the policy or position of ABN AMRO.

Resistance Factor Calibration of Drilled Shafts for Bridge Foundations

D. Bach, P.H.A.J.M. van Gelder, K.J. Bakker, and J.K. Vrijling
Delft University of Technology, Delft, The Netherlands

Abstract: Calibrating resistance factors for drilled shafts is to insure safety degrees for foundation structures with high load effects from a superstructure system with target reliability levels. As this is accomplished under conditions of uncertainty, probabilistic analyses are necessary in the development of such probability-based design methods. A method for load and resistance factor design (LRFD) will be presented, and reliability-based methods for calibrating the resistance factors are described in this paper. Methods which consist of first-order second moment (FOSM), first-order reliability method (FORM), and Monte Carlo simulation (MCS) are used to calibrate these factors for 16 cases of calculation, which are based on a drilled shaft database covering various types of soil, resistance prediction methods, and construction methods. The resistance factors are determined for a set of assigned load factors to meet specified target reliability indices. Moreover, correlation analyses between the determined resistance factors which are calibrated according to reliability methods are also considered herein. Through obtained results, some extra findings are illustrated in this paper.

1 Introduction

The allowable stress design (ASD), also called the working stress design (WSD) method, has been used in civil engineering since the early 1800s. Under ASD, the design load, which consists of the actual forces applied to the piles, has to be less than the resistance divided by a single factor of safety. This method has several shortcomings, the most significant of which is that it does not provide a consistent framework for incorporating the individual sources of risk into the design. In fact, each component of the load and the resistance has a different level of variability and uncertainty.

In the 1950s, the demand for the more economical design of piles brought about the use of the limit state design (LSD) method. Two types of limit states are usually considered, ultimate limit state (ULS), and serviceability limit state (SLS). ULS pertains to structural safety and involves structural collapse or, in relation to piles, the ultimate bearing capacity of soils. SLS pertains to conditions, such as excessive deformations and settlements or deterioration of the structure that would affect the performance of the structure under expected working loads. The format of limit state design equations involves the application of partial factors to increase the loads and to decrease the resistances. This approach represents a fundamental improvement over the single factor of safety in ASD because the partial factors are applied directly to the uncertain quantities of loads and resistances.

The partial factors were determined subjectively based on two criteria: (i) a larger partial factor should be applied to a more uncertain quantity; (ii) the partial factors should result in approximately the same dimensions as those from traditional practice. This approach did not satisfy one of the basic requirements of LSD because it is impossible to demonstrate the occurrence of each limit state (Brown et al. [6]). The next logical step in LSD has been to apply probabilistic reliability analysis to establish the partial factors, in order to account for the uncertainty and variability for loads and resistances. One of the advantages of this approach is that all components of the structure, including the foundations, can be designed to a uniform level of safety. The LSD method based on the probabilistic reliability analysis has been used increasingly with a new name as the load and resistance factor design (LRFD) method, in which the partial factors applied to loads are termed load factors and those applied to resistances are resistance factors. Each resistance factor is the product of a calibration study in which a limit state function (LSF) is evaluated to predict a specific component of resistance (e.g., side or base or both types of resistance) to a specified target reliability level.

As described by Withiam et al. [13], calibrating load factors and resistance factors can be carried out by the use of: (i) judgment; (ii) fitting to other codes or past practice; (iii) reliability-based analysis; or (iv) a combination of approaches. Only the third approach, reliability-based analysis, satisfies the objective of LSD, and establishes load and resistance factors to achieve a defined target reliability level. Several comprehensive works based on the reliability analysis were conducted for the resistance factor calibration, for example, FOSM was used by Barker et al. [5], FORM was used by Paikowsky et al. [12] and MCS was utilized in the works of Allen et al. [2] and Abu-Farsakh and Yu [1].

In this paper, resistance factors are calibrated according to different reliability-based methods. A database, which involves sixteen cases of calculation of axially loaded drilled shafts, is collected and computed under the ultimate limit state for strength I. Each case is represented by a soil type, a resistance prediction method and a construction method. The resistance factors are calibrated with specified target reliability levels and different span lengths of bridges. From the obtained results, the relationships between resistance factors and statistical parameters of the resistance are formulated. Furthermore, the correlations between resistance factors calibrated by reliability methods are presented and discussed as well.

2 Reliability-Based Design Methods

According to Ayyub et al. [4], there are two primary approaches for the reliability-based design: (i) load and resistance factor design (LRFD); and (ii) direct reliability-based design. The LRFD approach is called the level I reliability method. Level I reliability methods use partial safety factors (PSF's) that are reliability based; but the methods do not require explicit use of the probabilistic description of the random variables. The direct reliability-based design approach can include level II and/or level III reliability methods. Level II reliability methods (e.g. FOSM, FORM) are based on the moments (mean and variance) of random variables, and sometimes, with a linear approximation of non-linear limit state functions. Level III reliability methods such as numerical integration according to the Riemann procedure, MCS, use the complete probabilistic characteristics of the random variables.

2.1 Reliability-based design philosophy

The reliability-based design procedure requires defining limit state functions that correspond to limit states for significant failure modes. A general form for the limit state function for a structural component is given by:

$$g = R - Q \tag{1}$$

Where g is the limit state function, R is the resistance (or strength), and Q is the load effect on the structural component. The failure is defined in the region where g is less than zero or R is less than Q, that is $g < 0$ or $R < Q$. Whereas, the safety is defined in the region where g is greater than zero or R is greater than Q, that is $g > 0$ or $R > Q$.

The reliability-based design approach assumes the resistance R and the load Q to be random variables. The frequency distributions, permanently called the

probability density functions (PDF's), of random variables are shown in Fig. 1.

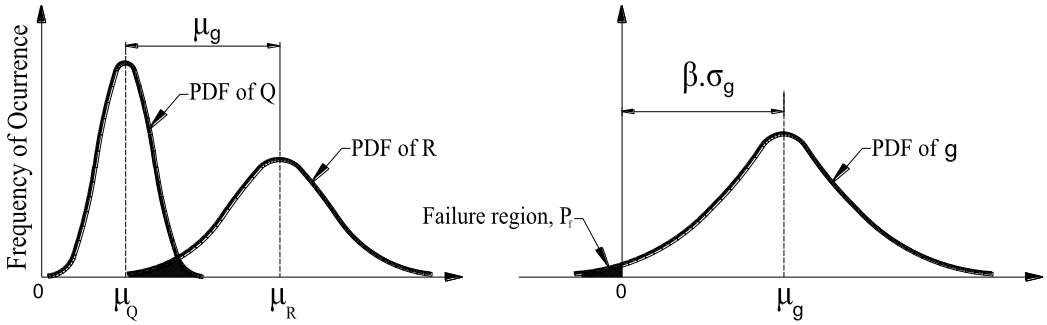

Figure 1. Reliability concepts: distribution of load and resistance, probability of failure and reliability index.

If *R* is greater than *Q*, there will be a safety margin. However, unless *R* is greater than *Q* by a large amount, there is always a probability that *Q* may exceed *R*. This is illustrated by the shaded area in Fig. 1 where the two curves for *R* and *Q* overlap. Because of the variability in both resistance and load effects, there is always a probability of failure, P_f, that can be defined as:

$$P_f = P(g < 0) = P(R < Q) \tag{2}$$

The probability of safety (or reliability), P_s, is given by the following expression:

$$P_s = P(g > 0) = P(R > Q) = 1 - P_f \tag{3}$$

The probability of failure can also be expressed conveniently in terms of a reliability index, denoted by β, which represents the distance measured in standard deviations between the mean safety margin, μ_g , and the failure limit $g = 0$.

The design of any structural component must provide for adequate safety regardless of what philosophy of design is used. Reliability and risk measures can be considered as performance measures, specified as target reliability levels (denoted by target reliability indices, β_T*'s*). The selected reliability level of a structural component reflects the probability of failure of that component (see Table 1). These levels can be set based on implied levels in the currently used design practice with some calibration, or based on the cost-benefit analysis.

Table 1. Relationship between target reliability index and probability of failure

Target reliability index, β_T	Probability of failure, P_f
2.0	0.1
2.5	0.01
3.0	0.001
3.6	0.0001
4.1	0.00001
4.6	0.000001

2.2 Load and resistance factor design (LRFD)

The load and resistance factor design states that a factored (reduced) resistance of a structural component is larger than a linear combination of factored (magnified) load effects as given by a following general format:

$$R \geq \sum_{i=1}^{n} \gamma_i Q_i \tag{4}$$

Where ϕ is the resistance factor, R is the nominal (or prediction) resistance, γ_i is the load factor for the ith load component, and Q_i is the nominal (or design) value for the ith load component. Generally, the higher the uncertainty associated with a load, the higher the corresponding load factor; and the higher the uncertainty associated with the resistance, the lower the corresponding resistance factor. These factors are calibrated using reliability methods based on the probabilistic characteristics of basic random variables for load effects and the resistance including statistical and prediction (or modelling) uncertainties. The factors are calibrated to meet target reliability indices that were selected based on assessing previous designs. This process of developing the LRFD rules to meet target reliability indices that are implicit in current practices is called code calibration.

2.3 Resistance factor calibration based on first-order second moment method (FOSM)

Based on FOSM and assumed lognormal distributions for the resistance, Barker et al. [5] determined the resistance factor as follows:

$$\phi = \frac{\lambda_R \left(\sum \gamma_i Q_i \right) \sqrt{\dfrac{1 + COV_Q^2}{1 + COV_R^2}}}{\sum Q_i \exp\left\{ \beta_T \sqrt{\ln\left[\left(1 + COV_R^2\right)\left(1 + COV_Q^2\right) \right]} \right\}} \tag{5}$$

In which λ_R is the mean of resistance bias factor; COV_Q and COV_R are the coefficient of variation of the load and resistance bias factors, respectively; β_T is the target reliability index. When just dead and live loads are considered, Eq. 5 can be rewritten as:

$$\phi = \frac{\lambda_R\left(\frac{\gamma_D Q_D}{Q_L} + \gamma_L\right)\sqrt{\frac{1 + COV_{QD}^2 + COV_{QL}^2}{1 + COV_R^2}}}{\left(\frac{\lambda_{QD} Q_D}{Q_L} + \lambda_{QL}\right)\exp\left\{\beta_T\sqrt{\ln\left[\left(1 + COV_R^2\right)\left(1 + COV_{QD}^2 + COV_{QL}^2\right)\right]}\right\}} \quad (6)$$

Where γ_D and γ_L are the dead load and live load factors, respectively; Q_D/Q_L is the dead to live load ratio; λ_{QD} and λ_{QL} are the dead load and live load bias factors, respectively. The dead to live load ratio varies with the span length of bridges. Hansell and Viest [8] determined these ratios indicated in Table 2 for the LRFD approach.

Table 2. Relationship between dead load to live load ratio and span length

Span length (m)	9	18	27	36	45	60	75
Ratio Q_D/Q_L	0.52	1.04	1.56	2.07	2.59	3.46	4.32

The actual loads transferred from the superstructure to the foundations are, by and large, unknown. The load uncertainties are taken, therefore, as those used for the superstructure analysis. The probabilistic characteristics of the dead load, Q_D, and live load, Q_L, are assumed to be those used by Nowak [10] with the following load factors and normal distributions shown in Table 3.

Table 3. Load factors and probabilistic characteristics for dead and live loads

Type of load	Load factor, γ	Bias factor, λ	Coefficient of variation, COV	Distribution
Dead load	1.25	1.05	0.10	Normal
Live load	1.75	1.15	0.20	Normal

Both λ_R and COV_R for a certain case of calculation are computed through the theoretically predicted resistance, R_{Pi}, and the measured nominal resistance R_{Mi}. The measured nominal resistance was defined as the load corresponding to a displacement that is equal to 5% diameter of drilled shafts or the plunging load in static load tests (O'Neill and Reese [11]), whichever comes first. Paikowsky et al. [12] evaluated that this criterion provides a reliable and simple failure interpretation. For the mean of resistance bias factor:

$$\lambda_R = \frac{\sum_{i=1}^{N} \lambda_{Ri}}{N} \tag{7}$$

Here $\lambda_{Ri} = R_{Mi}/R_{Pi}$, and N is the number of considered drilled shafts. The standard deviation of resistance bias factor is determined as:

$$\sigma_R = \sqrt{\frac{\sum_{i=1}^{N} (\lambda_{Ri} - \lambda_R)^2}{N-1}} \tag{8}$$

Finally, the coefficient of variation of resistance bias factor is given as:

$$COV_R = \frac{\sigma_R}{\lambda_R} \tag{9}$$

2.4 Resistance factor calibration based on first-order reliability method (FORM)

The first-order reliability method (FORM) is a convenient tool to assess the reliability of a structural component. Based on the Hasofer and Lind [9] approach, the present studies using the FORM provide a means for calculating the partial safety factors, ϕ and γ_i, as indicated in Eq. 4 for a target reliability index β_T . In design practice, there are usually two types of limit state, which are ULS and SLS. Both types can be represented generally by the following limit state function:

$$g(X) = g(X_1, X_2, \ldots, X_n) \tag{10}$$

In which X is a vector of basic random variables, X_i, for the resistance and loads. The limit state is defined when $g(X) = 0$, and therefore, failure occurs as $g(X) < 0$. The target reliability index, β_T, is defined as the shortest distance from the origin to the failure surface in the reduced coordinates at the most probable failure point on that surface, this point called the design point, x_i^*, at which the joint probability density function of the vector X is greatest.

In the space of the reduced variables, the designs at different target reliability indices may be viewed as corresponding to satisfying different failure surfaces represented by varying distances to the origin β_T (see Fig. 2). The most general design format is to apply the partial safety factors, $\overline{\gamma_i}$, to the basic design variables, these factors may be apply to the respective mean values (Ang and Tang [3]); thus,

$$g(\overline{\gamma_1}\mu_{X_1}, \quad \overline{\gamma_2}\mu_{X_2}, \ldots, \overline{\gamma_n}\mu_{X_n}) = 0 \tag{11}$$

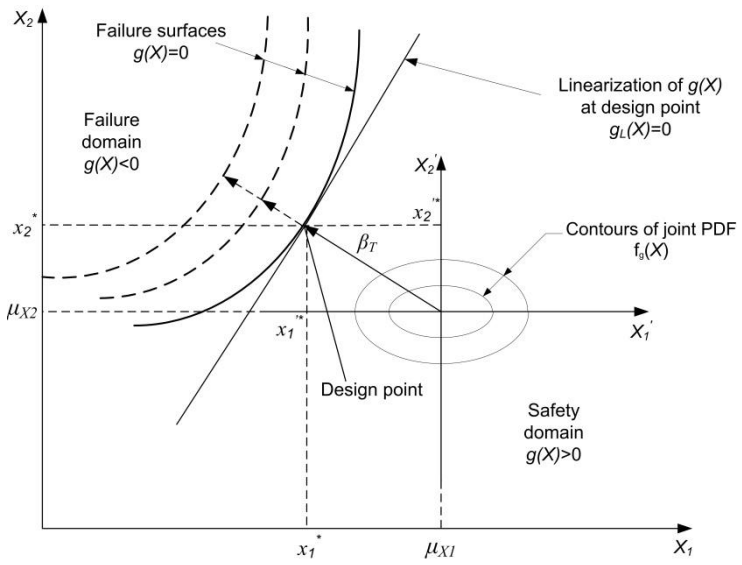

Figure 2. Relationship of partial factors to a design point

From Eq. 11, $\overline{\gamma_i}\,\mu_{Xi}$ should be on the failure surface; in particular, it may be at the most probable failure point. Hence, the required partial safety factors are:

$$\overline{\gamma_i} = \frac{x_i^*}{\mu_{X_i}} \tag{12}$$

Therefore, the determination of the required safety factors is also a problem of determining the most probable failure point x_i^*. The computational steps to determine the safety factors for a specified target reliability index, β_T, are as follows:

- Step 1: in the regular coordinate system, assume a design point, x_i^*, and in the reduced coordinate system, obtain corresponding point, $x_i'^*$, using a transformation:

$$x_i'^* = \frac{x_i^* - \mu_{X_i}}{\sigma_{X_i}} \tag{13}$$

Where μ_{Xi} and σ_{Xi} are the mean value and the standard deviation of basic random variable X_i, respectively. The mean value of the vector of basic random variables is often used as an initial value for the design point.

- Step 2: if the distribution of basic random variables is non-normal, approximate this distribution with an equivalent normal distribution at the design point, having the same tail area and ordinate of the probability density function, that is an equivalent mean:

$$\mu_{X_i}^N = x_i^* - \Phi^{-1}\left[F_{X_i}(x_i^*)\right]\sigma_{X_i}^N \tag{14}$$

and an equivalent standard deviation:

$$\sigma_{X_i}^N = \frac{\phi\left\{\Phi^{-1}\left[F_{X_i}(x_i^*)\right]\right\}}{f_{X_i}(x_i^*)} \tag{15}$$

Where $\mu_{X_i}^N$ and $\sigma_{X_i}^N$ are the mean and standard deviation of the equivalent normal distribution for variable X_i, respectively. $F_{Xi}(x_i^*)$ and $f_{Xi}(x_i^*)$ are the original cumulative distribution function (CDF) and original probability density function (PDF) of variable, X_i, evaluated at the design point x_i^*, respectively. Φ and ϕ are the CDF and PDF of the standard normal distribution, respectively.

- Step 3: set $x_i'^* = -\alpha_i^* \beta_i$, in which α_i^* is the direction cosine determined as follows:

$$\sum\left(\left(\frac{g}{(X_i'}\right)^2\right) \tag{16}$$

Where:

$$((g/(''(''X_{\downarrow}i^{\uparrow\prime}))_{\downarrow} *= ((g/(''(''X_{\downarrow}i^{\uparrow}))_{\downarrow} * \sigma_{\downarrow}(X_{\downarrow}i)^{\uparrow}N \tag{17}$$

- Step 4: a new design point obtained as:

$$x_i^* = \mu_{X_i}^N - \alpha_i^* \beta_T \sigma_{X_i}^N \tag{18}$$

In general, the determination of x_i^* requires an iterative solution. Steps 1 to 3 are repeated until convergence of α_i^* is achieved. Then, through Eq. 12, the resistance factor, ϕ, and the load factors, γ_i, are obtained as:

$$\phi = \frac{r^*}{\mu_R} \tag{19}$$

and:

$$\gamma_i = \frac{q_i^*}{\mu_{Q_i}} \tag{20}$$

Where r^* and q_i^* are the design points of resistance and loads, respectively. μ_R and μ_{Qi} are the mean values of resistance and loads, respectively. The resistance factor is generally less than one, whereas the load factors are greater than one.

As specified by Paikowsky et al. [12], for a given target reliability index and probability distributions for resistance and loads, the partial safety factors determined by the FORM approach may differ with failure mode. For this reason, the calibration of the partial safety factors is to maintain the same values for all loads at different failure modes. In the case of geotechnical codes, the resistance factor calibration is performed for a set of load factors already specified in the structural code (see Section 2.3). Thus, the load factors are fixed, the following algorithm is used to determine the resistance factor only:

- For a given target reliability index, probability distributions and statistical parameters of load and resistance variables, compute mean resistance using FORM.
- With the mean value of resistance computed above, the resistance factor, ϕ, can be revised for a given set of load factors as follows:

$$\phi = \frac{\sum_{i=1}^{n} \gamma_i \mu_{Q_i}}{\mu_R} \tag{21}$$

2.5 Resistance factor calibration based on Monte Carlo simulation (MCS)

This paper follows the calibration procedure based on MCS as recommended by Allen et al. [2] to determine the resistance factor of drilled shafts. The dead and live loads are considered abiding the strength I ultimate limit state. Thus, the limit state function can be written as:

$$g = R_M - Q_{MD} - Q_{ML} \tag{22}$$

In which R_M, Q_{MD}, and Q_{ML} are the measured nominal resistance, the mean value of dead load and live load, respectively. Implement bias factors, λ_R, λ_{QD}, and λ_{QL} for the resistance, dead load and live load, respectively, we have:

$$g = R_P\lambda_R - Q_D\lambda_{QD} - Q_L\lambda_{QL} \tag{23}$$

Combine Eq. 4 into Eq. 23, after several transformations, the limit state function can be rewritten as:

$$g = Q_L\left(\frac{\gamma_D\frac{Q_D}{Q_L} + \gamma_L}{\phi}\lambda_R - \lambda_{QD}\frac{Q_D}{Q_L} - \lambda_{QL}\right) \tag{24}$$

Where all terms in Eq. 24 are the same as those aforementioned in Section 2.3.

MCS was used to generate random numbers that are needed to independently extrapolate the cumulative distribution function (CDF) value for each random variable in the calibration process. In this calibration, there are three random variables which are resistance, dead load and live load bias factors. The computation steps are as follows:

- Step 1: assign a target reliability index, β_T .
- Step 2: select a trial resistance factor, ϕ.
- Step 3: generate random numbers for each set of bias factors λ_R, λ_{QD} and λ_{QL}.
- Step 4: define the limit state function g as described in Eq. 24. Find the number of cases in which $g \leq 0$. The probability of failure is then computed as:

$$P_f = \frac{count(g \leq 0)}{N_S} \tag{25}$$

Where N_S is the number of simulations. In this paper, the number of simulations was used as $5x10^4$. The corresponding calculated reliability index, β, is then defined as:

$$\beta = -\Phi^{-1}(P_f) \tag{26}$$

Where Φ^{-1} is the inverse CDF of the standard normal distribution. If the calculated reliability index, β, is different from the specified target reliability index, β_T , the trial resistance factor, ϕ, in Step 2 should be changed and a new iteration needs to be repeated until $|\beta-\beta_T| \leq$ tolerance.

3. Case Study

3.1 Database for calibration

A database for axially loaded drilled shafts was collected from report NCHRP 507 (Paikowsky et al. [12]). Sixteen cases of calculation consisting of the number of considered pile cases, soil types, calculation methods, and construction methods are categorized in Table 4.

Table 4. Calculation cases for drilled shafts

No.	No. of pile cases	Soil type	Prediction method	Construction method[c]
1	12	Sand	FHWA[a]	Casing
2	9	-	-	Slurry
3	12	-	Reese & Wright (1977)	Casing
4	9	-	-	Slurry
5	13	Clay	FHWA	Casing
6	36	-	-	Dry
7	21	Sand+Clay	FHWA	Casing
8	11	-	-	Dry
9	9	-	-	Slurry
10	21	-	Reese & Wright (1977)	Casing
11	11	-	-	Dry
12	9	-	-	Slurry
13	46	Rock	Carter & Kulhawy (1988)	Mixed
14	30	-	-	Dry
15	46	-	IGM[b]	Mixed
16	30	-	-	Dry

[a,b]FHWA=Reese & O'neill (1988), IGM=O'neill & Reese (1999)
[c]Refer to O'neill & Reese (1999)

In order to calibrate resistance factors, statistical parameters and probability distributions for the resistance, dead load and live load have to be determined. As mentioned in Section 2.3, the statistical parameters and probability distributions for the dead load and live load were already estimated by Nowak [10] and shown in Table 3. Therefore, the next section will focus on the determination of probabilistic characteristics for the resistance. To avoid redundancy hereafter, cases of calculation will be denoted briefly by a group of words. For example, "Sand-RW-Slurry", that is, the soil type is the sand, the prediction is the Reese and Wright method, and the construction is the slurry method.

3.2 Probabilistic characteristics for resistance

Based on the collected database, apply Eqs. 7, 8, and 9 to calculate the mean, standard deviation and coefficient of variation of resistance bias factors, respectively. Assume that the probability distribution of the resistance bias factors is lognormal. In the next step the Kolgomorov-Smirnov test (K-S test) will be used to verify the fitness of the empirical cumulative distribution function, F_E, against the fitted cumulative distribution function, F_F . The K-S test seeks how close the F_E is to the F_F . Thus, the K-S test statistic, D_N, is simply the largest (vertical) distance between F_E and F_F across all values of the resistance bias factor. The K-S test will be satisfactory as the adjusted K-S test statistic is less than the critical value:

$$\left(\sqrt{N} + 0.12 + \frac{0.11}{\sqrt{N}}\right) D_N \leq CV \tag{27}$$

In which N is the number of calculated resistance bias factors; it is also the number of considered pile cases. D_N is the K-S test statistic. CV is the critical value which has a value of 1.358 corresponding to a significance level of 5%. A selected result of Rock-IGM-Mixed is indicated in Fig. 3 for demonstration purpose. The graphs on Fig. 3a are the histogram and probability density function (PDF) of the bias factors which are assumed to follow the lognormal distribution. The graphs on Fig. 3b are the empirical cumulative distribution function, F_E, and fitted cumulative distribution function F_F . In this case, the determined adjusted K-S test statistic is 0.562, much less than 1.358, and satisfies the requirement of the K-S test. Hence, the lognormal distribution attributed to the resistance bias factors is acceptable. The results for the remaining fifteen cases of calculation are also satisfactory with the K-S test and are shown in Table 5. The largest value of the adjusted K-S test statistic is 0.763 for the case of Sand-FHWA-Slurry and the smallest one is 0.342 for the case of Sand+Clay-FHWA-Casing.

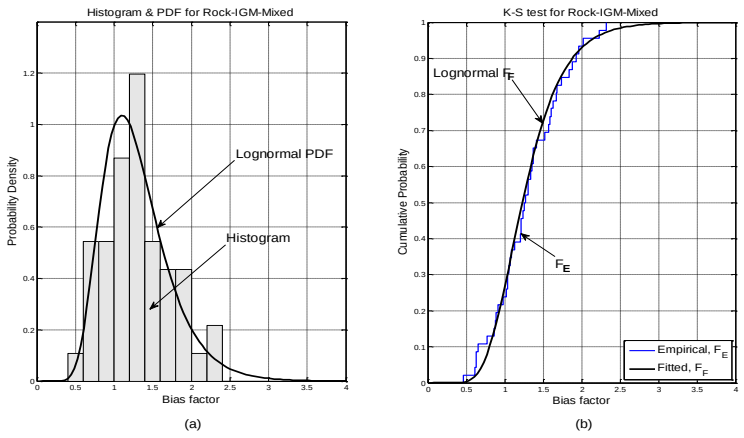

Figure 3. The K-S test for Rock-IGM-Mixed

Regarding the number of pile cases needed for probability analyses, Fenton and Griffiths [7] suggested that if sufficient data are available, generally, at least 20 observations are needed for each dataset. If so, there are nine out of the sixteen cases of calculation in Table 5 that have a number of pile cases less than 20. Paikowsky et al. [12] evaluated that one of the major difficulties with respect to the code calibration is the lack of data. We consider this problem as a type of uncertainty when using probabilistic analysis methods. From Table 5, it is easily recognized that the calculation cases with the sufficient number of pile cases (i.e., from 21 to 46 pile cases) have K-S test statistics smaller than those of calculation cases with the lack of data (i.e., only from 9 to 13 pile cases).

Also, the bias factors, λ_R, represent the difference level between the measured nominal resistance and the theoretically predicted resistance. If a prediction method has a bias factor larger than one, that is, this method is an underpredicted method, and vice versa, a method is overpredicted when its bias factor is smaller than one. In addition, the coefficient of variation of bias factors, COV_R, is an important parameter which presents a level of uncertainty in modelling of a prediction method. Therefore, one method which has a bias factor of one and a coefficient of variation of zero is a perfect prediction method. In Table 5, the FHWA prediction method for sandy soil and the casing construction (Sand-FHWA-Casing) is the most underpredicted method with a bias factor of 2.270. Conversely, the FHWA method used for the clayey soil and the dry construction (Clay-FHWA-Dry) is the most overpredicted method with a bias factor of 0.797. Similarly, the RW method has a coefficient of variation of 0.231 for the sandy+clayey soil and the slurry construction (Sand+Clay-RW-Slurry), but this method has a coefficient of up to 0.695 for the sandy soil and the same construction method (Sand-RW-Slurry). For a prediction method, the values of these parameters will vary in conjunction with the quantity as well as the quality of the data collected, that is, the more good data, the more precise the prediction method.

Table 5. Statistical parameters and K-S test results for resistance bias factors

No.	Calculation case	No. of pile case	λ_R	σ_R	COV_R	D_N	ATS^*
1	Sand-FHWA-Casing	12	2.270	1.000	0.441	0.165	0.595
2	Sand-FHWA-Slurry	9	1.614	1.122	0.695	0.242	0.763
3	Sand-RW-Casing	12	1.650	0.944	0.572	0.117	0.422
4	Sand-RW-Slurry	9	1.033	0.718	0.695	0.161	0.507
5	Clay-FHWA-Casing	13	0.835	0.399	0.478	0.143	0.539
6	Clay-FHWA-Dry	36	0.797	0.296	0.371	0.079	0.482
7	Sand+Clay-FHWA-Casing	21	1.039	0.297	0.286	0.072	0.342
8	Sand+Clay-FHWA-Dry	11	1.322	0.359	0.272	0.158	0.549
9	Sand+Clay-FHWA-Slurry	9	1.288	0.333	0.259	0.209	0.660
10	Sand+Clay-RW-Casing	21	0.951	0.325	0.342	0.105	0.496
11	Sand+Clay-RW-Dry	11	1.206	0.365	0.303	0.149	0.517
12	Sand+Clay-RW-Slurry	9	1.158	0.268	0.231	0.199	0.628
13	Rock-CK-Mixed	46	1.229	0.504	0.410	0.108	0.746
14	Rock-CK-Dry	30	1.350	0.584	0.433	0.112	0.626
15	Rock-IGM-Mixed	46	1.298	0.437	0.337	0.081	0.562
16	Rock-IGM-Dry	30	1.400	0.478	0.342	0.082	0.462

*Adjusted K-S Test Statistic

3.3 Resistance factor calibration

The calibration is performed for sixteen cases of calculation according to three reliability methods as FOSM, FORM, and MCS. In order to evaluate the variability (sensitivity) of the resistance factor, target reliability indices are assigned as 2.0, 2.5, 3.0, and 3.5; which correspond to the target probabilities of failure as 0.1, 0.01, 0.001, and 0.00023 (see Table 1); a range of the dead load to live load ratios, Q_D/Q_L, is taken from 0.52 to 4.32; which correspond to the bridge span lengths from 9 m to 75 m (see Table 2).

The statistical parameters for the dead load and live load are shown in Table 3, the probability distribution for both is normal. The statistical parameters for the resistance are shown in Table 5, the probability distribution for the resistance is lognormal.

For the purpose of demonstration and comparison, four cases of calculation with various types of soil, resistance prediction methods and construction methods are chosen. The results are shown in Figs. 4, 5, and 6 according to FOSM, FORM, and MCS, respectively.

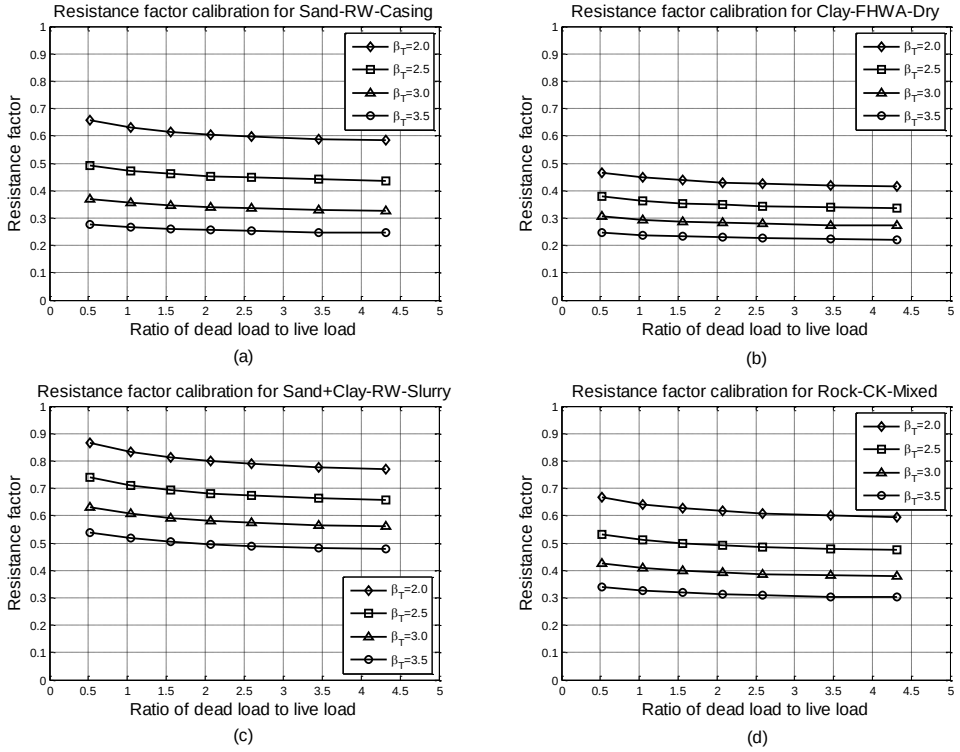

Figure 4. Resistance factors calibrated by FOSM

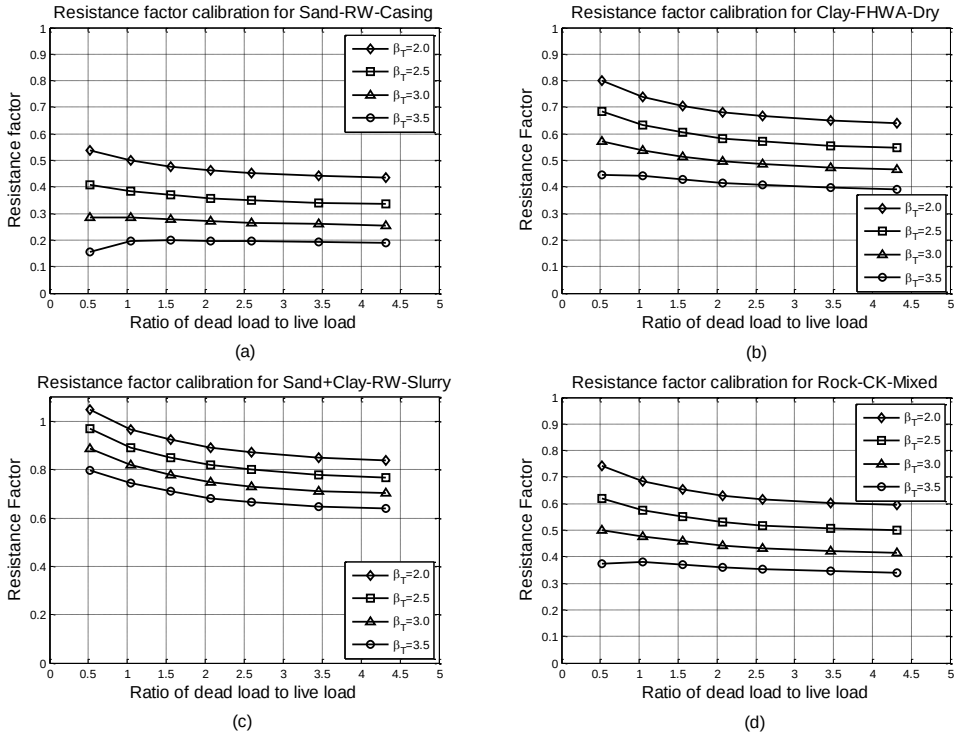

Figure 5. Resistance factors calibrated by FORM

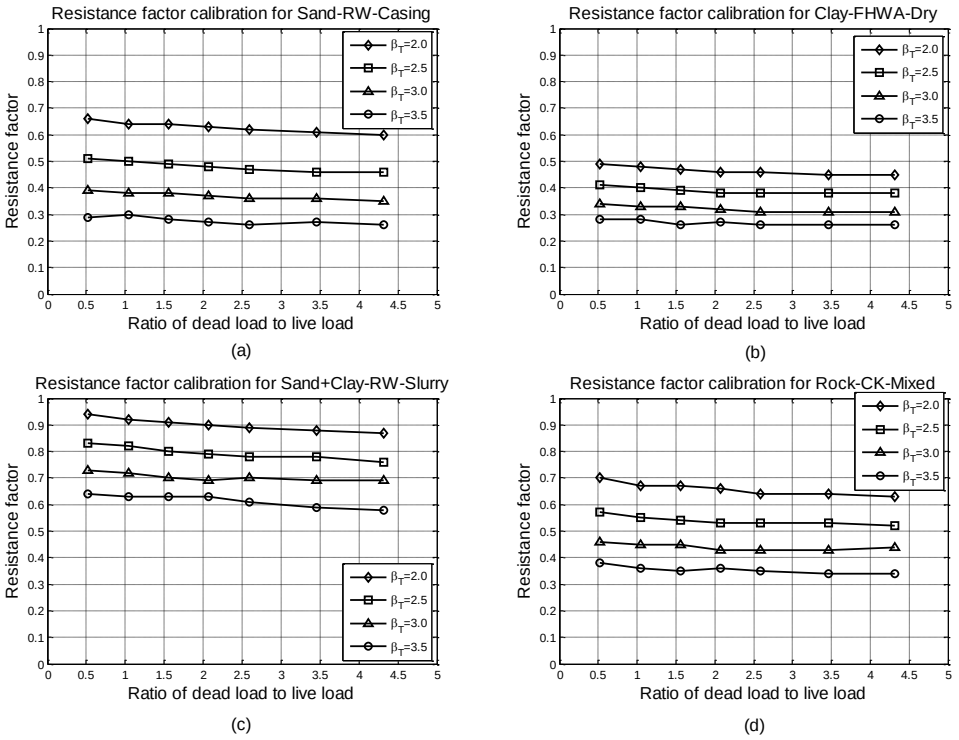

Figure 6. Resistance factors calibrated by MCS

Based on the graphs, several general observations can be made as follows:

- Clearly, the larger the target reliability index, the smaller the resistance factors.
- The resistance factors calibrated by FOSM, FORM, and MCS are in relative agreement with one another. Intuitively, the correlation of the resistance factors created between FOSM and MCS is better than that between FOSM and FORM as well as between FORM and MCS.
- According to FOSM and MCS, the value of resistance factor gradually decreases with the increase of the dead load to live load ratio and reaches a stable value when this ratio is larger than 3.0 (see Figs. 4, 6). While the value of the resistance factor according to FORM with β_T = *3.5* starts to reveal an inverse tendency; the value gradually increases with the increase of the ratio and also achieves a stable value when this ratio is larger than 3.0 as well (see Figs. 5a, b, d).

One issue arising herein is that of which target reliability index will be selected for practical designs. Based on the review of the studies, the survey of common practice, and the evaluation of several authors, Paikowsky et al. [12] recommended the use of the target reliability indices in conjunction with capacity evaluation methods of single piles as follows:

- For redundant piles, defined as 5 or more piles per pile cap, the recommended probability of failure is 0.01, corresponding to a target reliability index of 2.33.
- For non-redundant piles, defined as 4 or fewer piles per pile cap, the recommended probability of failure is 0.001, corresponding to a target reliability index of 3.0.

Hence, the values of the calibrated resistance factors for all sixteen cases of calculation shown in Table 6 are taken with the target reliability indices as 2.5 and 3.0 only; and the dead load to live load ratio is given herein as 3.46 (i.e., larger than 3.0).

Table 6. Resistance factors with target reliability indices, $\beta_T = 2.5$ and 3.0

				FOSM		FORM		MCS	
No.	*Calculation case*	λ_R	COV_R/λ_R	β_T=2.5	β_T=3.0	β_T=2.5	β_T=3.0	β_T=2.5	β_T=3.0
1	Sand-FHWA-Casing	2.270	0.194	0.82	0.65	0.47	0.38	0.80	0.69
2	Sand-FHWA-Slurry	1.614	0.430	0.33	0.23	0.25	0.18	0.34	0.25
3	Sand-RW-Casing	1.650	0.347	0.44	0.33	0.34	0.26	0.46	0.36
4	Sand-RW-Slurry	1.033	0.673	0.21	0.15	0.25	0.18	0.22	0.16
5	Clay-FHWA-Casing	0.835	0.573	0.28	0.22	0.43	0.34	0.31	0.24
6	Clay-FHWA-Dry	0.797	0.465	0.34	0.27	0.56	0.47	0.38	0.31
7	Sand+Clay-FHWA-Casing	1.039	0.275	0.34	0.27	0.68	0.61	0.61	0.53
8	Sand+Clay-FHWA-Dry	1.322	0.206	0.70	0.59	0.71	0.63	0.80	0.70
9	Sand+Clay-FHWA-Slurry	1.288	0.201	0.70	0.59	0.73	0.66	0.81	0.70
10	Sand+Clay-RW-Casing	0.951	0.359	0.43	0.35	0.60	0.52	0.48	0.40
11	Sand+Clay-RW-Dry	1.206	0.251	0.60	0.50	0.66	0.58	0.68	0.58
12	Sand+Clay-RW-Slurry	1.158	0.200	0.66	0.57	0.78	0.71	0.78	0.69
13	Rock-CK-Mixed	1.229	0.334	0.48	0.38	0.51	0.42	0.53	0.43
14	Rock-CK-Dry	1.350	0.321	0.50	0.39	0.48	0.39	0.54	0.44
15	Rock-IGM-Mixed	1.298	0.260	0.60	0.49	0.60	0.52	0.67	0.56
16	Rock-IGM-Dry	1.400	0.244	0.64	0.52	0.60	0.52	0.71	0.59

Based on a set of comprehensive results shown in Table 6, firstly we realize that the correlation between the values of the resistance factor by FOSM and MCS is better than that by FOSM and FORM as well as MCS and FORM. Secondly, we can evaluate the reliability level of a prediction method in a combination of a certain soil type and construction method. If we choose the results according to MCS with $\beta_T = 2.5$ as an example, we will readily see that the FHWA method is consistent for the sandy soil and the casing construction method ($\phi = 0.80$) in case Sand-FHWA-Casing, but that is not suitable for the slurry construction method ($\phi = 0.34$) in case Sand-FHWA-Slurry. Similarly, using the IGM method in case Rock-IGM-Dry ($\phi = 0.71$)

clearly has a higher reliability level than the use of the CK method for the same conditions of soil and construction ($\phi = 0.54$) in case Rock-CK-Dry.

Since the input data of the dead load and live load were fixed and commonly used for all cases of calculation, the question is to find a relationship between the given resistance factors and the statistical parameters of the resistance. Aside from the statistical parameters mentioned above, a ratio of COV_R to μ_R is proposed and implemented into Table 6. Relationships between the resistance factor, ϕ, versus μ_R, σ_R, COV_R and ratio $\mathrm{COV_R}/\mu_\mathrm{R}$ are shown in Fig. 7a. We see that the relationships between ϕ versus μ_R, σ_R, and COV_R are not clear; while the one between ϕ and the ratio COV_R/μ_R (denoted by a bold line) is more apparent, the resistance factor increases with the decrease of this ratio.

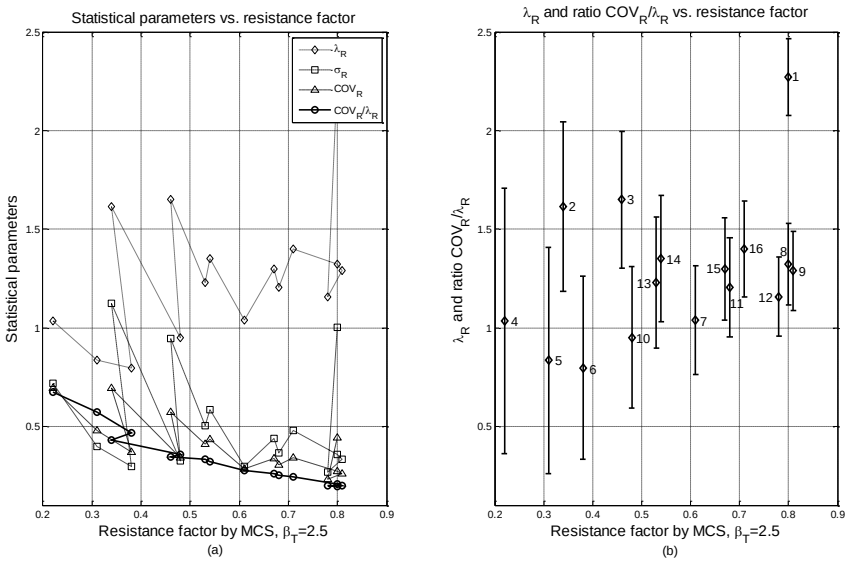

Figure 7. Relationship of resistance factor vs. statistical parameters of resistance

Fig. 7b also describes the relationships between ϕ versus μ_R and the ratio COV_R/μ_R by another manner via error bars. The middle point ordinate of an error bar denotes the mean value of μ_R and the length from this point to both ends of the error bar represents the value of the ratio COV_R/μ_R. The error bars with the smaller ratio fall into positions that have larger values of ϕ. Calculation cases number 1, 8 and 9 with the small ratios (around 0.20) have the same resistance factors ($\phi = 0.80$), and vice versa, case number 4 with the largest ratio (0.673) leads into the smallest resistance factor ($\phi = 0.22$). We consider cases number 1, 8, 9, and 12 which have the same ratios (approximately 0.20). This results in the same resistance factors with the value about 0.80, although the values of μ_R of these cases vary considerably from 1.158 (case number 12) up to 2.270 (case number 1). The ratio COV_R/μ_R is likely to affect strongly the resistance factors. However, it should be noted

that this effect is only obtained from the results by MCS, while FOSM and FORM do not express clearly this one.

The relationship between ϕ versus the ratio COV_R/μ_R is also considered with respect to FOSM and FORM. Figs. 8a, b, and c describe this relationship for FOSM, FORM, and MCS, respectively. Generally, all three methods give the same tendency, that is, the resistance factor increases with the decrease of the ratio, but the correlation of each has relative discrepancies. MCS and FOSM create a quite good correlation between ϕ and the ratio, but there still exist some points at which the value of fluctuates slightly. Whereas, FORM does not produce a good correlation; there are many points where the values of ϕ fluctuate considerably, and these fluctuation amplitudes, generally, reduce gradually with the decrease of the ratio.

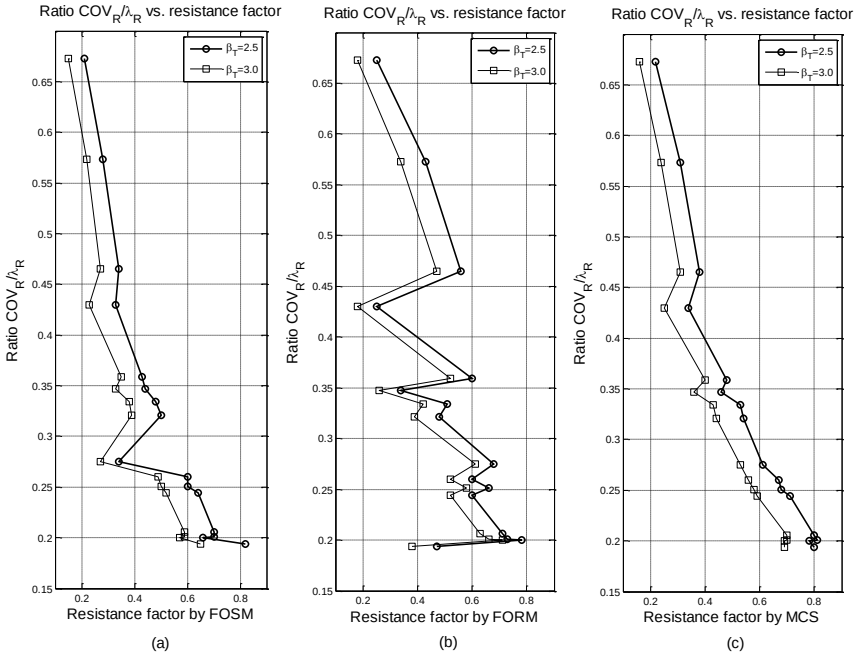

Figure 8. Relationship of resistance factor vs. COV_R/λ_R for reliability methods

3.4 Correlation analyses

The relationships between the resistance factors obtained by the different reliability methods need to be checked. Based on the correlation analyses and the robust regression method, these relationships are quantified and expressed in terms of numerical values and functional relations. The data for analyses are taken from Table 6. The analysis results are shown in figs. 9a, b, and c as follows:

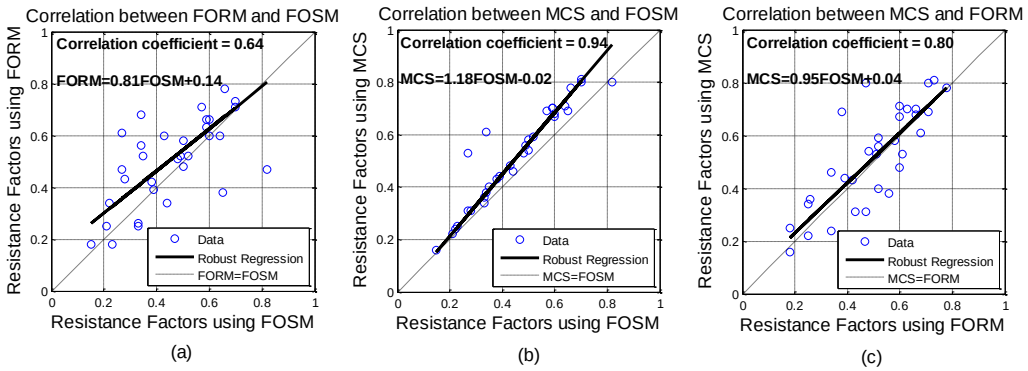

Figure 9. Correlation analyses of resistance factors for reliability methods

Based on the results described in Fig. 9, we see that:

- The correlation coefficients between method couples of FORM-FOSM, MCS-FOSM, and MCS- FORM are 0.64, 0.94, and 0.80, respectively. Through these coefficients, it can be confirmed quantitatively that the correlation level between MCS and FOSM is better than that between FORM and FOSM as well as between MCS and FORM.
- According to the functional relations, MCS and FORM produce resistance factors consistently higher than those obtained by FOSM. Further, both MCS and FORM produce the resistance factors which have relative agreement values with each other.

4. Conclusions

This paper has presented the resistance factor calibration according to three reliability methods: FOSM, FORM and MCS followed the LRFD method. A database of drilled shafts was collected and used for this purpose. Sixteen cases of calculation were considered comprising various resistance prediction methods, soil types and construction methods. In the scope of this paper, only the ultimate limit state of strength I for axially loaded drilled shafts is used, other limit states are not mentioned herein.

The limit state function used only includes the total resistance, dead load, and live load. The probabilistic characteristics for the dead load and live load were taken from the design criterion for superstructures with the assigned values. For the resistance, the statistical parameters were calculated and the theoretical (fitted) probability distribution was selected and checked by the Kolmogorov-Smirnov test.

The resistance factors were calibrated according to the different target reliability indices and dead to live load ratios. Based on a set of results, conclusions drawn from the study are as follows:

1. A larger target reliability index results in smaller resistance factors.
2. The value of the resistance factor decreases gradually with the increase of the dead to live load ratio and reaches a stable value when this ratio is larger than 3.0. However, there was a discrepancy with respect to FORM, when the target reliability index is larger than 3.5, then the value of resistance factor increases gradually with the increase of the ratio and also reaches a stable value as this ratio is also larger than 3.0.
3. Through Table 6, a design engineer can choose a prediction method that has a consistent reliability level with respect to a prescribed soil condition and a specified construction method.
4. The value of the resistance factor increases gradually with the decrease of the ratio of the coefficient of variation to the mean of the resistance bias factor. In this study, MCS was used to derive this observation.
5. MCS and FORM produce resistance factors consistently higher than those obtained by FOSM. With regard to the correlations between the methods, MCS and FOSM have a good correlation with a correlation coefficient of 0.94.
6. MCS has indicated to be a powerful and confident tool aiming to solve probabilistic problems in civil engineering.

ACKNOWLEDGEMENTS

This study is mainly funded by Project 322 of the Vietnam Ministry of Education and Training and partly supported by CICAT and the Section of Hydraulic Engineering, Delft University of Technology, the Netherlands.

REFERENCES

[1] Abu-Farsakh, M. Y.; and Yu, X.: *Interpretation criteria to evaluate resistance factors for axial load capacity of drilled shafts*. Transportation Research Record: Journal of the Transportation Research Board, 2202(1), 20-31. (2010)

[2] Allen, T. M.; Nowak, A. S.; and Bathurst, R. J.: *Transportation research circular E-C079: Calibration to determine load and resistance factors for geotechnical and structural design*. Technical report, Transportation Research Board, Foundations of Bridges and Other Structures Committee, General Structures Committee. 2005. Washington, D.C.

[3] Ang, A. H.-S.; and Tang, W. H.: *Probability Concepts in Engineering Planning and Design-Decision Risk and Reliability*. Volume II. John Wiley and Sons, 1984

[4] Ayyub, B. M.; Assakkaf, I. I.; and Atua, K.: *Reliability-based load and resistance factor design (LRFD) of hull girders for surface ships*. Naval Engineers Journal, 112(4), 279-296. (2000)

[5] Barker, R. M.; Duncan, J. M.; Rojiani, K. B.; Ooi, P. S. K.; Tan, C. K.; and Kim, S. G.: *National cooperative highway research program - Report 343: Manuals for the design of bridge foundations*. Technical report, Transportation Research Board, National Research Council. 1991. Washington, D. C.

[6] Brown, D. A.; Turner, J. P.; and Castelli, R. J.: *Federal highway adminitration - Report No. FHWA-NHI-10-016: Drilled shafts: Construction procedures and LRFD design methods*. Technical report, National Highway Institute, Federal Highway Administration, US Department of Transportation. 2010. Washington, D.C.

[7] Fenton, G. A.; and Griffiths, D. V.: *Risk Assessment in Geotechnical Engineering*. John Wiley and Sons, 2008

[8] Hansell, W. C.; and Viest, I. M.: *Load factor design for steel highway bridges*. AISC Engineering Journal, 8(4), 113-123. (1971)

[9] Hasofer, A. M.; and Lind, N. C.: *An exact and invariant first-order reliability format*. Journal of Engineering Mechanics, 100(EM1), 111-121. (1974)

[10] Nowak, A. S.: *National cooperative highway research program - Report 368: Calibration of LRFD bridge design code*. Technical report, Transportation Research Board. 1999. Washington, D. C.

[11] O'Neill, M. W.; and Reese, L. C.: *Federal highway administration - Report No. FHWA-IF-99-025: Drilled shafts: Construction procedures and design methods*. Technical report, Federal Highway Administration. 1999. Washington, D.C.

[12] Paikowsky, S. G.; Birgisson, B.; McVay, M.; Nguyen, T.; Kuo, C.; Baecher, G. B.; Ayyub, B. M.; Stenersen, K.; O'Malley, K.; Chernauskas, L.; and O'Neill, M.: *National cooperative highway research program - Report 507: Load and resistance factor design (LRFD) for deep foundations*. Technical report, Transportation Research Board. 2004. Washington, D. C.

[13] Withiam, J.; Voytko, E.; Barker, R.; Duncan, J.; Kelly, B.; Musser, S.; and Elias, V.: *Federal highway administration - Publication No. FHWA-HI-98-032: Load and resistance factor design (LRFD) for highway bridge substructures*. Technical report, National Highway Institute, Federal Highway Administration, US Department of Transportation. 1998. Washington, D.C.

Reliability and Risk Analysis of Concrete Bridges for Hazard Scenarios

Vazul Boros, Balthasar Novák
Institute for Lightweight Structures and Conceptual Design,
University of Stuttgart

Abstract: Bridges are essential, yet also vulnerable parts of the infrastructure. They are subject to natural disasters, traffic accidents and terrorist attacks, moreover they generally require significant resources and time to be repaired or replaced. In this research critical reinforced and prestressed concrete bridges were to be identified. Based on a complex probabilistic model the reliability index was assessed for several hazard scenarios considering four different traffic scenarios. An approximation by the Monte Carlo method forms the core of the reliability analysis, however the variance of the approximation can be reduced effectively, by considering the model uncertainty factors analytically. The introduced method is demonstrated on the example of two representative bridges with five hazard scenarios. Based on the results of the Monte Carlo method an approximation of the reliability index, considering also the additional safety due to the redistribution of moments in statically indeterminate structures, is presented. The Monte Carlo method also enables the risk analysis of the different hazard scenarios, taking into account the consequences of failure. These results provide valuable tools for proprietors and operators of traffic infrastructure to reach important ethical and economic decisions. Some interesting insights of the research on the combination of different time-dependent actions and the assessment of the reliability index of systems with several correlated limit states are shown.

1 Introduction

The highway network plays an essential part in a country's economy and social life. Its continuous and undisrupted operation is vital for our society. The probably most vulnerable components of the road infrastructure are bridges

and tunnels. These structures not only act as bottle-necks in the highway system, but also have to face a number of different hazards. Bridges can be affected by vehicle impact against vital structural components such as cables or pillars. Due to the rising percentage of heavy traffic and growing average vehicle weight these impact loads have to be revised regularly. The effect of climate change on structures has to be taken into account, too. It results in higher wind velocities, increased temperatures and rainfall, thus causing storms, floods and other natural disasters. Finally, another ever greater threat to important infrastructure components is represented by terrorist attacks.

The aim of the German research project "Protection of Critical Bridges and Tunnels in a Road Network" (SKRIBT in German) was, to investigate the effects of these hazard scenarios on bridges and tunnels and to develop effective protection measures and strategies as described in [1]. The objective was to rank different types of structures according to their criticality and thus enable traffic administrations to identify their most vulnerable structures. Subsequently, suitable protection measures had to be identified and their effect on the criticality of the structure had to be assessed.

The objectives of the research project required the assessment of the criticality of a structure-hazard combination with suitable indicators. This is also essential for the examination of protection measures, as the reduction of criticality due to a protection measure describes its efficiency. Three main aspects have been considered regarding the criticality of a structure: effects on road users, influence on the road network and structural aspects. All three main aspects have been investigated in detail in the research project, yet this paper addresses the assessment of the criticality of the structure, in particular of reinforced and prestressed concrete bridges.

2 Probabilistic model

The probabilistic model is based on the traditional separation of actions and resistances common to structural engineering. After careful considerations and extensive literature review basic variables have been selected for both sides.

2.1 Resistances

Regarding resistances mainly material properties had to be considered as basic variables. Table 1 provides an overview of the selected variables and the main parameters of the corresponding distribution functions. The distribution functions for the basic variables have been assumed according to various references, for the prestressing steel the permit of the cables [2] provided information regarding the requirements towards material quality. A correlation between the compressive strength and the modulus of elasticity of concrete has been considered in accordance with SIX [3]. The modulus of elasticity has been regarded as constant for reinforcement and prestressing steel. An eccentricity of vertical loading has been considered for pillars. Model uncertainty factors, accounting for random effects neglected in models and simplifications in the mathematical relations according to the JCSS Probabilistic Model Code [4] have been considered, too.

Table 1. Basic variables for resistances

Variable	Distribution	Mean	Standard deviation	Reference
Compressive strength of concrete	Lognormal	43 MPa	5 MPa	[3]
Modulus of elasticity of concrete	Lognormal	33282 MPa	4992 MPa	[3]
Yield stress of reinforcement	Normal	560 MPa	30 MPa	[4]
Modulus of elasticity of reinforcement	Constant	205 GPa	-	[4]
Ultimate strength of prestressing steel	Normal	1876 MPa	64,5 MPa	[2]
Modulus of elasticity of prestressing steel	Constant	195 GPa	-	[2]
Eccentricity of load on pillar	Normal	0 mm	21 mm	[4]
Factor of model uncertainty for bending	Lognormal	1,2	0,15	[4]
Factor of model uncertainty for shear	Lognormal	1,0	0,1	[4]
Factor of model uncertainty for normal forces	Lognormal	1,0	0,05	[4]

2.2 Actions and loads

Modeling actions and loads required more advanced considerations. It had to be distinguished between permanent actions, such as self weight and variable actions, as for example traffic loads or temperature differences. The factor for self weight has been applied to each construction section separately. Also ground settlements have been considered for each pair of pillars individually. Wind actions, based on the evaluation of statistical data recorded in Germany for the past decade, were applied on pillars. The effect of climate change proved to be negligible on the linear temperature differences according to [5], therefore temperature differences have been considered based on FRENZEL et

al. [6]. For the mechanical properties of soil SPAETHE [7] suggest the Beta distribution, hence this was chosen for ground settlements. Model uncertainties have been implemented into the calculation models for actions also. The main characteristics of the probabilistic models for actions other than traffic loads are shown in Table 2.

Table 2. Basic variables for actions and loads

Variable	Distribution	Mean	Standard deviation	Reference
Self weight factor	Normal	1,0	0,1	[3]
Positive temperature difference	Weibull	3,62 K	2,2 K	[6]
Negative temperature difference	Weibull	-2,59 K	1,59 K	[6]
Ground settlements	Beta	1,0 cm	0,3 cm	[7]
Wind velocity	Weibull	10,54 m/s	3,94 m/s	[5]
Factor of model uncertainty for bending	Lognormal	1,0	0,1	[4]
Factor of model uncertainty for shear	Lognormal	1,0	0,1	[4]

In order to reproduce the traffic loads on the bridge, complex traffic simulations were carried out. The simulations were developed on the basis of statistical data acquired in traffic measurements on German highways by KASCHNER et al. [8]. This simulation method has also been used to support the development of new traffic load models for the German National Annex to the EN 1991-2 [9]. Four traffic scenarios have been considered:

- Traffic scenario I - Current traffic on German highways
- Traffic scenario II - Increase in maximum permissible weight of lorries and addition of mobile crane
- Traffic scenario III - Twofold swell of vehicle numbers
- Traffic scenario IV - Twofold swell of vehicle numbers, increase in maximum permissible weight of lorries and addition of mobile crane

One scenario accounts for the current traffic on German highways according to the above mentioned measurements, assuming an average daily traffic of 60.000 vehicles / day with approximately 10.000 vehicles / day heavy traffic. The other three scenarios consider different prognosticated changes in the traffic composition, such as a swell in vehicle numbers or an increase in vehicle loading and they considers additionally a small percentage of exceptionally heavy vehicles like mobile cranes of 72 t. The main parameters of the bimodal normal distribution function for vehicle weights of different vehicle types and the composition of heavy traffic for the different scenarios are presented in Table 3.

Table 3. Parameters of basic variables for vehicle weights and traffic composition

Vehicle type	Portion (%)	Mean (kN)	Standard deviation (kN)	Portion (%)	Mean (kN)	Standard deviation (kN)	I/III Share (%)	II/IV Share (%)
Type 8	49	59,6	14,6	51	91,7	44,0	11,0	10,9
Type 33	20	190,3	23,2	80	208,4	73,9	5,0	4,9
Type 41	69	276,8	59,5	31	414,5	32,5	17,0	16,9
Type 97	34	156,7	18,8	66	211,4	52,8	8,0	7,9
Type 98	62	259,6	92,0	38	405,3	24,8	59,0	-
Type 98 (modified)	62	259,6	92,0	38	526,9	24,8	-	58,9
Mobile crane	100	720,0	63,3	-	-	-	-	0,5

Additional basic variables for the traffic simulations included the distance between vehicles and probabilities for simulating traffic congestion on the bridge. The distance between the axles for each vehicle type and the distribution of loads on the axles have been regarded as constant. The different vehicle types with the distances between axles are presented in Figure 1.

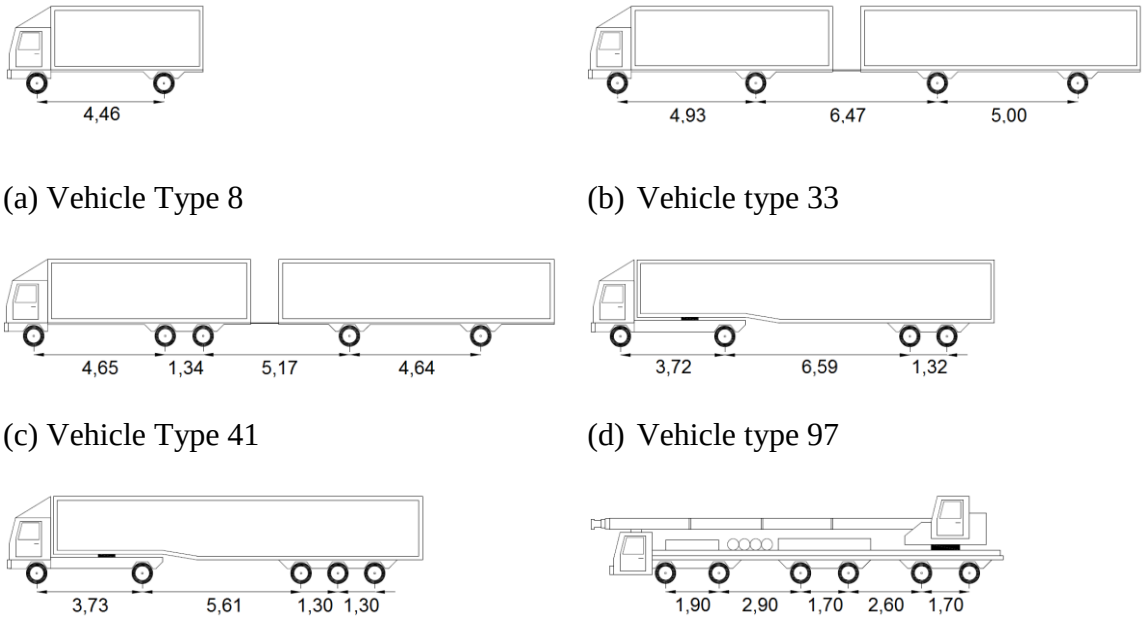

(a) Vehicle Type 8 (b) Vehicle type 33

(c) Vehicle Type 41 (d) Vehicle type 97

(e) Vehicle Type 98 (f) Mobile crane

Figure 1. Vehicle types with distances between axles

3 Reliability analysis

3.1 Method of model uncertainties

The Monte Carlo method has been implemented to determine the risk and reliability indicators in question. In order to improve the accuracy of the Monte

Carlo simulation a special method considering the model uncertainties, has been developed. The technique is similar to the importance sampling method, which utilizes prior information about which domain of the possible values of basic variables contributes most to the probability of failure, and achieves a variance reduction by centering the simulation on this area as described in FABER [10]. In an analogous way the applied method considers only those values of the model uncertainties which result in the failure of the structure.

For each of the basic variables, with the exception of model uncertainties, n different possible realizations according to the corresponding population function are generated. Thereafter the resistance and action forces can be calculated for each of these realizations. The limit state function for one realization can be stated as

$$R_i \cdot \theta_R - E_i \cdot \theta_E \geq 0 \tag{1}$$

with R_i resistance forces for the *i.* simulation
E_i action forces for the *i.* simulation
θ_R model uncertainty factor for resistances
θ_E model uncertainty factor for actions

The model uncertainty factors follow the logarithmic normal distribution, therefore they can be substituted by the exponents of normally distributed variables U_R and U_E.

$$R_i \cdot e^{U_R} - E_i \cdot e^{U_E} \geq 0 \tag{2}$$

$$e^{U_R - U_E} \geq \frac{E_i}{R_i} \tag{3}$$

As the exponential function is strictly increasing, the inequality has to be also valid for the natural logarithm of both sides.

$$U_R - U_E \geq \ln\left(\frac{E_i}{R_i}\right) \tag{4}$$

The variables U_R and U_E being normally distributed, their difference has to be normally distributed also. Therefore the probability of the limit state function not being fulfilled can be calculated as the value of this normal distribution at $\ln(E_i/R_i)$. The corresponding probability of failure for this realization of basic variables can then expressed as

$$\hat{P}_{f\,i} = \Phi\left(\frac{\ln\left(\frac{E_i}{R_i}\right) - \left(\mu_{U_R} - \mu_{U_E}\right)}{\sqrt{\sigma_{U_R}{}^2 + \sigma_{U_E}{}^2}} \right) \tag{5}$$

with $\hat{P}_{f\,i}$ probability of failure for the $i.$ simulation

$\Phi(\cdot)$ standard normal distribution function

μ_{U_R} mean value of variable U_R

μ_{U_E} mean value of variable U_E

σ_{U_R} standard deviation of variable U_R

σ_{U_E} standard deviation of variable U_E

By this equation each realization in the simulation provides an estimate of the failure probability for the investigated limit state. The overall failure probability considering all n simulations can be expressed as

$$\hat{P}_f = \frac{1}{n}\sum_{i=1}^{n} \hat{P}_{f\,i} \tag{6}$$

The variance of the failure probability can then be calculated in analogy to the importance sampling technique by

$$Var\left[\hat{P}_f\right] = \frac{1}{n-1}\left(\frac{1}{n}\sum_{i=1}^{n} \hat{P}_{f\,i}{}^2 - \hat{P}_f\right) \tag{7}$$

In comparison the variance of the crude Monte Carlo method can be estimated according to RACKWITZ [11] by

$$Var\left[\hat{P}_f\right] = \frac{\sqrt{n \cdot \hat{P}_f \cdot \left(1 - \hat{P}_f\right)}}{n \cdot \hat{P}_f} \approx \frac{1}{\sqrt{n \cdot \hat{P}_f}} \tag{8}$$

In both cases the variance is dependent on the number of simulations and the probability of failure which of course can also be expressed by the reliability index. In Figure 2 the variances obtained by the method of model uncertainties for different limit states and the variance of the crude Monte Carlo method according to Equation (8) are plotted.

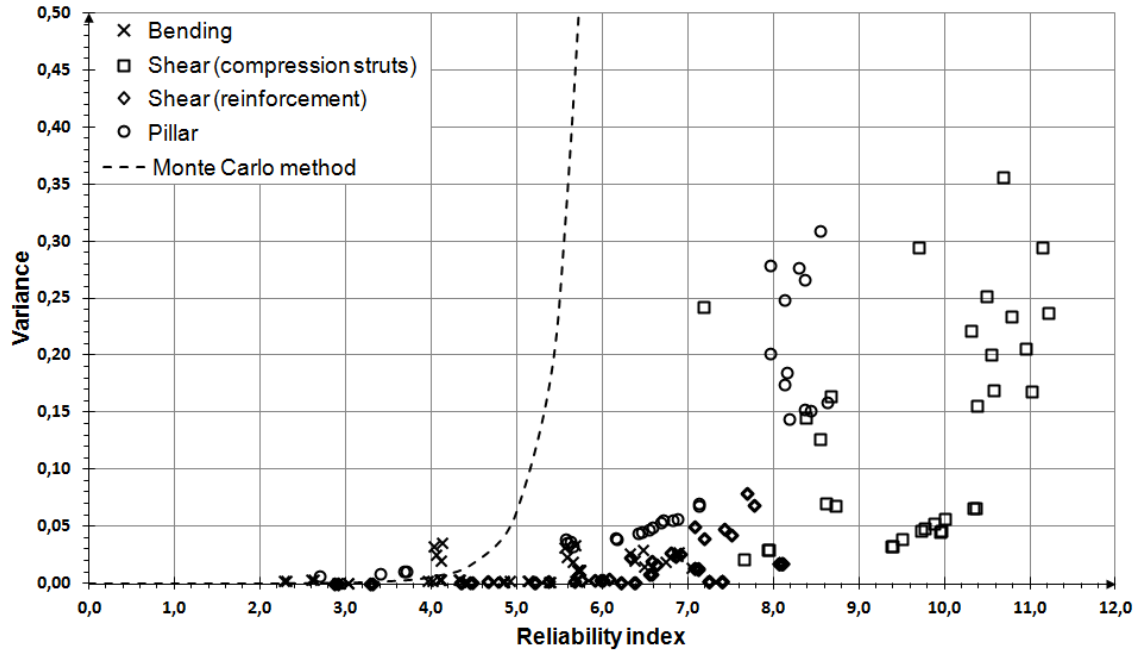

Figure 2. Variance of the estimate for the probability of failure

The introduced method proved effective in improving the accuracy of the estimation for the probability of failure, as the variance for the dominant limit states of shear and bending could be reduced to less than 0,07.

3.2 System reliability analysis

Once the probability of failure had been determined using the method of model uncertainties for each limit state, the overall probability of failure for the bridge has to be calculated. The combined reliability of a structure with several different limit states can be calculated according to a system model as shown for example on a statically indeterminate continuous beam in Figure 3.

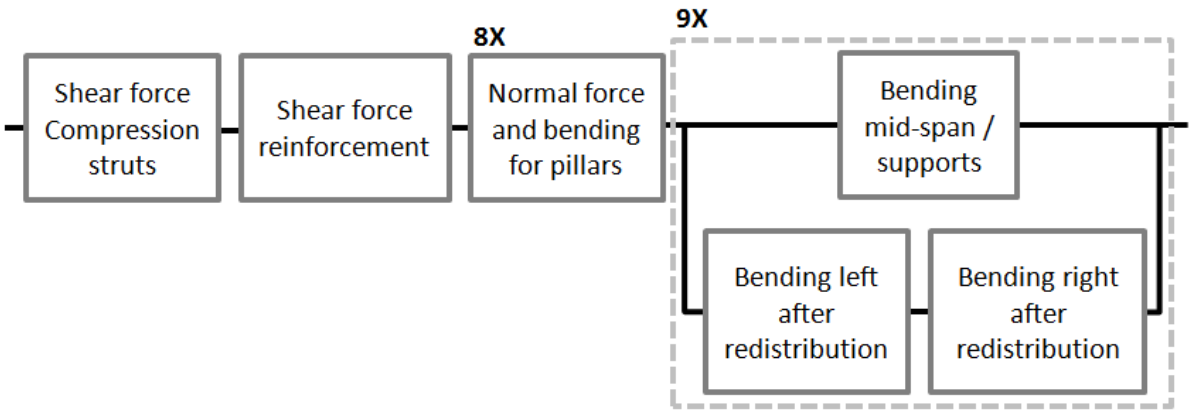

Figure 3. Example of system model for statically indeterminate structure

The different failure modes are to be considered as series systems, as exceeding any of the limit states would result in failure. The redistribution of moments in the statically indeterminate structure can be modeled by a parallel system, as the failure of one cross-section due to bending does not result in a system failure, provided that both neighboring cross-sections can take the additional loads after redistribution.

The JCSS Probabilistic Model Code [4] provides recommendations for first-order approximations and first-order reliability bounds for series and parallel systems. The first-order approximation for series systems is given by

$$P_{fsys} = 1 - \Phi_m \left(\overline{\beta}; \overline{\overline{\rho}} \right) \tag{9}$$

with Φ_m multi-variate standard normal distribution function
$\overline{\beta}$ vector of component reliability indices
$\overline{\overline{\rho}}$ correlation matrix between safety margins

The upper bound for series systems is

$$P_{fsys} \le Min\left(\sum P_j ; 1 \right) \tag{10}$$

with P_j failure probability of the $j.$ component

In analogy the first-order approximation for parallel systems is given by

$$P_{fsys} = \Phi_m \left(\overline{\beta}; \overline{\overline{\rho}} \right) \tag{11}$$

The upper bound for parallel systems is

$$P_{fsys} \le Min\left(P_j \right) \tag{12}$$

In order to asses the accuracy of these upper bounds the difference between the first-order approximation and the upper bound has been investigated on a simple system with two components. For the two components equal reliability indices were assumed. This reliability index was varied in the range of 1 to 6 and the difference between the upper bound and the first-order approximation has been calculated for seven different correlation coefficients both for series and parallel systems. The results are shown in Figure 4.

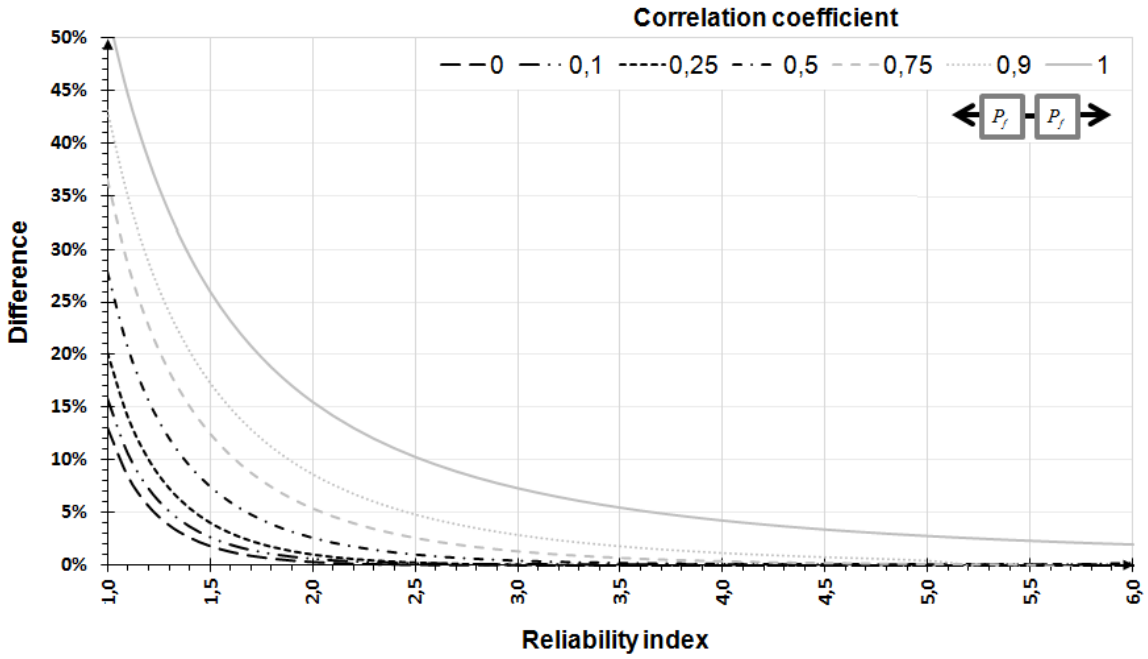

(a) Series system

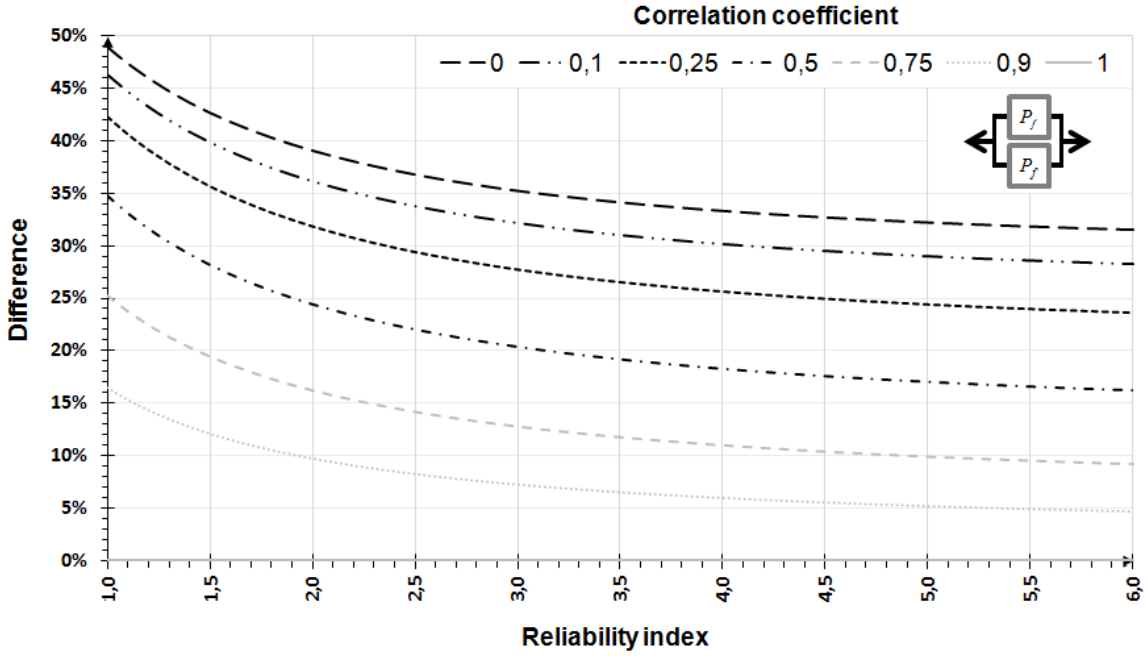

(b) Parallel system

Figure 4. Accuracy of approximation by upper bound for different types of systems

It can be seen that for series systems the upper bound provides a good approximation, especially for high reliabilities and low correlation coefficients, as typically present in the reliability analysis of structures. For parallel systems the difference is rather significant and diminishes only slightly with increasing reliability index. Further investigations of BOROS [12] have shown that we

can obtain similar results even if the two components have different failure probabilities. Therefore we can conclude that for series systems the upper bound provides acceptable results, however for parallel systems disregarding the correlations by using the upper bound may results in considerable inaccuracy in the results.

Consequently to be able to asses the additional safety of statically indeterminate structures due to the redistribution of moments with parallel systems, the correlation between the neighboring cross-sections has to be considered. For this reason this correlation had been calculated via statistical analysis and was implemented in the calculation of the reliability index.

3.3 Superposition of time-dependent loads

Two methods are commonly used to obtain the maximum load resulting out of the superposition of two time-dependant actions. Turkstra's rule suggests that the maximum value of the sum of two independent load processes occurs when one of the processes attains its maximum value as described in TURKSTRA et al. [13]. This rule is known to provide a good approximation with reasonable effort however it may underestimate the combination of the actions in question. As an alternative the maximum of the sum of two loads can be assessed by considering them according to the Ferry Borges-Catanheta model as a sequence of independent identically distributed random variables acting for a given time interval according to GHOSN et al. [14]. This way for each time interval the loads can be added and the maximum value within the observation period can be obtained. In the present research both methods have been investigated and compared for the combination of traffic loads and temperature differences regarding the limit states of bending and shear. The result is displayed in Table 4.

Table 4. Comparison of methods for superposition of time-dependent loads

Comparison criteria	Bending	Shear
Ratio of identical results	70,7 %	55,6 %
Mean value of difference	1,0 %	1,2 %
1 % quantile of difference	9,0 %	7,2 %

It can be observed, that both methods provide the same result in most of the cases and mean value of the difference is around 1 %, thus mostly verifying the assumption of Turkstra's rule. It has to be remarked however that with low probability higher differences can be observed, too.

4 Results

4.1 Reliability analysis

The introduced method is demonstrated on two bridges with 5 hazard scenarios. These case studies were carried out on two different structures: a single span prestressed concrete slab and a prestressed concrete continuous beam with five spans and a double-webbed T-beam cross-section. These can be regarded as fairly representative, as beams and slabs account for more than two thirds of bridges in the German highway network. The structures were designed according to the valid German standards at the time of construction. As a reference scenario the reliabilities have also been calculated for the undamaged structures, too. The reliabilities have been assessed with the method of model uncertainties for the five hazard scenarios combined with each of the four traffic scenarios. For the continuous beam the additional safety due to the redistribution of moments in the statically indeterminate structure was also calculated. These results are displayed in Table 5.

Table 5. Reliability indices for different hazard and traffic scenarios

Hazard / traffic scenario	Without redistribution				With redistribution			
	I	II	III	IV	I	II	III	IV
Single span slab damage in mid-span	4,12	4,11	4,12	4,11	-	-	-	-
Single span slab damage at support	5,74	5,73	5,74	5,73	-	-	-	-
Continuous beam damage in mid-span	5,69	5,60	5,66	5,57	6,29	6,26	6,28	6,25
Continuous beam collapse of a pillar	4,09	4,01	4,08	3,98	4,48	4,36	4,45	4,34
Continuous beam damage at support	6,49	6,25	6,50	6,33	6,51	6,26	6,52	6,36

The results show a small difference between the different traffic scenarios, yet a moderate decrease in reliability can be observed for prognosticated traffic. Due to the redistribution of moments an increase in the reliability can be detected for the statically indeterminate continuous beam, however the increase is rather small for some scenarios. This is mostly due to the limit state of shear becoming more significant than bending.

4.2 Risk analysis

The method of model uncertainties enabled the assignment of an estimate for the failure probability to each of the traffic situations on the bridge generated from the basic variables of the traffic simulation. For each traffic situation however the consequences of failure in terms of affected human lives can be

easily assessed if we allow for some basic assumptions on the number of passengers for trucks and cars. In this research each truck was assumed to hold one and each car to hold two people. Thus it became possible to estimate the risk for each of the different hazard and traffic scenarios. The results are displayed in Figure 5 in logarithmic scale.

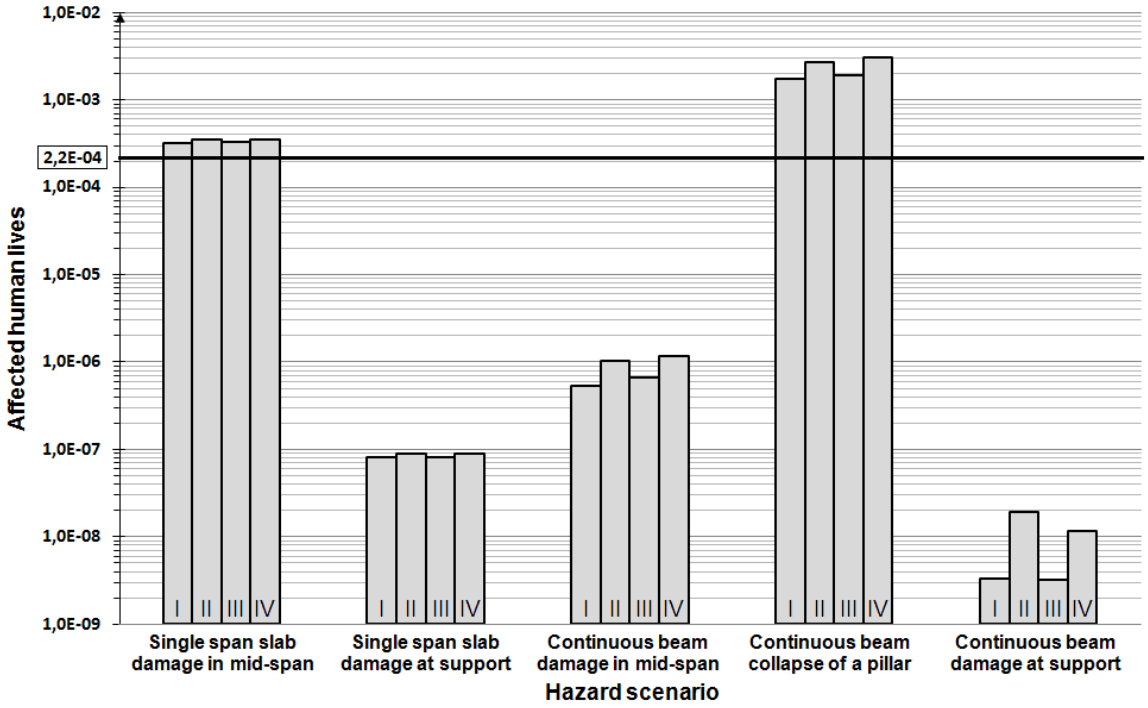

Figure 5. Results of risk analysis

The risk of the hazard scenarios can be compared for example to the yearly mortality rate among motorist: $2{,}2 \cdot 10^{-4}$ according to CURBACH et al. [15]. We can observe that two of these scenarios have a risk which is close or above this value for all traffic scenarios. Based on this comparison proprietors and operators of traffic infrastructure can make informed decisions in identifying critical scenarios and considering suitable protection measures.

5 Conclusions

A method was introduced to assess the reliability index and risk of different types of concrete bridges for hazard scenarios. These indicators proved suitable to identify critical structures. The additional safety of statically indeterminate structures due to the redistribution of moments could be implemented into the calculation. Some interesting insights on the combination of different time-dependent actions were also gained.

6 Literature references

[1] SKRIBT Schlussbericht: *Schutz kritischer Brücken und Tunnel im Zuge von Straßen*, Empfehlungen zur Maßnahmenanwendung für Brücken und Tunnel, in Vorbereitung

[2] Allgemeine bauaufsichtliche Zulassung Z-12.3-29, Spannstahllitzen St 1570/1770 aus 7 kaltgezogenen, glatten Einzeldrähten, Deutsches Institut für Bautechnik, 2004

[3] Six, M.: Sicherheitskonzept für nichtlineare Traglastverfahren im Betonbau, *Deutscher Ausschuss für Stahlbeton Heft 534*, 2003

[4] Joint Committee on Structural Safety, *Probabilistic Model Code*, 2001

[5] FE 89.0232/2009/AP Schlussbericht, Auswirkungen des Klimawandels auf bestehende Spannbetonbrückenbauwerke, 2011

[6] Frenzel, B. et al.: Bestimmung von Kombinationsbeiwerten und -regeln für Einwirkungen auf Brücken, *Forschung Straßenbau und Straßenverkehrstechnik Heft 715*, Typo-Druck-& Verlaggesellschaft, Bonn, 1996

[7] Spaethe, G.: *Die Sicherheit Tragender Baukonstruktionen*, Springer, Wien, 1992

[8] Kaschner, R. et al., Auswirkungen des Schwerlastverkehrs auf die Brücken der Bundesfernstraßen, *Berichte der Bundesanstalt für Straßenwesen Heft B 68*, Verlag für neue Wissenschaft, Bremerhaven, 2009

[9] FE 15.451/2007/FRB Schlussbericht, Anpassung des DIN-Fachberichtes „Einwirkungen auf Brücken“ an endgültige Eurocodes und nationale Anhänge einschließlich Vergleichsrechnung, 2009

[10] Faber, M. H.: *Risk and Safety in Engineering*, ETH Zürich, 2009

[11] Rackwitz, R.: *Zuverlässigkeit und Lasten im konstruktiven Ingenieurbau – Teil I: Zuverlässigkeitstheoretische Grundlagen*, Technische Universität München, 2006

[12] Boros, V.: *Zur Zuverlässigkeitsanalyse von Massivbrücken für außergewöhnliche Bedrohungsszenarien*, Universität Stuttgart, 2012 - Dissertation

[13] Turkstra, C. J. et al.: Load Combinations in Codified Structural Design, *Journal of the Structural Division, Proceedings of the American Society of Civil Engineers* 106 (1980), S. 2527-2543

[14] Ghosn, M. et al.: *National Cooperative Highway Research Program Report 489*, Design of Highway Bridges for Extreme Events, Transportation Research Board, Washington D. C., 2003

[15] Curbach M. et al.: Die Sicherheit von Brücken im Vergleich zu anderen Risiken, *12. Dresdner Brückenbausymposium - Planung, Bauausführung und Ertüchtigung von Massivbrücken*, Dresden, 2002, S. 197

Probabilistic Analysis Based on S-version Finite Element Method of Surface Crack Growth

MRM Akramin[1], AK Ariffin[1], M Kikuchi[2], S Abdullah[1],
N Nikabdullah[1], MS Shaari[1]
[1]Faculty of Mechanical Engineering and Built Environment,
Universiti Kebangsaan Malaysia, Selangor, Malaysia.
[2]Tokyo University of Science, Yamazaki, Noda, Chiba, Japan.

Abstract: The complexity of 3D surface crack growth behavior is investigated by the S-version Finite Element Method. The research work is focused on cyclic load, which gives an absolute picture of reality in an engineering world. The Monte Carlo method is embedded with S-version Finite Element Method for reliability analysis of the structural system with a mixture of random and interval parameters and loadings. The purpose of employed the Monte-Carlo method is to determine the reliability of the structure. Thus, mean values and standard deviations of uncertain parameters need to be computed. The generated uncertain parameters by Monte-Carlo method are used for analysis in S-version Finite Element Method. The S-version Finite Element Method is performed by superposed the local dense finite element mesh on the global coarse finite element mesh. An adaptive mesh refinement method is implemented, which allows local refinement of the mesh without introducing a transition region. Based on S-version Finite Element Method results, probabilistic analysis is conducted. Probabilistic analysis represents the uncertainty in modeling studies. It can offer the opportunity to view the impact of the uncertain parameters statistically. Variabilities of material properties are presented in a probabilistic analysis by using statistical distribution functions. The probability of failure which is caused by uncertain loads and material properties in the structure is estimated. Numerical example is presented to show that probabilistic analysis based on S-version Finite Element Method simulation provides accurate estimates of failure probability. The comparison shows that the combination between S-version Finite Element Method analysis and probabilistic analysis provide a simple and realistic of quantify the failure probability.

1 Introduction

The existence of surface crack has been a major problem in pressurized thick-walled cylinders and nuclear reactor structural. Surface crack as well frequently found in aeronautical panel, cylinder of an extrusion press, riveted aeronautic reinforcement and pressure vessel. The most happen to be in semielliptical form. Due to the complexity of the three-dimensional surface crack, many researchers have used numerical approximation to obtain the stress intensity factor. Thus, numerical calculation is one of the best remedy to solve the complexity. Various methods have been developed such as Finite Element Method, Extended-Finite Element Method and others. In this research work, S-version Finite Element Method (s-FEM) was implemented for calculation of the stress intensity factor.

The s-FEM has been applied to diverse application ranges such as heat affected zone material [1, 2], corrosion cracking [3], crack closure effect [4] and composite material [5]. Various types of load behavior [6-9] as well have been an issue in the numerical implementation. The most striking one is the fatigue load since the fatigue load represented a real case study in an engineering world. Fatigue load is a major fracture cause in a structure due to long term cyclic load. The integrity of the structure can be questioned when a crack was discovered in a structure. Sustainability of the structure needs to evaluate in order to avoid a fiasco, especially when a crack detected.

Therefore, in this study s-FEM is developed together with an analysis of residual fatigue life. The prediction of fatigue crack growth rate is based on Paris law. The crack surface introduced into the structure is considered. In s-FEM 3-dimensional simulation model, fatigue load is applied throughout the process. Experimental works were carried out to validate the simulation analysis data. The crack paths from simulation and experiment were compared and discussed briefly. Afterward, the change of the stress intensity factors along the cycle was investigated based on simulation results.

2 Methodology

The s-FEM was implemented in this study. Figure 1 shows the s-FEM concept. The coarser mesh was generated for global mesh while a denser mesh was used at near the crack tip area. Crack tip area was taken into account during the implementation of local mesh. On the global mesh, Ω^G crack tip area was neglected temporarily.

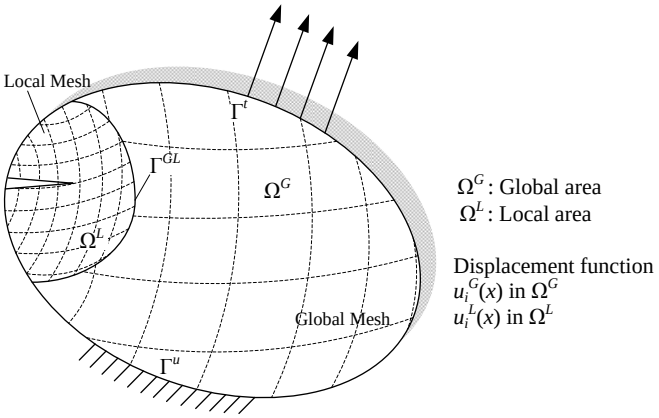

Figure 1. Concept of s-FEM.

After the local mesh, Ω^L was overlaid on the global mesh, a complete structure is ready to be modeled. The size of local mesh area is crucial to be decided since the propagation of crack is affected by the calculation of the displacement function. The displacement on overlaid area was summed from global and local mesh as shown below:

$$u(x) = \begin{cases} u^G(x) & x \in \Omega^G - \Omega^L \\ u^G(x) + u^L(x) & x \in \Omega^L \end{cases} \tag{1}$$

On the other hand, the strain of the superimposed area was calculated as below:

$$\varepsilon(x) = \varepsilon^G(x) + \varepsilon^L(x) \tag{2}$$

Afterward, the relationship between stress and strain was implemented in virtual work equation and indicates by equation:

$$\int_\Omega \left\{\delta\varepsilon^G\right\}^T [D] \left\{\varepsilon^G\right\} d\Omega^{G-L} + \int_\Omega \left(\left\{\delta\varepsilon^G\right\}^T + \left\{\delta\varepsilon^L\right\}^T [D] \left(\left\{\varepsilon^G\right\} + \left\{\varepsilon^L\right\}\right)\right) d\Omega^L$$

$$- \int_\Gamma \left\{\delta u^G\right\}^T \{f\} d\Gamma^{G-L} - \int_\Gamma \left(\left\{\delta u^L\right\}^T + \left\{\delta u^L\right\}^T\right) \{f\} d\Gamma^L = 0 \tag{3}$$

The final matrix form for s-FEM is:

$$\begin{bmatrix} K_{GG} & K_{GL} \\ K_{LG} & K_{LL} \end{bmatrix} \begin{Bmatrix} u_G \\ u_L \end{Bmatrix} = \begin{Bmatrix} F_G \\ F_L \end{Bmatrix} \tag{4}$$

where

$$[K_{GL}] = \int_{\Omega^L} \left[B^G\right]^T [D] \left[B^L\right] d\Omega^L$$

$$[K_{LL}] = \int_{\Omega^L} \left[B^L\right]^T [D] \left[B^L\right] d\Omega^L$$

The $[K^{GL}]$ matrix represented the stiffness matrix of the superimposed area, and $[B]$ is the displacement-strain matrix. By computing the final form of s-FEM matrix, displacement for each node can be obtained. The displacement for global and local mesh for each node was calculated simultaneously. The global mesh not affected by the changing of local mesh size. Re-meshing process can be generated for local area alone since the region of interest is at the crack tip area. Figure 2 shows the global mesh with boundary condition and combination of local and global mesh. During the crack growth simulation, local mesh's size was expanded and stress intensity factor (SIF) begun to calculate.

The SIF was obtained based on calculation of energy release rate as shown below:

$$K_I = \sqrt{EG_I}, \quad K_{II} = \sqrt{EG_{II}}, \quad K_{III} = \sqrt{2\mu G_{III}} \tag{5}$$

where E is the modulus young during plane stress condition and equal to $E/(1-\nu^2)$ for plane strain condition. ν and μ are Poison's ratio and shear modulus respectively. SIF and energy release rate were used in crack growth simulation since the failure occurred in a linear elastic fracture mechanic's region.

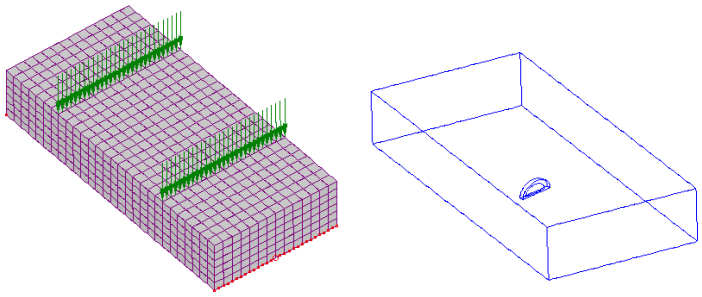

(a) (b)

Figure 2. (a) Global mesh and (b) local mesh overlaid on global in wireframe view.

The energy release rate was evaluated by virtual crack closure method (VCCM). Displacements and nodal forces as shown in Figure 3 are required, in order to calculate accurately the energy release rate. The VCCM for 20 nodes of hexahedron element was computed by:

$$G_{Total} = \frac{1}{2\Delta w^J} \sum_{I=1}^{5} C^I \nu_i^I P_i^I \tag{6}$$

where I is referred to node number around the crack tip as shown in Figure 3. Constant C^I is depicted as:

$$C^1 = C^2 = \frac{w^J}{w^{J+1} + w^J}, \quad C^3 = 1, \quad C^4 = C^5 = \frac{w^J}{w^{J-1} + w^J} \tag{7}$$

Meanwhile, the energy release rate for non-symmetric local mesh was computed differ from equation (6) since the arrangement of crack front elements were not symmetric. The energy release rate for non-symmetric local mesh which implemented by [10] were employed in this study.

$$G_{Total} = \frac{1}{2\left[S_1^J - \frac{1}{4}\left(S_1^J - S_2^J\right)\right]} \int_{S_1^J} \sigma_{3i}(r)\nu_i(\Delta - r)dS_1^J \tag{8}$$

where S_1^J and S_2^J are the plane's area at the crack front as shown in Figure 3. The σ_{3i} and ν_i are the stress and displacement respectively at the crack face.

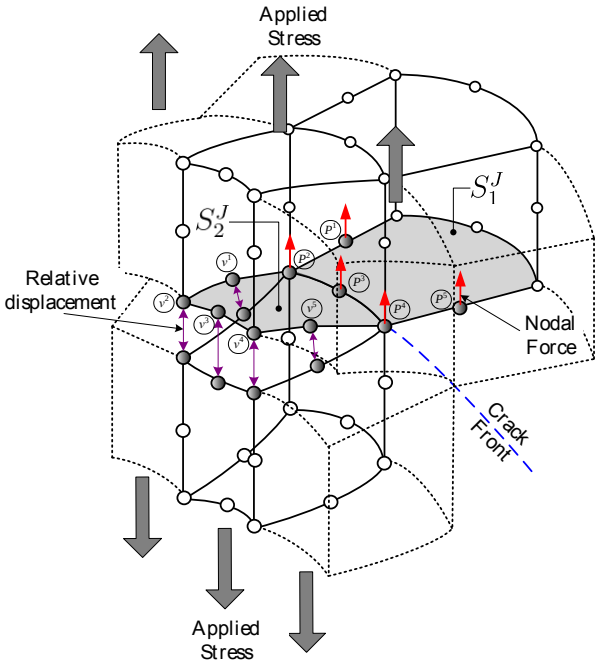

Figure 3. Virtual crack closure method for local mesh with curved crack front.

The value of ΔK is representing by:

$$\Delta K_{eq} = \frac{\Delta K_I}{2} + \frac{1}{2}\sqrt{\Delta K_I^2 + 4\left(1.155\Delta K_{II}\right)^2 + 4\left(\Delta K_{III}\right)^2} \tag{9}$$

3 Probabilistic Fatigue Life Analysis

Prediction of fatigue life is a challenging problem in engineering design. As well as maintenance and inspection services which are exposed to the uncertain parameter in material, external condition such as load and structural geometry itself. Therefore, an analysis considering all uncertain parameter is needed.

Probabilistic fatigue life predictions were performed by using Monte-Carlo. The material parameter, crack length and the initial crack size are deemed as the random variable. The parameters' distribution is varied for each of geometry as shown in Table 1. The fatigue life analysis was performed in s-FEM utilizing the crack closure method and the appropriate specimen. The code was written in C language. Parameters for the input induced closure model for Al 7075-T6 were based on work by [11]. The distributions for input parameters were developed from available literature data for aluminum 7075-T6.

In probabilistic analysis, Paris coefficient, *C* of Al 7075-T6 was represented by mean 6.54×10^{-13} m/cycle with a standard deviation of 4.01×10^{-11} m/cycle. The distribution was assumed to be lognormal distribute based on the assumption made in the literature [11]. No standard deviation for fatigue power parameter, *n* since it was set as deterministic. The reason behind this was to control the acceleration of the crack growth in numerical calculation. Deterministic value of fatigue power parameter was computed since to monitor the sensitivity of remaining distributed variable.

Young's modulus was treated as a normal distribution as the variable changed accordingly during the real application. Young's modulus also has small coefficient of variation and became the main reason for selecting Gaussian as the distribution.

4 Experiment

The surface crack was introduced by using four point bending test which conducted on the 0°, 15° and 45° specimens. Throughout the study, the aluminum alloy, A7075-T6 was chosen as the material of the specimen. The specimens were imposed on two steps, which are the initial step and after pre crack step. The differences between initial and after pre crack steps are the protuberance and the dimension of the specimen after pre crack introduced.

Table 1. Input distribution for the model

Variable	Distribution	Mean	Standard deviation
Tensile Strength, Ultimate	Deterministic	764 MPa	0
Young's modulus, *E*	Normal	71.7 GPa	10.34
Tensile Strength, Yield	Deterministic	691 MPa	0
Paris coefficient, *C*	Lognormal	6.54×10^{-13} m/cycle	4.01×10^{-11}
Fatigue power parameter, *n*	Deterministic	3.8863	0
Threshold value, ΔK_{th}	Lognormal	5.66 MPa.$m^{0.5}$	0.268
Initial crack length, *da*	Lognormal	0.23 mm	0.05

Firstly, a notch was introduced at the protuberance by using Electric Discharge Machining (EDM) with 1 mm depth as shown in Figure 4(a). Then, first fatigue test was performed by pure mode I load. A four point bending test was conducted. Due to the load, crack propagated inside the protuberance starting from the notch. The fatigue test continued until the crack reached 2 mm mark on the flat plate, as shown in Figure 4(b). After 2 mm surface crack was appeared at the flat plate, the protuberance was removed and the specimens were cut according to the certain angle. Figure 5 shows the dimension of the specimen according to the angle subjected.

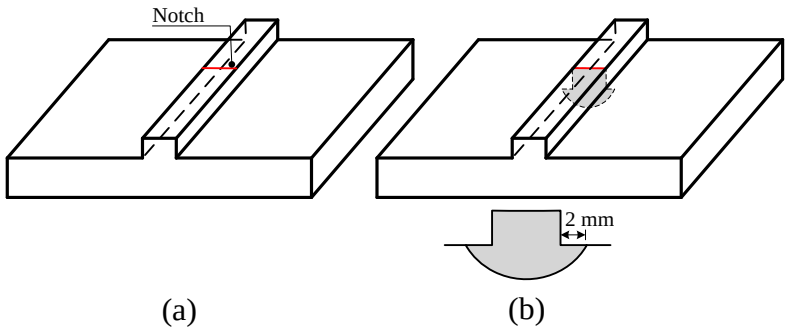

Figure 4 Specimen (a) before fatigue test (b) after first fatigue test with surface crack.

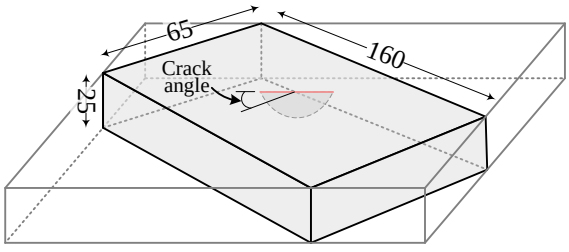

Figure 5 Dimension of specimen in mm.

Second fatigue test was conducted by four point bending as well as shown in Figure 6. The distance of loading points was 70 mm, and cracked area was subjected to uniform bending moment. Due to inclination of crack surface, ΔK_I and ΔK_{II} exist near the specimen sur-

face. ΔK_I and ΔK_{III} exist at the deepest point of surface crack. Stress ratio 0.1 was used. To measure the change of surface crack shape, beach mark was introduced by stress ratio R=0.8.

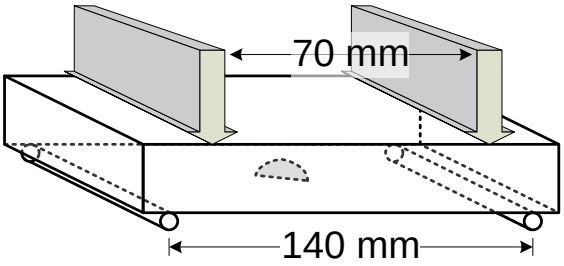

Figure 6 Four point bending test.

5 Results and Discussion

The uncertain inputs data was generated according to its distribution with respect to mean and standard deviation value as shown in Figure 7. The frequency of each random parameter represented the distribution. Each parameter's computations were compared with the best fit cumulative distribution function. The parameters were shown that, it was generated according to its distribution function.

The 95% confidence bounds of data inputs shown in Figure 8. All data inputs; Young's modulus, Paris coefficient, threshold value and initial crack length were generated within the two standard deviation of each parameter. It showed the capability of developed s-FEM code to generate random variables according to certain distribution.

In Figure 9, the simulation results for growth of the surface crack were compared with experimental results. The notch introduced at the early stage of the experimental process was shown clearly in this figure as an initial for crack to growth. After the cyclic load was applied on the specimen, the pre-cracking was generated as shown in the plot. The pre-cracking area was drawn in the graph. Crack growth for experimental works was started to be observed after pre-cracking's area. The same initial conditions introduced for numerical model. As well as the size of pre-cracking area was modelled in local mesh. In this figure, variations of crack growth shown as the results of the randomness of uncertain parameters. It showed all possibilities that crack tend to growth with respect to certain random parameters.

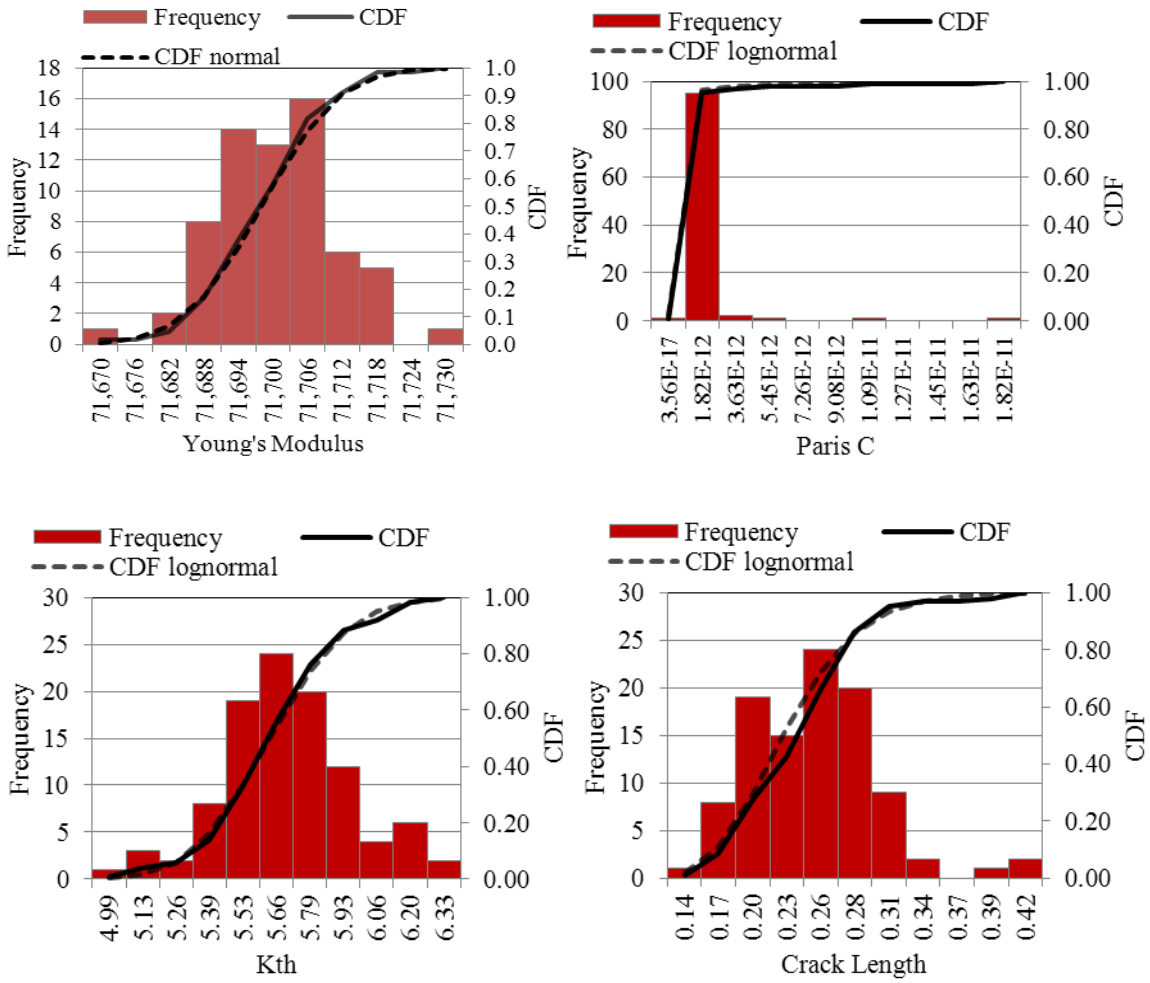

Figure 7 Data inputs distribution.

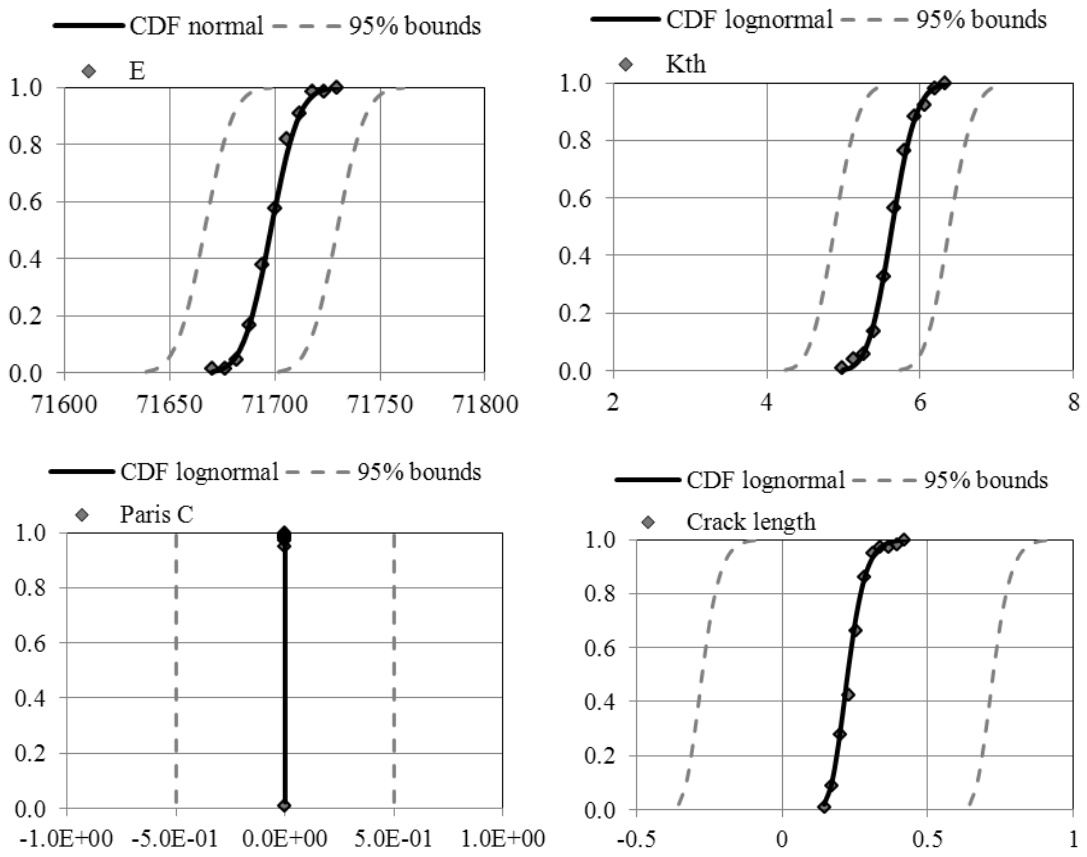

Figure 8 The 95% confidence bounds of data inputs.

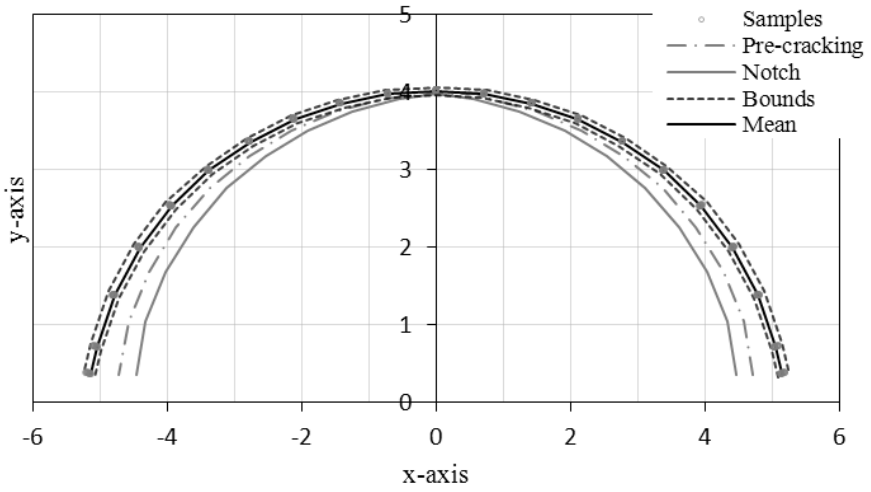

Figure 9 Comparison of *x-y* axis of crack growth.

Constant amplitude fatigue simulation data on 100 samples of four point bending specimens of aluminium A7075-T6 plates were computed. Each sample was tested under the same maximum loads of 40 kN. Figure 10 shows the histogram for specimen to fail. It showed that more than 80% failure occurred in between $5x10^7$ cycles. For material such as aluminium A7075-T6, which does not show any fatigue limit in S-N curve is essential to determine the failure cycle and probability of failure as shown in Figure 11.

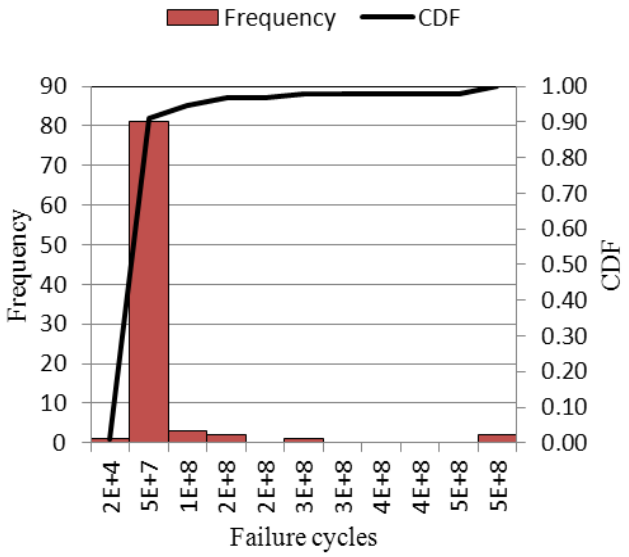

Figure 10 Histogram and predicted cumulative distribution function of cycles for specimen to fail.

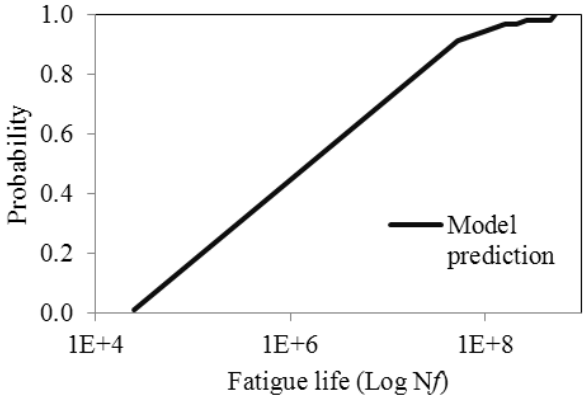

Figure 11 Probability of fatigue life for model prediction

6 Conclusion

The s-FEM simulation with auto-mesh generation and fully automatic fatigue crack growth system was implemented. Experimental works were compared with simulation results and indicate that the findings were close with the actual case. The crack path from experiment showed that the crack tends to grow to elliptical shape. Probability of failure and failure cycle were determined in the developed source code in order to emphasis the capability of the numerical simulation.

7 Reference

[1] Kikuchi, M.; Wada, Y.; Shimizu, Y.; Li, Y.: Crack growth analysis in a weld-heat-affected zone using S-version FEM. *International Journal of Pressure Vessels and Piping*, 90–910 (2012), P. 2-8.

[2] Kikuchi, M.; Wada, Y.; Shimizu, Y.; Yulong, L.: Crack growth analysis in weld-heat affected zone using S-Version FEM. *American Society of Mechanical Engineers, Pressure Vessels and Piping Division*. 2010 P. 401-406.

[3] Kikuchi, M.; Wada, Y.; Shmizu, Y.; Li, Y.: Stress corrosion cracking analysis under thermal residual stress field using S-FEM. *Key Engineering Materials* 462-463 (2011), P. 431-436.

[4] Kikuchi, M.; Wada, Y.; Maitireyimu, M.; Sano, H.: Closure effect on interaction of two surface cracks under cyclic bending. *American Society of Mechanical Engineers, Pressure Vessels and Piping Division*. 2010 P. 415-421.

[5] Angioni, S.L.; Visrolia, A.; Meo, M.: Combining X-FEM and a multilevel mesh superposition method for the analysis of thick composite structures. *Composites Part B: Engineering*, 432 (2012), P. 559-568.

[6] Kikuchi, M.; Wada, Y.; Suga, K.: Surface crack growth simulation under mixed mode cyclic loading condition. *Procedia Engineering*. 2011 P. 427-432.

[7] Kikuchi, M.; Wada, Y.; Ohdama, C.: Effect of KIII on fatigue crack growth behavior. *American Society of Mechanical Engineers, Pressure Vessels and Piping Division*. 2010 P. 407-413.

[8] Kikuchi, M.; Wada, Y.; Suga, K.; Ohdama, C.: Effect of KIIIon fatigue crack growth behavior (factory roof and fatigue crack growth rate). *Nihon Kikai Gakkai Ronbunshu, A Hen/Transactions of the Japan Society of Mechanical Engineers, Part A*, 76772 (2010), P. 1674-1680.

[9] Kikuchi, M.; Maitireymu, M.; Sano, H.: Study on fatigue crack growth criterion 1st report, paris' law of a surface crack under pure mode i loading. *Nihon Kikai Gakkai Ronbunshu, A Hen/Transactions of the Japan Society of Mechanical Engineers, Part A*, 76764 (2010), P. 516-522.

[10] Okada, H.; Higashi, M.; Kikuchi, M.; Fukui, Y.; Kumazawa, N.: Three dimensional virtual crack closure-integral method (VCCM) with skewed and non-symmetric mesh arrangement at the crack front. *Engineering Fracture Mechanics*, 7211 (2005), P. 1717-1737.

[11] Liu, Y.; Mahadevan, S.: Probabilistic fatigue life prediction using an equivalent initial flaw size distribution. *International Journal of Fatigue*, 313 (2009), P. 476-487.

Influence of soil heterogeneity on geotechnical performance and uncertainty: a stochastic view on EC7

Michael A. Hicks, Jonathan D. Nuttall
Section of Geo-Engineering, Faculty of Civil Engineering and Geosciences,
Delft University of Technology, Netherlands

Abstract: The spatial variability of soil properties affects soil behaviour and geotechnical performance. It also leads to uncertainty in design due to incomplete knowledge about the ground conditions. This paper demonstrates how the Random Finite Element Method (RFEM) may be used to quantify the performance of geotechnical structures within a probabilistic framework, so accounting for the impact of heterogeneity on structure response, while, at the same time, quantifying the uncertainty. In particular, it is shown that RFEM provides a self-consistent framework for understanding the concept of characteristic property values in Eurocode 7, as well as providing a means by which reliability-based characteristic values may be determined. The procedure is demonstrated for a 3D slope stability problem. Characteristic values are shown to be problem dependent and a function of two competing factors: the spatial averaging of properties along potential failure surfaces, which reduces the coefficient of variation of the property values; and the tendency of failure mechanisms to follow the path of least resistance, which causes an apparent reduction in the property mean.

1 Introduction

Soils exhibit spatial variability of material properties. This spatial variability, frequently referred to as heterogeneity, is anisotropic, often depth-dependent and occurs at multiple scales: at the very small scale, as seen in the arrangement of solid particles of sand or in the arrangement of fibres in fibrous materials such as peat; at the decimetre to metre scale, as observed in CPT

soundings within soil layers; and at larger scales too, for example as seen in the geological layering of soils of different types. Spatial variability influences fluid flow, material behaviour and "global" geo-structural response. It also leads to uncertainty in ground conditions and thereby to uncertainty in design (HICKS [5]).

This paper focuses on the spatial variability of soil properties that occurs within so-called uniform layers and adopts a probabilistic approach to quantifying the uncertainty that arises through having incomplete information about the ground conditions. Hence soil properties are defined in statistical terms and geotechnical performance is defined probabilistically; for example, in terms of reliability, the probability of failure not occurring. This is in contrast to traditional deterministic analysis based on single "representative" soil property values, which leads to factors of safety for which there is no information regarding probability of failure.

The paper considers the issue of spatial variability within the context of characteristic soil property values advocated in Eurocode 7 (EC7) (CEN [1]). It is shown that stochastic analysis may be used as an aide to understanding the philosophy and nature of characteristic values, as well as providing a framework for deriving reliability-based values in line with EC7 (HICKS [6], HICKS & SAMY [10]). This is based on linking random field theory for generating spatial property distributions with finite elements for computing geo-structural response, an approach often referred to as the Random Finite Element Method (FENTON & GRIFFITHS [3]). The procedure for deriving characteristic values is demonstrated for a 3D slope stability problem. The results also provide insight into the influence of spatial variability on the performance of geotechnical structures.

2 Extracts from Eurocode 7

The importance of accounting for the variability of soils is highlighted in Section 2.4.5.2 of Eurocode 7, "Characteristic values of geotechnical parameters" (CEN [1]). Table 1 lists some of the main clauses, including: Clause (4)P, which highlights the spatial nature of soil variability, the uncertainty this causes and the problem-dependency of characteristic values; Clause (7), which emphasises the importance of the mean over the domain of influence; Clause (8), which considers the special case of local failure; and Clause (11), which considers the use of statistical methods.

Table 1. Extracts from Section 2.4.5.2 of Eurocode 7 (CEN [1])

No.	Clause
(4)P	The selection of characteristic values for geotechnical parameters shall take account of the following: ● geological and other background information, such as data from previous projects; ● the variability of measured property values and other relevant information, e.g. from existing knowledge; ● the extent of the field and laboratory investigation; ● the type and number of samples; ● the extent of the zone of ground governing the behaviour of the geotechnical structure at the limit state being considered; ● the ability of the geotechnical structure to transfer loads from weak to strong zones in the ground.
(7)	The zone of ground governing the behaviour of a geotechnical structure at a limit state is usually much larger than a test sample or the zone of ground affected in an in situ test. Consequently the value of the governing parameter is often the mean of the range of values covering a large surface or volume of the ground. The characteristic value should be a cautious estimate of this mean value.
(8)	If the behaviour of the geotechnical structure at the limit state considered is governed by the lowest or highest value of the ground property, the characteristic value should be a cautious estimate of the lowest or highest value occurring in the zone governing the behaviour.
(11)	If statistical methods are used, the characteristic value should be derived such that the calculated probability of a worse value governing the occurrence of the limit state under consideration is not greater than 5%. NOTE: In this respect, a cautious estimate of the mean value is a selection of the mean value of the limited set of geotechnical parameter values, with a confidence level of 95%; where local failure is concerned, a cautious estimate of the low value is a 5% fractile.

HICKS [6] gave a detailed review of Section 2.4.5.2 by explaining selected clauses, clarifying the relationship between clauses and addressing areas of potential confusion. In particular, the paper focussed on the statistical definition of a characteristic value given in Clause (11) and explained how it is, despite first appearances, completely consistent with Section 2.4.5.2 as a whole, including Clauses (7) and (8) and the footnote to Clause (11). For this purpose, HICKS [6] argued that the Random Finite Element Method provided a self-consistent framework for quantifying and understanding the response of geotechnical structures given soil heterogeneity, and for deriving characteristic values satisfying the requirements of Eurocode 7 as demonstrated previously by HICKS & SAMY [10].

Clause (11) states that "the characteristic value should be derived such that the calculated probability of a worse value governing the occurrence of the limit state under consideration is not greater than 5%". This implies a mini-

mum level of reliability of 95% regarding response of the structure (before application of partial safety factors) and appears to contradict Clauses (7) and (8) and the footnote to Clause (11) which focus on property values rather than structure response. However, HICKS [6] used Figure 1 to demonstrate that the latter are merely special cases of Clause (11).

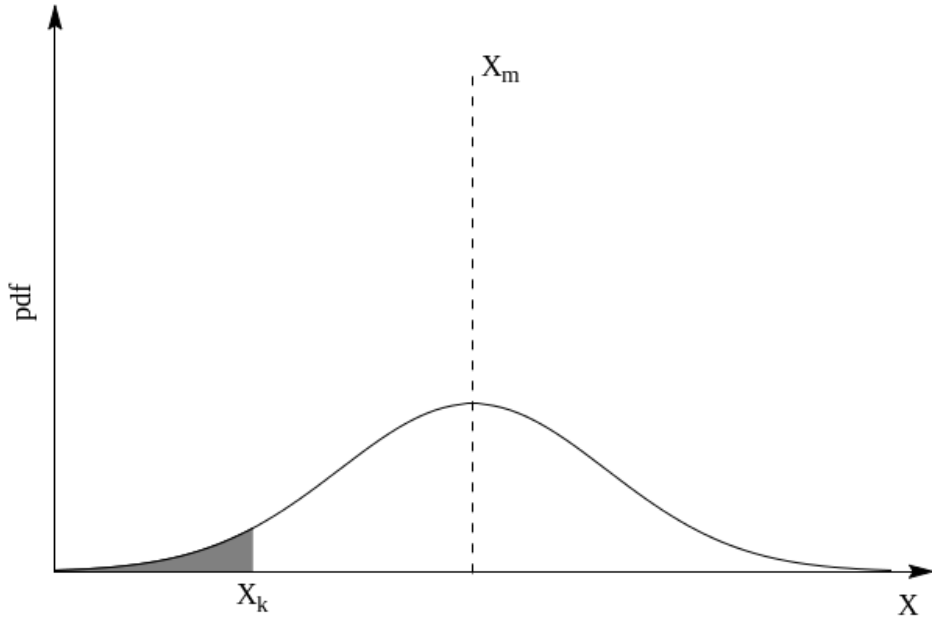

(a) Basic definition of X_k

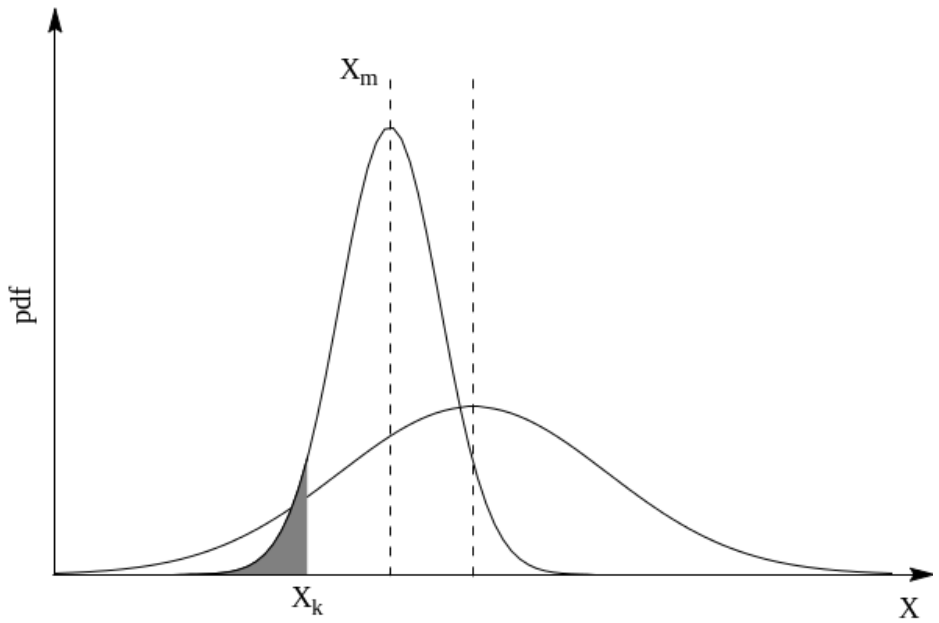

(b) General definition of X_k

Figure 1. Derivation of characteristic property values satisfying Eurocode 7 (HICKS [6]).

2.1 Reliability-based characteristic values

Figure 1(a) shows the probability density function of a material property X, which, to simplify the illustration, is assumed to be normal with a mean value X_m. The simplest way to derive a reliability-based characteristic value X_k is to proportion the area under the distribution as indicated. However, this is not consistent with Clause (11) as it merely defines a value of X_k for which there is a 95% probability of a larger value.

Figure 1(b) gives a more general derivation of X_k that is consistent with Clause (11) and, by association, with all other clauses in Section 2.4.5.2. This involves proportioning the area under a modified distribution of X that has been back-figured from the response of the geotechnical structure itself. The modified distribution is narrower than the underlying property distribution due to the averaging of property values over potential failure surfaces. It is also shifted to the left, due to the tendency for failure to propagate through weaker zones. Hence, although it may be reasonable to take a conservative estimate of the mean property value over a potential failure surface as the characteristic value for that mechanism, this mean will generally be smaller than the mean of the underlying property distribution. Variance reduction methods may therefore give an unsafe solution if no account is taken of the reduction in the mean.

HICKS [6] explained how the modified property distribution is a function of the underlying distribution, the spatial correlation of property values, the problem being analysed and the quality and extent of site investigation data. Moreover, the modified distribution has two limits:

- When the spatial scale of fluctuation is very small relative to the problem domain there is much averaging of soil properties, so that the standard deviation approaches zero and the mean tends to the mean of the underlying distribution. In this case a cautious estimate of the mean is appropriate, as advocated by Clause (7) and the first part of the footnote to Clause (11).

- When the spatial scale of fluctuation is very large relative to the problem domain there is a very large range of possible solutions, so that the modified distribution approaches the underlying distribution. In this case Clause (8) and the second part of the footnote to Clause (11) are relevant.

HICKS [6] also explained how the modified property distribution in Figure 1(b) may be derived for general problems. This is based on the work of

HICKS & SAMY [10], who proposed a solution strategy for deriving reliability-based characteristic values based on the Random Finite Element Method and demonstrated its use in analysing a 2D slope stability problem. This paper extends this earlier work by illustrating the process for a 3D slope.

3 Modelling spatial variability

The spatial variability of soil properties is herein modelled by random fields generated using Local Average Subdivision (FENTON & VANMARCKE [4]). The pointwise variability of the material property (in this case, undrained shear strength) is represented by a normal distribution and by the property mean and standard deviation, whereas the spatial variability is represented by the scale of fluctuation θ which is a measure of the distance over which material properties are significantly correlated (VANMARCKE [16]). Due to the process of deposition in natural soils and engineering construction, the horizontal scale of fluctuation is generally much larger than the vertical scale of fluctuation, as has been reported and modelled for example by HICKS & SAMY [9-11].

4 Numerical example

The method for deriving characteristic values is illustrated through analysing an idealised 3D slope stability problem; specifically, a 45° clay slope of height 5 m and length 100 m, resting on a firm base and characterised by a spatially varying undrained shear strength c_u. Figure 2 shows the problem geometry and mesh details. These are the same as used by HICKS & SPENCER [12] and SPENCER & HICKS [14], who conducted a detailed investigation into the influence of the horizontal scale of fluctuation on potential failure mechanisms and slope reliability, and HICKS et al. [7] who investigated the volumes of soil associated with potential slides. The mesh comprises 8000, 20-node finite elements, each using $2 \times 2 \times 2$ Gaussian integration and having dimensions of $1.0 \times 1.0 \times 0.5$ m (except for along the sloping surface where elements have been distorted to fit the problem geometry). The base of the mesh is fixed, whereas the back face is on rollers preventing displacement in the x direction. Both ends of the mesh are on rollers allowing only vertical movement; HICKS & SPENCER [12] found that preventing movement in the x direction avoided a bias in failures near these locations and validated the boundary condition through analysing slopes of different length.

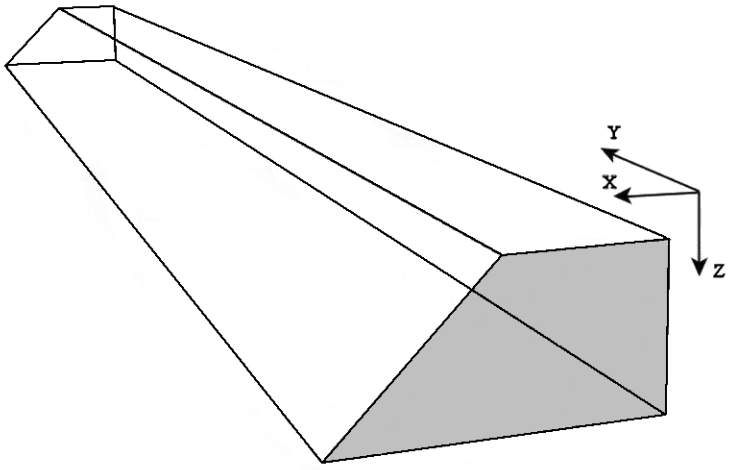

(a) Isometric projection

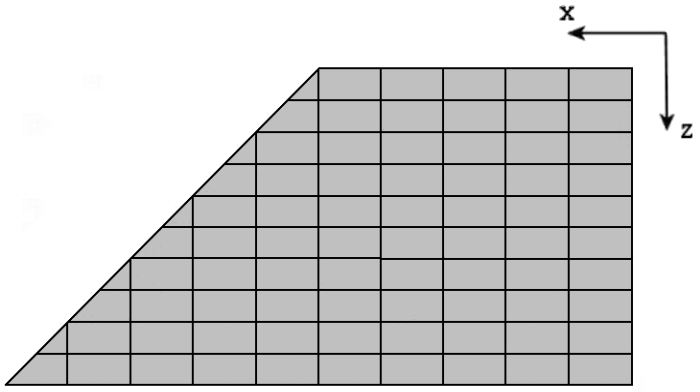

(b) Cross-section through mesh

Figure 2. Slope geometry and finite element mesh details (HICKS & SPENCER [12]).

In this investigation the clay is modelled by a linear elastic, perfectly plastic soil model. The model's elastic component is defined by a Young's modulus, E = 100000 kPa, and Poisson's ratio, ν = 0.3, whereas the plastic component comprises a Von Mises failure surface. The undrained shear strength is modelled by a normal distribution with a mean of 40 kPa and a standard deviation of 8 kPa. The vertical scale of fluctuation is θ_v = 1.0 m, whereas a range of possible values has been considered for the horizontal scale of fluctuation θ_h.

4.1 Methodology

For each value of θ_h a Monte Carlo simulation has been carried out, comprising 250 realisations. Each realisation involves two steps: (a) the generation of

a random field of c_u, using the statistics of c_u and Local Average Subdivision; and (b), the finite element analysis of the slope by applying gravity loading to generate the in situ stresses, assuming a soil unit weight of 20 kN/m^3.

The second step also uses the strength reduction method for finding the factor of safety F of the slope. Hence, each Monte Carlo simulation results in a distribution of factors of safety, from which a distribution of "effective" values of undrained shear strength may be back-figured; in this case, through relating F and effective c_u via the slope stability number (TAYLOR [15]).

4.2 Results and evaluation

Figure 3 shows the distribution of computed factors of safety for a degree of anisotropy of the heterogeneity of $\theta_h/\theta_v = 48$, as well as a fitted normal distribution. The tendency for failure to follow the weakest path results in most factors of safety lying below the deterministic factor of safety ($F = 2.47$) for a slope with $c_u = 40$ kPa. Figure 4 shows the back-figured distribution of effective c_u and compares it with the underlying distribution of c_u, demonstrating that the effective distribution has a lower mean and standard deviation than the underlying distribution.

Figure 5 summarises the results for all analyses, by plotting the mean and standard deviation of the effective c_u as a function of θ_h/θ_v and comparing these results with the underlying mean and standard deviation. For a degree of anisotropy of 1, the scale of fluctuation is small in all directions relative to the slope height. This causes failure mechanisms to propagate almost equally through weak and strong zones alike, thereby leading to considerable averaging of material properties, and to a mean approaching 40 kPa and a standard deviation approaching zero. In this case, HICKS & SPENCER [12] demonstrated a tendency for a 2D failure mechanism consistent with that for a 2D deterministic analysis based on the mean c_u (referred to as "Mode 1" failure).

As the horizontal scale of fluctuation increases, failure mechanisms develop through weaker zones resulting in discrete 3D "Mode 2" failures (HICKS & SPENCER [12]). This results in a decrease in the mean and an increase in the standard deviation of the effective c_u.

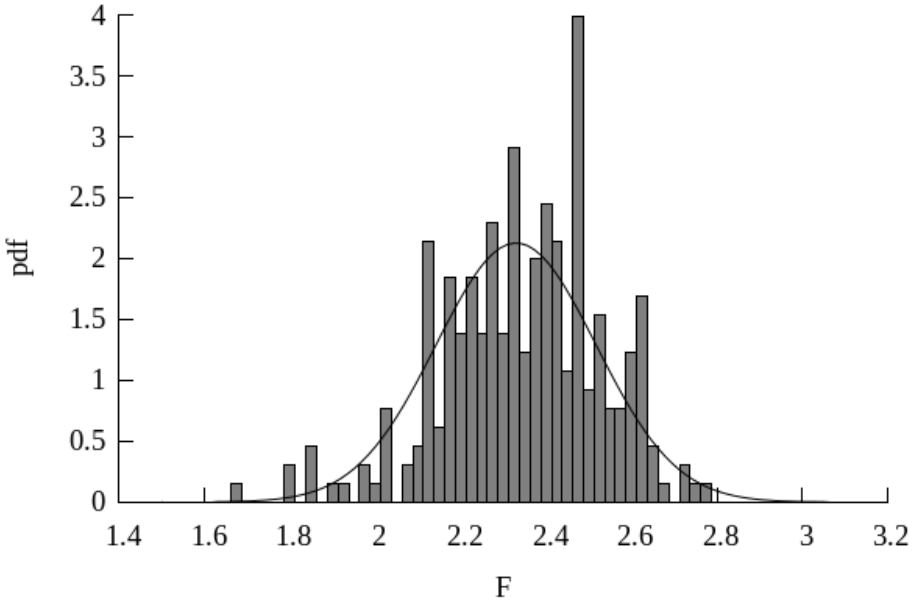

Figure 3. Distribution of factor of safety for $\theta_h/\theta_v = 48$.

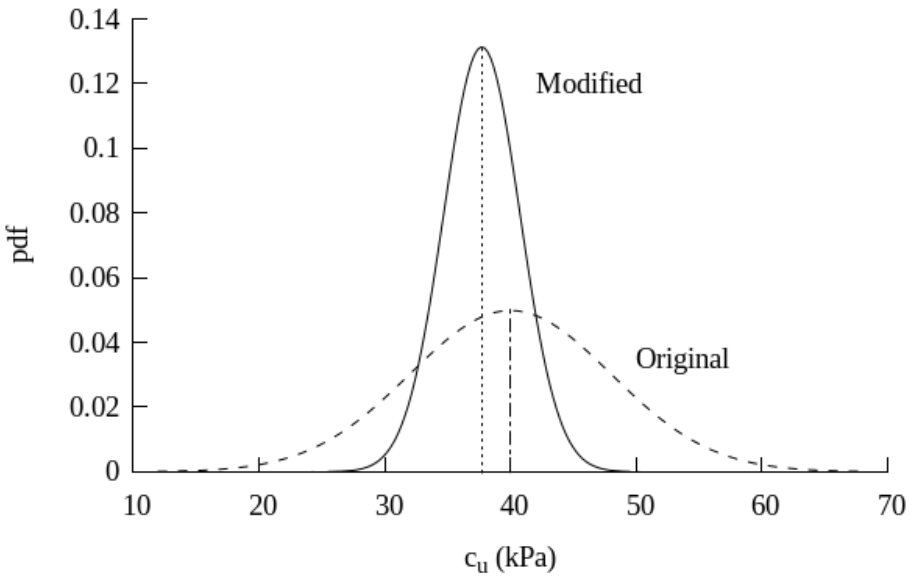

Figure 4. Distribution of "effective" c_u for $\theta_h/\theta_v = 48$.

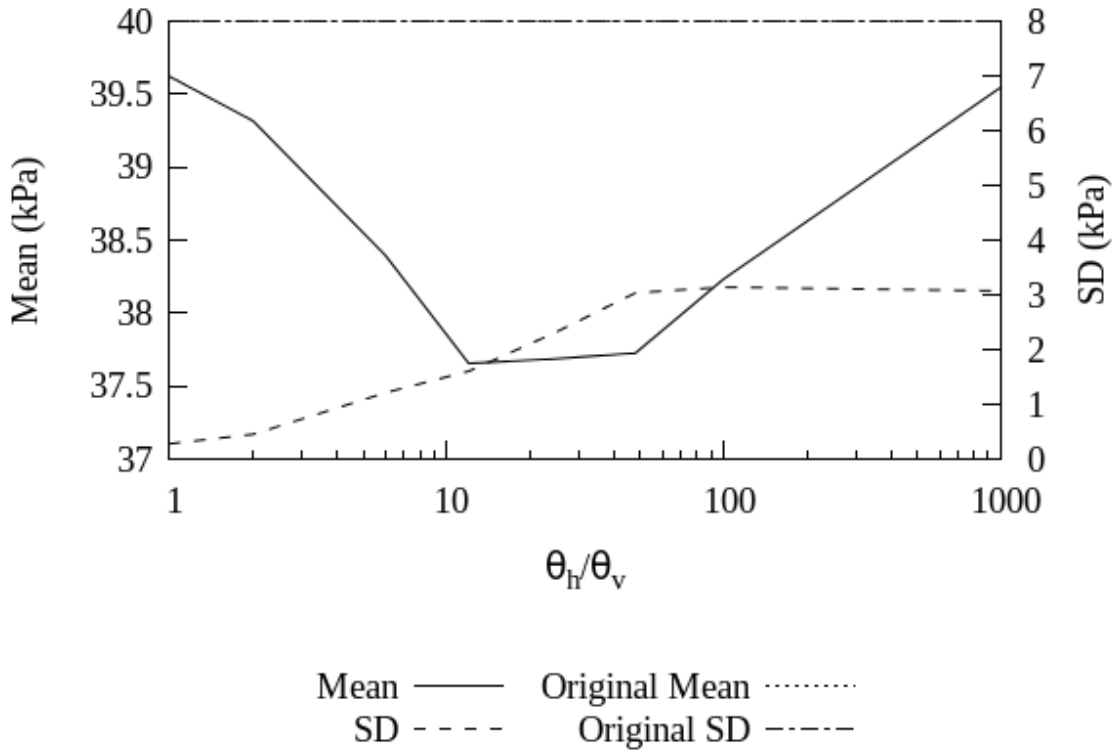

Figure 5. Influence of θ_h/θ_v on the mean and standard deviation of "effective" c_u.

Finally, as the horizontal scale of fluctuation exceeds about half the length of the slope, in this case represented by $\theta_h/\theta_v = 50$, the tendency for discrete failures reduces due to the influence of the mesh boundaries; at the same time there is an increasing tendency for 2D "Mode 3" failures initiating at depths influenced by the distribution of the weak and strong "layers" (HICKS & SPENCER [12]). This results in the mean approaching the underlying mean of 40 kPa. However, even though the standard deviation reaches a maximum of around 3 kPa, it remains well below the underlying standard deviation of 8 kPa due to the small value of θ_v causing considerable averaging of property values in the vertical direction.

Figure 6 shows typical 3D deformed mesh and *x*-displacement contours at failure for Modes 1, 2 and 3. However, these are purely illustrative; HICKS et al. [7] and HICKS & SPENCER [12] highlighted the wide range of failure mechanisms possible when accounting for three-dimensional effects, especially for the most probable failure mode, Mode 2.

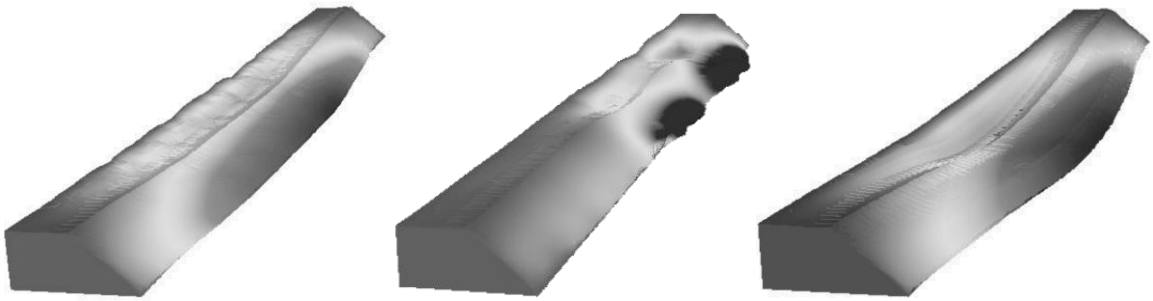

(a) Mode 1 (b) Mode 2 (c) Mode 3

Figure 6. Deformed meshes and contours of *x*-displacement for typical failure mechanisms.

4.3 Further comments

As indicated in the earlier discussion regarding Figure 1(b), reliability-based characteristic values are derived by proportioning the area under the probability distributions of effective c_u, such as that shown in Figure 4. It is clear that the distribution of c_u from which the characteristic value is obtained is narrower and has a lower mean than the underlying property distribution, for the reasons discussed earlier. There are two further points worthy of note:

- Although there is only a modest reduction in the mean for the example presented in this paper, this is largely due to the simplicity of the problem itself. For example, HICKS & SAMY [9-11] showed that weak zones can have a greater influence in problems in which there is an underlying depth trend in the statistics (as is often the case). Moreover, HICKS & ONISIPHOROU [8] investigated the influence of spatial variability of sand state on the liquefaction potential of an underwater slope and showed that, for realistic degrees of anisotropy of the heterogeneity, slope stability was often governed by the weakest zones. In their investigation, a deterministic analysis based on the mean sand state gave an upper bound solution.

- The modified soil property distributions quantify the uncertainty in the structure response due to lack of knowledge of the soil spatial variability. This led HICKS [6] to highlight two practical questions: "(a) what is the required intensity of in situ testing to give reasonable estimates of the soil property statistics; and (b), how may the uncertainty in geotechnical performance be reduced through the optimal use of available data?" A start on

addressing these issues has been made by VAN DEN EIJNDEN & HICKS [2] and LLORET-CABOT et al. [13].

5 Conclusions

The influence of spatial variability of soil properties on geotechnical performance and uncertainty has been demonstrated for an idealised 3D slope stability problem. As previously discussed by HICKS [6] and demonstrated by HICKS & SAMY [10], the Random Finite Element Method may be used as a basis for understanding and determining reliability-based characteristic values in line with the requirements of Eurocode 7 (CEN [1]). HICKS [6] highlighted that the modified property distribution, from which characteristic values should be derived, is different to the underlying property distribution in two respects: (a) it is narrower due to the averaging of properties over potential failure surfaces; and (b), it has a reduced mean due to the tendency for failure to follow the path of least resistance. This observation has been supported by the results in this paper, reinforcing the view that variance reduction methods may give an unsafe solution if no account is taken of the reduction in the mean.

References

[1] CEN: *Eurocode 7: Geotechnical design. Part 1: General rules, EN 1997-1*. European Committee for Standardisation (CEN), 2004.

[2] Eijnden, A.P. van den; Hicks, M.A.: Conditional simulation for characterizing the spatial variability of sand state. In: Pietruszczak, S.; Pande, G.N. (Eds.): *Proceedings of the 2nd International Symposium on Computational Geomechanics*. Dubrovnik, Croatia, 2011, 288–296.

[3] Fenton, G.A.; Griffiths, D.V.: *Risk assessment in geotechnical engineering*. John Wiley and Sons, 2008.

[4] Fenton, G.A.; Vanmarcke, E.H.: Simulation of random fields via Local Average Subdivision, *Journal of Engineering Mechanics, ASCE* 116 (1990), 1733–1749.

[5] Hicks, M.A. (Ed.): *Risk and variability in geotechnical engineering*. Thomas Telford, London, 2007.

[6] Hicks, M.A.: An explanation of characteristic values of soil properties in Eurocode 7. In: Arnold, P.; Fenton, G.A.; Hicks, M.A.; Schweckendiek, T.; Simpson, B. (Eds.): *Modern geotechnical design codes of practice: development, calibration and experiences*. IOS Press, 2012, in press.

[7] Hicks, M.A.; Chen, J.; Spencer, W.A.: Influence of spatial variability on 3D slope failures. In: Brebbia, C.A.; Beriatos, E. (Eds.): *Proceedings of the 6th International Conference on Computer Simulation Risk Analysis and Hazard Mitigation*. Kefalonia, Greece, 2008, 335–342.

[8] Hicks, M.A.; Onisiphorou, C.: Stochastic evaluation of static liquefaction in a predominantly dilative sand fill. *Géotechnique* 55 (2005), 123–133.

[9] Hicks, M.A.; Samy, K.: Influence of heterogeneity on undrained clay slope stability. *Quarterly Journal of Engineering Geology and Hydrogeology* 35 (2002), 41–49.

[10] Hicks, M.A.; Samy, K.: Reliability-based characteristic values: a stochastic approach to Eurocode 7. *Ground Engineering* 35 (2002), December, 30–34.

[11] Hicks, M.A.; Samy, K.: Stochastic evaluation of heterogeneous slope stability. *Italian Geotechnical Engineering* 38 (2004), 54–66.

[12] Hicks, M.A.; Spencer, W.A.: Influence of heterogeneity on the reliability and failure of a long 3D slope. *Computers and Geotechnics* 37 (2010),

[13] Lloret-Cabot, M.; Hicks, M.A.; Eijnden, A.P. van den: Investigation of the reduction in uncertainty due to soil variability when conditioning a random field using Kriging, *Géotechnique Letters* 2 (2012), in press.

[14] Spencer, W.A.; Hicks, M.A.: A 3D finite element study of slope reliability. In: Pande, G.N.; Pietruszczak, S. (Eds.): *Proceedings of the 10th International Symposium on Numerical Models in Geomechanics*. Rhodes, Greece, 2007, 539–543.

[15] Taylor, D.W.: Stability of earth slopes. *Journal of the Boston Society of Civil Engineers* 24 (1937), 197–246.

[16] Vanmarcke, E.H.: *Random fields: Analysis and synthesis*. The MIT Press, Cambridge, Massachusetts, 1983.

Uncertainty Analysis of stiffness prediction for pile group models

Bastian Jung[a)], Henning Stutz[a)], Gudio Morgenthal[b)], Frank Wuttke[c)]
[a)] Research Training Group 1462,
[b)] Chair of Modelling and Simulation - Construction,
[c)] Chair of Geomechanical Modelling,
Bauhaus-Universität Weimar

Abstract: This paper presents a quantification of different vertical and lateral pile group models. Therefore the chosen models are briefly introduced. The uncertainty quantification for the total model uncertainty is then introduced. This total model uncertainty is a combination of the model uncertainty and the parameter uncertainty. After the introduction of the models and the uncertainty analysis the investigated geometry and the stochastic input parameters are described. The methodology is applied to the above-mentioned applications and the results therefore are discussed.

1 Introduction

Model uncertainty is an important model property which has to be considered for a reliable and therefore safe model application. DITHNDE et al. [3] stated, that uncertainty analyses are essential especially in foundation engineering. MOST [6] shows for the prediction and simulation of an appropriate structural behaviour it is significant to consider a model choice evaluation including the evaluation of the complexity and the prediction capability of the models. For example, the research of SCHMOOR et al. [16] about the influence of the variability of soil and load parameters according a monopile does not take this source of uncertainty into account. Taking this model prognosis uncertainty into account can support the model selection process and can be the basis for subsequent simulations like the above-mentioned reliability analyses [16].

Nowadays in bridge engineering, the use of integral or semi-integral structures is rising. This new development needs a holistic modelling of the complete structure. One major part of these engineering structures is the

surrounding soil at the abutments and the pile-soil-pile interaction of the pier foundations. Deflections and rotations of the foundation defined by their stiffness prediction can reduce restraining forces in the structure in comparison to the fixed foundation boundary conditions [11]. This paper focuses on different models for the prediction of the vertical and lateral stiffness of pile group foundations and their quantification of the total model uncertainty.

1.1 Vertical pile group models

Vertical loading on pile groups can be analysed using analytical solutions and numerical techniques like the Finite Element Method or the Integral Equation Analysis. A rather high number of different models for each methodology exist, which differ in their considered phenomenon for the piles, their interaction in the group and the soil conditions. The research of RANDOLPH et al. about the behaviour of single piles [13] and pile groups [14] is cited in almost every publication afterwards and can be renowned as a fundamental approach to determine the vertical stiffness of piles and piles groups. The interaction between the piles is dependent on the displacement field arising from the settlement of a loaded ("source") pile and therefore the piles follow the free-field displacement generated by their neighbours, as an assumption (superposition of individual pile displacement field). The model could be applied to any general geometry of the pile group. The only restriction being that all the piles must be embedded to the same depth. The soil behaviour is modelled as a linear-elastic material defined by the shear modulus which is assumed to vary linearly with depth and a constant Poisson´s ratio.

MYLONAKIS et al. [7] used this model as their basis for further investigations. The analytical formulation is based on the Winkler model of soil reaction for determining the vertical interaction factors between two piles embedded in multi-layered soil. In order to analyse this interaction, the interplay between the adjacent ("receiver") pile and the soil subjected to this displacement field is additionally considered, in comparison to RANDOLPH et al. [14]. Axial pile rigidity and the soil reaction at the pile tip tend to reduce the settlement based on the assumption by [14].

In order to develop a practical design approach by determining nomogram, RUDOLF [15] defined a numerical model for pile groups which take into account the partial safety concept. This model is developed based on extensive parameter studies complemented by the results of extended analytical methods. The soil is modelled as a bi-linear material with a failure criteria defined by Mohr-Coulomb.

Table 1 shows the different phenomenon criteria's and the corresponding input parameters of the considered models. If the pile behaviour is assumed to be rigid, there is no need for defining a modulus of elasticity for the pile. Therefor this parameter is not considered in the model by RANDOLPH et al. [14] and the model by RUDOLPH [15]. The soil parameter friction angle, dilatancy and cohesion are needed for the description of the Mohr-Coulomb material model. They are exclusively included in the nonlinear soil model by RUDOLPH [15] and are not necessary for the other models, which assume linear-elastic soil behaviour.

Table 1. Characteristics of pile models considered due to vertical loading.

		RANDOLPH et al. [14]	MYLONAKIS et al. [7]	RUDOPLH [15]
pile behaviour		rigid	compressible	rigid
soil behaviour		linear-elastic	linear-elastic	bi-linear Mohr-Coulomb failure criteria
soil stratification		homogenous	multi-layered	multi-layered
pile Young´s modulus	E_p	-	+	-
soil Young's modulus	E_s	+	+	+
soil shear modulus	G_s	+	+	+
Poisson ratio	ν_s	+	+	+
friction angle	φ	-	-	+
dilatancy	ψ	-	-	+
cohesion	c	-	-	+
earth pressure at rest coefficient	K_0	-	-	+

1.2 Lateral pile group models

Static lateral loaded pile groups have been under investigation since the early sixties. There are a multitude of different models in existence to predict the lateral deflection behaviour of pile groups. An overview is given by OOI et al. [8] and OOI et al. [9]. In the following section, two different approaches are investigated for lateral loaded pile groups.

The lateral loaded pile model developed by RANDOLPH [12] can be used with an interaction approach by POULOS [10] for laterally loaded pile groups. RANDOLPH [12] presented simple analytical solutions for laterally loaded piles. These analytical solutions are obtained by curve-fitting of the results of Finite Element Analyses of laterally loaded piles. Therefore, RANDOLPH [12] assumed that the piles are embedded in an elastic soil medium. Under this as-

sumption a power law relationship was developed. These solutions can be applied for deflection u and the rotation θ at the soil surface. This lateral load pile model is extended by using the interactions factor concept from POULOS [10] which is modified by to RANDOLPH [12] to predict the lateral pile group behaviour.

The second lateral load model considered was developed by DUNCAN et al. [2]. This model uses the concept of *p-y* analysis. The Characteristic Load Method (CLM) approximates the results of the nonlinear p-y analyses. This model was developed using an amount of different *p-y* calculations to express the results in a dimensionless relationship. These factors can be used to predict the deflections and maximum moments of lateral load piles. For the analysis of pile group behaviour, the CLM *p-y* multiplier is used by MOKWA et al. [5]. For the computation, a revised form of these *p-y* multiplier are used by BRETTMANN et al. [1].

Both models are used for different back calculation of filed load tests and 1g scale test and show their application possibilities. Table 2 shows the different effects and phenomena which can be reproduced with both considered laterally loaded pile models. The essential input parameter shows that the models differ in major parts.

Table 2. Characteristics of pile models considered due to lateral loading.

		RANDOLPH [12]	DUNCAN [2]
pile behaviour		flexible	flexible
pile head behaviour		fixed/free head	fixed/free head
soil behaviour		elastic	nonlinear *p-y*
Young's modulus		may vary with depth	may vary with depth
shear modulus		may vary with depth	may vary with depth
Possion's ratio		constant with depth	constant with depth
horizontal stiffness		possible	possible
rotational stiffness		possible	not possible
pile Young´s modulus	E_p	+	+
soil Young´s modulus	E_s	+	+
soil shear modulus	G_s	+	+
Possion´s ratio	ν_s	+	+
friction angle	φ	-	+
effective unit weight	γ'	-	+
Rankine coefficient of passive earth pressure	K_P	-	+

2 Geometry and parameters for different pile group applications

Two different types (denoted by I and II) for the geometry of the pile group are analyzed, see Fig. 1. A pile group with only one row of piles (I) in longitudinal direction of a bridge on the one hand and beyond this, a square group (II) of piles is investigated in the next section. Both types of pile foundation can be found for different types of bridge constructions. The type (II) generates more lateral stiffness in comparison to the type (I). Therefore the type (II) is applied for the classical decoupled beam bridges (decoupling between superstructure and substructure using bearings). In contrast to this, the type (I) is used commonly for semi-integral and integral bridges in order to reduce the horizontal stiffness of the foundation, which can reduce restraining forces in the entire structure (often a critical design criteria for integral bridges).

Homogenous soil as a large graded and compact sand (SW) is defined for both configurations of the pile groups. Ongoing research about the influence of the soil stratification, different types of soil, varying pile properties (length, diameter) and other pile group geometries are not part of this paper.

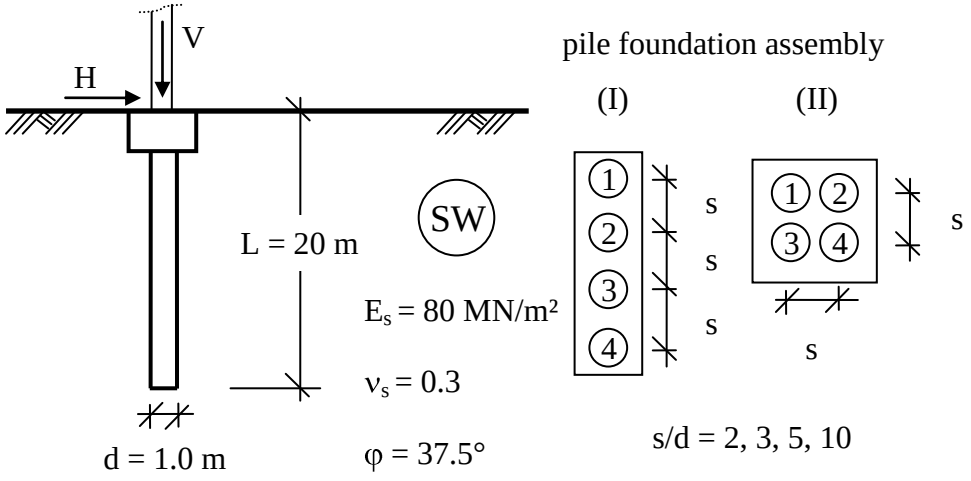

Figure 1. Geometry of pile groups and soil conditions

The length of the pile is estimated using a pre-design method for static pile formulations to consider that the pile will be long enough to carry the vertical and horizontal load of a 3 span (36.95 m – 41.00 m – 32.35 m) semi-integral concrete box girder bridge.

3 Uncertainty analysis of different pile group models

3.1 Stochastic Input Parameter

The stochastic input parameters are chosen as artificial data to show the general methodology for the uncertainty quantification for pile group models. The different input parameters and their distribution, mean, coefficient of variation and the correlation matrix is shown in Table 3.

Table 3. Probabilistic input parameters of pile and soil properties.

Material Property		Distribution	Mean value	CV	Correlation Matrix			
					E_p	E_s	ν_s	φ
pile Young´s modulus	E_p	Log Normal	30000 MN/m²	0.15	1.0	0	0	0
soil Young's modulus	E_s	Log Normal	80 MN/m²	0.20	0	1.0	0.7	0.4
Poisson ratio	ν_s	uniform	0.28…0.32	-	0	0.7	1.0	0
friction angle	φ	Log Normal	37.5	0.20	0	0.4	0	1.0

3.2 Uncertainty Quantification

The uncertainty analysis considers the complexity of the models (epistemic uncertainty) and the influence of uncertain input parameters concerning the model output (aleatoric uncertainty). A reference model is used in order to evaluate the deterministic differences in the prognosis and to determine therefore the epistemic uncertainty. Experimental data could be used for this purpose, but usually a lack of specific experimental data exist in the design process of engineering structures. Therefore the most complex model of the considered models is fixed as a benchmark for the simplified models. Through the highest complexity, the accuracy for describing the physical phenomena should be highest, as an assumption. The model uncertainty is defined as:

$$CV_{model,K_i} = \frac{\left|K_{complex} - K_i\right|}{1.645} \tag{1}$$

with i partial model (considered model) and
K predicted stiffness of the model.

The difference in the model output between a simplified model in relation to the complex model (reference model) is in the 90%-CI of the complex one, as an assumption.

The quantification of the parameter uncertainty is simulated with 5000 scatter material properties of the pile and the soil (see Table 3).

Latin Hypercube Sampling [4] is used as an effective sampling strategy. The correlation between the input parameters is considered inside the sampling. The parameter uncertainty is defined as:

$$CV_{parameter,K_i} = \frac{\sigma_{K_i}}{\mu_{K_i}} \tag{2}$$

with σ standard deviation of the model output,
μ mean value of the model output,
i partial model (considered model) and
K predicted stiffness of the model.

The total uncertainty is based on the idea of [6] and defined as:

$$CV_{total,K_i} = \sqrt{CV_{model,K_i}^{\ 2} + CV_{parameter,K_i}^{\ 2}} \tag{3}$$

with CV_{model} model uncertainty expressed by the coefficient of variation according the model output and
$CV_{paramater}$ parameter uncertainty expressed by the coefficient of variation according the model output.

4 Results of the deterministic and probabilistic model evaluation

4.1 Uncertainty quantification for vertical loading

The deterministic solution for the vertical stiffness of the pile group (see Fig. 2a)) show, that the prognosis for elastic loading is quite similar according to the considered models. Influenced by the different distance between each of the piles inside the group in relation to the pile foundation assembly (I) or (II), the interaction factors are different and therefore the resulting vertical stiffness is not constant between both configurations. The interaction is higher in the quadratic assembly (II) compared to the assembly with all piles in one row (I) and consequently the stiffness of (I) is higher compared to (II). The non-linear model by RUDOLPH [15] was chosen as reference model because of the highest model complexity. Therefore the model of RUDOLPH [15] has no model uncertainty. The model uncertainty of RANDOLPH et al. [14] and

MYLONAKIS et al. [7] is in the range of $CV_{model,vertical,elastic} < 0.02$ and the parameter uncertainty for all s/d-ratios is in the range of $CV_{parameter,vertical,elastic} \sim 0.20$ for all considered vertical pile foundation models. Hence, the resulting total uncertainty is mainly influenced by the parameter uncertainty of the model and is the range of $CV_{total,vertical,elastic} \sim 0.20$ as it is shown in Fig. 2(b).

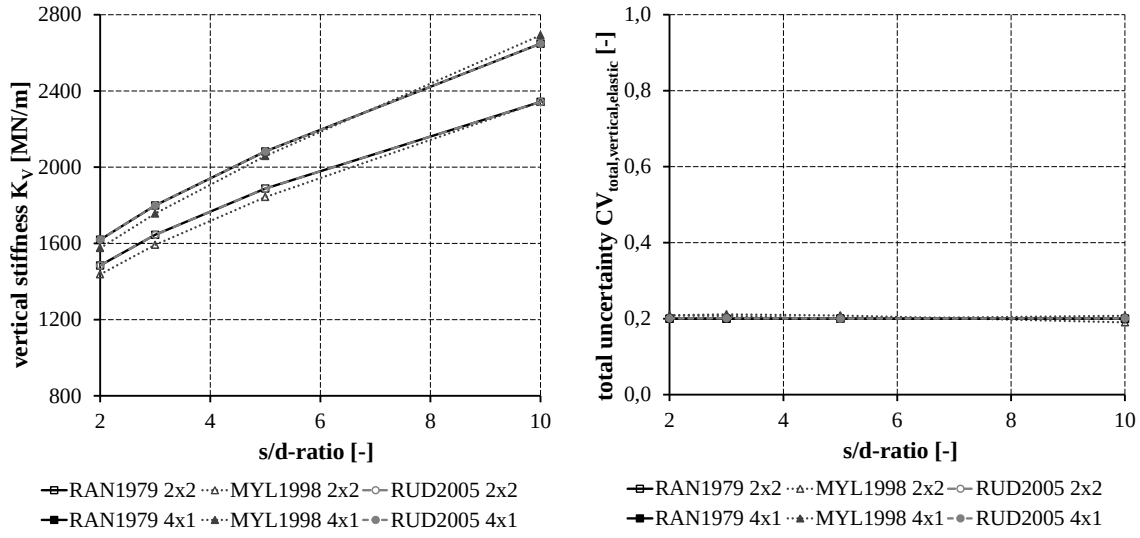

(a) Deterministic vertical stiffness of the considered models as a function of the ratio pile space / pile diameter (s/d)

(b) Total Uncertainty of the vertical pile models as a function of the s/d-ratio

Figure 2. Vertical stiffness prediction and total uncertainty in case of elastic loading

In comparison to the linear loading and according to the results of the uncertainty, a nonlinear vertical loading influences strongly the vertical stiffness and in consequence the uncertainty of the pile foundation stiffness prediction, see Fig. 3(a). The models by RANDOLPH and WROTH [14] and MYLONAKIS and GAZETAS [7] assume linear-elastic soil behaviour and therefore, the vertical stiffness is independent on the loading conditions. The results according to the deterministic vertical stiffness shown in Fig. 3(a) are the same compared to Fig. 2(a) for the above-mentioned models. The approach by RUDOLPH [15] considers a bi-linear behaviour of the soil with the Mohr-Coulomb failure criteria. Therefore, the stiffness can be decreased in a large amount for nonlinear loading of the pile foundation. In this example, the loading for the pile foundation was 25 MN in order to force high nonlinear effects in the soil. The linear prognosis of the more simplified models overestimate enormously the stiffness, which results in a high model uncertainty for both linear models $0.20 < CV_{model,vertical,nonlinear} < 0.65$. The nonlinear model by RUDOLPH [15] was

chosen as the reference model. The parameter uncertainty for the linear models [7,14] is exactly the same for the nonlinear loading as for the linear loading. For the complex nonlinear model [15], the parameter uncertainty increases significantly up to $CV_{parameter,vertical,nonlinear} \sim 0.45$. Taking into account the model uncertainty and parameter uncertainty leads to the total uncertainty for the considered vertical pile models due to nonlinear loading (see Fig. 3). The results for short ratios between the pile spacing (s) and the diameter of the pile (d) determine a slight difference in the uncertainty of the model prognosis. In contrast, for higher s/d-ratios the difference between the nonlinear and linear models increases.

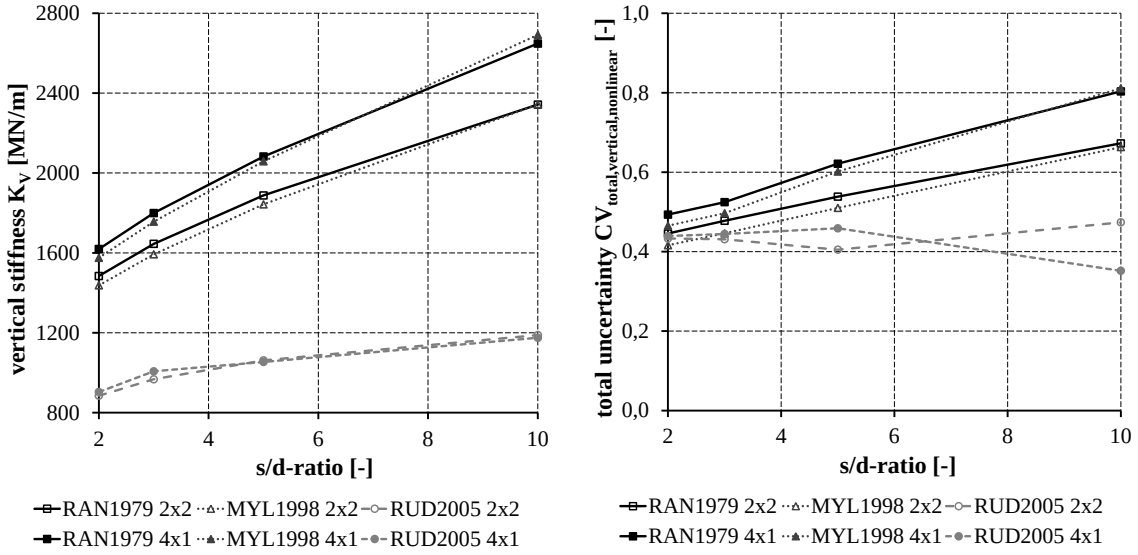

(a) Deterministic vertical stiffness of the considered models as a function of the ratio pile space / pile diameter (s/d)

(b) Total Uncertainty of the vertical pile models as a function of the s/d-ratio

Figure 3. Vertical stiffness prediction and total uncertainty in case of nonlinear loading

4.2 Uncertainty quantification for lateral loading

In the case of the laterally loaded pile group models, the deterministic solution for the horizontal stiffness of the pile group is shown in Fig. 4(a). Quite significant differences in the stiffness prediction are obvious. The nonlinear model by DUNCAN et al. [2] was chosen as the reference model. The model uncertainty is in the range of $CV_{model,lateral,elastic} \sim 0.60$ for the squared pile group (II) and $CV_{model,lateral,elastic} \sim 0.13$ for the row of piles (I). The parameter uncertainty for the RANDOLPH [12] model is for various s/d-ratios between the range of $CV_{parameter,lateral,elastic} \sim 0.05 - 0.17$ for the squared (II) and the row pile

group (I). The DUNCAN et al. [2] model shows a parameter uncertainty $CV_{parameter,lateral,elastic} \sim 0.36 - 0.39$ for both pile group assemblies. The resulting total uncertainty of both models is shown in Fig. 4(b).

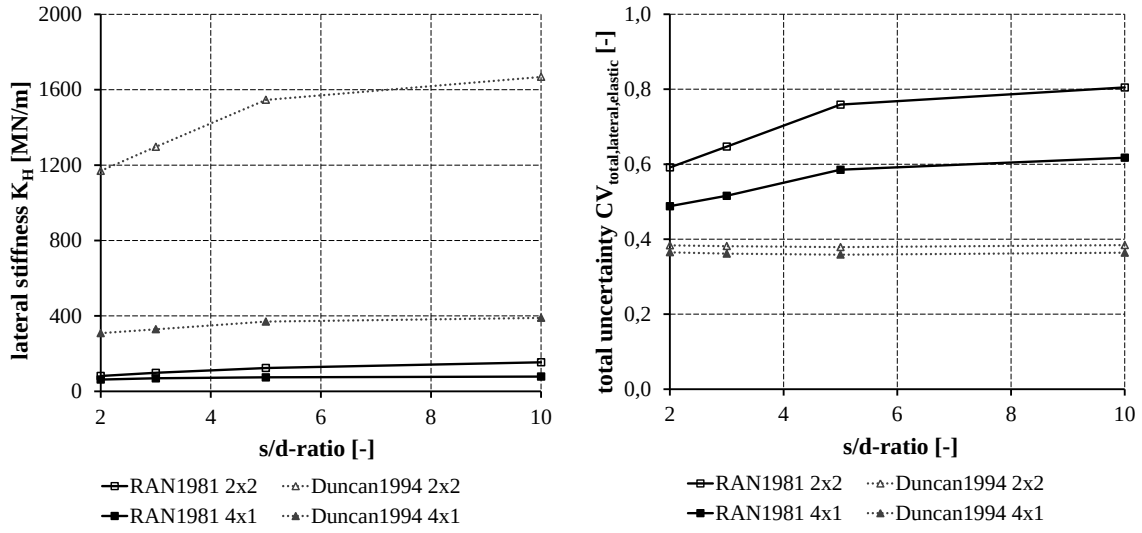

(a) Deterministic lateral stiffness of the considered models as a function of the ratio pile space / pile diameter (s/d)

(b) Total Uncertainty of the lateral pile models as a function of the s/d-ratio

Figure 4. Lateral stiffness prediction and total uncertainty in case of linear loading

In comparison to the elastic loading and the results according to the uncertainty, a nonlinear loading strongly influences the lateral stiffness of the pile foundation (see Fig. 5(a)). In contrast to the elastic loading, both models show a similar behaviour for the two different pile group geometries (I) and (II). The deterministic nonlinear lateral stiffness (see Fig. 5) is decreased compared to their elastic stiffness (see Fig. 4). In this example, the lateral nonlinear loading for the pile foundation was 0.45 MN in order to force nonlinear effects in the model response. The linear prognosis of the more simplified model by RANDOLPH [12] underestimates the stiffness, which results in a high model uncertainty for this linear model $0.13 < CV_{model,lateral,nonlinear} < 0.40$. The parameter uncertainty for the model by RANDOLPH [12] is exactly the same for the elastic and nonlinear loading by both different pile group assemblies. For the nonlinear model by DUNCAN et al. [2], the parameter uncertainty is approximately constant around $CV_{parameter,lateral,nonlinear} \sim 0{,}40$ for both pile group geometries. Taking into account the model uncertainty and parameter uncertainty leads to the total uncertainty of the considered lateral pile models due to nonlinear loading (see Fig. 5(b)), which is quite high for the model by

RANDOLPH [12]. The parameter uncertainty of this model is rather small, but the model uncertainty is high, due to the simplicity of the model compared to the model by DUNCAN et al. [2].

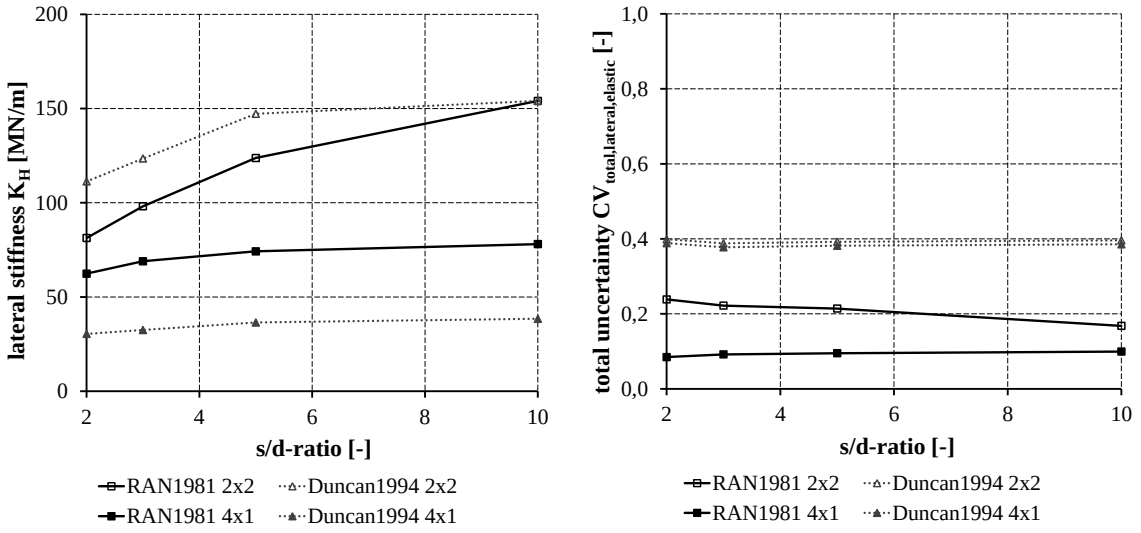

(a) Deterministic lateral stiffness of the considered models as a function of the ratio pile space / pile diameter (s/d)

(b) Total Uncertainty of the lateral pile models as a function of the s/d-ratio

Figure 5. Lateral stiffness prediction and total uncertainty in case of nonlinear loading

The results for narrow ratios between the pile spacing and the diameter of the pile determine a difference in the uncertainty of the model prognosis. The model by DUNCAN et al. [2] shows for the nonlinear loading a better total uncertainty of ~ 0.30 compared to the model by RANDOLPH [12] from ~ 0.46 - 0.80. This result is in contrast to the model uncertainty of the pile group behaviour under elastic loading.

5 Conclusions

The uncertainty of the stiffness prediction for pile foundation models with different pile assemblies is analysed quantitatively. This evaluation includes the model prediction error of simplified models in relation to a reference model. Therefore the model uncertainty is used which express these difference as a coefficient of variation CV_{model}. More and more input parameter for higher order models (sophisticated models) can force a second uncertainty in the prediction of the model, which is called the parameter uncertainty $CV_{parameter}$. Taken both effects into account leads to the total uncertainty of the

considered models CV_{total}. This total uncertainty is an expression for the prediction quality of the model response.

The vertical and lateral stiffness prognosis of the pile foundation models are used as the target value for the uncertainty analysis. This model output couples the bridge structure with the soil and foundation conditions in order to achieve a simulation model of the entire structure.

As well as for vertical and lateral models this prediction and uncertainty is strongly dependent on the loading condition. Either the loading forces linear or nonlinear reaction in the models will change the uncertainty of the model prediction. For example, the vertical stiffness prediction of the considered models for a loading condition which leads to an elastic response differs only slightly. In contrast, a significant difference for nonlinear loading conditions can be observed for those vertical pile models. The ratio between the pile spacing and the pile diameter has a lesser influence for the vertical models in comparison to the lateral models.

As an outlook here, the described models and methodology will be applied in a holistic model for an entire integral or semi-integral bridge to show the importance of the stiffness prediction of the pile foundation (model class) in interaction with other model classes, like creep, shrinkage, material modelling of concrete, temperature loading and geometric nonlinearities. Furthermore, the complete model is evaluated and the global model quality will be assessed using graph theory and sensitivity analyses.

6 References

[1] Brettman, T.; Duncan, J. M.: Computer application of CLM lateral load analysis to piles and drilled shafts *J. Geotech. Geoenviron. Eng.* 120 (1996), pp. 496-498

[2] Duncan, J. M.; Evans, L. T. and Ooi, P. S. K.: Lateral load analysis of single piles and drilled shafts *J. Geotech. Geoeviron. Eng.* 120 (1994), pp. 1018-1033

[3] Dithinde, M.; Phoon, K. K.; De Wet, M. and Retief, J. V.: Charaterization of model uncertainty in the static pile design formula *J. Geotech. Geoeviron. Eng.* (2011), pp.70-85

[4] McKay, M. D.; Beckman, R. J.; Conover, W. J.: A comparison of three methods for selecting values of input variables in the analysis of output from a computer code. *Technometrics* (1979)

[5] Mokwa, R. L.; Duncan, J. M.: Laterally Loaded Pile Group Effects and p-y Multipliers *ASCE Geotechnical Special Publication* No 113, (2001), pp. 728-742.

[6] Most, T.: Assessment of Structural Simulation Models by Estimating Uncertainties due to Model Selection and Model Simplification. *Computers and Structures* 89 (2011), pp. 1664–1672

[7] Mylonakis, G.; Gazetas, G.: Settlement and additional internal forces of grouped piles in layered soil. *Géotechnique* 48 (1998), pp. 55–72

[8] Ooi, P. S. K.; Chang, B. K. F. and Wang, S.: Simplified lateral load analyses of fixed-headed piles and pile groups *J. Geotech. Geoeviron. Eng.* 130 (2004), pp. 1140-1151

[9] Ooi, P. S. K.; Duncan, J. M.: Lateral load analysis of groups of piles and drilled shafts *J. Geotech. Geoeviron. Eng.* 120 (1994), pp. 1034-1050

[10] Poulos, H. G.: Behavior of laterally loaded piles: II Pile groups *Journal of Soil Mechanics and Foundations Division* SM 5 (1971), pp. 733-750

[11] Raithel, M..; Kempfert, H.-G.; Leusink, E.: Geotechnische Problemstellungen bei der Ausführung von semi-integralen Brückenbauwerken am Beispiel der Fahrbachtal- und Glattbachtalbrücke. *7. Brückenbau Symposium.* Dresden, pp. 1-12

[12] Randolph, M.F.: The response of flexible piles to lateral loading. *Geotechnique* 31 (1981), pp. 247-259

[13] Randolph, M. F.; Wroth, C. P.: Analysis of deformation of vertically loaded piles. *Journal of the Geotechnical Engineering Division* 104 (1978), pp. 1465–1488

[14] Randolph, M. F.; Wroth, C. P.: An analysis of the vertical deformation of pile groups. *Géotechnique* 29 (1979), pp. 423–439

[15] Rudolf, M.: Beanspruchung und Verformung von Gründungskonstruktionen auf Pfahlrosten und Pfahlgruppen unter Berücksichtigung des Teilsicherheitskonzeptes. Universität Kassel: self-publishing company, 2005 – Dissertation

[16] Schmoor, K.; Achmus, M.: On the influence of the variability of soil parameters on the behaviour of laterally loaded piles in sand. *Proceedings of the 9th International Probabilistic Workshop* (2011)

Point Estimate Method vs. Random Set – A case study in Tunnelling

A. Nasekhian [*], H.F. Schweiger[**], T. Marcher [***]
[*]Dr. Sauer & Partners Ltd., London
[**]Graz University of Technology, Graz
[***]ILF Consulting Engineers, Rum/Innsbruck

Abstract: The international insurance industry has suffered several hundred million US$ compensation for large losses in the tunnelling industry in the last three decades. Certainly a variety of causes may be considered for the losses; nevertheless, causes originating from uncertainties, lack of knowledge or insufficient data prior to tunnel construction cannot be overlooked. Therefore, modern concepts dealing with uncertainties (e.g. reliability analysis, risk management and sensitivity analysis) have to be introduced into common engineering practice, especially for large underground structures. It seems that there is a demand to utilise simple mathematical concepts regarding uncertainties in tunnel engineering and to introduce simple and user-friendly frameworks for analysing and designing underground structures. This paper aims to compare the results of two uncertainty models, namely the Point Estimate Method (PEM) and the Random Set Method, against the measurements for a tunnel problem. The shortcomings and merits of the methods are highlighted and the conditions under which both approaches can lead to similar results, considered to be useful in engineering practice, are demonstrated.

1 Introduction

In this paper, two selected non-probabilistic and probabilistic methods with the potential of being combined with numerical methods – without requiring any modification to the core of the numerical code – are investigated. It is demonstrated that useful information can be provided for more rational engineering judgment and decision making in tunnelling. As it can be seen in a possible classification of non-deterministic analysis methods portrayed in

Figure 1, non-deterministic methods are divided into two main categories, non-probabilistic and probabilistic methods (Nasekhian 2011). In this paper one method from each category of the non-deterministic methods has been selected. Although, due to the characteristics of information usually available in tunnelling problems, the Random Set Approach is favoured by the authors to deal with uncertainties, the Point Estimate Method is still appealing in engineering practice because of its lower number of computer realisations required.

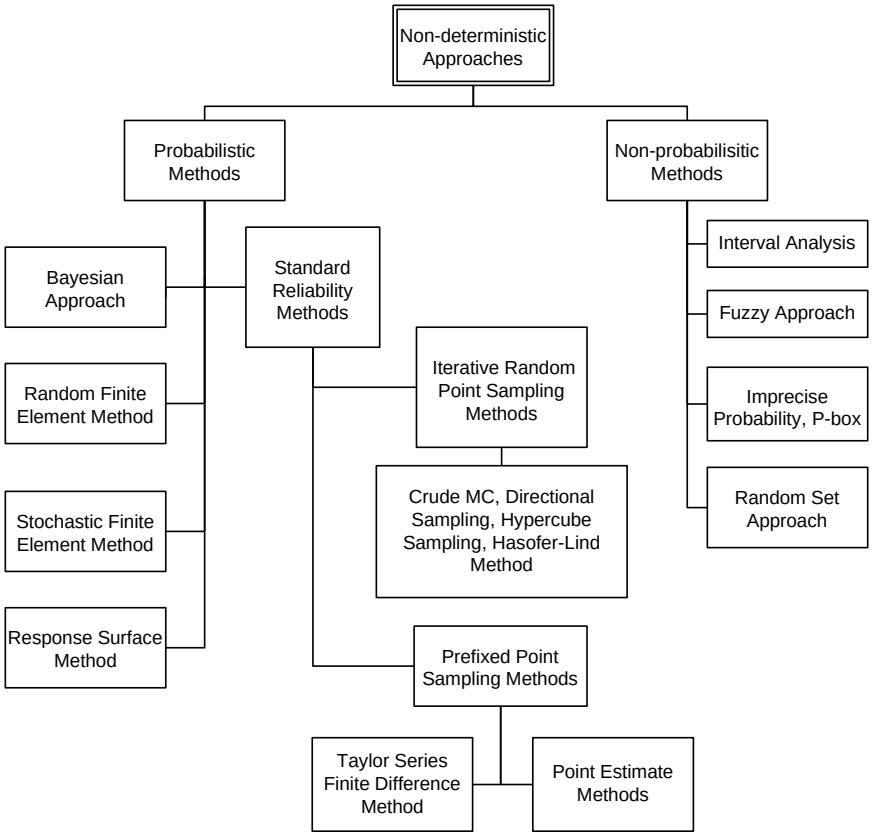

Figure 1. Classification of non-deterministic approaches (Nasekhian 2011)

2 Random Set Approach

In short, in random set analysis, set valued information (focal elements) and probability measures (probability assignments) are combined together leading to probability bounds in terms of discrete cumulative distribution functions (CDF). The bounds encompass any distribution compatible with the existing data including the actual distribution. The Random set procedure maps the inputs onto the system response, also in terms of probability bounds. This approach has many similarities to other non-probabilistic methods depicted in

Figure 1 such as the fuzzy set and p-box approach. For instance, both random set and fuzzy set approaches are supported by set theory and interval analysis that would be an integral part of their solution procedure. However, in Random Set the independence of the individual information sources are preserved while in the p-box approach a set is randomly taken by the Monte-Carlo process at each simulation.

The random set is attractive in the sense that it enables engineers to consider both "aleatory" and "epistemic" types of uncertainty. In tunnel engineering, due to the linear nature of tunnel projects, usually very limited results from investigation programs are available at the beginning of the design stage, which leads to very sparse and scarce data. Consequently, the geotechnical properties mostly appear in ranges without probability measures attributed across the ranges. In such conditions, the random set approach is proposed and preferable.

The applicability and efficiency of Random Set Finite Element Method (RS-FEM) in geotechnical practice and tunnelling have been demonstrated in several publications e.g. Peschl 2004, Schweiger et al. 2007, Nasekhian 2011, Nasekhian & Schweiger 2011. The basics and the mathematical framework of the Random Set are extensively discussed in the literature, e.g. Dubois and Prade 1991 and Tonon et al. (2000), and are not repeated herein.

3 Point Estimate Method

The Point Estimate Method (PEM) is one of the probabilistic methods. In brief, the probability distribution of input parameters is substituted by single values and their respective predefined weights. The uncertainty model is evaluated with the predefined sampling points and as a result, the statistical moments of system responses that are of interest, are estimated.

This method is favourable in the sense of simplicity (from a practical point of view) as well as its relatively low number of simulations, although there are limitations and some of these are addressed in this paper.

In PEM, the Reliability analysis of a geotechnical problem in connection with numerical models can be broken down into a limited number of deterministic finite element calculations based on the number of predetermined points given by the method. In this sense, PEM is similar to the Random Set Finite Element Method. PEM is appealing in terms of the number of required realisa-

tions comparing to the RS-FEM. There are two main distinguishable approaches for the point estimate method: first, Rosenblueth's approach (Rosenblueth, 1975) and its modified method given by his followers (e.g. Harr 1989) that attempt to save computational cost by reducing the number of prefixed sampling points. In a research undertaken by Thurner (2000), it turned out that the approach proposed by Zhou and Nowak (1988) employing the $2n^2+1$ integration rule (ZN-III) -*n* is the number of basic variables- results in an optimum compromise between accuracy and computational effort. Hence, in the present work this approach is adopted.

3.1 Advantages and shortcomings of PEM

The accuracy of PEM generally varies from exact to approximate statistical parameters of a target value depending on the complexity of the mapping function and the number of points included in the calculations. The result of Rosenblueth's PEM is precise for sums of uncorrelated or correlated variables (Alén, 1998) while in the case of more complex functions the degree of accuracy drops. However, it can be sufficiently accurate in many practical situations (Harr, 1996; Baecher and Christian, 2003). According to Alén (1998) the more linear the function is, the more accurate the method probably is, also the error given by the PEM-approximation is on the safe side. However, the latter comment is not true for all types of limit state functions (especially in association with Rosenblueth methods; see work of Eamon et al. (2005)). Yet Baecher and Christian (2003) state "The method is reasonably robust and is satisfactorily accurate for a range of practical problems, though computational requirements increase rapidly with the number of uncertain quantities of interest". Nasekhian (2011) has addressed the accuracy of PEM on some basic polynomial and non-polynomial functions. Furthermore, it is anticipated that random set results encompass the distribution of the system response obtained from PEM. Regarding the Point Estimate Method, particularly ZN-III, the following advantages are pointed out:

- The simplicity of the method, which allows engineers to benefit from it with limited knowledge of probability theory.
- It gives reasonable accuracy in the estimate of the mean (the most accurate result) and variance of polynomials and most complex functions. Correlations between random variables can also be considered.
- It is a favourable method in terms of the number of FE calculations compared to the Random Set Finite Element Method. Random set analysis with the total number of calculations ($4n$) – given 2 sources of information for each basic variable – leads to

a significantly larger computational effort in comparison with that of ZN-III ($2n^2+1$) in cases where the number of basic variables is more than 3 (Fig. 2).

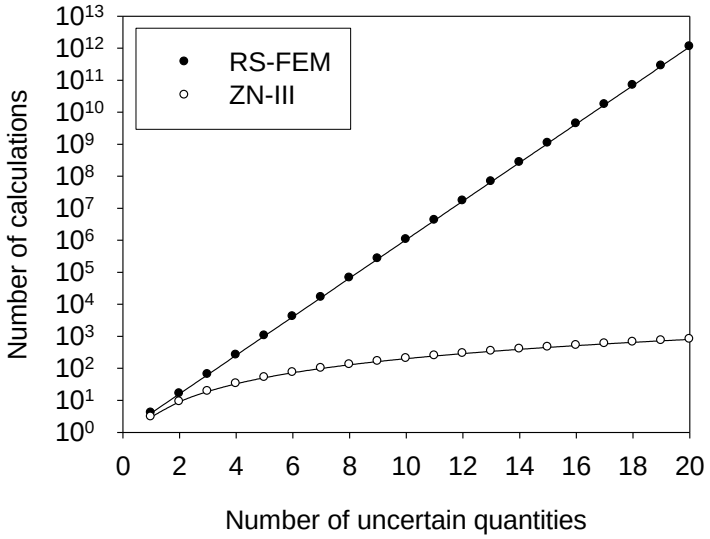

Figure 2. Comparison of RS-FEM with ZN-III in terms of the number of realisations

Despite many appealing points regarding PEM, there are main disadvantages as follows:

- PEM yields only the statistical parameters of the system response but no information concerning the shape of the response distribution. Therefore a subjective assumption is needed in this regard, which may affect the probability of failure obtained by this method.

- The method has severe limitations in handling large numbers of variables because difficulties may arise in the determination of meaningful points in the input space.

4 Application to Tunnel Excavation

A tunnel application was chosen for the purpose of comparison between RS-FEM and PEM. The 460 m long tunnel located in Germany with a typical horse-shoe shaped section and dimension of 15×12.3 m width and height respectively, is constructed according to the principles of the New Austrian Tunnelling Method (NATM), and is divided into three main excavation stages: top-heading, bench and invert. The overburden along the tunnel axis starts from 7.5 m in the portal region to a maximum of 25 m. However, a section with the overburden of 25 m was selected herein. The relevant tunnel geometry including some model specifications are depicted in Figure 3. Approximately 900 15-noded triangular elements were employed in the 2D finite

element model using Plaxis software (Brinkgreve et al. 2008) and the Mohr-Coulomb failure criterion is chosen as the constitutive model.

The random set input variables utilised in RS-FEM are summarised in Table 1. The probability share, $m(A)$, (or probability assignment) of both sets are identical. E_{rm} is the elastic modulus of the rock mass, φ and c are the Mohr-Coulomb strength parameters. It is noted that both sets chosen for the stress relaxation factor (R_f values) are based on expert's opinion. This factor is usually employed in order to account for 3D-effects in a 2D analysis. In addition, the R_f values for different stage constructions are correlated to each other, for example the left extreme value of top-heading's R_f is used with the corresponding lower values of relaxation factors for bench and invert. Some selected results of the RS-FEM analysis are presented in the next sections along with the PEM results for the sake of comparison. Further details about the manner of obtaining RS-FEM results are referred to other publications of the authors e.g. Nasekhian and Schweiger (2011).

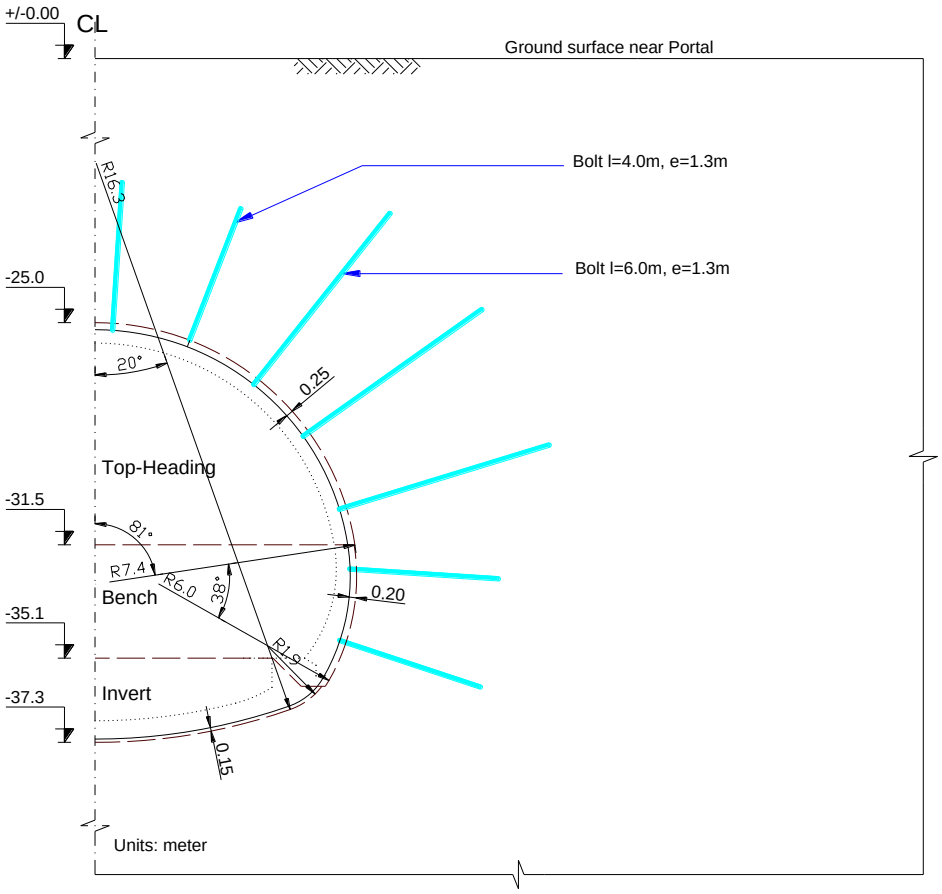

Figure 3. Specifications of the tunnel geometry and supports

Table 1. Random set parameters used in RS-FEM analysis

Var.	$m(A)$	E_{rm}	R_f T.H.	R_f Bench	R_f Invert	φ	c
Units	[-]	[MPa]	[-]	[-]	[-]	[°]	[kPa]
Set 1	0.5	1300-2300	0.4-0.6	0.3-0.5	0.2-0.4	22-32	450-750
Set 2	0.5	1900-3400	0.3-0.5	0.2-0.4	0.1-0.3	24-34	1000-1600

4.1 Providing distribution functions equivalent to random sets

In order to apply PEM, it is necessary to have a probability distribution function for each random variable. Due to the lack of test results and limited sampling, it was not feasible to build an accurate Probability Distribution Function (PDF) of the considered random variables. In addition, in order to be able to compare PEM results with those of RS-FEM, the uncertainty of the input should be matched with each other, which is difficult and is achievable only to a limited extent. In this situation Nasekhian (2011) has proposed 3 alternatives to provide a PDF of basic variables that match the random set input. The approach used in this work is discussed below.

4.1.1 The selection of a best fit to a uniform distribution

In this alternative, first a uniform distribution is constructed whose left and right extreme values are respectively medians of left and right random set bounds (rectangular distribution in Fig. 4). Then, typical and well-known distributions are fitted to the obtained distribution and depending on the shape of the random bounds and the variable itself, an appropriate distribution for further analysis can be selected. The approach was applied to the friction angle using Triangular, Normal and Lognormal distributions as depicted in Figure 4. In this particular case where the CDF of the variable is very coarse, a considerable discrepancy between the different distribution types occurs and engineering judgment is necessary.

Although the random set exhibits some kind of symmetry on the right and left bounds, the selection of Lognormal looks more reasonable since it covers the whole range of random set values and it is also a commonly used distribution for the friction angle because it always gives positive values. When there is

abundant information and the random set bounds are smoother, the appropriateness of this approach emerges.

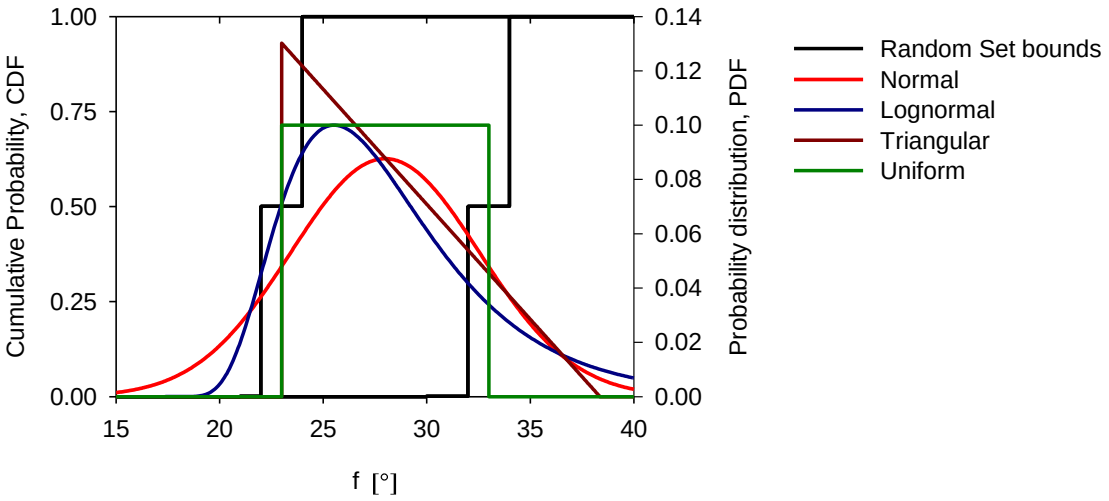

Figure 4. Distribution of friction angle equivalent to the random set

The approach has been applied to other random variables of the problem whose results are illustrated in Figure 5.

For each random parameter some judgment has been carried out as follows:

Elasticity modulus: Lognormal distribution shows skewness to the left inspired by the random set; it also covers the entire range of the random set rather well. Triangular and Uniform distributions do not entirely cover the random set.

Cohesion: Normal distribution is chosen since it has a better coverage on the whole random set than the others, and also shows no skewness or predisposition to the left or right just like the corresponding random set.

Relaxation factor: Normal distribution is adopted since there is no evidence that the relaxation factor has any sort of skewness. On the other hand, Normal distribution covers the range of the random set quite well and takes some values out of the range into account (ones with a very small probability value), which places the results on the safe side.

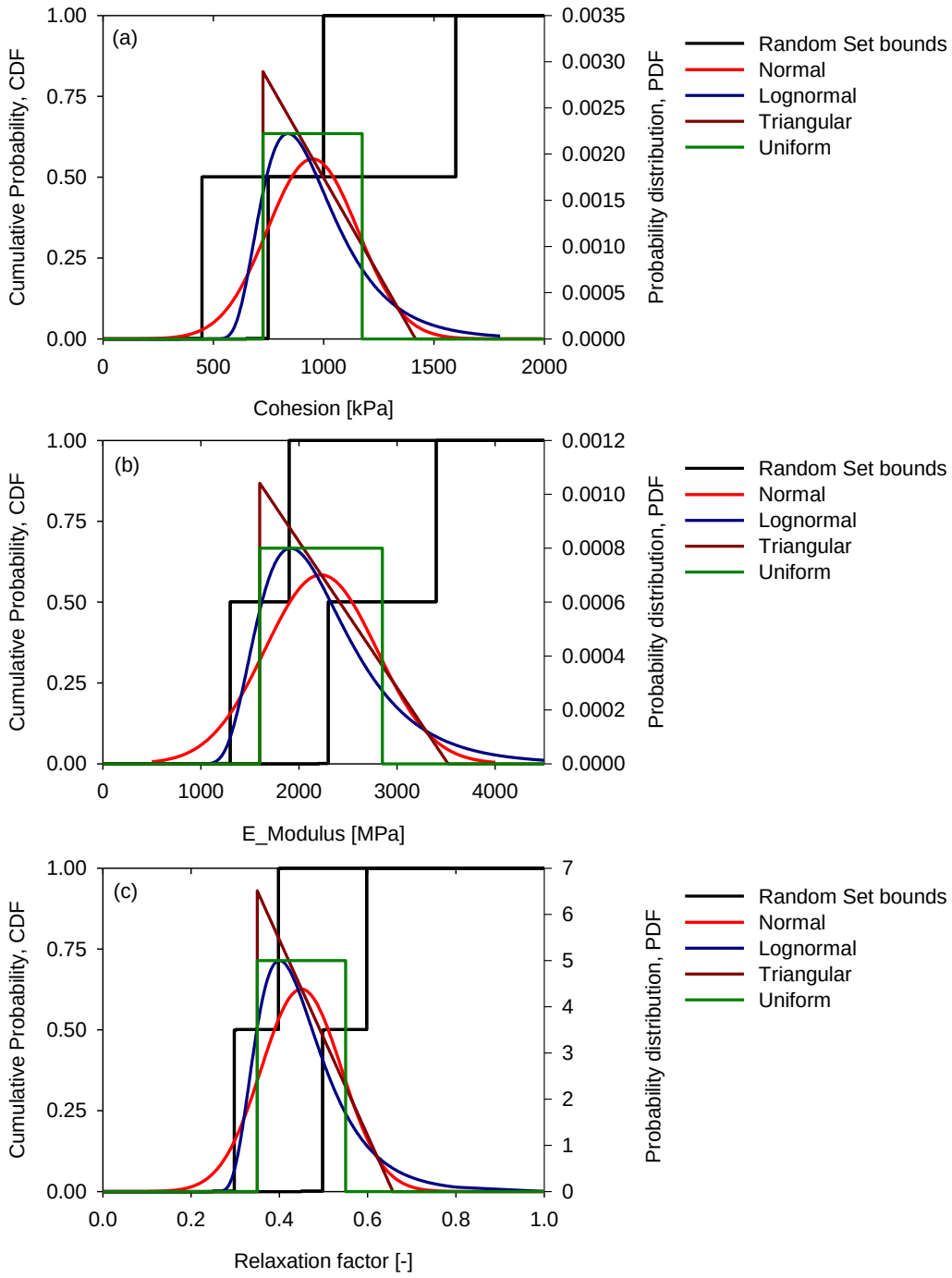

Figure 5. Equivalent distribution to the random set for basic variables,
a) cohesion b) elastic modulus c) relaxation factor

According to the above discussion, detailed information about the probability distribution of the four basic random variables selected for PEM analysis is given in Table 2.

Table 2. Basic random variables and the respective PDF details

Basic variable	Unit	Distribution type	Mean	Standard dev.	COV %
Friction angle, φ	degree	Lognormal	28	5	17.8
Elasticity modulus, E	MPa	Lognormal	2256	631	28
Cohesion, c	kPa	Normal	950	205	21.6
Relaxation factor, R_f	-	Normal	0.45	0.09	20

5 Calculation Results

The input parameters are given in Table 2. No correlations between basic random variables have been taken into account. According to the ZN-III integration rule the numerical model of the tunnel based on the sampling points has to be evaluated 33 times. Eight realisations can be left out since the respective weights are zero; therefore, the number of calculations decreases to 25 realisations. The number of calculations in comparison with the random set approach (256 realisations required) is considerably lower and can be considered as an advantage of PEM.

The following results have been selected for comparison:

1. Vertical displacement of the tunnel crown (Uy-A)
2. Vertical & horizontal displacement of the side wall (Uy-B & Ux-B)
3. Maximum normal force and moment in the lining.

The basic statistical moments of the results have been tabulated below (Tab. 3) and for instance, the results of crown displacement and maximum moment in the lining are illustrated in Figure 6 with the corresponding RS-FEM p-boxes overlaid. For each result, two commonly used distributions, namely Normal and Lognormal have been assumed corresponding to the estimated statistical moments given in Table 3.

Based on the mean (μ) and standard variation (σ) of the results, Table 3 gives the extremes of the 86% confidence interval ($\mu \pm 1.8\sigma$), regardless of the distribution type (Pukelsheim, 1994). They show a good conformity with the range of the most likely values given by RS-FEM.

Table 3. Statistical moments of the selected results and the range of the most likely values given by RS-FEM

	Response Unit	U_y-A mm	U_x-B mm	U_y-B mm	Normal Force kN.m/m	Moment kN/m
PEM results	Average (μ)	2.5	0.58	1.5	264	12.2
	Stand. dev. (σ)	0.8	0.14	0.4	78	2.6
	μ+1.8σ	3.9	0.83	2.2	405	16.9
	μ-1.8σ	1.2	0.33	0.7	124	7.5
RS-FEM	Upper limit	3.9	0.77	2.2	407	16.8
most likely range	Lower limit	1.6	0.44	1.0	164	7.3

Generally, the most likely values in the Random Set results are defined as values with the highest probability of occurrence, where the slope of the corresponding cumulative distribution function is steepest. For the purpose of simplification, it is assumed that the most likely results are those values whose cumulative probabilities at the lower and upper bound are less and higher than 0.5 respectively. In this research, it turned out that the range $\pm 1.8\sigma$ could encompass the range of the most likely values given by RS-FEM, although this finding should be confirmed by further investigation and more examples. As it can be seen in Figure 6, results such as displacements and internal forces show a good conformity with the RS-FEM results in the sense that PEM's results are supposed to present the 'true' distribution of the system response and should not exceed the random set bounds.

From the probability theory (Pukelsheim, 1994), it is known that the interval $\pm 1.8\sigma$ represents the 86% confidence interval irrespective of what distribution the target variable has, on condition that the distribution is unimodal. If it goes beyond 3σ, a very small probability of the occurrence of such an event is expected, or in other words, it should be practically 'unlikely' since the interval $\pm 3.0\sigma$ theoretically encompasses at least 95% of the expected results.

The two-step discrete cumulative probability distribution of the measurements implies that only the measurements of two tunnel cross sections were available. As it can be seen from Figure 6a, both measured values of the tunnel crown could be captured by the interval $\pm 1.8\sigma$.

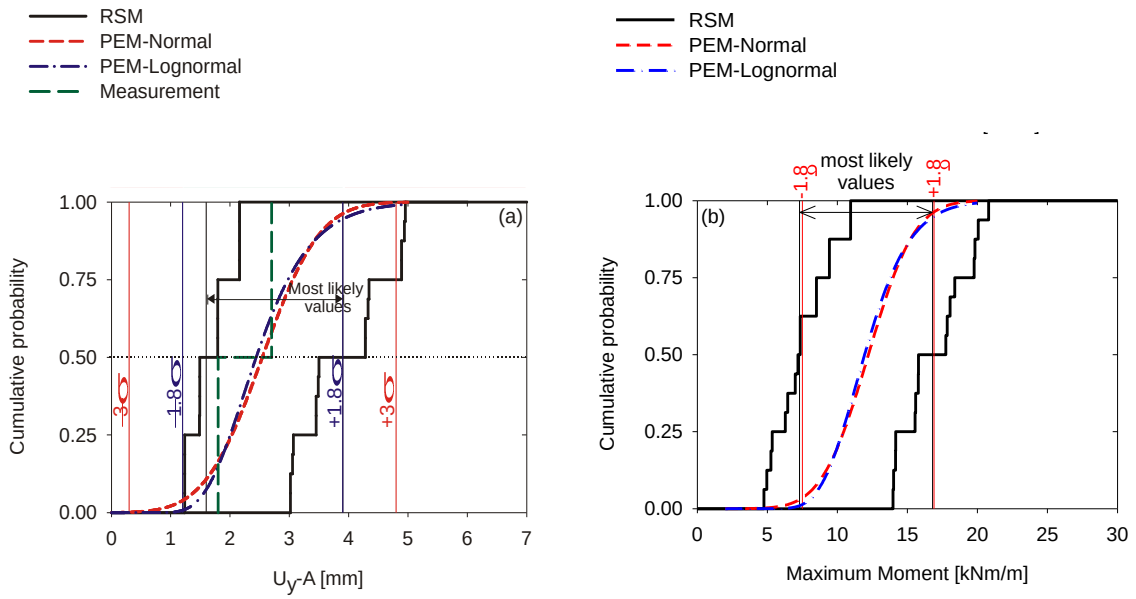

(a) vertical displacement at the tunnel crown

(b) maximum moment in the tunnel lining

Figure 6. Comparison of PEM with RS-FEM results.

6 Summary and conclusion

Both RS-FEM and PEM were applied to a real case tunnel problem. A process of obtaining a probability distribution consistent with the corresponding random set p-box was proposed. The results of PEM in comparison with RS-FEM were satisfactorily consistent. The number of FE calculations required by PEM is significantly lower than those in the random set method especially as the number of basic random variables increases. Furthermore, it was found that in all results, the range of $\pm 1.8\sigma$ with respect to the mean value encompasses the range of most likely values estimated by RS-FEM. This range theoretically represents an interval at least with 86% confidence.

RS and PEM methods both produce a common range of results, although their input and assumptions are clearly different, and thus difference in results have to be expected. When the soil/rock data parameters are abundantly available, their probability distributions are definable with sufficient accuracy, thus applying PEM is advantageous in this case. However, this paper showed that even in the case of having set valued input parameters without knowing the probability of occurrence across the sets, it is possible to draw a similar conclusion from PEM.

7 References

[1] Alén, C. (1998) *On Probability in Geotechnics*: *Random Calculation Models Exemplified on Slope Stability Analysis and Ground-Superstructure Interaction*. Department of Geotechnical Engineering, Chalmers University of Technology. Dissertation.

[2] Baecher, G.B.; Christian, J.T. (2003) *Reliability and Statistics in Geotechnical Engineering*. New York: Wiley & Sons.

[3] Brinkgreve, R.B.J.; Broere, W. (2008) PLAXIS, Finite element code for soil and rock analyses, *users manual*. Version 9, Rotterdam: Balkema.

[4] Dubois, D.; Prade, H. (1991) Random sets and fuzzy interval analysis. *Fuzzy Sets and Systems*, Vol. 42, 87-101.

[5] Eamon, C.D.; Thompson, M.; Liu, Z. (2005) Evaluation of accuracy and efficiency of some simulation and sampling methods in structural reliability analysis. *Structural Safety*, Vol. 27, No. 4, 356-392.

[6] Harr, M.E. (1989) Probabilistic estimates for multivariate analyses. *Applied Mathematical Modelling*, Vol. 13, No. 5, 313-318.

[7] Nasekhian, A.; Schweiger, H.F. (2011) Random Set Finite Element Method application to tunnelling. *Int. J. Reliability and Safety*, Inderscience Publishers, 5(3/4), 299-319

[8] Nasekhian, A. (2011) *Application of Non-probabilistic and Probabilistic Concepts in Finite Element Analysis of Tunnelling*. Institute for Soil Mechanics and Foundation Engineering, Graz University of Technology, Dissertation.

[9] Peschl, G.M. (2004) *Reliability Analyses in Geotechnics with the Random Set Finite Element Method*. Graz University of Technology, Dissertation.

[10] Pukelsheim, F. (1994) The Three Sigma Rule. *The American Statistician*, Vol. 48, No. 2 , 88-91.

[11] Rosenblueth, E. (1975) Point estimates for probability moments. *Proc. Nat. Acad. Sci.* USA, Vol. 72, No. 10, 3812-3814.

[12] Schweiger, H.F.; Peschl, G.M.; Pöttler, R. (2007) *Application of the random set finite element method for analysing tunnel excavation*. Georisk 1, S. 43-56.

[13] Thurner, R. (2000) *Probabilistische Untersuchungen in der Geotechnik mittels Deterministischer Finite Elemente-Methode*, Institut für Bodenmechanik und Grundbau, TU-Graz, Dissertation.

[14] Tonon, F.; Bernardini, A.; Mammino, A. (2000) Reliability analysis of rock mass response by means of Random Set Theory. *Reliability Engineering & System Safety*, Vol. 70, No. 3, 263-282.

[15] Zhou, J.; Nowak, A.S. (1988) Integration formulas to evaluate functions of random variables. *Structural safety*, Vol. 5, No. 4, 267-284.

Classification of warning systems for natural hazards

Martina Sättele, Michael Bründl (1), Daniel Straub (2)
(1) Research Group Avalanche Dynamics and Risk Management, WSL Institute for Snow and Avalanche Research SLF, Davos
(2) Engineering Risk Analysis Group, TU München, Munich

Abstract: Intensified efforts are being made to establish warning systems as efficient components of an integrated risk management strategy for natural hazards. While testing and reliability analyses are well established procedures for active protection measures such as dams, rockfall nets and galleries, methods and conventions for evaluating the reliability of warning systems are lacking. To incorporate warning systems as standard measures of an integrated risk management strategy for natural hazards, their reliability must be quantifiable. The aim of this contribution is to establish appropriate reliability quantification methods for warning systems by classifying them according to characteristics relevant to assessing their reliability. Firstly, chief natural hazard processes in Switzerland in need of warning systems are selected and system relevant process characteristics such as the role of the geographical disposition of the event site, trigger events and dynamic process parameters are clarified. In three examples the influence of the process characteristics on the monitoring possibilities with respect to the system lead time is illustrated. A system classification is suggested, which classifies the systems in i) threshold systems, ii) expert systems and iii) model-based expert systems. The classification is applied to 52 warning systems in Switzerland and for each system class typical characteristics such as the lead time, the geographical range, the degree of human influence vs. technical influence and direct vs. indirect monitoring possibilities are identified. The classification allows a structured identification of reliability criteria for each class and is a first step towards development of a method for quantifying the reliability of warning systems for natural hazards.

1 Introduction

Integrated risk management aims to mitigate the risk caused by natural hazards to persons, animals, infrastructures and to achieve protection goals through the application of approved mitigation measures. Thereby, risk to an object i associated with a scenario j is a function of [3]:

p_j probability of occurrence of scenario j ,

pe_{ij} presence probability of object i in scenario$j$,

V_{ij} vulnerability of object i in scenario j,

A_i value of object i .

Warning systems mitigate the overall risk level by reducing pe_{ij} and with sufficient warning time V_{ij} can be reduced [10]. One of the first automated warning system in Switzerland is the snow avalanche detection system in "Mahnkinn", commissioned by a railway company in 1953 [20]. Since then, the use of viable warning systems has increased considerably, and warning systems have been established by a number of different institutions according to different needs specific to various natural hazard processes all over Switzerland. To date the systems are often installed as prototypes where technical developments are tailored to specific projects and there is little standardisation between systems [11]. In order to incorporate warning systems as standard measures in an integrated risk management strategy for natural hazards, their reliability must be quantifiable. Warning systems are complex technical systems and to efficiently access their reliability requires an holistic system approach considering the system design and the technical failures as well as the natural hazard process characteristics and the human influences. A system classification is the first step towards such a method, since it allows the identification of system reliability criteria in a structured manner. At present a recognized classification of this kind does not exist.

Glantz [8] discusses system types and classification criteria, but argues that even a simple definition for the term warning system is not practical and thus limits the system diversity, the space for interpretations and the opportunity for future system advancements. The Swiss Federal Office for Civil Protection distinguishes between warning, which is a notification to authorities, and alarm, which is issued directly to general public [6]. According to the United Nations Office for Disaster Risk Reduction [14], a warning system is "a set of capacities needed to generate and disseminate timely and meaningful warning information to enable individuals, communities and organizations threatened by a hazard to prepare and to act appropriately and in sufficient time to reduce

the possibility of harm or loss". Monitoring is a part of warning, but it does not include automatic issued warning possibilities and is thus no warning system [8]. Bell et al. [2] classify warning systems in monitoring, expert and alarm systems, but emphasize that a sharp system classification is not convenient. These approaches and ideas are the starting point for the development of the classification proposed in this paper.

2 Hazard processes and warning systems in Switzerland

The geography of Switzerland implicates that natural hazards often involve water or mass movement processes. The landscape is characterised through rivers and more than 1500 lakes, and the Alps cover 60% of the country [22,23]. The most frequent events in Switzerland are forest fires, earthquakes, floods, (thunder) storms, rock and snow avalanches, debris flows, rock/ block and ice falls, permanent landslides, flash floods and glacier lake outburst floods (GLOF) [21]. Floods, hail and storm have been causing the highest property damages since 1990 [13], while the number of flood, debris flow, landslide and rockfall damages between 1972 and 2007 were dominated by six major flood events [12]. They caused over 50% of the total damages recorded and were mainly triggered through long-lasting rain fall [12]. Permanent landslides, debris flows and rockfalls caused 64 fatalities while floods caused 46 deaths between 1972 and 2007 (Rockfall events have only be recorded since 2002). Snow avalanches have the highest fatality rate with about 25 deaths each winter, of which a great number are self-inflicted by mountaineers and off-piste skiers [12].

The range of warning systems identified in four Cantons of Switzerland (Bernese Oberland, Grison, Ticino and Valais) mainly covers the variety of hazard processes identified (Figure 1). The documentation and analysis of these 52 active warning systems is the basis for the classification. Thereof are four systems operated by specialist departments on a national scale (Federal Office for the Environment (FOEN) - flood, MeteoSchweiz - meteo hazards, Swiss Seismological Service (SED) - earthquake, WSL Institute for Snow and Avalanche Research SLF - snow avalanches). The identified systems are installed for ten different hazards processes and classified following the suggestion from Dikau and Weichselgartner [4].

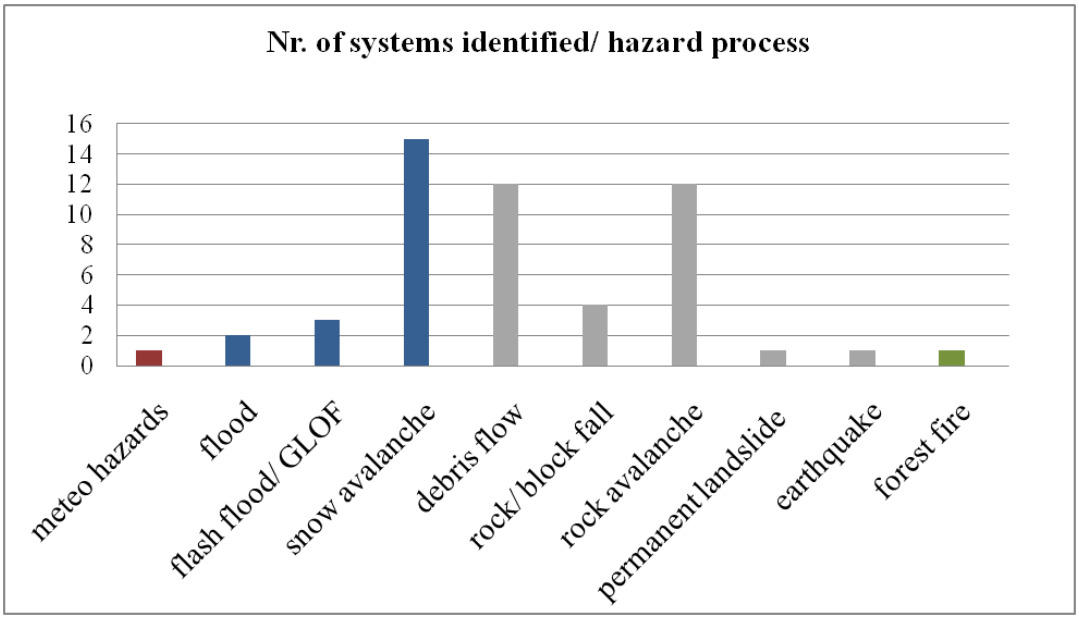

Figure 1. Number of systems identified for different hazard processes.

3 Hazard process characteristics and system monitoring possibilities

3.1 Hazard process characteristics

Natural hazard processes can be divided into an initiating *hazard event* and a resulting *damaging event* in the case that objects of value are hit. Each hazard event is characterised through its process characteristics. The *basic disposition* determines the general and long-term potential for a hazard process of a certain area. It is defined through parameters such as the topography, geology, geomorphology, hydrology and vegetation. The *variable disposition* is characterised by time dependent parameters such as state of vegetation, rain, snow and temperature changes. The basic disposition determines if an area is endangered and the variable disposition when and how often events take place[18]. Keefer [15] lists common *trigger events*, which are pre-events that activate main hazard events, such as precipitation, snow melt, frost actions, human-induced cutting of slopes, weathering processes, deposition of material on slopes, changing in ground water conditions, surface drainage, blasting, tectonic deformation and earthquakes. For an event to occur both triggers and the variable disposition must be critical and coincide [18]. Each hazard process itself is marked through specific *dynamic process parameters*.

For example, the basic disposition of a debris flow torrent could be characterised by the presence of a glacier, a terrain with steep slope and curvature, while the variable disposition depends on the availability of additional loose debris material. Trigger events can be short and intensive precipitation, long

rainy periods, intense snow and ice melting, hail and outburst of sub-surface flows or a combination of them. For debris flows, characteristic dynamic process parameters are flow depth, velocity, volume and density [9].

3.2 System monitoring possibilities

Warning systems monitor different hazard process characteristics. The choice of the monitoring parameters depends on the hazard process and determines the system lead time (Figure 2). Two situations can be distinguished:

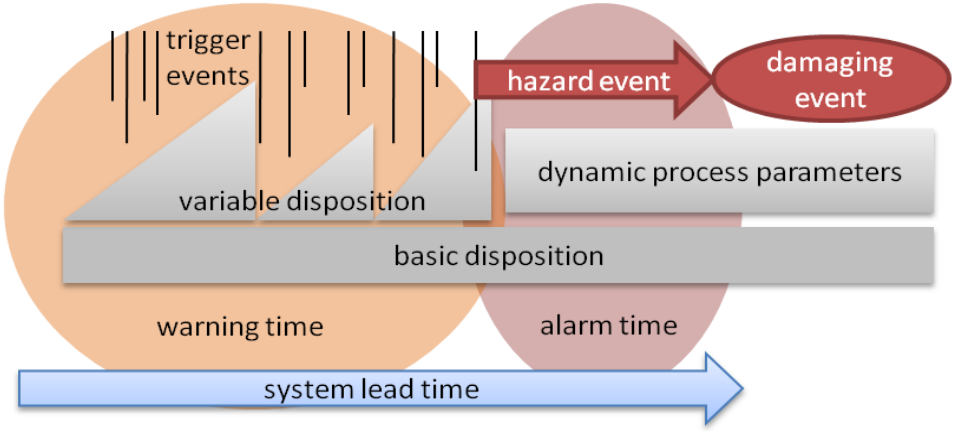

Figure 2. Reliability relevant hazard process characteristics and monitoring parameters. Figure aligned to [26].

1. System lead time = alarm time: the system directly monitors the dynamic process parameters during the ongoing hazard event. The alarm time is less or equal to the event time. Thus, the alarm time depends on the velocity of the process and the distance between the warning system and endangered objects.

2. System lead time = warning time + alarm time: the system monitors direct or indirect changes in the disposition or indirect trigger events. The potential warning time is the time between the appearances of the changes in disposition and triggers until the start of the damaging event. The lead time is the warning plus the alarm time.

The geographical coverage of a system is defined as the area covered by the monitoring system. The system coverage can be international, national, regional or local (catchment and endangered objects below). The geographical resolution is the minimum area that can be monitored.

Dikau and Weichselgartner [4], Felgentreff and Glade [5], Keller and Blodgett [16] and Lang et al. [19] discuss speed and duration, warning times as well as the geographical range of different hazard processes. We discuss

the influence of process characteristics on the system monitoring parameters in the following three examples.

The Swiss Federal Institute for Forest, Snow and Landscape Research (WSL) operates a local debris flow warning system at Illgraben in Canton Valais. The system aims to detect ongoing events by monitoring specific dynamic process parameters. Geophones and radars are controlled by a logger, which initiates an alarm if certain thresholds for ground motion and water level are exceeded. This alarm automatically triggers acoustic and optic signals to warn the population in the catchment area. Additionally, authorities responsible for managing the hazard are informed directly and data of the event is stored in a database. Here the lead time is equal to the alarm time [1].

A local rock avalanche system was installed at Preonzo in Canton Ticino which was able to provide sufficient warning time of an event in May 2012. Prediction of the release time was possible through monitoring the variable disposition [7]. Rock avalanches, although spontaneous events [24], have typically long warning times, as they start with visible cracks, move slowly and accelerate over time [17]. In Preonzo extensometers and a theodolite were installed to directly measure pre-failure movements of the rock-mass at regular intervals. An alarm was sent to the authorities and geologists whenever a specific velocity threshold was exceeded. The decision about further actions was made by the experts after analysing the input data. The acceleration of the rock-mass was evaluated in simple models to predict critical failure. Final evacuation decisions were made based on these models and information drawn from indirect rain data. The lead time incorporated the warning time.

The national avalanche warning system operated by SLF issues information about the avalanche danger level for specific alpine regions and the Jura daily at 5pm as forecast for the following day during the winter. Avalanche forecasters use measurements of snow height, amount of fresh snow, air and snow temperature, solar radiation, wind direction and wind speed. This data inputs are crucial for judging the snowpack stability and the release of avalanches, because they affect the variable disposition. The data are collected from 180 automatic measuring stations and observers in the field. In addition, experts consult meteorological forecasts and complex snowpack models for generating two public and daily avalanche bulletins. The lead time incorporates the warning time [25].

4 System classification and application

We propose a generic classification that takes into account the monitoring possibilities and distinguishes between three system types i) threshold systems, ii) expert systems and iii) model-based expert systems. The classification has some similarities to the one given by Bell [2], but is more refined and does not incorporate monitoring systems. Expert and alarm systems are further differentiated according to certain system characteristics. The application of the classification on 52 systems identified in Switzerland revealed that each system class incorporates similar system characteristics (Table 1).

Table 1. Classification of the 52 systems identified in Switzerland. Individual system characteristics which derivate from the typical characteristic for a certain system class are illustrated in grey font.

Type / Characteristics	Threshold (34)	Expert (14)	Model-based expert (4)
system lead time	alarm (34)	warning/ alarm (13) alarm (1)	warning/alarm (4)
geographical coverage	national (2) regional (1) local (31)	national (1) local (13)	national (3) regional (1)
geographical resolution	local (34)	local (14)	regional (4)
type of monitoring	direct (33)	direct (14) indirect (7)	indirect (4)
first decision instance	threshold (33)	threshold (14)	threshold (1) no (3)
final decision instance	threshold (33)	expert (14)	experts (4)
model-based decision	no (33) complex models (1)	simple model (14)	complex models (4)
automated actions	yes (34)	no (14)	no (4)
warning levels	one (21) multiple (13)	one (6) multiple (8)	multiple (4)
information receiver	endangered object (33) public (1) authorities (31) system operator (33)	endangered object (14) public (6)	interest groups (4) public (4) authorities (4)

Threshold systems are systems with small lead times on the order of minutes or seconds, installed for spontaneous natural hazard processes such as debris

flows, snow avalanches, rock/ block and ice falls, GLOFs and flash flood. The geographical coverage and resolution is local. Dynamic process parameters are directly monitored in the field. A threshold determines if an alarm is issued e.g. in the form of colored or flashing lights or acoustic signals. Alarm signals are automatically provided in one or multiple states of alarm to the endangered objects, authorities and system operators.

Expert systems are installed for processes with longer lead times such as rock avalanches and permanent landslides and have lead times on the order of minutes to years. The systems installed are site specific and thus the geographical coverage and resolution of the systems is local. The parameters monitored in the variable disposition are direct changes similar to the real process parameters. The alarm is not issued automatically or with direct signals. Experts decide on necessary action plans by evaluating the monitored data and by using simple models. In addition, data is collected from parameters that are indirectly related to the process such as rain data. In most cases, systems include different alarm levels and the data is made available only to those responsible for managing natural hazards. For systems in Canton Ticino all data are collected on a server and provided to the general public on a website.

Model-based expert systems aim to make spontaneous hazard processes predictable. The alarm time is complemented with a warning time and hence a lead time in the range of hours and days is reached. Immense sensor networks offer national or regional system coverage. The input data are mainly gained through indirect monitoring parameters influencing the variable disposition and trigger data. They are further processed in complex models and resulting in final products (e.g. bulletins) published on a regular base for general public and affected institutions.

Each system class can be described though a typical system design which is influenced by the identified characteristics. The design describes the monitoring choice, the decision instances and their tresholds, expert and model dependencies, data management and alternatives for implementing measures of the integrated risk managment strategy (Figure 3).

Five out of 52 systems do not explicitly fit into one system class. The national SED earthquake detection system is a typical example of such a system. By counting the number of instances in which the system complies with the characteristics of any class, the appropriate class can be identified. Thus, the SED system is classified as a threshold system, which is based on complex models covering a national area. Another edge case system in the threshold system

class is the CERTAS flood reporting system, which consists of a network of 38 local measuring stations that directly issue alarms to customers, if certain

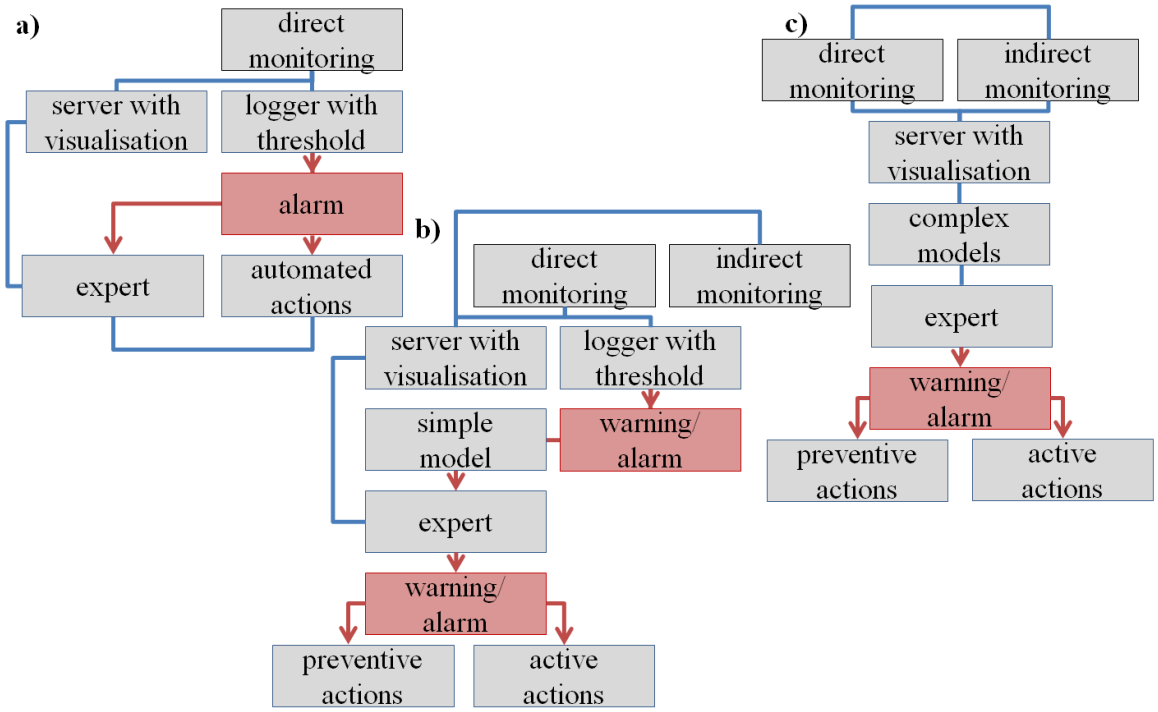

Figure 3. System designs: a) threshold, b) expert and c) model-based expert system.

water level thresholds are exceeded. A similar threshold approach is employed in the BLS rockfall system with a regional coverage. A rockfall system operated by the Swiss Federal Railway Company has a short lead time similar to threshold systems, but complies in most characteristics with an expert system, because an expert is consulted and makes the final decision within seconds. The reason is that false alarms would cause high financial losses to the company. The FireLess system was recently installed by WSL, on a regional scale in Canton Ticino and Canton Valais, to predict forest fires and is classified as model-based expert system, even though it is issuing an alarm to the experts if a threshold is exceeded.

5 Identification of reliability criteria

The overall reliability of a warning system is strongly related to the assigned system characteristics per class and the resulting design (Figure 4).

The reliability of threshold systems mainly depends on the threshold and the implementation of automated actions. The human influence and the technical complexity are low. Uncertain parameters are technical and data-related factors. The following reliability criteria can be derived for this class:

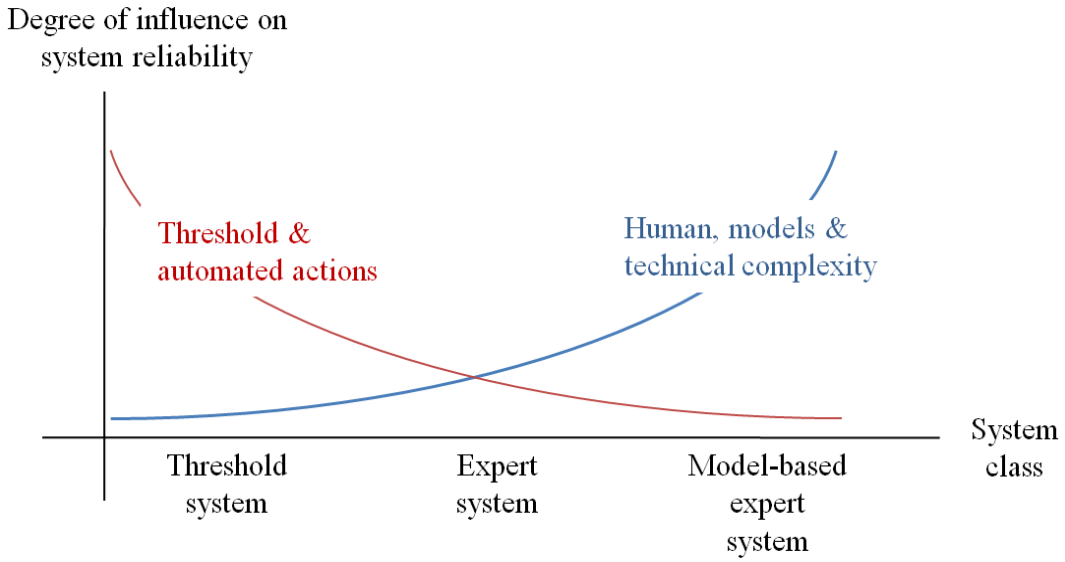

Figure 4. System types and the influence of reliability relevant characteristics on the system reliability.

- The monitoring of the correct dynamic process parameters is ensured through the right choice of sensor type, redundancies and their ideal position and fixation.
- A suitable threshold value should be chosen. A high threshold leads to missed events and a low leads to false alarms.
- The logger is functional. Power supply at remote sites is required, technical failure is reduced to a minimum and communicated automatically.
- The alarm transmission from the detection area to the endangered objectives is reliable, ideally redundant and controlled.
- The functionality of the alarm facilities/ equipment is ensured and controlled.
- The technical complexity and the number of interfaces between the system components are kept to a minimum.

The reliability of expert systems is mainly influenced by the predefined threshold and the decisions of the experts. Automated actions are not directly implemented and the technical complexity is moderate. Uncertain parameters are technical, human, data-related and organisational factors. The detection of an event depends on the same reliability criteria as for the threshold system, but is also dependent on the following criteria:

- The data is transmitted to a server and made available to the experts.
- The experts experience is high and their risk attitude neither too high nor too low.
- The quality of models used is high and the indirect data are interpreted correctly.
- Preventive and active actions are implemented in a timely manner.
- The endangered objects are reached in a timely manner.

The reliability of model-based expert systems is independent from thresholds and the implementation of automated actions, but incorporates high human influences, complex models and a high technical complexity. Uncertain parameters are technical, human, data-related, organisational- and standardisation-related factors. In addition to the factors illustrated above further criteria are relevant for the system reliability:

- Networks of several hundred sensors require a complex data management e.g. redundant servers and clear work and decision processes.
- The data format and measuring stations should be standardised, to minor the influence of measuring failures, because the same failures occur in each measurement and hence the data stay valid and comparable.

6 Conclusion

Warning systems for natural hazards can be classified as i) threshold systems, ii) expert systems and iii) model-based expert systems. The application of the classification has revealed that each system class can be described by typical system characteristics resulting in a typical system design. Systems that do not explicitly fit into one system class can be classified to the class with the highest compliance and variations can be described within the defined characteristics.

The classification does not limit the space for interpretation and further enhancement of warning systems, but allows a structured determination of reliability relevant criteria for each class. General influences on the overall system reliability could be identified for each class, before reliability criteria could be derived from the typical system characteristics. The characteristics of the monitored hazard process determines the system lead time and drastically influences the system characteristics, design and hence the system reliability criteria. The classification and the derived reliability criteria are essential inputs to develop a method for quantifying the overall reliability of warning systems. In the next step each system class will be further analysed on a subsystem level to identify appropriate reliability methods.

7 Acknowledgements

This study is part of a research project, supported by the Swiss Federal Office for Civil Protection (FOCP). The authors want to thank the FOCP for financial support and the members of the steering group for valuable comments. We also want to thank all system stakeholders such as geologists, authorities who are responsible for the management of natural hazard, system operators, manufacturer and railway companies for their valuable input and the time and energy they spend on field visits. Lorenz Meier (GEOTEST; SLF), Hansueli Gubler (ALPUG GmbH), Giorgio Valenti (Cantonal geologist Ticino), Christoph Graf (WSL), Maren Salz (SLF) and James Glover (SLF) are acknowledged for constructive discussions and relevant input to this study.

8 References

[1] Badoux, A.; Graf, C.; Rhyner, J.; Kuntner, R.; McArdell, B.W.: A debris-flow alarm system for the Alpine Illgraben catchment: design and performance. *Natural hazards* 49 (3), (2009), p. 517-539

[2] Bell, R.; Mayer, J.; Pohl, J.; Greiving, S.; Glade, T.: *Integrative Frühwarnsysteme für gravitative Massenbewegungen (ILEWS): Monitoring, Modellierung, Implemenierung*. Essen: Klartext Verlag, 2010

[3] Bründl, M.: *Risikokonzept für Naturgefahren - Leitfaden*. Bern: Nationale Plattform für Naturgefahren PLANAT, 2009

[4] Dikau, R.; Weichselgartner, J.: *Der unruhige Planet: Der Mensch und die Naturgewalten*. Darmstadt: Wissenschaftliche Buchgesellschaft, 2005

[5] Felgentreff, C.; Glade, T.: *Naturrisiken und Sozialkatastrophen*. Berlin: Springer Verlag, 2008

[6] Fuchs, C.: Warnen, alarmieren, informieren – eine Tour d'Horizon. *BEVÖLKERUNGSSCHUTZ*, 3 (2009), p. 7-9

[7] GEOPRAEVENT: *Interferometrische Radarmessungen in Preonzo/TI.* URL http://www.geopraevent.ch/?page_id=370. last retrieved: 07.08.2012

[8] Glantz, M.: *Unsable Science 8: Early warning systems: Do's and Don'ts.* Report of Workshop held 20-23 October 2003 in Shanghai, China. Boulder: National Center for Atmospheric Research, 2004

[9] Iverson, R.M.; Vallance, J.W.: New views of granular mass flows. *Geology* 29(2) (2001), p.115-118

[10] Gubler, HU.: Personal communication, 25.11.2011. Davos: Alpug GmbH

[11] Hattenberger, D.; Wöllik, A.: Naturgefahren- Mess-und Frühwarnsysteme: Einzelne rechtliche Aspekte. *Baurechtliche Blätter: bbl* 11(3) (2008), p. 89-101

[12] Hilker, N.; Badoux, A.; Hegg, C.: The Swiss flood and landslide damage database 1972–2007. *Natural Hazards Earth System Science* 9 (2009), p. 913–925

[13] IRV Interkantonaler Rückversicherungsverband: *Durchschnittlicher Anteil der Ursachen an der Schadenhöhe im Zeitraum 2002 - 2011*. URL http://irv.ch/IRV/Services/Statistik/Elementar/Ursachen.aspx, last retrieved: 06.08.2012

[14] ISDR: *A terminology on disaster risk reduction.* URL http://www.unisdr.org/files/7817_UNISDRTerminologyEnglish.pdf. last retrieved: 06.08.2012

[15] Keefer, D.K.: Earthquake-induced landslides and their effects on alluvial fans. *Journal of Sedimentary Research 69* (1999), p. 84-104

[16] Keller, E.; Blodgett. R.: *Natural Hazards - Earth`s Processes as Hazards, Disasters, and Catastrophes*. New York: Pearson Education, Inc., 2008

[17] Keusen, HR.: Warn-und Überwachungssysteme (Frühwarndienste). In: Rageth, T. (ed.)*: Frühwarndienste-Stand der Kenntnisse und Anwe*ndungen. Glarus: FAN Forstliche Arbeitsgruppe Naturgefahren, 1998, p.1-34

[18] Kienholz, H.: Early Warning systems related to Mountain Hazards. In: Zschau J.; Küppers, A.(ed.) *Early Warning Systems for Natural Disaster Reduction*. Potsdam: Springer, 2003, p. 555-564

[19] Lang, P.; Munier, H. Böhm, T.; Deutscher Wetter Dienst (ed.): *Anleitung zur Nutzung von Konrad: Das Verfahren zur schnellen Erkennung und Verfolgung sommerlicher Unwetter mittels Wetterradar*. ULR http://www.meteo.life-rostam.de/KonRad-Benutzerhandbuch.pdf. last retrieved: 08.08.2012

[20] Lehnherr, A.: Personal communication, 08.12.201. Bern: BLS AG

[21] PLANAT Nationale Plattform Naturgefahren: *Wissen.*
URL http://www.planat.ch/de/wissen/. last retrieved: 02.08.2012

[22] Russi, T.; Ammann, W.; Brabec, B.; Lehning, M.; Meister R.: Avalanche Warning Switzerland 2000. In: Zschau J. ; Küppers, A.(ed.*): Early Warning Systems for Natural Disaster Reduction*. Potsdam: Springer, 2003, p. 569-577

[23] Spreafico, M.; Weingartner, R.: *Hydrologie der Schweiz - Ausgewählte Aspekte und Resultate*. Berichte des BWG, Serie Wasser Nr. 7. Bern: Bundesamt für Wasser und Geologie BWG, 2005

[24] Varnes, D.J.: *Landslide Hazard Zonation: a review of principles and praxis*. Paris: Unesco, 1984

[25] WSL Institute for Snow and Avalanche Research SLF: *Avalanche Warning.* URL www.slf.ch/forschung_entwicklung/lawinen/lawinenwarnung/index_EN. last retrieved:22.08.2012

[26] Zimmermann, M.; Mani, P.; Gamma, P.; Gsteiger, P.; Heiniger, O.; Hunziker, G.: *Murganggefahr und Klimaänderung: ein GIS-basierter Ansatz: Projektschlussbericht im Rahmen des Nationalen Forschungsprogrammes" Klimaänderungen und Naturkatastrophen*. Schlussbericht NFP 31. Zürich: vdf Hochschulverlag AG an der ETH, 1999

Random Field Methods in Robustness Analysis

Veit Bayer
dynardo – dynamic software and engineering GmbH, Weimar

Abstract: Any structure is subjected to natural random scatter of its properties, caused by, e.g., production tolerance, material scatter or random loads. Scattering properties may have significant influence on the performance or safety of the structure. Such random properties which are distributed over the structure can be simulated and/or analysed with help of random field theory. By this methodology, it is possible to analyse the cause of scatter, find critical locations on the structure and quantify the influence on the performance. In consequence, quality requirements can be formulated and robustness can be enhanced. Several methods in this context for data reduction, decomposition, simulation and analysis are explained and demonstrated by real application examples.

1 Introduction

In industrial product development, along with the increasing application of CAE methods, there is a trend also of increasing use of optimization methods. In structural engineering, sophisticated analysis tools and high performance materials lead to weight savings and reduction of cross sections. However, deterministic computer simulations assume ideal conditions, while in reality any structure is subjected to natural random scatter of its properties, i.e. scatter of material properties, production tolerances, random loads or operation conditions. Optimized structures in particular tend to react sensitive towards scattering properties or external influences, so the performance (or usability, e.g. vibration behaviour) or safety degrades, compared to the deterministic, idealized case.

Therefore it is paramount to perform a robustness or safety assessment taking stochastic properties into account. In the context of robustness or safety assessment, the probability that the structure takes over an inadmissible state defined by quality or legal requirements is calculated. Unlike safety analysis, robustness assessment regards events of relatively high probability of occurrence and is often substituted by the analysis of variances of the performance instead of probabilities (WILL [16], BUCHER [6]).

Random properties such as mentioned above are often distributed over the observed structure. They can be modelled and/or analysed with help of random field methods, as explained in the following section. Sources of spatial scatter which have to be regarded as random fields are, for example:

- Deviations from the designed geometry are measured by photogrammetric methods, i.e. laser or high resolution video – based scanners. Hence the production tolerance is given as measured geometry random field.

- CAE tools allow the simulation of a production process (e.g., casting or sheet metal forming) with random process parameters within a robustness assessment. The result is a sample set of finite element models with random properties.

Based on such data, the random field computations are sketched as follows (BAYER [2]):

- Analysis of spatial scatter. This allows locating critical points with high scatter and, by correlation analyses, to find the cause of scatter.

- Simulation of random fields. A random field is modelled based on empirical data and/or model assumptions. On this basis a set of imperfect structures is generated and fed into the CAE solver process in order to obtain a meaningful robustness assessment.

In the following section, the basic theory and methodology for random field analysis and simulation will be explained. Application examples demonstrate the utilization of this methodology in section 3.

2 Random fields

2.1 Theoretical basics

We observe a continuous, arbitrarily shaped structure. A property of the structure, e.g. geometry, material, or external load, which spatial domain of definition is the structure itself, takes over a random value at any point of observation. In other words, at any point the property is a random variable. This is expressed mathematically by the random function $H(\mathbf{r})$, wherein $\mathbf{r} \in \Re^3$ is the position vector to a point on the structure. A set of *realizations* of the random field, obtained by measurement or simulation, forms the *ensemble*. Fig. 1 shows a schematic of a random field defined on a beam structure.

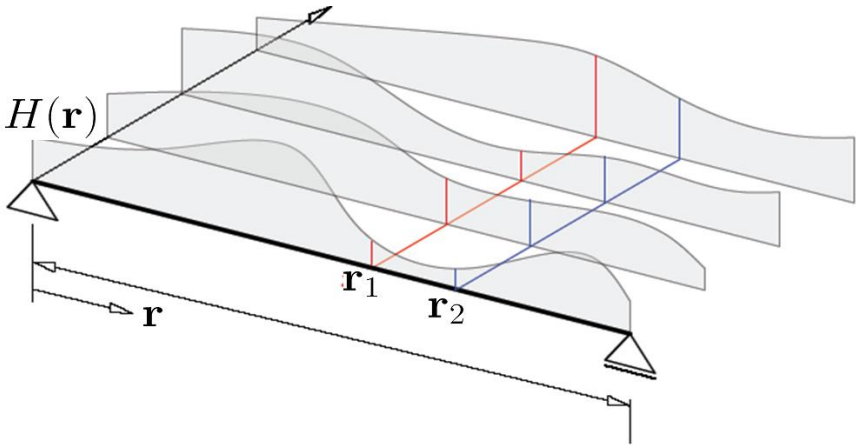

Figure 1: Schematic of realizations of a 1D random field.

A random variable may be defined by distribution type and statistical moments. It is commonly assumed that one random property has the same distribution type all over the structure; however the statistic moments may be different at any location. The random variables at different locations may be statistically dependent, expressed by Pearson's coefficient of correlation.

If it is further assumed that the distribution type is Gaussian, then mean values, standard deviations and correlation coefficients suffice to fully define random variables. The spatial distribution on the structure is defined by the mean function and correlation function (see VANMARCKE [15])

$$\mu_H(\mathbf{r}) = \mathrm{E}[H(\mathbf{r})] = \int_{-\infty}^{\infty} h f_H(\mathbf{r})\, dh \tag{1}$$

$$R_{HH}(\mathbf{r}_1, \mathbf{r}_2) = \mathrm{E}[H(\mathbf{r}_1)H(\mathbf{r}_2)] = \int_{-\infty}^{\infty}\int_{-\infty}^{\infty} h_1 h_2 f_H(\mathbf{r}_1, \mathbf{r}_2, h_1, h_2)\, dh_1 dh_2 \qquad (2)$$

The latter is not equivalent to Pearson's coefficient of correlation. This can be derived from the correlation function by subtracting the mean values at $\mathbf{r}_1$, $\mathbf{r}_2$ and dividing by the respective standard deviations.

Two special cases shall be mentioned here:

2.1.1 Homogeneous random field

A homogeneous random field is characterized by constant moments throughout the structure. It is comparable to a stationary random process. If this holds for the functions of mean values and standard deviations only,

$$\mu_H(\mathbf{r}) = const;\ \sigma_H(\mathbf{r}) = const;\ \forall \mathbf{r} \qquad (3)$$

and if also the correlation function is independent of the reference location (but on the difference vector between each two locations),

$$R_{HH}(\mathbf{r}, \mathbf{r} + \boldsymbol{\xi}) = R_{HH}(\boldsymbol{\xi}) \qquad (4)$$

then the random field is called *weak sense homogeneous*. Since a Gaussian distribution is fully defined by second moment characteristics, the above definitions will fulfil also strict homogeneity in the Gaussian case.

2.1.2 Isotropic random field

A random field is called weak sense homogeneous and *isotropic*, if the correlation function is independent also from the relative position of each pair of observed locations, but still depends on the absolute distance:

$$R_{HH}(\mathbf{r}, \mathbf{r} + \boldsymbol{\xi}) = R_{HH}(\|\boldsymbol{\xi}\|) \qquad (5)$$

For simulation of an artificial, homogeneous isotropic random field one defines a (one–dimensional) correlation coefficient function over the distance $\rho(\|\xi\|)$. This function must be positive definite. The ξ-value of the centre of gravity of the area beneath the function is a typical characteristic called *correlation length*.

2.2 Discretization

For any application in the context of computer aided engineering (CAE), the continuous functions which define the random field have to be discretized. Since the observed structure is given in discretized form by CAE methods (FEM, CFD, etc.), it is instrumental to choose the same mesh for random field discretization. Geometry random fields (manufacturing tolerances) are modelled as shifts of node coordinates, element properties (such as e.g. material, or residual strains), element mid points or integration points are chosen. However, if the random field is modelled based on measured data, usually the data have to be transformed into the model coordinate system and mapped onto a common reference mesh.

As result of discretization, one obtains a finite number *n* of random variables, pooled in the random vector $\mathbf{X} = \{X_i(\mathbf{r}_i)\}_{i=1,\dots,n}$. The mean value function becomes the mean vector $\boldsymbol{\mu}_\mathbf{X} = \{\mathrm{E}[X_i(\mathbf{r}_i)]\}_{i=1,\dots,n}$. Variances and correlations are given by the covariance matrix

$$\mathbf{C}_{XX} = \{\mathrm{E}[(X_i - \mu_{X_i})(X_j - \mu_{X_j})]\}_{i,j=1,\dots,n} \tag{6}$$

The covariance matrix is, unlike typical finite element matrices, fully occupied. Since each node or element of the structure is associated to a random variable, the dimension of the covariance matrix becomes too high to be treated on the computer in a feasible way, with respect to both memory and computing time for decomposition (see following section). In order to mitigate this, a mesh coarsening algorithm has been proposed by BAYER [1] which keeps the topology (relative refinement) of the original mesh. Data are mapped from the original mesh to the random field discretization by local averaging. For later post-processing on the original mesh, special interpolation techniques are adapted from MOST et al. [9]. Although this is always a loss of information, which is noted as a smoothing effect, it can be shown (as in BAYER [3]) that in most cases the characteristics of the random field are retained.

2.3 Spectral representation

As mentioned, the random variables which constitute a random field are usually correlated. An equivalent set of independent random variables (in the weak sense) has to be found for two purposes. For the simulation of artificial random fields, random number generators are able to handle independent var-

iables only. These have to be transformed to the physically meaningful, "real world" variables. If the random field data are obtained e.g. by a manufacturing process simulation, and the statistical relations between the input process parameters and the resulting random fields shall be analyzed, then the decomposition of the random field into independent components helps to isolate different effects and analyse correlations between the input and output side of the process.

The random field shall be written as a Fourier-type series expansion, introduced as Karhunen – Loève – series in PAPOULIS [13]:

$$\widehat{H}(\mathbf{r}) = \sum_{i=1}^{\infty} Y_i \, \varphi_i(\mathbf{r}) \tag{7}$$

The ortho-normal basic functions φ_i in eq. (7) are determined as the eigenfunctions of the correlation function, eq. (2).

We observe the *discrete, Gaussian, zero-mean* random field, i.e. the mean values may be subtracted before decomposition and if required, added to each realization later again. Then the covariance matrix, cf. eq. (6), contains the complete stochastic characterization of the random field. It can be shown, that the basic functions in this case are the eigenvectors of the covariance matrix. The eigenvalue analysis reads

$$\mathbf{\Phi}^T \mathbf{C}_{XX} \mathbf{\Phi} = \mathrm{diag}\{\lambda_i\} \tag{8}$$

In eq. (8), $\mathbf{\Phi}$ is the matrix of eigenvectors stored in columns. The coefficients Y_i in eq. (7) are also Gaussian distributed, zero-mean, and independent (GHANEM et al. [8]. The standard deviations of the Y_i are computed as the square roots of the eigenvalues of $\mathbf{C}_{XX}$. Hence by

$$Y_i := \mathcal{N}(0\,;\sqrt{\lambda_i}\,;\rho_{i\neq j}=0) \tag{9}$$

one defines a new set of random variables and obtains a series expansion of the original random field $\mathbf{X}$ consisting of deterministic "shape functions", i.e the eigenvectors, and random, independent amplitudes Y_i.

$$\widehat{\mathbf{X}} = \mathbf{\Phi}\mathbf{Y} \tag{10}$$

If statistical data distributed on a structure are given (either by CAE simulation or measurement), then with help of the inverse transformation of eq. (10) it is possible to compute the corresponding sample of amplitudes.

$$\widehat{\mathbf{Y}} = \mathbf{\Phi}^T \mathbf{X} \tag{11}$$

The series expansion approach offers another opportunity for data reduction. The eigenvalues are usually stored by the solver in a sorted manner, so it is easy to choose those variables Y_i which contribute most to the total scatter of the random field. As experience from practical application, a drastic reduction of the number of random variables is possible that way. This is always a numerical advantage in simulation, but also helps to isolate the most relevant effects in data analysis.

The truncation of the series expansion is nevertheless an approximation. A measure of the approximation quality was introduced by BRENNER [5] as the so-called *variability fraction*, defined as the ratio of the sum of variances of the random variables considered to the total variance of the discrete random field. When the dimensions of the original data grid and the random field discretization differ, then both numerator and denominator of this ratio must be normalized to the respective number of points (BAYER et al. [4]).

$$\begin{aligned} \frac{\sum_{i=1}^{N_\lambda} \lambda_i}{\operatorname{trace}(\mathbf{C}_{XX})} &\equiv \frac{\sum_{i=1}^{N_\lambda} \lambda_i \Big/ \dim(\mathbf{C}_{XX})}{\operatorname{trace}(\mathbf{C}_{XX}) \Big/ \dim(\mathbf{C}_{XX})} \\ \frac{\sum_{i=1}^{N_\lambda} \lambda_i}{\sum_{j=1}^{N_{\text{supports}}} \sigma_j^2} &\Rightarrow \frac{\sum_{i=1}^{N_\lambda} \lambda_i \Big/ \dim(\mathbf{C}_{XX})}{\sum_{j=1}^{N_{\text{supports}}} \sigma_j^2 \Big/ N_{\text{supports}}} \end{aligned} \tag{12}$$

3 Applications

3.1 Simulation of geometric tolerances

In the first application example, NUNES et al. [11] show the simulation of geometric tolerances of a car chassis part. The task was to examine the influence of the random geometry on the dynamic behaviour and therefore on the tendency of noise emission during brake.

From a 3D-scan we obtained the geometry of one real specimen as a triangularized geometry in STL-format. The deviations of this measured geometry to the finite element model were computed. The exact measure would be the distance normal to the surface through each point (node) of the reference model. Since the number of measured points is far larger than the number of nodes, the direct distance to the nearest neighbour, which is found by the approximate nearest neighbour (ANN) algorithm, is used instead.

One measurement was taken only; hence a statistical survey of an ensemble of data sets at each node is not possible. Assuming ergodicity (VANMARCKE [15]), the statistics pooling the values at all nodes into one sample were computed. With a homogeneous variance obtained such and an assumed correlation function (see sections 2.1.1 ff.), an artificial, but realistic random field for geometric deviations was modelled.

Within a robustness analysis, Monte Carlo methods were applied to generate samples of the random field parameters, create imperfect parts with random geometry and put them into the CAE model of the entire chassis and brake system. For each sampled structure, the brake squeal tendency was computed with help of complex modal analysis.

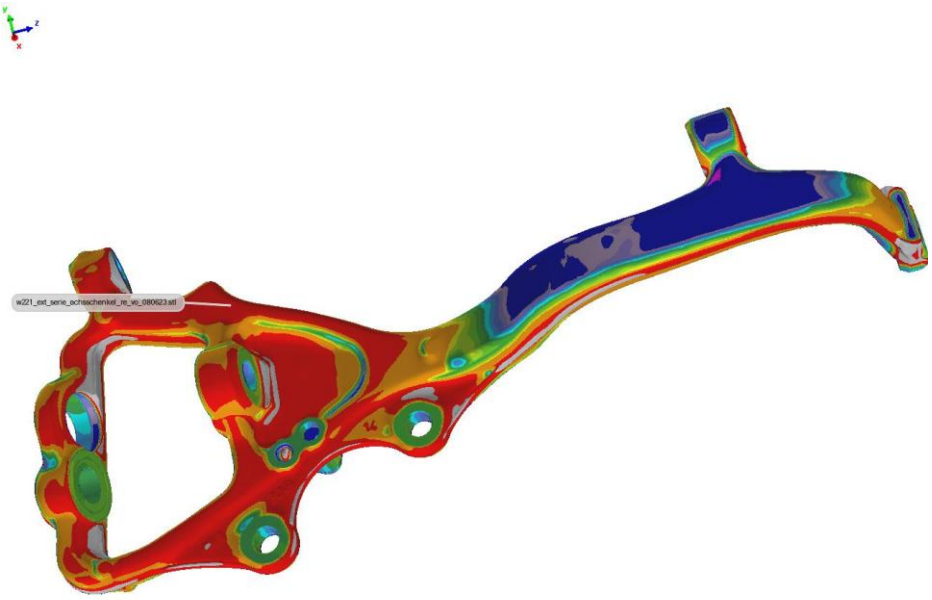

Figure 2: Measured geometry of car chassis part (NUNES et al. [11]).

By robustness analysis it was found that for the measure of brake squeal tendency, the mean value was above the deterministic value of the design geometry at a frequency near 2 kHz, with a coefficient of variation of 0.32. Near 6 kHz there was a smaller, yet significant coefficient of variation and difference of mean to deterministic value. Thus it could be shown that geometric manufacturing tolerances of the part seen in figure 2 have a significant influence on noise emission of the brake system.

3.2 Crash analysis

The analysis of spatially scattering data with help of the random field methodology shall be demonstrated by an example from crash analysis (BAYER et al. [4]). During the development of a load bearing part of a car body, figure 3, a buckling phenomenon was observed experimentally, which could not be seen by deterministic computational analysis. In the scope of a stochastic robustness analysis, parameters of the crash load case were introduced as random variables, as well as properties of this and other parts in the load path, such as sheet thickness and material strength. The stochastic structural properties were obtained from a previous forming simulation with random process parameters. Within the crash robustness analysis, 150 structures with random structural properties and load parameters were sampled and calculated.

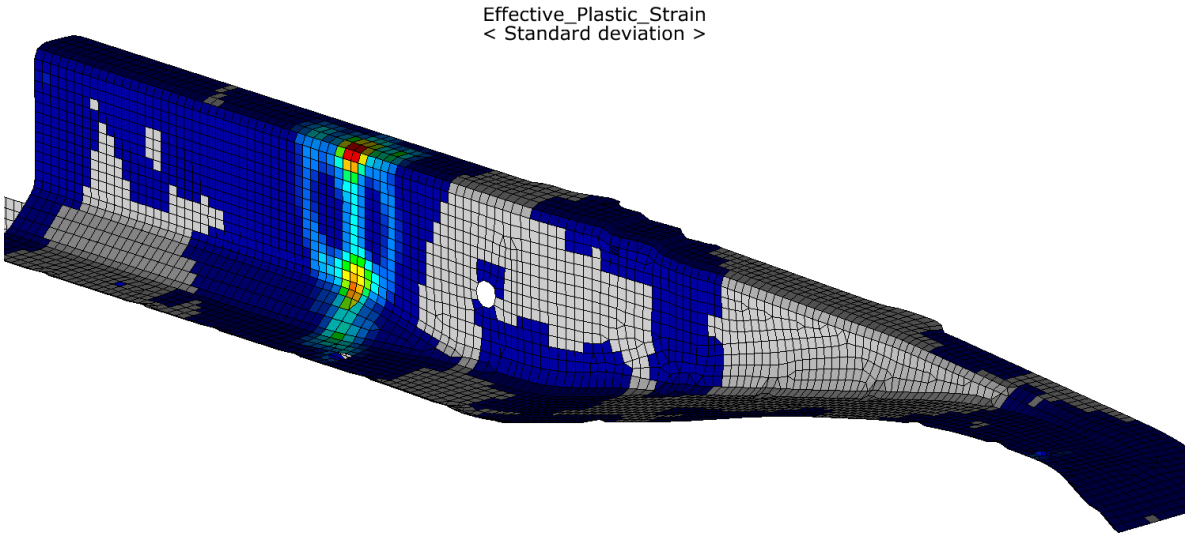

Figure 3: Standard deviations of plastic strain of a load bearing car part after crash robustness analysis (BAYER et al. [4]).

The scatter of plastic strains which is plotted in figure 3 corresponds to the observed buckling deformation. As it was explained in section 2.3, the spatial scatter of the plastic strain was decomposed into “scatter shapes”; the respective samples of random amplitudes were computed following eq. (11). The random amplitudes were statistically surveyed and related to the input random variables.

Figure 4 shows the first three scatter shapes and their contributions to the total scatter of plastic strain given in percent, cf. eq. (12). It is seen that with three random amplitudes of the Karhunen – Loève – expansion only, in contrast to ca. 5000 original variables (one for each finite element), it is possible to represent 98 % of total scatter. This demonstrates the efficiency of the random field parametric proposed here.

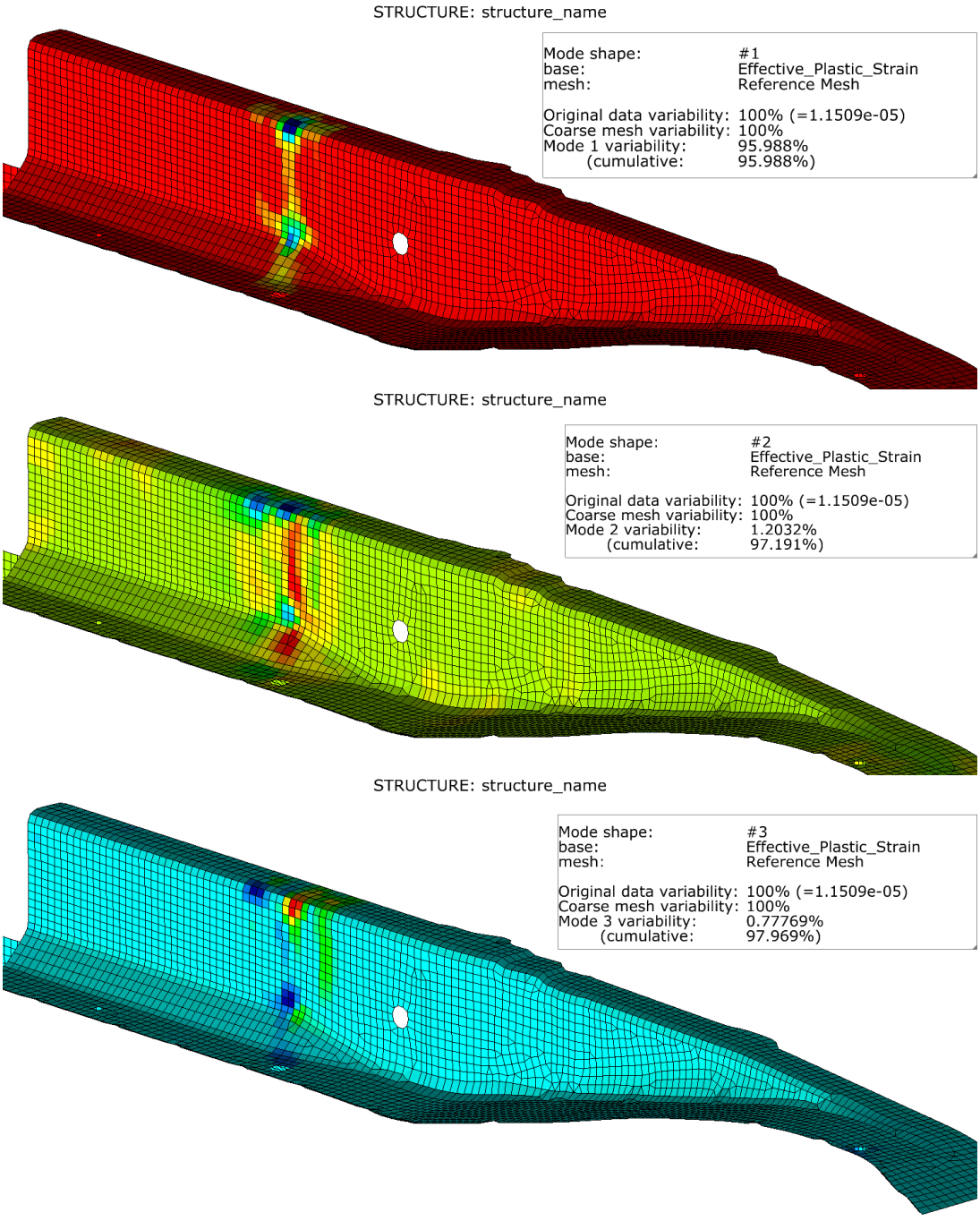

Figure 4: First three scatter shapes of plastic strain.

The algorithm *Metamodel of Optimal Prognosis* (MoP) of optiSLang (MOST et al. [10]) was applied to relate the samples of the first three amplitudes to the random parameters of the crash analysis. This algorithm uses the samples of input – output sets as supports and fits a powerful interpolation model. As

further result, one obtains the prognosis quality of the entire metamodel (Coefficient of Prognosis – CoP) and the relative influences of the scatter of the random inputs on the scatter of the amplitudes. These values are shown in figure 5 as bar chart. The most relevant random input parameters which cause the scattering plastic strains can be identified. Hence requirements on the design of the part and quality assurance could be formulated and the problem was mitigated.

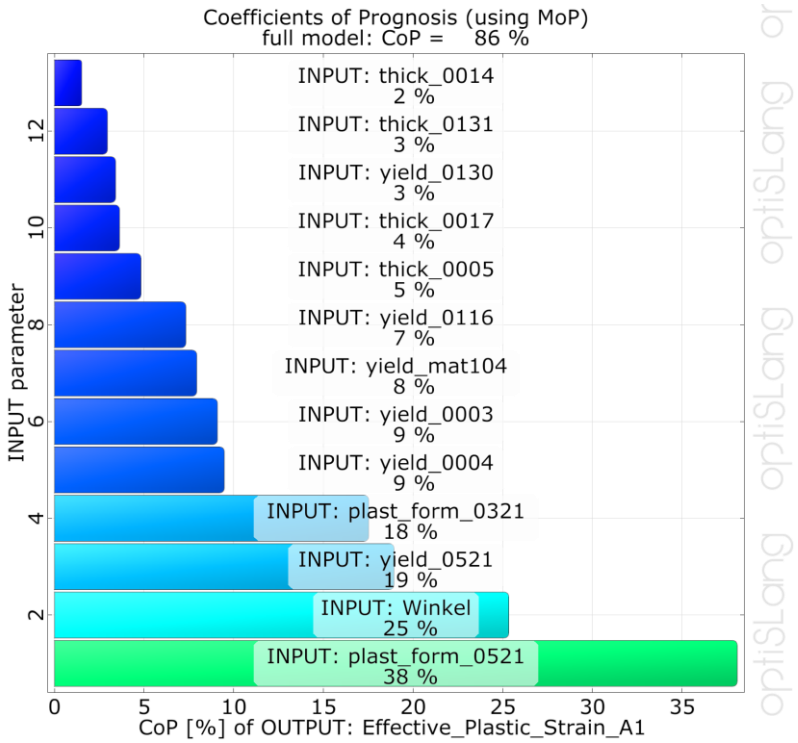

Figure 5: CoP values of the optimal metamodel for the first amplitude of plastic strains.

4 Final remarks

In the present article it is demonstrated, how scattered data which are spatially distributed on structures (such as material properties, geometric tolerances etc.) can be analysed by random field methodology. Such data are obtained by measurements of specimen or by stochastic robustness analyses of CAE processes, e.g. manufacturing process simulations.

The data can be decomposed into “scatter shapes” of a random field. Already the visualization of the most important (by means of contribution to the total variation) scatter shapes helps to understand “mechanisms” of spatial scatter.

By further statistical analysis of the respective amplitudes and their relation to the random inputs, expressed as correlations, coefficients of determination of a regression model or coefficients of prognosis of a MoP, the cause of scatter can be identified.

It is also possible to model and sample random fields on the basis of empirical data and/or model assumptions. With these artificial random fields, structural parts with random properties are generated and fed into a CAE analysis. In that way it is possible to study the sensitivity of a structure towards spatially distributed random properties or loads.

Dynardo offers the software SoS (Statistics on Structure) for the analysis of spatially scattering data. Statistical characteristics of the data can be plotted on the structure, as well as the scatter shapes of the decomposed random field. Samples of the respective random amplitudes can be exported as optiSLang result file for further statistical analyses, in particular the relations to input parameters, as it was demonstrated in the example of section 3.2.

5 Literature

[1] Bayer, V.; Roos, D.: Efficient Modelling and Simulation of Random Fields. *6th International Probabilistic Workshop*, Darmstadt 2008.

[2] Bayer, V.: Random Fields in Statistics on Structure. *Weimar Optimization and Stochastic Days 7.0*, Weimar 2010.

[3] Bayer, V.: Random Fields – Applications in Robustness Analysis. *Weimar Optimization and Stochastic Days 8.0*, Weimar 2011.

[4] Bayer, V.; Will, J.: Zufallsfelder in der Robustheits- und Zuverlässigkeitsbeurteilung von Bauteilen. *SIMVEC 2010 – Berechnung und Simulation im Fahrzeugbau*. VDI, Baden-Baden 2010.

[5] Brenner, C.E.: *Ein Beitrag zur Zuverlässigkeitsanalyse von Strukturen unter Berücksichtigung von Systemuntersuchungen mit Hilfe der Methode der Stochastischen Finite Elemente*. Dissertation, Leopold Franzens Universität Innsbruck 1995

[6] Bucher, C.: Basic concepts for robustness evaluation using stochastic analysis. *EUROMECH Colloq. Efficient Methods of Robust Design and Optimization*, London 2007

[7] Bucher, C.: *Computational Analysis of Randomness in Structural Mechanics*. Taylor & Francis, London 2009

[8] Ghanem, R.; Spanos, P.D.: *Stochastic Finite Elements – a Spectral Approach*. Springer, New York, Berlin 1991

[9] Most, T.; Bucher, C.: A moving least square weighting function for the elementfree galerkin method which almost fulfills essential boundary conditions. *Structural Engineering and Mechanics* 21, 2005

[10] Most, T.; Will, J.: Metamodel of optimized prognosis (MoP) - an automatic approach for user friendly parameter optimization. *Weimar Optimization and Stochastic Days 6.0*, Weimar, 2009

[11] Nunes, R.; Will, J; Bayer, V.; Chittepu, K.: Robustness Evaluation of brake systems concerned to squeal noise problem. Weimar *Optimization and Stochastic Days 6.0*, Weimar 2009.

[12] Dynardo GmbH: *optiSLang – the Optimizing Structural Language*, User's Manual Version 3.1. Weimar 2009

[13] Papoulis, A.: *Probability, Random Variables, and Stochastic Processes*. McGraw–Hill, New York 1991

[14] Dynardo GmbH: *SoS – Statistics on Structure*, User's Manual Version 2.3.5., Weimar 2011

[15] Vanmarcke, E.: *Random Fields: Analysis and Synthesis*. MIT Press, Cambridge, USA, 1983

[16] Will, J.: State of the art - robustness in CAE-based virtual prototyping processes of automotive applications. Weimar *Optimization and Stochastic Days 4.0*, Weimar 2007

Probabilistic Assessment of Concrete Creep Models under Repeated Loading Considering Measurement Uncertainty

Hem Bahadur Motra[a], Andrea Dimmig-Osburg[b] and Joerg Hildebrand[c]
[a]Graduiertenkolleg 1462, Bauhaus-Universität, Weimar Germany
[b]Department of Polymer Binder and Building Materials, Bauhaus-Universität Weimar, Germany
[c]Department of Simulation and Experiment, Bauhaus-Universität, Weimar, Germany

Abstract: The aim of this paper is to present the analysis of the influence of some input variables on the creep deformation in concrete for various models, namely BP model, Whaley and Neville model, modified MC90 for cyclic loading and modified Hyperbolic function for cyclic loading. Creep causes increased deflection in concrete structures and changes the stress distribution with in elements. The benefits of an accurate prediction model of creep yields a safer design: a structure with minimum cracking, extended life and durability. The error in determining the input variables and model itself can produce significant changes in creep prediction values. The variability influence of input random variables on the cyclic creep was studied by means of the stochastic uncertainty and sensitivity analysis method. All input parameters were considered to be random variables. The Latin Hypercube Sampling (LHS) numerical simulation method (Monte Carlo type method) was used. It has been found by the stochastic sensitivity analysis that the cyclic creep deformation variability is most sensitive to the Elastic modulus of concrete, compressive strength, mean stress, cyclic stress amplitude, number of cycles, in that order. Further, it is observed that the uncertainties of the creep prediction for all models are compared and reveal significant differences. Due to the consideration of three types of uncertainty which are included in uncertainty quantification: (i) natural variability in loading materials properties; (ii) data uncertainty due to measurement errors; and (iii) modelling

uncertainty and errors during cyclic creep analysis, a measure for the total variation of the model response is achieved. The study finds that the BP, modified Hyperbolic and modified MC90 are the best performing models for cyclic creep prediction - in that order.

1. Introduction

It is a well-known fact that the repeated loading of concrete causes irreversible deformations GAEDE [8] and KERN *et al.* [13] called cyclic creep. The experimental knowledge of this phenomenon is still rather limited but yet quite sufficient for numerical prediction. When the principle of superposition is used to estimate cyclic creep, the creep under cyclic loading of many repetitions is significantly under-estimated. The reason behind this problem is that, the cyclic creep is a non-linear phenomenon and principle of superposition is no longer valid BAŽANT [1] and GVOZDEV [9]. The micro pre-stress solidification theory, mechanical deformation theory, the viscous flow theory, the plastic flow theory, the seepage of gel theory and the micro cracking theory can be explained by the unidirectional non-linear creep under dynamic loading, which is proposed by BAWEJA *et al*. [4], WHALEY *et al.* [24] and SUTER *et al.* [19]. This study can be of importance for structures such as bridges carrying high traffic loads, structures carrying heavy vibrating machinery, ocean oil platform and other such complex structures.

Creep and shrinkage are the most uncertain mechanical properties of concrete. The stochastic aspects of these physical phenomena should therefore taken into account in structural analysis and design. Structural responses have thus far been treated as deterministic values in this study, although it was acknowledged that the prediction models are marked with a certain degree of statistical variation. Material and environmental parameters were also taken into account with their expected mean value, but in reality they are also subjected to statistical variation and prediction errors. Moreover, civil engineering constructions are naturally subjected to variability; from many origins: their dimensions, their construction processes, and their exposure to several loadings. Among these variables, which influence the behaviour of a structure and; thus, its lifespan, some introduce a variability on the material characteristics, evolving with time and are not necessarily homogeneous in the whole structure, whereas some others create a variability on the loading itself, which the structure is subjected to.

For all these aforementioned reasons, modelling the input parameter in a probabilistic context makes sense SUDRET [18]. The uncertainty that affects the input parameter may be of various kinds. They are usually classified as follows:

- *Aleatoric uncertainty*: is an inherent variation associated with the physical or natural variability in the phenomenon under consideration. As an examples, the number-of-cycles-to-failure of a samples specimen subjected to fatigue loading shows aleatoric uncertainty, since the very life time of the specimens of the same materials subjected to the same experimental conditions varies one to the other SUDRET [18].

- *Epistemic uncertainty*: is an uncertainty that is due to a lack of knowledge of quantities or processes of the system and is also referred to as subjective uncertainty, reducible uncertainty, and model from uncertainty. As an example, the lack of experimental data to characterize new materials and processes, poor understanding of coupled physics phenomena. Further, the compressive strength of concrete of a given shows scattering.

For the quantification of measurement uncertainties (as defined in the ISO/IEC Guide 98-3 (2008a)) [11], namely the uncertainty based on a statistical analysis of observations and the uncertainty derived from a process equation physically describing the measurement process. Both types of measurement uncertainties are utilized for the derivation of a posterior measurement uncertainty by Bayesian updating. This facilitates the quantification of a measurement uncertainty using all available data of the measurement process. The measurement uncertainty models derived are analysed through a sensitivity study and are discussed in detail resulting in an identification of the most relevant sources of measurement uncertainties THOENS [21].

Sensitivity Analysis (SA) techniques will perform better for specific type of models. Sampling based methods are examined to scatter plots given by HELTON [10]. One method of importance in the measurement of models by considering the uncorrelated and correlated parameters is proposed by XU *et al*. [23]. The distinction between uncorrelated and correlated contribution of uncertainty for an individual variable is very important and output response and the input variables is approximately linear in this method. Method XU *et al*. [23] is used in this present work.

2. Cyclic creep models

Several experimental and mathematical models have been developed for estimating cyclic creep strain. The most widely used mathematical models are the BP [2] models, NEVIELLY [24] model. Modified MC90/EC2 [5] and modified Hyperbolic function [17], experimental cyclic creep models: GAEDE [8], KERN *et al*. [13], NEVILLE et al. [24], SUTER *et al*. [19]. This study also includes these four mathematical models.

Based on the test data, Whaley and Neville models have shown that the cyclic creep strain can be expressed as the sum of the two strain component, a mean strain component and a cyclic strain component. We consider uniaxial stress described as:

$$\sigma = \sigma_0 + \frac{1}{2}\Delta \sin(2\pi\omega t) \tag{1}$$

Where $\sigma =$ mean stress; $\frac{1}{2}\Delta =$ cyclic stress amplitude; and $\omega =$ circular frequency. The mean strain component is the creep strain produced by the static mean stress $(\sigma_m)=(\sigma_{max} - \sigma_{min})/2$. The additional cyclic creep component was found to dependent on both mean stress (σ_m) and the stress range $(\Delta)= (\sigma_{max} - \sigma_{min})$. They proposed the following predictive equation for the total cyclic creep strain:

$$\varepsilon(t - t_0) = 129\sigma_m(1 + 3.87\Delta)t^{\frac{1}{3}} * 10^{-6} \tag{2}$$

$$\Phi\ t - t_0\ = \frac{1}{\sigma}\left[\varepsilon_{el}\ t_0\ + \varepsilon\ t - t_0\ \right] = \frac{1}{E_c\ t_0} + \frac{\varepsilon\ t - t_0}{\sigma} \tag{3}$$

Where $\varepsilon\ (t - t_0)$ is the cyclic creep strain, σ_m is the mean stress expressed as a fraction of the compressive strength; and Δ is the stress-range expressed as a fraction of the compressive strength and $\Phi\ (t - t_0)$ is the creep function.

The above-noted static and dynamic components of dynamic creep are a function of time. It can be expressed as a function of a number of cycles also.

$$\varepsilon(t - t_0) = 129\sigma_0 t^{\frac{1}{3}} + 17.8\sigma_0 \Delta N^{\frac{1}{3}} \tag{4}$$

BP model takes into consideration both shrinkage strain and mechanical strain. According to the BP model, cyclic creep function $(t - t_0)= \varepsilon/\sigma_{mean}$, where ε is the strain mean level of cycle, is as follows:

$$\phi(t-t_0)=\left[\frac{1}{E}+C_{oc}(t-t_{oc})+C_d(t-t_0-t_d)g\sigma-C_p(t-t_o-t_d)\right]f\sigma \tag{5}$$

Where,

$$C_{oc}(t-t_0)=\frac{\varphi_1}{E_0}(t_0^{-m}+\alpha)(1+k_\omega\varphi_\sigma\sigma_{pp}^2\omega^n(t-t_0)^n \tag{6}$$

and this equation modified:

$$\phi(t,t_0,\sigma)=q_1+F(\sigma)\left[C_{0c}(t,t^{'}+C_d(t_{dc},t^{'},t_0)+C_p(t_{dc,}t^{'},t_0)\right] \tag{7}$$

In which t_{dc} can be calculated as:

$$t_{dc}=t^{'}+(t-t^{'})\left[1+10\omega^{\frac{1}{4}}\Delta^2F^3\sigma_{\max}\right] \tag{8}$$

Here ω is the frequency *(Hz)*, k_ω is the empirical constant and the function $F(\sigma_{max})$ is the nonlinearity over proportionality factors.

The long-time material model presented in the 1990 CEB Model Code MC90 [5] was chosen as the model. Static creep tests within the previously mentioned and the modified by TERJE *et al*. [20] cyclic creep function is defined as:

$$\phi(t-t_0)=\frac{1}{E_c(t_o)}+\frac{\varphi_c(t-t_0)}{E_c(28d)}+\frac{\varphi_{cc}(t-t_0)}{E_c(28d)} \tag{9}$$

In these expression $\varphi_c\ (t - t_o)$ is the static creep ratio and φ_{cc} is the cyclic creep ratio, *t'* the concrete age at loading and *t* the actual time. The cyclic creep ratio is defined as:

$$\varphi_{cc}(t-t_0)=\beta(t_0)\beta(f_{cm})\beta(S_m)\beta(\Delta)\varphi_{cc}\beta(N,\omega) \tag{10}$$

In this expression f_{cm} is the average compressive cylinder strength at 28 days; S_m the ratio between the mean stress and the concrete strength at the start of testing; Δ the relative stress amplitude; N is the number of load cycles and ω is the frequency $N=(t-t_0)\omega$

$$\beta(N,\omega)=N^n1=((t-t_0)86400\omega)^n-1, with, n=0.022 \tag{11}$$

The general expression for cyclic creep term is then written as:

$$\varphi_{cc}(t-t_0)=1.39\beta(t_0)\beta(f_{cm}81+10.5(S_m-0.4)^2)\Delta(N^n-1) \tag{12}$$

The hyperbolic function from German code 1045-1 or DAfStb booklet 525 DIN5 [6] modified by SCHWABACH [17] and give the final equation as:

$$\varphi(t-t_0)=\left(\frac{t-t_0}{a+(t-t_0)}\right)^b \varphi_\infty(t_0)=\left(\frac{t-t_0}{a+(t-t_0)}\right)^b * c * \frac{1}{d+t_0^e} \tag{13}$$

$$c=\varphi_{RH} * \beta(f_{cm})=\left(1+\frac{1-\frac{RH}{100}}{0.1*h_0^{\frac{1}{3}}}*\left(\frac{35}{f_{cm}}\right)^{0.7}\right)*\left(\frac{35}{f_{cm}}\right)^{0.2}*\left(\frac{16.8}{f_{cm}^{\frac{1}{2}}}\right) \tag{14}$$

3. Sources of uncertainty

The uncertainty modelled by stochastic variables can be divided in the following groups:

3.1 Physical uncertainty

Physical or inherent uncertainty is related to the natural randomness of a quantity, for example, the uncertainty in the material and environmental input parameter, or in the yield stress due to production variability.

3.2 Measurement uncertainty

Measurement uncertainty is the uncertainty caused by imperfect measurements of for example, a geometrical quantity. It is possible to characterize three types of uncertainty during the measurement of the cyclic creep measurements: (i) uncertainty related to measurements, (ii) uncertainty due to the positioning of the gauges and (iii) uncertainty due to the installation.

Uncertainty in the measurement can be given starting from the data obtained during the calibration. The calculation method of measurement uncertainty is discussed in Section 4.1.

3.3 Statistical Uncertainty

Statistical uncertainty is due to limited sample sizes of observed quantities. A stochastic quantity has one more property: a probability (density) distibution. When doing a finite set of measurements, one can construct a histogram from those measurements.

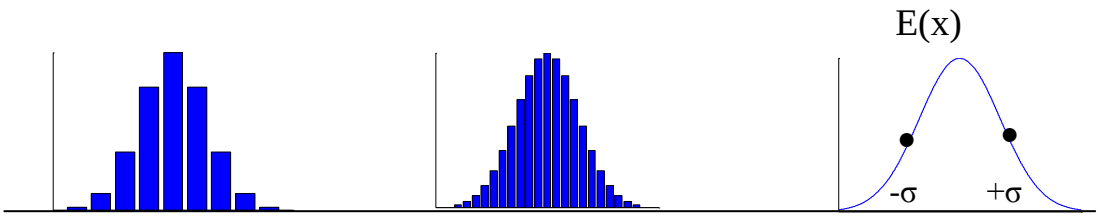

Figure 1. Few observation… more observation theoretical limit

It should be noted that when the number of measurements increases, the histogram will become more and more detailed, and in the limit become a smooth function. This theoretical limit is called the stochastic quantity probability density distribution function, distribution function for short. The Figure 1 shows the quantity of observation and limit of expectation is a histogram.

3.4 Model Uncertainty

Model uncertainty is the uncertainty related to imperfect knowledge or idealizations of the mathematical models used or uncertainty related to the choice of probability distribution types for the stochastic variables. Even when there occurs no measurement uncertainty (or when it is negligible), there may be some discrepancies between the predicted and observed values in most situations. This is called model error or uncertainty.

4. Uncertainty quantification in measurement

4.1 Measurement uncertainty using Bayes method

The experimental results may be assessed using strategies based on conditional probability concepts. These concepts are founded on Bayes' theorem, which is introduced by Thomas Bayes.

$$P(B_j|A) = \frac{P(A|B).P(B_j)}{\sum[P(A|B_i).P(B_i)]} \tag{15}$$

Where,

B_j is a state of the unknown quantity

B_i is the set of all states of the quantity, including B_j
A is the observed data (sample)
" | " is read as "given"

A necessary condition for Bayes' theorem is that the probability of observing any particular data outcome for a given state $P(A \mid B_j)$ must be known. This information is often available from laboratory testing, product literatures, or past experiences. Information about an input quantity X consists of a series of indications regarded as realizations of independent, identically distributed random variables characterized by a PDF, but with unknown mean and variances. Calculation proceeds in two steps:- first, a non-informative joint prior- (pre-data) PDF is assigned to the unknown mean and variances. This joint prior PDF is then updated, based on the information supplied by the series of indications, to yield a joint posterior (post-data) PDF for the unknown parameters, which is shown in Figure 2. The desired posterior PDF for the unknown mean is then calculated as a marginal PDF by integrating over the possible values of unknown variances. The updating is carried out by forming the product of a likelihood function and the prior PDF. The likelihood function is the product of functions, one function for each indication, and is identical in form, e. g., to a Gaussian PDF with expectation equal to the indication and variance formally equal to the unknown variance.

Figure 2 plots are shown for the prior and the posterior probability density for mean observed cyclic creep function.

The parameter of the cyclic creep models mean (μ) and standard deviation (σ) are considered as uncertain to account for the assignment uncertainty. A prior probability density function for this parameter is derived by calculating the individual probability densities, Equation 16 and measurement uncertainty model (M_c) THOENS [21].

$$f'(\mu,\sigma|M_c) = f(M_c|\phi(t-t_0)) \tag{16}$$

The likelihood estimate of the parameters is derived based upon observations of the measurement process and defined with Equation 17.

$$L(\mu,\sigma|\phi(t-t_0) = \prod_{j=1}^{n} f(\phi_0|\mu_j,\sigma_j) \tag{17}$$

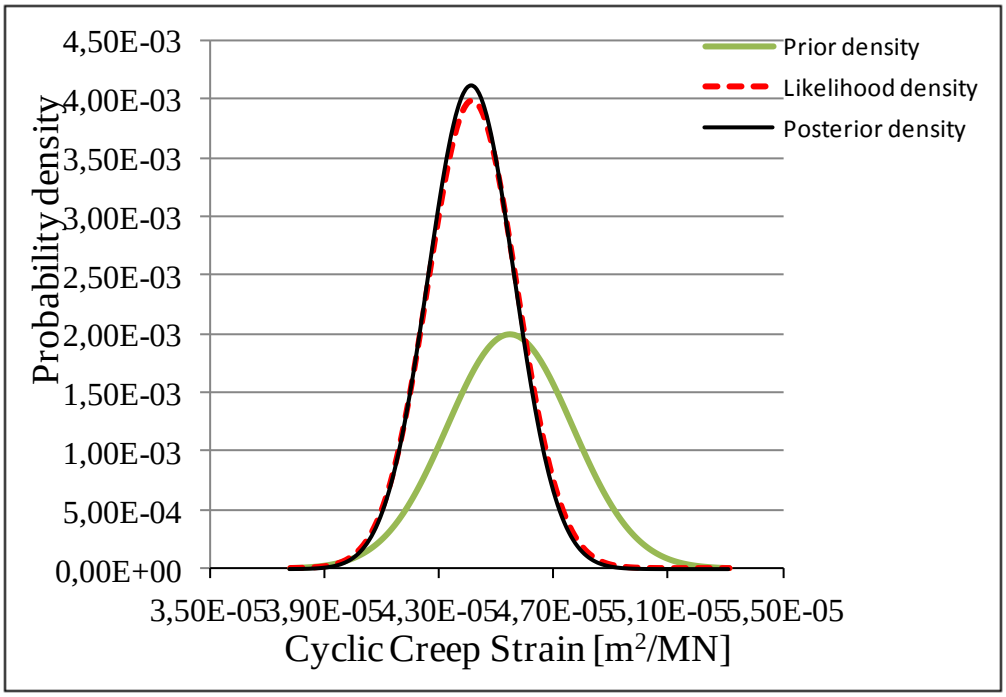

Figure 2. Illustration of prior and posterior probability density for the observed mean of cyclic creep. Also the likelihood for the test results is shown.

The posterior distributions of the parameters are derived based on Bayesian updating, which is given in Equation 18.

$$f(\phi(t-t_0) = \int_{-\infty}^{+\infty} f(\phi(t-t_0 \,|\, \mu,\sigma).f(\mu).f(\sigma) d\mu d\sigma \tag{18}$$

The measurement uncertainty obtained by observation has different boundary conditions associated with the probability models calculated separately. The process equation based measurement uncertainty is seen as the accumulation of prior knowledge of the measurement process. It becomes clear that the measurement uncertainty for a specific application is not exactly determinable and that furthermore, both concepts for the determination of the measurement uncertainty have their different boundary conditions and their limitation THONES [21].

In order to carry out the Bayesian updating by running the program in MATLAB, for *n_digit =1* it performed 10^6 evaluations of the different models until the stabilization of the results. It gives the estimate cyclic creep with associated standard uncertainty, measurement uncertainty, ($CV_{\varphi,\beta)}$ *or* $u(E(_x))$, for simplification in this work (standard uncertainty $u(E(_x))$, is written as measurement uncertainty ($CV_{\varphi,\beta}$), which is shows in Table 1, last row with a shortest 95% coverage interval In this work, is the method of calculating the measurement error and predicted values to consider measurement uncertainty with the goal of facilitating enhanced evaluation of cyclic creep models. The basis of this method was the

theory that cyclic creep models should not be evaluated against the values of measured data, which are uncertain, but against the inherent measurement uncertainty. Especially for; the deviation calculation of the probability distribution of measured data; the value of internal uncertainty is assumed.

Table 1. Uncertainties in cyclic creep models

Model	BP	mod. MC90	mod. Hyperbolic	Neville
$U(E(_{model}))$	0.283	0.306	0.300	0.380
$U(E(_{internal.}))$	0.080	0.080	0.080	0.080
$U(E(_{posterior}))$	0.062	0.086	0.093	0.121

4.2 Sensitivity analysis (SA)

The objective of SA is to identify critical inputs variables of a model and to quantify how input uncertainty impacts model outcomes. The sensitivities are solved at nominal values, cannot take account of the variation effect of the input variables, and thus those sensitivities are local. Compared with the local sensitivity, the uncertainty importance measure is defined as the uncertainty in the output can be apportioned to different sources of uncertainty in the model input, and the importance measures is also called global sensitivity. XU *et al.* [23] Method is used in this paper and method is approximately linear output response and input variables. For a model $y = (x_1, x_2, x_3 .... x_i .... x_k)$ and the main effect of each variable, the model can be simplified as follows:

$$y = \beta_0 + \sum_i^K \beta_i x_i + e \tag{18}$$

For detailed information see the reference XU *et al*. [23].

5. Input parameter Uncertainty and Sensitivity analysis of Cyclic Creep Function

Main statistic properties of concrete are given in Table 2.

The input variables correlation of the BP is shown in Tables 3.

Table 2. Statistic properties of the input variables

Variables	Mean	Std	CoV	Distribution	Models*	Sources
$f_{c,28}$	52.00 MPa	3.12	0.06	Log-normal	1,2,3,4	[22]
f_d	50.70 MPa	3.00	0.06	Log-normal	1,2,3,4	Assumed
$E_{ci,\,28}$	34144 Mpa	3414.4	0.1	Log-normal	1,2,3,4	[22]
$E_{c,d}$	33290 MPa	3329.0	0.1	Log-normal	1,2,3,4	Assumed
Humidity	0.65 [-]	0.026	0.04	Normal	1,2,3	[7]
Cement content	362 kg/m^3	36.20	0.1	Normal	1,3	[15]
Water-cement ratio	0.50 [-]	0.05	0.1	Normal	1	[15]
sand-cement ratio	5.16 [-]	0.516	0.1	Normal	1	[15]
Frequency	9 Hz	0.72	0.08	Normal	1,3	Assumed
Mean stress	$0.35f_c$ [-]	0.035	0.1	Normal	1,2,3,4	Assumed
Stress amplitude	$0.3f_c$ [-]	0.03	0.1	Normal	1,2,3,4	Assumed
Number of cycles	10^6 Number	80000	0.08	Normal	1,2	Assumed
a	318.22	31.82	0.1	Normal	3	Assumed
b	0.3	0.03	0.1	Normal	3	Assumed

**1 = BP, 2 = modified MC90/CE 2 , 3 = modified Hyperbolic , 4 = Neville*

Taking into account the input variables real correlation of model Neville the input variables increase significantly $CV_{par,cr,cyc}(t - t_0) = 0.08$ may cause this effect-strong correlation of strength and young modulus of elasticity. Comparing the total uncertainty of the models from Figure 3, we conclude that the model and, in comparison of all models, BP has the lowest total uncertainty $CV_{par,cr,cyc}(t - t_0) = 0.30$ and model Neville has highest total uncertainty $CV_{par,cr,cyc}(t - t_0) = 0.40$. The models mod. MC90, mod. Hyperbolic and Neville are based on the experimental data and also, assumed strain-time equation always satisfactorily fit the experimental data, so that long-term values cannot be estimated with confidence. Generally, the longer the times over which creep have actually been measured the better the prediction. The *CV* in the initial time of loading shows a higher figure and decreases with increasing time; because the initial time shows more uncertainty in measurement. The most important variable at short-time creep is model uncertainty factor for all models.

Table 3. Correlation matrix BP

Variables	*RH*	*c*	*w/c*	*a/c*	k_s	f_c	ω	Δ
RH	1	0	0	0	0	0	0	0
c		1	-0.4	-0.4	0	0.4	0	0
w/c			1	0	0	-0.4	0	0
a/c				1	0	-0.4	0	0
k_s					1	0	0	0
f_c	Symm.					1	0	0
ω							1	0
Δ								1

Total model quality *(MQ)* can be used to balance the better response of the model to its uncertainty in order to select the model that is most for a certain response. Figure 4 shows the time-dependent model quality. *MQ* which is dependent upon total uncertainty considering the correlated input quantities. The *MQ* is slight time dependent. For this reason the time interrogation according to KEITEL [12] and results given in Figure 4. In all these comparisons, model BP is found to be the best. *CEB-MC90/EC2* model (CEB 1990), which modifies its original model *MC90/EC 2*, TERJE *et al*. [21] by co-opting key aspects of cyclic loading (the mean stress and stress amplitude function and dependence on the number of cycles would simply mean a loading frequency), comes out as the second best. Considerably worse but the third best overall is seen to be the modified Hyperbolic model. Since the current Neville model, labelled Neville, is the simplest, introduced in 1973 on the basis of Neville's research (Neville *et al*. 1973), it is not surprising that it comes out as the worst because it is based on only four variables and therefore there is no consideration of concrete composition and environmental variables.

The results for application of the measurement uncertainty with the calculation of total uncertainty (as represented by four *CoV* values from 0.30 to 0.40) and distribution measured and predicted value for example data sets appear subsequently. The discussion focuses on the calculation of model quality based on calculated with incorporates both measurement uncertainty and model uncertainty.

Figure 5 display the sensitivity indices of different correlated and uncorrelated inputs of model BP. The model BP sees a more time dependent sensitivity indices over the time. The main reason behind this is the increased combination of time function with the input quantities. It is seen that the most sensitive quantities turn out to be concrete strength. In the second place is the content of the cement when quantities are assuming the uncorrelated. Further, the stress amplitude and frequency is the third and fourth influence quantities. The influence of water- cement ratio, aggregate-sand ratio and humidity are also considerable. The concrete strength is most dominating quantities when considering the quantities correlation. The second dominant quantity is the cement content and stress amplitude. The sensitivity indices of cement content and stress amplitude show a small decrease with increasing time. In the cyclic parameter is observed that there are considerable influences.

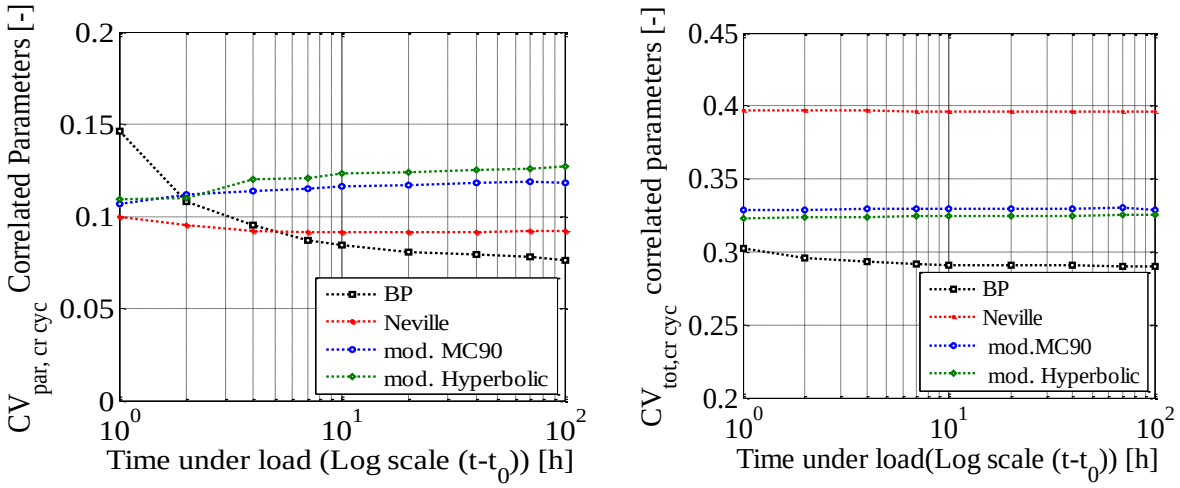

Figure 3. Input variables and model uncertainty of cyclic creep prediction

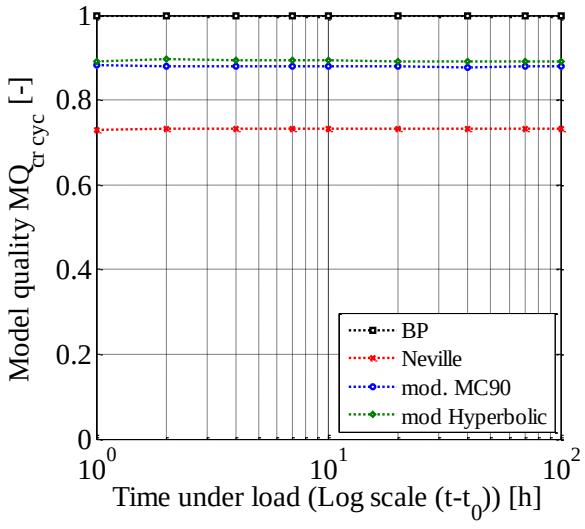

Figure 4. Model quality (MQ) of cyclic creep prediction

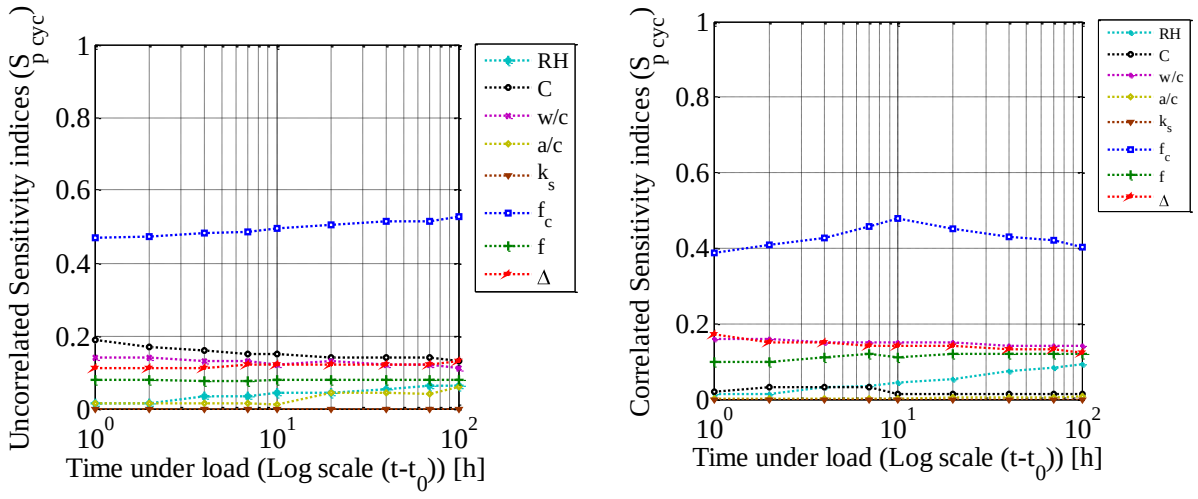

Figure 5. Uncorrelated and correlated sensitivity indices of model BP

6. Conclusion

In the present study, a probabilistic framework is suggested for the prediction of the cyclic creep of plain concrete considering four different cyclic creep models. Different sources of uncertainty- physical variability, data uncertainty, and model error/uncertainty- were included in the cyclic creep analysis. The input quantities which derive the cyclic creep such as, elastic modulus, concrete strength, mean stress, cyclic stress amplitude, number of cycle, humidity, cement content, water-cement ratio, sand-cement ratio, geometric factor have been considered as random variables. The uncertainty and sensitivity analysis is computed using the LHS sampling technique.

It is seen from the uncertainty analysis that the complex cyclic creep model BP has the good MQ and less uncertainty but the simple model Neville has higher uncertainty and lower model quality. In contrast, the complex model needs computational effort and more input variables. Stochastic sensitivity analysis is performed to determine the predominant factor amongst the input variables, which influences the cyclic creep prediction. It is observed that cyclic creep is more sensitive to the elastic modulus and strength of concrete, followed by mean stress, stress amplitude, frequency, cement content, humidity, water- cement ratio, in that order. Further, the present study of cyclic creep models results in some interesting points. The most of the creep analysis is only sustained load; the cyclic loading effect is neglected. Cyclic effect, neglected so far, might be non-negligible for long span bridges with many lanes or with a dense traffic of heavy trucks. This may cause the excessive time-dependent deflection of concrete structures. The concrete structure can lose their stiffness by (i) the degrada-

tion of concrete, (ii) the creep of concrete etc. The relation between the frequency of the structure and its age is important for the study of the long-term behaviour of materials, possibly for the detection of its damage. Of significance is the change of the modulus of elasticity of concrete due to cyclic creep.

Also, the proposed approach for UQ and SA is applicable to several engineering disciplines and the domain of cyclic creep analysis was used only as an illustration to develop the methodology. In general, the proposed methodology provides a fundamental framework in which multiple models can be connected through a Bayes network and the confidence in the overall model prediction can be assessed quantitatively.

Acknowledgment

This research is supported by the German Research Institute (DFG) via Research Training Group ”Evaluation of Coupled Numerical Partial Models in Structural Engineering (GRK 1462)”, and is gratefully acknowledged by the authors.

References

[1] Bažant, Z.P. : *Creep of concrete in structural analysis*, SNTL (State Publ. House of Techn Lit.), Prague 1966

[2] Bažant, Z. P.; Panula, L.: *Practical prediction of time-dependent deformation of concrete (Part IV: Cyclic creep, nonlinearity and statistical scatter)* J. Mat. Struct. 1979, 12 (69), pp. 175-183

[3] Bažant, Z. P.; Kim, J. : *Improved prediction model for time-dependent deformation of concrete: (Part 5- Cyclic load and cyclic humidity),* J. Mat. Struct. 1992, 25. pp 163-169

[4] Bazant , Z. P.; Hauggaaed A. B.; Baweja S.; Ulm F. J.: *Microprestress-solidification theory for concrete creep. I: Aging and drying effects,* Journal of Engineering Mechanics, vol. 123, 11, p. 1188-1194, 1997a

[5] CEB - *Comite Euro-International du Beton: CEB-FIP Model Code 1990 / Comite Euro-International du Beton.* 1993. - Technical Report 43

[6] DIN: *DAfStb Heft 525: Erläuterungen zur DIN 1045-1. Deutscher Ausschuss für Stahlbeton DAfStb,*1 Auflage, 2003, September

[7] Diamantidis, D.; Madsen, H.; Rackwitz, R.: *On the variability of the creep coefficient of structural concrete*. Mater Constr 1984, 17(100):321-8

[8] Gaede, K.: *Über die Festigkeit und die Verformung von Beton bei Druck-Schwellbeanspruchung. Deutscher Ausschuss für Stahlbeton*, Heft 144, Berlin 1962, Vertrieb durch Verlag von Wilhelm Ernst und Sohn.

[9] Gvozdev, A. A. : *Creep of concrete. In Mekhanika Tverdogo Tela (Conference Proc.)* Acad. Sci. USSR, Nauka Moscow 1966, pp. 137-152

[10] Helton, J. C.; Davis, F. J.: *Latin hypercube sampling and the propagation of uncertainty in analyses of complex systems*. Reliability Engineering & System Safety 2003;81(1):23–69.

[11] International Organization for Standardization, ISO/IEC Guide 98-3:2008 – Uncertainty of Measurement - Part 3: Guide to the Expression of Uncertainty in Measurement (GUM), ISO, 2008

[12] Keitel, H.: *Evaluation Methods for the Prediction Quality of Creep Models of Concrete*, Bauhaus-Universität Weimar, Dissertation, 2011

[13] Kern, E.; Mehmel, A. : *Elastische und Plastische Stauchungen von Beton infolge Druckschwell-und Standbelastung, Deutsche*. Ausschuss für Stahlbeton, Heft 153, W. Ernst, Berlin 1962

[14] Li, G. H.; Bažant, Z. P.: *Unbiased Statistical Comparison of Creep and Shrinkage Prediction Models*. In: ACI Materials Journal, 105(6) (2008)

[15] Madsen, H.; Bažant, Z.: *Uncertainty analysis of creep and shrinkage effects in concrete structures*. ACI J B 1983; 80:116–27

[16] Mckay, M. D.; Beckman, R. J.; Conover, W. J.: *Comparison of 3 Methods for Selecting Values of Input Variables in the Analysis of Output from a Computer Code*. Technometrics 1979;21(2):239–245

[17] Schwabach, E.: *Verformungs- und Degradationsverhalten von niederzyklisch uniaxial druckbeanspruchtem Beton.* Dissertation an der Fakultt Bauingenieurwesen der Bauhaus-Universitt Weimar, 2005

[18] Sudret, B.: *Uncertainty propagation and sensitive analysis in mechanical models and contribution to structural reliability and stochastic spectral methods*, Universite Blaise Pascal, Clermont-Ferrand, 2007

[19] Suter, G.T.; Mickleborough, N. C. : *Creep of concrete under cyclically varying dynamic loads.* Cement and Concrete Research, Vol. 5, No. 6, 1975. Pp.565-576

[20] Terje, K.; Gordana, P.: *Material model for high strength concrete exposed to cyclic loading ,* Fracture mechanics and concrete structures Edited by Z.P Bažant, 1992

[21] Thoens, S.: *Monitoring based Condition Assessment of Offshore Wind Turbine Support Structures*, Dissertation ETH Zurich, 2011

[22] Vrouwenvelder, T.: *Probabilistic model code*. 12th draft. Tech. rep. Joint Committee on Structural Safety. 2002

[23] Xu, C.; Gertner, G. Z.: *Uncertainty and Sensitivity Analysis for Models with Correlated Parameters.* In: Reliability Engineering and System Safety, 2008, 93 , S. 1563-1573 7, 61

[24] Whaley, C. P.; Neville, A. M. : *Non-elastic deformation of concrete under cyclic compression*. Magazine of Concrete Research. Vol. 25, No. 84. September 1973 pp. 145-154

Fuzzy and statistical conformity criteria for compressive strength according to EN 206-1

Izabela Skrzypczak
Institute of Geodesy, University of Technology, Rzeszow

Abstract: Statistical conformity criteria for compressive strength of concrete for small sample size n=3 are matter of the debate. Statistical criteria can have prejudicial effects to both - producer and client. In the code this is taken into account by choosing of optional decision for the acceptance of batch of concrete. These ones are checked from the economical and statistical decision of view. Statistical and fuzzy method of quality control, and especially compliance criteria for concrete recommended in code EN 206-1 and fuzzy criteria based on the fuzzy sets are presented and discussed.

1 Introduction

In order to achieve a sufficient level of the reliability required for a concrete structure the strength distribution and parameters of concrete supplied to a construction site should be in accordance with the assumptions specified in the design. Thus in each lot of concrete the conformity of the compressive strength should be verified using an adequate conformity criteria. Statistical conformity criteria specified in different codes and standards [1, 2, 3] are usually compounded of two elements and can be expressed as follows:

$$\bar{x} \geq f_{ck} + k_1 \quad \text{and} \quad x_{min} \geq f_{ck} - k_2 \tag{1}$$

where $\bar{x}, x_{min}$ are the sample mean and minimum value of the compressive strength of concrete, f_{ck} is the characteristic value of the concrete compressive strength specified by the producer, k_1, k_2 are parameters that depend on different circumstances, for example: $k_1 = \lambda s_n$, $\lambda = (1.4 \div 1.87)$; λ is the parameter that depends on the tolerance limit and the fractile considered, s_n is the sampling standard deviation, or $k_1 = (1 \div 5)$ MPa and $k_2 = (1 \div 5)$ MPa [5].

In the European Standard EN 206-1 [1] the statistical compliance criteria for compressive strength of concrete for continuous production are given as follows:

- for n=3 of results in the group

$$f_{cm} \geq f_{ck} + 4 \ , \ f_{ci} \geq f_{ck} - 4 \qquad (2)$$

- for n≥15 of results in the group

$$f_{cm} \geq f_{ck} + 1{,}48\sigma \ , \ f_{ci} \geq f_{ck} - 4 \qquad f_{ci} \geq (3) f_{ck} - 4$$

These criteria are far from perfection and there is always the risk that the suitable lot of concrete can be rejected (producer's risk and loss) or that the defective lot can be accepted (contractor's or/and investor's risk).

Compound compliance criteria of type (2) raises many questions, so the analysis reference is made to the sample size n = 3 using the methods of statistical and fuzzy. The paper presents an analysis and assessment of the quality and safety associated with the use codes compliance criteria for compressive strength of ordinary concrete of one kind. Method was used for analysis of random Monte Carlo simulation and the theory of fuzzy numbers using fuzzy statistical methods.

2 OC- curves (operating-characteristic curves)

Performance and efficiency of the statistical conformity criteria are investigated using the operation characteristic curves (OC curves). The probability of acceptance P_a is calculated by means of numerical simulation using the Monte Carlo technique and simulation programs.

The simulation programs for this purpose were elaborated for normal distribution with several known standard deviation, obtaining the operating characteristic curves shown in Figures 2 and 3 for compressive strength criteria specified in PN- EN 206-1. Similar procedure has been adopted by Taerwe [7].

OC curves calculated of single criterion and compound criterion. Denote by:

- A - the event. that $\bar{x}_n \geq f_{ck} + 4$,
- B - the event. that $x_{\min} \geq f_{ck} - 4$

and $\overline{A}, \overline{B}$ - opposite event for A, B. Each group of three simulated strength values can be classified. In one of the mutually exclusive subsets of the sample: AB, $\overline{A}B$, $A\overline{B}$, $\overline{A}\overline{B}$.

The probability of acceptance of compound criteria can be evaluated in this relationship:

$$P_a = P(AB) \Rightarrow P_a = 1 - P(\overline{A}B) - P(A\overline{B}) - P(\overline{A}\overline{B}) \quad (4)$$

For standard deviation 4,86 MPa and n = 3, the contributions of the different subset to the probability of rejection are show in Figure 2.

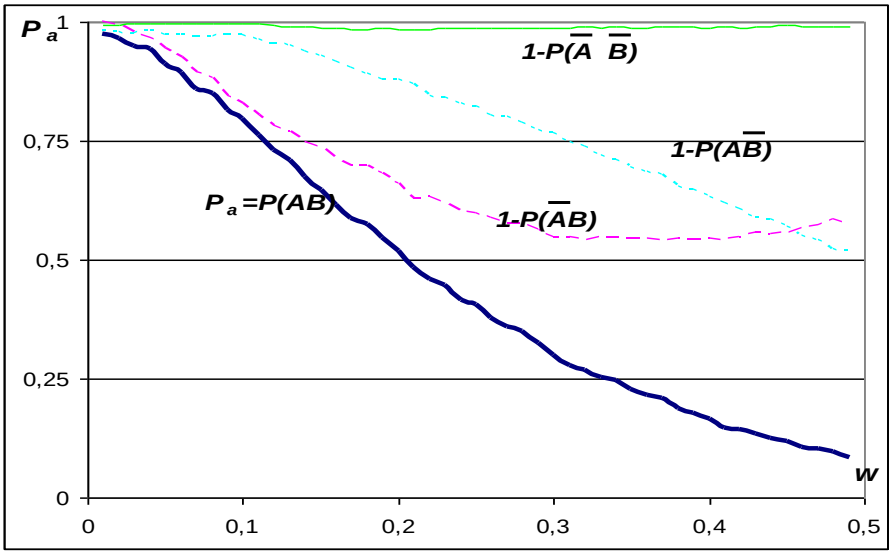

Fig.1. Contributions to the probability of rejection of criterion $\bar{x}_n \geq f_{ck} + 4$, $x_{min} \geq f_{ck} - 4$ for σ=4,86MPa, n=3

2.1 Analysis on the basis of OC-curves

Using Monte Carlo [2,7,8] simulation technique OC-curves for the compound criterion of conformity were investigated for three different types of distribution of the compressive concrete strength: N, different standard deviation σ_{fc} of concrete strength and small sample size: n= 3. The total number of simulation N = 100000 were used to obtain OC curves in all case.

The following conformity criteria were used:

- for the sample size n = 3; $f_{cm} \geq f_{ck} + 4$ and $f_{ci} \geq f_{ck} - 4$.

Comparisons of the rules for judging the quality of concrete (OC curves) with boundaries for unsafe and uneconomic regions have been presented by figures 3 and 4. These regions were given as mathematical basis and justification by Taerwe [6,7].

Taerwe's definition of the boundary of the unsafe region is:

$$w \cdot P_a = 500 \tag{5}$$

and of the uneconomic region is:

$$\frac{w}{100 - P_a} = 0{,}05 \tag{6}$$

These boundaries are shown on Figure 2 as dashed lines.

If conformity rule gives an operating characteristic that passes through the unsafe region than the protection it gives the specifier would be too weak. If a rule gives an operating characteristic that passes through the uneconomic region it causes producers to use excessively large margins, even then, accept high risks of non-conformity [6].

OC curve for criteria (2) shown in Fig.3 to Fig.4 for samples n=3 for normal (N) distributions with known standard deviation.

Prediction accuracy of statistical acceptance criteria has been determinate with use of normal distribution. Taking the compliance compound criterion into consideration, higher values of acceptance probability P_a correspond to lots of bigger strength variability. The lower probability of acceptance has been for N distributions of higher strength variability.

High values of probability of acceptance have been of productions with more than 5% of defects, which can be around 80% in some cases. For standard conformity criteria probability of acceptance of all is higher, the higher is standard deviation of concrete compressive strength. It may lead to increasing of mean concrete strength at growing spread causing groundless costs of a producer. Conformity criterion of concrete compressive strength for small sample size discourages from concrete production with small scatter.

selection of materials, concrete design and production, inspection and control, test results. Only one type of restricted information connected with numerical measurements, namely the values of standard deviation and minimum strength are taken into consideration in the statistical conformity criteria. The wide information on the composition, production, placing, curing and testing of concrete is mostly qualitative, verbal, subjective and imprecise. Statistical procedures ignore this type of data. Application of the fuzzy sets theory and approximate reasoning scheme enables to take advantage of qualitative and quantitative information, sharp and vague data for conformity assessment of concrete strength.

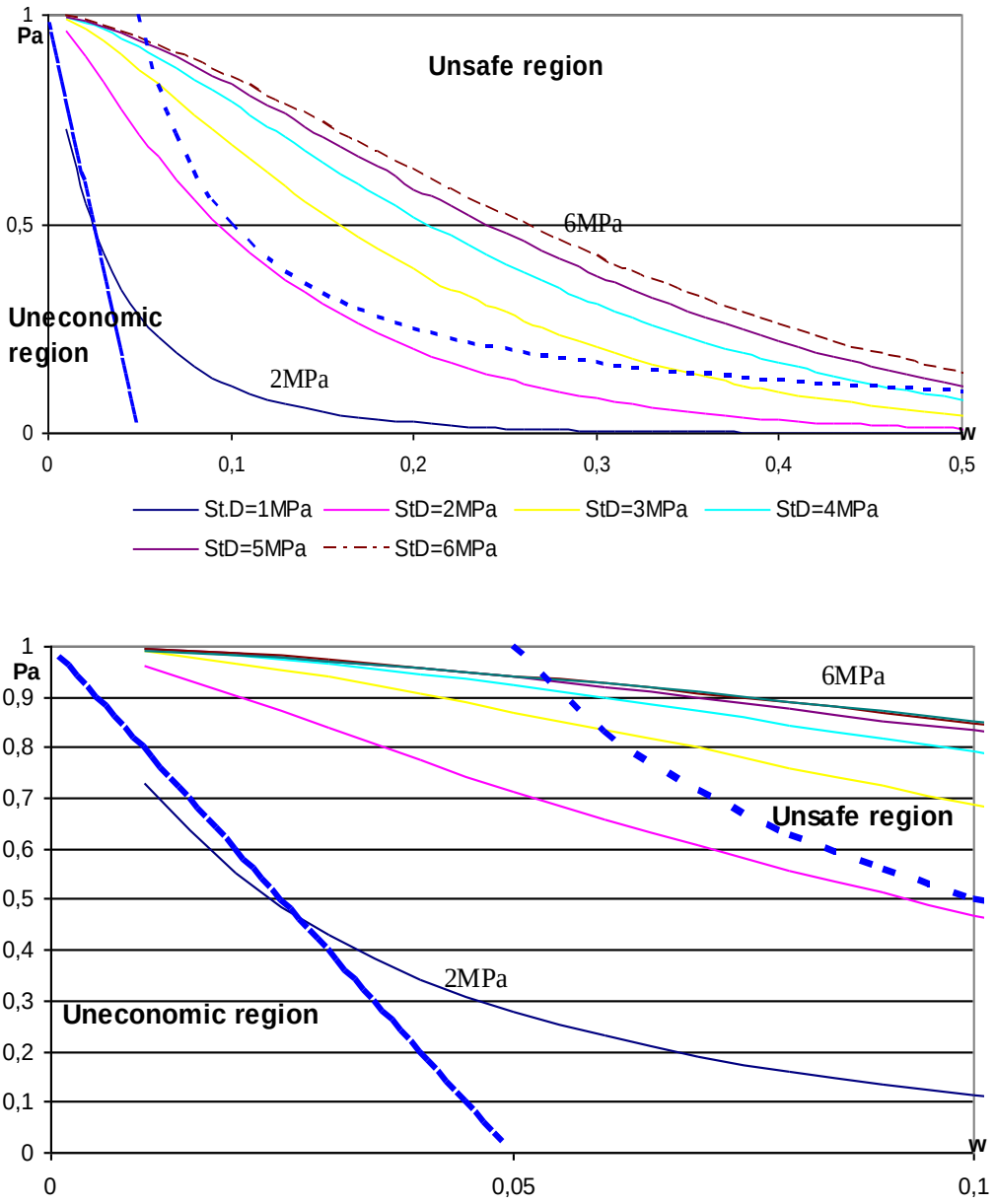

Fig.2. Compliance criteria for group *n=3* samples with known standard deviation and for compound criterion $f_{cm} \geq f_{ck} + 4$ and $f_{ci} \geq f_{ck} - 4$

When reviewing the batch of material based on a sample of small size and population of defects greater than 5% - (for unsafe region) may be helpful the statistical-fuzzy compliance criteria.

3 Compliance criteria with the fuzzy-statistical approach

The information sources available for conformity assessment of concrete strength include recorded data and other documents necessary to maintain and regulate the quality of concrete in conformity with specification, for instance:

Compressive strength of concrete f_c, fulfilling the compound compliance criterion can be inscribed by using a fuzzy set:

$$f_c = [\mu_{f,C}(f_{cm}), f_c], \quad \mu_{f,C}: F_c \rightarrow [0,1] \tag{7}$$

Where: $\mu_{f,C}(f_{cm})$ is the membership function assigning degree of the fuzzy set membership f_c (from the interval [0,1]) to each element of the strenght set $f_c \in F_c$.

The code compound criterion of conformity of produced concrete lot with projected class may have the following form:

- for sample size n = 3:

$$\left.\begin{array}{l} f_{cm} \geq f_{ck} + 4 \\ f_{ci} \geq f_{ck} - 4 \end{array}\right\} = K \tag{8}$$

- for sample size n = 15:

$$\left.\begin{array}{l} f_{cm} \geq f_{ck} + 1{,}48\sigma \\ f_{ci} \geq f_{ck} - 4 \end{array}\right\} = K \tag{9}$$

Where: K is the fuzzy value (of μ_{fc} (f_{cm}) membership function), which should be established for determined classes of concrete on the ground the fuzzy-statistical experiment.

3.1. Fuzzy-statistical analysis for compressive strength of concrete

The three-phase method (fuzzy-statistical) has been used to determine membership functions of test characteristics [6, 7]. Random variables ξ and η were defined. Every experiment determines a pair of numbers ξ and η, where ξ is demarcation point for considered and lower class of concrete and η is demarcation point for considered and higher class concrete. Variable (ξ ,η) can be assumed as a two-dimensional random variable. Then trough sampling it is possible to obtain $p_\xi(x)$ and $p_\eta(x)$ as marginal probability distributions. In general, ξ and η follow a normal distribution $\xi \rightarrow N(m_\xi, \sigma_\xi)$ and $\eta \rightarrow N(m_\eta, \sigma_\eta)$.

The membership function for i-class of concrete can be described below:

$$\mu_{Ci}(f_{cm}) = \int_{-\infty}^{f_{cm}} p_\eta(f_{cm})\, df_{cm} = F\left(\frac{f_{cm} - m_\eta}{\sigma_\eta}\right) \tag{10}$$

The membership function for considered and less i- class of concrete can be described by the following formula:

$$\mu_{Ci-1}(f_{cm}) = \int_{f_{cm}}^{+\infty} p_{\xi}(f_{cm})\,df_{cm} = 1 - F\left(\frac{f_{cm} - m_{\xi}}{\sigma_{\xi}}\right) \tag{11}$$

Contrast, the fuzzy membership functions considered and higher i- class of concrete has follow form:

$$\mu_{Ci+1}(f_{cm}) = 1 - \int_{f_{cm}}^{+\infty} p_{\xi}(f_{cm})\,df_{cm} - \int_{-\infty}^{f_{cm}} p_{\eta} f(f_{cm}) \tag{12}$$

$$\mu_{Ci+1}(f_{cm}) = 1 - \left[1 - F\left(\frac{f_{cm} - m_{\xi}}{\sigma_{\xi}}\right)\right] - F\left(\frac{f_{cm} - m_{\eta}}{\sigma_{\eta}}\right) \tag{13}$$

The final form of the formula is:

$$\mu_{Ci+1}(f_{cm}) = F\left(\frac{f_{cm} - m_{\xi}}{\sigma_{\xi}}\right) - F\left(\frac{f_{cm} - m_{\eta}}{\sigma_{\eta}}\right) \tag{14}$$

Where:

$$F(z) = \frac{1}{\sqrt{2\pi}} \int_{-\infty}^{z} \exp(-0{,}5z^2)\,dz \tag{15}$$

With the membership functions for different classes of concrete, and the mean value of compressive strength for neighboring classes estimated based on random simulation, we can calculate the degree of membership values of the considered batch of concrete to different classes. Depending on the value of $\mu_{f,Ci}(f_{cm})$, we can decide on the inclusion of lots of concrete to the appropriate class of concrete. This decision may be more or less conservative, depending on its impact on the qualitative assessment of the produced concrete and the impact on the requirements of safety, quality and economics.

4. Examples with application of fuzzy-statistical method

Compliance criteria given in the formulas (1) were performed by the computations method: generating 100 000 random groups of size *n=3* in accordance with normal distribution, generating class of concrete (concrete classes of the three neighboring classes of concrete $C_{i\,-1}$, C_i, $C_{i\,+\,1}$ with 1/3 probability), generating standard deviation and defective fraction. To generate random numbers with standard normal distribution, the method Box and Muller [5] was used. The table of probability distribution of random vector (ξ , η) and the histogram of marginal probability distributions, for the considered and lower

class of concrete and one for the considered and higher class of concrete, were built. Graphs of the density function of boundary probability distributions $p_\xi(f_{cm})$ and $p_\eta(f_{cm})$ are the basis for the designation of membership function for each class of concrete.

On the basis of simulations for the concrete class C16/25, generating 100 000 random groups of size n = 3 in accordance with normal distribution, marginal density functions of distributions and fuzzy membership functions were estimated for each class of concrete.

The marginal probability distributions $p_\xi(x)$, $p_\eta(x)$ and the plot of original and modified membership function of concrete class C16/20 and neighboring classes (C12/15, C20/25) are presented by the Fig. 3.

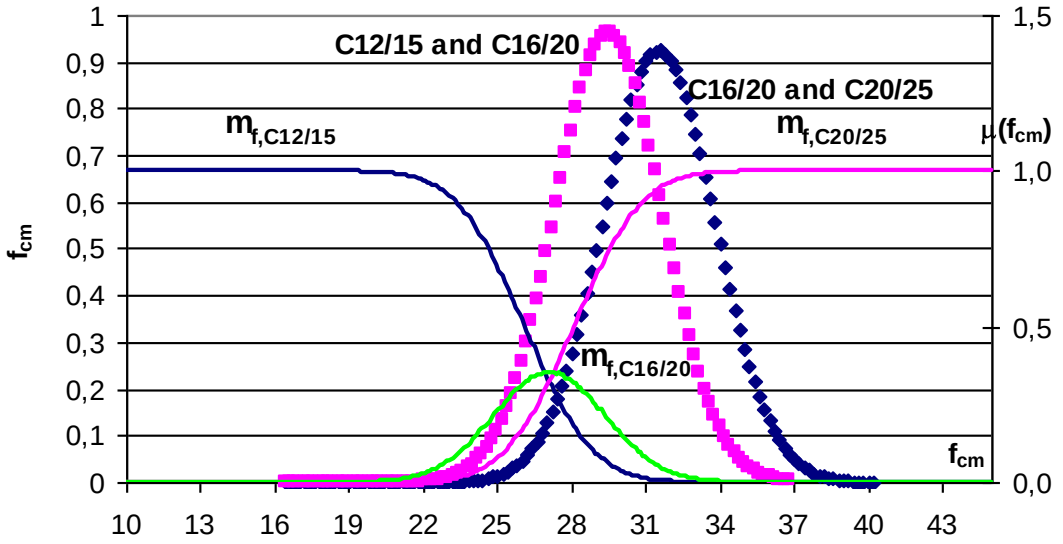

Fig.3. The membership function of f_{cm} concrete classes for concrete class C12/15, C16/20 and C20/25

The plot for membership function of concrete class does not accept value 1,0 [Fig. 3]. This suggests that concrete class division is too numerous.
The analysis was conducted for the second-class concrete getting the results of the confirmatory foundation about too numerous classes of concrete.
Class of concrete C16/20 (sample size $n=3$, $\mu_{,Ci}(f_{cm})$) were considered to estimate the membership function of the fuzzy value of concrete classes. Assuming the normal distributions of demarcation points $\xi \rightarrow N(m_\xi, \sigma_\xi)$ and $\eta \rightarrow N(m_\eta, \sigma_\eta)$ of concrete class C8/10 and C16/20, and C16/20 and C25/30, respectively, mean values $m_\xi = 10{,}19$ MPa, $m_\xi = 21{,}72$ MPa and standard deviation $\sigma_\xi=3{,}29$ MPa and $\sigma_\xi=2{,}18$ MPa were estimated. Then the membership function of value of test coefficient for concrete class C16/20 was calculated according to formulas 10,11,14 and 15 which is presented on the Fig. 4.
We can accept batch of concrete, with values of:

- f_{cm}=15,8 MPa compressive strength with the confidence level 0,82 to the concrete class C16/20
- f_{cm} as values from intervals (10; 15,8) MPa with the confidence level from interval (0,5; 0,82) to the concrete class C16/20 or to C8/10,
- f_{cm} as values from intervals (15,8; 22) MPa with the confidence level from interval (0,08; 0,5) to the concrete class C25/30.

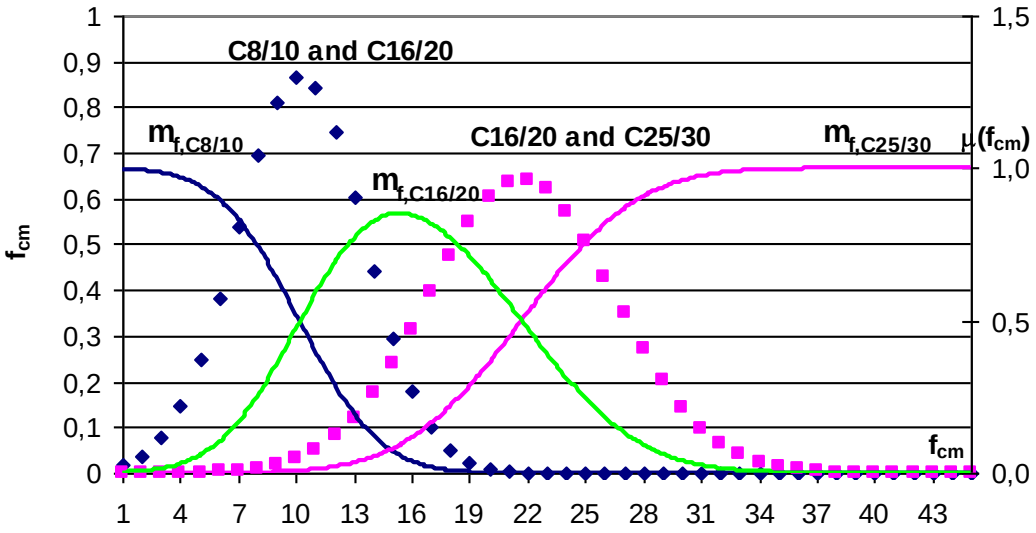

Fig.4. The membership function of f_{cm} concrete classes for concrete class C8/10, C16/20 and C25/30 (the analysis for the second-class concrete)

4 Conclusions

Defects and deficiencies of the pure statistical criteria of conformity evaluation give reasons for finding a new solutions. Uncertainties related to the assessment and classification of concrete strength leads to apply a fuzzy measures of safety in the designing and analysis of building structures. It is base of the formulation of the fuzzy-statistical classification procedures for produced concrete. This innovative approach, which allows taking into account the opposing requirements - in case of producer and client - of safety, quality, economy. Application of fuzzy-statistical methods gives possibility of taking more reasonable decision on the concrete classification.

5 Literature

[1] PN-EN 206-1:2003, *Polish Standard, Concrete – Part 1: Specification, performance, production and conformity*, [in Polish], PKN, Warszawa 2003

[2] Comité Euro-International du Beton, CEB-FIB Model Code 1990, Bulletin d'Information No. 213-214, Lausanne, May 1993

[3] EN 206:2000, *European Standard, Concrete – Part 1: Specification, performance, production and conformity*, CEN, Brussels, 2000

[4] Brandt S., *Analiza danych*, Wydawnictwo Naukowe PWN, Warszawa, 1998

[5] Brunarski L.: *Criteria of the agreement of the characteristic strength of building materials in codes PN-EN-ISO*, Prace ITB-Kwartalnik, No. 4 (124), Warsaw, 2002

[6] T.A. Harrisom, *Guidance on the application of the EN 206-1 conformity rules*, www.bca.org.uk, April 2001

[7] L. Taerwe, *Evaluation of compound compliance criteria for concrete strength*, Materials and Structures, 21, 1988, 13-20

[8] L. Taerwe, R. Caspeele, Conformity control of concrete: some basic aspects, Proceedings 4-th International Probabilistic Symposium, Berlin, 2006, 57-70

[9] Sz. Woliński, *Statystyczne i rozmyte kryteria zgodności wytrzymałości betonu na ściskanie, Problemy naukowo-badawcze konstrukcji z betonu*, Politechnika Krakowska, Monografia 247, Kraków 199, s. 51-57

Quantifying the structural safety of concrete slabs subjected to the ISO 834 standard fire curve using full-probabilistic FEM

Ruben Van Coile, Robby Caspeele, Luc Taerwe
Magnel Laboratory for Concrete Research, Ghent University, Ghent

Abstract: Finite Element Models (FEM) allow to incorporate the structural interaction between different sections and possible stress redistributions, enabling a more economic (performance-based) design. However, the uncertainty with respect to material and geometrical properties can have a significant influence on the obtained safety level, especially when the structure is exposed to accidental loads such as fire. Using a Latin Hypercube Sampling procedure (LHS) and the Finite Element software package ATENA, the safety level of a simply supported concrete slab exposed to fire is assessed. The structural fire resistance time is calculated, and a comparison is made with results obtained from a simplified full-probabilistic cross-section calculation method developed by the authors in a previous contribution.

1 Introduction

Although numerous studies are available with respect to the safety level of concrete structures, the behaviour of the safety level during fire is most often not considered. Nevertheless, a full-probabilistic methodology for calculating the safety level during fire is very useful for a quantitative comparison of design alternatives and for considering more detailed (or updated) information regarding material properties and geometrical properties into the design or verification process.

For simplified cross-section analyses of concrete elements during fire crude Monte Carlo simulations (MC) can be used, as applied in **Fehler! Verweisquelle konnte nicht gefunden werden.** and [22]-[23]. The probability of failure P_f can be assessed as the frequency with which the resistance effect R is smaller than the load effect E:

$$P_f = P\ R < E\ = \frac{N_{R<E}}{N_{total}} \tag{1}$$

with $N_{R<E}$ Number of simulations where R is smaller than E.
N_{total} Total number of simulations.

The reliability index β is consequently calculated as:

$$P_f = \Phi\ -\beta \tag{2}$$

with $\Phi(.)$ The cumulative normal distribution.

Reliability studies can be performed by combining MC simulations with Finite Element Models (FEM) for assessing the response of structural elements to fire loads (see e.g. [18], [19]), but many authors indicate that the computational efforts are too large for practical purposes [2], [15]. Therefore, more computationally effective methodologies have been proposed for such reliability analyses, e.g. the Response Surface Method [8] and [13], or a FORM analysis combined with the Finite Difference Method or the Direct Differentiation Method [7]. However, from a practical perspective all of these methods have significant drawbacks, e.g. a large number of required simulations or a difficult implementation in existing commercial Finite Element software packages. The sampling procedure known as Latin Hypercube Sampling (LHS) [16] seems a promising alternative which balances computational efficiency with simple practical implementation in existing FEM.

In this contribution LHS is used to determine the mean and coefficient of variation of the bending moment capacity M_R of a concrete slab exposed to fire. By assuming a lognormal distribution for M_R and using the standard First Order Reliability Method (FORM), a reliability index β is calculated in compliance with EN 1990 [4]. Furthermore, the proposed methodology allows for an exact calculation of the fire resistance time t_R, as defined by EN 1992-1-2 [5] by:

$$M_{Rd,fi,t} \geq M_{Ed,fi,t} = M_{Ed,fi} \quad \text{for } t \leq t_R \tag{3}$$

With $M_{Rd,fi,t}$ the bending moment capacity during fire at t minutes of exposure to the ISO 834 [11] standard fire curve, and $M_{Ed,fi,t}$ the bending moment induced by the design loads during fire.

2 Application of Latin Hypercube Sampling to the reliability analysis of concrete structures

Some of the variables involved in a structural analysis of concrete elements during fire are highly uncertain. Therefore the stochastic representation of these input variables X_i should be taken into account and a reliability study should be performed.

When using crude Monte Carlo simulations for the uncertainty propagation the uncertainty of the input variables X_i is translated into the uncertainty with respect to the output variable Y by repeated random sampling [1]. For each random vector $\bar{X}_j = X_{1,j}, X_{2,j}, ..., X_{n,j}$ of the n input variables X_i, Y_j is calculated by (4) and the mean value of the response can be estimated by (5). The required number N of random simulations in order to achieve a reliable estimation of $\hat{\mu}_Y$ is however too large to use in combination with Finite Element Models [15].

$$Y_j = g\left(\bar{X}_j\right) = g\left(X_{1,j}, X_{2,j} .. X_{n,j}\right) \tag{4}$$

with g(.) The response operator.

$$\hat{\mu}_Y = \bar{Y} = \frac{\sum_j Y_j}{N} \tag{5}$$

While maintaining the simple implementation of MC simulations, the Latin Hypercube Sampling procedure significantly reduces the number of required simulations N by ensuring that even for a very small number of samples the entire domain of the cumulative distribution function of the input variables X_i is represented, i.e. the Latin Hypercube Sampling procedure subdivides the entire domain of possible values for each stochastic variable X_i in N (the number of simulations) subsequent areas with equal probability. Within each area a random value of X_i is generated and combined with similarly generated values of the other input variables to compose the random vector $\bar{X}_j$. An example of this subdivision of the cumulative distribution function for the input

variable X_i and the subsequent random sampling in each interval is given in Figure 1 for a LHS with 10 samples.

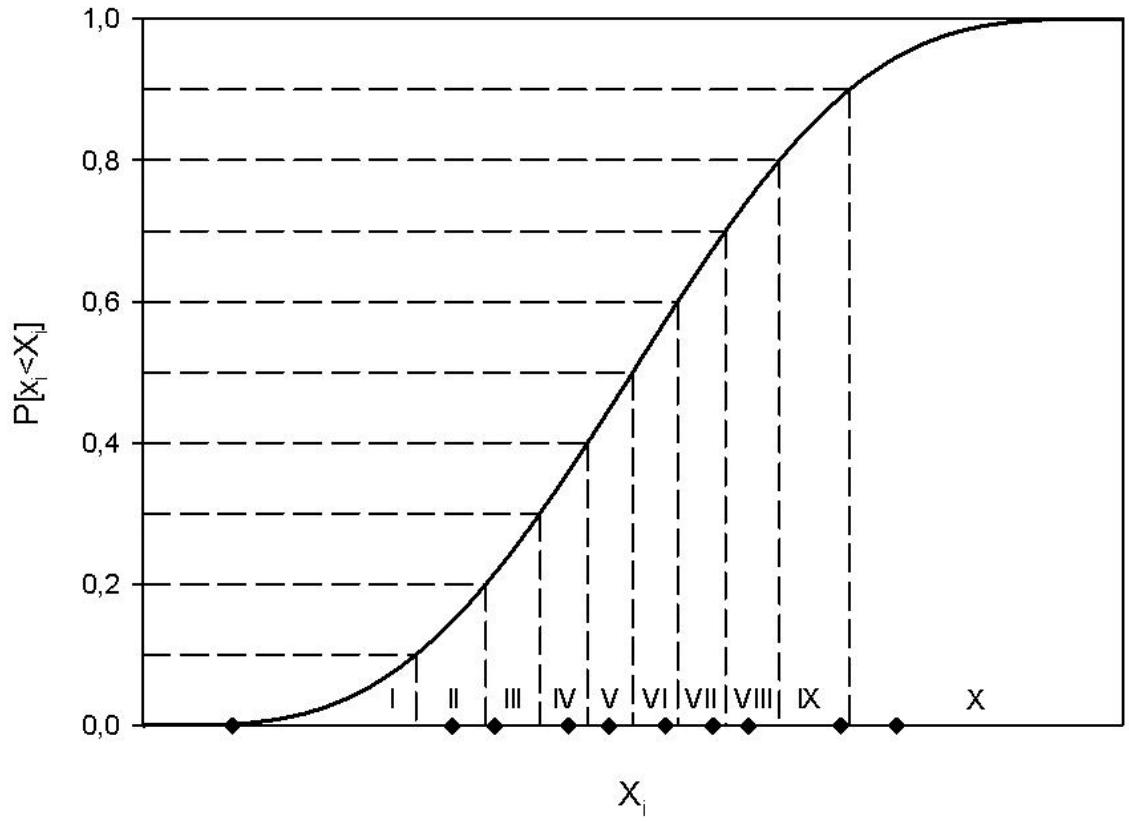

Figure 1. Latin Hypercube Sampling procedure for a single random variable X_i

The subdivisions of X_i are designated I to X and in each of these areas a random value of X_i is selected (represented by the dot on the X_i-axis). Combining the random samples of each variable X_i into a random vector $\bar{X}_j$ requires the composition of a Latin Hypercube and a Cholesky decomposition in order to avoid spurious correlations.

A detailed description of the application of LHS to structural reliability analysis is given by OLLSON ET AL. [16].

Similar to the situation for crude MC simulations, the stochastic distribution of the output variable Y can be fitted to a chosen distribution (e.g. normal or lognormal) and an estimation of the mean μ_Y and coefficient of variation δ_Y or standard deviation σ_Y can be calculated according to well-known estimation methods such as the Method of Moments or the Maximum Likelihood Method [3].

For the set of N simulations performed by LHS, the sample moment m of order r can be calculated by (6) [14] and consequently the mean μ_Y and standard deviation σ_Y can be estimated by (7) and (8) in accordance with the Method of Moments [3].

$$m_r = \frac{1}{N}\sum_j Y_j^r \tag{6}$$

$$\hat{\mu}_Y = m = \frac{1}{N}\sum_j Y_j \tag{7}$$

$$\hat{\sigma}_Y^2 = \hat{\mu}_{Y,2} - \hat{\mu}_{Y,1}^2 = m_2 - m_1^2 = \frac{1}{N}\sum_j Y_j^2 - \hat{\mu}_Y^2 \tag{8}$$

In this study the maximum bending moment capacity of a concrete slab exposed to fire is assessed using the Finite Element software package ATENA. The following procedure is carried out for each of the N LHS simulations:

1. The LHS samples of the stochastic variables are implemented
2. The slab is subjected to its self-weight
3. The slab is exposed to the ISO 834 standard fire curve for t minutes
4. A load-displacement test is simulated while maintaining the temperature distribution in the slab
5. Steps 1 to 4 are repeated for different fire exposure durations t

By determining the maximum load bearing capacity for different values of t, the evolution of the bending moment capacity $M_{R,fi,t}$ during fire is determined for each of the N slabs. The mean and standard deviation of $M_{R,fi,t}$ is assessed through (7) and (8). In this study a lognormal distribution for the bending moment capacity is assumed.

3 Methodology for calculating the reliability index and the fire resistance time

3.1 Calculation of the reliability index

For a concrete slab exposed to fire the limit state function for bending can be expressed by (9), taking into account that the event of a fire does not affect the applied load on the concrete slab, in accordance with EN 1992-1-2 [5].

$$Z = K_R M_{R,\,fi,t} - K_E M_E \tag{9}$$

with $M_{R,fi,t}$ The bending moment capacity during fire.
M_E The bending moment induced by the loads
K_R The model uncertainty of the resistance effect
K_E The model uncertainty of the load effect

A reliability index β_{slab} is calculated from (9) by a FORM analysis. The bending moment capacity $M_{R,fi,t}$ is approximated by a lognormal distribution with mean and coefficient of variation determined by the FEM LHS calculations.

For a concrete slab with a uniformly distributed permanent load g_k (characteristic value) and only a single uniformly distributed variable load q_k (characteristic value), the load ratio χ of the variable load to the total load is defined by (10) and M_E equals $M_Q + M_G$, which is correct for a statically determined concrete slab.

$$\chi = \frac{q_k}{q_k + g_k} = \frac{M_{Qk}}{M_{Qk} + M_{Gk}} \tag{10}$$

with M_{Gk} Bending moment induced by g_k.
M_{Qk} Bending moment induced by q_k.

Under ambient design conditions (i.e. at 20°C) and assuming $M_{Rd} = M_{Ed}$, the design value of the bending moment capacity can be calculated by (11), adapted from EN 1990 [4].

$$M_{Rd} = M_{Gk} \max\left\{\left(\gamma_G + \psi_0 \gamma_Q \frac{\chi}{1-\chi}\right); \left(\xi\gamma_G + \gamma_Q \frac{\chi}{1-\chi}\right)\right\} \tag{11}$$

with γ_G Partial factor for the permaenent load.

ψ_0 Combination factor
γ_Q Partial factor for the variable load
ξ Reduction factor for unfavorable permanent loads

According to GULVANESSSIAN et al. [6], the permanent load's characteristic value can in general be assumed equal to its mean value. Thus, M_{Gk} is equal to its mean value μ_G and for a given slab configuration (11) defines μ_G as a function of the load ratio χ.

The standard deviation σ_G of the bending moment induced by the permanent load, and the mean value μ_Q and standard deviation σ_Q of the bending moment induced by the variable loads are calculated through equations (12)-(14), as suggested in the literature study by HOLICKY and SYKORA [9]. For the bending moment M_G induced by the permanent loads a normal distribution is used, while for the bending moment M_Q induced by the variable load a Gumbel distribution is assumed [9].

$$\sigma_G = 0.1\mu_G \tag{12}$$

$$\mu_Q = 0.6M_{Qk} \tag{13}$$

$$\sigma_Q = 0.35\mu_Q \tag{14}$$

The model uncertainty K_E of the load effect follows a lognormal distribution with a mean value of 1 and a standard deviation of 0.1 [9].

It is not clear which model uncertainty K_R would be appropriate for non-linear FEM analysis of concrete elements. For a simplified cross-section calculation, the model uncertainty K_R can be approximated by a lognormal distribution with mean 1.1 and standard deviation 0.1, based on [10]. Further in this paper a lognormal model uncertainty K_R with mean 1.05 and coefficient of variation 0.1 will be proposed for the FEM calculations. This proposed model uncertainty lies within the boundaries for the model uncertainty for FEM as suggested by SCHLUNE ET AL. [17].

3.2 Evaluation of the design format of EN 1992-1-2 and calculation of the fire resistance time t_R

EN 1992-1-2 [5] defines the structural fire resistance time t_R by (3). The partial factors for the calculation of $M_{Rd,fi,t}$ and $M_{Ed,fi}$ are equal to 1 and a combination factor ψ_{fi} is prescribed for the variable load.

It is unclear which safety level corresponds with this design format of EN 1992-1-2. However, for a given slab configuration one can calculate a limit value for the reliability index which is implicitly determined by (3). If the reliability index β_{slab} drops below this implicit limit value, the fire resistance time is reached. The implicit limit value is a function of the time t of fire exposure and will be designated $\beta_{limit,EC,t=tR}$.

Similar to equation (11), the mean bending moment μ_G* can be calculated for a given slab configuration and load ratio χ under the assumption $M_{Rd,fi,t} = M_{Ed,fi,t}$ and considering the load combination $M_{Gk} + \psi_{fi} M_{Qk}$:

$$M_{Rd,fi,t} = \mu_G^* \left(1 + \frac{\chi}{1-\chi} \psi_{fi} \right) \tag{15}$$

with ψ_{fi} Combination factor in case of fire defined by EN 1992-1-2 [5].

The distributions of M_Q^* and M_G^* can similarly be calculated as in equations (12)-(14). Implementing these distributions in the limit state function (9) for the time t results in:

$$Z^* = K_R M_{R,fi,t} - K_E \; M_Q^* + M_G^* \tag{16}$$

Consequently, the limit value $\beta_{limit,EC,t=tR}$ for the reliability index is determined by a FORM calculation.

This methodology allows for an objective evaluation of the design format of EN 1992-1-2. The following procedure is used for a given slab configuration:

1. For a given time t the design value of the bending moment capacity during fire $M_{Rd,fi,t}$ is calculated.

2. The maximum allowable load according to EN 1992-1-2 is determined by $M_{Rd,fi,t} = M_{Ed,fi,t}$.

3. The probabilistic distributions of the permanent load and the variable load are determined by (12)-(15).

4. The reliability index $\beta_{limit,EC,t=tR}$ is calculated for the limit state function (16) by a FORM calculation.

By comparing $\beta_{limit,EC,t=tR}$ for different exposure times t one can evaluate whether or not a similar safety level is obtained by the design format of EN 1992-1-2 for different t_R. By comparing $\beta_{limit,EC,t=tR}$ for different slab configurations one can assess whether the safety level pursued by the design format of EN 1992-1-2 is dependent on the slab configuration. Furthermore, one can calculate the impact of a larger uncertainty of e.g. the concrete cover on the safety level at the fire resistance time.

4 Case study

For a concrete slab with probabilistic models according to Table 1, a FEM is developed in the commercial Finite Element software package ATENA developed by Cervenka Consulting. The sampling procedure described by OLSSON ET AL. [16] is applied to determine the input parameters corresponding to 10 different LHS samples for the slab.

Table 1. Probabilistic models for the slab configuration

Symbol	Name	Dimension	Distribution	Mean	Standard Deviation
h	thickness	mm	Normal	200	5
f_c (20°C)	20°C concrete compressive strength; f_{ck}(20°C) = 20 MPa	MPa	Lognormal	25.4	2.7
f_y(20°C)	20°C steel yield stress; f_{yk}(20°C) = 500 MPa	MPa	Lognormal	581.4	40.7
c	concrete cover	mm	Beta	35	2
A_s	bottom reinforcement area	mm²	Normal	801	16
$k_{fc(\theta)}$ [22]	concrete compressive strength reduction factor at temperature θ	-	Beta	θ-dependent	θ-dependent
$k_{fy(\theta)}$ [22]	steel yield stress reduction factor at temperature θ	-	Beta	θ-dependent	θ-dependent
K_R	model uncertainty of the resistance effect	-	Lognormal	method-dependent	method-dependent
K_E	model uncertainty of the load	-	Lognormal		

effect	1	0.1

Initially, every slab is subjected to its self-weight only. Then, the slab is exposed to the ISO 834 standard fire curve for a specified fire duration. Finally, a load-displacement analysis is carried out while maintaining the temperature distribution in the slab in order to determine the maximum bending moment capacity of the slab configuration at a given duration of exposure to the ISO 834 standard fire curve. This procedure is repeated for every one of the 10 LHS samples for different fire exposure times, i.e. every 60 minutes of exposure.

The calculated bending moment capacity as a function of the exposure time to the ISO 834 standard fire curve for a LHS sample set of 10 slabs is presented in Figure 2.

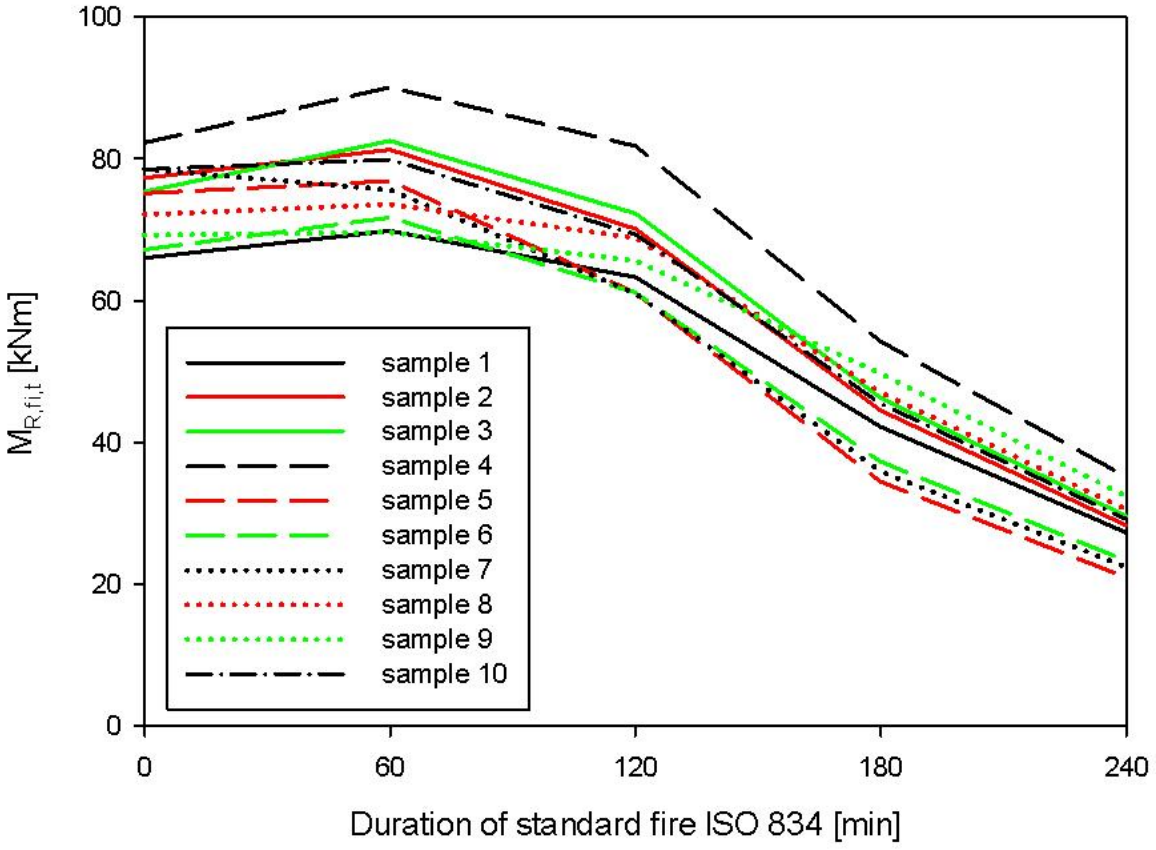

Figure 2. Bending moment capacity $M_{R,fi,t}$ as a function of the exposure time to the ISO 834 standard fire curve for 10 LHS Finite Element simulations

Since the curves in Figure 2 are not parallel, the response to the fire exposure differs for the different slabs. This primarily results from a difference in reinforcement temperature and reinforcement yield stress during fire due to the stochastic characteristics of the concrete cover and the reduction variable $k_{fy(\theta)}$ for the steel yield stress at elevated temperatures.

In order to assess the repeatability of the simulations other sets of LHS FEM were carried out for the same slab configuration of Table 1, each with a new calculation of the Latin Hypercube input parameters in accordance with the procedure described by OLSSON ET AL. [16]. A comparison for the mean $\mu_{MR,fi,t}$ and coefficient of variation $\delta_{MR,fi,t}$ is presented in Figure 3, together with results for an identical slab configuration taken from [21] where Monte Carlo (MC) simulations were used together with a simplified cross-section calculation procedure adapted from [22].

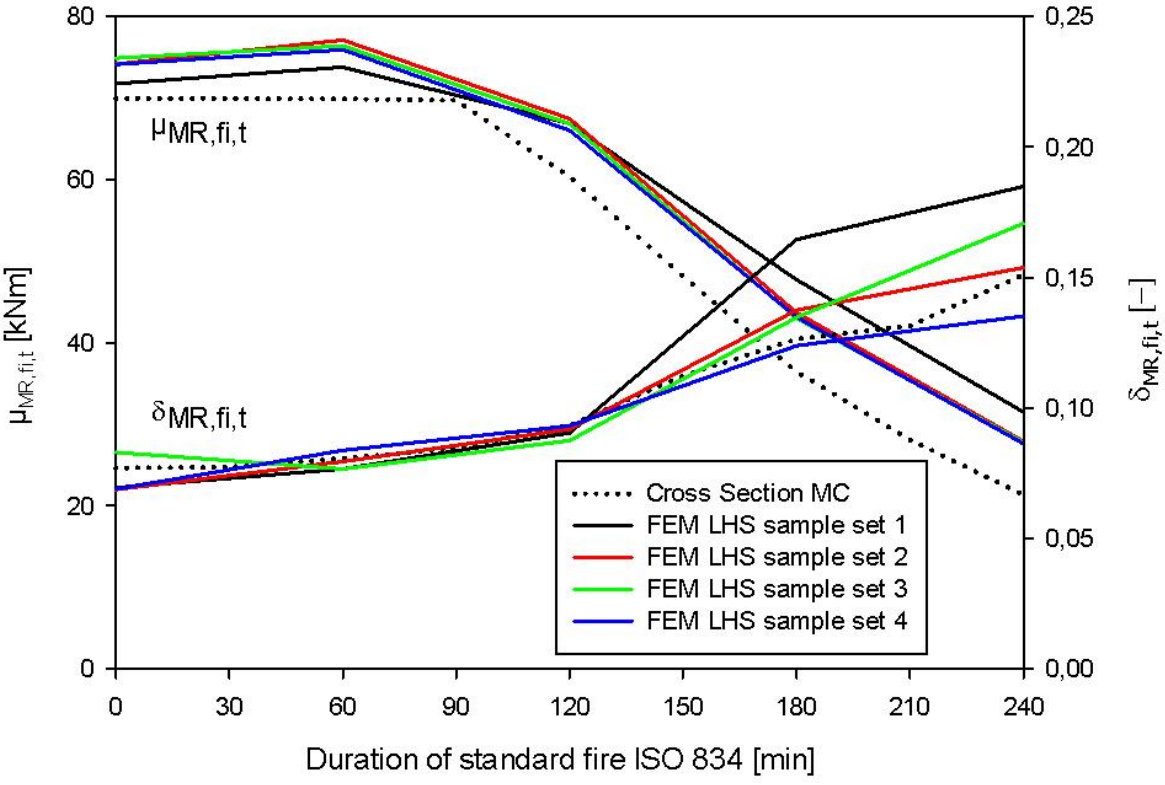

Figure 3. Mean bending moment capacity $\mu_{MR,fi,t}$ and coefficient of variation $\delta_{MR,fi,t}$ for the cross section calculation method and the FEM LHS method

The LHS FEM estimations of the mean bending moment capacity $\mu_{MR,fi,t}$ are very similar for all four LHS procedures carried out. Similarly, up to 120 minutes of fire exposure there is only a minor difference for the four LHS

procedures with respect to the coefficient of variation $\delta_{MR,fi,t}$. There is however a larger scatter with respect to $\delta_{MR,fi,t}$ for fire exposure times exceeding 120 minutes. It is suggested that a small number of samples for the LHS procedure is sufficient for calculations at lower temperatures, but a larger number of samples may be required to have a more accurate estimation of the coefficient of variation during fire.

As can be expected the non-linear FEM calculations indicate a higher average bending moment capacity than calculated by the simplified cross-section calculations. Furthermore, the strength reserve found by the FEM calculations as compared to the simplified calculation increases from 5% at 0 minutes of exposure to approximately 35% at 240 minutes of exposure. It is concluded that the use of a FEM can have significant advantages for the calculation of concrete elements exposed to fire.

There is no clear difference in coefficient of variation $\delta_{MR,fi,t}$ for the cross section MC simulations and the LHS FEM. However, a larger number of samples may be required to have a better estimation of the coefficient of variation for the LHS FEM procedure.

Assuming a lognormal distribution for the bending moment capacity, equations (9) and (16) can be evaluated. It is however unclear which model uncertainty K_R is appropriate for non-linear FEM analysis [20]. If one calibrates K_R for the specific slab configuration investigated in this paper so that the reliability index β_{slab} for the LHS FEM procedure is approximately equal to β_{slab} for the simplified MC procedure at 20°C (i.e. at 0 min of exposure to the ISO 834 standard fire curve), a lognormal distribution with mean 1.05 and standard deviation 0.1 can be proposed, which lies within the boundaries for the model uncertainty for FEM as suggested by [17]. In Figure 4 the reliability index at 0 minutes of exposure (i.e. at 20°C) for the four LHS of 10 samples each and the simplified MC calculation (1000 samples) are presented.

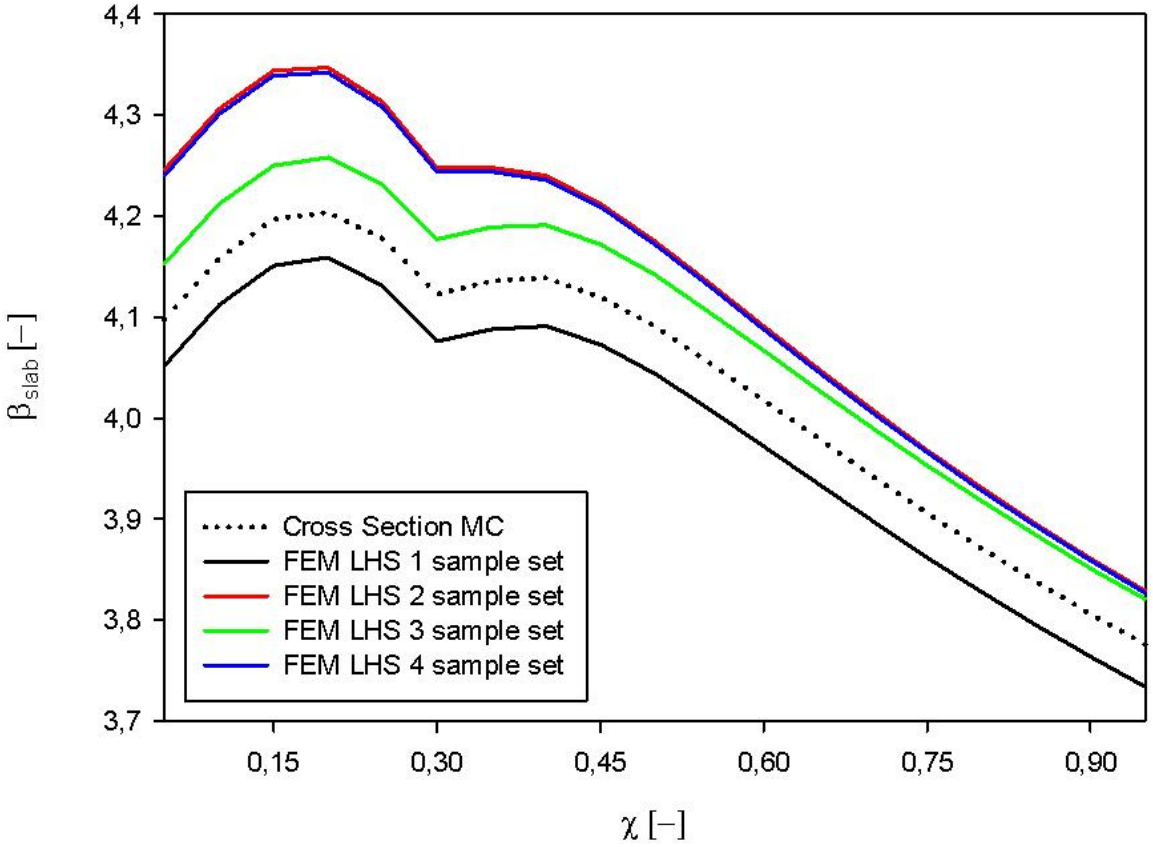

Figure 4. Reliability index at 20°C as a function of the variable to total load ratio χ, for the cross section calculation method (1000 samples) and the FEM LHS method (10 samples)

For this specific situation of LHS FEM calculations the K_R with mean 1.05 and coefficient of variation 0.1 can be considered appropriate.

The results of the evaluation of equations (9) and (16) are presented in Figure 5.

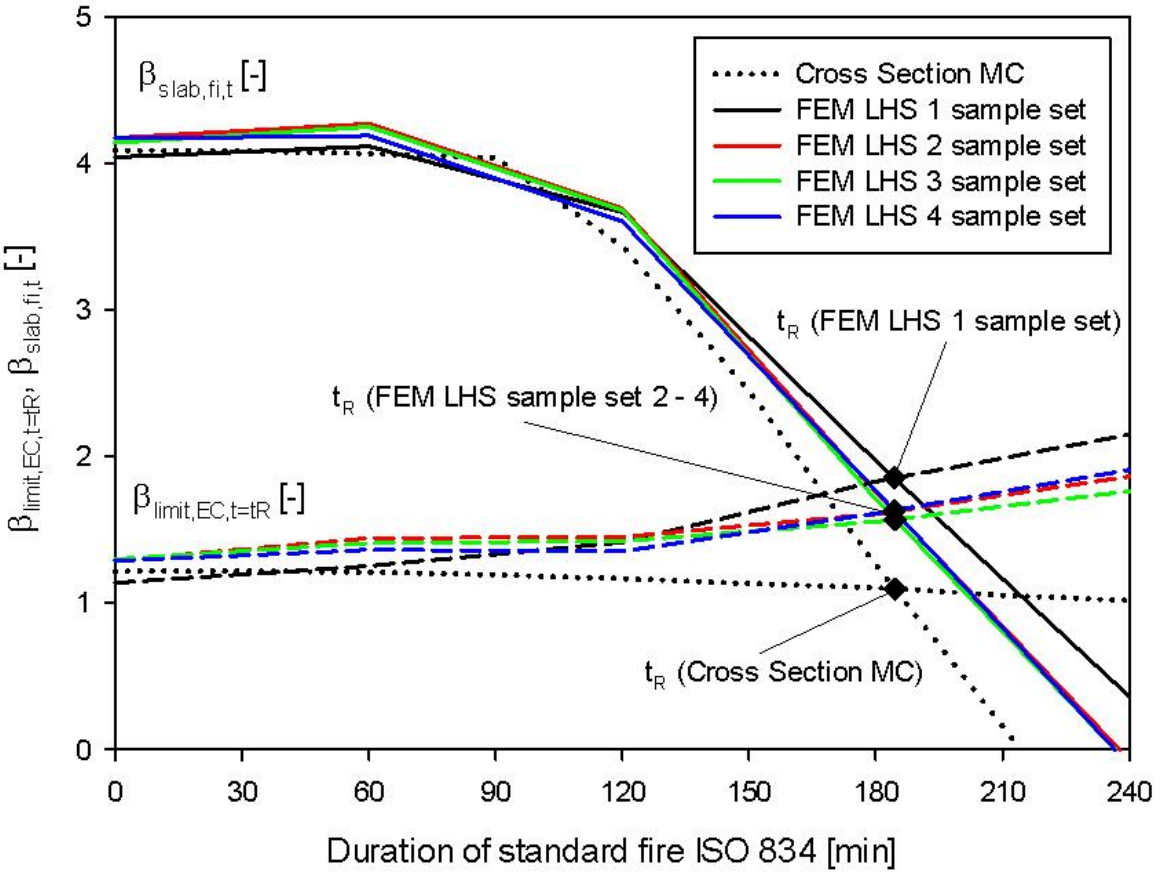

Figure 5. Evolution of $\beta_{slab,fi,t}$ and $\beta_{limit,EC,t=tR}$ as a function of the ISO 834 exposure time and calculated fire resistance time t_R for different calculation methods ($\chi = 0.5$)

As expected, the calibration of the model uncertainty K_R results in a similar reliability index β_{slab} for both calculation procedures (LHS FEM and simplified cross section MC) up to 90 minutes of exposure to the ISO 834 standard fire curve. However, for exposure times larger than 120 minutes, the LHS FEM calculations indicate a higher reliability index $\beta_{slab,fi,t}$.

A large difference is found with respect to the implicit Eurocode limit value for the reliability index $\beta_{limit,EC,t=tR}$. For the simplified cross section MC simulations a reduction of $\beta_{limit,EC,t=tR}$ is found during fire exposure which indicates that according to the cross section MC method the Eurocode design value for the bending moment capacity corresponds to a less conservative characteristic value of the actual bending moment capacity during fire. However, in the FEM calculations considerable strength reserves were found as compared to the simplified cross section calculations (i.e. in Figure 3 the estimation of the mean bending moment capacity by the FEM calculations is significantly higher than the estimation by the cross section calculations). This results in an

increase of $\beta_{limit,EC,t=tR}$ during fire, which indicates that according to the FEM calculations, the Eurocode design value during fire corresponds with a more conservative characteristic of the distribution of the bending moment capacity.

It should be noted that using the model uncertainty K_R for FEM calculations proposed by JCSS [12], i.e. a lognormal distribution with mean 1.2 and coefficient of variation 0.15 (standard deviation 0.18) results in a significantly higher estimation of the reliability index at exposure times larger than 120 minutes. Therefore, the model uncertainty proposed by JCSS is found to be unsafe for these specific calculations. A literature study on model uncertainties by SYKORA ET AL. [20] illustrates that there is currently no consensus on the model uncertainty to be used for FEM calculations.

The structural fire resistance time t_R is determined by the intersection of $\beta_{slab,fi,t}$ and $\beta_{limit,EC,t=tR}$. In Figure 5 $\beta_{slab,fi,t}$ is defined by the assumption that $M_{Rd} = M_{Ed}$ at ambient conditions (i.e. at 20°C). Both calculation methods and all LHS FEM calculations result in approximately the same fire resistance time t_R, but a difference is found for the reliability index at the fire resistance time. It is concluded that the proposed methodology allows for an objective comparison of different design alternatives with respect to the fire resistance time t_R, irrespective of the calculation procedure used. This property can be of interest for structural fire safety engineering when using FEM to design equivalent solutions to prescriptive codes based on simple cross section calculations. The FEM calculations indicate a higher reliability index β at the fire resistance time as compared to simplified cross section calculations. Therefore FEM calculations of concrete elements exposed to fire can constitute considerable advantages when performing a reliability optimization.

5 Conclusions

- The combination of Latin Hypercube Sampling and non-linear Finite Element Models is found to be an efficient calculation procedure for the analysis of concrete elements exposed to fire.
- At 20°C the mean bending moment capacity calculated by the FEM procedure is only slightly higher than the one determined by a simplified cross-section calculation. However, during fire the FEM calcula-

tions result in a significantly higher bending moment capacity, indicating that FEM calculations for concrete elements exposed to fire can have considerable advantages for design.

- There is currently no consensus on the model uncertainty K_R for the resistance effect to be used for non-linear FEM calculations at 20°C. A lognormal distribution with mean 1.05 and coefficient of variation 0.1 is proposed for the specific situation investigated, chosen according to the suggestions found in literature. However it is questionable whether the same model uncertainty is appropriate at elevated temperatures.

- A probabilistic procedure for the calculation of the structural fire resistance time t_R is proposed which allows for an objective comparison of different design alternatives. With respect to t_R, the proposed methodology is found to be independent of the calculation method used (Finite Element Model or simplified cross section calculation method). However, the FEM calculations indicate a higher reliability index β at the fire resistance time as compared to simplified cross section calculations. Therefore FEM calculations of concrete elements exposed to fire can constitute considerable advantages when performing a reliability optimization.

6 Acknowledgements

RUBEN VAN COILE is a Research Assistant of the FWO Research Foundation Flanders. The authors wish to thank the FWO for the financial support on the research project "Probabilistic Formulation of the structural reliability of concrete structures subjected to fire in relation to risk-based decision making and risk-transfer mechanisms".

7 References

[1] Ang, A.H.-S.; Tang, W.H., *Probability concepts in engineering (2nd edition)*. John Wiley & Sons, 2007

[2] Au, S.K.; Wang, Z.-H.; Lo, S.-M.: Compartment fire risk analysis by advanced Monte Carlo simulation. *Engineering Structures*, 29 (2007), p. 2381-2390

[3] Benjamin, J.R.; Cornell, C.A.*: Probability, Statistics and Decision for Civil Engineers*. McGraw-Hill, 1970

[4] CEN.: *European Standard EN 1990: Eurocode 0: Basis of structural design*. Brussels, 2002

[5] CEN.: *European Standard EN 1992-1-2: Eurocode 2: Design of concrete structures: Part 1-2: Structural fire design*. Brussels, 2004.

[6] Gulvanessian, H.; Calgaro, J.-A.; Holický, M.: *Designer's guide to EN 1990: Eurcode 0: Basis for structural design.* Thomas Telford, 2002

[7] Guo, Q.; Jeffers, A.E.: Finite Element Reliability Analysis for Structural Safety Evaluation in Fire. In: Fontana, M.; Frangi, A.; Knobloch, M. (eds): *Proceedings of the 7th International Conference on Structures in Fire*. Zürich, 2012, p. 469-478

[8] Hasofer, A.M.; Qu, J.: Response surface modelling of monte carlo fire data. *Fire Safety Journal* 37 (2002), p. 772-784

[9] Holický, M.; Sýkora, M.: Stochastic models in analysis of structural reliability. *Proceedings of the International Symposium on Stochastic Models in Reliability Engineering, Life Sciences and Operation Management*. Beer Sheva, 2010

[10] Holický, M.; Retief, J.V.; Dunaiski, P.E.: The reliability basis of design for structural resistance. *Proceedings of the Third International Conference on Structural Engineering, Mechanics and Computation (SEMC)*. Cape Town, 2007

[11] ISO 834, *Fire Resistance Tests – Elements of Buildings Construction – Part I - General Requirement*, 1999

[12] Joint Committee on Structural Safety: *JCSS Probabilistic Model Code*, www.jcss.byg.dtu.dk, Zürich, 2006

[13] Kang, S.-C.; Koh, H.-M.; Choo, J.F.: An efficient response surface method using moving least squares approximation for structural reliability analysis. *Probabilistic Engineering Mechanics*, 25 (2010), p. 365-371

[14] Keramat, M.; Kielbasa, R.: Latin Hypercube Sampling Monte Carlo Estimation of Average Quality Index for Integrated Circuits. *Analog Integrated Circuits And Signal Processing* 14 (1997), p. 131-142

[15] Novák, D.; Vorechovský, M.; Lehký, D.; Rusina, R.; Pukl, R.; Cervenka, V.: Stochastic nonlinear fracture mechanics finite element analysis of concrete structures. *Proceedings of the 9th International Conference on Structural Safety and Reliability (ICOSSAR)*. Rome, 2005, p. 781-788

[16] Olsson, A.; Sandberg, G.; Dahlblom, O.: On Latin Hypercube Sampling for Structural Reliability Analysis. *Structural Safety* 25 (2003), p. 47-68

[17] Schlune, H.; Plos, M.; Gylltoft, K.: Safety formats for nonlinear analysis tested on concrete beams subjected to shear forces and bending moments. *Engineering Structures*, 33 (2011), p. 2350-2356

[18] Shi, K.; Guo, Q.; Jeffers, A.E.: Stochastic analysis of structures in fire by Monte Carlo simulation. In: Wald, F; Horová, K.; Jirku, J. (eds.): *Proceedings of the Application of Structural Fire Engineering Conference (ASFE)*. Prague, 2011, p. 355-360

[19] Sidibé, K., Duprat, F., Pinglot, M. and Bourret, B., Fire Safety of Reinforced Concrete Columns, *ACI Structural Journal*, 97 (2000), p. 642-647

[20] Sýkora, M.; Cervenka, V.; Holický, M.: Assessment of model uncertainties in the analysis of reinforced concrete structures. In: Naprstek, J.; Fischer, C. (eds): *Proceedings of the 18th International Conference on Engineering Mechanics*. Svratka, 2012

[21] Van Coile, R.; Caspeele, R.; Taerwe, L.: Global Resistance Factor for Concrete Slabs exposed to Fire, In: Fontana, M.; Frangi, A.; Knobloch, M. (eds): *Proceedings of the 7th International Conference on Structures in Fire*. Zürich, 2012, p. 775-784

[22] Van Coile, R.; Annerel, E.; Caspeele, R.; Taerwe, L.: Assessment of the safety level of concrete slabs during fire. *Fire Safety Science – Proceedings of the 10th International Symposium*. Maryland, 2011, 1115-1124

[23] Van Coile, R.; Caspeele, R.; Annerel, E.; Taerwe, L.: Assessment of the reduction of the safety level of concrete slabs during fire. In: Gucma, L.; Van Gelder, P.; Proske, D. (eds.): *Proceedings of the 8th International Probabilistic Workshop*. Szczecin, 2010, p. 61-72

Reliability of a crankshaft by using Markov chain model with a probabilistic approach.

Nik Abdullah Nik Mohamed, Salvinder Singh Karam Singh
Faculty of Engineering and Built Environment, Department of Mechanical Engineering, Universiti Kebangsaan Malaysia, Malaysia.

Mohd Salmi Md Noorani
Faculty of Science and Technology, Universiti Kebangsaan Malaysia, Malaysia.

Abstract: This paper describes the probabilistic method of using Markov chain model to determine the reliability of the crankshaft based on the Weibull distribution. The crankshafts are constantly subjected to cyclic loading which will tend to display the effects of fatigue which is stochastic in nature. The bending stresses are due to self-weight of the piston, connecting rod and other components or misalignment of the piston and torsion stress. Therefore, the fatigue failures generally are of the rotating bending type and torsional based on the nature of its working condition. The Markov chain model was constructed and the probability method was selected to represent the bending and torsion loads acting on the crankshaft for a range of operating hours. The criteria for probability loading for bending would be higher compared to torsion because the initial loading for the crankshaft is bending due to its working condition. Based from the Markov chain model, the shape and scale parameter was calculated and was used to determine the Weibull probability density function, cumulative distribution function, hazard rate and hazard rate-reliability. It was observed from the characteristic of the Weibull shape parameter that the failure due to bending-torsion was an increasing failure rate (IFR) with the mean load to failure (MLTF) 3.4 MPa. This can be seen from the behaviour of the crack that shows it propagates from the fillet region towards the oil seal at a 45 degree angle.

1 Introduction

In this paper, the concept of probabilistic approach will be introduced by using the Markov chain model in determining the failure of a crankshaft based on bending and torsional loading. The aim of this paper was to develop the reliability and statistical analysis on the crankshaft by using the Markov chain model based on the applied loads. The development of the probabilistic approach by using this model provides an alternative method in determining

the failure of the crankshaft, whereby this model looks at a sequence of events, and analyzes the tendency of one event to be followed by another.

From the developed Markov chain model, a new sequence of random but related events, which will look similar to the original event, was generated. The model developed was useful in analyzing dependent random events - that is, events whose likelihood depends on what happened last over a transition time.

Bending and torsion are main types of loading that will occur on the crankshaft. The failures acting on the crankshaft are generally of the torsional and rotating bending based on the nature of its working condition. The operating condition of the crankshaft is that it will rotate at 720 degree for a complete 4-stroke cycle which consist of the intake, combustion, power and exhaust stoke. During the combustion and power cycle the pressure acting on the piston head will be the highest where the compressed air–fuel mixture will be ignited, usually by a spark plug, which in return will be ignited due to the heat generated from the air-fuel mixture during the compression stroke. This resulting massive pressure from the combustion of the compressed fuel-air mixture forces the piston back down toward bottom dead centre based on operating procedure of the crankshaft.

Salvatore et al. [12] mentioned that the reliability of the crankshaft is the construction of the model that can be represented by the time to failure of the crankshaft based on the distribution of load. From the reliability point of view, it is possible that the crankshaft has influence on other sub-components of the vehicle such as the connecting rod and the engine block. This can be used in characterising the reliability dynamics of the crankshaft.

Hyun Jung et al. [5] mentioned that the crankshaft is the core element of the engine of a vehicle, that transforms the translation motion generated by combustion to rotational motion. Therefore the failure of crankshaft can cause serious damage to the engine even though the crankshaft must be designed to last a lifetime of an engine. Hyun Jung et al. [5] also did mention that practical case and investigation revealed that bending stress is much serve than torsion. The fillet region is the highest point of stress on the crankshaft due to loads from bending and torsion simultaneously. The failure due to cracks at the fillet region starts from the fillet region and will propagate along the journal to the oilseal due to irregularities during the manufacturing process.

Asi [10] mentioned that the main reason of failure in a crankshaft is due to the cyclic loading during rotation on its axis. The crankshaft is normally subjected to bending stresses due to self-weight of the piston, connecting rod

and other components or misalignment of the piston and torsion stress. Even though the crankshaft is manufactured to have mechanical properties with high strength, high toughness and good machining ability by using ductile cast iron with spheroidal graphite mentioned by Asi [10], but the failure of the crankshaft is still unavoidable due to the cyclic loading. Therefore the crankshaft which is under constant cyclic loading will tend to display fatigue due to the type of loading (bending, torsion, reverse bending) applied on it.

The crankshaft undergoes constant amplitude loading during the intake and exhaust cycle of the piston and variable amplitude loading during the compression and power cycles due to the combustion pressure that is acting on the head of the piston. The main reason for failure of the shaft is due to the initiation of cracks, which begins at the fillet region of the crankshaft and propagates towards the oil seal at the journal by using the finite element (FE) technique as performed by Taylor et al. [3]. The FE method was done to determine the hot zones (which would be the most probable) by using various sizes of mesh and comparing it with the experimental data. The hot zones were used to estimate the region where crack would most likely initiate and propagate based on the stress concentration. Any dependent or independent loading (bending and torsion) acting on the crankshaft will result in stress field with 2 extremes:

1. Magnitude of the principal stresses.
2. Direction of the principal stresses.

Experimental analysis such as SEM, fractography, tensile test, hardness test, chemical analysis, x-ray analysis (EDAX) and visual examination was conducted to determine the failure of the crankshaft based on the operating hours as shown in [1,6,9,10,11,13,17]. It can be concluded from the experimental analysis that the failure time varies based on the cyclic loading acting on the crankshaft and where the failure time occurred are very random between the operating hours due to the load applied and the material properties of the crankshaft.

Silva [6] stated that the mechanical fatigue failure of the crankshaft was because of high stress concentration due to high cycle and low stress and that varies based on the type of cyclic loading. This type of failure is due to misalignment of the shaft, originating rotating-bending or vibration due to some problem with the main bearing or incorrect fillet sizes. Figure 1 shows the location and direction of the crack where the depth of a notch behaves as a crack.

Figure 1.Crack propagation in the crankshaft [10].

The lumped model method was developed by Becarra et al. [7], where this model is a simplified method of assuming that the system is in a rigid body and there are interactions between each rigid body in the form of kinematic pair or springs or dampers. The simplifying assumptions in this model are:

1. Objects are rigid bodies.
2. Interactions between rigid bodies take place via kinematic pairs (*joints*), springs and dampers.

By using this method, the crankshaft was divided into various degrees of freedom depending on the number of pistons and analysed individually based on the loads. These individual results will be combined to determine the harmonic torsional due to radial loads of the cylinder pressure transmitted by the piston and connecting rod. By doing this, it allows a dynamic analysis on the shaft to be calculated by considering the bending-torsional loads.

As a conclusion, various methods such as FE method, experimental analysis and the lumped model method had been carried out by previous researches to model the failure of the crankshaft. The significance between all these studies is that the failure of the crankshaft was due to torsion given bending loads.

2 Methodology

The failure of the shaft can be mathematically modelled in the conditional probability where the probability of failure for the crankshaft is due to torsion (T) given bending (B) during operating condition as shown in equation (1).

$$P(T|B) = \frac{P(T \cap B)}{P(B)} \quad (1)$$

Since failure is random, therefore the failure of the system would be stochastic in nature. The Markov chain model has the property to provide information for future state, where the future state is independent of the past

state given that we know the present state, which has the similar properties of the crankshaft under operating condition.

The Markov chain model for loading on the crankshaft system was set in two states, i.e. bending and torsion as shown in Figure 2. This model is in the recurrent state whereby the loading of bending and torsion will be repeating over time.

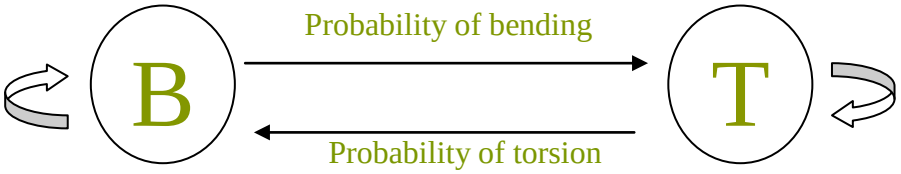

Figure 2. Markov chain state diagram of the crankshaft

The probabilistic equation of the Markov chain from Figure 2 can be modelled as a memoryless condition based on equation (2), where it describes the probability (P_r) of going from the bending state to the torsion state and vice versa was based only on the given present state regardless of its past condition.

$$P_r\{X_1 = T|X_0 = B\} = P_r\{X_{n+1} = T|X_n = B\} \quad (2)$$

Each probability matrices of bending (P_B) and torsion, (P_T) is set to be independent of each other where each of the probability of failure due to bending and torsion is a compliment of each other. In other words, for each P_T, it will contain the remaining P_B and vice-versa for P_T, as shown in equation (3).

$$P_r = \begin{cases} P_B = 1 - P_T \\ P_T = 1 - P_B \end{cases} \quad (3)$$

The torsion loading would only start to take effect when the crankshaft is in the operating condition, due to rotation on its axis. Hence, the probability matrix for the crankshaft (P) based on the operating hours (n) can be illustrated in equation (4).

$$P = \begin{bmatrix} P_T & P_{TB} \\ P_{BT} & P_B \end{bmatrix}^n \quad (4)$$

The Chapman-Kolmogorov method as shown in equation (5) was derived to observe the changes that would over the loading states as time increases whereby the outcome of each transition time is independent on its initial condition. This was done to observe was there any steady state condition for the probability matrix provided.

The importance for a steady state condition was to observe the changes of the states over a given period of time as in the tendency of the probability to diverge from an independent state to a dependent state.

$$P_{BT}^{(n)} = \sum_{k=0}^{m} P_{Bk}^{(m)} P_{kT}^{(n-m)} \text{ ; where } 1 \leq m \leq n-1 \quad (5)$$

The probability for bending and torsional loading will be acting independently in this transition time where the present situation is not dependent on the past. Therefore, the expected value E(X), for the bending-torsion loading over the transition time can be calculated by determining the probability vector (μ) as the initial condition together with the loading vector (L) of maximum and minimum loads acting on the crankshaft based on equation (6).

$$E(X) = \mu . P^{n}[L] \quad (6)$$

From equation (6), the shape parameter (β) and scale parameter (θ), can be derived to determine the type of Weibull distribution, hazard rate function (λ), and mean load to failure (MTLF) as shown in equation (7) and (8).

$$\lambda(L) = \frac{\beta}{\theta}\left(\frac{L}{\theta}\right)^{\beta-1} \quad (7)$$

$$MLTF = \theta\Gamma\left(1+\frac{1}{\beta}\right) \quad (8)$$

An important aspect of the Weibull distribution is how the values of the shape parameter and the scale parameter affect the distribution characteristics as in the shape of the probability density function, the reliability and the failure rate. The Weibull provides a good model for failure as it considers a variety of shape parameter.

3 Results and Discussion

The experimental data collected shown in Table 1 was for 2 cycles; power and combustion cycle.

Table 1. Experimental results for loading on each RPM. (Data from UTP DI CNG: UKM)

RPM	Minimum Load (MPa)	Maximum Load (MPa)
1000	1.00×10^5	5.23×10^6
2000	1.00×10^5	6.10×10^6
3000	1.06×10^5	6.50×10^6
4000	1.08×10^5	6.90×10^6
5000	1.09×10^5	7.50×10^6
5400	1.09×10^5	8.00×10^6

This is because during the combustion and power cycle the pressure acting on the piston head will be the highest where the compressed air–fuel mixture will be ignited resulting massive pressure from the combustion of the compressed fuel-air mixture forces the piston back down toward bottom dead centre.

The intake and exhaust data were neglected because the piston is working at a minimal and constant loading as shown in Figure 3.

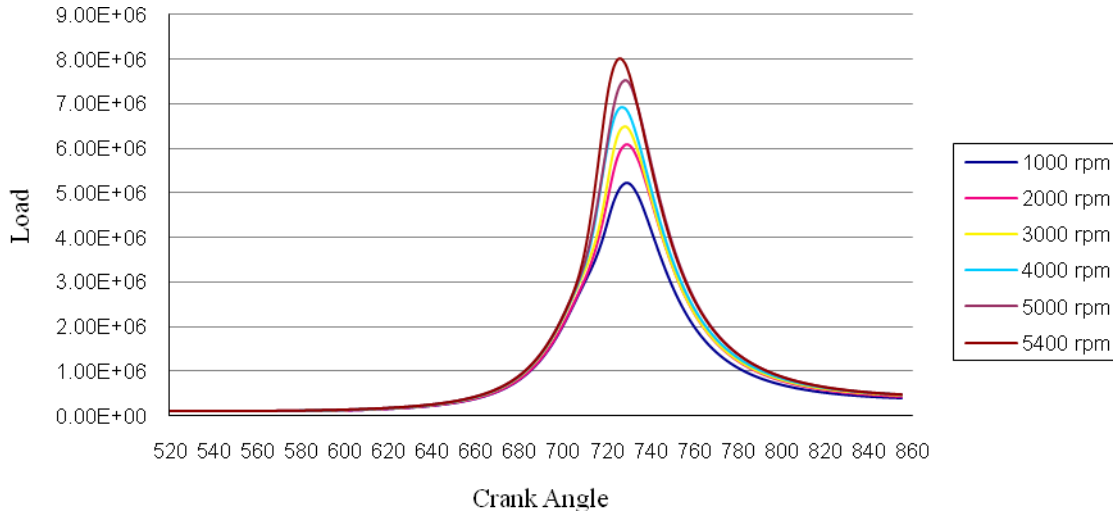

Figure 3. Loading on the crankshaft based on the crank angle of the piston

The crankshaft is subjected to various pressures but generally needs to be analyzed in two positions. Firstly, failure may occur at the position of maximum bending; this may be at the centre of the crank or at either end. In such a condition the failure is due to bending and the pressure in the cylinder is maximum as stated in [3,14]. Secondly, the crank may fail due to twisting, so the connecting rod needs to be checked for shear at the position of maximal twisting. The pressure at this position is the maximal pressure, but only a fraction of maximal pressure as stated by Asi [10].

The probability of bending should be higher compared to the probability of torsion as the failure of the crankshaft would begin from bending state due to its pre load due to the self-weight and misalignment of the piston. Therefore the expected value from equation (6) was used to simulate a statistical analysis based on the experimental loading as shown in Table 2.

Table 2. Simulated results from loading for each RPM from equation (3).

RPM	Minimum Load (MPa)	Maximum Load (MPa)	Mean Load (MPa)	Std. Dev. (MPa)
1000	1.06×10^5	5.20×10^6	2.68×10^6	1.16×10^6
2000	1.06×10^5	6.06×10^6	3.12×10^6	1.35×10^6

3000	1.14×10^5	6.46×10^6	3.33×10^6	1.45×10^6
4000	1.16×10^5	6.86×10^6	3.53×10^6	1.54×10^6
5000	1.18×10^5	7.45×10^6	3.83×10^6	1.67×10^6
5400	1.18×10^5	7.90×10^6	4.08×10^6	1.79×10^6

The expected value equation used has the ability to provide statistical analysis with an error ranging from 5-10% as it was shown in 2. This error is considered minimal as it is assumed that the errors occurred due to geometry dimension of the shaft, size of the fillet on the journal and irregularities during the manufacturing process as shown by [1,4-7,10,11,15] through their experimental analysis.

The probability density function (PDF) and cumulative distribution function (CDF) as shown in Figure 4 were plotted to observe the distribution of the simulated data.

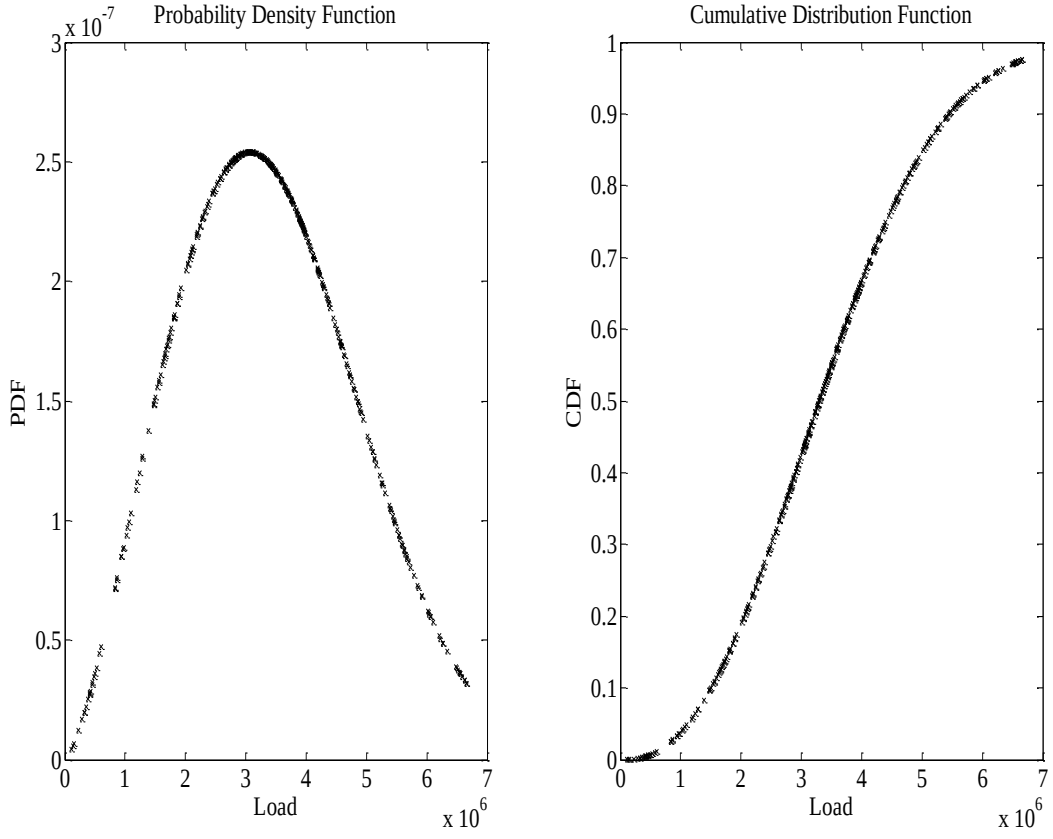

Figure 4. Distribution of the loads

Based from the shape (β) and scale parameter (θ) of the distribution, the MTLF can be calculated and is shown in Table 3.

Table 3. Shape and scale parameter under operating condition from 1000-5400 RPM

RPM	Shape Parameter (β)	Scale Parameter (θ)	MLTF (MPa)	Mean Load (MPa)
1000-5400	2.4	3.85×10^6	3.40×10^6	3.48×10^6

The various shape parameters influences the hazard rate whereby it provides information regarding the behaviour of the failure process in Table 4 as it was shown by Ebeling [2].

Table 4. Shape parameter properties.

Shape Parameter	Properties
$0 < \beta < 1$	Decreasing failure rate
$\beta = 1$	Exponential distribution
$0 < \beta < 1$	Increasing failure rate, concave
$\beta = 1$	Rayleigh distribution
$\beta > 2$	Increasing failure rate, convex
$3 \leq \beta \leq 4$	Increasing failure rate, approaches normal distribution; symmetrical

By comparing the shape parameter obtained from Table 3 and its properties from Table 4, it can be concluded that the crankshaft has that increasing failure rate as shown in Figure 5.

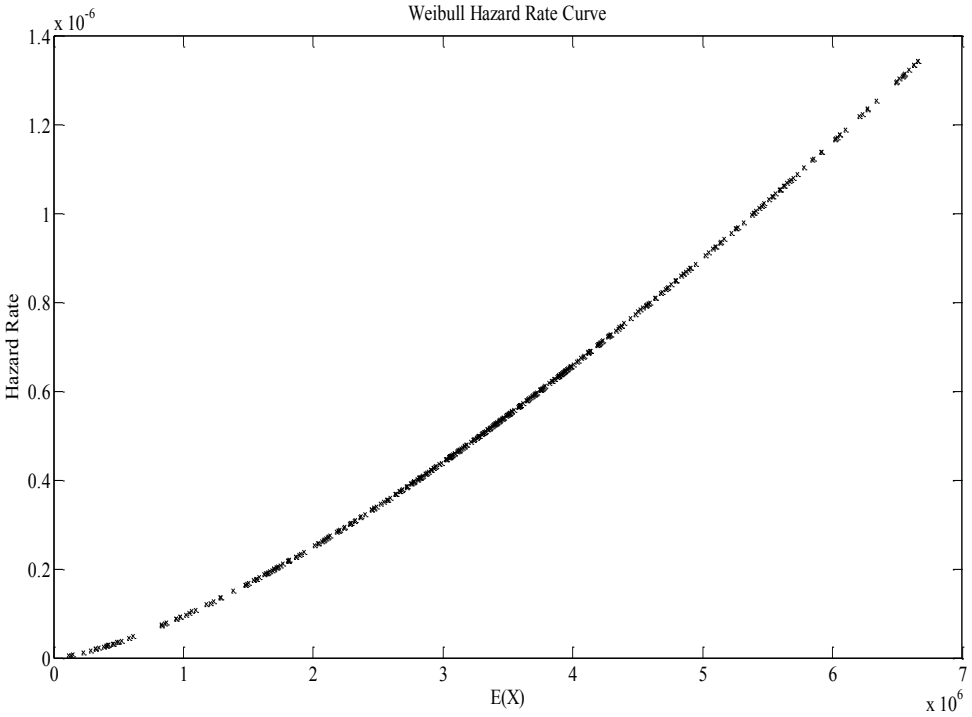

Figure 5. Distribution of the expected loads, E(X).

The reason for an increasing failure rate will affect the reliability of the crankshaft as shown in Figure 6. This was due to fluctuation of loading during

power and combustion cycles with a high number of cycles during operating condition, impurities of the material and misalignment of the connecting rods .

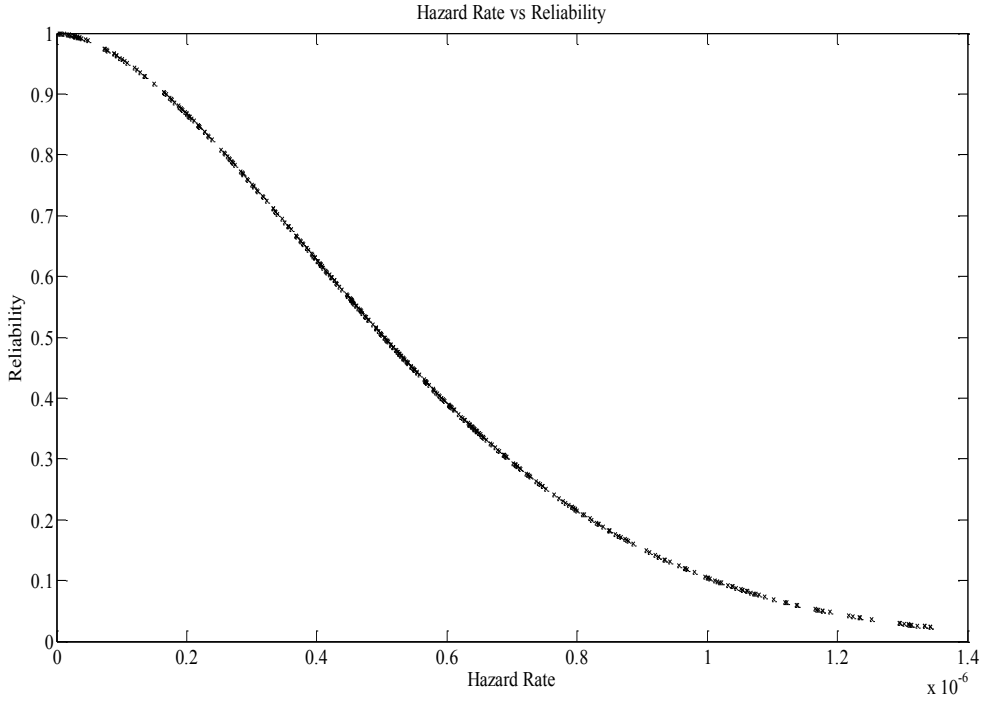

Figure 6. Reliability- Hazard Rate

The Weibull probability plot as shown in Figure 7 was constructed to observe the probability of failure on the crankshaft over the expected load.

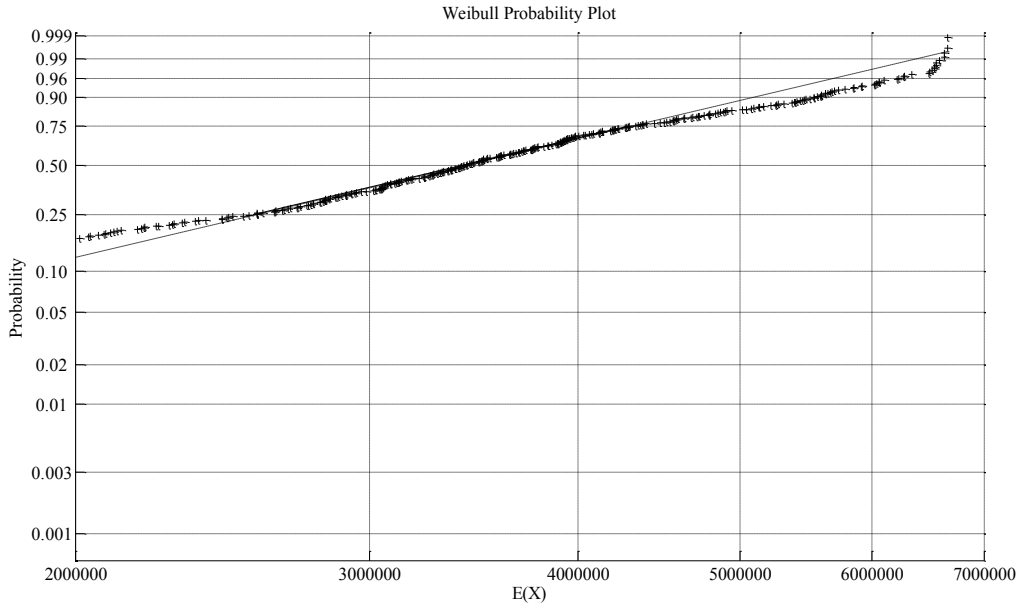

Figure 7. Weibull probability plot

As indicated from Table 4, hazard rate with $\beta < 1$ have a failure rate that decreases with load, also known as infantile or early-life failures where as hazard rate with β close to or equal to 1 have a fairly constant failure rate, indicative of useful life or random failures. Finally hazard rate with $\beta > 1$ have a failure rate that increases with time, also known as wear-out failures. These comprise the three sections of the bathtub curve as shown in Figure 8 whereby a hazard rate with $\beta < 1$, $\beta = 1$ and $\beta > 1$ was plotted to show the behaviour of failure for the crankshaft.

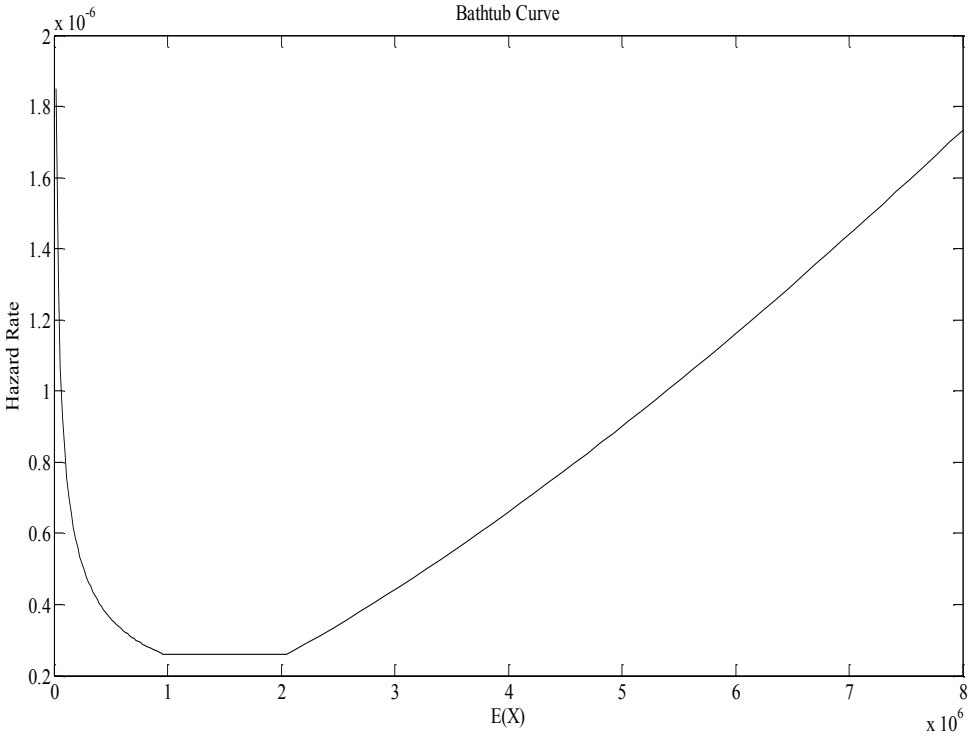

Figure 8: Bathtub curve for the crankshaft

4 Conclusion

The Markov chain model was developed as an alternative method in determining the failure on the crankshaft due to bending and torsional loading. The model has an error of 5-10% after comparing it with the experimental results whereby this model was able to perform reliability and statistical analysis compared to the experimental works done. This error was considered minimal as the errors occurred were due to geometric shape of the crankshaft, radius of the fillet and irregularities during the manufacturing process.

It can be concluded from the reliability analysis on the crankshaft due to loading was the characteristic of the Weibull shape parameter. It was observed that failure due to bending-torsion has properties of an increasing

failure rate (IFR) with the mean load to failure (MLTF) 3.4 MPa. This can be seen from the physical behaviour of the crack that shows it propagates from the fillet region towards the oil seal at a 45 degree angle.

5 Acknowledgement

This study has been funded by the Ministry of Higher Education, Malaysia and thanks to the Centre of Automotive Research, University Kebangsaan Malaysia for providing the necessary information regarding to this study.

6 References

[1] Changli Wang, Chengjie Zhao and Deping Wang. Analysis of an unusual crankshaft failure. *Engineering Failure Analysis* (2005), 12(3): 465-473.

[2] Charles E. Ebeling. *Introduction to Reliability and Maintainability Engineering*. MCGraw-Hill International Editions. 1997

[3] D. Taylor, W.Zhou, A.J. Cielapowicz and J. Devlukia. Mixed mode fatigue from stress concentrations: an approach on equivalent stress intensity. *International Journal of Fatigue* (1999),21(2):173-178.

[4] Dawn An, Joo-Ho Choi, Nam H. Kim and Sriram Pattabhiraman. Fatigue life prediction based on Bayesian approach to incorporate field data into probability model. *Structure Engineering and Mechanics* (2011),37(4):427-442.

[5] Do-Hyun Jung, Hong-Jin Kim, Young-Shik Pyoun and Alisher Gafurov. Reliability prediction of fatigue life of a crankshaft. *Journal of Mechanical Science and Technology* (2009), 23:1071-1074.

[6] F.S. Silva. Analysis of a vehicle crankshaft failure. *Engineering Failure Analysis* (2003), 10(5):606 -616.

[7] J.A. Becarra, F.J. Jimenez, M. Torrez, D.T. Sanchez and E. Carvajal. Failure Analysis of reciprocating compressor crankshafts. *Engineering Failure Analysis* (2011),18(2):735-746.

[8] Julien Chiquet, Nikolaos Limnios and Mohamed Eid. Piecewise deterministic Markov processes applied to fatigue crack growth. *Journal of Statistical Planning and Inference* (2009), 139(5):1657-1667.

[9] M.A. Alfares, A.H. Falah and A.H. Elkholy. Failure analysis of a vehicle engine crankshaft. *Journal of Failure Analysis Prevention* (2007), 7:12-17.

[10] Osman Asi. Failure analysis of a crankshaft made from ductile cast iron. *Engineering Failure Analysis* (2006), 13(8):1260-1267.

[11] R.K. Pandey. Failure of diesel engine crankshaft. *Engineering Failure Analysis* (2003), 10(2):65-175.

[12] Salvatore Distefano and Antonio Peliafito. Reliability and avaliability of dependent dynamic system with DRBD's. *Reliability Engineering and System Safety* (2009), 94(9):1381-1393.

[13] S.K. Bahumik, R. Rangaraju, M.A. Venkataswamy, T.A. Baskaran and M.A. Parameswara. Fatigue fracture of crankshaft of an aircraft engine. *Engineering Failure Analysis* (2002), 9:255-263.

[14] W.F. Wu and C.C. Ni. Probabilistic models of fatigue crack propagation and their experimental verification. *Probabilistic Engineering Mechanics* (2004), 19(3):247-257.

[15] W.Y. Chien, J.Pan, D.Close and S.Ho. Fatigue analysis of crankshaft under bending with consideration of residual stresses. *International Journal of Fatigue* (2005), 27(1):1-19.

[16] Xuanyang Lei, Guicai ZhPang, Ji Chen, Song Xigeng and Guangming Dong. Simulation on the motion of crankshaft with a slant crack in crankpin. *Mechanical Systems and Signal and Processing* (2007), 21:502-513.

[17] Zissimos P. Mourelatos. A crankshaft system model for structural dynamic analysis of internal combustion engines. *Computers and Structures* (2001),79:2009-2027.

Probabilistic assessment of existing structures

Milan Holický, Miroslav Sýkora
Klokner Institute of the Czech Technical University in Prague, Prague

Abstract: Assessment of existing structures is in many aspects different from that taken in designing new buildings. Effects of the construction process and subsequent life of the structure, during which it may have undergone alteration, deterioration, misuse, and other changes to its as-built (as-designed) state, must be taken into account. That is why the assessment of existing structures often requires application of sophisticated probabilistic methods, as a rule beyond the scope of traditional design practice. Updating of probabilities and design values of basic parameters seem to provide effective tools in the assessment of existing structures.

1 Introduction

Assessment of existing structures is becoming a more and more important and frequent engineering task. Continued use of existing structures is of a great significance due to environmental, economic and socio-political benefits, growing larger every year. These aspects are particularly relevant to tall buildings that always constitute a great social, economic and often also architectural value. General principles of sustainable development regularly lead to the need for extension of the life of a structure, in majority of practical cases in conjunction with severe economic constraints.

That is why the assessment of existing structures often requires application of sophisticated methods, as a rule beyond the scope of traditional design codes. Nevertheless, apart from few national codes, three International Standards ISO 2394 [1], ISO 13822 [2] and ISO 12491 [3], related to the assessment of existing structures, have been recently developed. Additional information may be found in a number of scientific papers and publications, for example by Melchers [4], and Ellingwood [5]. Submitted paper is primarily based on previous study by Holicky [6].

The approach to the assessment of an existing structure is in many aspects different from that taken in designing the structure of a newly proposed building. The effects of the construction process and subsequent life of the structure, during which it may have undergone alteration, deterioration, misuse,

and other changes to its as-built (as-designed) state, must be taken into account. However, even though the existing building may be investigated several times, some uncertainty in behaviour of the basic variables shall always remain. Therefore, similarly as in the design of new structures, actual variation in the basic variables describing actions, material properties, geometric data and model uncertainties is taken into account by partial factors or other appropriate code procedures.

In general, an existing structure may be subjected to the assessment of its actual reliability in case of:

- rehabilitation of an existing constructed facility during which new structural members are added to the existing load-carrying system;
- adequacy checking in order to establish whether the existing structure can resist loads associated with the anticipated change in use of the facility, operational changes or extension of its remaining working life;
- repair of an existing structure, which has deteriorated due to time dependent environmental effects or which has suffered damage from accidental actions, for example, earthquake;
- doubts concerning actual reliability of the structure.

Under some circumstances assessments may also be required by authorities, insurance companies or owners or may be demanded by a maintenance plan.

The main general principles of the assessment may be summarized as follows:

- Available scientific knowledge and know-how including currently valid codes should be applied; historical practice and provisions valid in the time when the structure was built (designed) should be used as guidance information only;
- Actual characteristics of structural material, action, geometric data and structural behaviour should be considered; original documentation including drawings should be used as guidance material only.

The first principle should be applied in order to achieve similar reliability level as in case of newly designed structures. The second principle should avoid negligence of any structural condition that may affect actual reliability (in favourable or unfavourable way) of a given structure.

Most of the current codes are developed assuming the concept of limit states in conjunction with the partial factor method. In accordance with this method, which is mostly considered here, basic variables are specified by characteristic or representative values. The design values of the basic variables are determined on the basis of the characteristic (representative) values and appropriate partial factors.

It follows from the second principle that a visual inspection of the assessed structure should be made whenever possible. Practical experience shows that

inspection of the site is also useful to obtain a good feel for actual situation and state of the structure.

As a rule the assessment need not to be performed for those parts of the existing structure that will not be affected by structural changes, rehabilitation, repair, change in use or which are not obviously damaged or are not suspected of having insufficient reliability.

Thus, actual properties of basic variables describing actions, material properties, and geometric data are to be considered. In addition, expected social and economic consequences of a required intervention and possible structural failure should be taken into account. That is why the assessment of existing structures often requires application of sophisticated probabilistic methods, as a rule beyond the scope of traditional design practice.

The most important step of the probabilistic assessment itself is specification of the target reliability level (discussed by Holicky and Retief [7] during the previous International Probabilistic Workshop in Braunschweig), evaluation of inspection data and updating of prior information concerning all the basic variables. Target reliability should be determined on the basis of probabilistic optimization in conjunction with the probability updating. Typically the assessment of existing structures is a cyclic process in which the first preliminary assessment must be often supplemented by subsequent detailed investigations and assessment.

2 Basic variables

In accordance with the above-mentioned general principles, characteristic and representative values of all basic variables shall be determined taking into account the actual situation and state of the structure. Available design documentation is used as a guidance material only. Actual state of the structure should be verified by its inspection to an adequate extent. If appropriate, destructive or non-destructive inspections should be performed and evaluated using statistical methods.

For verification of the structural reliability using partial factor method, the characteristic and representative values of basic variables shall be considered as follows:

- Dimensions of the structural elements shall be determined on the basis of adequate measurements. However, when the original design documentation is available and no changes in dimensions have taken place, the nominal dimensions given in the documentation may be used in the analysis.

- Load characteristics shall be introduced with the values corresponding with the actual situation verified by destructive or non-destructive inspections. When some loads have been reduced or removed completely, the representative values can be reduced or appropriate partial factors can be adjusted. When overloading has been observed in the past it may be appropriate to increase adequately representative values.
- Material properties shall be considered according to the actual state of the structure verified by destructive or non-destructive inspections. When the original design documentation is available and no serious deterioration, design errors or construction errors are suspected, the characteristic values given in original design may be used.
- Model uncertainties shall be considered in the same way as in design stage unless previous structural behaviour (especially damage) indicates otherwise. In some cases model factors, coefficients and other design assumptions may be established from measurements on the existing structure (e.g. wind pressure coefficient, effective width values, etc.).

Thus reliability verification of an existing structure should be backed up by inspection of the structure including collection of appropriate data. Evaluation of prior information and its updating using newly obtained measurements is one of the most important steps of the assessment.

3 Probability updating

Using results of an investigation (qualitative and quantitative inspections, calculations, proof loading) the properties and reliability estimates of the structure may be updated. Two different procedures can be distinguished:

1. Updating of the structural failure probability.
2. Updating of the probability distributions of basic variables.

Direct updating of the structural reliability (procedure (1)) can formally be carried out using the basic formula of probability theory

$$P(F|I) = P(F \cap I) / P(I) \qquad (1)$$

with
- P probability
- F local or global failure
- I inspection information
- $\cap$ intersection of two events.

The inspection information I may consist of the observation that the crack width at the beam B is smaller than at the beam A. An example of probability updating using equation (1) is presented in Section 4.

The updating procedure of a univariate or multivariate probability distribution (procedure (2)) is given formally as

$$f_X(x|I) = C\, P(I|x)\, f_X(x) \qquad (2)$$

with $f_X(x|I)$ updated probability density function of X
$f_X(x)$ probability density function of X before updating
X basic variable or statistical parameter
C normalising constant
$P(I|x)$ likelihood function.

An illustration of equation (2) is presented in Figure 1. In this example updating leads to a more favourable distribution with a greater design value x_d than the prior design value x_d. In general, however, the updated distribution might be also less favourable than the prior distribution.

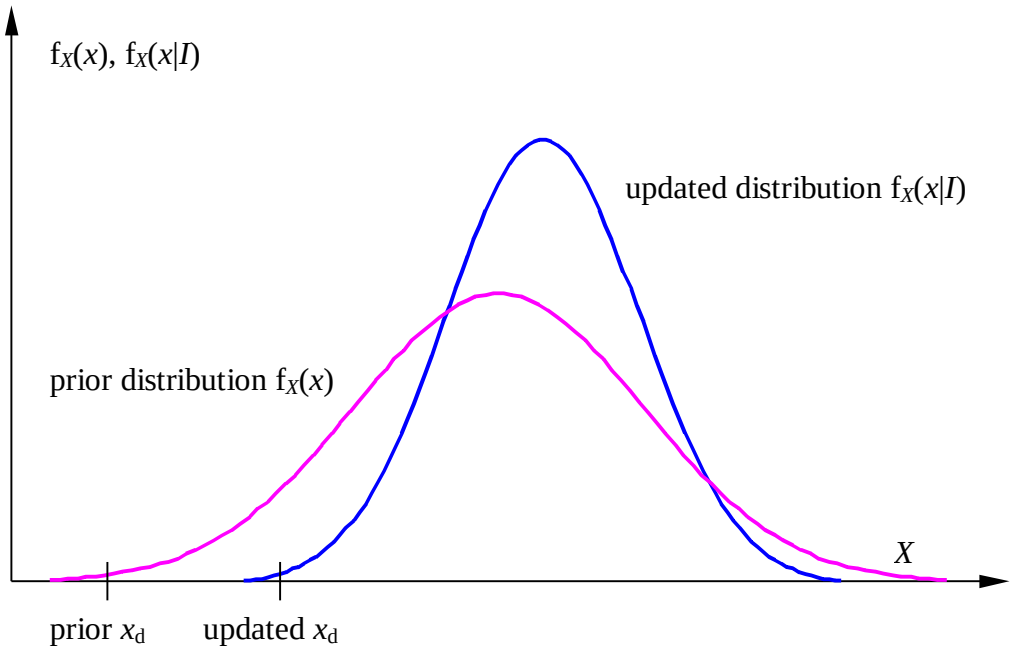

Figure 1. Updating of probability density function for an expected variable X.

The updating procedure can be used to derive updated characteristic and representative values (fractiles of appropriate distributions) of basic variables to be used in the partial factor method or to compare directly action effects with limit values (cracks, displacements). The Bayesian method for fractile updating is described in Sections 6 and 7. More information on updating may be found in ISO 12491 [3].

Once the updated distributions for the basic variables $f_X(x)$ have been found, the updated failure probability $P(F|I)$ may be determined by performing a probabilistic analysis using common methods of structural reliability

$$P(F|I) = \int_{G(X)\le 0} f_X(x|I)\, dx \qquad (3)$$

with $G(X) < 0$ failure domain ($G(X)$ being limit state function).

It should be proved that the probability P($F|I$), given the design values for its basic variables, does not exceed a specified target value.

4 Probability updating of a steel beam

This example of probability updating is adopted from [4,5]. Consider the limit state function G($\boldsymbol{X}$), where $\boldsymbol{X}$ is a vector of basic variables, and the failure F is described by the inequality G($\boldsymbol{X}$) < 0. If the result of an inspection of the structure I is an event described by the inequality $H > 0$ then using equation (1) the updated probability of failure P($F|\ I$) may be written as

$$\mathrm{P}(F|\ I) = \mathrm{P}(\mathrm{G}(\boldsymbol{X}) < 0|\ H > 0) = \mathrm{P}(\mathrm{G}(\boldsymbol{X}) < 0 \cap H > 0) / \mathrm{P}(H > 0) \qquad (4)$$

For example consider a simply supported steel beam of the span L exposed to permanent uniform load g and variable load q. The beam has the plastic section modulus W and the steel strength f_y.

Using the partial factor method the design condition $R_d - S_d > 0$ between the design value R_d of the resistance R and design value S_d of the load effect S may be written as

$$W f_{yk} / \gamma_M - (\gamma_G g_k L^2/8 + \gamma_Q q_k L^2/8) > 0 \qquad (5)$$

with f_{yk} characteristic yield strength
g_k characteristic (nominal) value of permanent load g
q_k characteristic (nominal) value of permanent load q
γ_M, γ_G, γ_Q partial factors of steel, permanent and variable load.

By analogy to equation (5) the limit state function G($\boldsymbol{X}$) follows as

$$\mathrm{G}(\boldsymbol{X}) = R - S = W f_y - (gL^2/8 + qL^2/8) \qquad (6)$$

where all the basic variables are generally considered as random variables described by appropriate probabilistic models.

To verify its reliability the beam has been investigated and a proof loading up to the level q_{test} is carried out. It is assumed that g_{act} is the actual value of the permanent load g. If the beam resistance is sufficient the information I obtained is described as

$$I = \{H > 0\} = \{W f_y - (g_{act} L^2/8 + q_{test} L^2/8) > 0\} \qquad (7)$$

with f_y actual steel strength
g_{act} actual permanent load determined reasonably accurately using non-destructive methods.

It follows from equation (4) that to determine the desired updated probability of failure $P(F|I)$ using equation (4) it is necessary to assess two probabilities $P(G(\boldsymbol{X})<0 \cap |H>0)$ and $P(H > 0)$

$$P(G(\boldsymbol{X}) < 0 \cap H > 0) = P[W f_y - (gL^2/8+qL^2/8) < 0 \cap W f_y - (g_{act}L^2/8 + q_{test} L^2/8)>0] \quad (8)$$

$$P(H > 0) = P(W f_y - (g_{act} L^2/8 + q_{test} L^2/8) > 0) \quad (9)$$

Additional assumptions concerning basic variables are then needed. Having the results of (8) and (9) the updated probability of failure $P(G(\boldsymbol{X}) < 0|H > 0)$ follows from equation (4).

Alternatively, considering results of the proof test, the probability density function $f_R(r)$ of the beam resistance $R = Wf_y$ may be truncated below the proof load as indicated in Figure 2. However the prove loading must be limited by an acceptable level (usually up to load effect corresponding to the serviceability level) to avoid damage of the structure during a test.

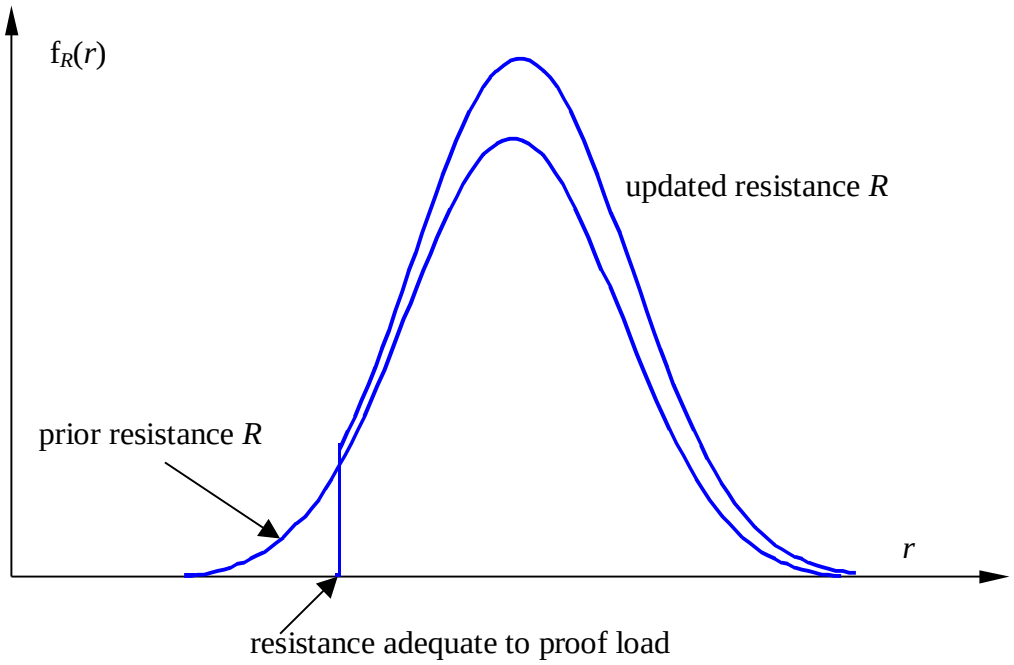

Figure 2 Truncated effect of proof loading on structural resistance.

Obviously, the truncation of structural resistance R decreases the updated probability of structural failure defined as

$$P(F) = P(R - S < 0) \quad (10)$$

and increase, therefore, the updated value of structural reliability.

5 Updating design values of basic variables

A more practical procedure is to determine updated design values for each basic variable (procedure (2)). For a resistance parameter X, the design value x_d can be obtained using operational formula given in ISO 2394 [1], ISO 12491 [3] and study [6]. For normal and lognormal random variable it holds

$$x_d = \mu(1 - \alpha\beta V) \quad (11)$$

$$x_d = \mu \exp[-\alpha\beta\sqrt{(\ln(1 + V^2)) - 0.5 \ln(1 + V^2)}] \quad (12)$$

with x_d updated design value of X
μ updated mean value
α FORM sensitivity factor
β target reliability index
V updated coefficient of variation of X.

Note that $\sqrt{\ln(1+V^2)} \approx V$ is equal to the standard deviation of the transformed variable $\ln(X)$.

The value of the target reliability index β is discussed by Holicky and Retief [7], the sensitivity factors α can be taken equal to those commonly used for new structures (the values −0.7 for the dominating load parameter, +0.8 for the dominating resistance parameter and the reduced values to 40 % for non-dominating variables are recommended in ISO 2394 [1]).

As an alternative to procedure (2), one might also determine the characteristic value x_k first and calculate the design value x_d by applying the appropriate partial factor γ_m

$$x_d = x_k / \gamma_m \quad (13)$$

For normal and lognormal random variable X the characteristic value x_k are

$$x_k = \mu(1 - k V) \quad (14)$$

$$x_d = \mu \exp[-k\sqrt{(\ln(1 + V^2)) - 0.5 \ln(1 + V^2)}] \quad (15)$$

with k = 1.645 (5% fractile of the standardised normal distribution) usually applied for the characteristic strength.

This procedure may be applied for all basic variables. However, for geometrical properties and variable loads also other distributions (in addition to the normal and lognormal distribution) are frequently applied.

Note that a lower acceptable reliability level can be specified by reducing β- values for probabilistic design and reducing γ- values in the partial factor method. For a material property X described by a normal or lognormal distribution the partial factor $\gamma_m = x_k / x_d$ may be estimated using equation

$$\gamma_m = (1 - k\,V) / (1 - \alpha\beta V), \quad \text{or} \quad \gamma_m = \exp[(-k + \alpha\beta)\sqrt{(\ln(1 + V^2))}] \tag{16}$$

which follows from general equations (11) to (15). All the symbols used in (16) are defined above. The second expression in (16) for γ_m is valid for the lognormal distribution; similar expressions may be derived for other distributions.

6 Bayesian fractile updating

Fractiles of basic variables can be effectively updated using the Bayesian approach described in ISO 12491 [3]. This procedure is limited here to a normal variable X only for which the prior distribution function $\Pi'(\mu,\sigma)$ of μ and σ is given as

$$\Pi'(\mu,\sigma) = C\sigma^{-1+\nu'+\delta(n')} \exp\left\{-\frac{1}{2\sigma^2}\left[\nu' s'^2 + n'(\mu - m')^2\right]\right\} \tag{17}$$

with C normalising constant
$\delta(n') = 0$ for $n' = 0$ and $\delta(n') = 1$ otherwise.

The prior parameters m', s', n', ν' are parameters asymptotically given as

$$\mathrm{E}(\mu) = m', \ \mathrm{E}(\sigma) = s', \ V(\mu) = \frac{s'}{m'\sqrt{n'}}, \ V(\sigma) = \frac{1}{\sqrt{2\nu'}} \tag{18}$$

while the parameters n' and ν' are independent and may be chosen arbitrarily (it does not hold that $\nu' = n' - 1$). In equation (18) $\mathrm{E}(\cdot)$ denotes the expectation and $V(\cdot)$ the coefficient of variation of the variable in brackets. Equations (18) may be used to estimate unknown parameters n' and ν' provided the values $V(\mu)$ and $V(\sigma)$ are estimated using experimental data or available experience.

The posterior distribution function $\Pi''(\mu,\sigma)$ of μ and σ is of the same type as the prior distribution function, but with parameters m'', s'', n'' and ν'', given as

$$\begin{aligned} n'' &= n' + n \\ \nu'' &= \nu' + \nu + \delta(n') \\ m''n'' &= n'm' + nm \\ \nu''(s'')^2 + n''(m'')^2 &= \nu'(s')^2 + n'(m')^2 + \nu s^2 + nm^2. \end{aligned} \tag{19}$$

with m sample mean
s sample standard deviation
n size of the observed sample
$\nu = n - 1$ number of degrees of freedom.

The predictive value $x_{p,\mathrm{pred}}$ of a fractile x_p is then

$$x_{p,Bayes} = m'' + t_p\, s''\sqrt{1+1/n''} \tag{20}$$

with t_p fractile of the *t*-distribution (see Table 1) with ν'' degrees of freedom.

If no prior information is available, then $n' = \nu' = 0$ and the characteristics m'', n'', s'', ν'' equal the sample characteristics m, n, s, ν. Then equation (20) formally reduces to so-called prediction estimates of the fractile given as

$$x_{p,\text{pred}} = m + t_p\, s\,\sqrt{1+1/n} \tag{21}$$

t_p is again the fractile of the *t*-distribution with ν degrees of freedom (Table 1). Furthermore, if the standard deviation σ is known (from the past experience), then $\nu = \infty$ and s shall be replaced by σ.

Table 1 - Fractiles – t_p of the *t*-distribution with ν degrees of freedom

ν	$1-p$					ν	$1-p$				
	0.90	0.95	0.975	0.99	0.995		0.90	0.95	0.975	0.99	0.995
3	1.64	2.35	3.18	4.54	5.84	12	1.36	1.78	2.18	2.68	3.06
4	1.53	2.13	2.78	3.75	4.60	14	1.35	1.76	2.14	2.62	2.98
5	1.48	2.02	2.57	3.37	4.03	16	1.34	1.75	2.12	2.58	2.92
6	1.44	1.94	2.45	3.14	3.71	18	1.33	1.73	2.10	2.55	2.88
7	1.42	1.89	2.36	3.00	3.50	20	1.32	1.72	2.09	2.53	2.85
8	1.40	1.86	2.31	2.90	3.36	25	1.32	1.71	2.06	2.49	2.79
9	1.38	1.83	2.26	2.82	3.25	30	1.31	1.70	2.04	2.46	2.75
10	1.37	1.81	2.23	2.76	3.17	∞	1.28	1.64	1.96	2.33	2.58

7 Example of concrete strength

A sample of $n = 5$ concrete strength measurements having the mean $m = 29.2$ MPa and standard deviation $s = 4.6$ MPa is to be used to assess the characteristic value of the concrete strength $f_{ck} = x_p$, where $p = 0.05$. If no prior information is available, then $n' = \nu' = 0$ and the characteristics m'', n'', s'', ν'' equal the sample characteristics m, n, s, ν. The predictive value of x_p then follows from (20) as

$$x_{p,\text{pred}} = 29.2 - 2.13 \times \sqrt{\frac{1}{5}+1} \times 4.6 = 18.5 \text{ MPa}$$

where the value $t_p = -2.13$ is taken from Table 1 for $1 - p = 0.95$ and $\nu = 5 - 1 = 4$. When information from previous production is available the Bayesian approach can be effectively used. Assume the following prior information

$m' = 30.1$ MPa, $V(m') = 0.50$, $s' = 4.4$ MPa, $V(s') = 0.28$

It follows from equation (18)

$$n' = \left(\frac{4.6}{30.1} \frac{1}{0.50} \right)^2 < 1 \, , \; \nu' = \frac{1}{2} \frac{1}{0.28^2} \approx 6$$

The following characteristics are therefore considered: $n' = 0$ and $\nu' = 6$. Taking into account that $\nu = n - 1 = 4$, equations (19) yield

$$n'' = 5, \; \nu'' = 10, \; m'' = 29.2 \text{ MPa}, \; s'' = 4.5 \text{ MPa}$$

and finally it follows from equation (20)

$$x_{p,\text{Bayes}} = 29.2 - 1{,}81 \times \sqrt{\frac{1}{5} + 1} \times 4.5 = 20.3 \text{ MPa}$$

where the value $t_p = -1.81$ is taken from Table 1 for $1 - p = 0.95$ and $\nu = 10$.

In this example the resulting characteristic strength is greater (by about 10 %) than the value obtained by prediction method without using prior information. Thus, when previous information is available the Bayesian approach may improve (not always) the fractile estimate, particularly in the case of a great variance of the variable. In any case due caution should be paid to the origin of the prior information with regard to the nature of considered variable.

8 Concluding remarks

The main principles of the assessment of existing structures are:

- Currently valid codes for verification of structural reliability should be applied, historic codes valid in the period when the structure was designed, should be used only as guidance documents;

- Actual characteristics of structural material, action, geometric data and structural behaviour should be considered; the original design documentation including drawing should be used as guidance material only.

Typically, the assessment of existing structures is a cyclic process in which the first preliminary assessment is often supplemented by subsequent detailed investigations and assessment. A report on structural assessment prepared by an engineer should include a recommendation on possible intervention. However, the client in collaboration with the relevant authority should make the final decision concerning possible interventions.

The assessment of existing structures often requires application of sophisticated probabilistic methods, as a rule beyond the scope of traditional design practice. The critical step of the probabilistic assessment itself is specification

of the target reliability level discussed already during the previous International Probabilistic Workshop in Braunschweig. The other important steps of the whole assessment include evaluation of inspection data and updating of prior information concerning strength and structural reliability. It appears that a Bayesian approach can provide an effective tool. Described methods of probability updating are frequently used in assessment of existing structures. Two types of probability updating are generally applied:

(1) Updating of the structural failure probability.

(2) Updating of the probability distributions of basic variables.

The second type of updating seems to be more operational and effective. It enables to determine directly the design values of basic variables or updated partial factors that can be subsequently used in structural assessment.

9 Acknowledgements

This study project has been conducted within the project CZ/11/LLP-LdV/TOI/134005 Vocational Training in Assessment of Existing Structures, funded with support from the European Commission (programme Leonardo da Vinci). The paper reflects views only of the authors, and the Commission cannot be held responsible for any use which may be made of the information contained therein. Results of the project LG11043 have been utilised.

10 Literature

[1] ISO 2394: *General principles on reliability of structures*, 1998.

[2] ISO 13822: *Basis for design of structures -Assessment of existing structures*, 2008.

[3] ISO 12491: *Statistical methods for quality control of building materials and components*, 1998.

[4] Melchers R.E.: *Structural reliability analysis and prediction*. Wiley & Sons, 2001.

[5] Ellingwood B.R.: *Reliability-based condition assessment and LRFD for existing structures.* Structural Safety, 18 (2+3), 1996, 67-80.

[6] Holický M.: Assessment of existing structures. Chapter 9 of *Structural Safety and Its Quality Assurance*. Edited by B.R. Ellingwood and Jun Kanda. ASCE, 2005.

[7] Holický M., Retief J.: *Theoretical Basis of the Target Reliability*, IPW, Braunschweig, 2011, 91-101.

Stochastic material properties for different concrete types: An experimental investigation

Thomas Zimmermann, Katharina Haider & Alfred Strauss
Institute for Structural Engineering, University of Natural Resources and Life Sciences, Vienna, Austria

Abstract: Within this paper an experimental investigation on basic material parameters as well as fracture mechanical properties for different concrete types is presented. In total four different concrete types – C30/37 H, C25/30 B3, C25/30 XC1 GK16 and C20/25 XC1 GK16 – were investigated. The results of this investigation serve as a basis for further numerical assessment with respect to (a) define suitable stochastic models and (b) to carry out non-linear finite element analysis. An additional target was to capture the effects of testing procedure on the mechanical properties. The associated knowledge of these material parameters is an important issue for a realistic reliability assessment of both new as well as existing structures.

1 Introduction

Design, computation and construction of engineering structures are generally based on linear static analyses and on linear or multi-linear material models. In the new generation of design specifications, dispersion effects and associated uncertainties, e.g. in material properties, are covered in the so-called semi-probabilistic safety concept (SPSC) [3]. The SPSC guarantees desired reliability levels over the life-cycle of a structure by careful selection of (a) suitable safety factors for the resistance and for the action side, and of (b) load combination factors.

The SPSC provides for particular structures, using fractiles of material properties and loads as inputs, the means for a standardized verification of the usability and the static safety of the structures. The demanded general validity of the SPSC for a wide range of structure types gives rise to reliability levels that may turn out to be even higher than originally intended [13].

Moreover an accurate knowledge concerning the material behaviour and the available capacity of a structure can be used for further life-cycle analysis. In particular, optimized strategies and concepts for maintenance and revitalization over the life-time of a structure can be developed. If therefore also different cost factors are taken into account a valuation concept and decision concept for immediate and necessary future actions can be created. Investigations for different engineering structure can be found e.g. in [5] and [14]. However the knowledge of the scattering quantities and suitable stochastic models are necessary.

The determination of the statistics and probability distributions of the random variables describing material properties play an important role in the development of probabilistic based design specifications. The choice of the probability distribution chosen to represent the material property data will have a large effect on the calculated reliability. Assuming different distributions for the material properties can result in computed probabilities of failure that vary by over an order of magnitude. This is the result of the lower tail behaviour of different cumulative distribution functions, which has become known as the tail-sensitivity problem in structural reliability [2].

2 Laboratory tests

2.1 Materials and test setup

In general, the properties of concrete are characterized based on the compressive strengths according to EN 206-1, on the exposure classes and on the slump value. Nevertheless, the realistic modelling of structures requires the incorporation of (a) nonlinear effects in the analysis and material properties, which can be captured for e.g., concrete by a variable modulus of elasticity, E_c the compressive strength, f_c and the fracture energy, G_f, and of (b) uncertainties in material and geometrical properties caused by nature, manufacturing processes and curing among others. These requirements, together with the newly characterized concrete classes in the Eurocode concept, forces the interest in experimental investigations with commonly used concrete types, e.g. C25/30 according to EN 206-1 or Önorm B 4710-1_ENREF_17.

In particular, the standardized compressive test and the wedge splitting test were accomplished. These investigations were divided into four parts: (I) concrete C30/37 H, (II) concrete C25/30 B3, (III) concrete C25/30 XC1 and (IV) concrete C20/25 XC1. Table 1 shows the mixture for these different concrete types.

Table 1. Concrete mixture of series I – IV.

Concrete Properties	C30/37 H Dry [kg]	C25/30 B3 Dry [kg]	C25/30 XC1 GK16 Dry [kg]	C20/25 XC1 GK16 Dry [kg]
Aggregate 0-4 mm	5151.32	5367.53	7628.98	7168.01
Aggregate 4-16 mm	5842.26	4756.67	6299.69	5928.83
Aggregate 16-32 mm	1958.07	3393.72	-	-
Water content	1245.75	1211.53	1229.20	1280.25
Readyair L-300	2.30	5.23	-	-
Readyplast SP-SL1	18.67	-	-	-
Fibrin 315 pp-fibers	9.00	-	-	-
Cemplast	-	31.32	28.53	25.50
Fluamix C	584.53	524.47	471.53	392.47
CEM II A-M 42.5N	2285.91	2086.72	1903.94	1569.12
w/c	0.54	0.58	0.65	0.82
w/b	0.45	0.48	0.54	0.68

In order to determine the basic material parameters like compressive strength and modulus of elasticity *compressive tests* according to EN 206-1 were carried out. Test cubes had dimensions of 150 x 150 x 150 mm and were loaded with a gradual increase of the stress level until the maximum load was reached. The maximum load was defined as test load at which an increase within a time frame of 4 seconds was no longer possible.

The second testing procedure for the characterization of the stochastic concrete properties was the *wedge splitting test method*. Figure 1 illustrates the principle of the wedge splitting method for uniaxial loading of a disk-shaped specimen. A starter notch is cut into the rectangular groove of the specimen. The load transmission pieces (comprising rollers or roller bearings) are inserted into this groove, into which the slender wedge is then laid. The force P_v from the testing machine is transmitted via the load transmission pieces onto the wedge, leading to the splitting of the specimen. The friction between wedge and force transmission pieces is negligible and the splitting force P_h can be determined by means of a simple calculation. The displacement is determined at the height of the load application line on both sides by electronic displacement transducers which are attached to a metal frame. In contrast to a normal wedge splitting test [9], two hinge roller supports were located on the top of the specimen as shown in Figure 1. Two massive steel loading devices, both equipped with rollers on each side, were placed on top of the specimen. A stiff steel profile with two identical wedges was fixed at the upper plate of the testing machine. The wedges were entered between the rollers on each side, thereby applying a horizontal splitting force. P_h is the horizontal component of the force acting on the rollers, and is calculated by taking the wedge angle θ into consideration:

$$P_h = P_v / 2 \tan \theta \quad (1)$$

where P_h is the horizontal load, P_v is the applied vertical load, and θ is the wedge angle.

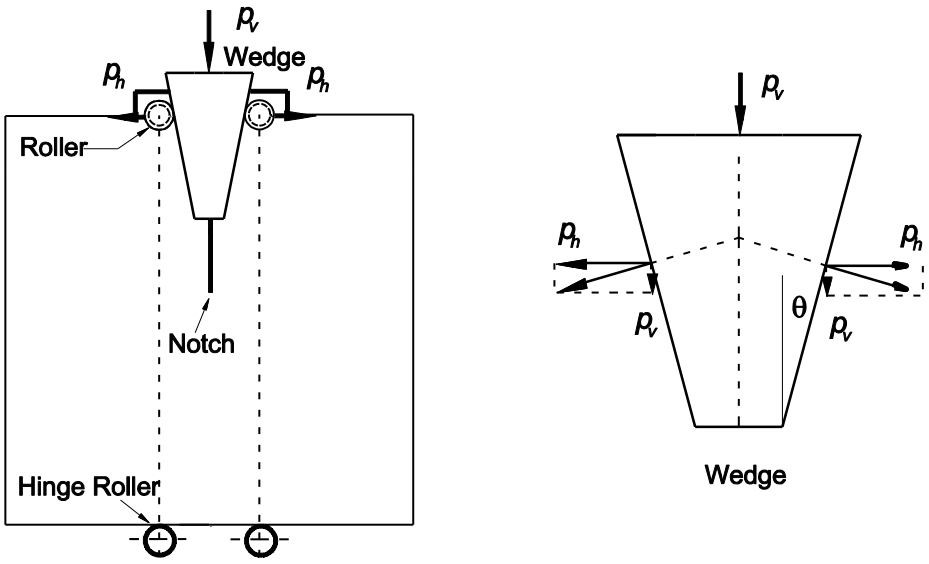

Figure 1: Specimen shape (a) and principle (b) of the wedge splitting test for uniaxial loading to obtain fracture energy.

2.2 Experimental results

From basic compressive tests the compressive strength f_c and the modulus of elasticity E_c are evaluated separately for each concrete class. Table 2 shows the results as well as descriptive statistical parameter.

Table 2. Experimental results of compressive tests all values are given in MPa.

I		II		III		IV	
E_c	f_c	E_c	f_c	E_c	f_c	E_c	f_c
34600	59.55	33000	47.95	39000	54.30	30300	39.20
36400	57.25	30500	46.90	35400	52.20	31600	40.90
33800	55.90	27600	45.15	35300	52.00	29100	38.65
36400	59.35	27900	45.00	32700	51.65	29800	38.70
41200	62.85	31600	48.50	35800	56.55	31100	39.70
31900	57.95	28900	48.15	34000	53.45	-	-
34400	61.00	31800	42.80	37600	52.75	32100	42.30
36900	61.10	30100	49.00	35900	58.20	32500	36.35
34100	52.05	36000	49.85	33400	49.65	32700	42.90
35522 [1)]	58.56	30822	47.03	35456	53.42	31150	39.84
2492 [2)]	3.05	2502	2.15	1869	2.47	1229	2.00
0.0702 [3)]	0.0522	0.0812	0.0457	0.0527	0.0462	0.0394	0.0501

1) mean value, 2) standard deviation, 3) coefficient of variation

The value G_f for the wedge specimen was calculated from the load-displacement curve using Eq. (2) [10]. Self-weight was not considered, be-

cause it is balanced with the reaction at the two bottom supports, as shown in Figure 1.

$$G_f = W / (D-N)B \tag{2}$$

Where W is the total work of the area under the load-deflection curve, and D, N, and B are the effective depth of the crack, notch length, and thickness of the specimen, respectively.

Figure 2 shows the load-deflection curves of the four investigated concrete mixtures.

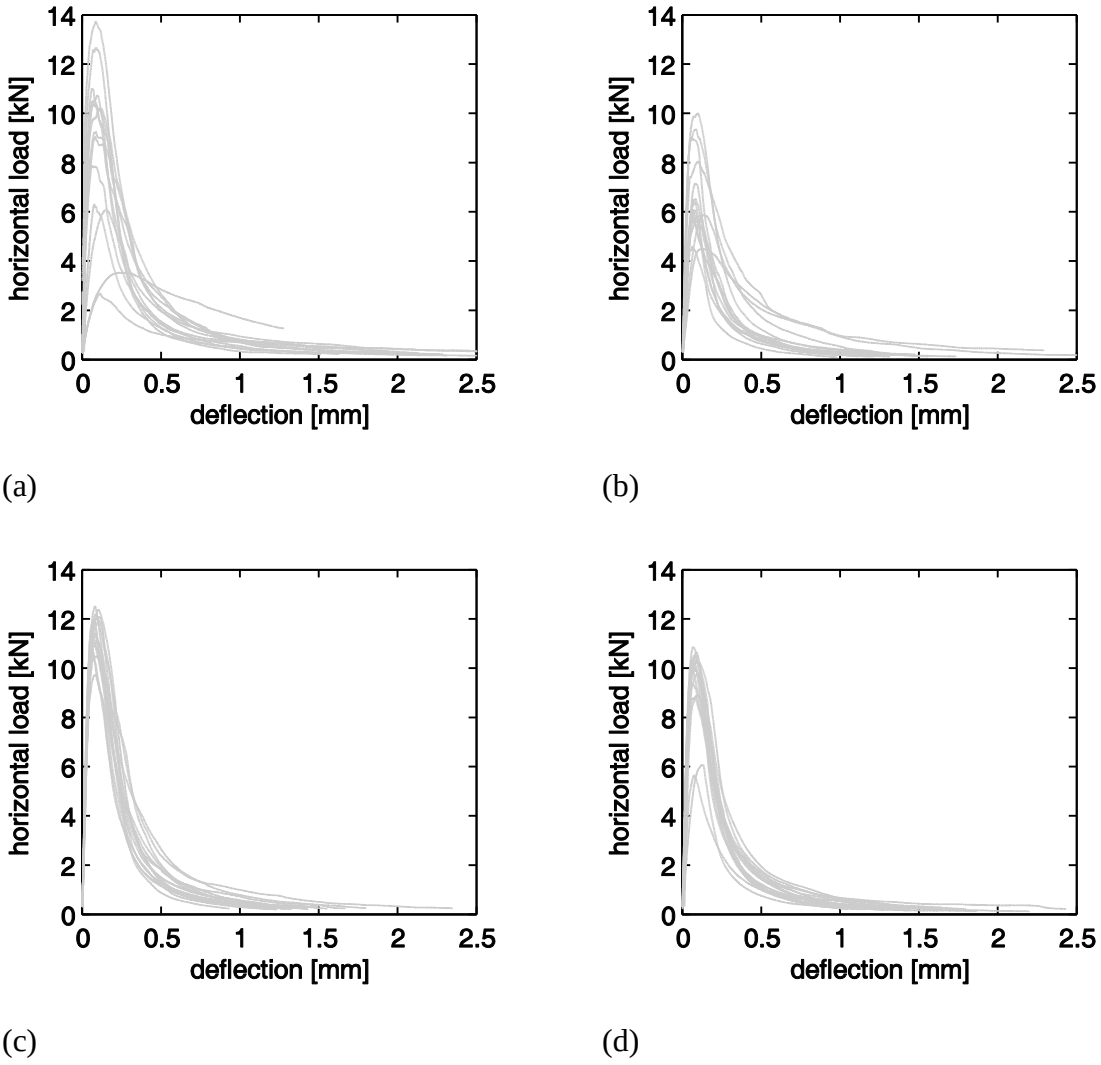

Figure 2: Load-deflection curves for (a) C30/37 H, (b) C25/30 B3, (c) C25/30 XC1 and (d) C20/25 XC1.

Table 3 shows the values of G_f as well as descriptive statistical parameters for the investigated concrete mixtures.

Table 3. Experimental results of wedge splitting tests all values are given in N/m.

I	II	III	IV
223.7	223.7	183.3	163.7
189.0	189.0	167.9	135.0
185.4	185.4	187.9	163.9
207.9	207.9	179.3	120.3
173.9	173.9	201.4	137.2
165.7	165.7	179.6	-
203.6	203.6	190.2	124.6
123.3	-	172.0	153.8
161.8	161.8	188.2	171.4
181.6 [1)]	188.9	183.3	146.2
28.13 [2)]	20.30	9.52	18.22
0.1549 [3)]	0.1075	0.0519	0.1246

1) mean value, 2) standard deviation, 3) coefficient of variation

3 Probabilistic models

Depending on the distribution function different procedures for the estimation of the unknown parameters have been used e.g. Method of Moments and Method of Maximum Likelihood. However choosing of the best fitted model to a given dataset was based on Kolmogorov Smirnov (KS) [1]. The fitting of suitable probability density functions to the obtained data set was done by using program FReET [6], [7].

Table 4. Recommended values of statistics and distribution functions.

item	pdf	mean [MPa]	std [MPa]	cov	skew-ness	excess
E_c I	Weibull max	35522	2643.3	0.07441	0.92819	1488
E_c II	Weibull max	30822	2654.1	0.08611	0.60009	0.47757
E_c III	Lognormal	35456	1982.5	0.05592	0.37134	0.24615
E_c IV	Weibull max	31150	1313.7	0.04217	-0.30699	-0.18949
f_c I	Weibull min	58.556	32.395	0.05532	-0.72044	0.79474
f_c II	Weibull min	47.033	2.282	0.04852	-0.92431	14732
f_c III	Weibull max	53.417	26.153	0.04896	0.57068	0.40901
f_c IV	Lognormal	39.838	21.335	0.05356	0.16082	0.04602
G_f I	Weibull max	181.59	29.834	0.16429	-0.53046	0.07344
G_f II	Weibull max	188.88	21.706	0.11492	0.24819	-0.12609
G_f III	Normal	183.31	10.093	0.05506	0	0
G_f IV	Weibull max	146.24	19.479	0.13320	-0.05244	-0.28935

As a result of the fitting process the data set can be represented in most cases by a Weibull distribution function. Using Weibull *max* or *min* is depending on the skewness of data. However in some cases also Lognormal or Normal distribution is a suitable distribution function to represent the experimentally ob-

tained data. It should be also taken into account that the accuracy of the fitting process is highly influenced by the number of samples, especially if probability density functions with more than two parameters are used.

4 Reliability assessment

In general, two basic analytical methods, FORM and SORM, can be used to estimate structural reliability [1]. Furthermore, numerical approximation techniques such as the Response Surface Method or Monte Carlo Sampling are available. It was verified that FORM reliability analyses provides in many cases an excellent approximation, even for nonlinear conditions. The design of any structure requires that its resistance R is greater than the load effect Q. This requirement (i.e., $R > Q$) is described by the limit state

$$g(\mathbf{X}) = R - Q = 0 \tag{3}$$

where $\mathbf{X} = \{X_1, X_2, \ldots, X_n\}^T$ = vector of random variables, $g(\mathbf{X}) = 0$ = limit state, and $g(\mathbf{X}) < 0$ is the failure region. The reliability index then is defined as

$$ß = (\mu_R - \mu_Q) / (\sigma^2_R + \sigma^2_Q)^{1/2} \tag{4}$$

where μ_R and μ_Q = mean resistance and mean load effect, respectively, and σ_R and σ_Q = standard deviations of both variables. If the resistance R and the load effect Q are normally distributed, $g(\mathbf{X})$ is normally distributed too and the probability of failure p_f can be determined as

$$p_f = \Phi(-ß) \tag{5}$$

where Φ = standard normal distribution. The calculation of the reliability index ß is a constrained optimization problem, where the closest point of the limit state surface with regard to the origin is searched in the standard normal space [12].

5 Conclusions

In order to determine experimentally the basic material parameters was well as fracture mechanical properties for different concrete types, four concrete types (C 30/37 H, C 25/30 B3, C25/30 XC1 GK16 and C20/25 XC1 GK16) were investigated.

The basic material parameters like compressive strength and modulus of elasticity were assigned by compressive tests according to EN 206-1. For the

characterization of the stochastic concrete properties for non-linear modelling purposes the wedge splitting test method was used.

After the laboratory tests the compressive strength f_c and the modulus of elasticity E_c were evaluated separately for each concrete class. Within this investigation the mean value, the standard deviation as well as the coefficient of variation was calculated.

With respect to the wedge-splitting tests for all investigated concrete mixtures the load-deflection curve was figured out and the descriptive statistical parameters out of the test results were calculated as well.

Afterwards, suitable probability density functions were fitted to the obtained data-set of the obtained material parameters by using program FReET. The best fitted probabilistic model was chosen by using the Kolmogorov Smirnov test.

Obtained data as well as fitted probabilistic models can serve as a basis for a further reliability assessment to calculate reliability index β and probability of failure p_f respectively.

6 Acknowledgement

The support of the experimental investigations by the project CZ.1.07/2.3.00/30.0005 of Brno University of Technology is gratefully acknowledged.

7 References

[1] Ang, A.H.-S.; Tang, W.H.: *Probability Concepts in Engineering*. John Wiley & Sons, Inc. 2007

[2] Ditlevsen, O.: *Uncertainty Modeling with Applications to Multidimensional Civil Engineering Systems*. McGraw-Hill International Book Co. New York, London, 1981

[3] Ellingwood, B.R.: Structural Reliability and Performance-Based Engineering, *Proceedings of the Institution of Civil Engineers: Structures and Buildings*, 161, 199-207, 2008

[4] EN 206-1 Concrete – Part 1: *Specification, Performance, Production and Conformity CEN/TC 104*.

[5] Frangopol, D.M.; Strauss, A.; Bergmeister, K.: Lifetime cost optimization of structures by a combined condition-reliability approach, *Engineering Structures*, 31(7): 1572-1580, 2009

[6] Novák, D.; Vořechovský, M.; Rusina, R.: *FReET v.1.6 – program documentation. User´s and Theory Guides*. Červenka Consulting, Czech Republic, http://www.freet.cz, 2011

[7] Novák, D.; Pukl, R.: Simulation of random behavior of engineering structures: From parameters identification to reliability assessment. *Proceedings of the 3rd International Symposium on Life-Cycle Civil Engineering*, IALCCE 2012

[8] ÖNORM B 4710-1 – Part 1: *Festlegung, Herstellung, Verwendung und Konformitätsnachweis*. 2003

[9] Petersson, P.E.: Fracture Energy of Concrete: Practical Performance and Experimental Results, *Cement and Concrete Research*, V.10, No.1, pp.91-101, 1980

[10] Rossi, P.; Brühwiler, E.; Chhuy, S.; Jenq, Y.S.; Shah, S. P, "Fracture Properties of Concrete as Determined by Means of Wedge Splitting Tests and Tapered Double Cantilever Beam Tests, " in: S. P. Shah, A. Carpentari (Eds.),Chapman & Hall, London, pp. 87-126. 1990

[11] Schneider, J.: *Sicherheit und Zuverlässigkeit im Bauwesen – Grundwissen für Ingenieure*. Stuttgart, Teubner, 1996

[12] Shinozuka, M.: Basic Analysis of Structural Safety. *Journal of Structural Engineering* 1109(3): 721-740, 1983

[13] Strauss, A.; Bergmeister, K.; Hoffmann, S.; Pukl, R.; Novak, D.: Advanced Life-Cycle Analysis of Existing Concrete Bridges, *Journal of Materials in Civil Engineering*, 20, 9-19, 2008

[14] Strauss, A.; Frangopol, D.M.; Bergmeister, K.: Assessment of Existing Structures Based on Identification, *Journal of Structural Engineernig*, ASCE, 136(1): 86-97, 2010

Development of a finite element model for masonry arch bridges incorporating stochastic material parameters

Alexander Krawtschuk, Thomas Zimmermann, Katharina Haider,
Alfred Strauss & Oliver Zeman
Institute of Structural Engineering, University of Natural Resources and Life Sciences, Vienna

Abstract: Due to the fact that historical arch bridges nowadays are one of the oldest infrastructural buildings which are still in usage, the estimation of the bearing capacity of these structures is quite important to companies responsible for maintenance. In most cases the material parameters and the geometrical shape are unknown which leads to an uncertainty in the determination of the bearing behaviour. Therefore, this contribution focuses on the development of a finite element model which aims for the detection of the most unfavourable geometrical form of a masonry arch bridge, which is presented in this contribution by means of a sensitivity analysis of a few arch shapes (circular, three-centre and parabolic shaped). As a second part, the contribution discusses the procedure of the calibration of an appropriate finite element model for further assessments. In addition the experimental program to determine the input parameters as well as to quantify stochastic properties is pointed out. By means of these stochastic material parameters the accuracy of the finite element model can be increased for a realistic and useable approach on existing historical arch bridges.

1 Introduction

Arch bridges made from nature stone nowadays are the oldest structures which are still in use on road and railway lines. With an average age of more than hundred years, these structures often are seen as historical important buildings. Most of them had been con-

structed during the great building period of roads and railways from the 1840ies to 1900. Lots of the considered nature stone bridges are constructed as circle or three centre curve, some of them also in a parabolic form or catenaries or cycloid. The height of the apex cover varies in a large range. When masonry was appropriated, usually sand, chalkstone or clay bricks were used. For most bridges no observations of the material parameter are available, as a result the stone and the mortar strengths are unknown. Under the usage of the German railway company, there are more than 8000 arch bridges yet, although at local roads there is an additional unknown number of them. In Austria, the railway network, especially along the southern railway line has around 1000 arch bridges in usage. In whole Europe, the stock of masonry railway bridges is estimated with around 70.000. In the course of route expansion plans in the past especially arch bridges have been replaced by new steel or reinforced concrete structures. Considerations of preservation, the budgetary situation of the rail and road operators, as well as a sustainable, efficient usage of resources and existing infrastructure are motivations to maintain and – if necessary – toughen up existing arch bridges. Therefore, the issues of sustainability, durability and serviceability become more important [4].

2 State of the art

The oldest existing arch bridges were designed based on experience. Later graphical methods for the static were available and approximation formulas based on the arch thrust line to design major geometrical parameters such as span, arch shape and arch thickness at the apex and the abutments were developed. These simplifying estimations can also now be useful to perform the bearing capacity of existing arch bridges on the basis of their geometrical parameters. Especially for old arch bridges which were designed for different loads at their design and construction date, these methods can be used as an first estimation for the current bearing capacity or the future use of these buildings. The recalculation of these buildings under the valid load approach enables the assessment of the bearing capacity and the suitability for an usage under nowadays valid load. Any necessary upgrading which considers the conservation of the existing structures both preserves the appearance of the arch bridges and saves costs. For the estimation of the bearing capacity as a result of a static recalculation, the knowledge of the construction and the material properties is required. If bridges are designed nowadays, e.g. made from reinforced concrete, steel or wood, these parameters are well known. In case of existing arch bridges made from stone, brick or rammed concrete, the material properties often cannot be identified, because too many factors influencing the bearing capacity [6].

The assessment of existing bridge structures can be used as a helpful method for the responsible organisations, e.g. road or railway maintenance companies, and the proper governments. In terms of the life cycle concept, the increasing axle loads, load restrictions, inspections, monitoring, maintenance measurements or even a replacement of the structures have to be considered. A conventional approach for the recalculation of arch bridges, the elasticity theory can provide results which differ significantly from the actual bearing capacity. The involvement of the wing walls and the interaction with the surrounding soil influence the capacity significantly. Therefore the issue of structure-soil-interaction as de-

picted in Figure 1 is particularly essential for arch bridges, however, calculations on the basis of existing studies cannot be performed correctly. These interactions can be summarized as follows:

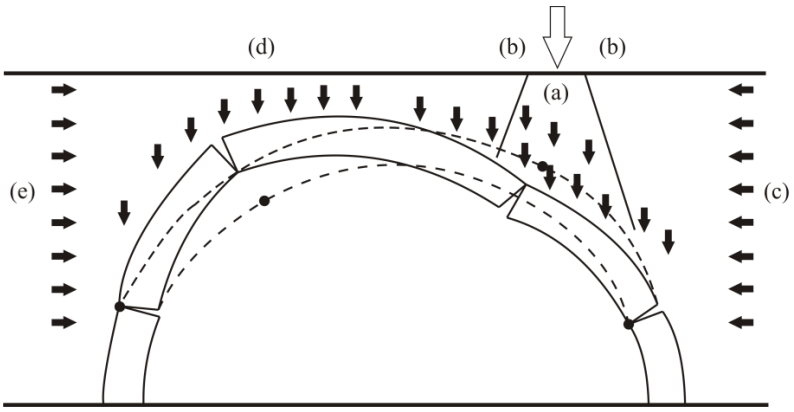

Figure 1: Structure – Soil – Interaction in accordance to UIC Code 778-3 [9]

(a) traffic load is distributed laterally over the depth, the distribution is dependent on the shear strength and stiffness of the backfill

(b) dead load of the backfill acts as a destabilizing force on the arch on the side loaded by the traffic load

(c) horizontal components on the loaded side of the arch as a result of the shear strength, stiffness, dead load of the backfill material and the traffic load

(d) stabilizing effect of the dead load of the backfill on the unloaded side of the arch

(e) horizontal components on the unloaded side of the arch as a result of the shear strength, stiffness, dead load of the backfill material and the traffic load

Practical considerations have shown that stone arches in combination with an appropriate structural state can have considerable reserves in their bearing capacity. Therefore they often reach the standards which are recommended nowadays. If the age of the structure is taken as a safety indicator, existing arch bridges show the convenience and the robustness of arch structures. Current tools of structural design are quite manifold and take account both geometrically and physically non-linear structural properties. Nevertheless, because the structural behaviour of natural stone masonry is quite complex due to various influence factors, it has not been possible to set up an appropriate model for masonry which considers all decisive effects up to now. The codes for proofing the bearing capacity and the serviceability only allow an overhead assessment of the resistance values. Thus there is a noticeable gap between the possibilities of mechanical modelling and the available safety proofs.

Current finite element (FE) programs serve a quite good approximation for modelling the material behaviour, as a result different models are implemented in these programs. In the calculation models, the spatial dimension of the arch structures is simplified to a cross sec-

tion of one meter. The most important point for a correct modelling is to identify the relevant meter-stripe and to describe the loadings correctly, particularly single loads in the transversal direction of the arch.

The well-known graphical methods with thrust line have been followed by analytical methods, particularly since the development of computational calculations. By means of elasticity and plasticity theory, the models were enhanced, although there is still no satisfactory solution approach for the issue of the discontinuous joint. Since a few years, some FE-Programs can bear with discontinuous joints, but these models require an enormous calculation effort. Additionally, there is the possibility that these models give completely wrong results, as a result of unknown boundary conditions.

3 Motivation and Method

In order to develop an appropriate numerical model for the assessment of masonry arch bridges the assessment procedure according to Figure 2 has been used. First of all in-situ measurements on the real structure under defined loading situations were carried out. Secondly, based on a survey of the real structure a FE-model was set up. Another input for the FE-model are results from laboratory tests in order to define the material properties. Afterwards the correlation between simulated (m_{si}) and measured (m_{ei}) reactions is calculated. If the accuracy between both values is in an appropriate state the FE-model is suitable for further investigations (life-time assessment, decision-making tool etc.), otherwise an update process has to be performed [8], [10].

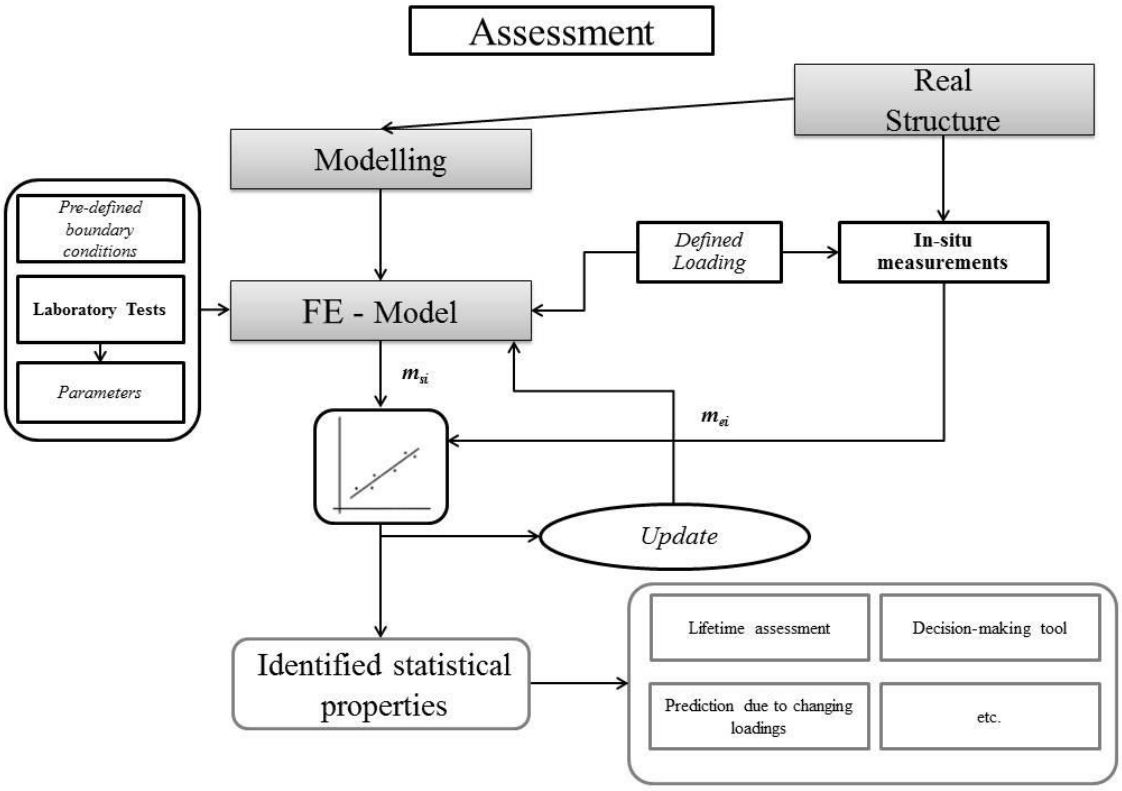

Figure 2: Assessment procedure for the FE-model setup.

4 Case study

The case study object is a historic masonry arch bridge located close to the city of Mattersburg, Austria. The so-called Rohrbach bridge consists of five arches and wing walls which imbed the structure to the surrounding earth dam. It is part of the Mattersburg Railway line from Vienna via Wiener Neustadt to Sopron in Hungary and was built from 1845 to 1847. The arches span over both a small rivulet and a local road with a span width of almost 6.0 m and an arch rise of 2.0 m at each arch. Primary the bridge was built for rail tracks into two directions, but just one was constructed, therefore there is an eccentric loading situation on the whole structure. The bridge consists of five arches which are made of masonry with a thickness of approximately 60 cm and has the shape of a three-centre shaped arch. Both, the spandrel walls, the wing walls, the springing and the abutments are made of limestone as it is shown in Figure 3. The parapet is also made from masonry, but this obviously does not have an influence on the bearing behaviour. The backfill material under the ballast could not be clarified which causes difficulties in modelling the bridge structure.

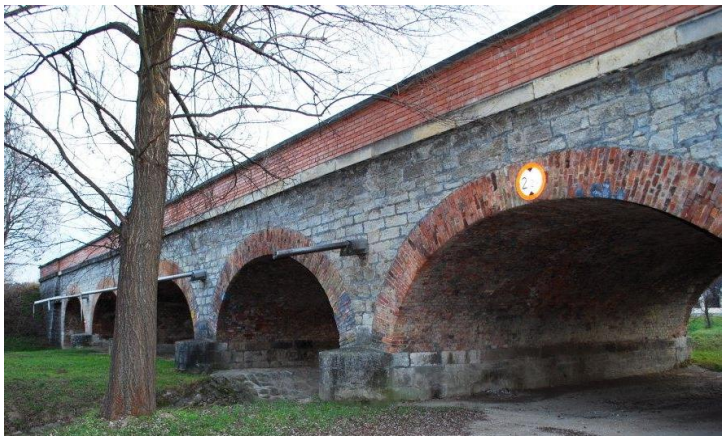

Figure 3: Case study object Rohrbach bridge.

4.1 Sensitivity analysis

Different idealized arch shapes were investigated due to vertical loading in order to obtain different internal forces as well as the thrust line. Thereby a *circular*, a *three-centre* and a *parabolic* shaped arch was set up in a simple computational model. The boundary conditions as well as the span (2.95 m) were equal for the three different shapes. The arch rise varied between 1.95 m and 2.95 m. The vertical loading was taken into account by an equally distributed load of 1 kN/m over the entire arch.

For the first investigated idealized shape it can be seen that the shape of the arch do not correspond with the thrust line because in the outer parts as well as in the middle part negative and positive moments are occurring. The more the support line deviates from the structural axis, the worse the load transfer behaviour in terms of normal forces. In the optimal case, the two lines are identical and the whole stress distribution is reduced to pure compression in the structure. Otherwise additional moments and shear forces arises.

Three-centre shaped arch was mainly chosen to decrease the height compared to a circular shaped arch. Thereby in the middle the occurring internal moments are similar to those by a parabolic shaped arch. In the outer parts it is closer to those occurring by a circular shaped arch.

The parabolic shaped seems to be the most appropriate shape for pure compression state. This is clearly represented by the distribution of the moment. In the middle part the behaviour is similar to the three-centre shaped arch. Moreover the resulting moments are only about 1/10 of the moments which occur within the other two investigated shapes. Hence the structure is stiffer than the other ones. This circumstance directly influences the further dimensioning process.

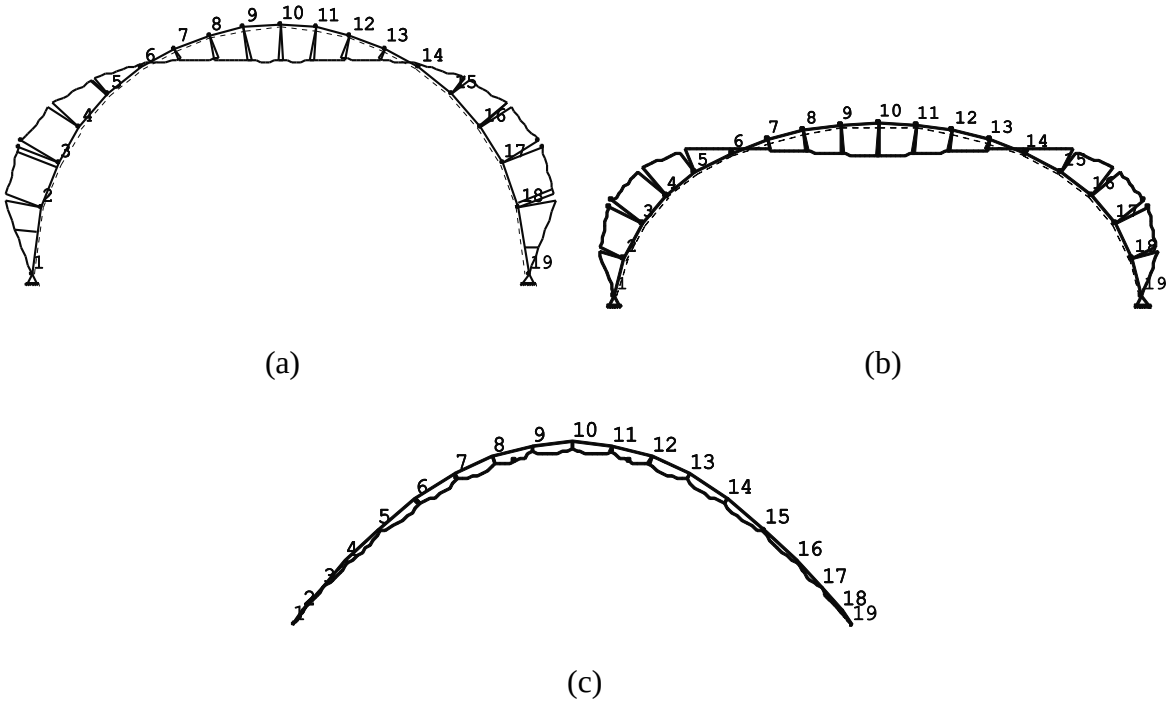

Figure 4: Distribution of internal moment for (a) circular, (b) three-centre and (c) parabolic shaped arch.

As it can be seen from Figure 4 the parabolic shaped arch is the most appropriate one to represent the ideal thrust line.

5 In-situ measurements and laboratory tests

The following section gives an overview of already conducted measurements as well as planed investigations.

5.1 In-situ measurements

The following not-destructive methods were used in order to get more information about size, build-up, density, form and homogeneity of individual parts of the structure. For the characterization of the subsurface of the structure and the backfill material a *ground penetration radar* was used. By means if this method it is possible to identify discontinuities at the structure and the backfill material. In order to virtualise the vibrations of the structure a *laservibrometer* was used. During the measurement time a vertical displacement from 0.05 to 0.40 mm was observed [1], [7]. The third non-destructive method was the *LVDT measurement*. The test setup contained of six pair wise fixed linear variable differential transformers (LVDT) to show the displacement related to a fixed point. Altogether 20 railcar crossovers were recorded in 10 different combinations of the measurement application. Finally 60 maximum values of the displacement were available for an adequate interpretation. The main items of the measurement setup were the linear variable differential trans-

formers. They should record the displacements of the thread rods caused by the reaction of the structure to the loading due to railcars.

From the obtained values of the measurement campaign it can be considered that the forces from the crown along the diagonals go down to the abutments and the springer [5].

5.2 Laboratory tests

To obtain basic material parameters as well as their scatter laboratory tests on single bricks were conducted. In a first test sequence compressive tests on normal sized bricks (25 x 12 x 6.5 cm) according to EN 772-1 [3] were carried out. The mean value of compressive strength results in f_b = 21.3 MPa, standard deviation s = 1.425 MPa and coefficient of variation cov = 0.0669. Based on this data the program FReET was used to fit a probability density function (pdf) to the given data set. To choose the most appropriate pdf the Kolmogorov Smirnov test statistic was used [1]. This results in a Weibull distribution with m = 21.3, s = 1.425, b = 27.607 MPa. Additionally, tests should be performed with different loading directions in order to obtain the compressive strength of bricks with respect to the loading direction.

Beside the small scale testing one arch of the Rohrbach bridge will be reconstructed in the scale 1:2. The arch will be built with bricks in compliance to the real structure and supported by artificial abutments. The backfill material can be varied with regards to its mixture.

6 Conclusions

In this contribution it is shown how on the base of adequate measurement data and surveying a FE-model of an existing masonry arch bridge can be set up for the evaluation process of the bearing capacity as well as to incorporate stochastic properties. To determine the most unfavourable shape of the arch a sensitivity analysis regarding the thrust line of three possible arch shapes was carried out. For an increase of the accuracy and the practicability of the model on the one hand laboratory tests were and are going to be performed to determine the correlation of the measured values on the real object and the measured values on a scale model; and on the other hand small scale tests on specimens taken from brick stones under variable angles. These variable angles determine the variable loading direction which occurs on existing structures. Based on test results performed under a vertical loading situation, which are already available, this extension to various angles will help to characterize the material parameters in an appropriate way.

7 Acknowledgement

The support of the experimental investigations by the project CZ.1.07/2.3.00/30.0005 of Brno University of Technology is gratefully acknowledged. Additionally the financial sup-

port by the research projects ILATAS and NANUB are acknowledged. Further we would like to thank Wienerberger for the provision of bricks for testing.

8 References

[1] Ang, A.H.-S.; Tang, W.H.: *Probability Concepts in Engineering*. John Wiley & Sons, Inc. 2007

[2] Dengg, F.; Mendlig K.; Krawtschuk A.: Performing of non-destructive measurement methods on existing arch bridge structures, *Proceedings of the 3rd International Symposium on Life-Cycle Civil Engineering*, IALCCE 2012

[3] EN 772-1: *Methods of test for masonry units – part 1: Determination of compressive strength*, 2000.

[4] Krawtschuk, A.; Strauss, A.; Wendner, R.; Zeman, O.: Inspection and Lifetime Assessment for Arch Bridges, in: Humberto Ramos R.; Guilherme Aris Parsekian (Eds.), *Proceedings of 15th International Brick And Block Masonry Conference*; ISBN: 978-85-63273-09-3, 2012

[5] Krawtschuk A.; Zeman, O.; Strauss, A.; Scheidl C.; Proske D.: Optimised monitoring concepts for historical masonry arch bridges, *Proceedings of the 3rd International Symposium on Life-Cycle Civil Engineering*, IALCCE 2012

[6] Proske, D.; van Gelder, P.: *Safety of Historical Arch Bridges*, Springer, Heidelberg, 2009

[7] Scheidl, C.; Chiari, M.; Kaitna, R.; Müllegger, M.; Krawtschuk, A.; Zimmermann, T.; Proske, D.: Analysis debris-flow impact models, based on a small scale modelling approach, *Surveys in Geophysics*, online first, 2012

[8] Strauss, A.; Krawtschuk, A.; Wendner, R.; Frangopol, D.M.; Bergmeister, K.: Monitoring based assessment of a jointless bridge. *Proceedings of 6th International Conference on Bridge Maintenance, Safety and Management*, IABMAS 2012, Italy, 2012

[9] UIC Code 778-3: *Recommendations for the inspection, assessment and maintenance of masonry arch bridges*, April 2011

[10] Zimmermann, T.; Krawtschuk, A.; Strauss, A.; Wendner, R.: Extreme value statistics for the life-cycle assessment of masonry arch bridges. *Proceedings of 6th International Conference on Bridge Maintenance, Safety and Management*, IABMAS 2012, Italy, 2012

Mitteilungen des Instituts für Geotechnik der Universität Stuttgart

Mitteilungen des Baugrundinstitutes Stuttgart
(Institut für Grundbau und Bodenmechanik)
der Universität Stuttgart
Hrsg.: Prof. Dr.-Ing. Dr. h.c. U. Smoltczyk

Nr. 01	Thamm, B. R.	(1974)	Anfangssetzungen und Anfangsporenwasserüberdrücke eines normalverdichteten wassergesättigten Tones
Nr. 02	Gußmann, P.	(1975)	Einheitliche Berechnung von Grundbruch und Böschungsbruch
Nr. 03	Feeser, V.	(1975)	Die Bedeutung des Kalziumkarbonats für die bodenphysikalischen Eigenschaften vom Löß
Nr. 04	Du Thin, K.	(1976)	Standsicherheit von Böschungen: Programm-Dokumentation
Nr. 05	Smoltczyk, U. Pertschi, O. Hilmer, K.	(1976)	Messungen an Schleusen in der UDSSR. Schleusennorm der UDSSR (SN 30365)

Nr. 06	Hilmer, K.	(1976)	Erddruck auf Schleusenkammerwände
Nr. 07	Laumans, Q.	(1977)	Verhalten einer ebenen, in Sand eingespannten Wand bei nicht-linearen Stoffeigenschaften des Bodens
Nr. 08	Lächler, W.	(1977)	Beitrag zum Problem der Teil-flächenpressung bei Beton am Bei-spiel der Pfahlkopfanschlüsse
Nr. 09	Spotka, H.	(1977)	Einfluß der Bodenverdichtung mittels Oberflächenrüttelgeräten auf den Erd-druck einer Stützwand bei Sand
Nr. 10	Schad, H.	(1979)	Nichtlineare Stoffgleichungen für Böden und ihre Verwendung bei der numerischen Analyse von Grundbau-aufgaben
Nr. 11	Ulrich, G.	(1980)	Verschiebungs- und kraftgesteuerte Platten-druckversuche auf konsolidierenden Böden
	Gußmann, P.		Zum Modellgesetz der Konsolidation
Nr. 12	Salden, D.	(1980)	Der Einfluß der Sohlenform auf die Traglast von Fundamenten

Nr. 13	Seeger, H.	(1980)	Beitrag zur Ermittlung des horizontalen Bettungsmoduls von Böden durch Seitendruckversuche im Bohrloch
Nr. 14	Schmidt, H.H.	(1981)	Beitrag zur Ermittlung des Erddrucks auf Stützwände bei nachgiebigem Baugrund
Nr. 15	Smoltczyk, U. Schweikert, O.	(1981)	Vorstudie über bauliche Alternativen für Durchgangsstraßen in Siedlungen
Nr. 16	Malcharek, K. Smoltczyk, U.	(1981)	Vergleich nationaler Richtlinien für die Berechnung von Fundamenten
Nr. 17	Gruhle, H.D.	(1981)	Das Verhalten des Baugrundes unter Einwirkung vertikal gezogener Ankerplatten als räumliches Problem des Erdwiderstandes
Nr. 18	Kobler, W.	(1982)	Untersuchungen über Böschungs- und Grundbruch bei begrenzten Lastflächen
Nr. 19	Lutz, W.	(1983)	Tragfähigkeit des geschlitzten Baugrunds neben Linienlasten

Nr. 20	Smoltczyk, U.	(1983)	Studienunterlagen "Bodenmechanik und Grundbau"; überarbeitete Ausgabe 1993
Nr. 21	Schweikert, O.	(1984)	Der Einfluß des Böschungswinkels auf die Berechnung des aktiven Erddrucks
Nr. 22	Vogt, N.	(1984)	Erdwiderstandsermittlung bei monotonen und wiederholten Wand-bewegungen in Sand
Nr. 23	Buchmaier, R.	(1985)	Zur Berechnung von Konsolidationsproblemen bei nichtlinearem Stoffverhalten
Nr. 24	Schad, H. Smoltczyk, U.	(1985)	Möglichkeiten der Böschungssicherung bei kleinen Baugruben
	Schad, H. Zoller, P.		Sonderkonstruktionen der Böschungssicherung
Nr. 25	Gußmann, P.	(1986)	Die Methode der Kinematischen Elemente
Nr. 26	Steinmann, B.	(1985)	Zum Verhalten bindiger Böden bei monotoner einaxialer Beanspruchung
Nr. 27	Lee, S.D.	(1987)	Untersuchungen zur Standsicherheit von Schlitzen im Sand neben Einzelfundamenten

Mitteilungen des
Instituts für Geotechnik der Universität Stuttgart
Hrsg.: Prof. Dr.-Ing. Dr. h.c. U. Smoltczyk

Nr. 28	Kolb, H.	(1988)	Ermittlung der Sohlreibung von Gründungskörpern unter horizontalem kinematischen Zwang
Nr. 29	Ochmann, H.	(1988)	Ebene Grenzzustände von Erdböschungen im stochastischen Sicherheitskonzept
Nr. 30	Breinlinger, F.	(1989)	Bodenmechanische Stoffgleichungen bei großen Deformationen sowie Be- und Entlastungsvorgängen
Nr. 31	Smoltczyk, U. Breilinger, F. Schad, H. Wittlinger, M.	(1989)	Beitrag zur Bemessung von Tunneln in offener Bauweise
Nr. 32	Gußmann, P. Schanz, T. Smoltczyk, U. Willand, E.	(1990)	Beiträge zur Anwendung der KEM (Erddruck, Grundbuch, Standsicher-heit von Böschungen)
Nr. 33	Gruhle, H.D.	(1990)	Der räumliche Erdwiderstand vor überwiegend horizontal belasteten Ankerplatten

Nr. 34	Henne, J.	(1995)	Zur Bewehrung von verformten Bodenschichten durch Einsatz zugfester Geokunststoffe
Nr. 35	Wittlinger, M.	(1994)	Ebene Verformungsuntersuchungen zur We-ckung des Erdwiderstandes bindiger Böden
Nr. 36	Schad, H.	(1992)	Zeit- und geschwindigkeits-abhängiges Materialverhalten in der Geotechnik – Experimentelle Erfassung und numerische Analyse
Nr. 37	Belz, I.	(1992)	Zur Ermittlung dynamischer Boden-kennwerte in situ aus der Systemantwort des Erregers
Nr. 38	Ma, J.	(1994)	Untersuchungen zur Standsicherheit der durch Stützscheiben stabilisierten Böschungen
Nr. 39	Smoltczyk, U.	(1994)	Sonderheft: 25 Jahre Lehre und Forschung in der Geotechnik
Nr. 40	Rilling, B.	(1994)	Untersuchungen zur Grenztragfähigkeit bindiger Schüttstoffe am Beispiel von Lößlehm

Mitteilungen des
Instituts für Geotechnik der Universität Stuttgart
Hrsg.: Prof. Dr.-Ing. P.A. Vermeer

Nr. 41	Vermeer, P.A.	(1996)	Deponiebau und Geotechnik
Nr. 42	Vermeer, P.A.	(1997)	Baugruben in Locker- und Festgestein
Nr. 43	Brinkmann, C.	(1998)	Untersuchungen zum Verhalten von Dichtungsübergängen im Staudammbau
Nr. 44	Fiechter-Scharr, I.	(1998)	Beeinflussung von Erdbaustoffen durch Beimischen eines organophilen Bentonits
Nr. 45	Schanz, T.	(1998)	Zur Modellierung des mechanischen Verhaltens von Reibungsmaterialien
Nr. 46	Akinrogunde, A.E.	(1999)	Propagation of Cement Grout in Rock Discontinuities Under Injection Conditions
Nr. 47	Vogt-Breyer, C.	(1999)	Experimentelle und numerische Untersuchungen zum Tragverhalten und zur Bemessung horizontaler Schraubanker
Nr. 48	Vermeer, P.A.	(1999)	Neue Entwicklungen in der Geotechnik

Nr. 49	Marcher, T.	(2002)	Resultate eines Versuchsprogramms an Beaucaire Mergel
Nr. 50	Marcher, T.	(2003)	Nichtlokale Modellierung der Entfestigung dichter Sande und steifer Tone
Nr. 51	Ruse, N.M.	(2004)	Räumliche Betrachtung der Stand-sicherheit der Ortsbrust beim Tunnelvortrieb
Nr. 52	Beutinger, P.H.	(2005)	Ein geotechnischer Beitrag zur Standsicherheit mobiler Bau-maschinen
Nr. 53	Wehnert, M.	(2006)	Ein Beitrag zur drainierten und undrainierten Analyse in der Geotechnik
Nr. 54	Möller, S. C.	(2006)	Tunnel induced settlements and forces in linings
Nr. 55	Benz, T.	(2007)	Small-Strain Stiffness of Soils and its Numerical Consequences
Nr. 56	Abed, A.	(2008)	Numerical Modeling of Expansive Soil Behavior

Nr. 57	Hintner, J.	(2008)	Analyse der Fundamentverschiebungen infolge vertikaler und geneigter Belastung
Nr. 58	Russelli, C.	(2008)	Probabilistic Methods applied to the Bearing Capacity Problem
Nr. 59	Peña Olarte, A.A.	(2008)	Influence of Particle Shape on the Global Mechanical Response of Granular Packings: Micromechanical Investigation of the Critical State in Soil Mechanics
Nr. 60	Neher, H. P.	(2008)	Zeitabhängiges Materialverhalten und Anisotropie von weichen Böden – Theorie und Anwendung
Nr. 61	Vermeer, P.A.	(2008)	Von der Forschung zur Praxis: Symposium zum 80. Geburtstag von Prof. U. Smoltczyk
Nr. 62	Satibi, S.	(2009)	Numerical Analysis and Design Criteria of Embankments on Floating Piles
Nr. 63	Lächler, A.	(2009)	Bedeutung herstellungsbedingter Einflüsse auf das Trag- und Verformungsverhalten von Schlitzwänden

Nr. 64	Möllmann, A.	(2009)	Probabilistische Untersuchung von Hochwasserschutzdeichen mit analytischen Verfahren und der Finite-Elemente-Methode

Mitteilungen des
Instituts für Geotechnik der Universität Stuttgart
Hrsg.: Prof. Dr.-Ing.habil. Ch. Moormann

Nr. 65	Moormann, Ch.	(2011)	7. Stuttgarter Geotechnik-Symposium
Nr. 66	Beuth, L.	(2012)	Formulation an Application of a Quasi-Static Material Point Method
Nr. 67	Moormann, Ch., Huber, M., Proske, D.	(2012)	Proceedings of the 10th International Probabilistic Workshop